THE UNIVERSITY *of* EDINBURGH

Biostratigraphy and Microfacies of the Cretaceous Sediments in the Indus Basin, Pakistan

BY

Suleman Khan

Thesis submitted for the degree of

Doctor of Philosophy

The University of Edinburgh

2012

Declaration

I declare that:

All material presented in this document was compiled and written by myself unless otherwise acknowledged.

Suleman Khan

2012

Acknowledgments

Hope has been the key for me during the entire period of my PhD. Thanks to Almighty Allah for giving me such a hope. Heartfelt thanks go to my supervisor, Professor Dick Kroon for his consistent help and guidance over the years. His kind suggestions have really helped me in completion of this thesis. I deeply acknowledge his friendly and enthusiastic attitude which helped me a lot as his student. I am also very thankful to my supervisors, Dr. Simon Jung and Dr. Susan Rigby for their help and suggestions.

My PhD study was supported by the Higher Education Commission (HEC) of Pakistan under the Faculty Development Programme of the University of Peshawar. I am very grateful to HEC, Pakistan and University of Peshawar K.P.K, Pakistan for sponsoring my PhD studies. I deeply acknowledge the School of GeoSciences, University of Edinburgh for sponsoring me through a partial scholarship that helped me in covering up the deficiency of my finances.

I am thankful to Dr. Stewart Molyneux, head of biostratigraphy laboratory in British Geological Survey (BGS) for arranging the palynological processing of some of my samples. Special thanks go to Dr. James Riding a renowned palynologist in the BGS, for providing a report of the preliminary findings of palynomorphs, and later on for his valuable comments on each dinoflagellate taxon identified in this study. David Batten, Emeritus Professor University of Manchester is acknowledged for his valuable comments on the spore and pollen taxa identified in this study. Special thanks go to Niels van Helmond a PhD student in the Utrecht University for running my sediments samples for TEX_{86} analysis.

I am also very thankful to friends and students i.e. Dr. Sajjad Ahmed, Hamad Ghani, Imran Ahmad, Hasaam, Fahad Alizai, Syed Wajid Hanif, Ibrahim Afridi, Rasheed, at the Department of Geology, University of Peshawar for their help in collection of field data. Special thanks go to a dear friend and an amateur geologist, Muhammad Altaf whose help and assistance in the field is worth mentioning. My friends and flat mates in Edinburgh i.e. Dr. Amjad Iqbal and Adil Hussain (PhD student) are thanked for providing a friendly environment and their help and support.

I am grateful to the technical staff of the Grant Institute University of Edinburgh for their help and assistance. Thanks to Colin Chilcott for his help in stable isotope analysis. Dr. Nicola Cayzer, John Craven are thanked for their help in using the microscope facilities. Thank you Mike Hall for your painstaking efforts in making hundreds of thin sections for me.

Finally I am deeply thankful to my mother (Khaima Bibi) and wife (Azra Bano) whose unconditional love and support always encouraged me in tense moments of my life.

Suleman Khan

To my parents and wife (Azra Bano)

Suleman Khan

Abstract

In this thesis I document the biostratigraphy of two Cretaceous sections in Pakistan, the Chichali Nala Section and the Moghal Kot Section. Furthermore, I document the stratigraphy of the so-called Oceanic Anoxic Events (OAEs) in the Moghal Kot Section. In addition, I establish potential links between the planktonic foraminiferal evolution and these OAEs in the Moghal Kot Section. Sea Surface Temperatures (SSTs) are established for the Valanginian time by using the TEX_{86} and $\delta^{18}O$ proxies in the Chichali Nala Section.

The new biostratigraphy of the Chichali Nala Section shows that the ages of the sediments are mainly Valanginian. The biostratigraphy of the Moghal Kot Section show ranges in age from the Early Aptian to Early Maastrichtian. Seven OAEs were recorded in the Moghal Kot Section based on the combined study of biostratigraphy, microfacies, and $\delta^{13}C$ analysis. These OAEs correlate well with previously documented OAEs elsewhere, therefore the new record of the OAEs in the Moghal Kot Section confirms the widespread occurrence of these events, possibly all global in nature.

A quantitative review of the planktonic foraminiferal evolution in the Moghal Kot Section indicates that the environmental changes along the OAE2 have strongly forced the evolution of the planktonic foraminifera. Conversely, no clear relationship is observed between other OAEs and planktonic foraminiferal evolution in the same section.

The SST results based on the TEX_{86} in the Chichali Nala Section show that the surface ocean was consistently much warmer (10-12 ^{o}C) than today at the paleolatitude of ~-35^{o} during the Valanginian time. Such warm conditions are also supported by the spore and pollen assemblages of the Chichali Nala Section. Collectively the two datasets indicate strongly that the Valanginian world was overall extremely warm. Such warming during the Valanginian is incompatible with previously suggested cooler conditions during this time period.

Table of contents

CHAPTER 1

1. Introduction

1.1 Project rationale

The aim of the project is to document the Cretaceous bio-carbon isotope stratigraphies, and microfacies of the Cretaceous sediments of the Indus Basin, Pakistan. These stratigraphies aid in the timing and identification of Oceanic Anoxic Events (OAEs), which have not been studied in Pakistani Cretaceous Sections as yet. The stratigraphies are collectively used to quantify evolutionary patterns of planktonic foraminifera in the Cretaceous.

1.2 Oceanic Anoxic Events (OAEs)

The OAEs are characterised by the deposition of anomalously high amounts of organic matter in sediments, which appear in the form of black shales (Schlanger and Jenkyns, 1976). In the literature, previously described major OAEs are the Toarcian Event in the Early Jurassic, the Weissert and Selli (OAE1a) Events in the Early Cretaceous and the Bonarelli Event (OAE2) in the Late Cretaceous (Takashima et al., 2006; see fig. 1.1).

The black shales associated with the OAEs can be explained by restricted oceanic circulation (Bralower & Thierstein, 1984) or high productivity (Pedersen & Calvert, 1990), or a combination of both (figs. 1.2 & 1.3). In the restricted oceanic circulation model, oxygen is not circulated to the bottom water, resulting in anoxic deep water conditions (fig. 1.3). In the high productivity model, a high amount of organic carbon is produced in the surface ocean, which gets partly preserved in the sediments (fig. 1.3).

The underlying cause of the OAEs is thought to be venting of greenhouse gases from submarine volcanism during plateau formation i.e. Large Igneous Provinces (Larson and Erba, 1999). These gases cause global warming, ocean acidification, ocean stratification, and an accelerated hydrological cycle (Jenkyns, 2010; Thierstein, 1979; Erba et al. 2004, see fig. 1.2).

The global warming caused by the venting of greenhouse gases is accompanied by ocean acidification (Jenkyns, 2010). Such acidification of global ocean may have been caused by volcanic derived input of CO2 and SO2 to the global oceans, or by methane release from upper slopes (Zachos et al., 2005; Jenkyns, 2010; Jahren et al., 2005; Hesselbo et al., 2000)

Most geochemical proxies for the past acidification are still under development. The most straightforward proxy is the decrease in the carbonate content (Hönisch et al. 2012) Therefore, past acidification events are recorded in geological records by a significant decrease in carbonate content.

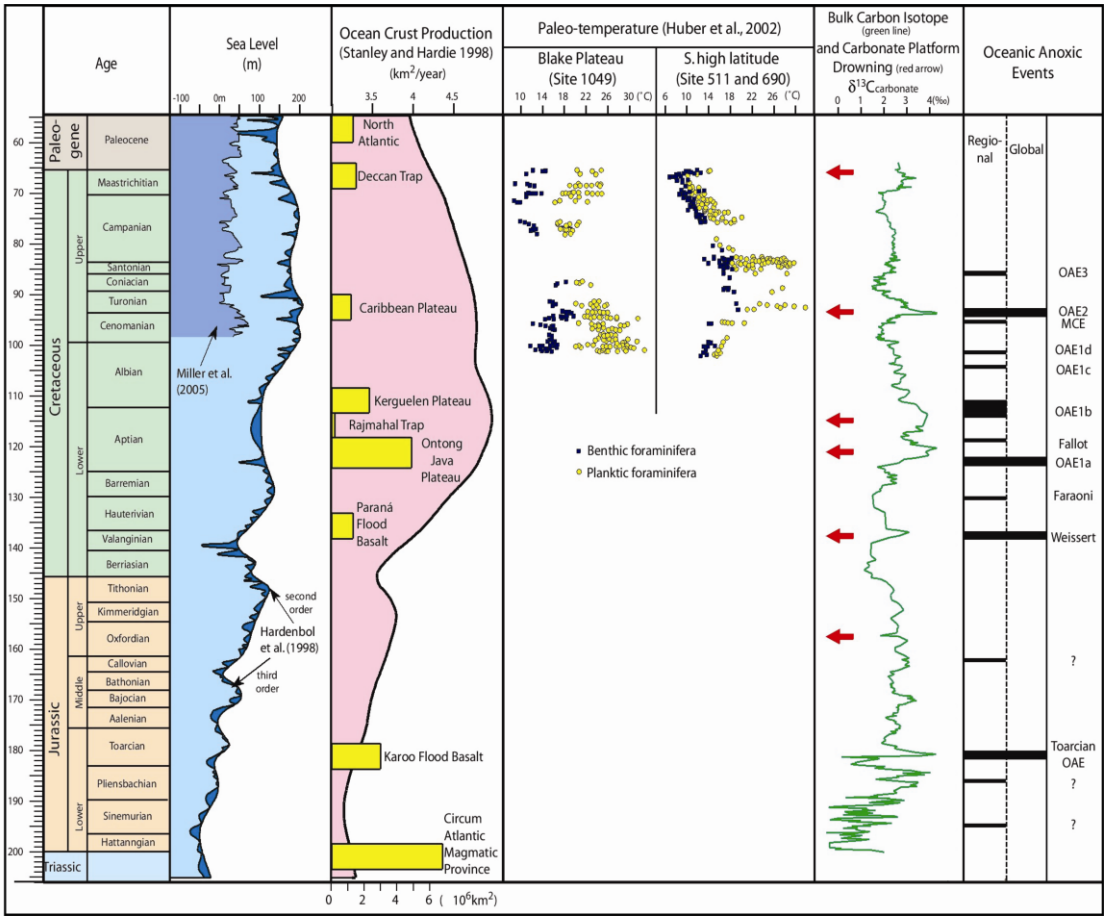

Figure 1.1: Showing regional and global OAEs, bulk carbon isotopes, paleo-temperature, sea level changes, oceanic-crust production, carbonate platform drowning, and paleo-temperature in Jurassic–Cretaceous, modified after Takashima et al. (2006).

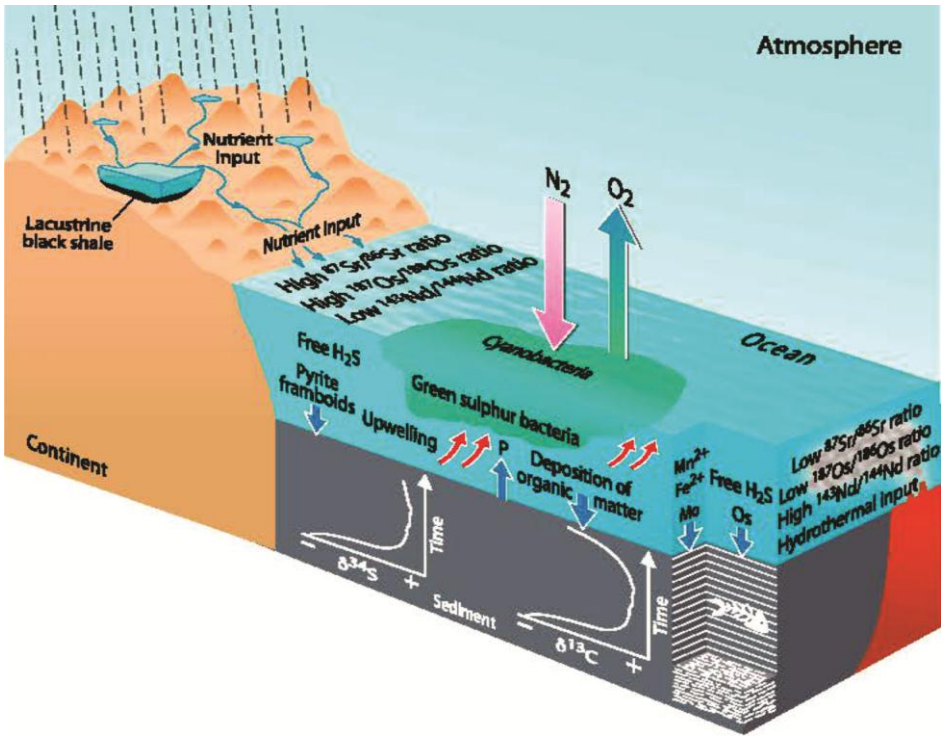

Figure 1.2: A model showing various geochemical processes associated with OAEs, modified after Jenkyns (2010).

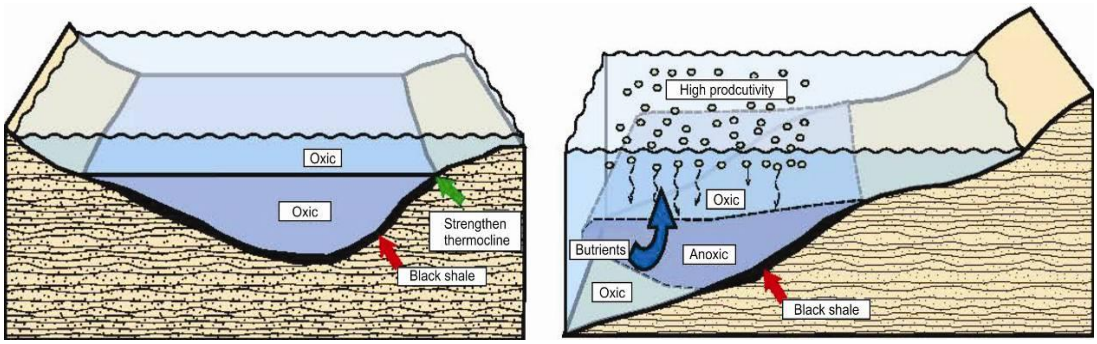

Figure 1.3: Showing two different models for black shale deposition: (left) the stagnant ocean model, and (right) the oxygen-minimum-layer model, modified after Takashima et al., (2006).

Carbon isotope stratigraphy is a useful tool for global correlation of Cretaceous sediments. Large carbon isotope excursions occur in the Cretaceous sediments, mostly coinciding with the OAEs. These carbon isotope excursions are not unidirectional across the OAEs, some OAEs are characterized by positive and others by negative excursions in $\delta^{13}C$, in both carbonate material and organic matter (Jenkyns, 2010; and references therein) (fig. 1.1). A positive shift in the carbon isotopes in the sediments across an OAE is explained by prolonged high productivity

in the oceans, resulting in sequestration of carbon enriched in ^{12}C in sediments (Scholle & Arthur, 1980), while a negative shift in the carbon isotopes across an OAE can be explained by methane release from the continental margins into the ocean-atmosphere system (Dickens et al. 1995; Hesselbo et al., 2000; Jahren et al. 2005), or by volcanic CO_2 release into the atmosphere (Menegatti et al., 1998). In this study, the carbon isotope stratigraphy of the Moghal Kot Section is shown.

The changing environmental conditions influenced evolution of the plankton across the OAEs in the Cretaceous (e.g. Leckie et al., 2002). Enhanced rates of speciation and extinction of the test secreting plankton occurred at or near these OAEs in various parts of the world's oceans (Leckie et al., 2002; Erbacher & Thurow, 1997). However, the evolutionary history of the planktonic foraminifera has not been studied in this part of the Eastern Tethys Ocean. In this study, a quantitative view of this history is presented.

1.3 Background to the study area

1.3.1 Geography

Geographically, Pakistan lies in South Asia and is bounded to the north by China and in the north-west by Afghanistan (fig. 1.4). Iran borders the country to the west, India to the east and the Arabian Sea is located to the south of Pakistan. Pakistan has a fascinating diverse landscape, varying from spectacular high mountains, broad plateaus, to vast plains and large deserts. The altitude decreases drastically from the north to the south and from west to the east in the country. The high altitude areas have a substantial role in dictating the climate of Pakistan. Based on temperature, Pakistan has been divided into hot, warm, mild, cool, and cold climates (Khan, 2010). The most significant factors which substantially affect the climate of the country e.g. Pakistan, are latitudinal location, proximity to sea level, continentality, marine influence in the extreme south, vegetation cover, and soil content (Khan, 2010).

1.3.2 Indus Basin

The Indus Basin is a large basin which stretches more in the north-south direction than in the east-west direction (fig. 1.4). The whole set of sedimentary rocks ranging from the Precambrian to Recent are exposed in the Indus Basin. The paleotopographic features such as the Sarghoda, Mari Jaisalmir, and Jacobabad Highs have influenced depositional patterns in this basin and hence these features subdivide the basin into two parts: the Upper Indus Basin (UIB), and the Lower Indus Basin (LIB), implying different lithofacies development in each (Kadri, 1995). The UIB is located between the Main Mantle Thrust (MMT) to the north and Sarghoda High to the south. The LIB extends from the Sarghoda High in the north to the Arabian Sea in the south. This LIB is further subdivided into the Middle Indus basin (MIB), or Sulaiman Basin, and the Southern Indus Basin (SIB). These two sub-basins of the LIB are in turn separated by the Jacobabad and Mari-Jaisalmir Highs. The Moghal Kot Section represents an integral part of the MIB. A brief subdivision of the MIB is given in the following paragraph.

1.3.2.1 Subdivision of the Middle Indus (Sulaiman) Basin

The Sulaiman Basin can be subdivided into the following areas from east to west: the Punjab Platform, the Sulaiman Depression, and the Sulaiman Fold Belt (Kadri, 1995; see fig. 1.5).

Punjab Platform: This is the eastern tectonically passive segment of the Sulaiman Basin, with no outcrops. It is a broad monocline which gently dips towards the Sulaiman Depression (Kadri, 1995). The data from wells drilled in this platform show various important stratigraphic pinch-outs in Pakistan (Kadri, 1995; see fig. 1.6). These stratigraphic pinch outs may act as possible stratigraphic traps for the future hydrocarbon exploration.

Sulaiman Depression: This longitudinally oriented depression, located in the front of the Sulaiman Fold Belt is shown by gravity data (Kadri, 1995). This depression becomes transverse (east-west) in its orientation in its southern domain (fig. 1.5). The west of the depression includes the Zindapir Inner Folded Zone, while the Mari Bugti

Inner folded Zone is located in its south (Kadri, 1995). The Punjab platform is located to the east of this depression.

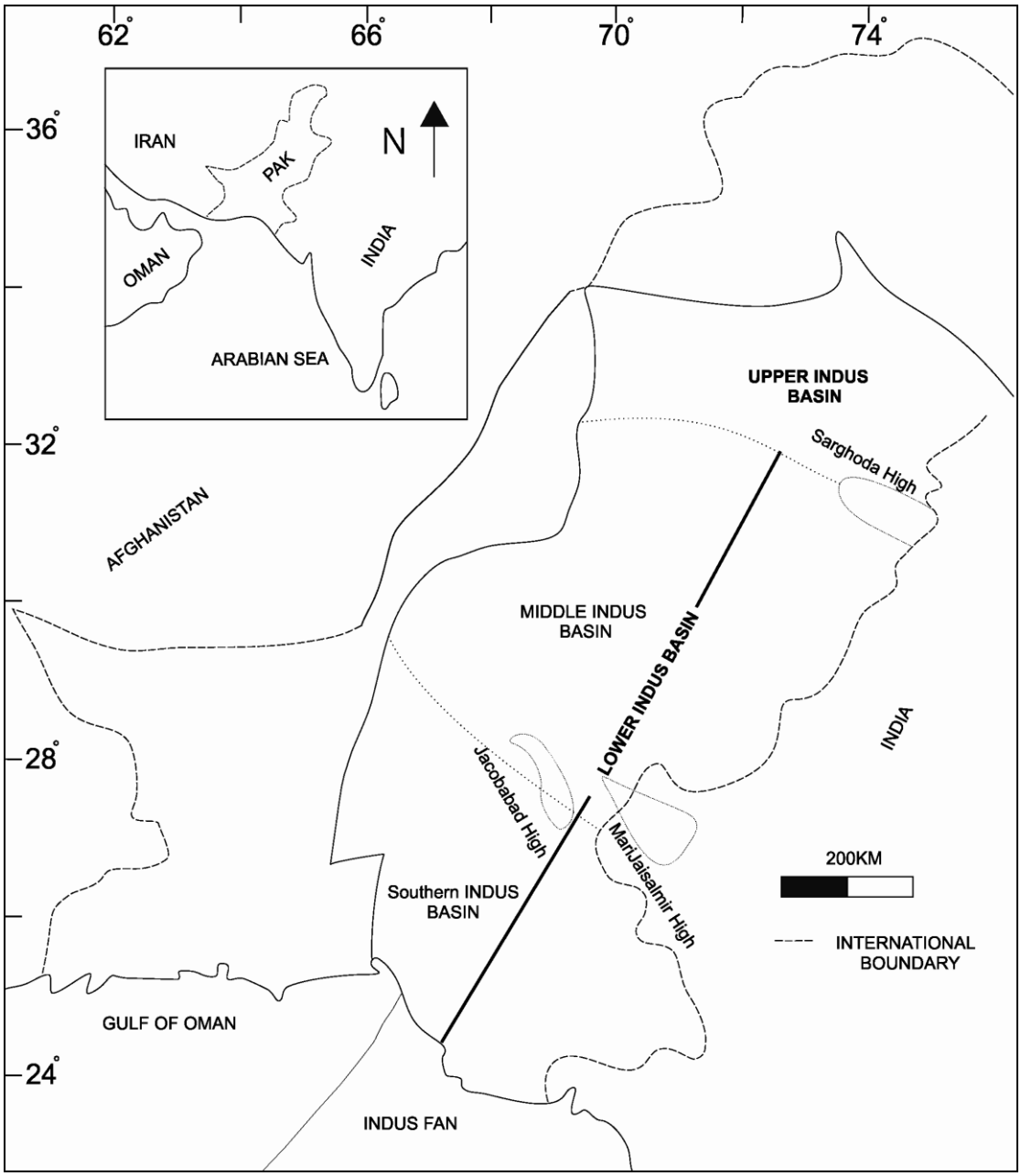

Figure 1.4: Map of Pakistan, showing the Indus Basin, modified after Banks & Warburton (1986) and Kadri (1995).

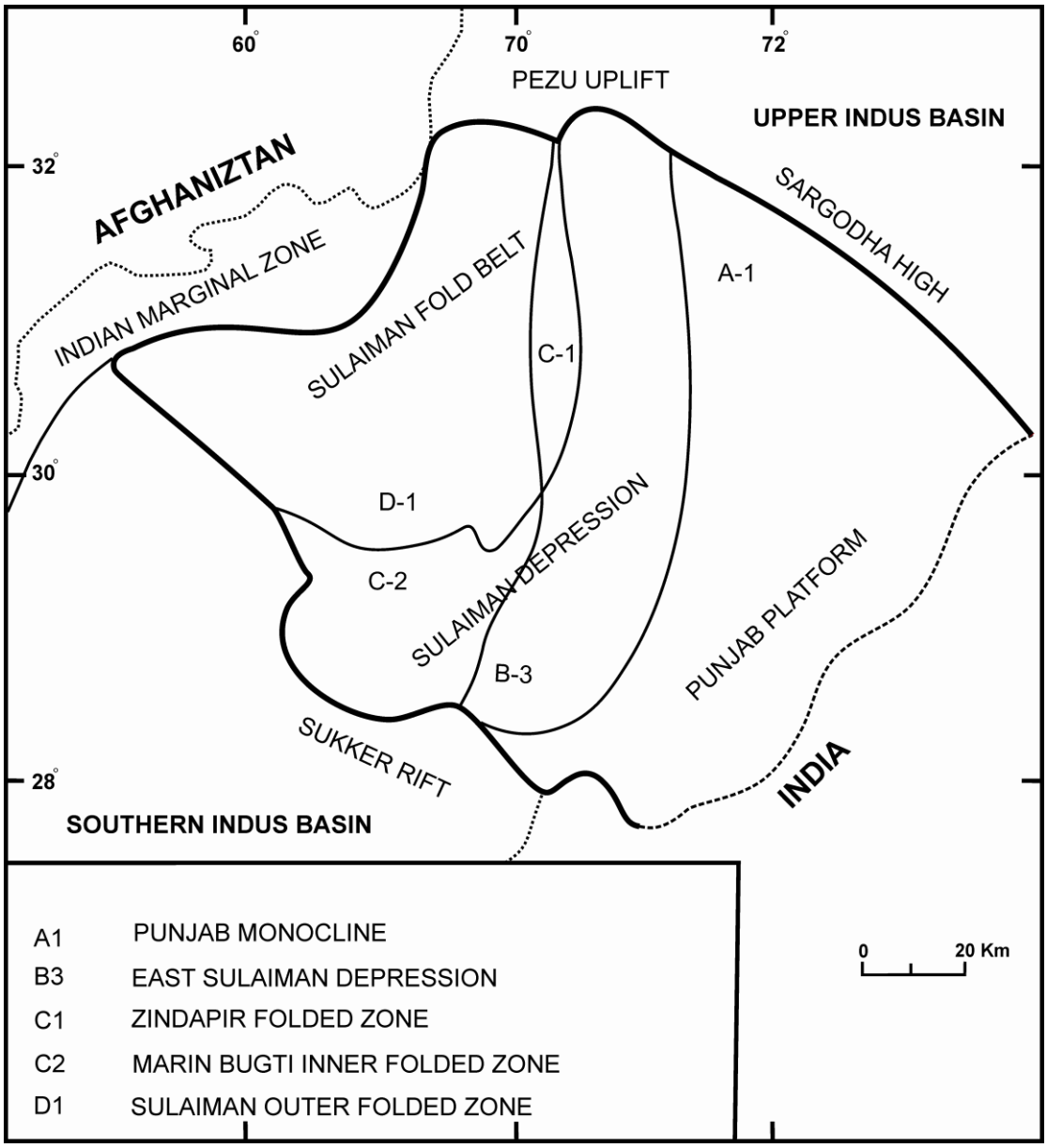

Figure 1.5: The subdivision of Middle Indus Basin after Kadri (1995).

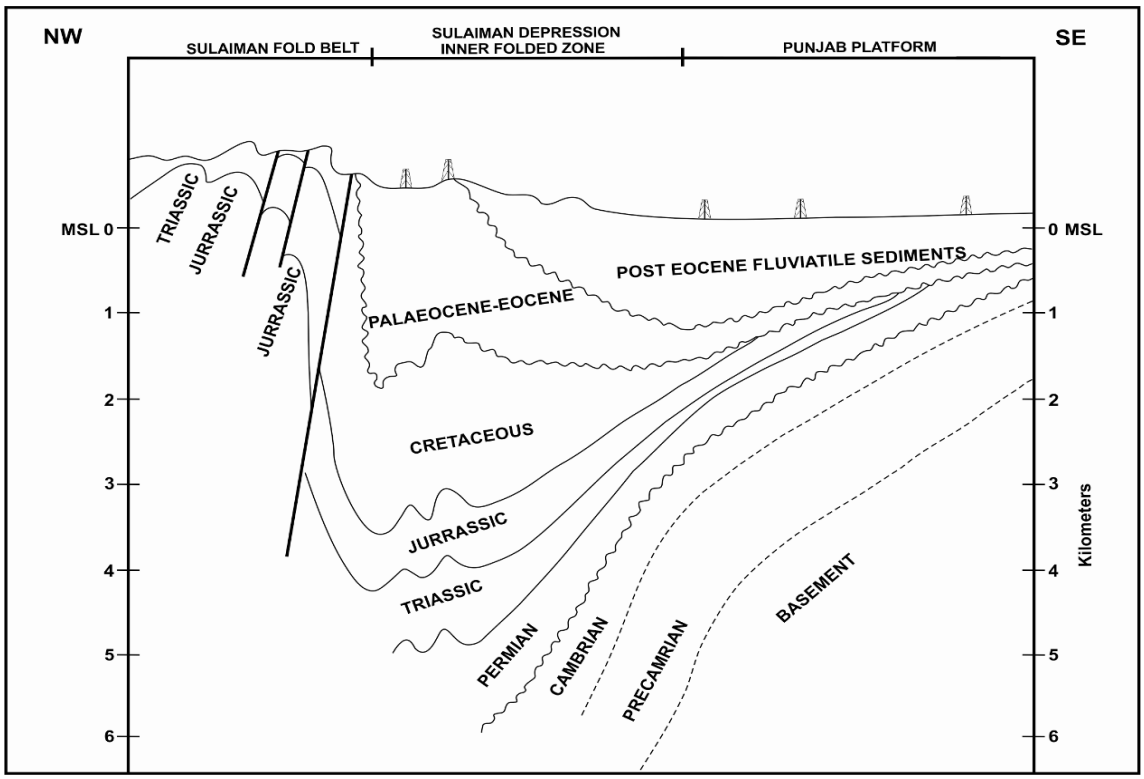

Figure 1.6: Regional Cross Section of the Middle Indus Basin, after, Kadri (1995).

Sulaiman Fold Belt: This major tectonic entity is formed as a result of the India and Afghanistan collision, which resulted in a large number of anticlines (Kadri, 1995). The lithofacies variations are very pronounced in sequences of the Sulaiman Depression and Sulaiman Fold Belt areas (Kadri, 1995). The Moghal Kot Section, key section for my stratigraphic study in this thesis, is the best section for studying the Jurassic to Palaeocene strata, because it is most complete.

1.3.3 Regional tectonics of Pakistan

The Himalayan orogeny which started in the Eocene time has dictated the regional tectonics of Pakistan. Pakistan occupies the western most part of the Indian Plate (fig. 1.4) and is therefore an integral part of the western Himalayas. The Himalayas extend from Burma all the way to northern India and Nepal into Pakistan (Gansser, 1981).

1.3.3.1 Northern tectonics of Pakistan

After rifting from the Gondwana continent, the Indian plate drifted to the north, and subsequently collided with Eurasia, which resulted in the spectacular Himalayas (Coward et al. 1986; Johnson et al. 1976). India started its northward drift (fig. 1.7) at 130 Ma, and intra-oceanic subduction in the north ultimately squeezed the Neo-Tethys (Johnson, 1976). The Kohistan Island Arc in Pakistan is part of the island arc system which had resulted due to this intra-oceanic subduction (figs. 1.8 & 1.9). After this island arc system was emplaced, the Tethys Ocean on the south of the Eurasia changed into back arc basins (Searle, 1991). In north Pakistan, such a back arc basin had closed after the Kohistan Island Arc collided with the Karakurm block (Eurasia) along a suture zone called the Main Karakurm Thrust (MKT) (Tahirkheli, 1982). This collision took place in Late Cretaceous between 102-75 Ma (Coward et al. 1986) (figs. 1.8 & 1.9). Afterwards, the Indian Plate collided with the Kohistan Island Arc along the MMT (figs. 1.8 & 1.9). This collision occurred about 55-50 Ma ago, and had significantly reduced the drift rate of the Indian Plate (Powell, 1979). Notably, the Indian Plate shows anticlockwise movement since 50-55 Ma (fig. 1.7).

After the final collision of India with Eurasia (Kohistan Island Arc in Pakistan), the propagation of the deformation towards the south had resulted in the regional thrusts

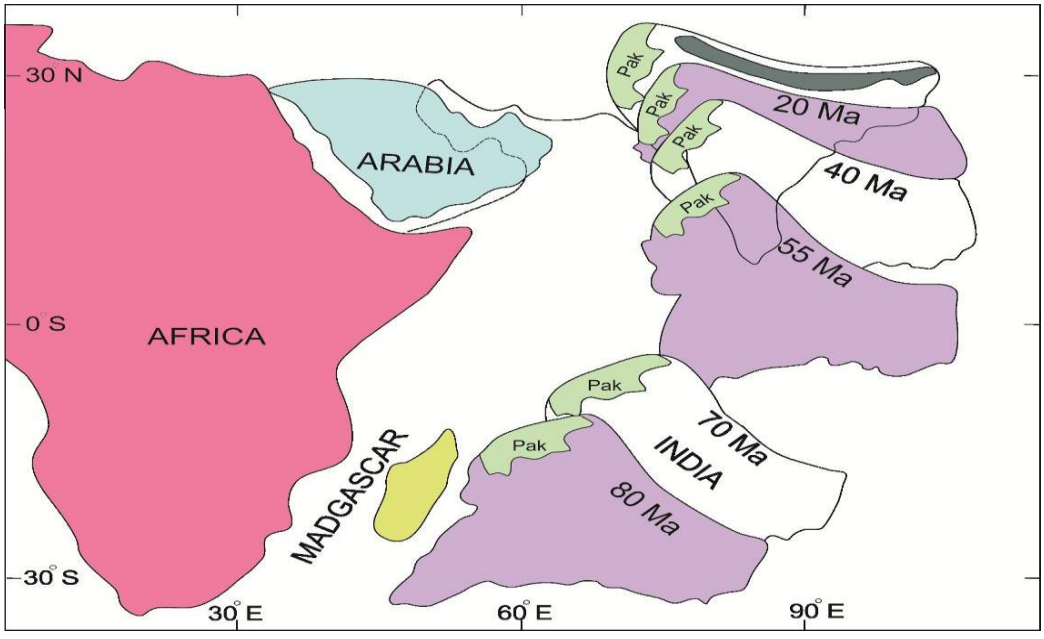

Figure 1.7: Map showing the northward drift of the Indian plate with anticlockwise rotation, modified after Kazmi & Jan (1997).

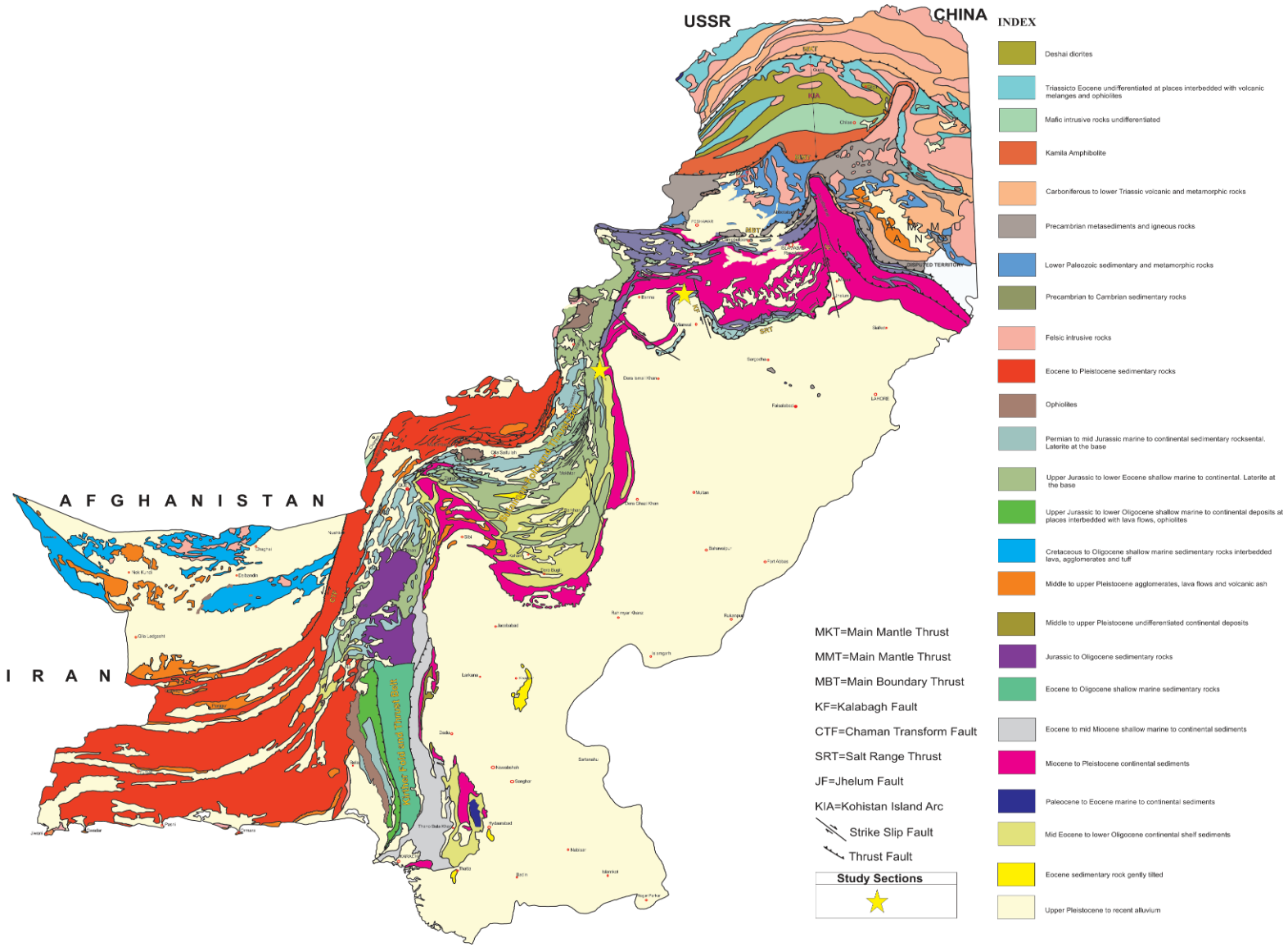

Figure 1.8: Tectonic map of Pakistan, showing major geological and tectonic features of Pakistan. The map is digitised after Kazmi & Rana (1982).

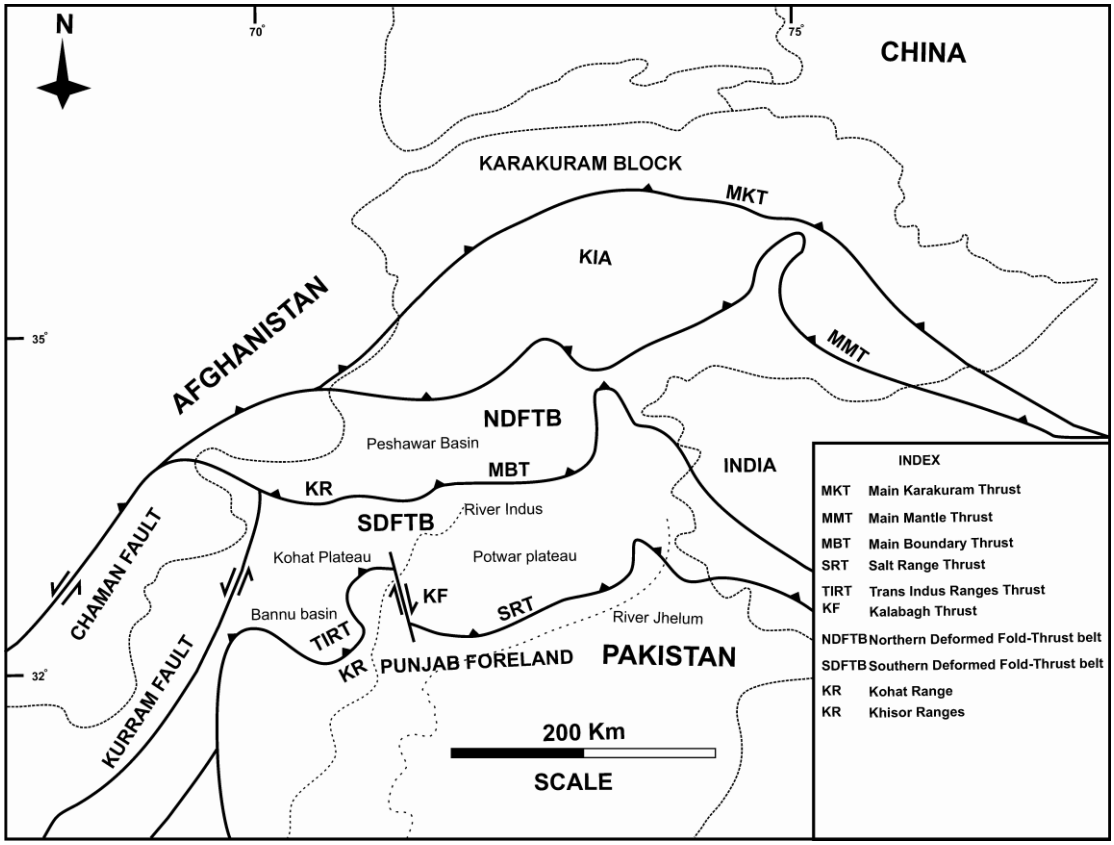

Figure 1.8: Tectonic map of north Pakistan, after Kazmi & Rana (1982).

i.e. the Main Boundary Thrust (MBT), and the Main Frontal Thrust (Salt Range Thrust in Pakistan) within the continental India (Kadri, 1995) (fig. 1.9).

The age of the final Indian plate-Asian plate collision is still controversial. Most workers agree on a proposed age of 50 to 55 Ma e.g. the paleomagentic data of Hinsbergen et al (2012) reconstructed from the sedimentary succession of the Indus Suture Zone (a zone of closure between the Indian plate and the Asian plate) suggests two stages of collision between the Indian and Asian plates, namely the first collision of the Tibetan-Himalaya micro-continent occurred with Asia at 50 Ma, and then the hard collision between India-Asia took place around 25-20Ma. This 25-20Ma age for the timing of the final Indian-Asian collision is the youngest age amongst the proposed ages for this collision. Interestingly, Bouilhol et al. (2013) have suggested a 40 Ma age for the India-Asia collision, based on field and isotopic data collected for understanding the spatial and temporal evolution of the Kohistan-Ladakh Island Arc. Therefore, based on this recent literature, a full picture of the

timing of the India-Asia collision is not clear as yet, however new paleomagentic and age data in future will help in addressing the controversy regarding the timing of this collision.

The severely deformed sedimentary, metasedimentary, and metavolcanics rock sequences of the zone between the MMT and MBT is known as the Northern Deformed Fold and Thrust Belt (fig.1.9). This deformed belt stretches all along the Kurram area in the west near Afghanistan to Kashmir in the east. The deformed sedimentary package of the zone between MBT and SRT is known as the Southern Deformed Fold and Thrust Belt (fig. 1.9). This belt can be further subdivided into the Potwar Plateau to the east and the Kohat Plateau to the west. These plateaus also have the status of the sub-basins of the UIB and are known as the Kohat and Potwar Basins (Kadri, 1995).

1.3.3.2 Western Tectonics of Pakistan

During the northern drift of the Indian Plate, it came in contact with the Afghan block in the west in the Late Cretaceous. During this time of the India-Afghanistan contact, significant amount of the Tethys Ocean was consumed already along the northern subduction zone (Bannert & Raza, 1992). On other hand the subduction zone between India and Afghanistan and the subsequent extrusion of the Afghan Block had resulted in the Katawaz Basin in the Late Cretaceous/Palaeocene (Jones, 1960; Kaever, 1967; Gansser, 1970; Cassaigneau, 1979). This basin developed further in the Late Palaeocene-Miocene (Badshah et al., 2000). After the development of the Chaman Transform Fault in the Miocene, the signs of deformation became more prominent in this Basin (Cassaigneau 1979). In Pliocene time, this basin closed completely, and the transpressional tectonics propagated further south, resulting in the formation of the Sulaiman and Kirthar Fold Belt (Cassaigneau, 1979; Haq & Davis, 1997) see figure, 1.8. The Chaman Transform Fault at the India-Afghanistan contact had both strike slip and thrust components. These components are, however, not simple. The sandbox model (fig. 1.10) shows

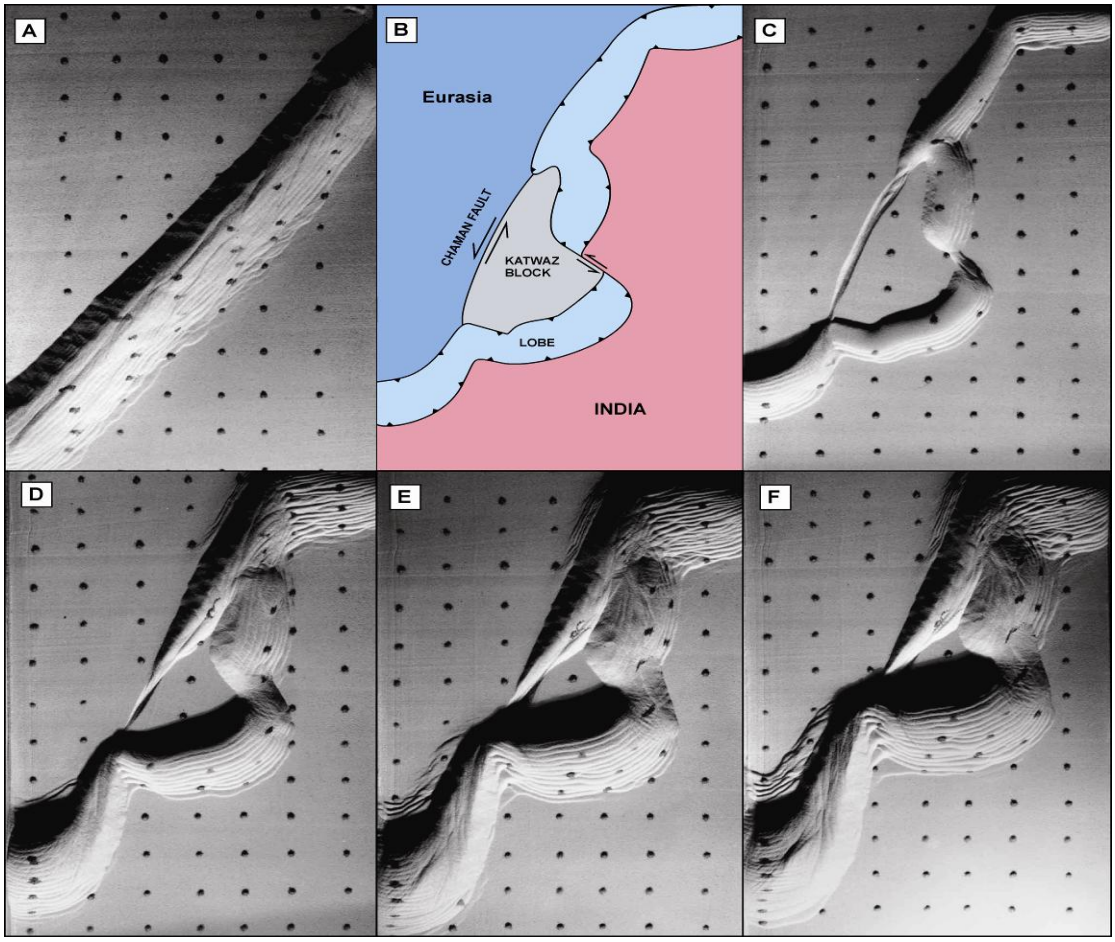

Figure 1.9: Plan view of sandbox model of the Sulaiman Fold Belt. A. Simple margin between Indian Plate and Afghan Block B. Margin having an intermediate block i.e. Katawaz Basin, between two plates. C, D, and E represent development of structures with ongoing convergence between Indian Plate (on the right) and Afghan plate (on the left) with an intermediate Katawz Basin (modified after, Haq & Davis, 1997)

that the plate motion vector between India and Afghanistan along the Chaman Fault cannot be explained simply by normal and parallel components of the vector to the plate boundary (Haq & Davis, 1997). Their model suggests that the complex strike slip and thrust faults of various orientations can only be explained if there is a continental block involved between the Indian Plate and the Afghan Block. They proposed the Katawaz Block is an intermediate crustal block between the Indian Plate and the Afghan Block (fig. 1.10). This intermediate block might have resulted in transpressional structures of the Sulaiman and Kirthar Fold Belts (Haq & Davis, 1997). The most important Moghal Kot Section for the current investigation is located in the Sulaiman Fold Belt of Pakistan, which is in turn part of the Middle Indus (Sulaiman) Basin.

1.4 Indus Basin Evolution during the Jurassic and Cretaceous

Regional tectonics is a fundamental controlling factor of sedimentary sequences. The tectonic activity affecting sedimentary sequences range from the major rift initiation to the in situ faulting inside the basin (McCann & Saintot, 2008). During the Mesozoic time the Indus Basin was located on the passive continental margin of the Indian Plate. The sedimentary sequences of the Indus Basin are therefore significantly affected by the Indian Plate collisional tectonics with Eurasia in the north and Afghan Block in the west.

During the Jurassic time a carbonate platform opened due to the rifting of passive continental margin of the Indian Plate (when the India-Madagascar Plate separated from the Afro-Arabia Plate; Smewing et al. 2002). The carbonates of the Samana Suk Formation and Chilten/Sulaiman Limestone were deposited on this platform in the Upper and Lower Indus Basins respectively (figs. 1.11).

The progradation of the Chilten/Sulaiman carbonate platform was driven by the thermal uplift of the Indian shield in middle Jurassic which lasted till the end of Jurassic (Smewing et al. 2002). This progradation has resulted in the subareal exposure of the Chilten/Sulaiman carbonate platform in the LIB, recorded as a thick laterite (figs. 1.11 & 1.12A). The middle Jurassic carbonates counter part of the Sulaiman/Chilten Limestone i.e. the Samana Suk Formation in the Upper Indus Basin (UIB) has also recorded this unconformity at the interface of the Saman Suk Formation and the overlying Chichali Formation.

During the Late Jurassic, deposition in the Indus Basin is recorded in the form of shelfal glauconitic sand and shale of the Chichali Formation in the UIB (figs. 1.11B & 1.12B) and organic rich clays/channelized sandstone of the Sembar Formation in the LIB suggests deposition in deltaic system (fig. 1.11B & 1.12C-D). The onset of these clastic strata is related to the transgression of the Tethys in Late Jurassic. This transgression is associated with the opening of the north-western margin of the Indian Plate along rift faults, before the separation of the India-Madagascar Plate from the Australia-Antarctica Plate (Besse & Courtillot 1988).

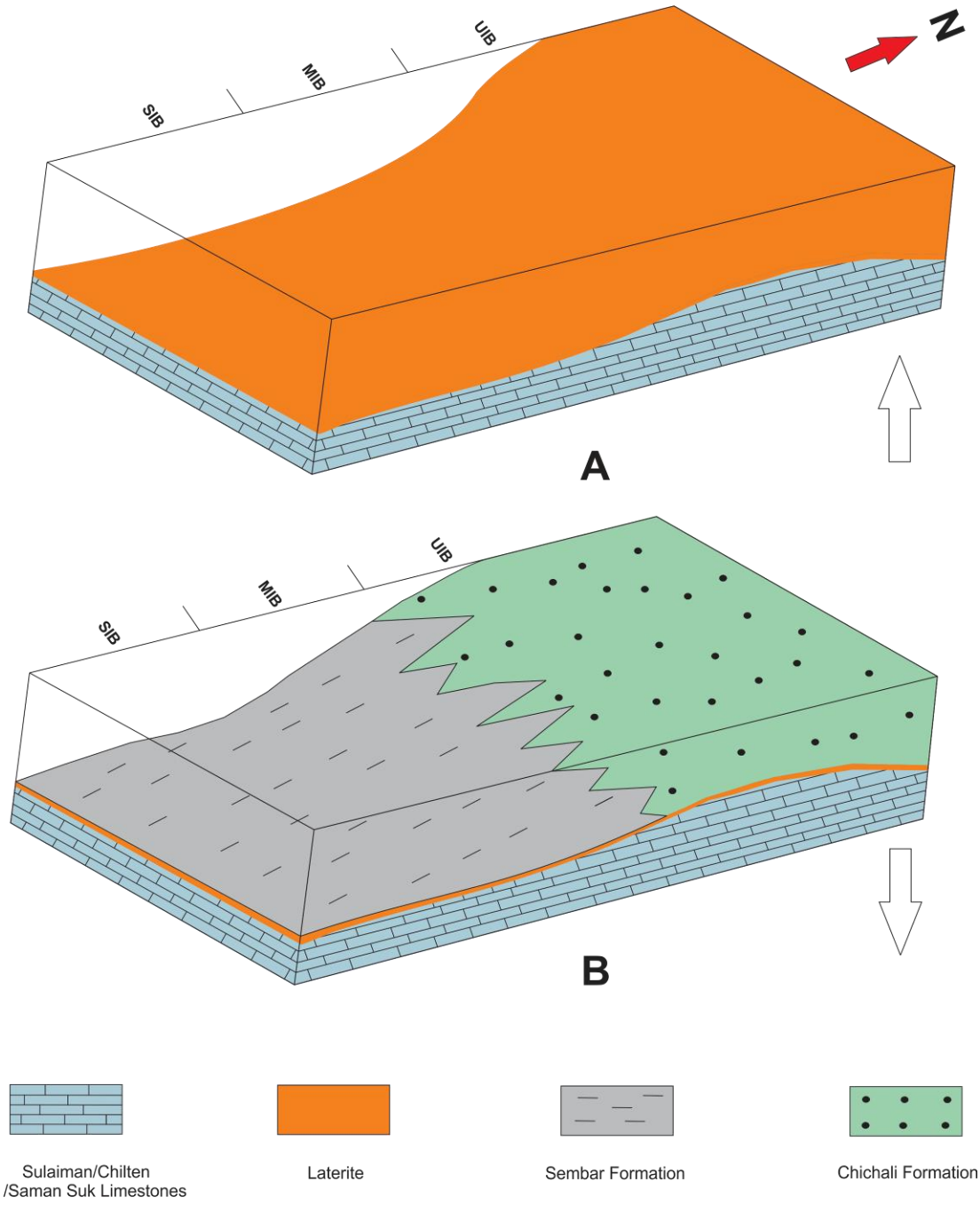

Figure 1.11: A. Exposure of the Jurassic carbonate platform due the thermal uplift of the Indian Shield in Middle to Late Jurassic B. The rifting of the passive continental margin of the Indian Plate in Late Jurassic caused flooding of the exposed platform and subsequent clastics deposition of the Chichali and Sembar Formation on the shelf during Late Jurassic to Early Cretaceous.

The source for the clastics is believed to the thermally uplifted eastern and southern margin of the Indian Shield (Smewing et al. 2002l; Hallam & Maynard). The clastic strata of the Chichali and Sembar Formations were continuously deposited till the Neocomian time (Shah, 2009). The time equivalent clastics of the Chichali and

Sembar Formations are also recorded in the Kachchh Basin of India, located in the SE of the Indus Basin (Fürsich & Pandey, 2003).

The increased eustatic sea level rise coupled with long span of denudation caused flooding of the Indian Shield in the LIB (Smewing et al. 2002) during the Early Aptian. In the Middle Indus Basin this flooding has caused the deposition of deeper pelagic carbonates of the Parh Limestone while synchronous deltaic Lumshiwal and Goru Sands were deposited in the UIB and SIB respectively (fig. 1.13A). These deltaic deposits lasted till the Albian time (Shah, 2009). The deltaic sediments in the UIB and SIB probably suggest the uplifted Indian Shield during Aptian-Albian time (Smewing et al. 2002).

In Late Cretaceous the pelagic carbonates facies of the Parh Limestone were also established in the SIB (fig. 1.13B), while synchronous pelagic carbonate facies of the Kawagarh Limestone were deposited in the UIB (Shah, 2009; Smewing et al. 2002). The Late Cretaceous is therefore a time of maximum retrogradation of the basin margin.

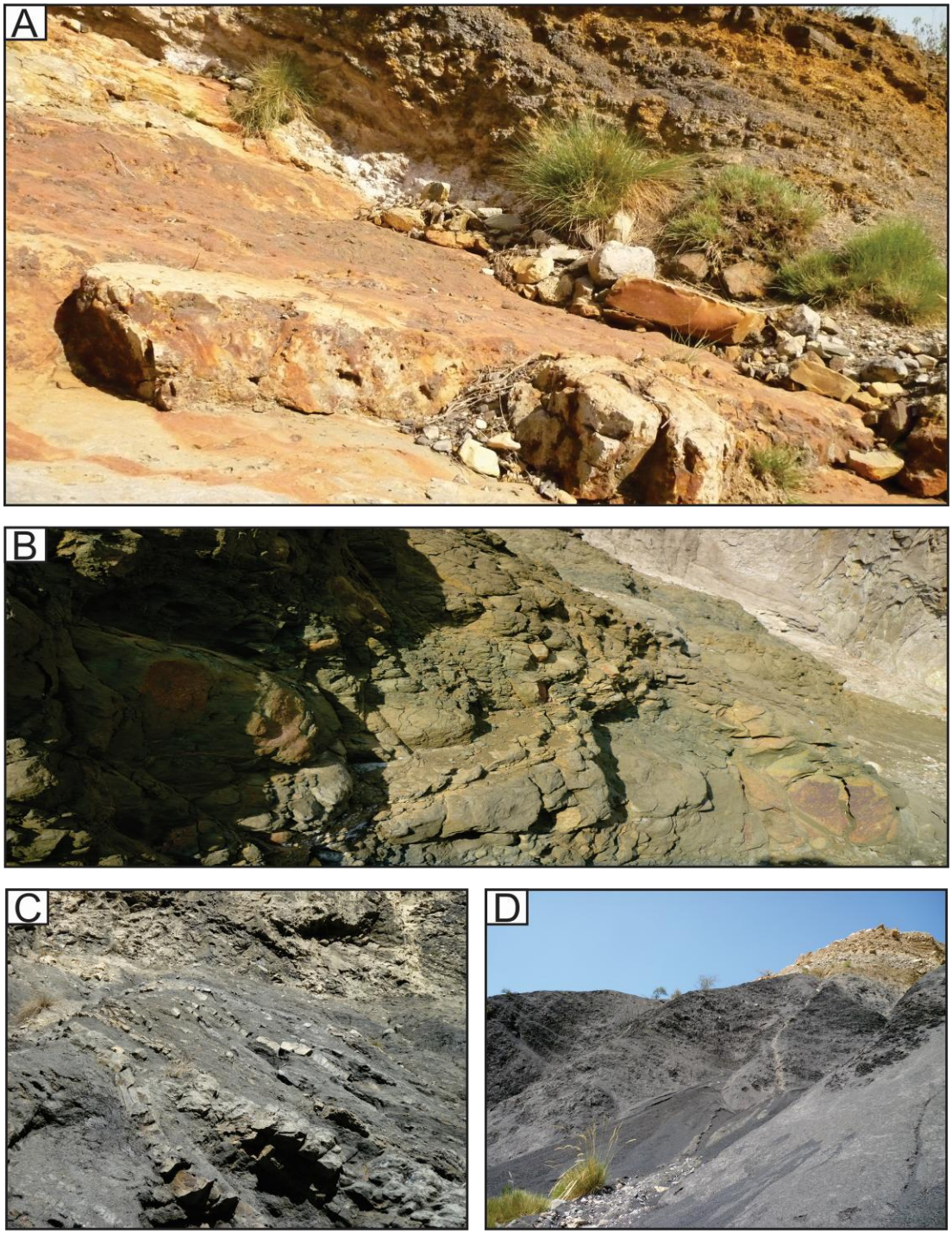

Figure 1.12: A. Late Jurassic laterite on top of the Sulaiman/Chilten Limestone B. Glauconitic sands of the Late Jurassic-Early Cretaceous Chichali Formation C. Delta Plain channelized sand and carbonaceous shales in the upper part of the Sembar Formation D. Prodelta carbonaceous shales of the Sembar Formation in the lower and middle parts of the Sembar Formation.

The carbonate breccias are recorded in the upper part of the Parh Limestone (fig. 1.14A &B). The upper part of the Parh Limestone is Late Cretaceous in age. These breccias may have formed by reworking of carbonate material from the normal fault

bounded highs caused by tectonic collapse of the western margin of the Indian Plate caused by obduction of Waziristan Ophiolites (Shafique, 2001).

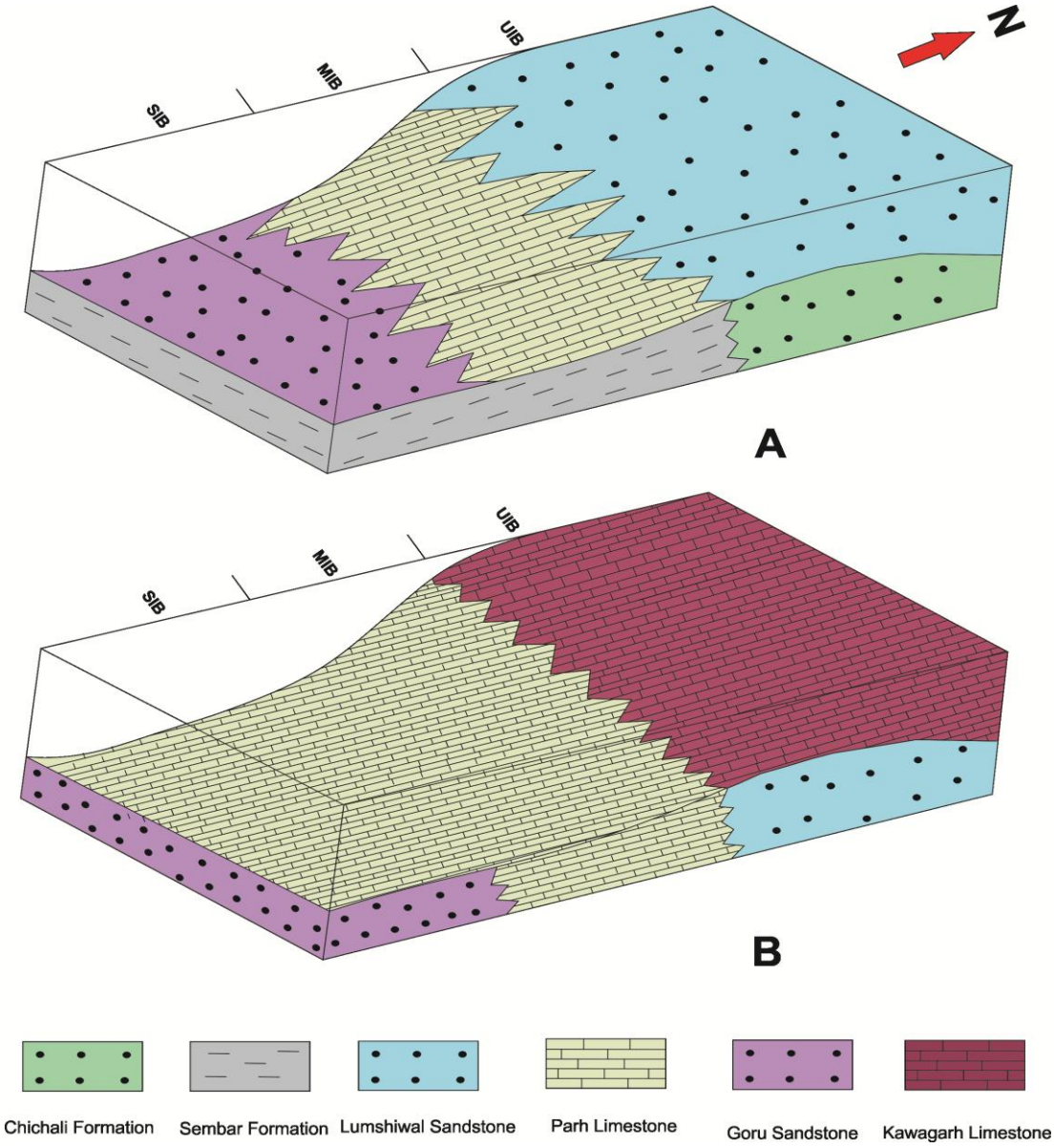

Figure 1.13: A. The flooding of the MIB during Aptian time induced the deposition of pelagic Parh Limestone, while synchronous deposition of deltaic deposits in the UIB and SIB suggest localised reworking of the Indian Shield B. Deepening of the whole Indus Basin in Late Cretaceous is recorded in the form of pelagic deposits of the Parh Limestone in the MIB and SIB and the Kawagarh Limestone in the UIB.

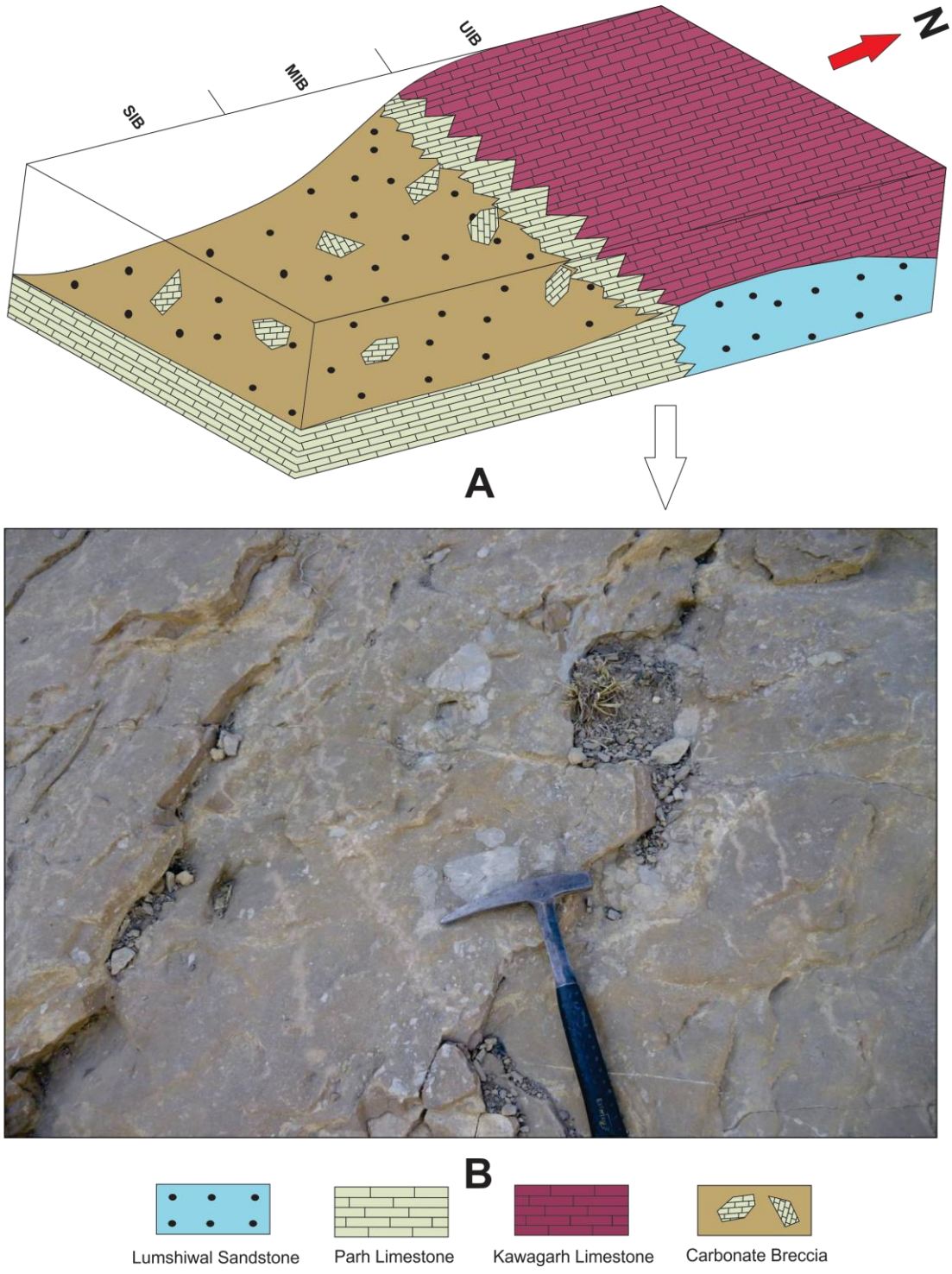

Figure 1.14: A & B shows the carbonate breccias formed due to the reworking of carbonate highs created by the tectonic collapse of the western margin of the Indian Plate by Late Cretaceous (Campanian) during ophiolite obduction.

1.5 Methodology

1.5.1 Field work

The Cretaceous rocks of Pakistan were deposited in the giant Indus Basin. This basin is divided into the Upper Indus Basin (UIB) and the Lower Indus Basin (LIB) as discussed earlier. In order to have an almost complete record of the Cretaceous sediments, and to understand lithofacies, biofacies, and paleoenvironmental changes throughout the Indus Basin, one section is selected from the UIB and one from the LIB. These two sections were sampled in three field sessions.

The first field session was carried out to describe and sample the Chichali Nala Section of the UIB from December 12th (2008) to January 14th (2009). In this field season, the clastic glauconitic strata of the Chichali Formation of the Early Cretaceous were sampled mostly at ~0.3 meter intervals. At the same time, a random collection of belemnite species was collected from each sample horizon where present.

The second field session was undertaken to sample the Moghal Kot Section of the LIB from October 16th to December 4th (2009). Due to the lack of systematic studies of stratigraphy and paleoenvironmental change events in the unique Moghal Kot Section of Pakistan, the aim of this field season was to sample the important organic rich horizons (black shales/limestones) of the Parh Limestone. In addition, samples were collected from the entire Formation for biostratigraphic purposes. A total of 40 samples were collected from the Parh Limestone in this field work. During this field season, the Chichali Formation was revisited to collect pieces of complete rostra of belemnite species throughout the entire section.

Preliminary results on the planktonic foraminiferal biostratigraphy and carbon isotope stratigraphy from the carbonate sequence of the Parh Limestone in the Moghal Kot Section of LIB (results from the second fieldwork), convinced me to return for another field work season in the LIB. Therefore, the third, final field season was carried out to sample in detail the Moghal Kot Section of the LIB between April 25 to May 23 (2010). In this field season, the Parh Limestone was sampled at much higher resolution. The ~100m Aptian (as determined from the previous samples) limestone section was sampled at 1m intervals. The black fissile hard calcareous shale at ~100m stratigraphic height was sampled at 0.5m intervals.

The 143m monotonous interbedded limestone and calcareous shale/marl sequence of the Albian (as determined from previous samples) was however sampled at low resolution (5-15 meter intervals) because of security risks and time constrains. The Cenomanian/Turonian (as determined from previous samples) boundary was sampled at centimetre scale in order to document the detailed biotic and carbon isotope response to the so called Bonarelli Event which is a global OAE. The Late Cretaceous strata above the Cenomanian-Turonian organic rich facies were sampled at ~4 meter intervals, although the black thinly laminated limestone at 340 m height was sampled at ~1m intervals.

1.5.2 Laboratory work

1.5.2.1 Foraminifera

The bulk of the laboratory work was carried out in the School of GeoSciences, University of Edinburgh. Some of the rock thin sections were prepared in the Department of Geology, University of Peshawar, Pakistan.

Thin Section: The indurated carbonate samples were processed for foraminiferal and microfacies analysis. 217 polished/unpolished thin sections were made in the thin section facility at the John Murray's Labs, School of GeoSciences, University of Edinburgh, and in the rock cutting laboratory of the University of Peshawar Pakistan.

Processing: Some of the limestone samples were also processed for the extraction of planktonic foraminifera. For this purpose the technique of Lirer (2000) was adopted, which is useful for the extraction of calcareous microfossils from the lithified limestones. In this technique, 80% acetic acid was used for the disintegration of limestones. The purpose of the use of weak acetic acid is to dissolve the matrix and it hopefully leaves the foraminifera in the residue, because their tests are comparatively robust against the acetic acid attack. To achieve this, 200 gm rock sample was fragmented into pieces of approximately 5 mm diameter. Then, these fragments were covered with the 80% acetic acid so that the level of acetic acid was 2 cm above that of the fragments level. The time for disintegration of limestones varied from 8 to 24 hours, depending on the type of limestone. The residues were sieved using mesh sizes of 250 µm, 150 µm, and 63 µm and then dried in the oven overnight at 75 degrees centigrade. In order to fully clean the foraminifera, hydrogen peroxide was added to the dried sieved samples, and then the samples were placed in the ultrasonic

bath for 1 to 2 hours. The samples were again sieved and dried in the oven, and then the samples were ready for picking and SEM photography.

Picking: The extracted planktonic foraminiferal species were picked with a zero size paint brush under the binocular microscope and were retained in a picking tray. The abundance and diversity of planktonic foraminifera in the acid treated samples were not the actual manifestation of foraminiferal species, because the acid has dissolved specimens of some of the species and the bulk of extracted specimens showed extreme damage when observed under the microscope, which hampers identification.

Photography: The specimens extracted from the 17 samples were mounted on the stubs under the binocular microscope for Scanning Electronic Microscopy. The stubs were gold plated and were kept in the sample chamber for photography. The photography of the foraminifera was carried out using the Scanning Electronic Microscope, Philips XL30CP, in two sessions each of 4 hours in the Grant Institute of Geology, University of Edinburgh. The voltage was kept constant at 20 kV. The polished thin sections were photographed by using the Nikon ECLIPSE E200 microscope in the microscopic laboratory at the Grant Institute of Geology, University of Edinburgh.

1.5.2.2 Cathodoluminescence photography of belemnites

The polished thin sections of the belemnites rostra were carbon coated before the photography. The cathodoluminescence photographs were taken by Scanning Electronic Microscope, Philips XL30CP with fitted Philips cathodoluminescence (CL) detector, at the Grant Institute of Geology, University of Edinburgh. The voltage was kept constant at 15 kV.

1.5.2.3 Palynomorphs

The slides of palynology were prepared by the British Geological Survey, and the Paly Parlour (private consultant) lab, South Wales. In BGS, 50g of each rock sample was crushed into 2-4mm size. In order to dissolve silicates, 100ml of 40% hydrofluoric acid was added to each sample and was left for 2 weeks in a fume hood. Afterward the samples were sieved at 10 µm and placed in warm HCL to dissolve the carbonates. Warm HCL treatment for carbonate dissolution after the HF is more effective than the cold HCL treatment prior to the HF treatment. Such kind of treatment has no effect on the palynomorphs. Then the samples were sieved again at

10 µm, while the fraction above 500 µm fraction was removed. Each sample was then washed in distilled water and one drop of PVA was added before mounting. The residue was mounted onto cover slips. When the residue was dried, the cover slips were mounted onto the slides with Elvacite.

In the Paly parlour lab, the samples were crushed to millimetre size, and then digested with 60 % hydrofluoric acid over night, and were sieved at 10µm. Then surprenant was oxidised for several minutes with 70% nitric acid and were sieved at 10µm. Then heavy liquid separation with 2g/cc zinc chloride solution was carried out to remove any remaining minerals and supernatant was sieved at 10µm. The palynofacies was mounted on a slide with PVA and Petropoxy 154 resin.

The palynomorphs were studied and photographed by the Nikon ECLIPSE E200 microscope in the microscopic laboratory at the Grant Institute of Geology, University of Edinburgh. The photographs were taken at 40X magnification.

1.5.2.4 Carbonates stable isotope analysis

Belemnites carbonate stable isotope analysis: Belemnites were prepared for analysis by washing them in ultrapure water and were allowed to air dry for twenty four hours as there is always a chance of losing some calcite in the form of carbon dioxide, if dried in oven. The fresh cut surfaces of the belemnites rostra were drilled by electric driller in order to get fresh carbonate for isotopic analysis.

Oxygen and carbon stable isotope analyses were performed on 0.03 - 0.2 mg sub-samples. The powdered carbonate samples were reacted with 100% orthophosphoric acid at 75 °C in a KIEL CARBONATE III preparation device and the resulting CO_2 was then analysed on a THERMO ELECTRON DELTA$^+$ ADVANTAGE stable isotope ratio mass spectrometer. The standard deviation for 15 analyses of a carbonate standard powder (COR1D) run in the period 13/05/09 and 29/06/09 was ± 0.06‰ for $\delta^{13}C$ and ± 0.06‰ for $\delta^{18}O$ respectively. The COR1D standards were run at the beginning, middle and end of a bulk carbonate samples run (number of samples in each run range from 34 to 38 normally). All carbonate isotopic values are quoted relative to VPDB.

Bulk carbonates stable isotopes: Bulk carbonates samples were prepared for analysis by drilling through the fresh cut surfaces of the limestone in order to extract fresh carbonate powder. Oxygen and carbon stable isotope analyses were performed on

0.02-0.1 mg sub-samples in the Grant Institute of Geology, University of Edinburgh. The carbonate samples were reacted with 100% orthophosphoric acid at 75 °C in a KIEL CARBONATE III preparation device and the resulting CO_2 was then analysed on a THERMO ELECTRON DELTA$^+$ ADVANTAGE stable isotope ratio mass spectrometer.

The standard deviation (n=61) of a powdered coral laboratory standard (COR1D, $\delta^{13}C$= -0.642, $\delta^{18}O$= -4.923) that was frequently run between bulk carbonate samples [between 01/04/10 and 20/03/12], was ± 0.05‰ for $\delta^{13}C$ and ± 0.08‰ for $\delta^{18}O$, respectively. The COR1D standards were run at the beginning, middle and end of a bulk carbonate samples run (number of samples in each run range from 34 to 38 normally). All carbonate stable isotopic values are quoted relative to VPDB.

Note: The standard deviation of the $\delta^{13}C$ and δ18O analysis recorded for each belemnite, and bulk carbonate sample is generally in the range 0.01 to 0.05‰. This standard deviation is based on eight measurements for each sample by the mass spectrometer.

1.5.2.5 TEX86 Analysis

Sample processing for biomarkers: Samples for biomarker analysis were prepared in the Organic Geochemistry Laboratory, Department of Earth Sciences, Utrecht University. In organic geochemistry it is of great importance to work 'clean'. This means that solvents used during the extraction and measurement of samples and cleaning of laboratorial equipment need to be checked for contamination (e.g. plasticizers). Every new bottle of solvents is checked for contamination by evaporating down 50ml redissolving this in 50µl, and injection on a gas chromatograph. When no contamination is found the solvents can be used. The most commonly used solvents in the laboratory include dichloromethane (DCM; CH_2Cl_2), methanol (MeOH, CH_3OH), *n*-hexane (C_6H_{14}), propanol (C_3H_8O) and ethyl acetate ($C_4H_8O_2$).

Another important lab procedure is the cleaning of glassware and other equipment (e.g. tweezers) that may come in contact with samples. First everything is washed under hot water with detergent. Afterwards it is soaked (at least overnight) in demineralised water containing 2-5% Extran. Subsequently it is rinsed three times with tap water and three times with demineralised water. Equipment is dried using an oven (120°C for 1-2 hours) or on a drying rack. Finally, openings of glassware are

sealed off with aluminium foil. Before using the glassware, it is rinsed two times with MeOH and two times with DCM. Generally, all lab work was performed according to regulations stated in the Laboratory manual Marine Organic Biogeochemistry NIOZ, Version 11, 2008.

For the analysis of biomarkers, of each sample 10 to 15 g of sediments were freeze dried and powdered using pestle and mortar. The sediments were extracted with a DCM: MeOH solvent mixture (9:1, v/v, 3 times for 5 minutes each) using an Accelerated Solvent Extractor (ASE, Dionex 200)* at 100°C and ca. 7.6 x 10^6 Pa. The resulting Total Lipid Extract (TLE) was evaporated to near dryness using a rotary evaporator under near vacuum. The TLE then was transferred to a 4 ml vial and dried under a continuous N_2 flow. Afterwards, 1 ml of DCM was added after which 0,2 ml (~20% of the TLE) was saved as archive. The other 'working part' was desulphurised. For the desulphurization cupper turnings were activated by adding a small amount of 2M HCl. The acid was pipetted off, and the cupper turnings were washed with demineralised water until the pH of the water was neutral. Afterwards the cupper turnings were washed twice with a small amount of methanol and DCM successively. Together with some DCM, the cupper turnings were added to the TLE, and after addition of a small stirring bar, the TLE was stirred overnight. The next day, the DCM layer was filtered over a small pipette filled with Na_2SO_4 to remove the CuS. The resulting desulphurised TLE was separated over a small column (Pasteur pipette) packed with activated Al_2O_3. Activation of the Al_2O_3 was performed by heating the Al_2O_3 in an oven for 2 hours at 150°C. Before the separation, the column was conditioned by flushing with one column volume of *n*-hexane : DCM 9:1 (v/v). The TLE was separated into an apolar fraction (e.g. *n*-alkanes), a ketone fraction (e.g. alkenones), a 'GDGT' fraction (the compounds used to calculate TEX86) and a polar fraction by eluting with three column-volumes of *n*-hexane: DCM 9:1 (v/v), ethyl acetate (v), DCM: MeOH 95:5 (v/v) and DCM : MeOH 1:1 (v/v) solvent mixtures, respectively.

GDGT analyses by HPLC-MS: The GDGTs analyses were done by HPLC-MS in the Department of Marine Organic Biogeochemistry, NIOZ Royal Netherlands, and Institute for Sea Research-Texel on 26th of January 2012. To the 'GDGT' fraction, 250 ng of the C46 GDGT internal standard was added. The polar fraction was ultrasonically dissolved in *n*-hexane: propanol (99/1, v/v) and filtered over a 0.45 µm mesh PTFE filter (ø 4mm) prior to analysis. GDGTs were analyzed using high

performance liquid chromatography/atmospheric pressure chemical ionization–mass spectrometry (HPLC/APCI-MS), according to methods of Hopmans et al. (2000, 2004), with minor modifications. Analyses were performed on an Agilent 1100 series/Hewlett-Packard 1100 MSD SL series instrument, equipped with auto-injection system and HP-Chemstation software. Separation was achieved on a Prevail Cyano column (150 mm x 2.1 mm, 3 μm; Alltech). The flow rate of the hexane:propanol (90:10, v/v) eluent was 0.2 ml min-1, isocratically for the first 5 min, thereafter with a linear gradient to 18% propanol in 45 min. Injection volume of the samples was 10 μl. To increase sensitivity, selective ion monitoring (SIM) of the protonated molecular ions of the GDGTs was used (cf. Schouten et al., 2007). Relative quantification of the GDGT compounds was achieved by integrating the peak areas in the mass chromatograms and comparison to the internal standard.

1.5.3 Graphic Software

The Corel Draw 14 graphic software was used for the construction of maps, charts, and plates.

1.6 Objectives

- To describe and sample sediments of the Chichali and Parh Limestones in the Upper and Lower Indus Basins, respectively.
- To establish detailed stratigraphy in the Chichali Formation based on dinoflagellates, spores and pollens. In addition, to establish Sea Surface Temperatures (SSTs) by using the TEX_{86} and $\delta^{18}O$ proxies.
- To establish detailed stratigraphy in the Parh Limestone based on planktonic foraminifera, linked to the global biozonation schemes of Caron (1985) and Sliter (1989). The biostratigraphy would help in defining the stratigraphic positions of the organic rich intervals in the Parh Limestone, which may corresponds to the OAEs, recorded elsewhere in the world.
- To carry out microfacies analysis of the Parh Limestone in order to record the sedimentological and biotic changes in the entire Parh Limestone, such changes may hint to OAEs.
- To establish stable isotope stratigraphies in both the Chichali and Parh Limestones.

- To place the black shale intervals, i.e. the OAEs, within the bio-carbon isotope stratigraphies of both the Chichali and Parh Limestones in this part of the Tethys Ocean.
- To quantify evolutionary patterns of the planktonic foraminifera across the OAEs in the Parh Limestone.

CHAPTER 2

2. Field Observations and Sampling Strategy

2.1 Introduction

In order to achieve the objectives of the current study (see Chapter 1 for detail), two stratigraphic sections i.e. the Chichali Nala and the Moghal Kot Sections were selected from the Indus Basin. The Indus Basin was an integral part of the Eastern Tethys. The mentioned two stratigraphic sections encompass almost whole of the Cretaceous, and are therefore important for understanding paloenvironmental changes as recorded in the Eastern Tethys. The detailed accounts of these stratigraphic sections are given below.

2.1.1 Chichali Nala Section

The Chichali Nala Section is part of the Surghar Range. The east-west trending Surghar Range represents the eastern extremity of the Trans Indus Ranges (TIR, see figure 2.1). The TIR are the mountain ranges on the west of the River Indus, while the Salt Range is on the east side of the river Indus. The Surghar Range was initially part of the Salt Range; however, the right lateral Kalabagh Strike Slip Fault truncated it to the north (see fig. 1.9, Chapter 1). The Kalabagh Fault is considered as an echelon splay of the Chaman Transform Fault (Treloar et al., 1992). Another school of thought consider it a lateral ramp of the Main Frontal Thrust (Butler et al., 1987), while some consider it a transpressional strike-slip fault (McDougall & Khan, 1990).

The entrance of the Chichali Nala Section is located at 32° 59" 36' N Latitude, and 71° 24" 14' E Longitude. It can be accessed by taking the metalled road from the Mianwali to Kalabagh, then heading on the partially metalled road from the Kalabagh to Chapri (12 km west of Kalabagh). The Chichali Nala (gorge) is 3 km east of the Chapri village, accessible through an un-metalled road. The Chichali Nala is also a pass which links the Punjab Province with the Khyber Pakhtunkhwa Province of Pakistan. The older rocks exposed in the Chichali Nala Section are Mesozoic while the Eocene rocks form the sky line on the distal end of the Chichali Nala Section (Ahmad et al. 1999). The Cretaceous rocks in this section comprise the Chichali Formation and the Lumshiwal Sandstone (Shah, 2009). This study focuses

on the stratigraphy of the Chichali Formation; hence it will be discussed in detail below.

Lithostratigraphy of the Studied Chichali Formation: The name Chichali Formation is introduced by Danilchick (1961). It is ~70 m thick in the study area; it is also the type section of this formation (figs. 2.2 & 2.3). Here, the formation is divided into three members (Shah, 1977). The lower member (~23m) is composed of organic rich sandy glauconitic shale interbedded with fine grained soft glauconitic sandstones (fig. 2.4A&D). In this lower member iron nodules are present (figs. 2.4A). The weathered surface of the rocks have a greenish colour due to the high glauconite content, while on fresh surfaces it is dark grey to black. The sediments of this member are riddled with belemnites (fig. 2.4B-D).

The middle member is ~19m thick. It is comprised of thick bedded, ridge forming, fine grained glauconitic sandstones (fig. 2.5A). The fresh colour of the rock surfaces is bright green, while the weathered colour is greenish. Abundant belemnites with minor ammonites are present here (figs. 2.5A &B).

The upper member is ~28m thick. This member is dominantly composed of soft dark green glauconitic sandstone, which lacks belemnites. The sandstone has mud cracks, filled with selenite in the lower half of the member, while iron nodules are present in the upper half of the member (figs. 2.6A&C-D, & 2.7) . Phosphate nodules are present throughout this member (figs. 2.5D & 2.6B). The basal most part of this upper member is composed of ~1.5m thick black shale, which lack belemnites (fig. 2.5C). This shale unit is in turn overlain by ~3m alluvium. Also, in the middle of this member at ~51m stratigraphic height there is a 1m thick black soft argillaceous sandstone/sandy shale interval. The lower contact of the Chichali Formation (33° 00" 09' N, 71° 24" 17' E) is disconformable with the Samana Suk Formation carbonates of the Late Jurassic. The upper contact (33° 00" 11' N, 71° 24" 15' E) with the Lumshiwal Formation is transitional (fig. 2.8).

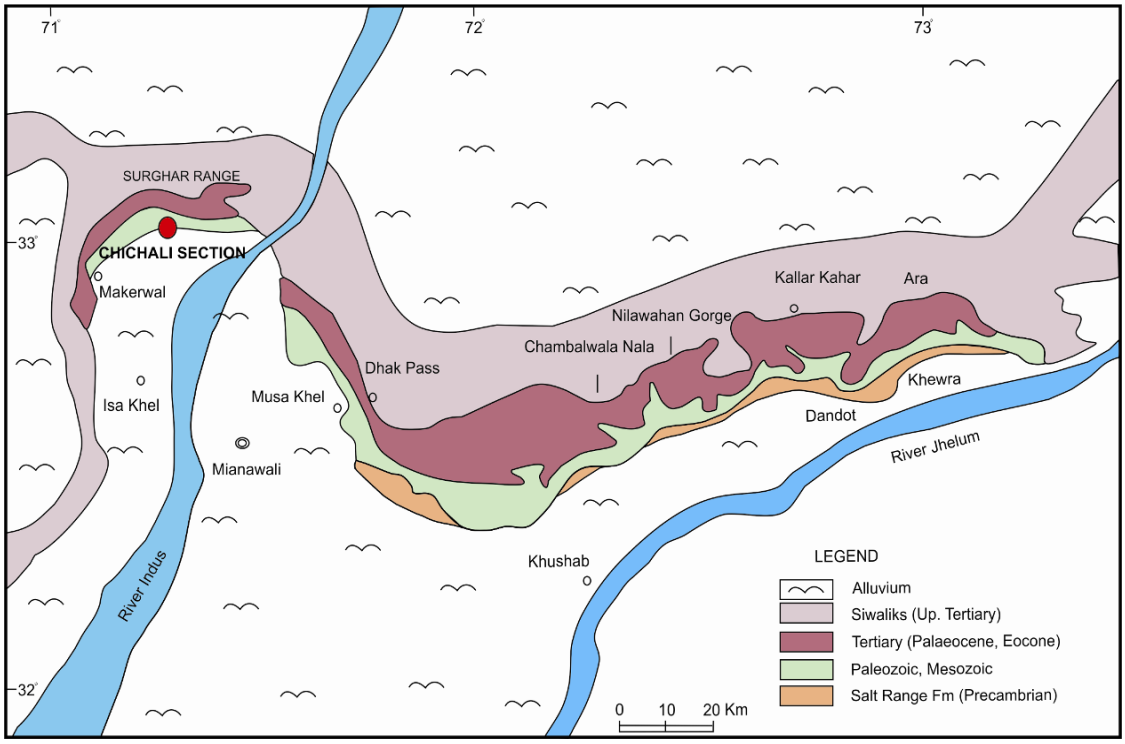

Figure 2.1: A geological map of the Salt Range and Trans Indus Ranges, showing the study area.

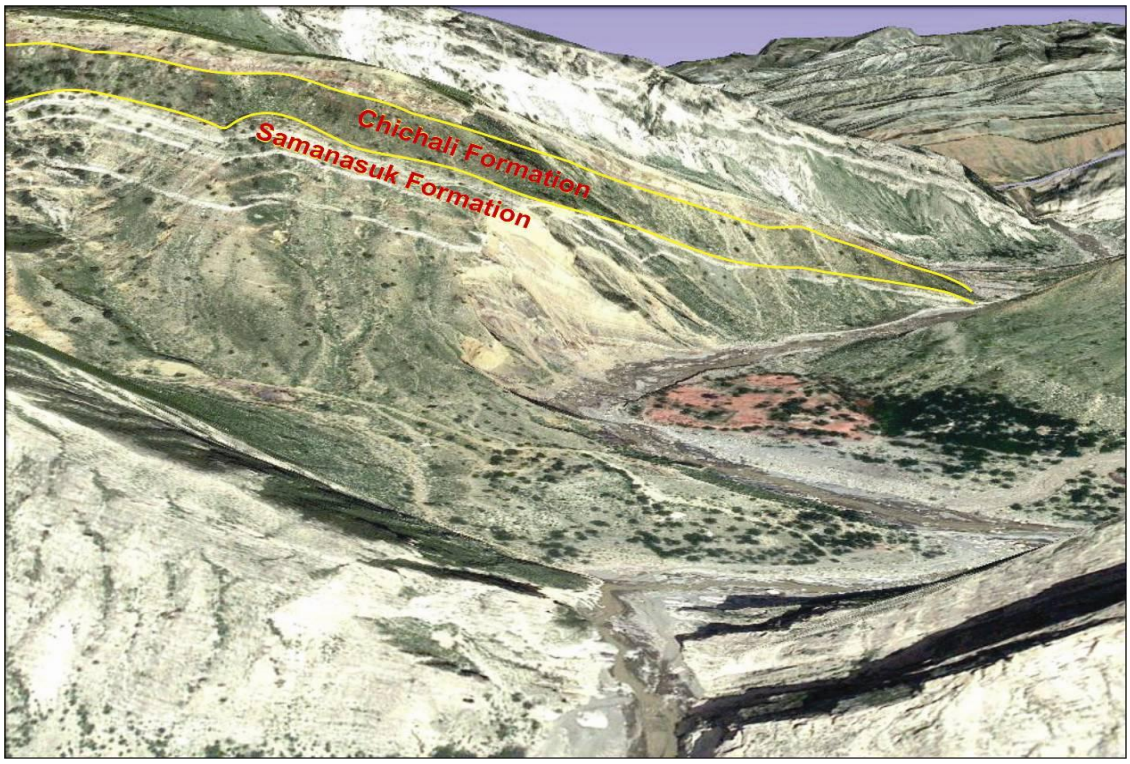

Figure 2.2: Panoramic view of the interior of the Chichali Nala Section, including the Chichali Formation.

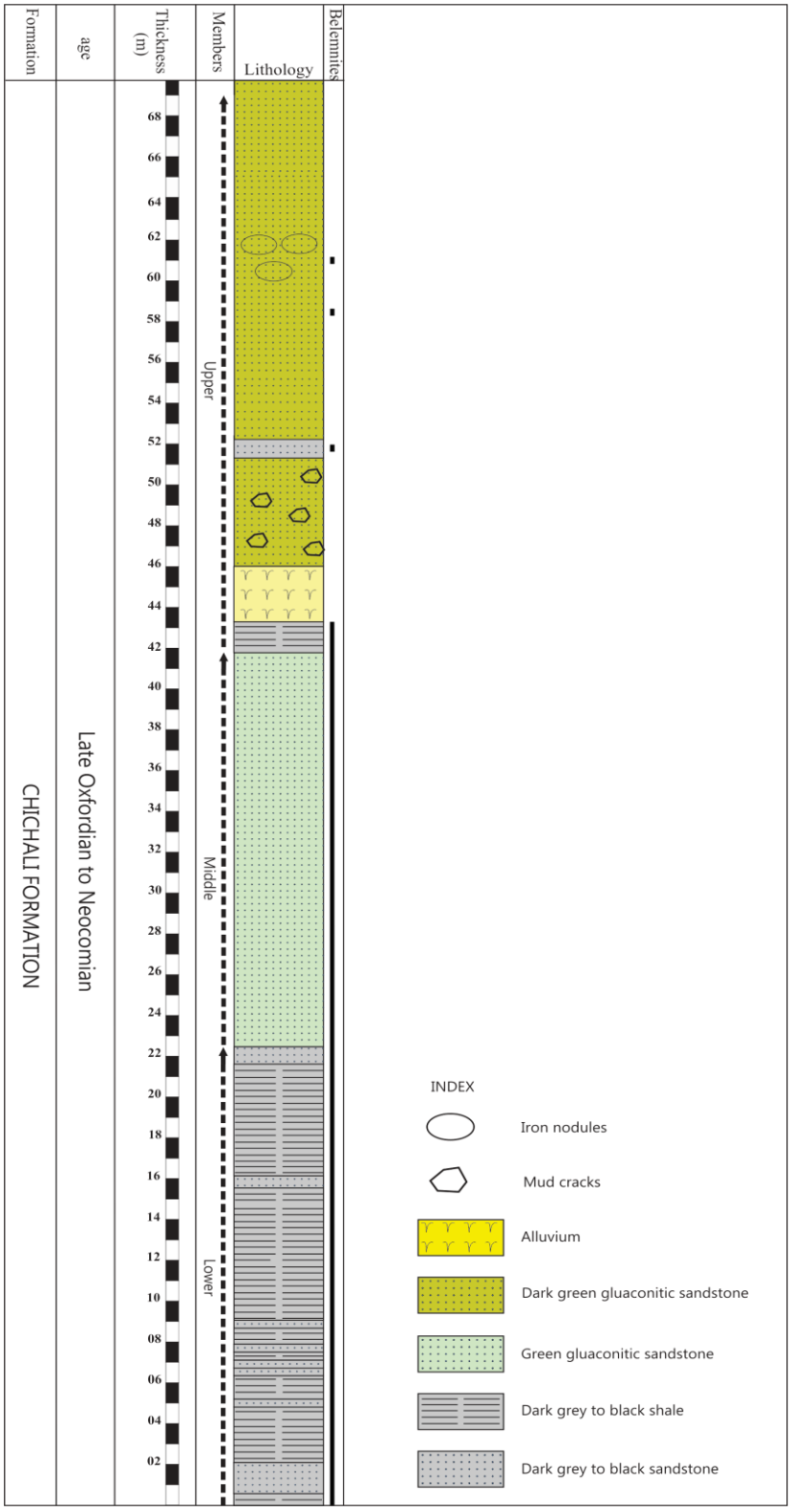

Figure 2.3: The stratigraphic chart of the Chichali Formation in the Chichali Nala Section. The age is after Shah (2009)

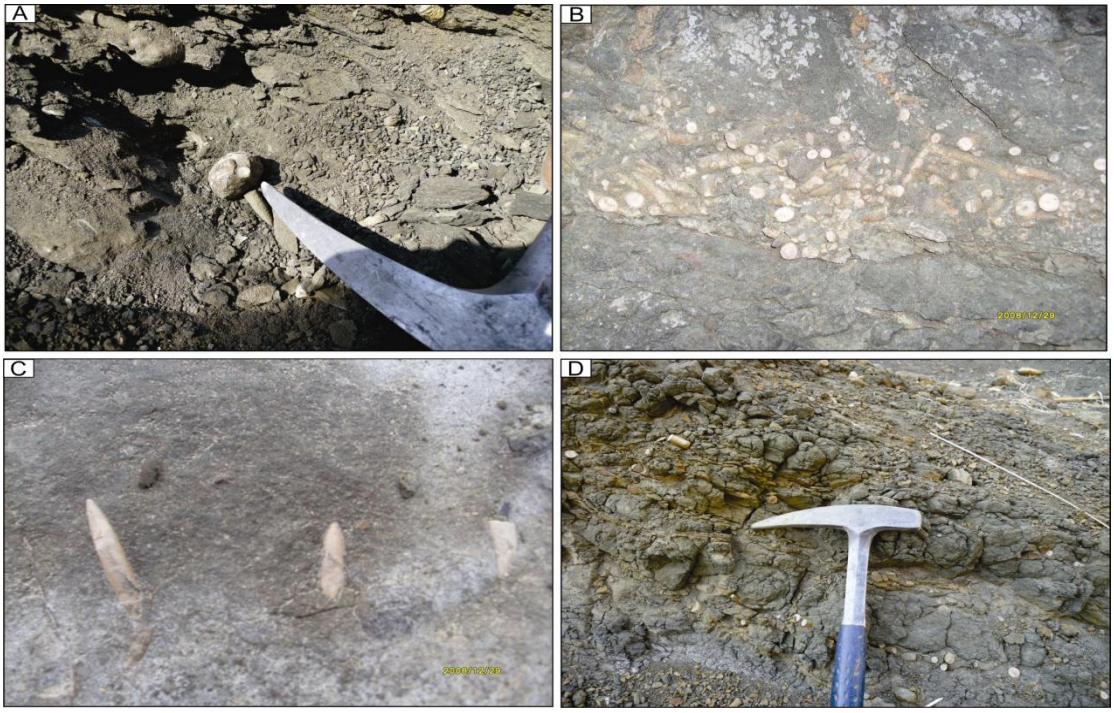

Figure 2.4: Stratigraphic details of the lower member of the Chichali Formation. A, Dark grey to black sandy shale with iron nodules; B, Tempestite bed of belemnites; C, Individual belemnites in the hard sandstone; D, Glauconitic soft sandstone bed.

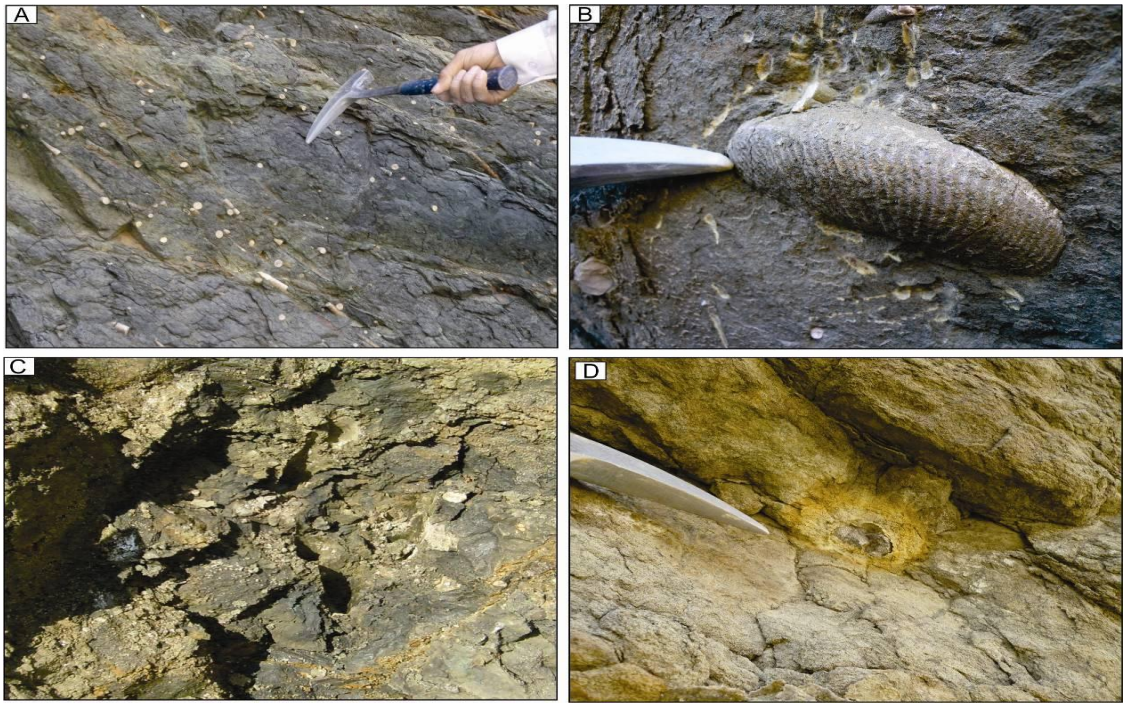

Figure 2.5: Details of the middle and upper members of the Chichali Formation. A, Glauconitic ridge forming sandstone of the middle member which is rich in belemnites; B, Ammonite in the sandstone of middle member; C, Close up of black shale in the basal part of the upper member; D, Weathered phosphate nodules in upper member.

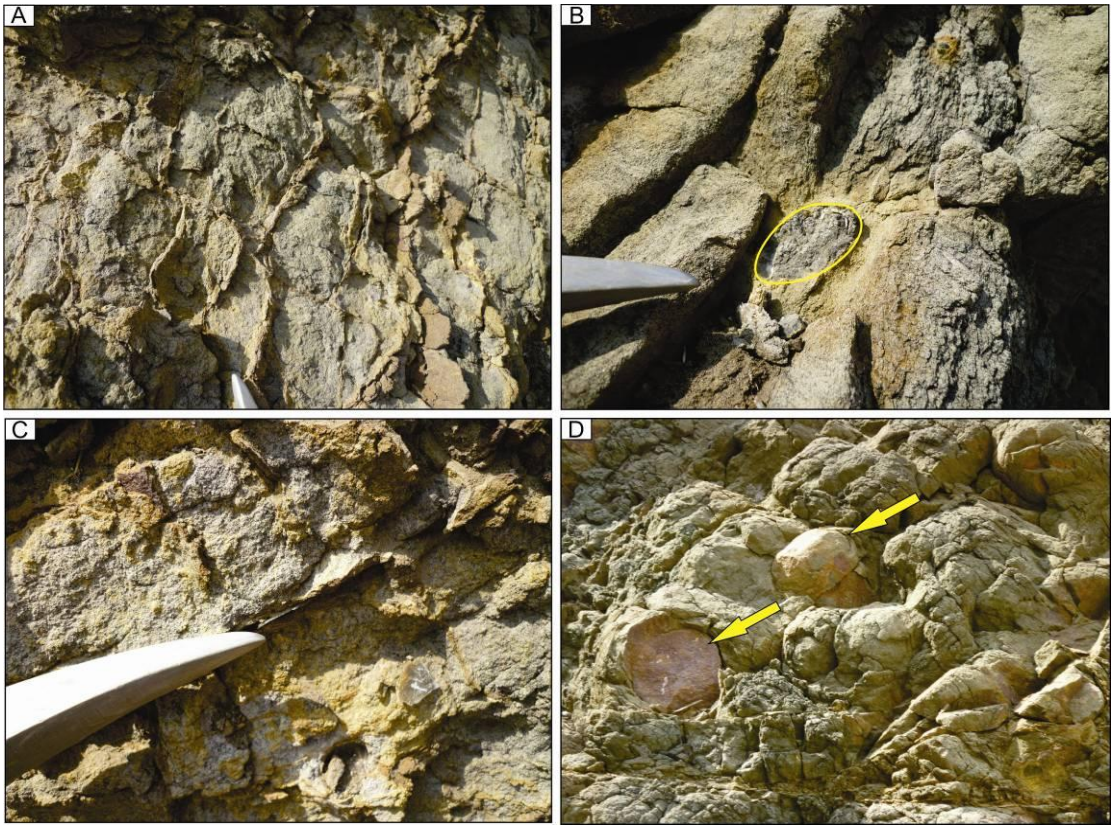

Figure 2.6: Details of the upper member of the Chichali Formation. A, Mud cracks in sandstone; B, Fresh phosphate nodules in glauconitic sandstone; C, Selenite development along the mud cracks; D, Hematite nodules in glauconitic sandstone

Figure 2.7: Hematite nodule in the glauconitic sandstone of the upper member of the Chichali Formation.

Figure 2.8: Upper contact of the Chichali Formation with the Lumshiwal Sandstone.

Age of the Chichali Formation: Variable ages have been assigned to this formation in different localities of the Upper Indus Basin including the Chichali Nala Section, i.e. Late Oxfordian to Neocomian age is assigned to the lower and middle members of this formation based on ammonoids (Spath, 1930; Fatmi, 1972; 1977). In the Spinghar, in north-western part of Pakistan, this formation ranges in age from the Tithonian to Aptian also based on ammonoids (Badshah et al., 2000). Masood et al. (2008) reported Upper Jurassic to Lower Cretaceous spores and pollens from the Chichali Formation in the Kala Chitta Range of Pakistan but there is no detailed biozonation.

Because the planktonic foraminifera and calcareous nannofossils are missing in this clastic marine section, palynomorphs are used in this study to reconstruct a detailed biostratigraphy.

2.1.2 Moghal Kot Section

The Moghal Kot Section is located in the Moghal Kot area. This area is part of the Frontier Region of Dera Ismail Khan (F.R.D.I. Khan) in the Khyber Pakhtunkhwa Province of Pakistan. In this area, a tribal belt occurs, known as the Federally Administered Tribal Areas (FATA). The FATA is further divided into Agencies and

Frontier Regions. Most of the matters in FATA are controlled by the people of these areas and therefore there is no police, resulting in security problems. It is because of these security risks that the Moghal Kot Section is not visited by the scientists very often and is therefore less explored. Geologically the Moghal Kot Section is part of the Sulaiman Range, and can be accessed through the metalled road from Dera Ismail Khan to Zhob (figs. 2.9 & 2.10).

The entrance of the Moghal Kot Section is located at 31° 26" 33' N Latitude and 70° 05" 00' E Longitude. The sedimentary rocks present in this section range from Jurassic to Palaeocene (Badshah et al. 2000). This study is based on the Cretaceous sediments of the Parh Formation, the lithostratigraphy of which is given below.

Lithostratigraphy of the Parh Formation: Blanford (1876) introduced the name Parh Limestone for the dominant limestone lithology in the Parh Range. In the Moghal Kot Section, Badshah et al. (2000) also mapped it as the Parh Limestone. However, here, the detailed lithostratigraphy shows that the limestone is interbedded with shales, and we call this unit the Parh Formation in this study (figs. 2.11 & 2.12). The limestone of the Parh Formation gradually grade downwards into the black shales of the Sembar Formation. The transitional contact between the two formations is mostly alluvium covered (fig. 2.12). The rounded carbonate concretions occur within the basal most part of the Parh Formation just above the contact between the two formations (fig. 2.13B, C & D). Note that the ages assigned in figures 2.14 to 2.17 are based on current study.

The Parh Formation is 384 meters thick in the study area (fig. 2.11). The lower part of the formation, with a thickness of 60 m, comprises thin to medium bedded limestone. On weathered surfaces, it is yellowish brown and on fresh surfaces it is dark grey to black in colour (fig. 2.14A).

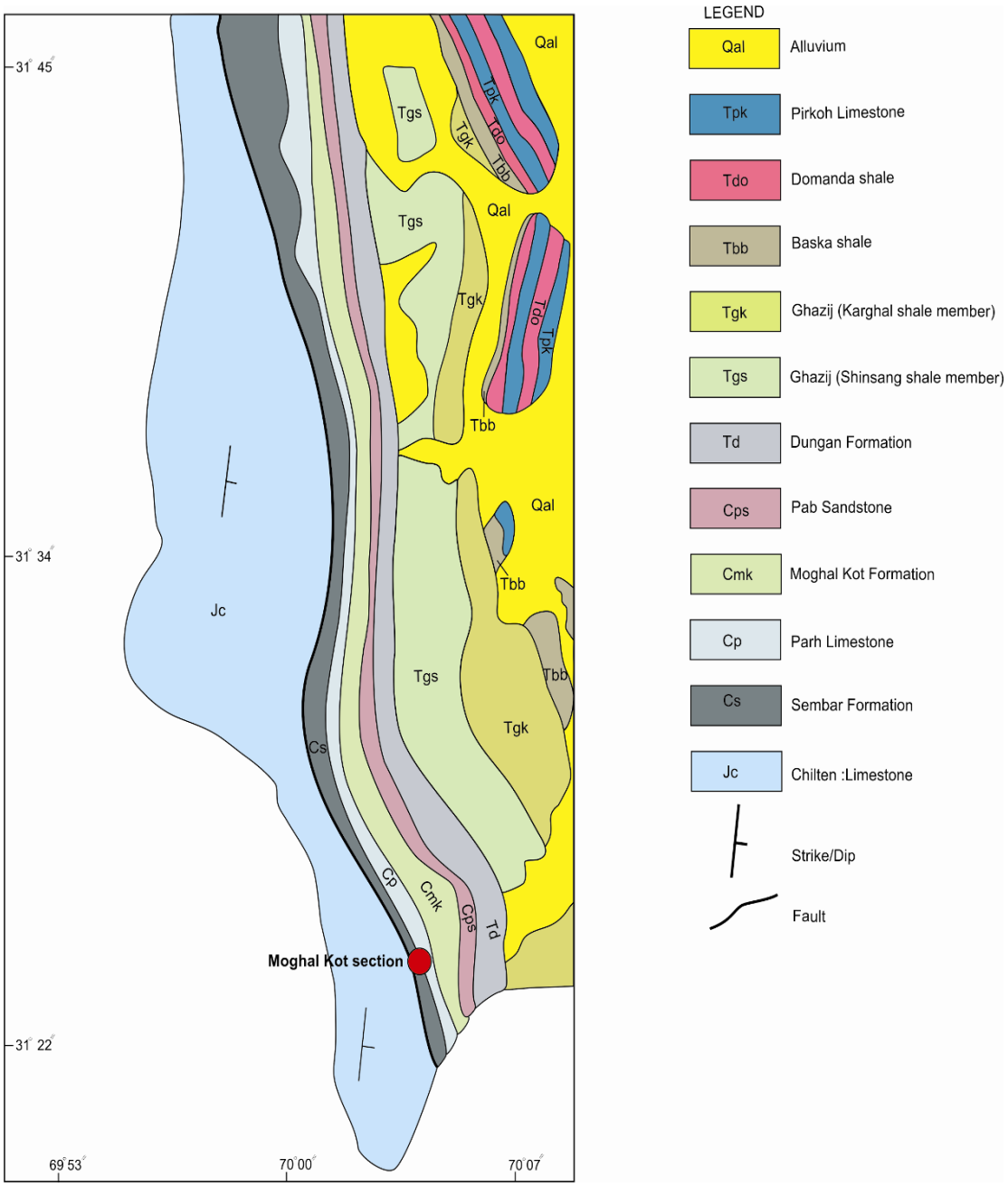

Figure 2.9: A Geological map of the Sulaiman Range, showing the location of the Moghal Kot Section, modified after, Badshah, et al. 2000.

Figure 2.10: A panoramic view of the entrance of the Moghal Kot Section.

This part includes pyrite and rare belemnites (fig. 2.14 B, C). The next unit, from 60 to 100m, is also thin to medium bedded limestone, whilst the colour of the limestone changes to grey (fig. 2.11). Some of the beds show sole marks at its base (fig. 2.14 D), which may represent sediment loading. Above this unit, 2 meter thick black fissile calcareous shale occurs (fig. 2.11). On top of this black shale, a 143 m thick monotonous interbedded very hard shale/marl and limestone sequence follows (figs. 2.11 & 2.15A). The shale/marl and limestone are bluish in colour. Above this unit, a ~62 m thick dark grey to black medium bedded limestone occurs, ranging in stratigraphic height from 246 to 308 m (fig. 2.11). It is in turn bounded by a 1m, thinly laminated black hard shale/limestone (figs. 2.11 & 2.15 B-C) which is further overlain by an approximately 4m thick interval of medium bedded laminated black nodular limestone (fig. 2.11 & 2.16A). The shale/limestone has pyrite inside it (fig. 2.15 D).

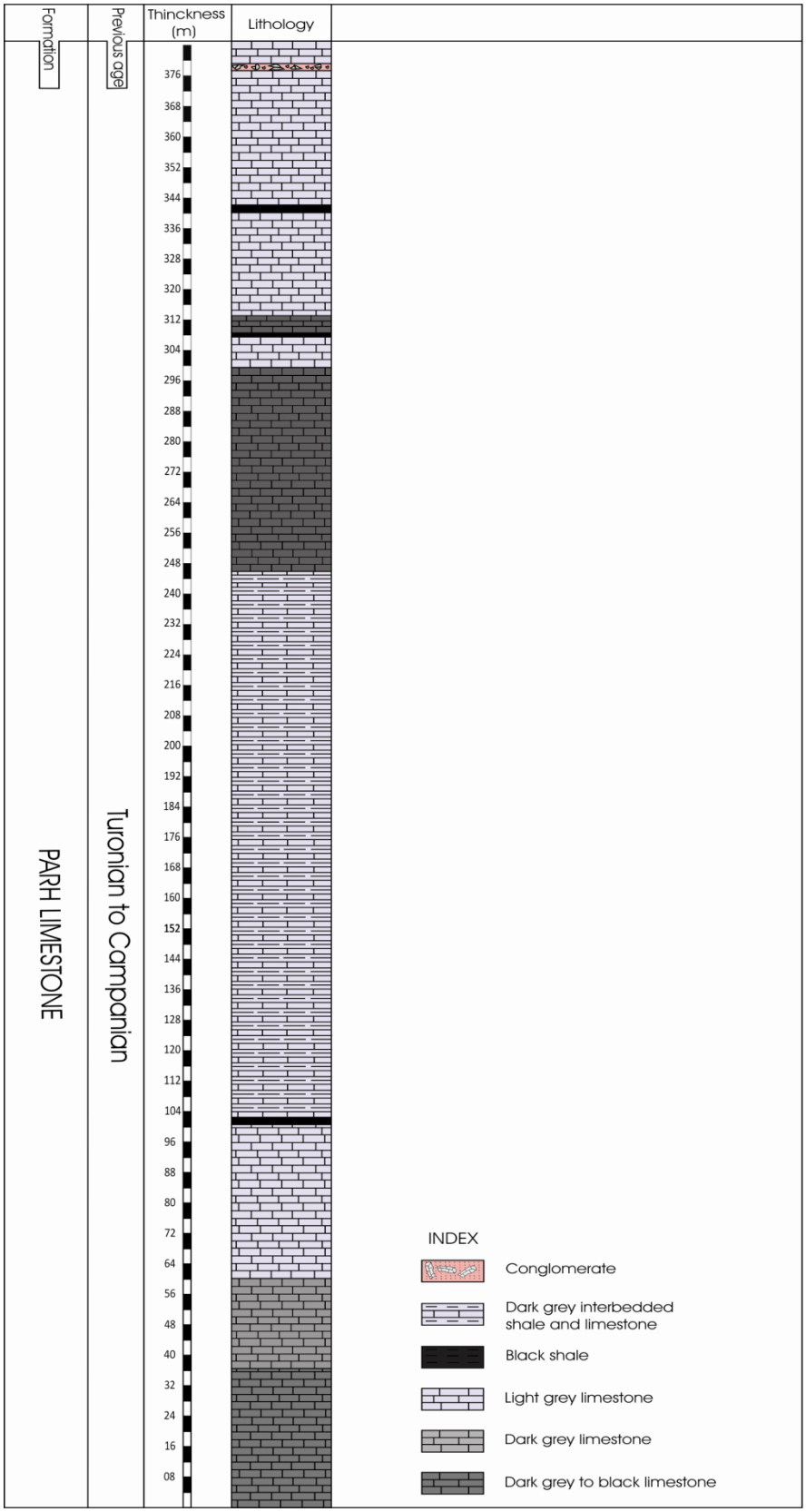

Figure 2.11: Stratigraphic chart of the Parh Formation in Moghal Kot Section, Sulaiman Range.

Figure 2.12: Panoramic view of the Parh Formation showing its major lithological units.

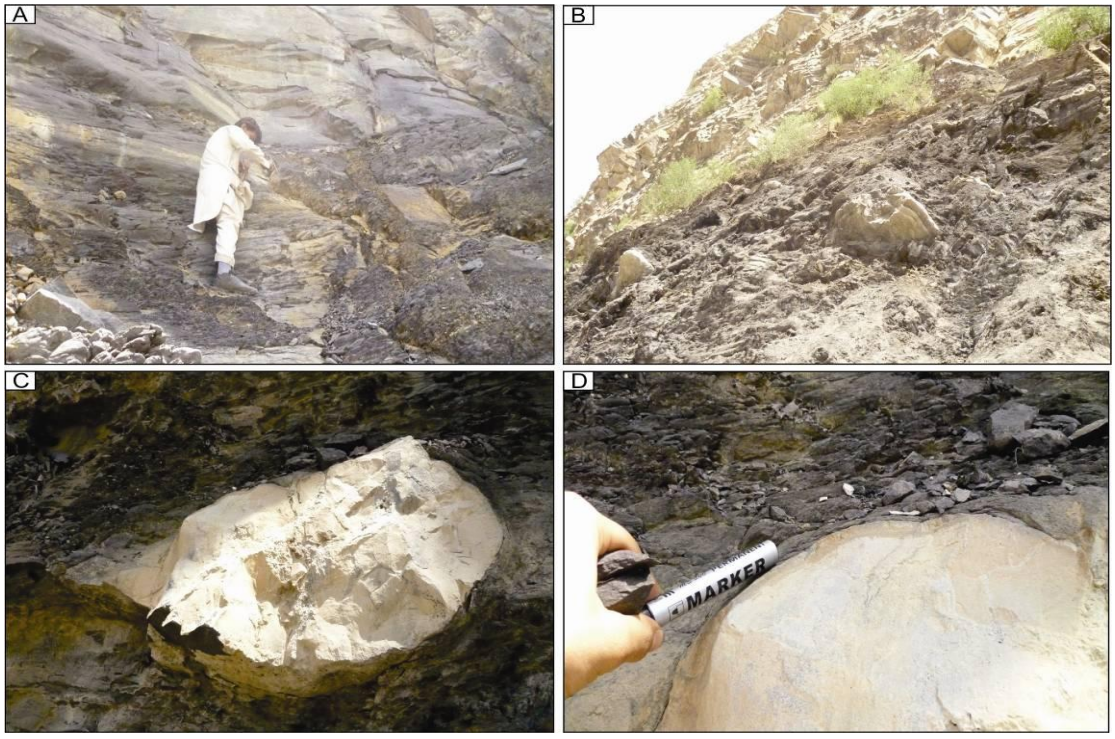

Figure 2.13: Details of the Parh Formation. A, Basal most part of the Parh Formation; B, The carbonate concretions in the basal most part of the Parh Formation; C, Close up of these lenticular Jurassic blocks; D, The Shale laminations wrap around these Jurassic limestone blocks.

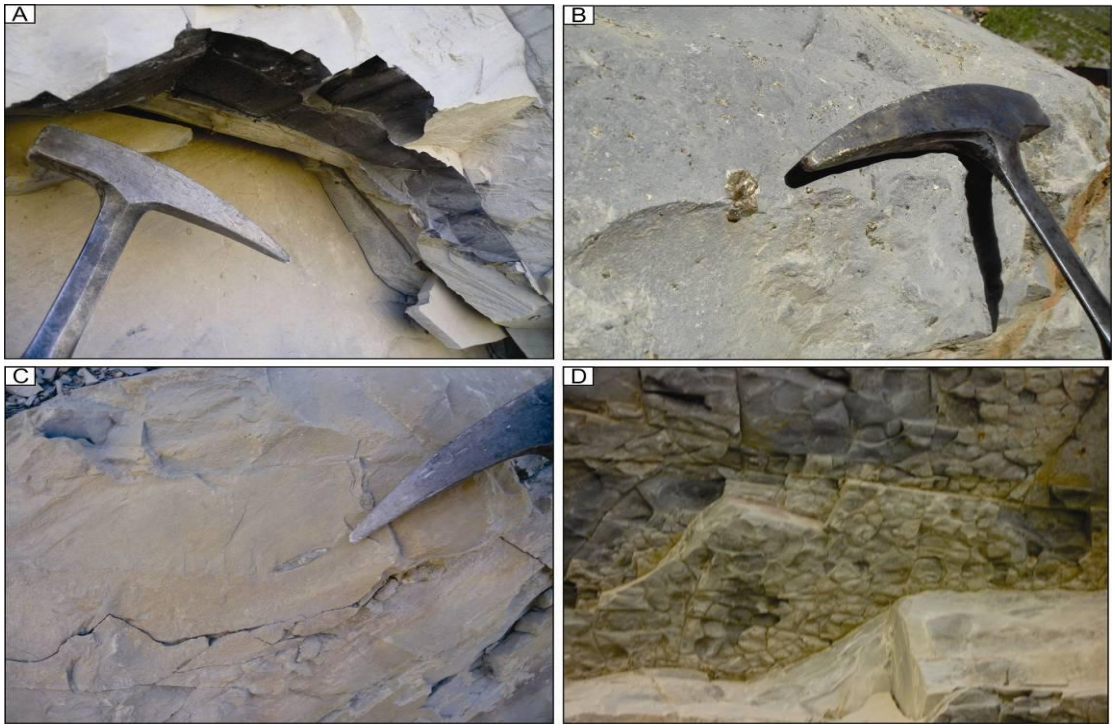

Figure 2.14: Details of the Parh Formation. A, Lower most Aptian dark grey to black limestone; B, Lower most Aptian limestone shows pyrite; C, Lower most Aptian limestone unit having scattered belemnites; D, Aptian limestone showing sole marks.

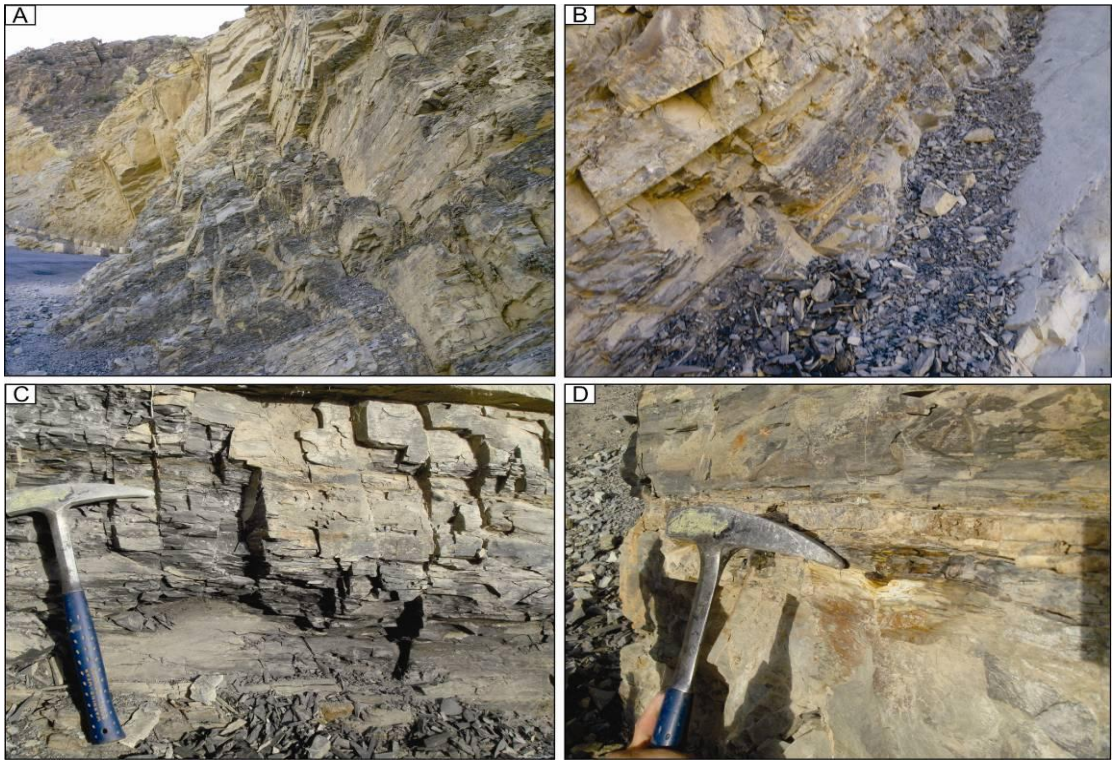

Figure 2.15: Details of the Parh Formation. A, Interbedded shale and limestone unit; B, Cenomanian-Turonian Black shale; C, Close up of the Cenomanian-Turonian Black fissile shale; D, Pyrite in the Cenomanian-Turonian black shale.

Upwards, the following unit, about 71 meters thick, comprises limestones, which are medium bedded (figs. 2.11 & 2.16B). These limestones generally have a blue colour.

However, a black band of thinly laminated limestone (~ 2m) occurs at about 340 meter stratigraphic height (fig. 2.16C). A brecciated unit (~ 2m) occurs at about 377 m height (fig. 2.17). The bedding of this limestone becomes thinner towards the top, just below the conglomerate (figs. 2.16D & 2.17).

The upper contact with the Moghal Kot Formation is transitional and conformable elsewhere, but here it is covered by alluvium (31° 26" 54' N, 70° 02" 28' E).

Age of the Parh Formation: The Parh Formation in most of the localities in the Lower Indus Basin overlies the Goru Sandstone, whereby in turn the Sembar Formation is below the Goru Sandstone. In the Moghal Kot Section, however, the Parh Formation directly overlies the Sembar Formation and thus the Goru Sandstone is missing (Smewing et al. 2002; Kazmi, 1988).

The established ages for the Parh Formation vary from place to place in the Lower Indus Basin. The sediments of the Parh Formation in the Kacha-Ziarat area, north-east Baluchistan, were assigned Barremian-Campanian (Kazmi, 1988). William (1959) stated that rocks of this formation are mainly Senonian (above Turonian but below Danian, based on planktonic foraminifera in the Gaj River Section of the Parh Range, which is the type locality of the Formation. Smewing et al. (2002) recorded a Santonian to Late Campanian age for this formation based on detailed biostratigraphic data from the exploration wells in the Southern Kirther Fold Belt. In the Moghal Kot Section (section for this study) Shafique (2001), while working on the tectonostratigraphic evolution of the north western Indian Plate, assigned a Turonian to Campanian age based on planktonic foraminifera to the Parh Formation. However he only collected five samples; hence a detailed biostratigraphy was not established for the Parh Formation.

Here, in this study I aim to establish a high resolution biostratigraphy based on planktonic foraminifera for the Parh Formation in the Moghal Kot Section.

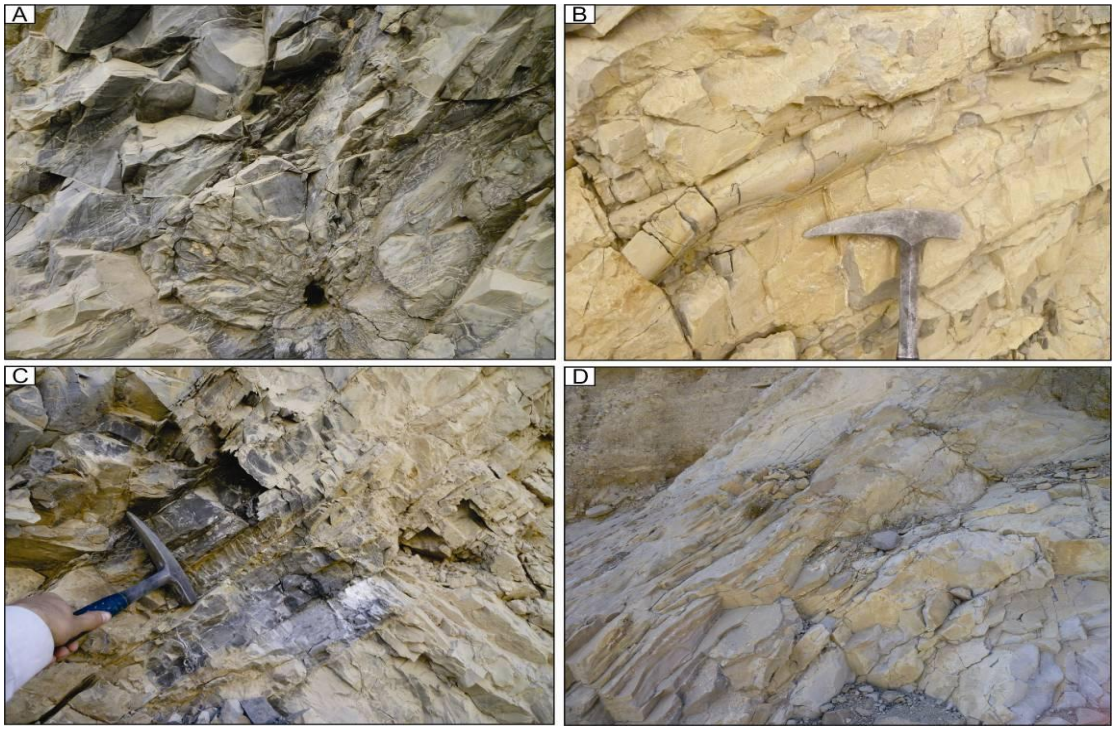

Figure 2.16: Details of the Parh Formation. A, Dark grey to slightly black laminated Turonian limestone; B, Thick belemnite rostrum in Campanian limestone; C, Campanian dark grey to black laminated black limestone; D, Thin beds of the Early Maastrichtian.

Figure 2.17: Close up of the Maastrichtian conglomerate in the upper most part of the Parh Formation.

CHAPTER 3

2. Microfacies of the Parh Formation

3.1 Introduction

To document the microfacies of the Parh Formation of the Moghal Kot Section, Middle Indus Basin Pakistan, 217 samples were collected and investigated. The microfacies analysis of the rock samples was carried out through microscopic examination of the thin sections. The texture, micro- and macro-carbonate constituents were analysed. Type, abundance, and size of the planktonic constituents (foraminifera, radiolarians, and calcispheres) along with other fossils groups (echinoderm spines and plates, calcareous algae, benthic foraminifera, sponge spicules, ostracodes), peloids and intraclasts were semi-quantitatively recorded to document the reliable microfacies history of these rocks. Presence and type of organic matter, pyritisation, and dolomitisation were also recorded for the interpretation of paleoenvironment. This was particularly important to identify the precise intervals that can be assigned to OAEs. The semi-quantitative data on the abundance of the carbonate constituents were recorded using the comparison Charts produced by Baccelle & Bosselini (1965).

The depositional environment of each microfacies is assigned on the basis of the texture, types of allochems, fauna, and other features such as tempestites (i.e. Flügel, 2004, Fig. 3.1)

3. 2 Microfacies

The microfacies of the Parh Formation are abbreviated as MP 1-MP 25 (figs. 3.2-3.27). M stands for Moghal Kot (the name of section), and P stands for Parh (name of the Formation), while the numbers 1-25 are the various microfacies recorded. The detail of each facies is given as below. The index for different biota and microfacies is given in figure 3.28, while the distribution of these microfacies within the Parh Formation, along with the sea level curve is given in figures 3.29 to 3.33.

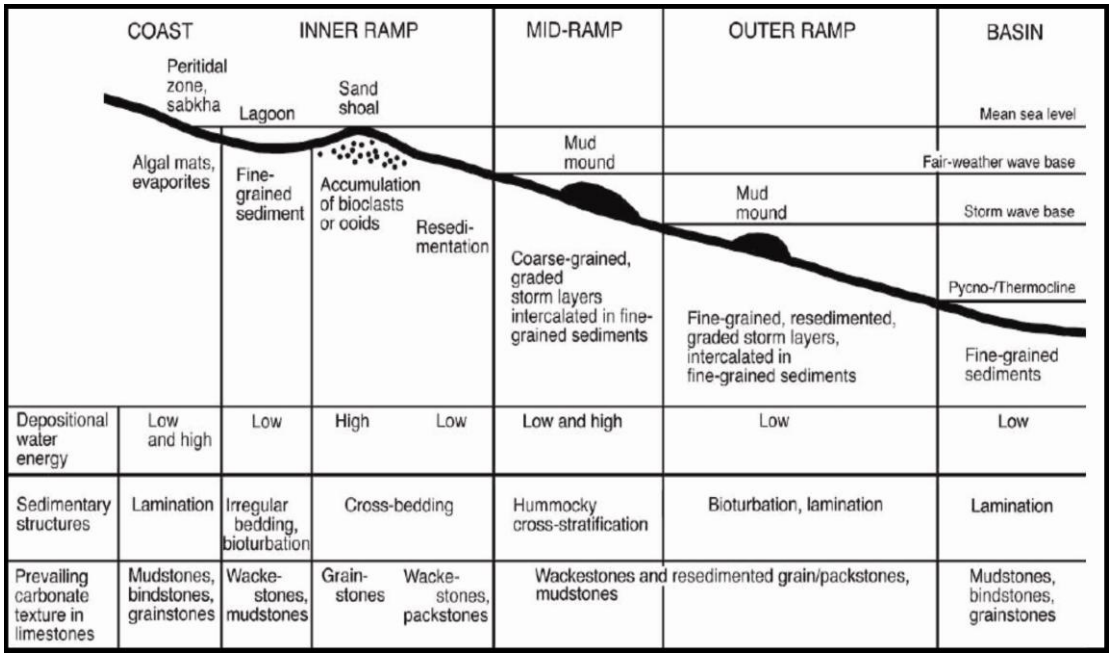

Figure 3.1: Generalized sketch of depositional environments in a ramp setting along with depositional textures and features such as bioturbation, laminations, algal mats (modified after Flügel, 2004).

In order to better understand the depositional history of the Parh Formation with emphasis on the OAE intervals important microfacies parameters such as organic matter, pyrite, clastic input, tempestites, burrows (bioturbation) are recorded. The pyrite and organic matter contents are scaled as minor, moderate and abundant based on visual estimation (see index in fig. 3.34). The burrows (bioturbation) and tempestites are marked as present or absent (see index in fig. 3.34). The clastic input to the basin is estimated from the input of the detrital quartz/lithoclasts to the basin. The presence of quartz between 0-5% is considered as minor, 5-15% as moderate, and >15% as abundant. The presence of the lithoclasts is also used in combination with quartz in order to document clastic input to the basin on the same scale of percentage. The distributions of all these parameters are given in figure, 3.35.

3.2.1 Microfacies of the Parh Formation

The details of the microfacies are discussed as below. The grains include all components of the Parh Formation which are coarser than the micrite i.e. Peloids, bioclasts, biota, detrital quartz, dolomite etc. The percentages of each component discussed below in the microfacies description, represent percent presence of that component in a total rock.

3.2.1.1 Organic-rich radiolarian wacke- to packstone MP 1 Microfacies, see also Figure 3.2

In thin section, these rocks can be classified as wacke- to packstone. The total relative abundance of grains ranges from 21 to 49%, with an average of 37%, while the micrite relative abundance ranges from 51% to 79%, with an average of 63%. The main constituents of this microfacies are calcitised radiolarians, their relative abundance ranges from 20 to 48%, with an average of 34%. The planktonic foraminifers have low relative abundances in this microfacies from 0.5 to 4%, with an average of 1%. The dominant genera of planktonic foraminifera are *Hedbergella*, *Globigerinelloides*, and *Ticinella*. Calcareous algae, echinoids, calcispheres, molluscs, benthic foraminifera, sponges, are very rare. The MP 1 Microfacies is rich in organic matter in the lower part of the sequence.

Paleoenvironment: The radiolarian-rich microfacies represents deposition of sediments in a deep basin (Flügel, 2004), hence the presence of dominant presence of radiolarians within MP1 Microfacies suggest deposition in the deep basin.

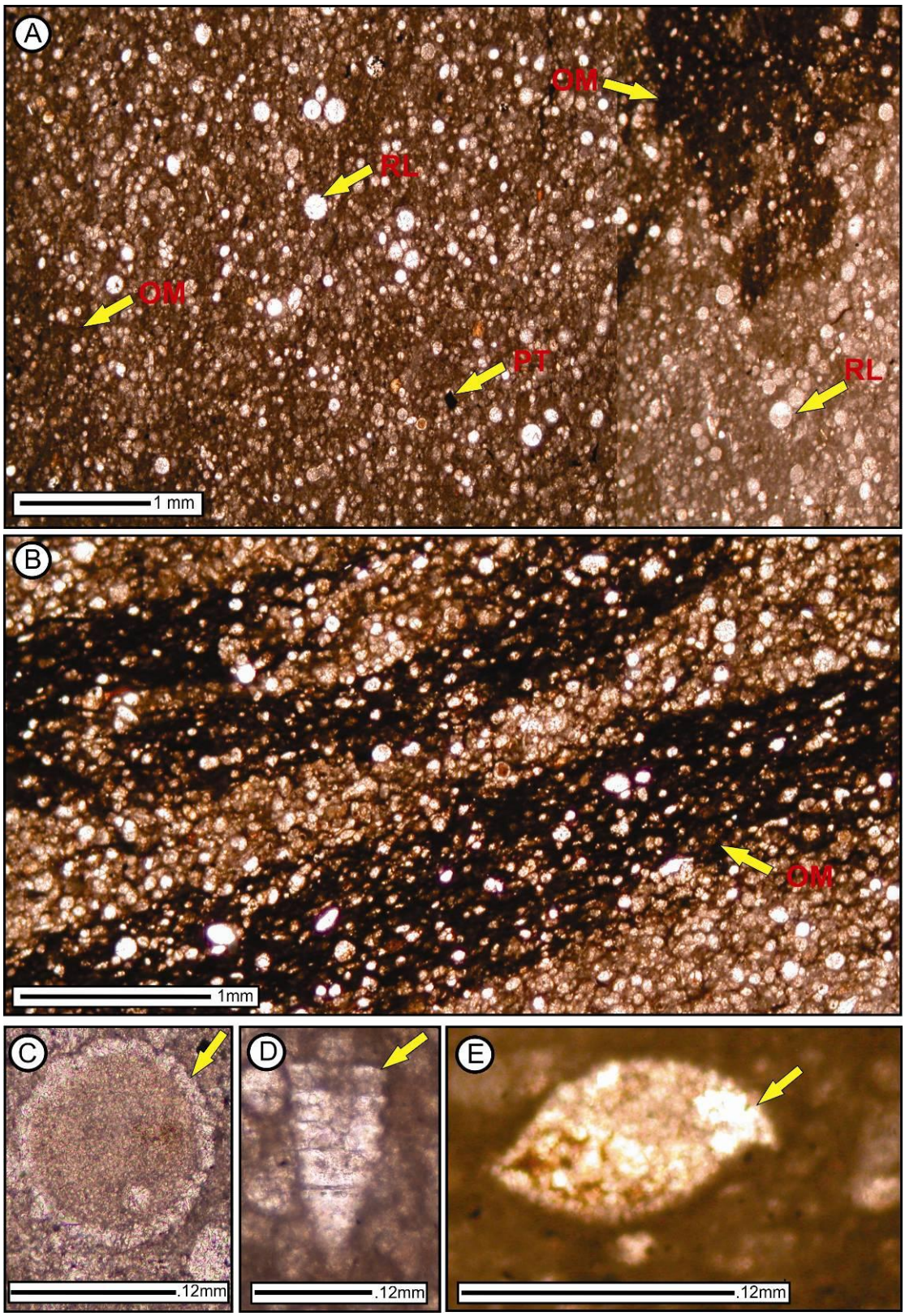

Figure 3.2: ***Organic-rich radiolarian wacke- to packstone (MP 1)*****: The frame work components of this microfacies are Radiolarians (**RL **in A; C; D; E), Pyrite presence (**PT **in A). Brown to dark brown Organic Matter is seen at different intervals in this microfacies (**OM **in A and B).**

3.2.1.2 Organic-rich mixed siliciclastic-carbonate wacke- to packstone MP 2 Microfacies, see also Figure 3. 3

The MP 2 Microfacies is composed of well sorted, angular quartz grains (15%). The carbonate angular lithoclasts (8%) float in the organic-rich micrite. These lithoclasts are broken and glauconitised after deposition. The glauconite usually forms in low turbulence and low temperature water conditions without much clastic influx to the basin (Lim et al. 2000). Also, slightly reduced water conditions are required with enough supply of iron and potassium (Odin & Matter, 1981; Hughes & Whitehead, 1987). Euhedral dolomite partially replaces calcite in the matrix as well as the carbonate intraclasts during burial diagenesis. The presence of stylolites and broken fossil shells indicate deep burial, while the presence of quartz indirectly confirms the presence of associated clay minerals (smectite). Hence, the burial has produced magnesium (smectite to illite conversion) which is a source for the dolomite formation. The dolomititisation may have been further enhanced by the sulphate reduction associated with organic matter, which makes the pore water more alkaline. This alkalinity aids in the dolomite formation.

To summarise, this facies is characterised by deposition of quartz and other carbonate lithoclasts in a carbonate matrix, glauconitisation of the framework components (lithoclasts and rare quartz), pressure solution, and formation of dolomite.

Paleoenvironment: The underlying MP 1 Microfacies was deposited in deep basin while the overlying MP 3 Microfacies was deposited in the outer ramp setting, hence the deposition of MP3 may also represent in outer ramp/deep basin. The clastic input can be explained by the presence of fluvio-deltaic input on the basin margin.

3.2.1.3 Hedbergella pack- to wackestone MP 3 Microfacies, see also Figure 3.4

The texture of the rock of the MP3 Microfacies ranges from pack- to wackestone under the microscope. The relative abundance of the grains ranges from 58% to 73%, with an average of 64%, while the combined micrite and organic matter range from 27% to 42%, with an average of 36%. The dominant components of the grains are the planktonic foraminifera which range from 22 to 30%, with an average of 27%.

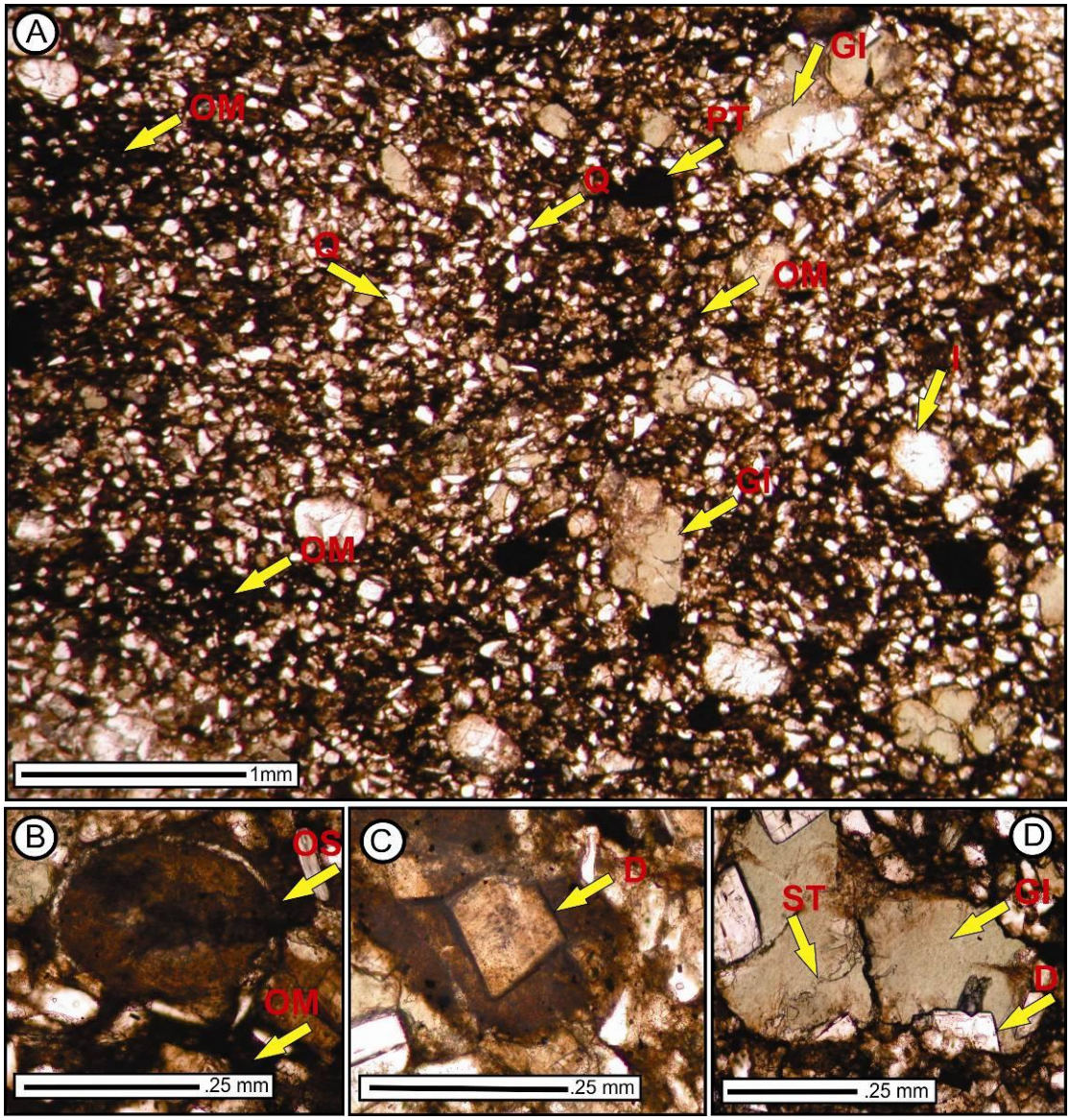

Figure 3.3: ***Organic rich mixed siliciclastic-carbonate wacke- to packstone (MP 2):*** **Note the well sorted angular quartz (**Q **in A), Pyrite (**PT **in A), brown to dark brown Organic Matter (**OM **in A), Intraclasts (**I **in A), partly to completely Glauconitic Intraclasts (**GL **in A; D), broken and micrititized ostracode (**OS **in B), Dolomite rhomb (**D **in C and D), Stylolites in broken glauconitised intraclasts (**ST **in D).**

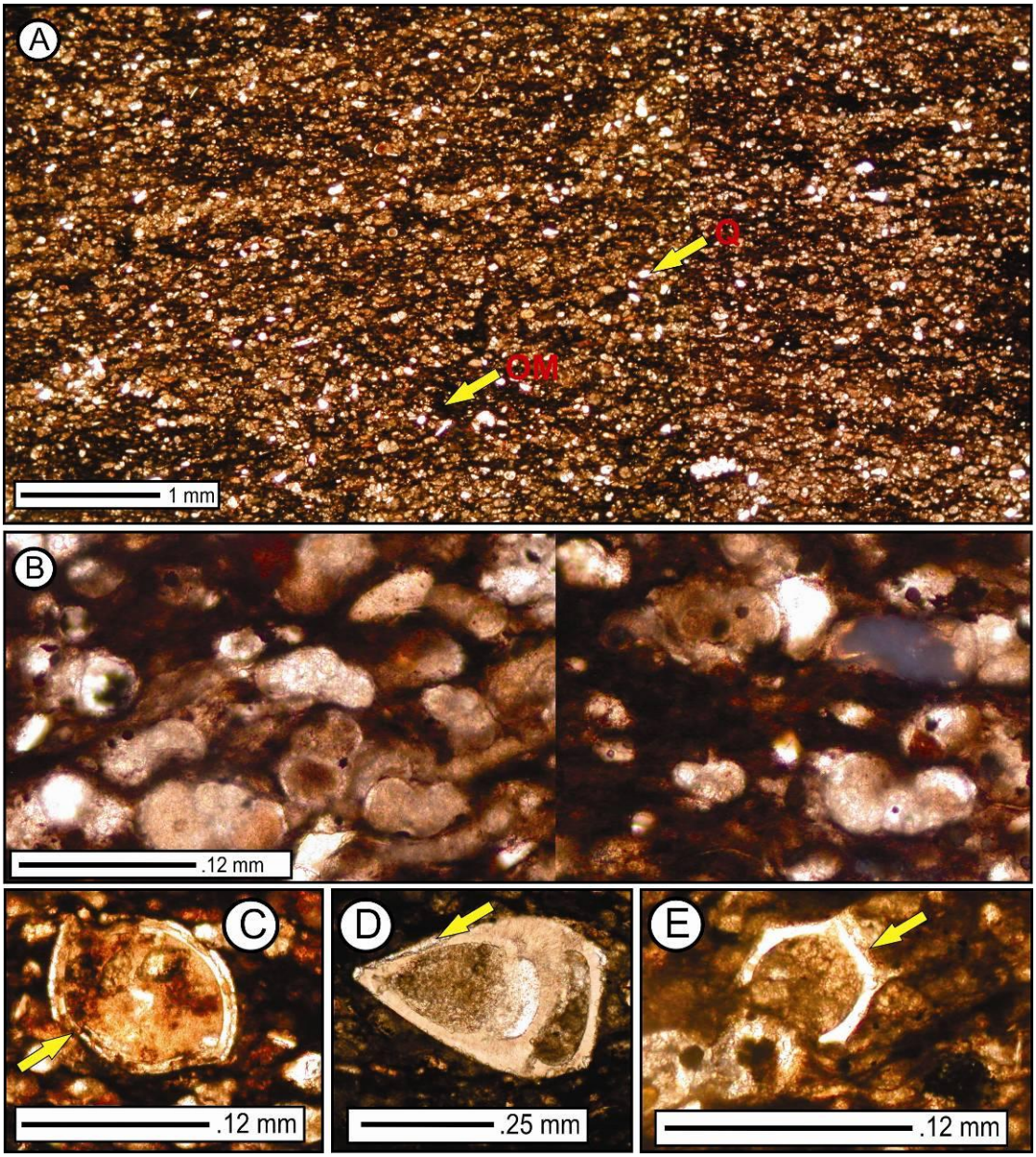

Figure 3.4: ***Hedbergella pack- to wackestone (MP 3):*** **The main constituent of the microfacies is** ***Hedbergella*** **(B), with amorphous Organic Matter (**OM **in A). The rare bored and micritised ostracode (C), bored and micritised benthic foraminifera (D) and Calcareous algae (E) are also present.**

The relative abundance of the echinoids ranges from 4 to 8%, with an average of 4%, while the radiolarians are present in low numbers, with an average of 3%. Ostracodes, algae, calcispheres, molluscs, benthic foraminifera, sponges form a very minor part of the rock. Well sorted, sub-rounded quartz makes up 2% of the whole rock. Intraclasts are very rare. The amorphous organic matter is distributed uniformly throughout this microfacies. These rock show minor to extensive pyritisation under the microscope. The pyrite is associated with the organic matter, probably formed

under anoxic conditions. Occasionally, the pyrite resides in faunal components. All the faunal components are bored and micritised on the margins and some of the fossils shells are internally partially replaced by neumorphic spar.

Paleoenvironment: The enriched planktonic foraminiferal sediments represent deposition in the outer ramp setting (Flügel, 2004). Therefore the major planktonic foraminiferal constituents within MP 3 Microfacies represent deposition in the outer ramp settings.

3.2.1.4 Mixed radiolarian-foraminifera wackestone MP 4 Microfacies see also Figure 3.5

The rocks of the MP4 Microfacies show a wackestone texture. The relative abundance of the grains ranges from 15 to 41%, with an average 25%, while the micrite ranges from 59-85%, with an average of 75%. The major component of this microfacies is the radiolarians, which range from 8-20%, with an average of 12%. The relative abundance of the planktonic foraminifera ranges from 5-13%, with an average of 9%. The echinoid, molluscs, calcispheres, benthic foraminifera, and sponges make only minor part of the rock. *Hedbergella* sp. and *Globigerinelloides* sp. are present in the lower part of the Parh Formation, while marginotruncanids, ***whiteinellids, and*** *Heterohelix* occur in the upper part of the sequence. Organic streaks are present throughout. The organic and pyrite enrichment is more conspicuous in the lower part of the Parh Formation.

Paleoenvironment: The combined occurrence of radiolarians and planktonic foraminifera suggests deposition in the outer-ramp setting (Heldt et al. 2008), hence the presence of both radiolarians and planktonic within MP 5 Microfacies, represent deposition in outer-ramp setting.

3.2.1.5 Organic-rich siliciclastic mixed peloidal-bioclastic wacke- to packstone MP 5 Microfacies, see also Figure 3.6

The texture of the MP5 Microfacies ranges from wacke- to packstones. The relative abundance of the grains in these rocks is on average 29%, while well sorted subangular to subrounded detrital quartz represents 8%. The remaining 63% comprises micrite and organic matter, their subdivision in terms of relative

abundance is not possible. Structureless elliptical to rounded peloids make up the 10% of the total rock, while the bioclasts represent 8%. These bioclasts are broken and are very small in sizes and hence a final conclusion on their affinity can't be drawn. However, molluscs and echinoderms clasts can be identified. The echinoderm spines and plates are degraded and show sweeping extinction (in cross light) due to wear and tear during its reworking. Benthic and planktonic foraminifera are very rare. The detrital quartz and bioclasts are differentially concentrated at places in matrix.

Paleoenvironment: The high percentage of the micrite represents deposition below storm wave base. The fine bioclasts along with peloids represent deposition in outer ramp settings (Wilson, 1975). The packstone patches of carbonate and quartz grains indicate concentration of the constituents of microfacies due to agitation induced by the storms. Therefore the MP 6 Microfacies was deposited in the outer ramp settings just below the storm wave base.

3.2.1.6 Organic-rich *Hedbergella-peloidal-radiolarian pack- to wackestone MP 6 Microfacies, see also Figure 3.7*

In thin section, the MP6 Microfacies has pack- to wackstone textures. The total relative abundance of grains ranges from 36 to 41%, with an average of 39%, while the combined relative abundances of micrite and organic matter range from 56 to 59%, with an average of 61%. The relative abundance of planktonic foraminifera ranges from 5 to 15%, with an average of 10%. Specimens belong to the genus *Hedbergella*. The relative abundance of radiolarians ranges from 4 to 10%, with an average of 7%. The relative abundance of elliptical peloids ranges from 5 to 10%, with an average of 7%. The echinoderm spines and plates make up 5% of the total rock. The average percentage of the smaller benthic foraminifera is 4%. The relative abundance of mollusc fragments ranges from 2.4 to 4%, with an average of 3%. The relative abundance of carbonate intraclasts ranges from 0.5 to 3%, with an average of 2%. Well sorted quartz grains make up 3% of the rocks whilst the calcareous algae are very rare and are less than 1%. The MP3 Microfacies contains high amounts of amorphous organic matter, which is distributed uniformly throughout the rock. The fossils are bored and micrite filled, on their periphery. The fossils are also replaced by spar internally.

Paleoenvironment: The high percentage of micrite indicates deposition below wave base. The presence of radiolarians and planktonic foraminifera represents the outer ramp environment (Heldt et al. 2008). Therefore the presence of both radiolarians and planktonic within MP 6 Microfacies, represent deposition below wave base in the outer ramp settings.

3.2.1.7 Laminated organic-rich peloidal pack- to wackestone MP 7 Microfacies, see also Figure 3.8

Under the microscope, the texture of the MP7 Microfacies is pack- to wackestone. The relative abundance of grains ranges from 46 to 52%, with an average of 49%, while the micrite together with organic matter ranges from 48 to 54%, with an average of 51%.

Paleoenvironment: The lack of shallow marine fauna and the laminated peloidal structures represent deposition in the outer ramp (Flügel, 2004) hence the MP 7 Microfacies was deposited in the outer ramp.

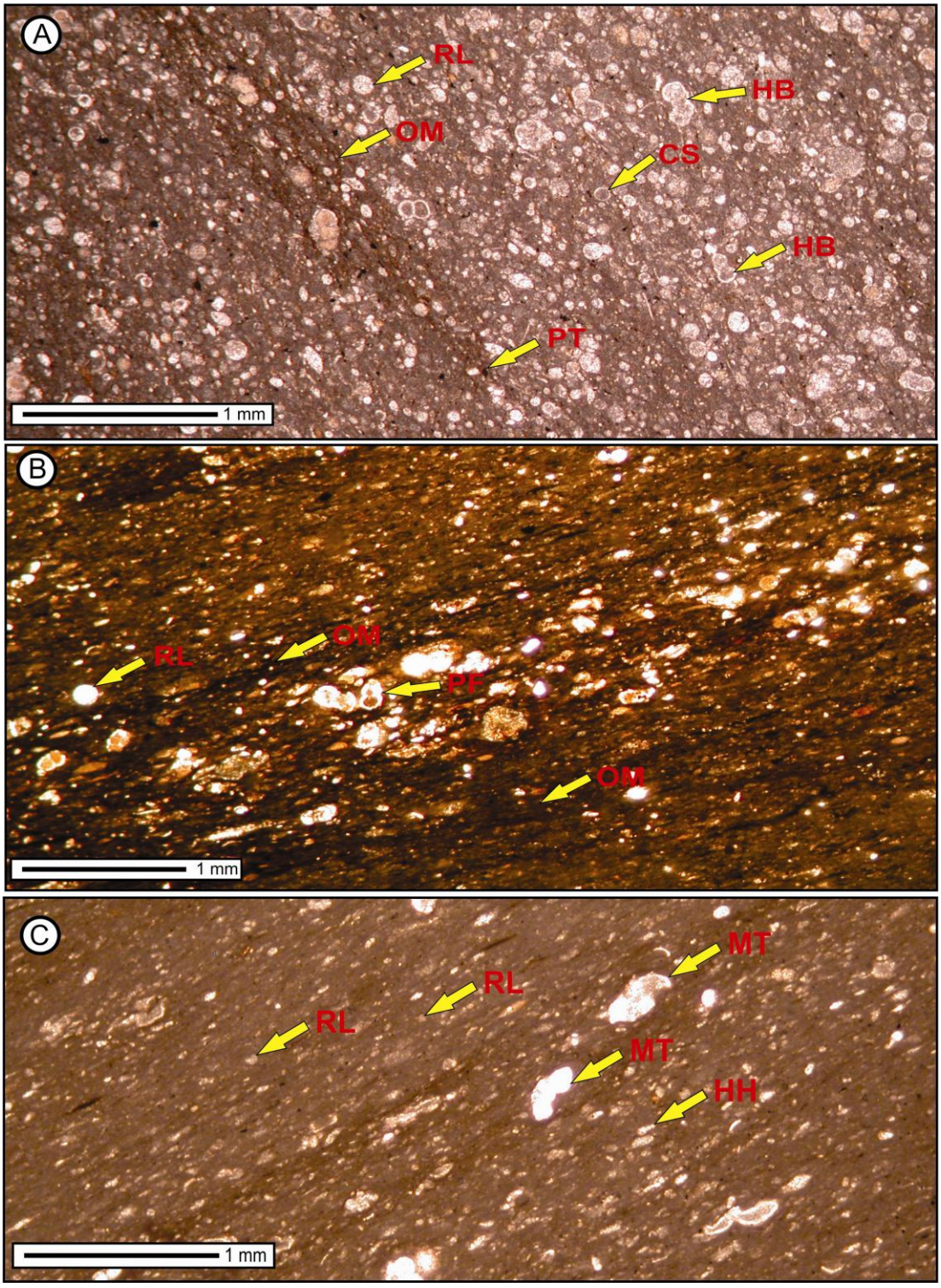

Figure 3.5: ***Mixed radiolarian-foraminifera wackestone (MP 4):*** **The dominant builders of this microfacies are Radiolarians (**RL **in A, B and C). The Planktonic Foraminifera (**PF **in B) contain** ***Hedbergella*** **(**HB **in A), and** ***Marginotruncana*** **(**MT **in B). Calcispheres are also present (**CS **in A), Pyrites are present (**PT **in A). Laminated Organic Matter (**OM **in A and B) is seen.**

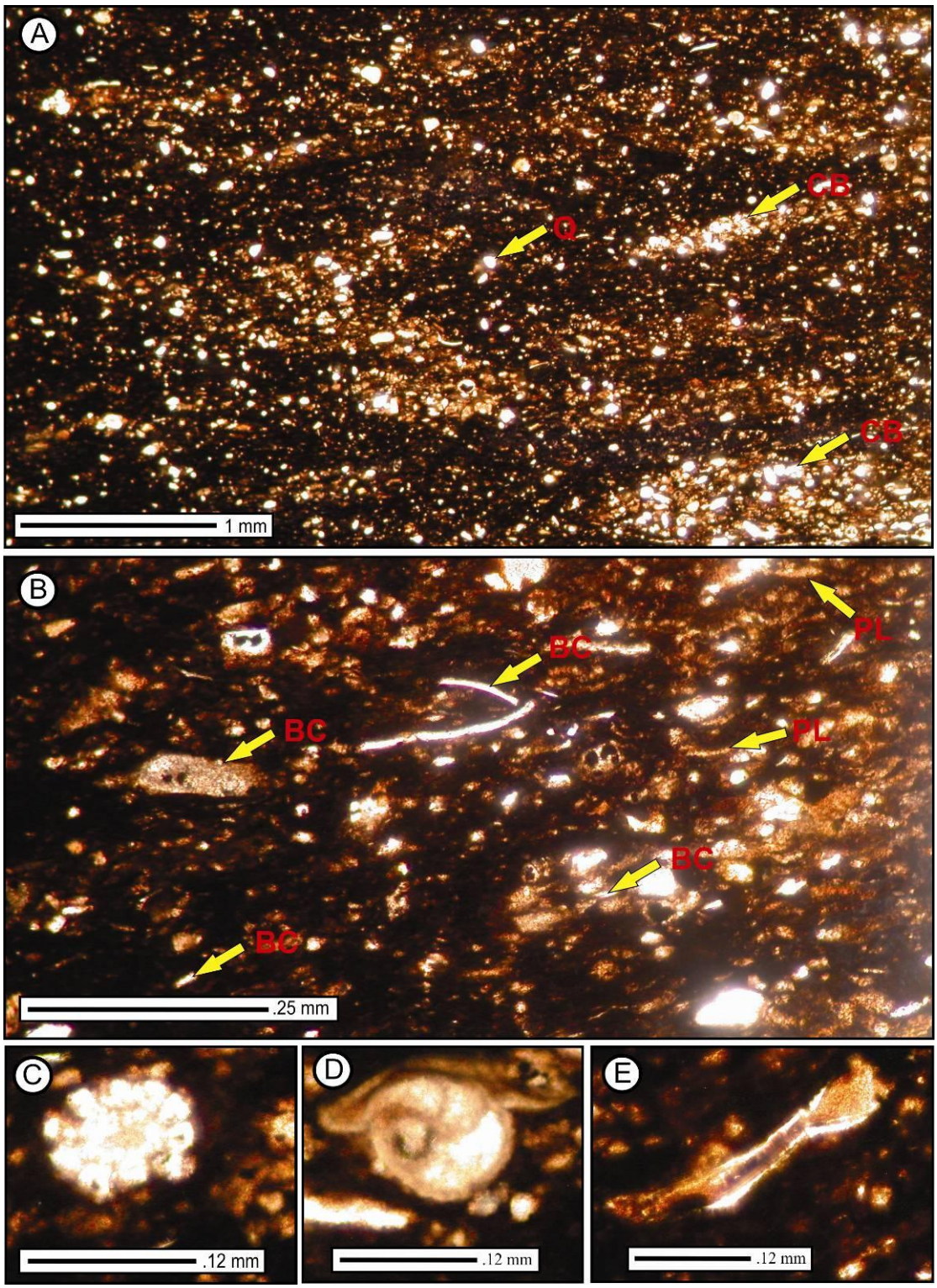

Figure 3.6: ***Organic-rich siliciclastic mixed peloidal-bioclastic wacke- to packstone (MP 5):*** **The main constituents of this microfacies are Peloids (**Pl **in B), Bioclasts (**BC **in B) with rare echinoderms (C) and smaller benthic foraminifera (D) and calcareous algae (E). Well sorted subrounded Quartz is present (**Q **in A). Concentred Bands of quartz and allochems deposited by storm (**CB **in A).**

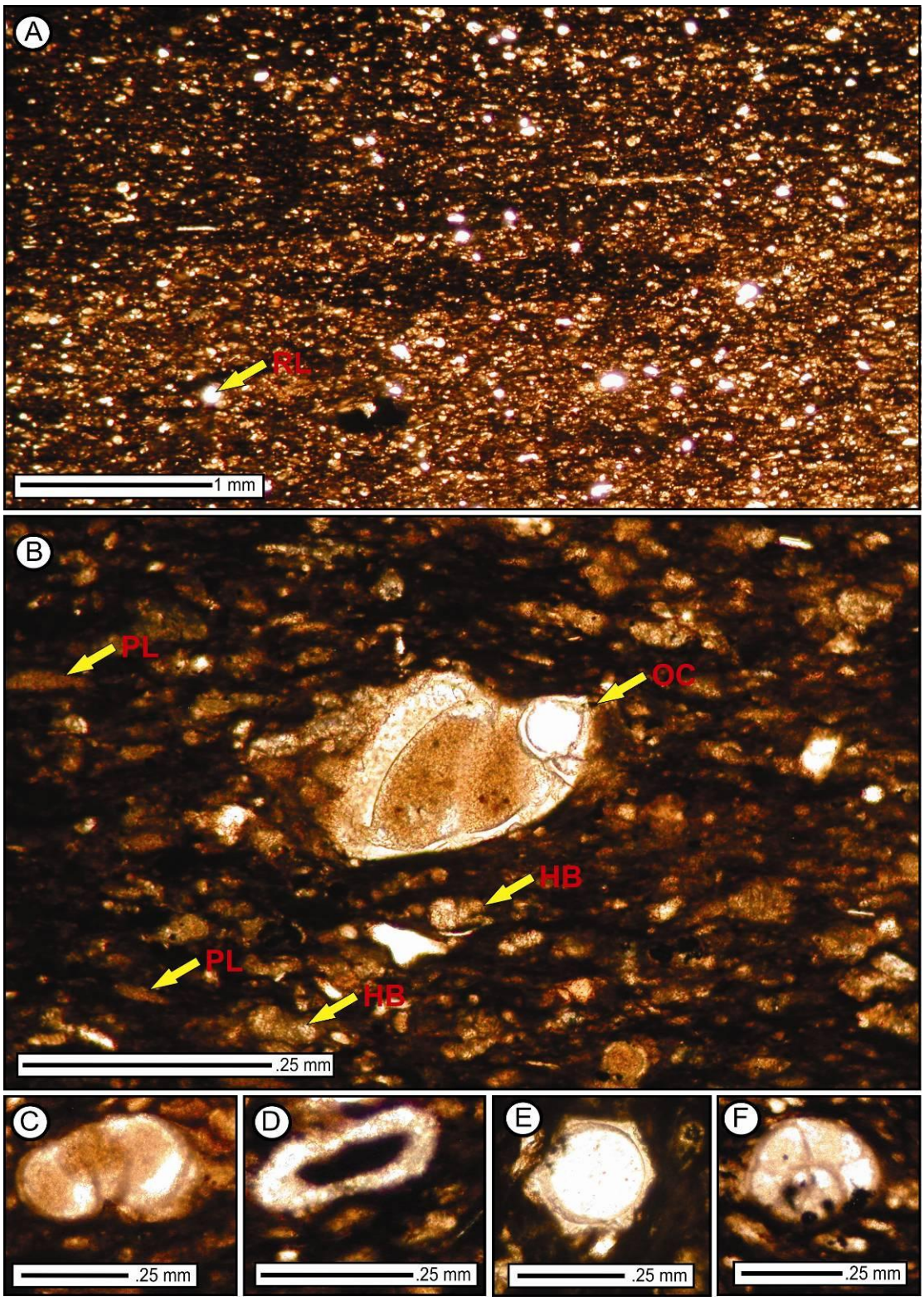

Figure 3.7: ***Organic-rich Hedbergella-peloidal-radiolarians pack- to wackestone (MP 6):*** **The grains of this microfacies consist of** ***Hedbergella*** **(**HB **in B; C), Peloids (**PL **in B), with minor Ostracodes (**OC **in B), Calcareous algae (D), Echinoderms spines (E), and small benthic foraminifera (F)**

3.2.1.8 Radiolarian-rich wacke- to mudstone MP 8 Microfacies, see also Figure 3.9

The MP8 Microfacies exhibits the wacke- to mudstone textures. The total relative abundance of the allochems ranges from 4 to 23%, with an average of ~12%, while the micrite ranges from 77 to 96%, with an average of 88%. The grains are dominantly composed of radiolarians which float in a carbonate matrix. The relative abundance of the radiolarians ranges from 0.5-21%, with an average of ~9%. Low numbers of planktonic foraminifera, ostracodes, calcareous algae, echinoderms, molluscs, sponges and benthic foraminifera are present. The planktonic foraminifera comprise *Hedbergella* and *Ticinella* sp.

Paleoenvironment: The mudstone texture and the presence of radiolarians indicate the deep basin environment (Flügel, 2004); therefore MP 9 Microfacies was deposited in deep basin.

3.2.1.9 Interlaminated mixed faunal pack- to mudstone MP 9 Microfacies, see also Figure 3.10

The MP9 Microfacies shows alternate laminations of the pack- to mudstone texture. The packstone texture is confined to laminated intervals which are thin as compared to the alternating mudstone intervals. The relative abundance of peloids and planktonic foraminifera range from 2 to 12% each, with an average of 7% and 9% respectively. The relative abundance of radiolarians ranges from 2% to 8%, with an average of 5%, Echinoderms make up 1 to 5%, with an average of 3%. Laminated organic matter is dominant in the mudstone interval, which is extensively pyritised. Minor burrows are present in the mudstone interval. The faunal components are worn from the margins due to boring and micritisation and internally they are partially replaced by neumorphic spar.

Paleoenvironment: The deposition of finer packstone and mudstone tempestite couplets represent deposition in the outer ramp environment (Mohseni & Aasm, 2004). Such tempestites show deposition close to the storm wave base, hence MP 9 Microfacies was deposited in the outer ramp close to the storm wave base.

3.2.1.10 Burrowed/bioturbated mixed biotic wacke- to mudstone MP 10 Microfacies, see also Figure 3.11

The texture of the rocks in thin section of the MP 10 Microfacies ranges from wack- to mudstones. The relative abundance of the grains ranges from 2 to 20%, with an average of 11%, while the micrite ranges from 80-98%, with an average of 89%. The dominant fauna are the radiolarians, which make up 4%, while the echinoderms are second in abundance with an average of 3%. The calcareous algae, sponges, planktonic foraminifera, molluscs, calcispheres, and ostracode represent a very minor fraction of the total rock in decreasing order of abundance. Small sized, well sorted and subrounded quartz grains make up about 1% of the total rock. The allochems dominantly show parallel orientation. The organic matter enrichment is common along the burrows.

Paleoenvironment: The mudstones with pelagic microfossils represent deposition in the outer ramp setting (Flügel, 2004); therefore MP 10 Microfacies was deposited in the outer ramp.

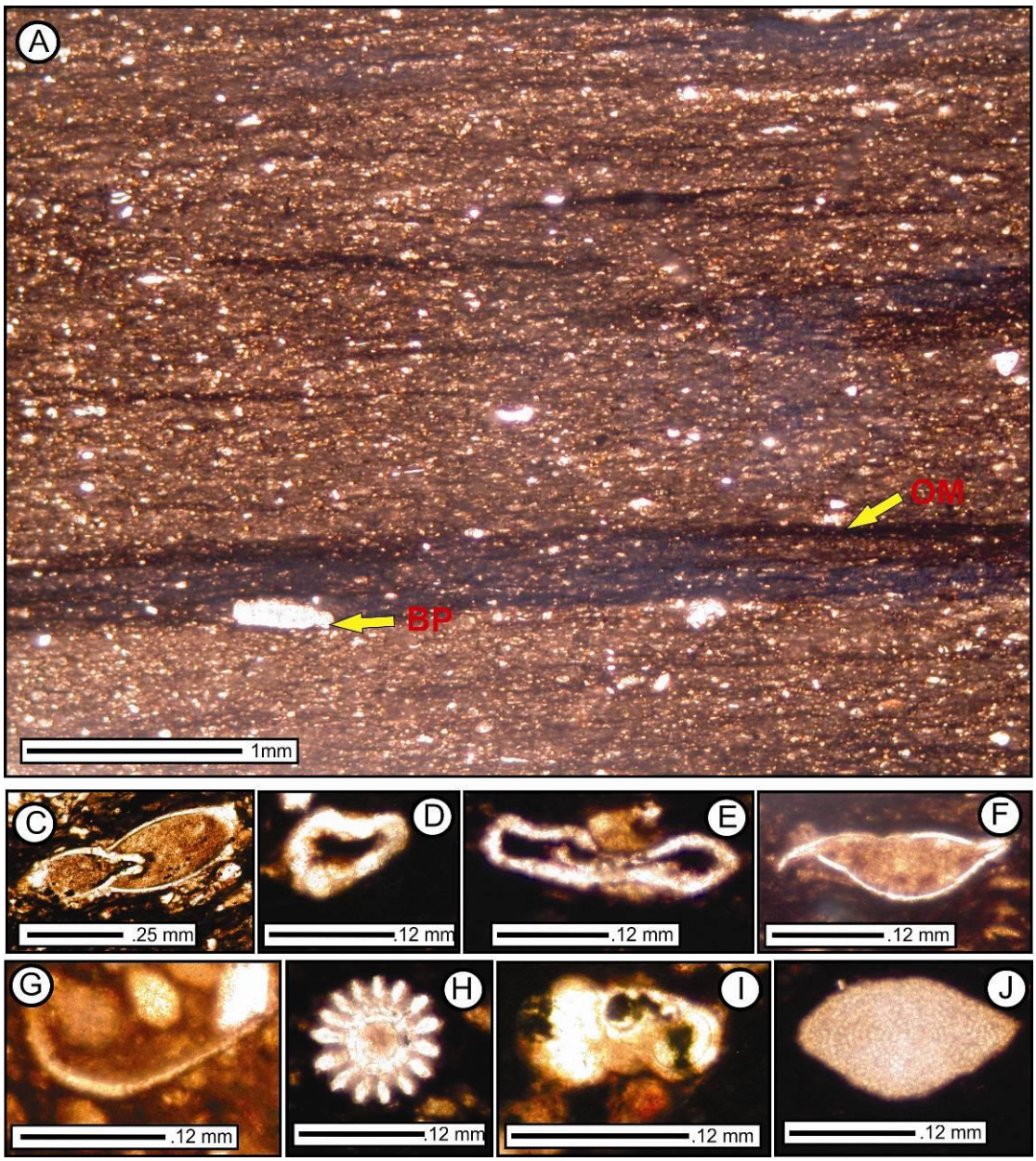

Figure 3.8: ***Laminated organic-rich peloidal pack- to wackestone (MP 7):*** **The main framework elements are peloids with minor calcareous algae (D and E), Ostracodes (F), echinoderm spines (H),** ***Hedbergella*** **(I), benthic foraminifera (C and J). Ostracode showing the geopetal fabric (G).**

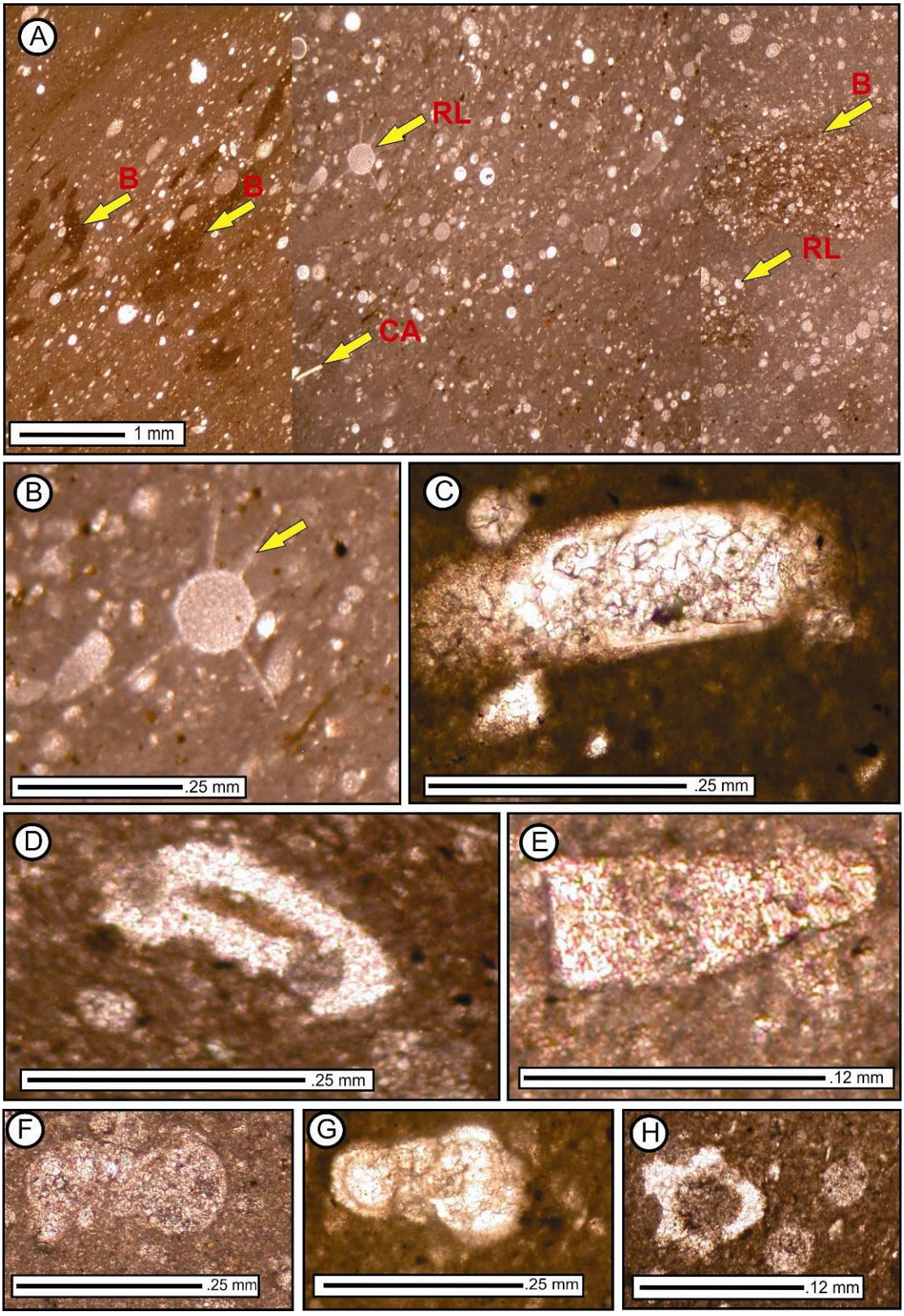

Figure 3.9: ***Radiolarian rich wacke- to mudstone (MP 8):*** **This microfacies is rich in Radiolarians (**RL **in A; B), and Burrows (**B **in A). Rare Calcareous Algae (**CA **in A; D; H), Echinoderms spines (C), Calcareous algae (D), Echinoderm plate (E),** ***Ticinella*** **sp. (F and G) are present.**

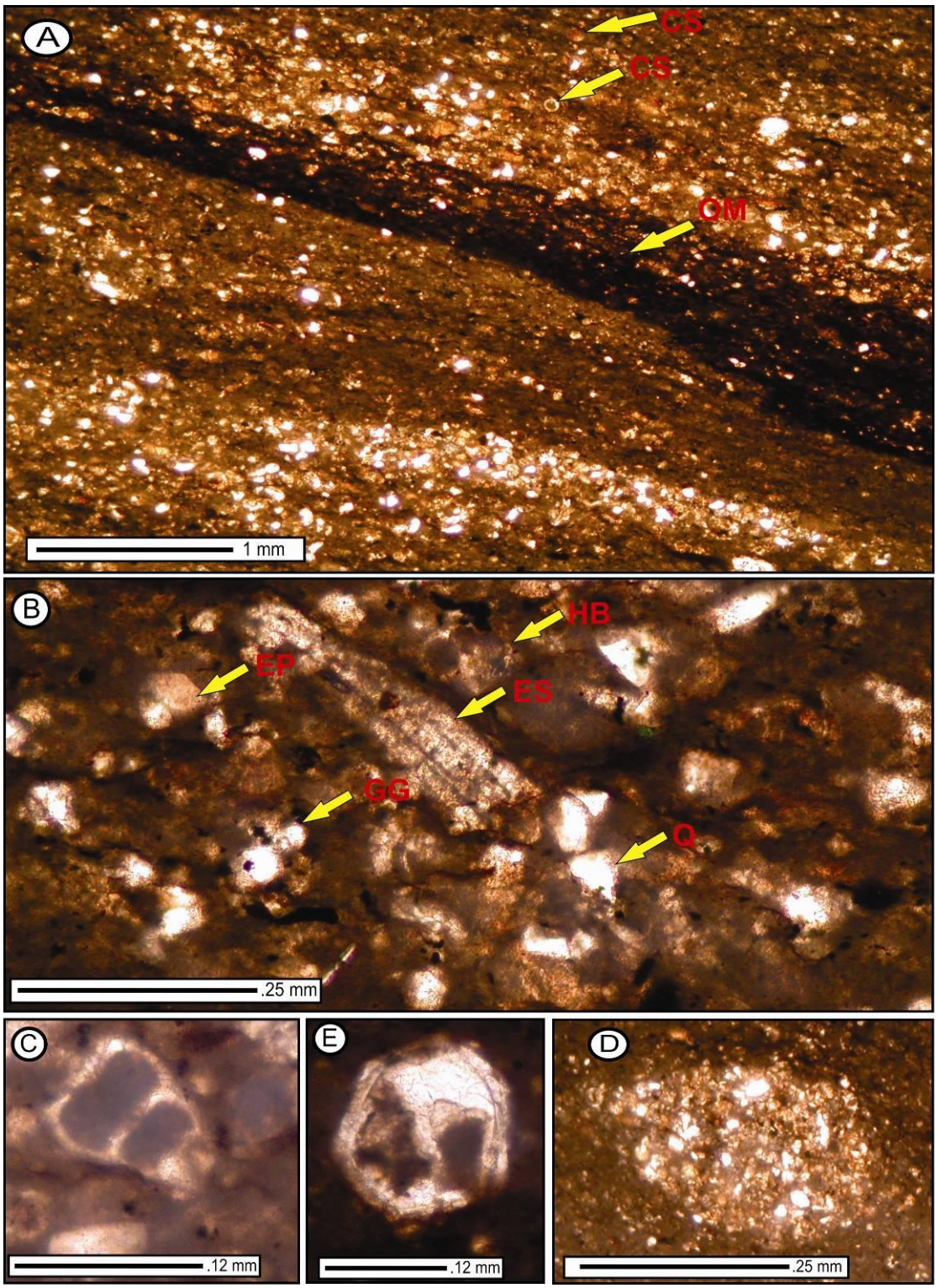

Figure 3.10: ***Interlaminated mixed faunal pack- to mudstone (MP 9):*** **This interlaminated microfacies has Organic Matter rich laminations (**OM **in A). Echinoderms Spines in the packstone laminae (**ES **in B), Echinoderm Plates (**EP **in B),** ***Globigerinelloides*** **(**GG **in B), angular Quartz (Q in B),** ***Hedbergella*** **(**HB **in B), Radiolarians (C), calcareous algae (E), mudstone laminae contains occasionally burrows (D).**

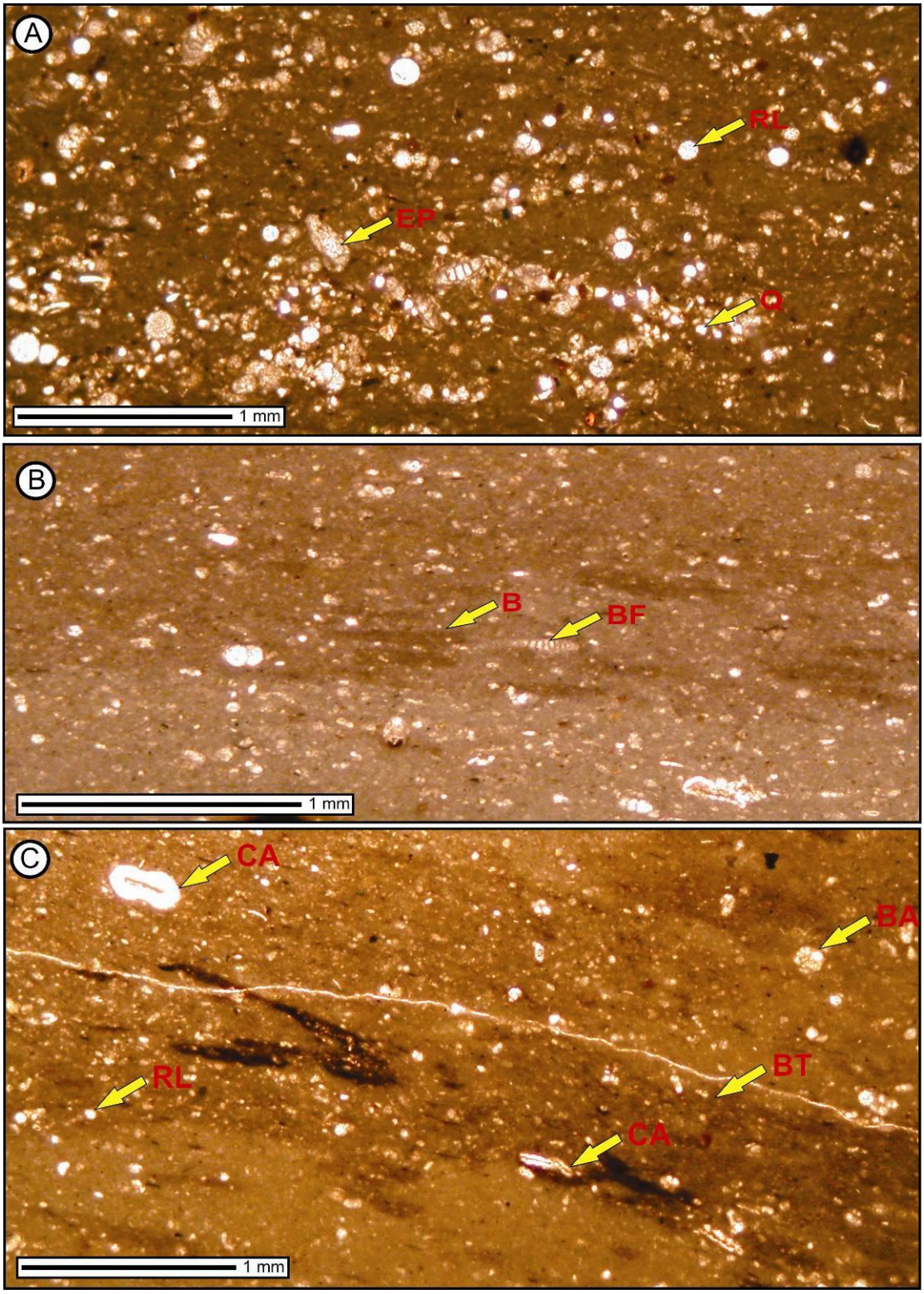

Figure 3.11: ***Burrowed/bioturbated mixed biotic wacke- to mudstone (MP 10):*** **The mixed biota include Echinoderm Plates (**EP **in A), Radiolarians (**RL **in A), Benthic foraminifera (**BF **in A, B, and C), Burrows (**B **in B), Calcareous algae (**CA **in C). Bioturbation is common (**BT **in C), well sorted subrounded to rounded Quartz present (**Q **in A).**

3.2.1.11 Burrowed/bioturbated mudstone MP 11 Microfacies, Fig. 3.12

The texture of the MP11 Microfacies is mudstone. It contains small amounts of grains, approximately 5%, while the rest of the rock is micrite. Minor planktonic foraminifera, algae, benthic foraminifera, sponges, calcispheres, molluscs, and echinoderms are present in most of the intervals. The burrows and bioturbation are common throughout these rocks. Some of burrows are elongated and are elliptical in shapes, while others are irregular. The microfacies is rich in organic matter at places.

Paleoenvironment: Mudstone with pelagic microfossils represents deposition in the outer ramp setting (Flügel, 2004); hence MP 11 Microfacies was deposited in the outer ramp.

3.2.1.12 Mixed bioclastic-foraminiferal wacke- to packstone MP 12 Microfacies, see also Figure 3.13

The rocks of the MP12 Microfacies show the wackestone texture under the microscope, although the packstone texture occurs in places. The relative abundance of the grains ranges from 32-46%, with an average of 42%, while micrite ranges from 54 to 68%, with an average of 58%. The fine bioclasts represent the bulk of the grains, their relative abundance ranges from 20-40%, with an average of 29%. The planktonic foraminifera range from 4 to13%, with an average of 9%. Other recognisable fauna includes calcispheres, benthic foraminifera, echinoids, ostracodes, molluscs, and sponges, although their abundances are rare. The bioclasts are often very small, which makes identification difficult. Quartz is a minor constituent about 1%.

Paleoenvironment: The fine bioclastic packstone having large planktonic foraminifera in association with minor benthic foraminifera represents deposition in the outer ramp environment (Heldt et al., 2008). The fine bioclasts of the current microfacies are interpreted to have been reworked from the inner-middle ramp environments and were deposited in the outer ramp.

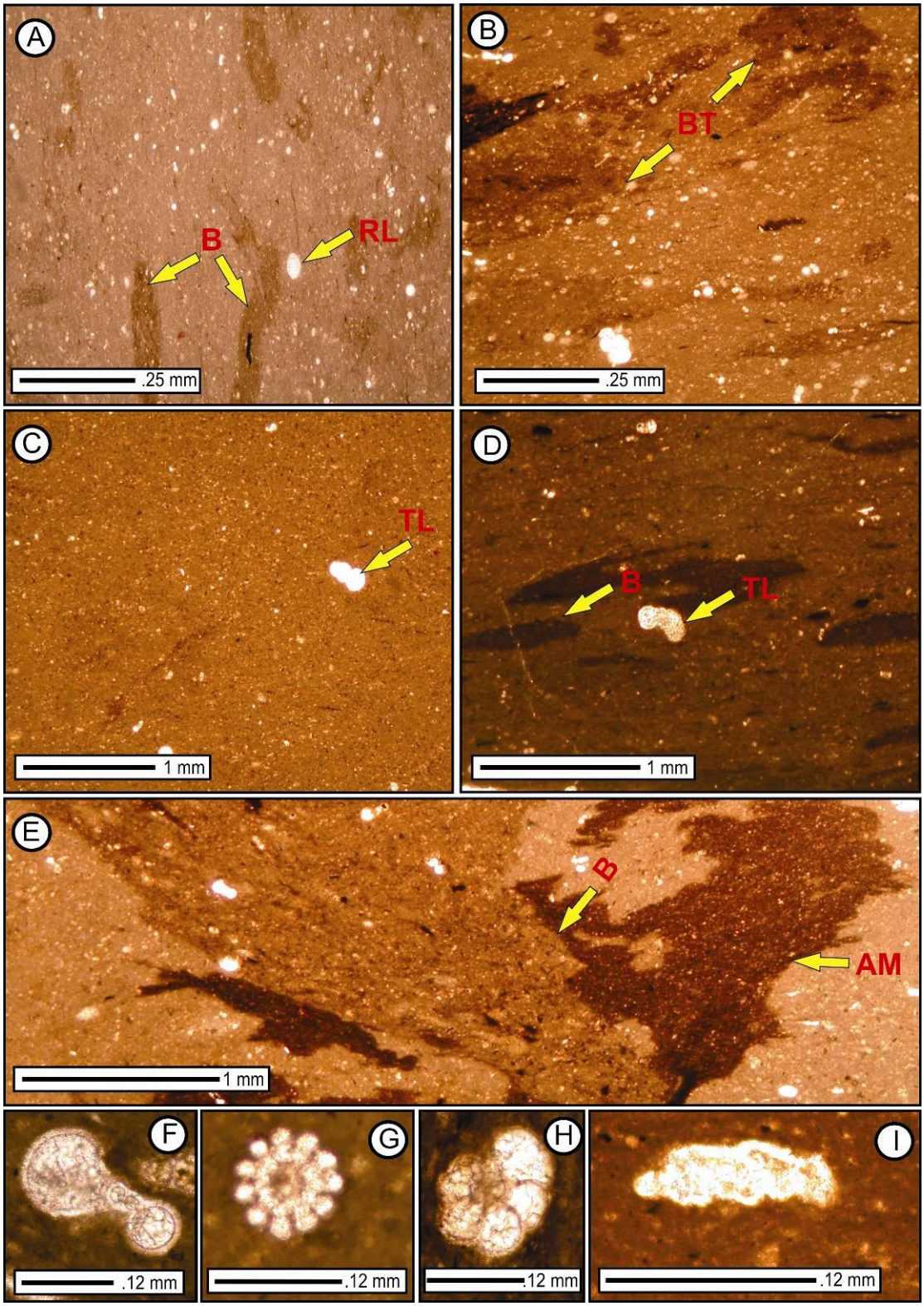

Figure 3.12: ***Burrowed/bioturbated mudstone (MP 11):*** **This mudstone facies have abundant Burrows (**B **in A, D, and E) and Bioturbation (**BT **in B). It also contains minor Radiolarians (**RL **in A), Ticinella (**TL **in C and D; F; H), echinoderms spines (G), and calcareous algae (I). Intraclasts of Algal Mats (**AM **in E) are also present.**

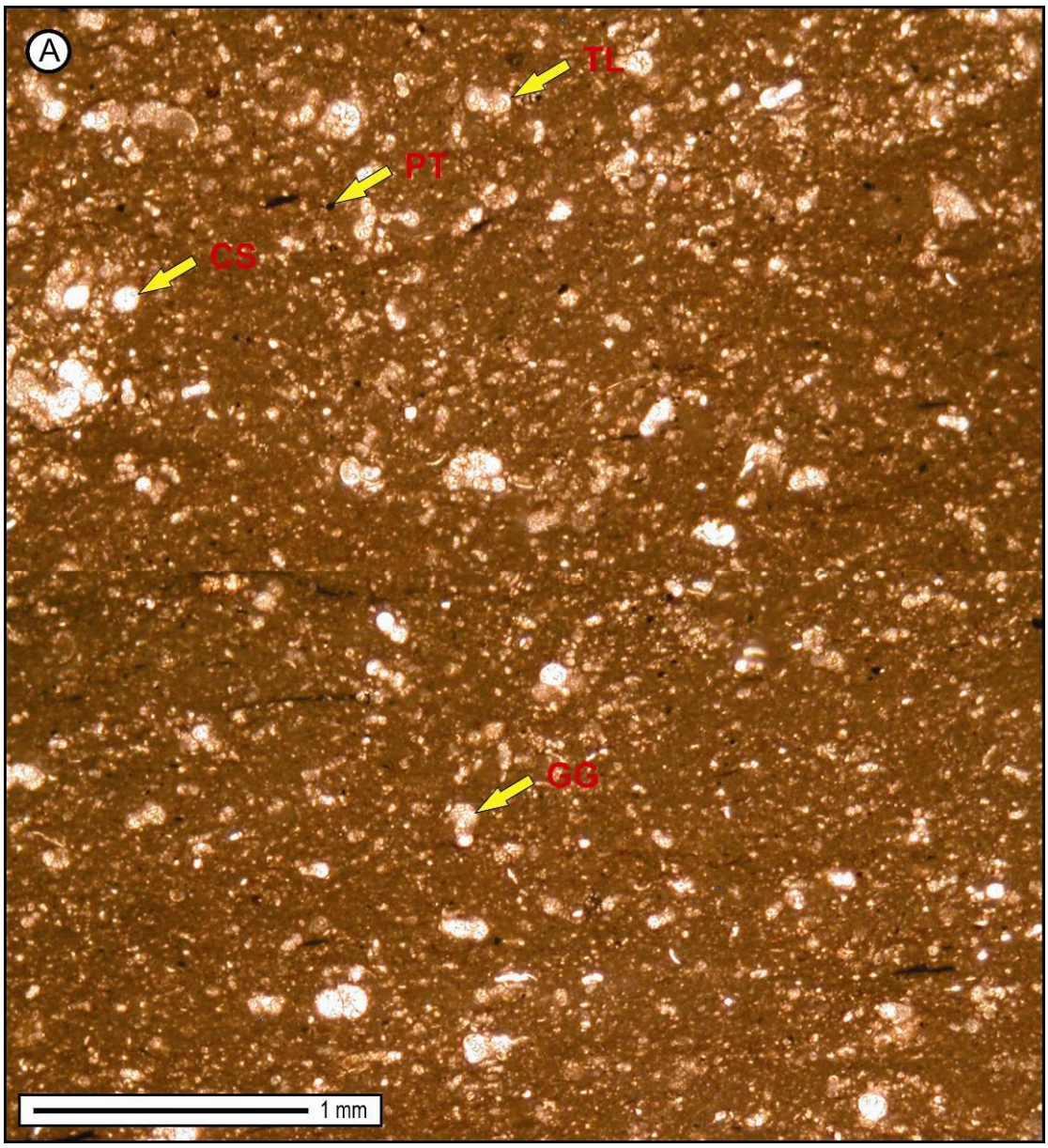

Figure 3.13: ***Mixed bioclastic-foraminiferal wacke- to packstone (MP 12):*** **The microfacies is mostly wackestone, which changes in places to packstone. The foraminifera contain *Ticinella* (**TL **in A), *Globigerinelloides* (**GG **in A). Minor Calcispheres (**CS **in A) are also present. Tiny Pyrite fambroids (**PT **in A) scattered throughout the microfacies.**

3.2.1.13 Mixed planktonic foraminiferal wacke- to mudstone MP 13 Microfacies, see also Figure 3.14

The texture of the MP13 Microfacies ranges from wackestone- to mudstone. The total relative abundance of grains of these rocks ranges from 19-38%, with an average of 28%, while the micrite ranges from 62-81%, with an average of 72%. The planktonic foraminiferal abundance ranges from 18-36%, with an average of 25%.

The *Rotalipora* are highly abundant, while *Praeglobotruncana*, *Ticinella*, *Heterohelix*, *Whiteinella*, *Globigerinelloides*, *Planomalina*, and *Dicarinella* are less abundant in decreasing order. Calcispheres and sponges are very rare. All the grains show parallel orientation. Banded amorphous organic matter is fair to rich in these rocks, while minor to extensive pyritisation is found in some intervals. The pyritisation is associated with microbial mat activity, indicating anoxic conditions in places.

Paleoenvironment: The deep marine *Rotalipora* mixed with diverse shallow marine planktonic foraminifera i.e. *Heterohelix*, *Whiteinella*, *Globigerinelloides* etc, and alternating mudstones couplets indicate deposition in the outer ramp environment (e.g. Lézin et al., 2012; Mohseni & Aasm, 2004) close to the storm wave base. Therefore similar environment of deposition is suggested for the MP 13 Microfacies.

3.2.1.14 Laminated Rotalipora wacke-/pack- to mudstone MP 14 Microfacies, see also Figure 3.15

The rocks of the MP14 Microfacies show alternating *Rotalipora* wacke- to packstones alternating with small planktonic foraminiferal mudstones. The relatively thin *Rotalipora*-rich laminations exhibit the packstone texture, while the thicker ones show the wackestone texture. The mudstone intervals show evidence of burrowing activity. The polygonal microbial mats are present. The total abundance of grains in this microfacies ranges from 44 to 62%, with an average of 56%, while the micrite ranges from 38-56%, with an average of 44%. The *Rotalipora* is the most dominant genus amongst the planktonic foraminifera. The *Rotalipora* ranges from 12-20% in abundance, with an average of 14%, while *Whiteinella* ranges from 1-14%, with an average of 6%. The *Praeglobotruncana*, *Dicarinella*, *Heterohelix* are rare. Algae, calciphere, molluscs, sponges are also rare, each below 1% on average.

Paleoenvironment: The tempestites, enriched in deep marine *Rotalipora* mixed with diverse shallow marine planktonic foraminifera, and alternating mudstones couplets, represent the outer ramp environment (e.g. Lézin et al., 2012; Mohseni & Aasm, 2004). The tempestites represent deposition close to the storm wave base. Storm agitated outer ramp environment of deposition is suggested for the MP 14 Microfacies.

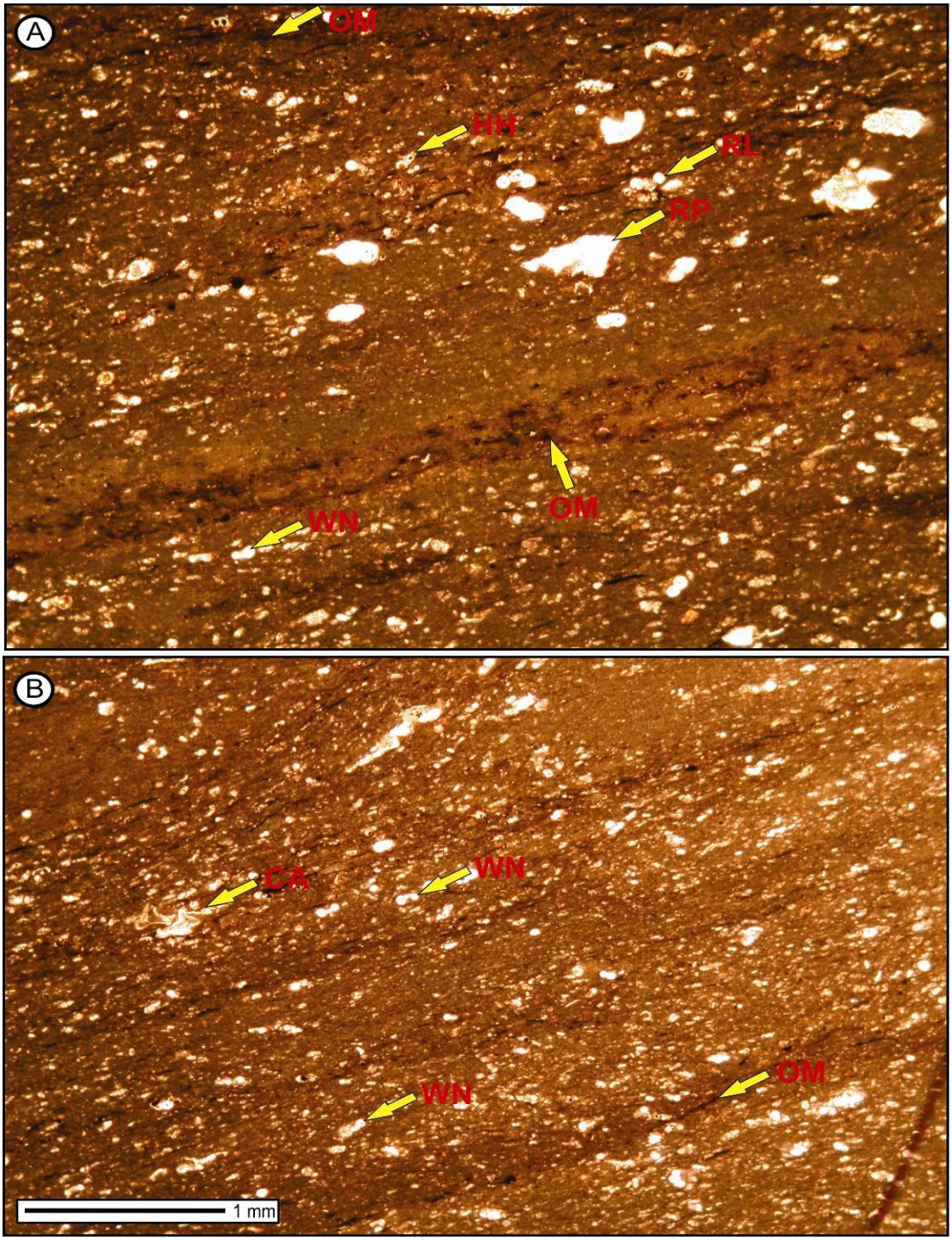

Figure 3.14: ***Mixed planktonic foraminiferal wacke- to mudstone (MP 13):*** **The microfacies show laminations. The planktonic foraminifera are concentrated in isolated laminae separated by laminae with no foraminifers or having less concentration of foraminifers. The Organic Matter (**OM **in A) is present as thin laminations. The planktonic foraminifera include** ***Rotalipora*** **(**RP **in A),** ***Heterohelix*** **(**HH **in A),** ***Whiteinella*** **(**WN **in A and B). Minor Radiolarians (**RL **in A) and Calcareous Algae (**CA **in B) are also present.**

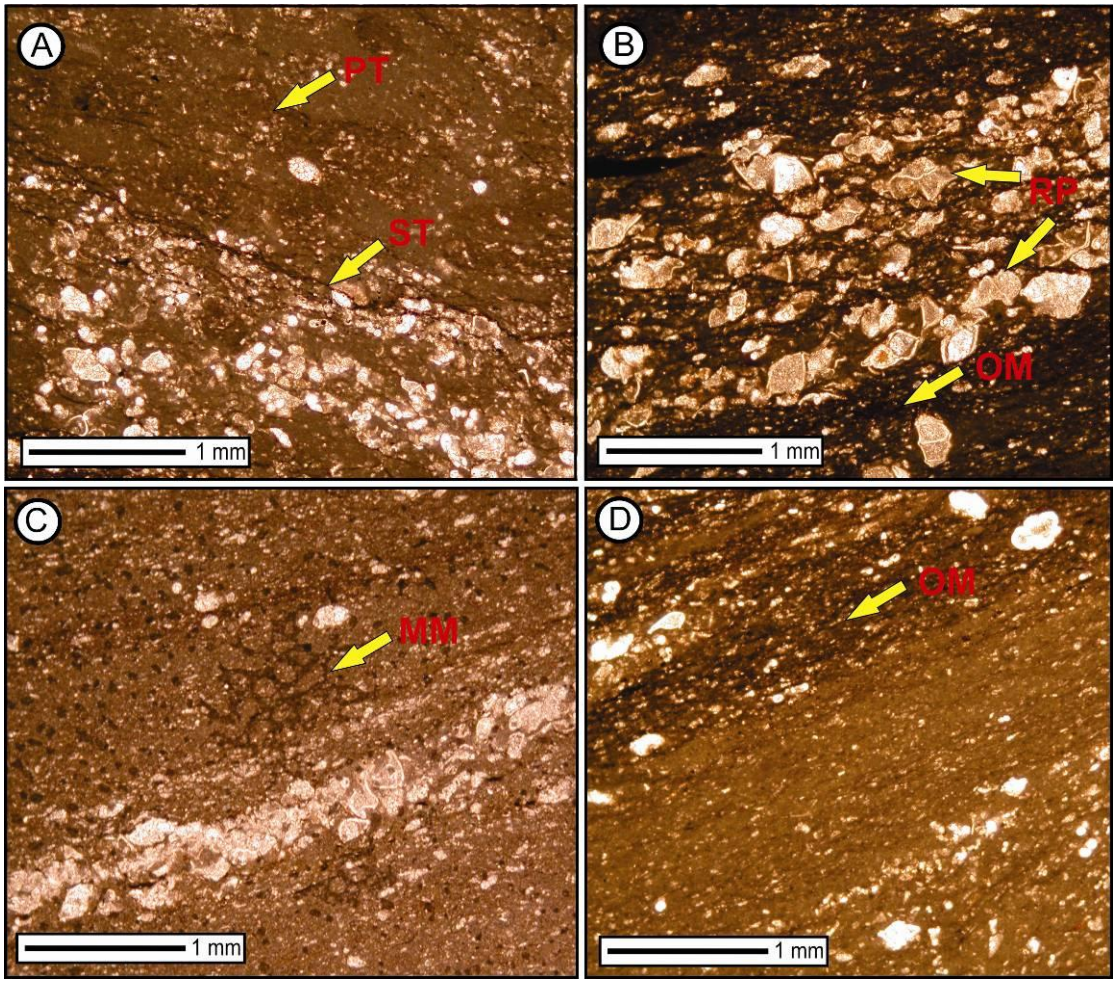

Figure 3.15: ***Laminated Rotalipora wacke-/pack- to mudstone (MP 14):*** **This microfacies is interlaminated between *Rotalipora* rich wackstone/Packstone and Mudstone. The dominant foraminifera are *Rotalipora* (**RP **in B), which occur in laminae of different thickness. The facies is also rich in laminated Organic Matter (**OM **in B). Microbial Mats (**MM **in C) are seen. Very small Pyrite fambroids are associated with microbial mats (**PT **in A). The microfacies show stylolitisates (**ST **in A).**

3.2.1.15 Mixed foraminifera-sponges wackestone MP 15 Microfacies, see also Figure 3.16

The rocks of the MP15 Microfacies exhibit the wackestone texture in thin section. The relative abundance of grains ranges from 24-50%, with an average of 37%, while the micrite ranges from 50 to 76%, with an average of 63%. The planktonic foraminiferal abundance ranges from 7-21%, with an average of 14%. The *Heterohelix* and *Rotalipora* are the dominant planktonic foraminiferal genera, while *Praeglobotruncana*, *Whiteinella* and *Dicarinella* are also present. The second most important faunal component of these rocks is monaxon sponge spicules, which make

up 8-10% of the total rock, with an average of 9%. Calcareous algae and calcispheres represent a very minor fraction of the whole rock.

Paleoenvironment: The association of sponge spicules with planktonic foraminifera restricts interpretation of the environment of deposition to the outer ramp (Wilson, 1975), hence outer ramp environment is suggested for the MP 15 Microfacies.

3.2.1.16 Rotalipora wackestone MP 16 Microfacies, see also Figure 3.17

The rocks of the MP16 Microfacies show the wackestone texture under the microscope. The total abundance of grains ranges from 41-46%, with an average of 42%, while the matrix ranges from 54-59%, with an average of 58%. The major component of the planktonic foraminifera is the genus *Rotalipora*, which ranges from 30-35% in abundance, with an average of 33%. The *Praeglobotruncana*, *Heterohelix*, and *Dicarinella*, represent minor portions of the planktonic foraminifera in decreasing order.

Paleoenvironment: Planktonic foraminifera-rich microfacies deposit in the outer ramp setting (Flügel, 2004); therefore similar environment of deposition is suggested for the MP 16 Microfacies.

3.2.1.17 Organic-rich peloidal packstone MP 17 Microfacies, see also Figure 3.18

These rocks are observed as black laminated shales/limestones at out crop. The rocks of the MP17 Microfacies are rich in peloids, the relative abundance of which ranges from 12-40%, with an average of 28%, while the fine grained well sorted silty quartz ranges from 1-5% with an average of 3%. The matrix is mixed micrite and clay. Due to the plastic nature of the clayey matrix the peloids are stretched due the overburden pressure. The calcareous algae represent a minute fraction of the rock, below 1%. Fine dolomite rhombs make up less than 1% of the total rock. This microfacies is enriched in organic matter. The bulk of the organic matter is in situ, while fine grained oxidised detrital organic matter, scattered throughout the microfacies is also recorded. Microbial mats are also present. Peloids deposited in the organic rich mudstone often in association with microbial mats have two origins. They are either formed as fecal pellets of organisms which digested the organic matter from the ingested mud and secrete these pellets as the non digestible fraction, or they are

formed by the biochemical precipitation within the microbial mats (e.g. Flügel, 2004).

Paleoenvironment: Organic- and peloidal rich packstone to wackstones associated with algal organic matter, and dolomite represent deposition in the intertidal setting (Flügel, 2004), hence MP 17 Microfacies was deposited in the intertidal setting.

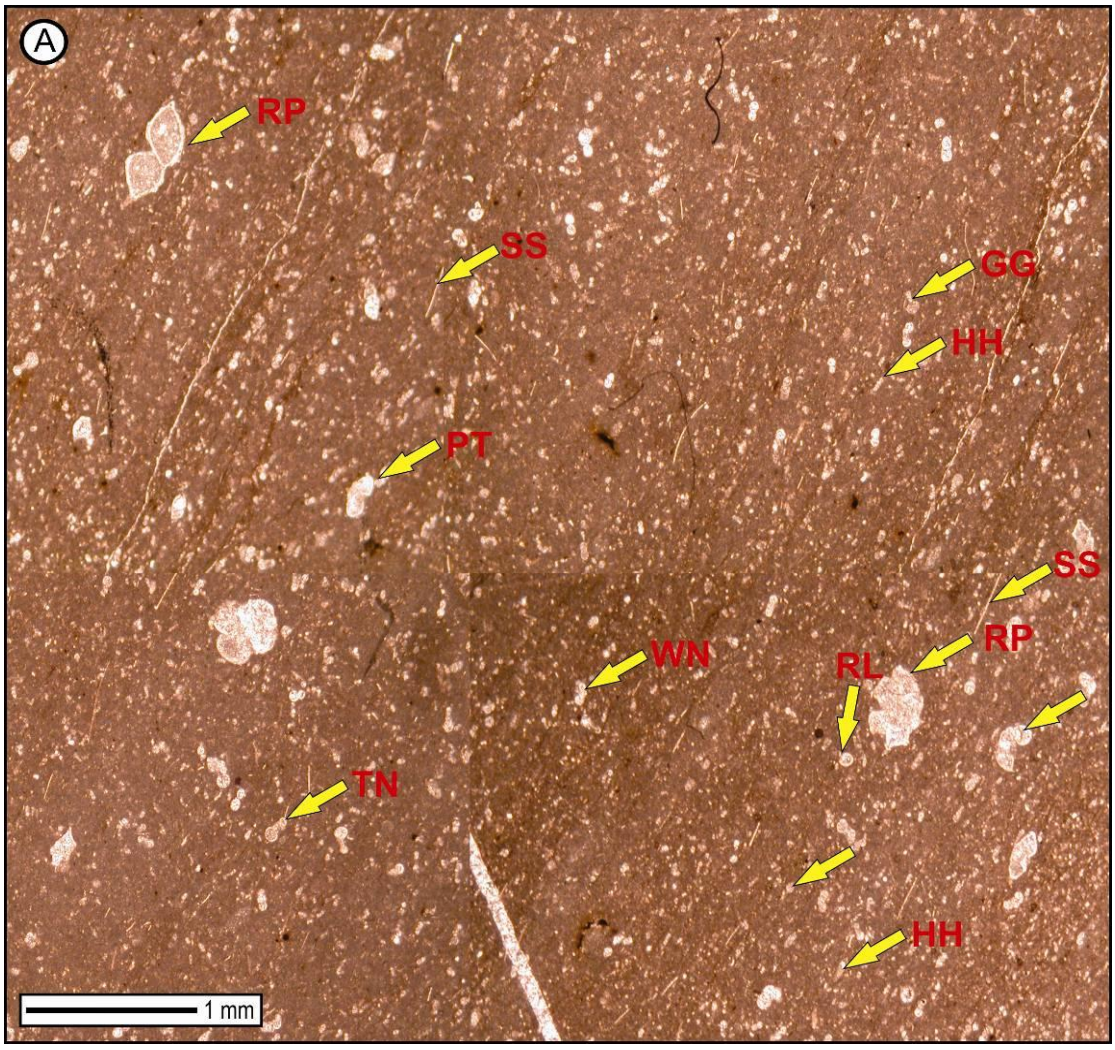

Figure 3.16: ***Mixed foraminifera-sponges wacke- (MP 15):*** **The smaller foraminifer of this microfacies includes *Globigerinelloides* (**GG **in A), *Heterohelix* (**HH **in A), and *Ticinella* (**TL **in A), *Whiteinella* (**WN **in A) while the larger planktonic foraminifera includes keeled *Rotalipora* (**RL **in A). The monoaxon sponge spicules are present throughout in microfacies.**

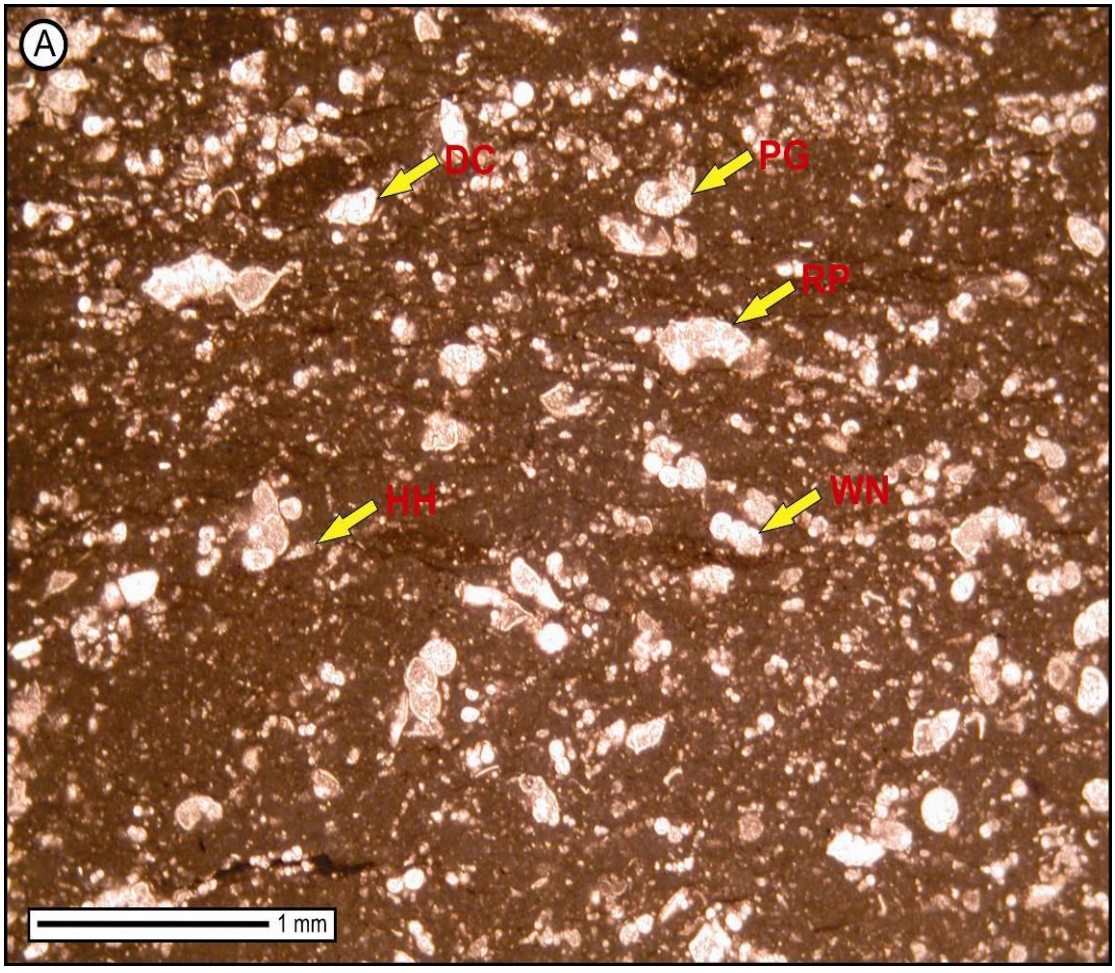

Figure 3.17: ***Rotalipora wackestone (MP 16):*** **This microfacies is rich in deep dwelling** ***Rotalipora*** **(**RP **in A), it also contains** ***Dicarinella*** **(**DC **in A),** ***Whiteinella*** **(**WN **in A),** ***Praeglobotruncana*** **(**PG **in A), and** ***Heterohelix*** **(**HH **in A).**

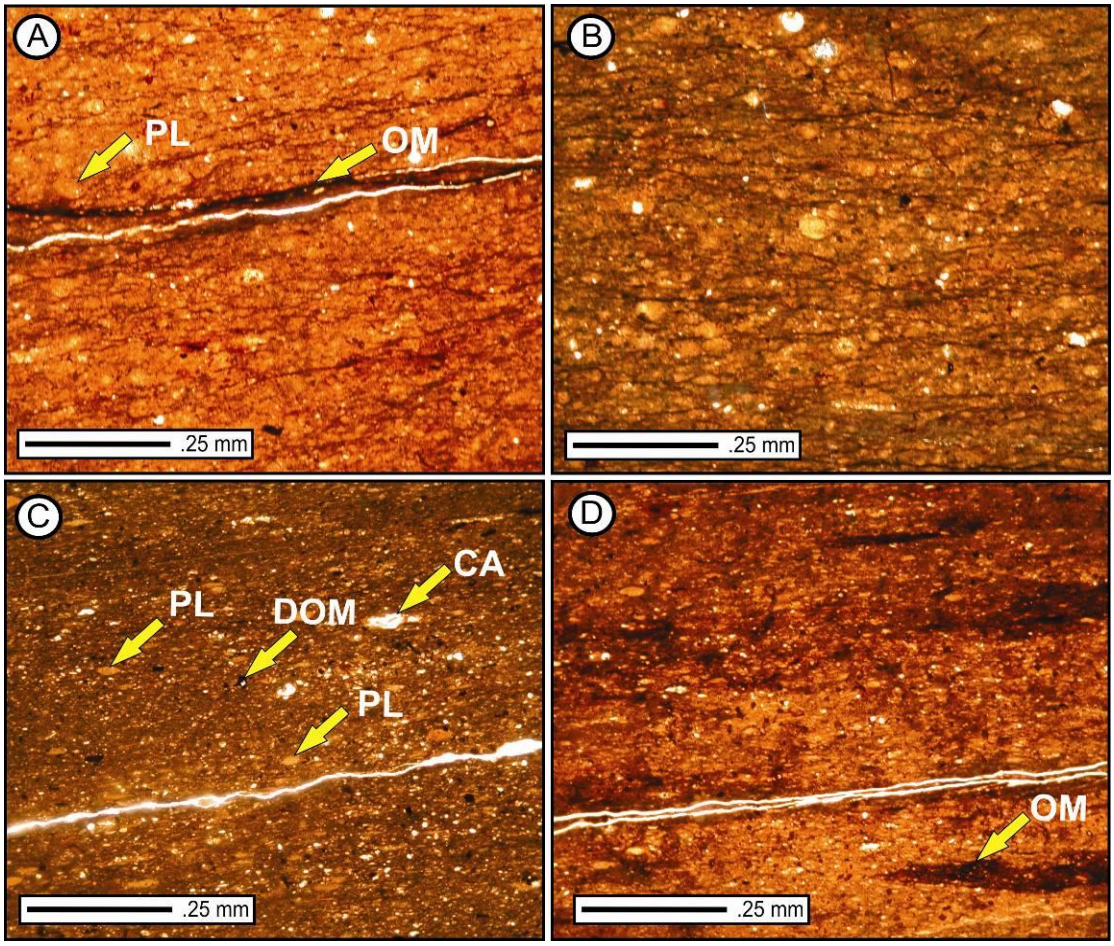

Figure 3.18: ***Organic-rich peloidal packstone (MP 17):*** **Rounded to stretched Peloids (**PL **in A, and C) are the dominant framework components of this microfacies. The Organic Matter is overall abundant which gives brownish to reddish colour to the microfacies but it is much concentrated at places (**OM **in A, C). Detrital Organic Matter (**DOM **in C) is also scattered. Rare Calcareous Algae (**CA **in C) are present.**

3.2.1.18 Organic-rich mudstone MP 18 Microfacies, see also Figure 3.19

These rocks are observed as black laminated shales/limestones at out crop. The rocks of the MP 18 Microfacies comprise finely laminated mudstone with abundant organic matter. The scattered peloids are stretched along the lamination planes. Rare calcareous algae and charophytes are present.

Paleoenvironment: The mudstone texture, fine laminations, lack of normal marine fauna, presence of rare calcareous algae and charophytes would indicate the quiet water lagoon environment of deposition within the inner ramp (e.g. Flügel, 2004). Therefore lagoonal environment of deposition is suggested for the MP 18 Microfacies.

3.2.1.19 Interlaminated silt- to mudstone MP 19 Microfacies, see also Figure 3.20

These rocks are observed as black laminated shales/limestones at out crop. The rocks of the MP19 Microfacies show interlaminated pack- to mudstone textures. The thin sections show alternating lighter coloured quartz-rich silty layers with dark organic-rich mudstone layers. On average, the small sized, well sorted, rounded to silty quartz ranges in abundance from 20% in the silty to 2% in the organic-rich mudstone layers. The in situ organic matter is abundant while the detrital organic matter is comparatively less in abundance and is scattered throughout the microfacies. Dolomite abundance ranges from 0-3% with an average of 2%. Pyritisation is minor to extensive in this microfacies.

Paleoenvironment: The mudstones to siltstone couplets, along with dolomite are common in the peritidal to muddy lagoon setting (Flügel, 2004); therefore similar environment of deposition is suggested for the MP 19 Microfacies.

3.2.1.20 Organic-rich fenestral mudstone MP 20 Microfacies, see also Figure 3.21

These rocks are observed as black laminated shales/limestones at out crop. The rocks of the MP 20 Microfacies show the mudstone texture, including rip up dark mud clasts. This mudstone is non-laminated and massive. The irregular fenestrae are present. Such irregular fenestrae are the result of either desiccation, or gas bubbles. These can also be formed as evaporative moulds, or replacement of grains such as evaporates (Flügel, 2004). The rip-up clasts are elongated and are elliptical in shape and occur in different sizes. Such clasts are formed due to the storm waves, which in turn were generated during the subsequent sea level rise, eroding the underlying intertidal to supratidal sediments.

Paleoenvironment: The organic-rich fenestral mudstones represent deposition in the intertidal setting (Flügel, 2004; Lehmann et al. 1998). Based on similar features intertidal environment of deposition is suggested for the MP 20 Microfacies.

3.2.1.21 Heterohelix, Marginotruncana, Whiteinella wacke- to mudstone MP 21 Microfacies, see also Figure 3. 22

The MP 21 Microfacies ranges from wacke- to mudstone in texture in thin section. The relative abundance of grains ranges from 3-31%, with an average of 20%, while

the micrite abundance ranges from 69-97%, with an average of 80%. Amongst the planktonic foraminifera *Heterohelix* abundance ranges from 1-12% with an average of 9%, while *Marginotruncana* makes up 4%, *Whiteinella* 3%, *Dicarinella* 2%, *Globigerinelloides* 2%, and *Helvetoglobotruncana helvetica* less than 1% on average, respectively. The calcareous algae, calcispheres, molluscs, and sponges have abundances less than 1% each.

Paleoenvironment: The planktonic foraminifera- rich microfacies indicates deposition in the outer ramp setting (Flügel, 2004); hence MP 21 Microfacies was deposited in the outer ramp.

3.2.1.22 Mixed silliciclastic-foraminiferal wackestone MP 22 Microfacies, see also Fig. 3.23

The MP 22 Microfacies shows the wackestone texture under the microscope. The relative abundance of grains ranges from 26-28%, with an average of 23%, while the micrite ranges from 72-74%, with an average of 73%. Amongst these grains moderately sorted, angular to sub-angular quartz represents 5% of the total rock. The genus *Globotruncana* presents 8% of the total rock, while *Heterohelix* is 3% and *Globigerinelloides* is 2%, respectively. The echinoderms represent 4% of the total rock while calcispheres and molluscs are each below 2%. Amorphous organic matter is distributed uniformly throughout this microfacies.

Paleoenvironment: The abundant planktonic foraminifera indicate deposition in the outer ramp environment (Flügel, 2004). The influx of silliciclastic would represent enhanced continental weathering. MP 22 Microfacies was therefore deposited in the outer ramp with significant siliciclastic input.

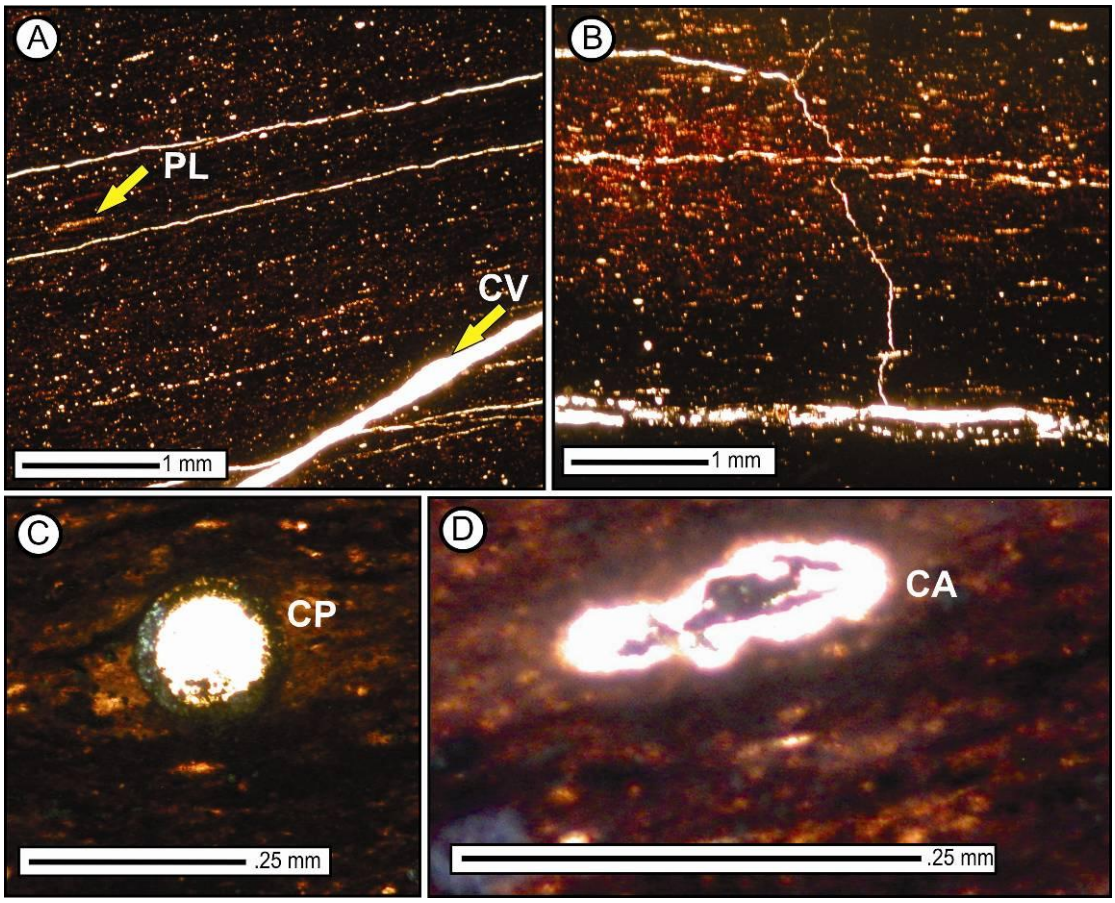

Figure 3.19: ***Organic-rich Mudstone (MP 18):*** **Thinly laminated organic-rich mudstone show thin stretched peloids (**PL **in A), rare Charophytes (**CP **in C), and Calcareous Algae (**CA **in D).**

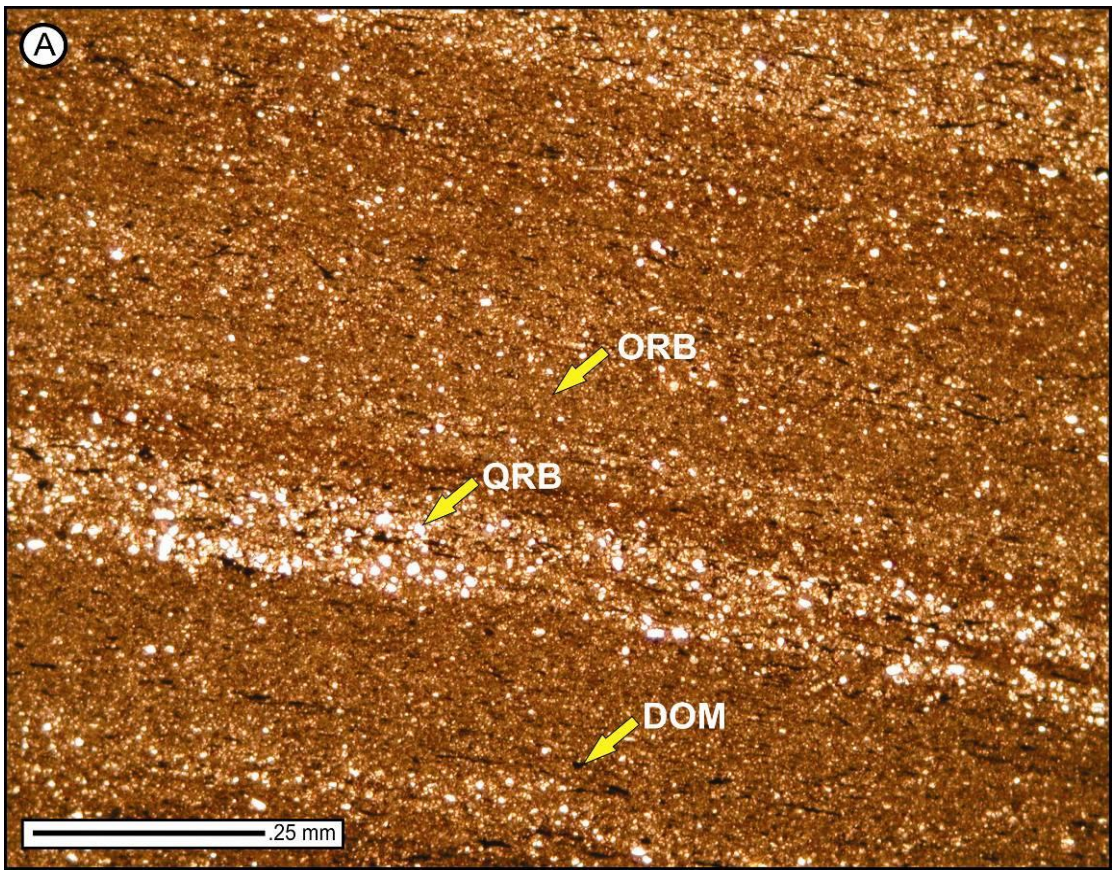

Figure 3.20: ***Interlaminated silt- to mudstone (MP 19):*** **This microfacies shows Quartz rich bands (**QRB **in A) of siltstone and Organic Rich Band (**ORB **in A) of mudstone. The in situ organic matter is dominantly present in association with Detrital Organic Matter (**DOM **in A)**

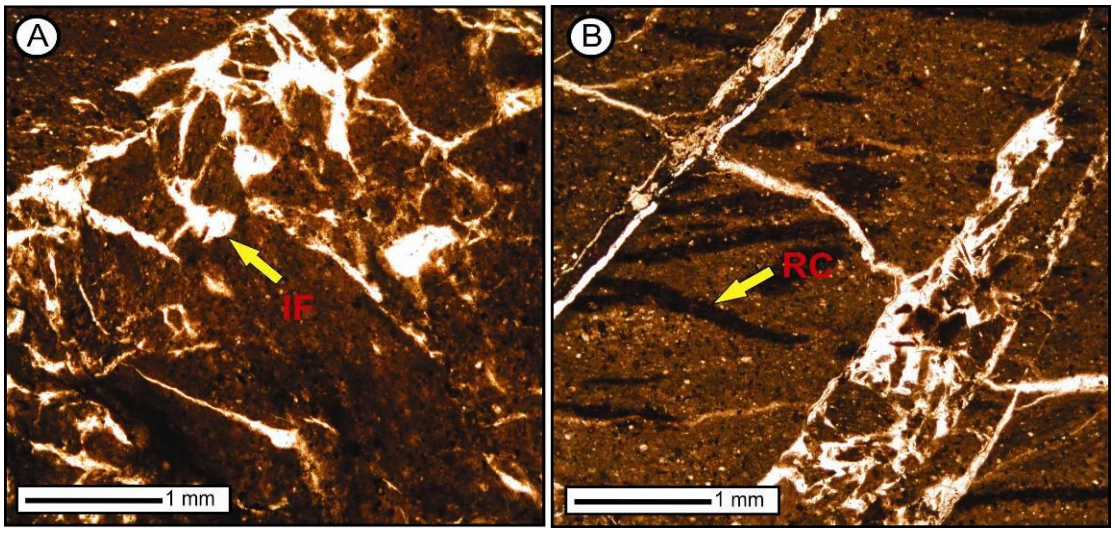

Figure 3.21: ***Organic rich fenestral mudstone (MP 20):*** **The irregular fenestrae (**IF **in A) are extensive in association with Rip up Clasts (**RC **in B) of organic rich mudstone.**

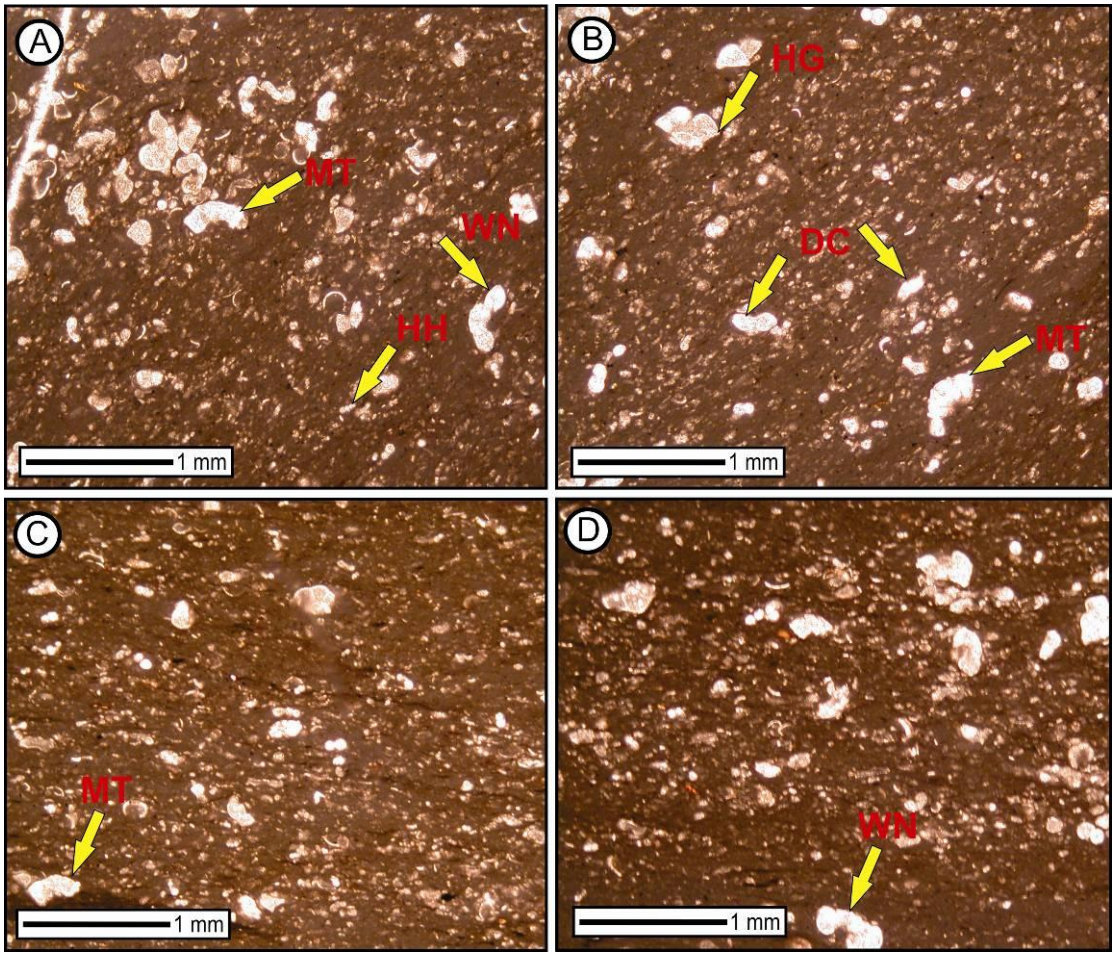

Figure 3.22: ***Heterohelix, Marginotruncana, Whiteinella wacke- to mudstone (MP 21):*** **The dominant component of this microfacies is** ***Heterohelix*** **(**HH **in A),** ***Marginotruncana*** **(**MT **in A, B, and C), and** ***Whiteinella*** **(**WN **in D). Minor** ***Dicarinella*** **(**DC **in B) and** ***Helvetoglobotruncana*** **(**HG **in B) are also present.**

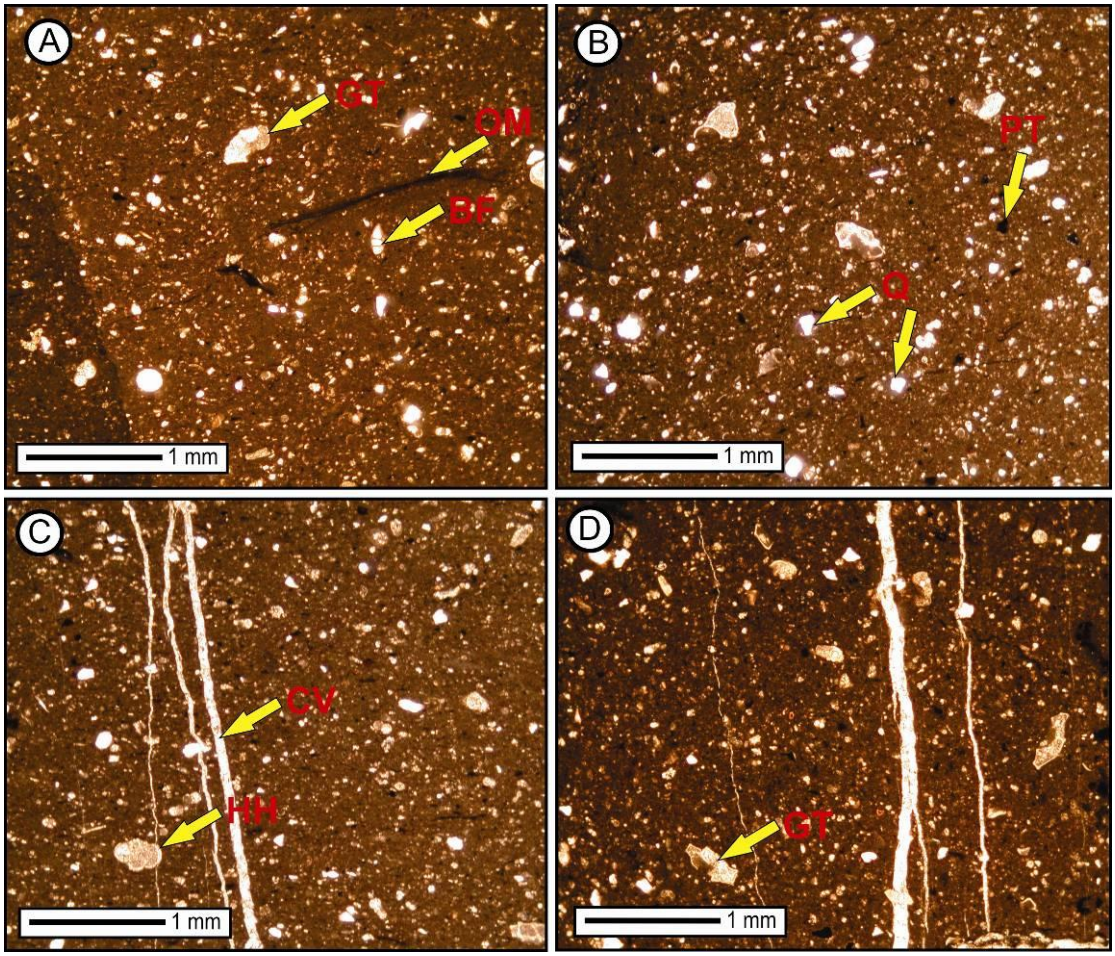

Figure 3.23: ***Mixed siliciclastic foraminiferal wackestone (MP 22):*** **This microfacies show angular to sub angular quartz (**Q **in B). The dominant planktonic foraminiferal species of these rocks is of *Globotruncana* (**GT **in A, D), *Heterohelix* (**HH **in C). It also have minor benthic foraminifera (**BF **in A), Pyritisation (**PT **in B) is present. The amorphous organic matter is present throughout the microfacies which give the reddish colour to it, although reworked oxidised Organic Matter (**OM **in A) is also observed.**

3.2.1.23 Heterohelix-Globotruncana wackestone MP 23 Microfacies, see also Figure 3.24

In thin section, the texture of the MP 23 Microfacies is wackestone. The total abundance of grains ranges from 23-45%, with an average of 38%, while the micrite abundance ranges from 55-77%, with an average of 62 %. Amongst the grains the *Globotruncana* abundance ranges from 5-15%, with an average of 11%, while the *Heterohelix* abundance ranges from 10-20%, with an average of 15% of the total rock. Sponges represent 4% of the total sediment, while molluscs, *Globigerinelloides*, calcispheres, echinoderms, and ostracodes represent a minor part of the microfacies in a decreasing order.

Paleoenvironment: Flügel (2004) stated that the keeled *Globotruncana* in association with *Heterohelix* indicates the open marine deep shelf environment which is equivalent to the outer ramp setting; hence MP 23 Microfacies was deposited in the outer ramp.

3.2.1.24 Globotruncana-Heterohelix wackestone MP 24 Microfacies, see also Figure 3.25

The MP 24 Microfacies comprises the wackestone texture. The relative abundance of allochems ranges from 35-52%, with an average of 44%, while the total micrite ranges from 48 to 65%, with an average of 56%. The *Globotruncana* is the dominant genus of the planktonic foraminifera, which ranges from 20-30% in abundance, with an average of 27%, while the *Heterohelix* ranges from 6-15% with an average of 10%. Molluscs and calcispheres, echinoderms, and *Globigerinelloides* represent a very minor component of the total rock in decreasing order, and their abundances are all below 2%.

Paleoenvironment: This microfacies has been deposited in the outer ramp setting (see Paleoenvironment of MP 23 Microfacies).

3.2.1.25 Quartz wacke MP 25 Microfacies, see also Figures 3.26-3.27

On the outcrop scale this facies is composed of thin bedded sandstone/conglomerate which incorporates widely scattered carbonate angular clasts. In thin section, this microfacies is composed of 50% medium to coarse quartz grains. The carbonate lithics makes 8% of the rock, while the other 42% is ferruginous clay in the matrix.

Paleoenvironment: The poor sorting of the whole rock coupled with presence of the carbonate grains and rare crinoidal plates represent deposition in shallow marine environment most probably in inner to middle ramp settings. This poorly sorted sandstone/conglomerate is most likely deposited as a slump of clastic deltaic sediments, in the middle/outer ramp settings. The carbonate angular clasts seen at outcrop scale indicate syndepositional tectonic activity within the basin. It is therefore concluded that these poorly sorted sands with floating brecciated carbonate clasts represent tectonically induced turbidites, derived from locally activated

structures within the basin. The turbiditic nature of these sediments is also confirmed by scouring of the underlying pelagic sediments (fig. 3.27).

3.2.2 Sea Level Changes

The purpose of constructing the sea level curve is to analyse the effect of sea level on the depositional sequences of the Parh Formation, particularly on the organic rich intervals. Generally the eustatic sea level changes are thought to be driven by tectonic and climate over varied time scale, while the global climate is in turn controlled by the Milankovitch cycles (Catuneanu, 2006). The local tectonics of the basin margin also influences the relative sea level changes, which in turn affect the sedimentary sequences of a particular basin.

The sea level curve constructed from the microfacies of the Parh Formation (see figs. 3.29-3.33) suggests that the sediments of the formation were deposited in outer ramp to deep basin environments. The pelagic nature of the Parh Formation makes it very useful for understanding the Cretaceous palaeoenvironmental changes preserved in this formation. It is interesting to note that drastic sea level falls are observed along two organic intervals at 308-309m and 376-384m respectively. Along these intervals the outer ramp microfacies are replaced by the tidal flats facies. Such drastic sea level changes can only be explained by the local tectonic imposed on the basin margin. The tidal flats are connected to the main land; hence the sediments of tidal flat settings are prone to meteoric diagenesis. Such diagenesis has the potential to destroy the primary isotopic signals; hence care will be taken in interpreting the isotopic signals along these two intervals in succeeding chapters.

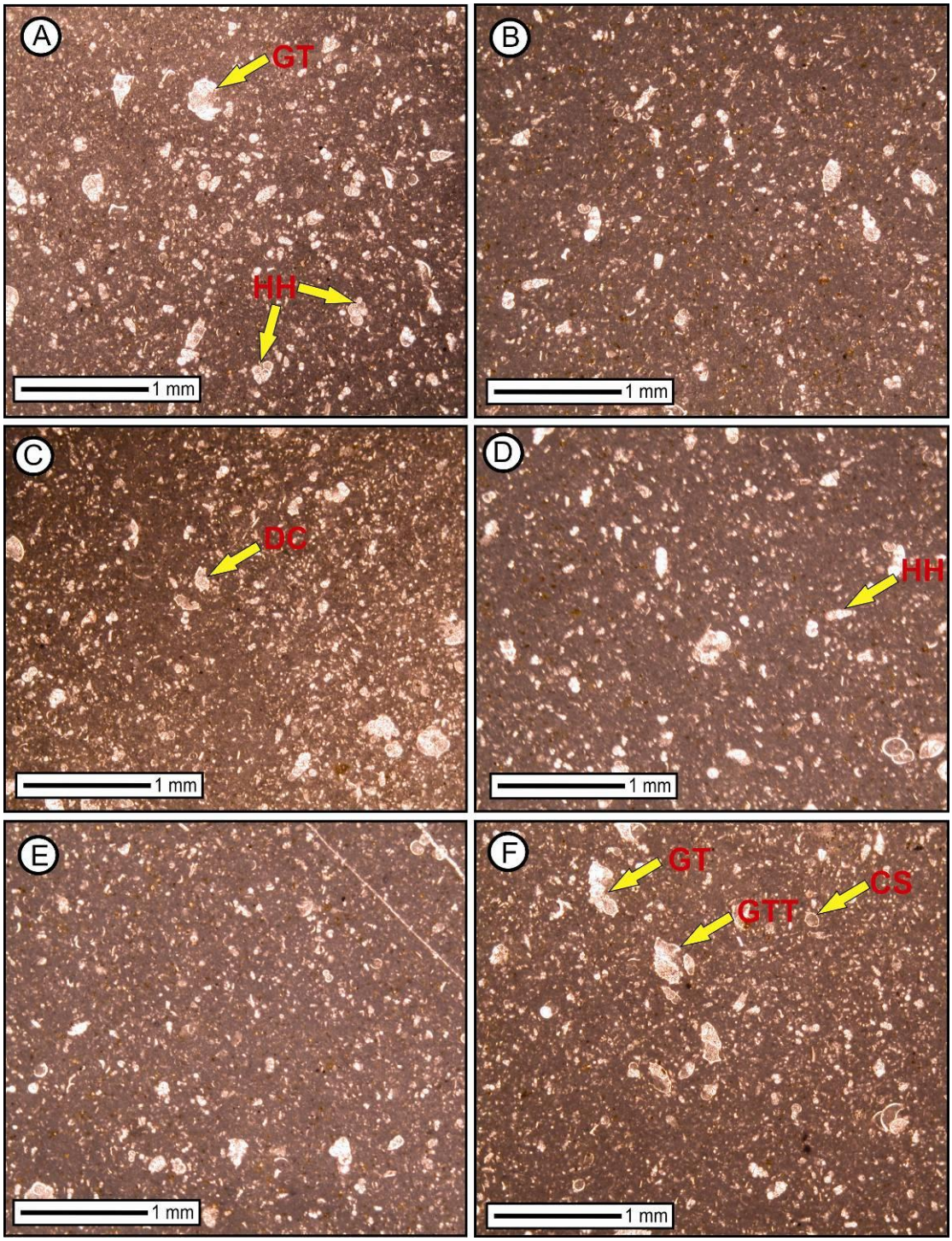

Figure 3.24: ***Heterohelix-Globotruncana wackestone (MP 23):*** **This microfacies have abundant** ***Heterohelix*** **(**HH **in A and D),** ***Globotruncana*** **(**GT **in A and F). Minor** ***Dicarinella*** **(**DC **in C),** ***Globotruncanita*** **(**GTT **in F), and Calcispheres (**CS **in F) are also seen.**

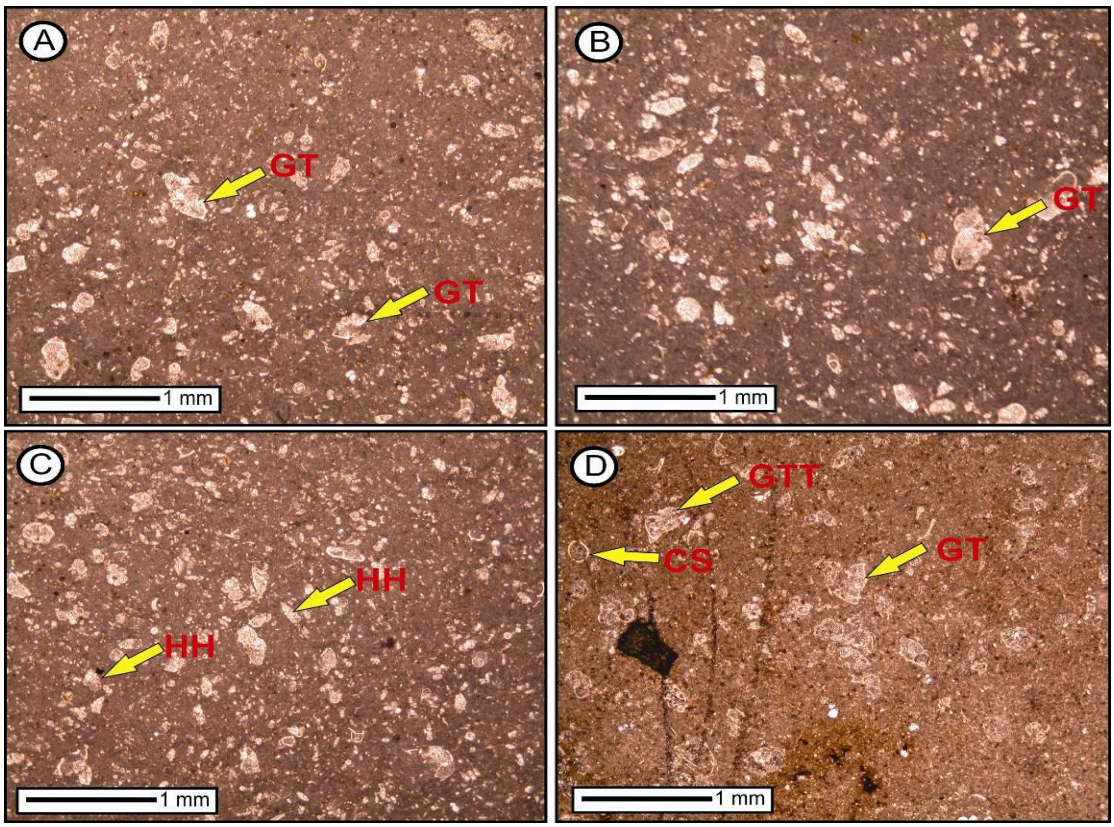

Figure 3.25: ***Globotruncana-Heterohelix wackestone (MP 24):*** **The** ***Globotruncana*** **(**GT **in A, B, and D) is the dominant builder of this microfacies. Second in abundance is** ***Heterohelix*** **(**HH **in C),** ***Globotruncanita*** **(**GTT **in D) and Calcispheres (**CS **in D) is also present.**

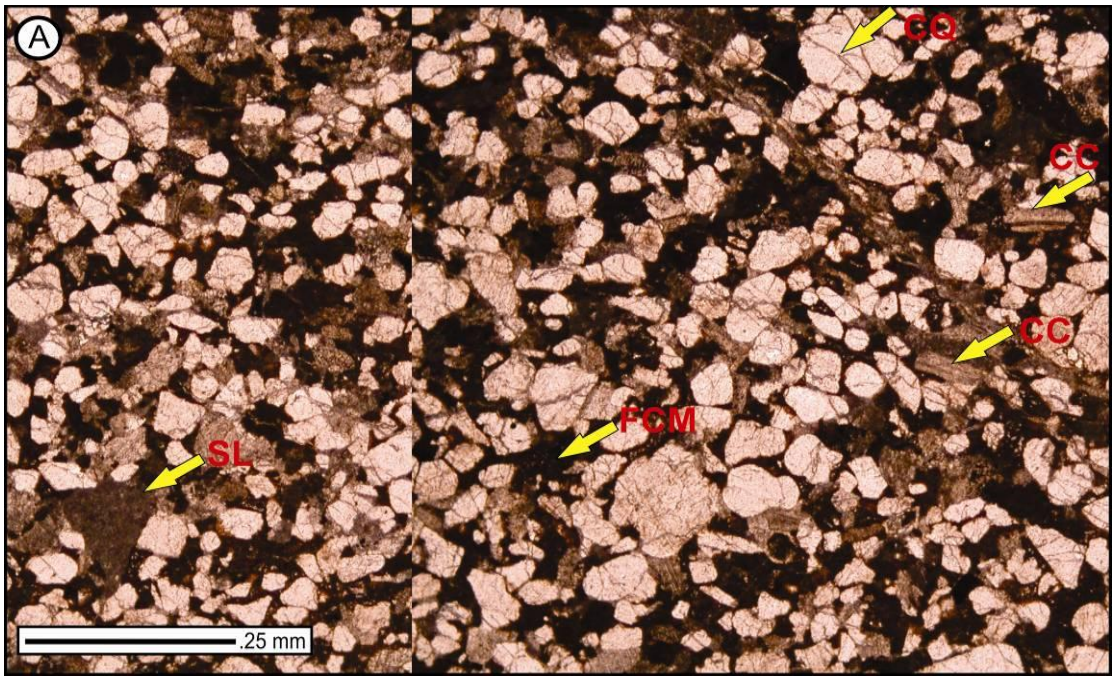

Figure 3.26: ***Quartz-Wacke (MP25):*** **The microfacies have angular to rounded Cracked Quartz (CQ), scattered angular Carbonate Clasts (**CC**), and rare Shale Lithics (**SL**); the Ferruginous Clay Matrix (**FCM**) is supporting all the grain types.**

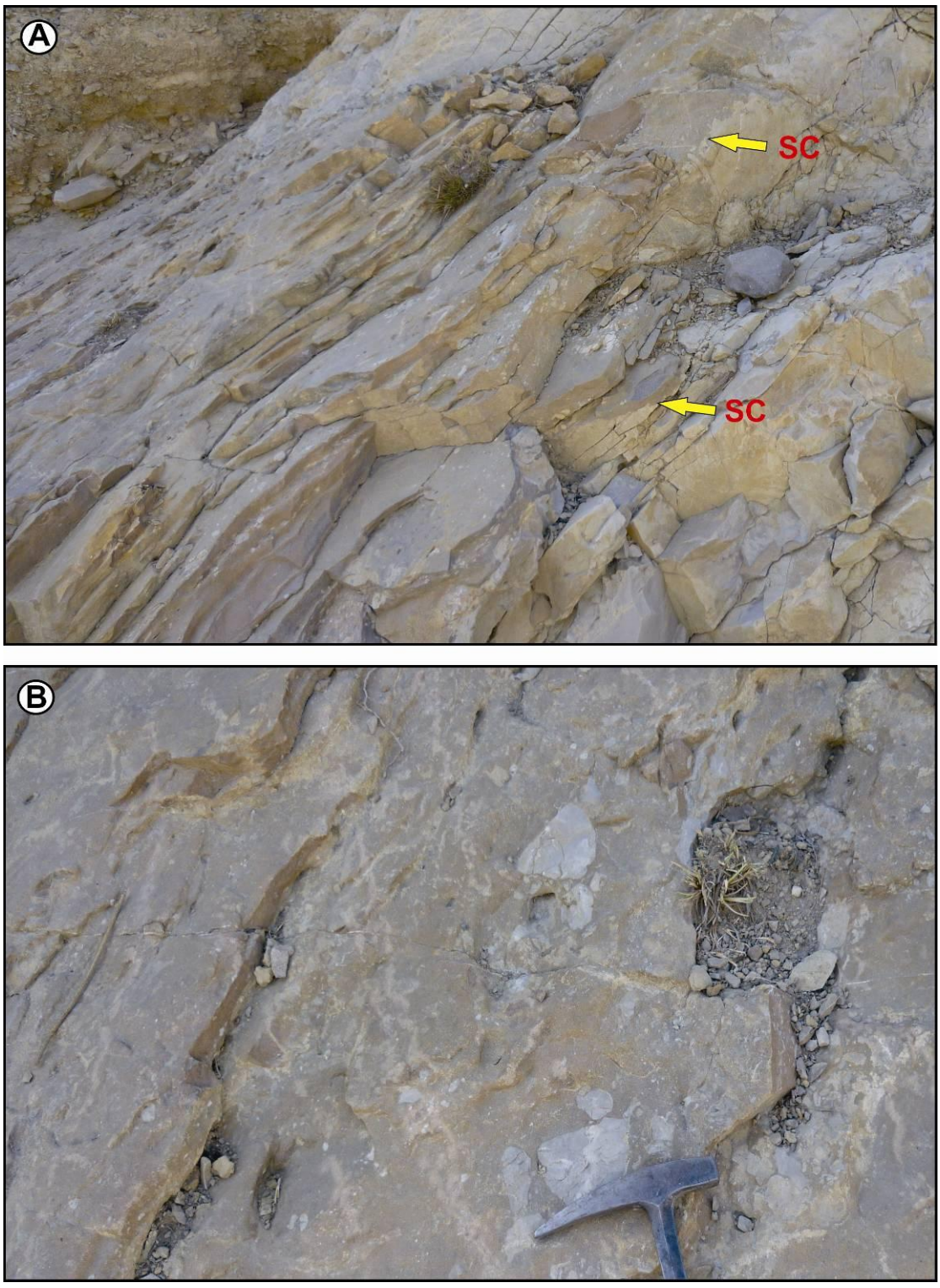

Figure 3.27: Plate showing the outcrop scale features of (Quartz-Wacke microfacies, MP25); A. Scored contact between the underlying pelagic sediments and overlying sandy deposits of MP25; B. Angular syntectonic carbonate clasts in the sandy matrix.

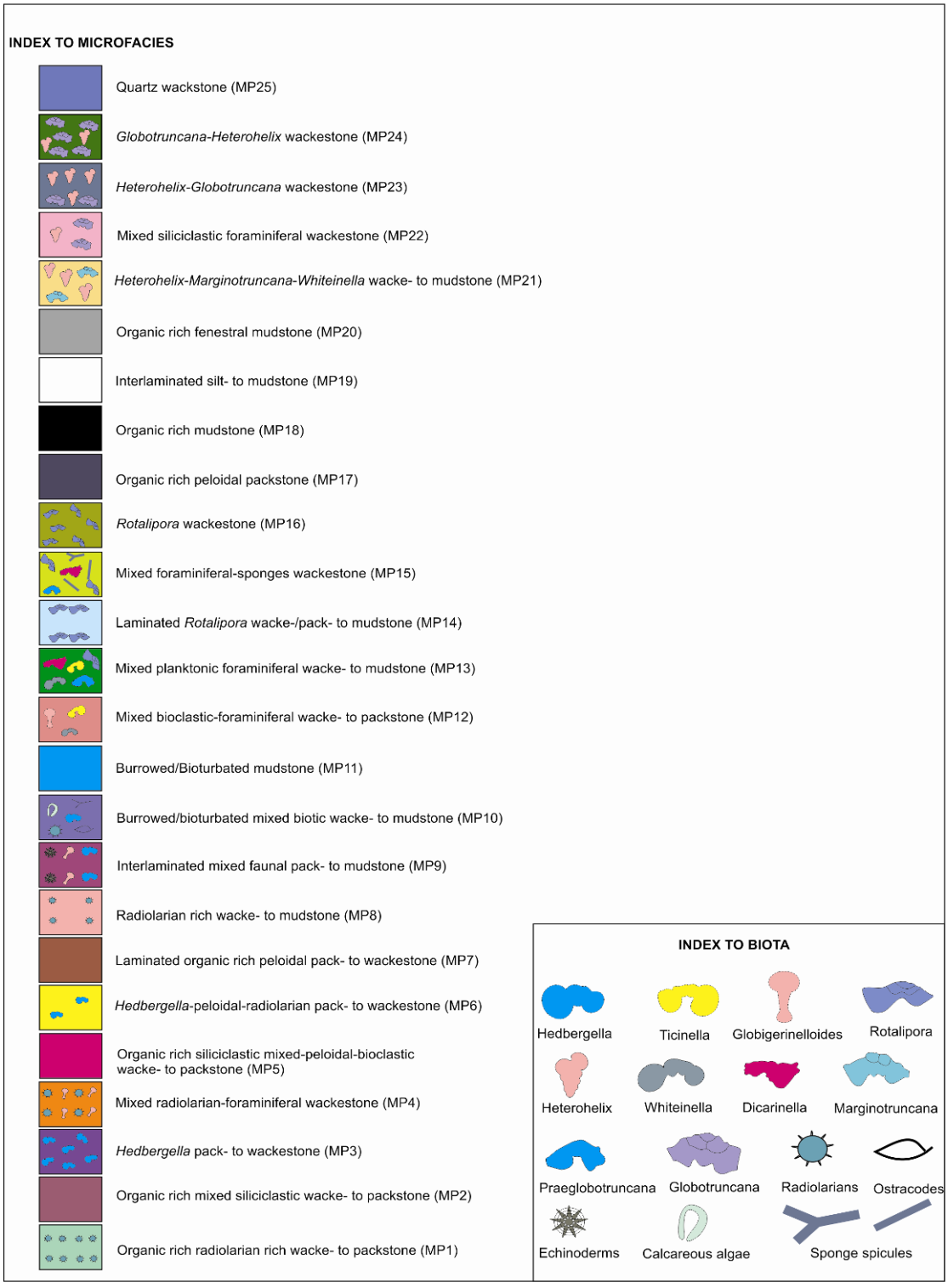

Figure 3.28: An index to the biota and microfacies types

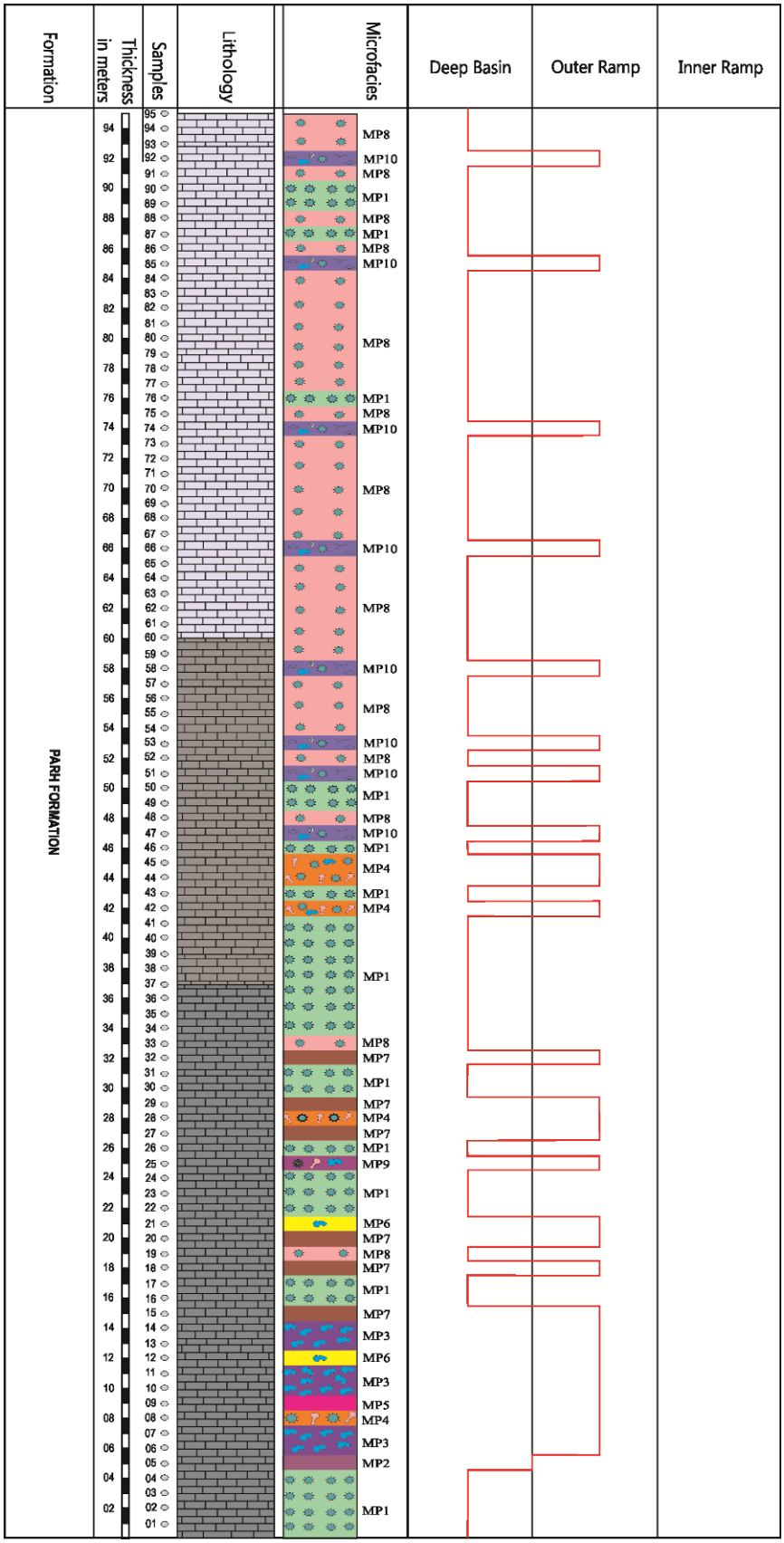

Figure 3.29: Chart showing the distribution of microfacies types in the Parh Formation.

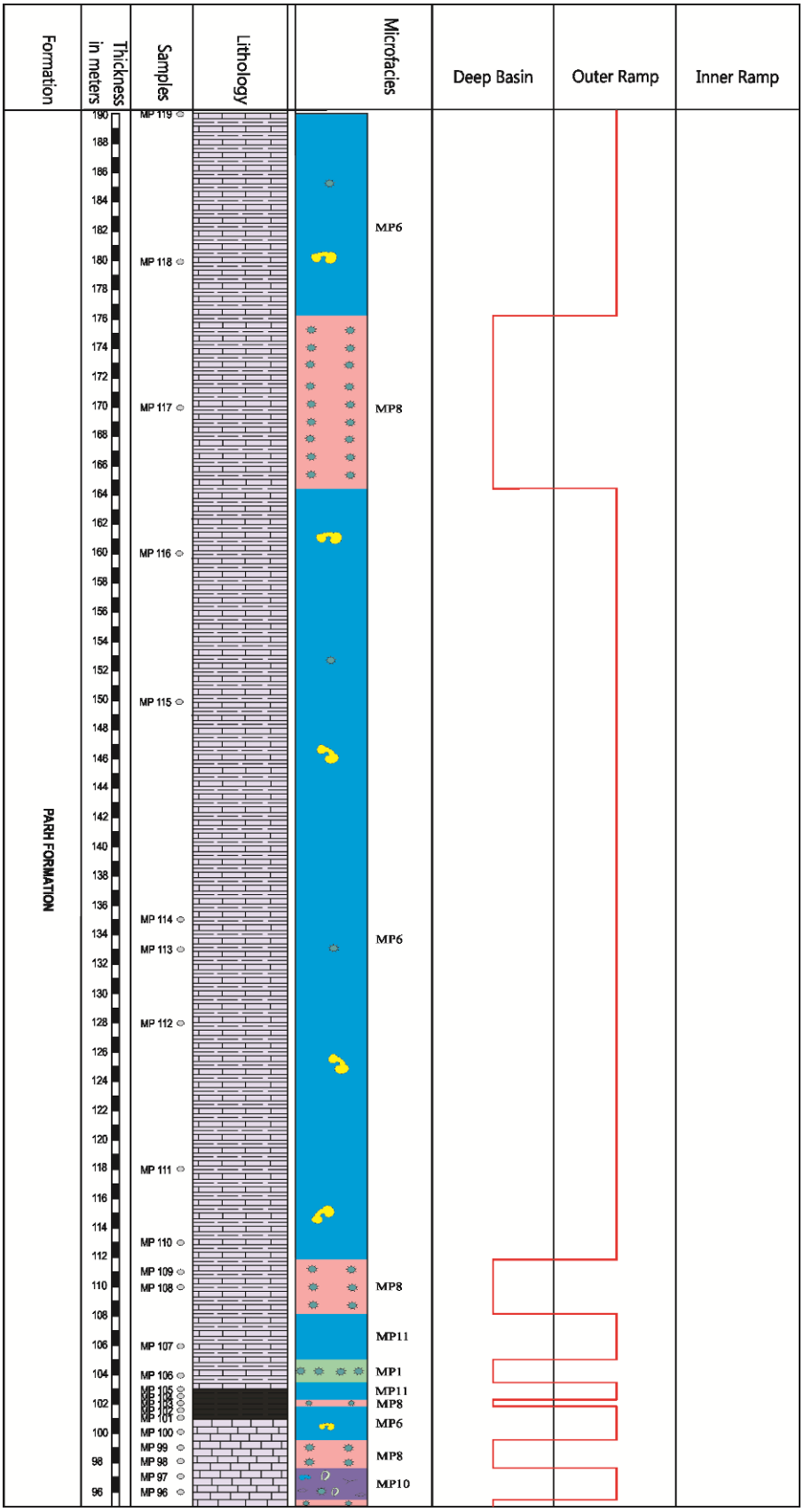

Figure 3.30: Chart showing the distribution of microfacies types in the Parh Formation.

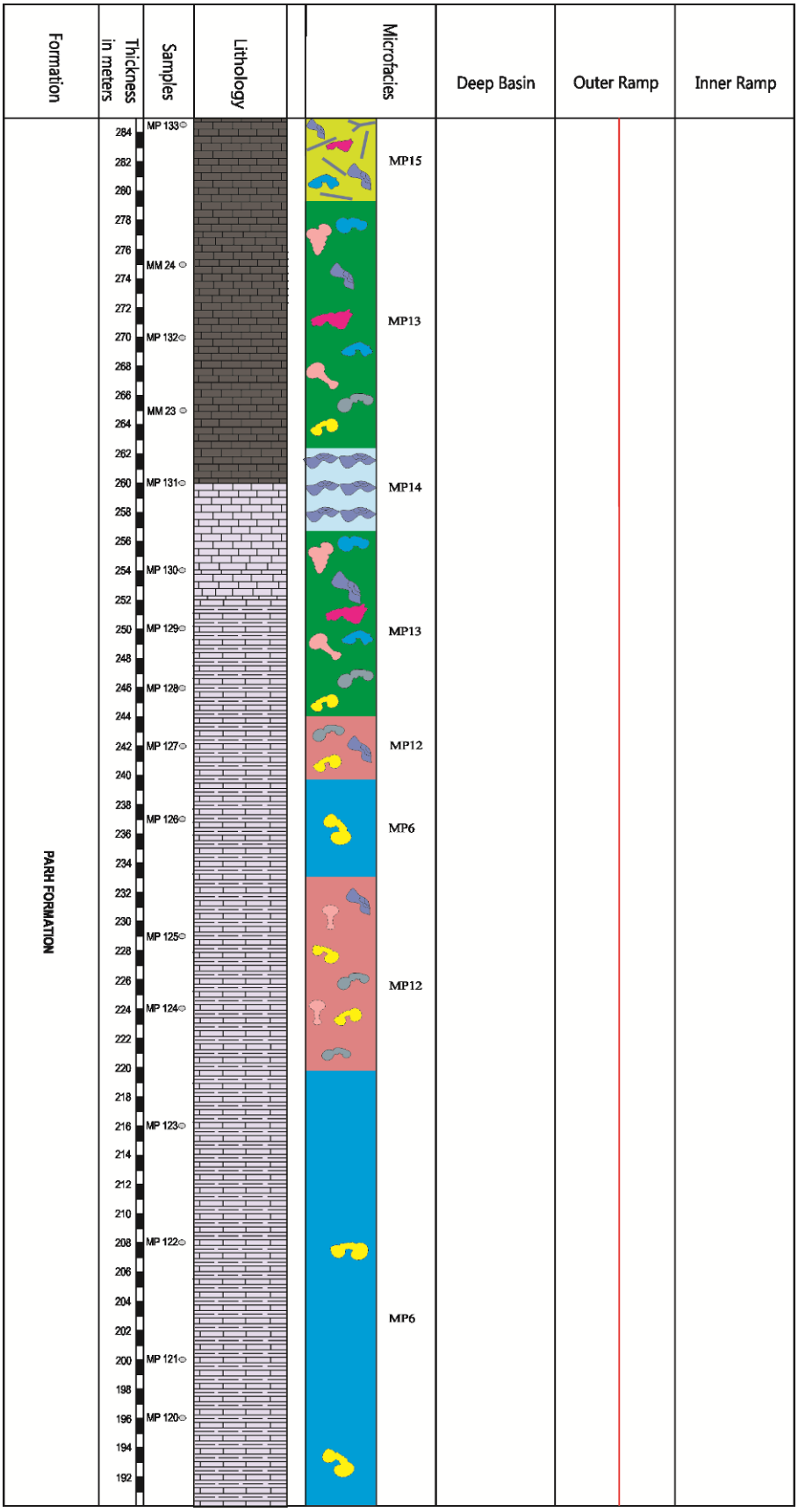

Figure 3.31: Chart showing the distribution of microfacies types in the Parh Formation.

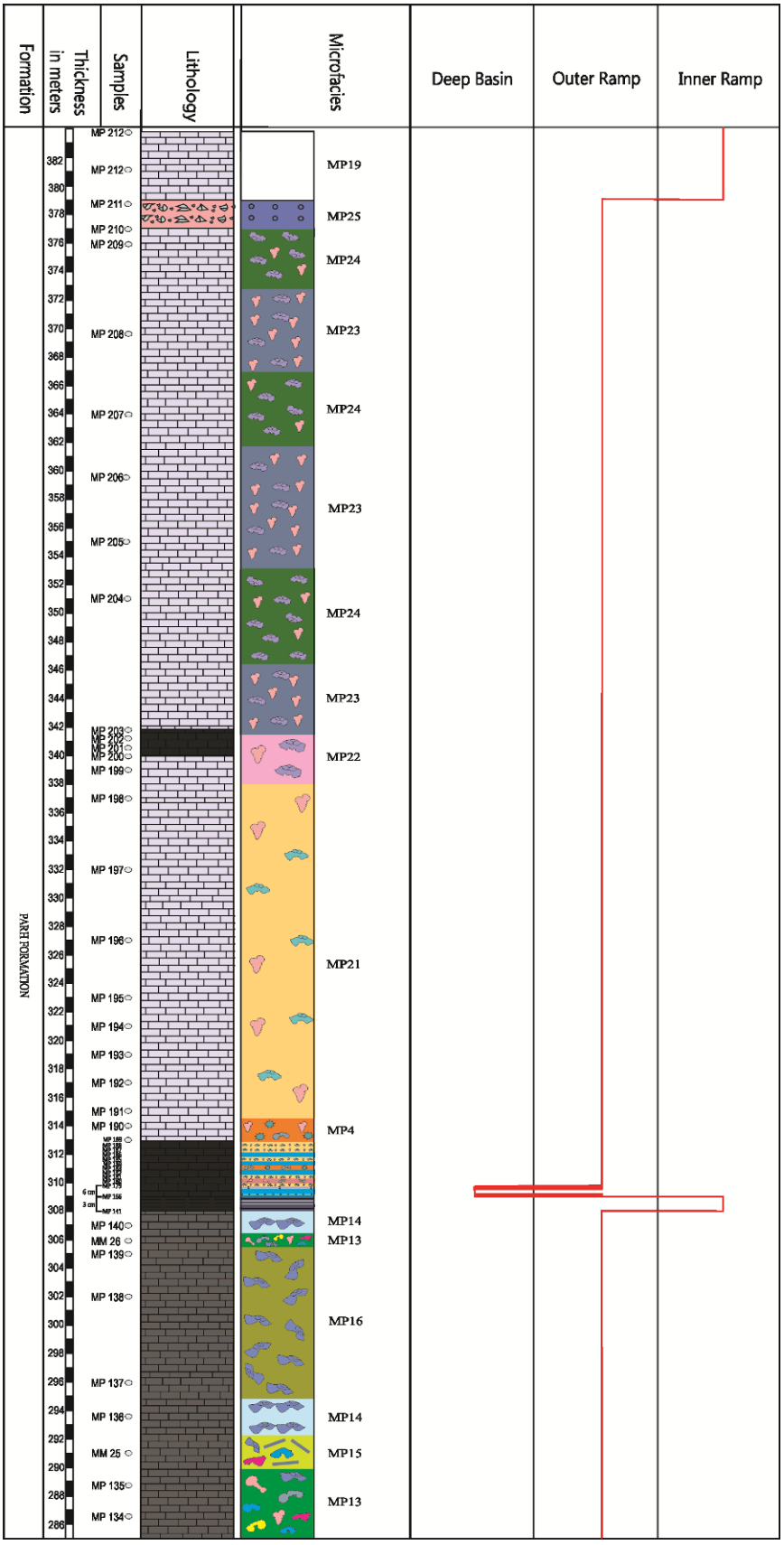

Figure 3.32: Chart showing the distribution of microfacies types in the Parh Formation.

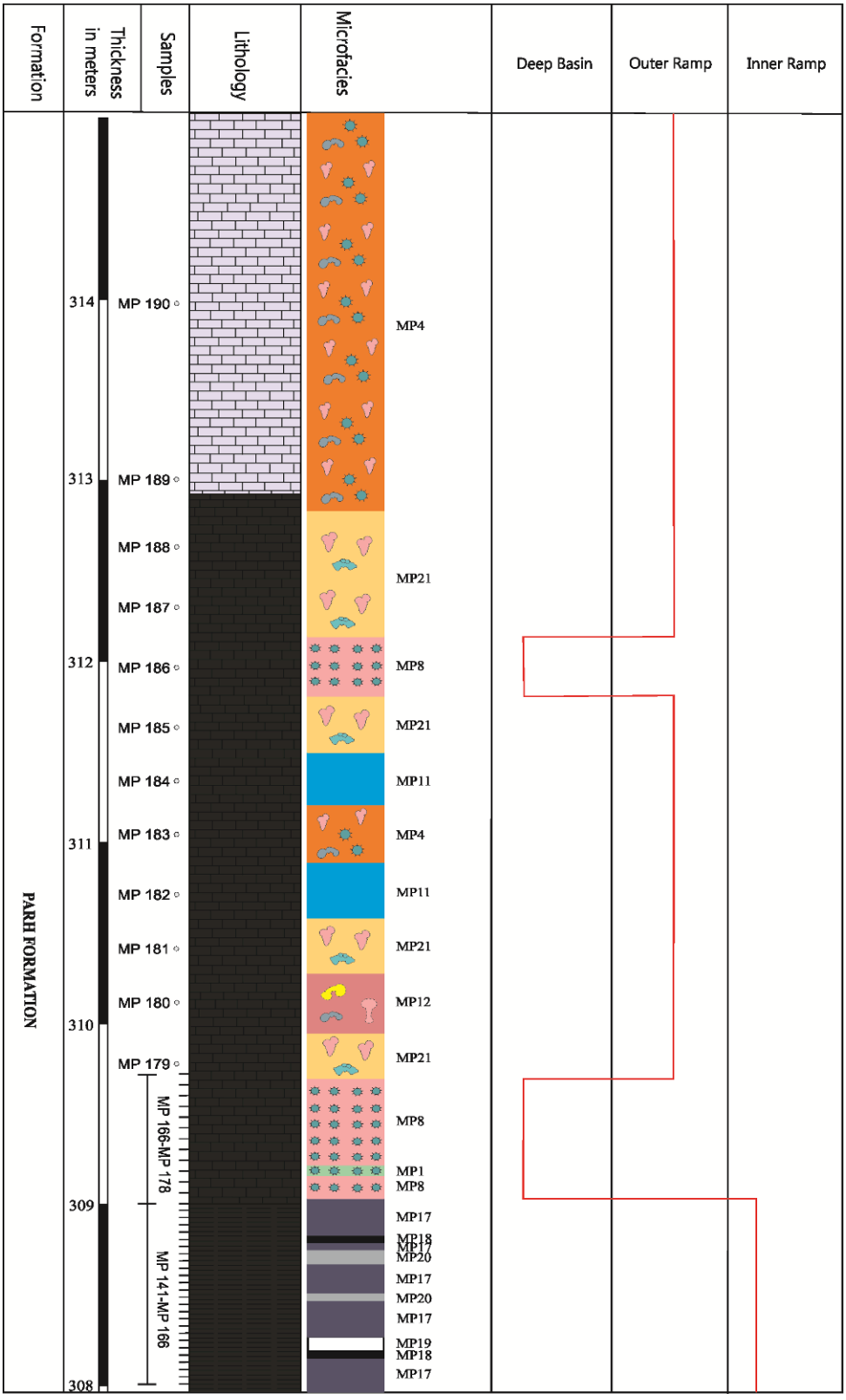

Figure 3.33: Chart showing the distribution of microfacies types in the 308-315 stratigraphic interval of the Parh Formation.

3.2.3 Microfacies parameters

In order to better understand the depositional history of the Parh Formation with emphasis on the OAE intervals, important microfacies parameters such as organic matter, pyrite, clastic input, tempestites, burrows (bioturbation) are recorded (fig. 3.35).

3.2.3.1 Organic matter and Pyrite (Fig. 3.35)

Both the high abundances of organic matter and pyrite represent anoxic water conditions, i.e. these intervals may represent the OAEs. Such organic rich intervals are recorded in the Parh Formation e.g. the lowermost interval (base of the section up to 32m) contains abundant organic matter. The next interval with abundant presence of organic matter along with minor occurrence of pyrite occurs at 44-45m. Upward the interval with abundant organic matter along with minor to moderate presence of pyrite occurs at 101-103m (see Microfacies MP6 & MP11). The moderate amounts of organic matter and pyrite are recorded at 244-274m along with the moderate presence of the pyrite (see Microfacies MP13 & MP14). Upwards, black shales/limestone in the interval 308-309m occurs with high abundance of organic matter and pyrite (see Microfacies MP17-MP20). The next organic rich interval is recorded at 340-342m with moderate to abundant amounts of pyrite (see Microfacies, MP22), while the uppermost interval, 379-384m, with abundant organic matter and pyrite is recorded in the Parh Formation (see Microfacies MP19).

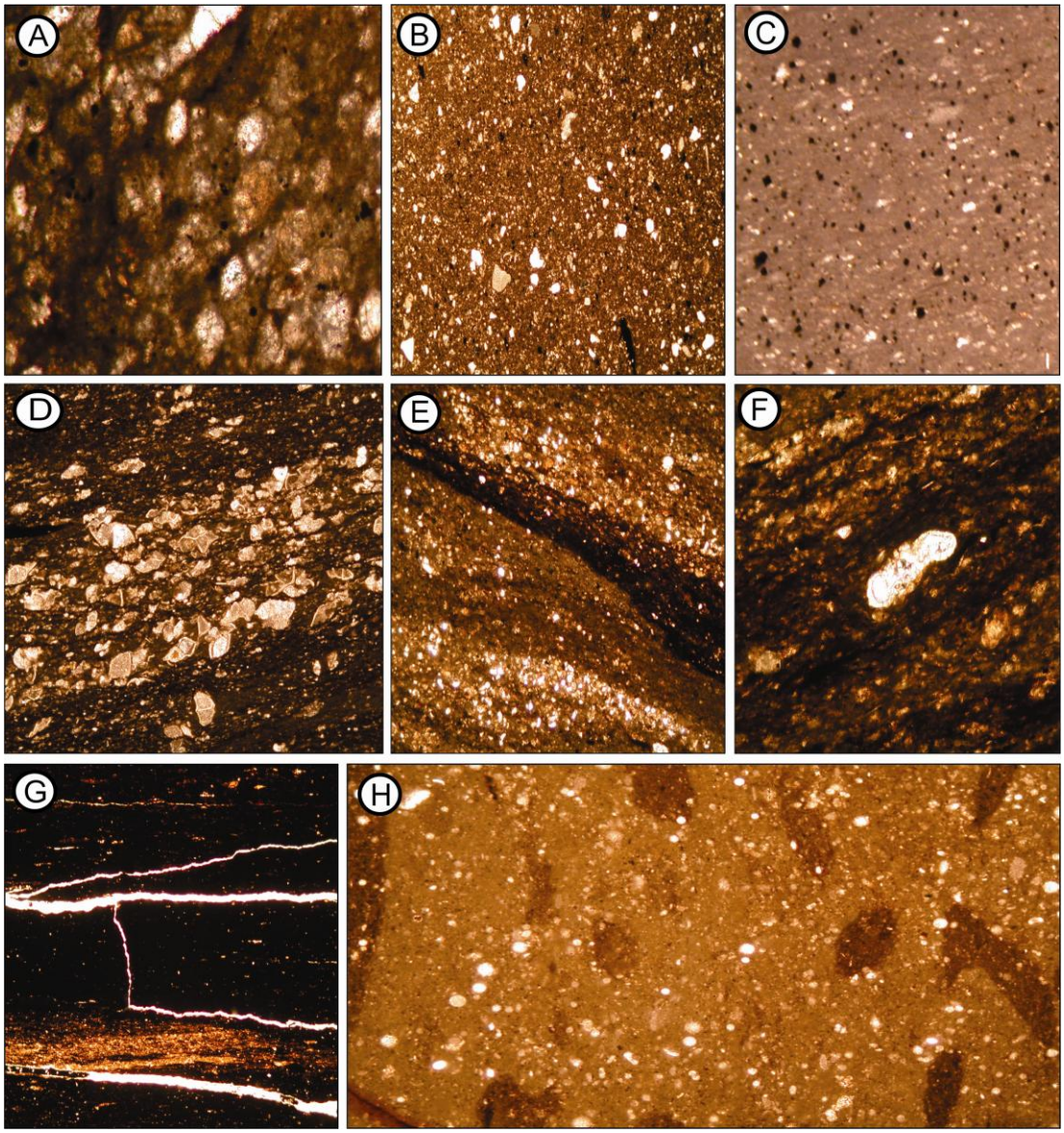

Figure 3.34: An index to the various microfacies parameters of the Parh Formation; A. Minor pyrite, B. Moderate pyrite, C. Abundant pyrite; D and E. Presence of Tempestites, while E also show minor organic matter; F. moderate organic matter; G. Abundant organic matter; H. presence of burrows.

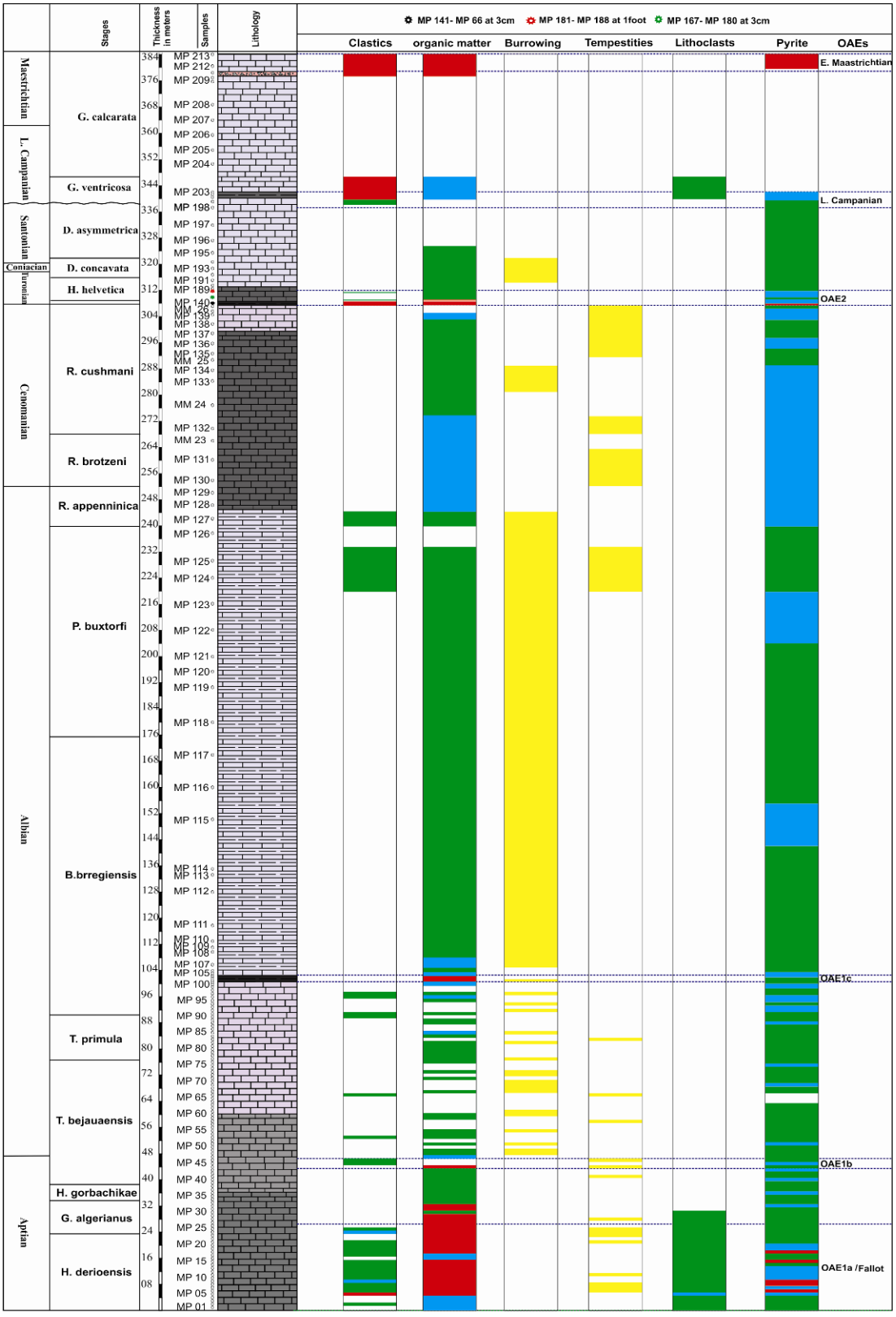

Figure 3.35: Showing the various microfacies parameters of the Parh Formation. The green colour represents minor presence; blue colour represents moderate presence, and the red colour represents abundant presence of the key elements. The yellow colour represents just the presence of tempestites and burrowing.

3.2.3.2 Clastics (Fig. 3.35)

The distribution pattern of the percentage of clastics is given in figure 3.35. It is of interest to note that periodic occurrences of moderate to abundant detrital quartz input occurred in the organic rich interval (base of the section to 25m), (see Microfacies MP2 & MP 5). Abundant detrital angular quartz is also recorded along the organic rich intervals at 308-309m, 340-342m, and 379-384m (fig. 3.35, see Microfacies MP19 & MP22). Therefore, increased clastic input mainly occurred during the early parts of the organic rich intervals. Such clastic input can be explained by increased run-off from the nearby continent during the deposition of these intervals.

3.2.3.3 Tempestites (Fig. 3.35)

In the Parh Formation tempestites occur periodically from the base of the section to 80m, and within the 220-308m interval. (fig. 3.35, see also Microfacies MP9 & MP 14). The periodic occurrence of the tempestites suggests storms within these intervals.

3.2.3.4 Burrowing (Fig. 3.35)

Burrowing activity is prominent in the 108-244m, 282-288m, and 313-322m intervals (fig. 3.35). In places, there is an enrichment of organic streaks along the margins of the burrows and inside (see Microfacies MP 10 & MP 11). This enrichment is caused by the concentration of the organic matter by the infilling of the depressed topographic features by organic rain from above. The abundance of burrows indicates oxygenated bottom water conditions. It is interesting to note that there is no burrowing activity in the organic rich intervals as a result of the anoxic conditions (see fig. 3.35).

3.3 Discussion

For details on the previous biostratigraphic ages of the Parh Formation see Chapter 2.The organic rich horizons within the Parh Formation are related to the organic rich intervals, which are found globally in the Cretaceous, and represent Oceanic Anoxic Events (OAEs, Schlanger and Jenkyns, 1976). Such OAEs have resulted in sharp

sedimentological and biotic changes in various Cretaceous sections (Föllmi, 2012 and Leckie et al., 2002).

The aim of this chapter is to look for such sedimentological and biotic changes along the organic rich horizons in the Parh Formation. The documentation of similar sedimentological and biotic changes from the Parh Formation will strengthen the idea that the organic rich intervals within the Parh Formation are the equivalents of the global OAEs.

The micofacies details of the Parh Formation indicate that the sediments of this formation are pelagic in nature and deposited on the outer ramp to deep basinal settings. Overall the pelagic nature of the Parh Formation makes it more appropriate for paloenvironmental studies because the open marine water are more stable in term of physical, chemical and biological processes. Therefore only severe environmental change can significantly affect the sedimentology, biota, and chemistry of the open marine environment. However significant sea level falls have been observed at some stratigraphic intervals (e.g. 308-309m and 379-384m see fig. 3.32) within the Parh Formation. Such sharp sea level changes could only be explained by the regional sea level fall due to tectonic uplifting.

The radiolarian-rich microfacies are dominant from the base of the section to 190m stratigraphic height. (see figs. 3.29-3.30). Generally the radiolarians are common in the eutrophic oceans with high primary productivity (Erbacher et al., 1996). The periodic occurrences of the radiolarians rich microfacies during this stratigraphic interval might have been controlled by the repeated eutrophication of oceans caused by the Milankovitch cycles.

The OAEs have resulted in the deposition of anomalous organic matter in short time span elsewhere (Schlanger and Jenkyns 1976; Scholle and Arthur; 1980; Coccioni et al., 1987 and Bréhéret, 1985). Therefore the organic rich intervals (0-32m, 44-45m, 101-103m, 308-309m, 340-342m, and 379-384m) within the Parh Formation may corresponds to such OAEs. The increased hydrological cycle during the OAEs may explain the reworked clastic sediments from continents to oceans (Jenkyns, 2003). It is interesting to note that the clastic input to the basin is recorded for most of the organic rich intervals of the Parh Formation (see fig. 3.35). It is also important to note that plankton crises are observed along the 101-103m, 308-309m, and 379-384m organic rich intervals. Such plankton crises are observed elsewhere, along the

OAEs of the Cretaceous (Erbacher et al., 1996 and Leckie et al, 2002). The abundance of burrows indicates oxygenated bottom water conditions. Although the burrowing activity is documented at various intervals within the Parh Formation (see fig. 3.35), it is interesting to note that there is no burrowing activity in the organic rich intervals most probably because of the anoxic bottom water conditions.

In summary, the concomitant occurrence of abundant organic matter and clastics at the same organic rich intervals, the lack of biotrubation along these organic rich intervals, and the plankton crises along some of the mentioned intervals, within the Parh Formation, suggest strongly that these organic rich intervals are the possible outcome of the OAEs. However the firm conclusions regarding the OAEs and their stratigraphic positions will be drawn after the integration of all stratigraphic information in the forthcoming chapters.

3.4 Conclusions

- The recorded microfacies MP1-MP25, coupled with the lack of reefal facies and other shallow marine facies suggest that the Parh Formation was deposited on a homoclinal ramp, mainly in the deep part of the ramp.

- The sea level curve constructed from the microfacies of the Parh Formation suggests that the sediments of the formation were deposited in outer ramp to deep basin. However it is interesting to note that drastic sea level falls are observed along organic intervals at 308-309m, and 379-384m.

- The radiolarian-rich microfacies are dominant from the base of the section to 190m stratigraphic height. The periodic occurrences of such radiolarians rich microfacies during this stratigraphic interval might have been controlled by the repeated eutrophication of oceans caused by the milankovitch cycles.

- Organic rich intervals (0-32m, 44-45m, 101-103m, 308-309m, 340-342m, and 379-384m) are recorded within the Parh Formation.

- Clastic input to the basin is recorded for most of the above organic rich intervals of the Parh Formation. Such clastic influx can be explained by the enhanced run off from the continents to the ocean basin.

- No burrowing activity is reported along the above organic rich intervals, most probably because of the anoxic bottom water conditions during the deposition of such intervals.

- Plankton crises are observed along the 101-103m, 308-309m, and 379-384m organic rich intervals. Similar plankton crises during the Cretaceous OAEs are reported by Leckie et al. (2002).

- All of the above data suggest strongly that the organic rich intervals within the Parh Formation are the result of the Cretaceous OAEs.

CHAPTER 4

3. Palynostratigraphy of the Chichali Formation

4.1 Introduction

The Chichali Formation is composed of glauconitic marine sandstone and organic-rich glauconitic marine shales. For the detailed description of the sedimentary log of the Chichali Formation, see figure 1.13 (Chapter 1). The sequence has been previously investigated using ammonites for biostratigraphy. The results were ranging from Late Oxfordian to Neocomian, however detail biozonation is still missing for the Chichali Formation (for a detailed discussion see Chapter 1). The aim of this chapter is to place the sedimentary sequence of the Chichali Formation into a reliable biostratigraphic framework based on dinoflagellates and associated spore-pollen assemblages. Furthermore the type of terrestrial vegetation will be reconstructed from the spore and pollen assemblages in the Chichali Formation. This vegetation will be used to comment on the terrestrial climate prevailing during the time of deposition of the formation. For these purposes, 14 samples were processed for palynomorphs.

4.2 Palyonostratigraphy

The use of palynomorphs in stratigraphy is called palynostratigraphy. Such palynomorphs includes dinoflagellates, spores and pollens etc. The dinoflagellates are mainly cysts producing marine protists. These cysts are preserved as fossils in sedimentary record, and are common since Late Triassic (Traverse, 2007). On the other hand a spore is the reproductive materials of fungi, plants (moss, ferns), and some bacteria. It can survive for a long period of time under unfavourable conditions. Pollen is fine to coarse powdery reproductive material produced by seed plants (gymnosperm and angiosperm), having a hard protective coat around it as a safeguard. The dinoflagellates, spores, and pollens are successfully used for stratigraphic purpose from various stratigraphic sections of Early Cretaceous, around the world (Li & Batten, 2004; Heilmann-Clausen, 1987; Helby et al., 1987). An attempt is made in this chapter to establish a reliable palynostratigraphy for the Chichali Formation.

The overall preservation of the palynomorphs in the Chichali Formation is moderate to poor. The extensive use of previous literature (Late Jurassic to Early cretaceous) from various stratigraphic sections around the world showing the illustrations of palynomorphs, proved very useful in current identification (i.e. Kotova, 1983; Riley & Fenton, 1984; Heilmann-Clausen, 1987; Helby et al., 1987; Riding & Thomas, 1988; Fensome, et al., 1991; Costa & Davey, 1992; Helby & McMinn, 1992; Fensome et al., 1993; Vijaya, 1997; Riding, et al., 1999; Schrank, 2005; Ziaja, 2006; Peyrot, et al., 2007; Traverse, 2007; Vijaya, 2009; Schrank, 2010; Lindström & Erlström 2011).

List of recorded dinoflagellates, spores, and pollens along with taxonomic notes are given in Appendix, 1. The recorded palynomorphs taxa are shown in plates 1-8. The presence/absence and range charts for the dinoflagellates are presented in figures 4.1-4.2, while the presence/absence and range charts for the spores and pollens are shown in figures 4.3-4.4.

Based on the recorded palynomorphs, two dinoflagellate and one spore-pollen biozone are introduced in this study (see figs. 4.1-4.4). The details of these biozones are given as follow.

Plate 1

Fig. 1, *Densoisporites velatus*, Sample CC 94
Fig. 2, *Densoisporites* cf. *velatus*, Sample CC 102
Fig. 3, *Densoisporites velatus*, Sample CC62
Fig. 4, *Alisporites thomasii*, Sample CC46
Fig. 5, *Alisporites* sp. Sample CC62
Fig. 6, *Arcuatipollenites ovatus*, Sample CC116
Fig. 7, *Podocarpidites* cf. *ellipticus*, Sample CC 105
Fig. 8, *Araucariacites australis*, Sample CC52
Fig. 9, *Araucariacites australis*, Sample CC12
Fig. 10, *Araucariacites australis*, Sample CC 102
Fig. 11, *Araucariacites australis*, Sample CC127
Fig. 12, *Araucariacites australis*, Sample CC12
Fig. 13, *Aratrisporites parvispinosus*, Sample CC 62
Fig. 14, *Inaperturopollenites* sp. Sample 46
Fig. 15, *Inaperturopollenites* sp. Sample, CC 12
Fig. 16, *Inaperturopollenites* sp. Sample CC12
Fig. 17, Trilete spore, Sample CC 46
Fig. 18, *Alisporites grandis*, Sample, CC 76
Fig. 19, *Ischyosporites punctatus*, Sample, CC 34
Fig. 20, *Concavisporites toralis*, Sample, CC 46
Fig. 21, *Classopollis triangulus*, Sample CC 94
Fig. 22, *Classopollis* sp. Sample, CC 76
Fig. 23, *Classopollis classoides*, Sample CC46
Fig. 24, *Concavisporites toralis*, Sample, CC 52
Fig. 25, Tetrad of *Classopollis* sp. Sample, LM 2
Fig. 26, *Concavisporites* sp. Sample, CC 52
Fig. 27, *Concavisporites* sp. Sample, CC 52
Fig. 28, C*oncavissimisporites variverrucatus*, Sample CC 46
Fig. 29, C*oncavissimisporites* sp. Sample, CC 12
Fig. 30, *Classopollis* sp. Sample, CC 12
Fig. 31, *Choanopollenites* sp. Sample CC 12

Note: Scale bar represent 31µm for all figures

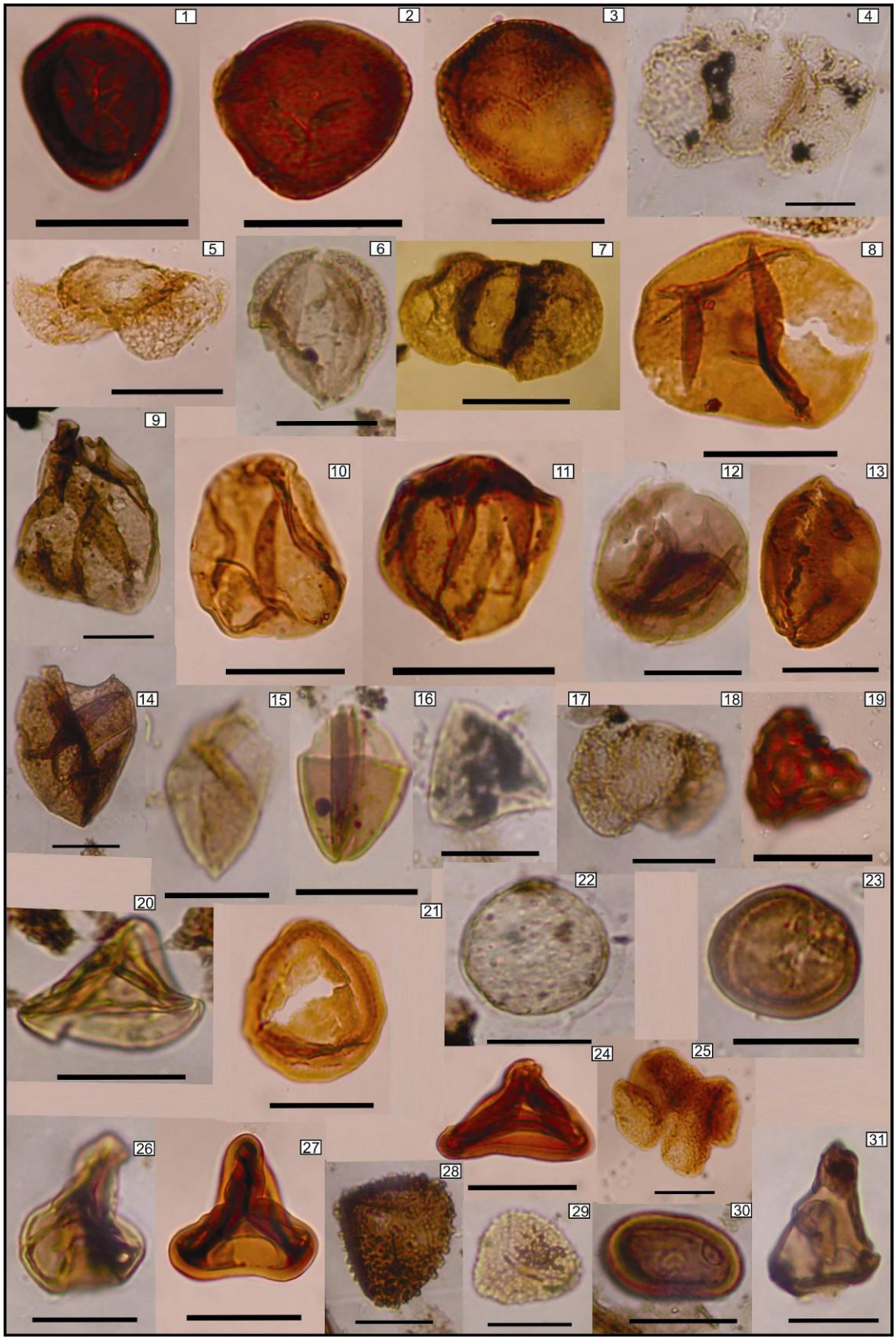
1
2
3
4
5
6
7
8
9
10
11
12
13
14
15
16
17
18
19
20
21
22
23
24
25
26
27
28
29
30
31

Plate 1

Plate 2

Fig. 1, *Cicatricosisporites* sp. Sample, CC 52
Fig. 2, *Cicatricosisporites* sp. Sample, CC 94
Figs. 3, 4, *Cicatricosisporites australiensis*, Sample, CC 46
Fig. 5, *Cicatricosisporites* sp. Sample, CC 62
Fig. 6, *Contignisporites* cf. *glebulentus*, Sample CC127
Fig. 7, *Cicatricosisporites* sp. Sample, CC 52
Fig. 8, *Cicatricosisporites* sp. Sample, CC 46
Fig. 9, *Cicatricosisporites hughesii*, Sample, CC 62
Fig. 10, *Cicatricosisporites* cf. *hughesii*, Sample, CC 62
Fig. 11, *Callialasporites* sp. Sample CC46
Fig. 12 *Callialasporites dampieri*, Sample, CC 12
Fig. 13, *Callialasporites dampieri*, Sample, CC 46
Fig. 14, *Callialasporites dampieri*, Sample, CC 102
Fig. 15, *Callialasporites dampieri*, Sample, CC 12
Fig. 16, *Callialasporites dampieri*, Sample, CC127
Fig. 17, *Callialasporites dampieri*, Sample, CC127
Fig. 18, *Callialasporites dampieri*, Sample, CC 102
Fig. 19, *Callialasporites dampieri-trilobatus*, Sample, CC 52
Fig. 20, *Callialasporites trilobatus*, Sample CC 12
Fig. 21, *Callialasporites trilobatus*, Sample
Fig. 22, *Callialasporites trilobatus*, Sample, CC 52
Fig. 23, *Callialasporites trilobatus*, Sample, CC 34
Fig. 24, *Callialasporites trilobatus*, Sample, C 94
Fig. 25, *Callialasporites turbatus*, Sample, CC 12
Fig. 26, *Callialasporites turbatus*, Sample CC 52
Fig. 27, *Callialasporites segmentatus*, Sample CC 94
Fig. 28, *Contignisporites multimuratus*, Sample, CC 34
Fig. 29, *Contignisporites fornicatus*, Sample, CC 34
Fig. 30, *Contignisporites* sp. Sample, CC 62
Fig. 31, *Contignisporites cooksoniae*, Sample, CC 62
Fig. 32, *Contignisporites glebulentus*, Sample, CC 34
Fig. 33, *Contignisporites* sp. Sample, CC 94
Fig. 34, *Contignisporites* sp. Sample, CC 62
Fig. 35, *Contignisporites* sp. Sample, CC 34
Fig. 36, *Contignisporites* sp. Sample, CC 62

Note: Scale bar represent 31µm for all figures.

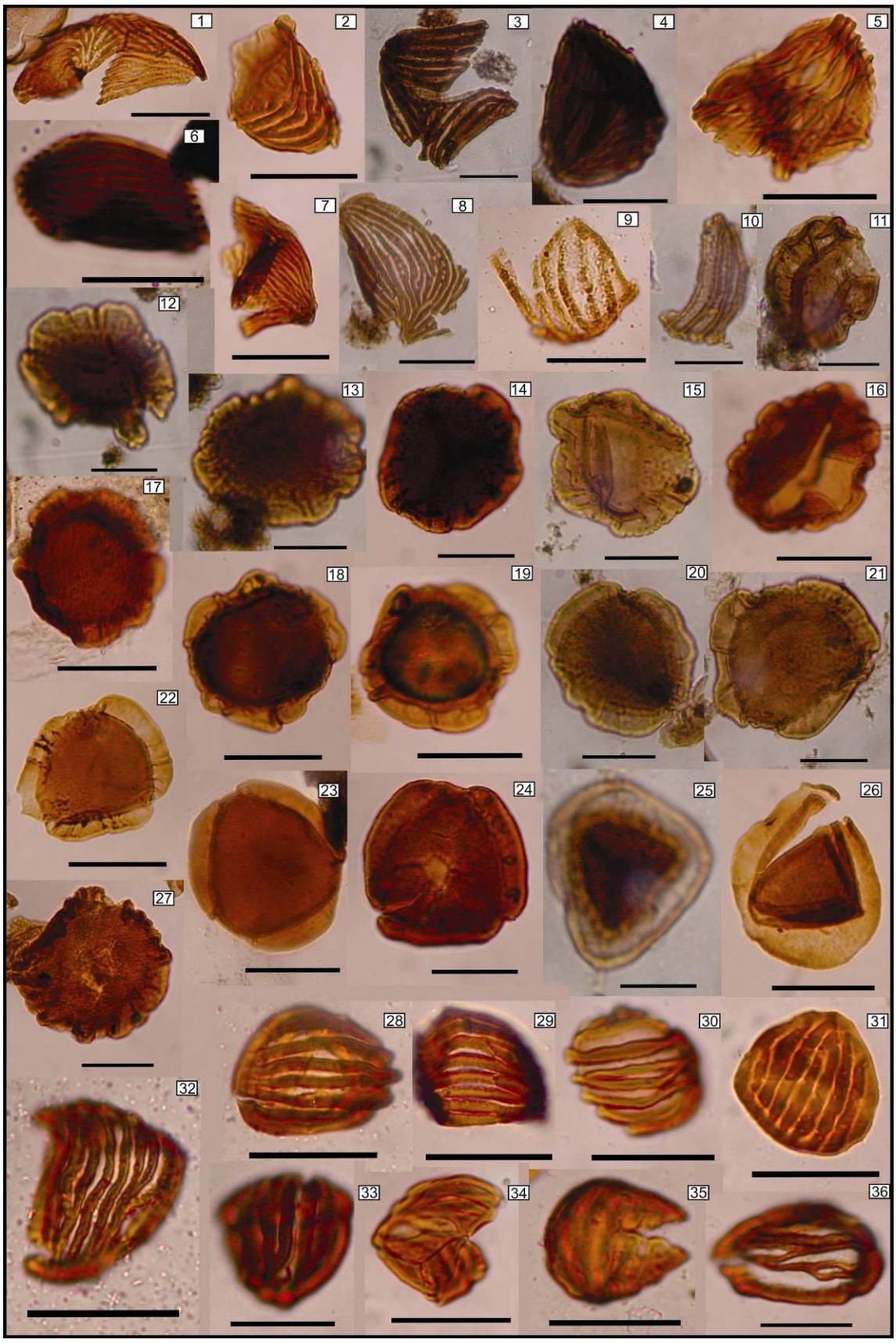
1
2
3
4
5
6
7
8
9
10
11
12
13
14
15
16
17
18
19
20
21
22
23
24
25
26
27
28
29
30
31
32
33
34
35
36

Plate 2

Plate 3

Fig. 1, *Cycadopites* sp. Sample CC 34
Fig. 2, *Cycadopites* sp. Sample CC 94
Fig. 3, *Cycadopites* sp. Sample CC 76
Fig. 4, *Cycadopites* sp. Sample LM 1
Fig. 5, *Cyathidites australis*, Sample CC 102
Fig. 6, *Cyathidites australis*, Sample CC 46
Fig. 7, *Cyathidites australis*, Sample LM 1
Fig. 8, *Cyathidites minor*, Sample CC 46
Fig. 9, *Cyathidites australis*, Sample CC 116
Fig. 10, *Cyathidites minor*, Sample CC 46
Fig. 11, *Cyathidites australis*, Sample CC 76
Fig. 12, *Classopollis* sp. Sample CC 76
Fig. 13, *Araucariacites australis*, Sample CC 34
Fig. 14, *Ceratosporites equalis*, Sample CC 102
Fig. 15, *Triplanosporites* sp. Sample CC 46
Fig. 16, *Classopollis* sp. Sample CC 46
Fig. 17, *Classopollis* sp. Sample CC 12
Fig. 18, *Deltoidospora* sp. Sample CC 52
Fig. 19, *Gleicheniidites senonicus*, Sample CC 12
Fig. 20, *Gleicheniidites* sp. Sample CC 12
Fig. 21, *Gleicheniidites* sp. Sample CC 116
Fig. 22, *Gleicheniidites* sp. Sample CC 76
Fig. 23, *Gleicheniidites* sp. Sample C 46
Fig. 24, *Gleicheniidites rasilis*, Sample CC 76
Fig. 25, *Gleicheniidites rasilis*, Sample CC 76
Fig. 26, *Gleicheniidites senonicus*, Sample CC 76
Fig. 27, *Gleicheniidites* sp. Sample CC 52
Fig. 28, *Gleicheniidites senonicus*, Sample CC 12
Fig. 29, *Gleicheniidites* sp. Sample CC 102
Fig. 30, *Gleicheniidites senonicus*, Sample CC 94
Fig. 31, *Verticipollenites gibbosus*, Sample CC 52
Fig. 32, *Dictyophyllidites* sp. Sample CC 62
Fig. 33, *Cicatricosisporites* sp. Sample CC 12

Note: Scale bar represent 31µm for all figures

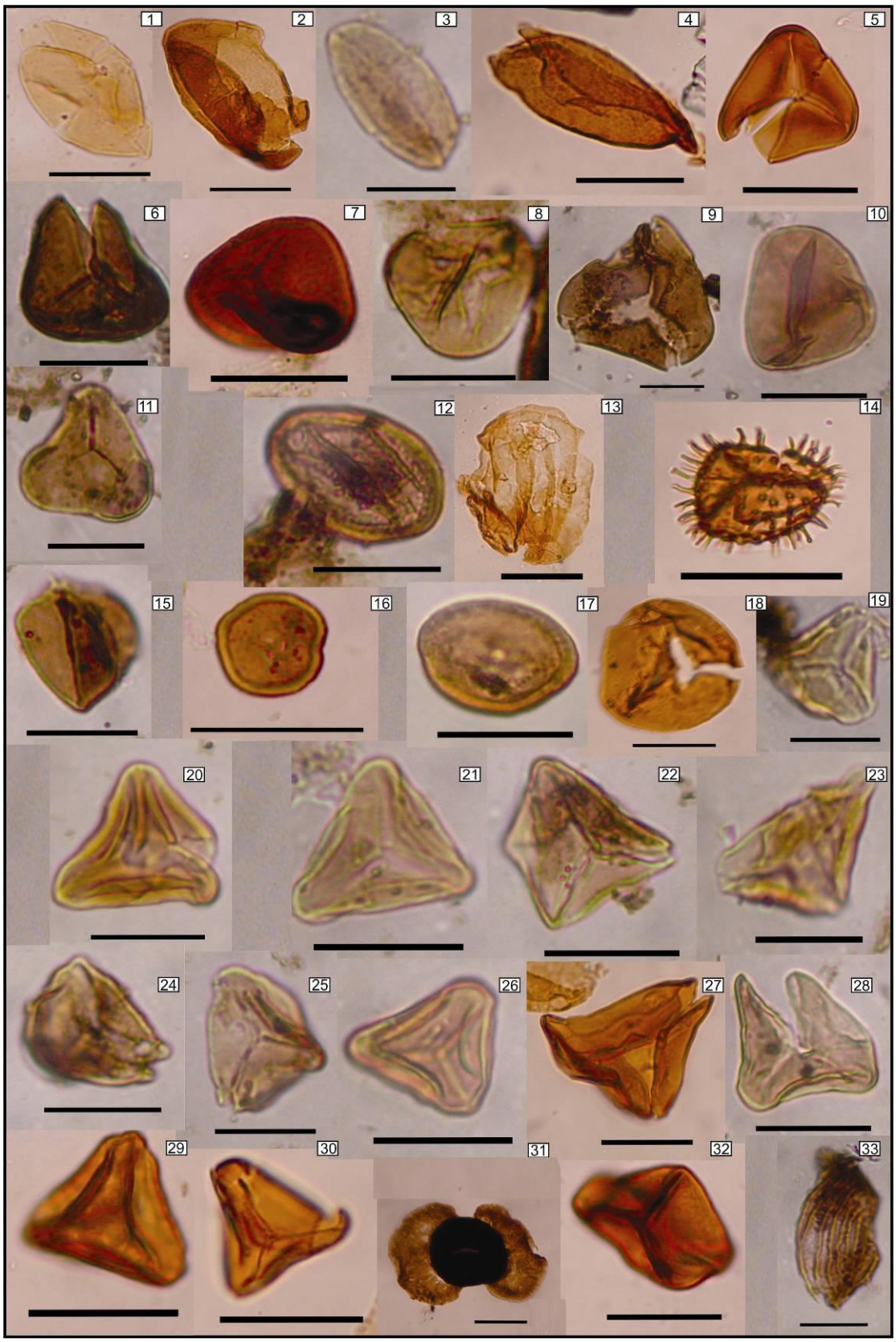
1
2
3
4
5
6
7
8
9
10
11
12
13
14
15
16
17
18
19
20
21
22
23
24
25
26
27
28
29
30
31
32
33

Plate 3

Plate 4

Fig. 1, 2, *Gleicheniidites* sp. CC 12
Fig. 3, *Gleicheniidites senonicus,* Sample CC 46
Fig. 4, *Gleicheniidites senonicus,* Sample CC 76
Fig. 5, *Sestrosporites pseudoalveolatus,* Sample LM 1
Fig. 6, *Classopollis martinottii,* Sample CC 94
Fig. 7, Gymnosperms verrucate monosulcate pollen grain, Sample CC 12
Fig. 8, *Klukisporites* cf. *pseudoreticulatus,* Sample CC 34
Fig. 9, *Ischyosporites* cf. *punctatus* Sample CC 62
Fig. 10, *Klukisporites* sp. Sample CC 52
Fig. 11, *Ischyosporites variegatus,* Sample CC 52
Fig. 12, *Ischyosporites* sp. Sample CC 52
Fig. 13, *Matonisporites equiexinus,* Sample CC 34
Fig. 14, *Monosaccites* sp. Sample CC 94
Fig. 15, *Jugella* sp. Sample CC 12
Fig. 16, *Matonisporites* sp. Sample LM 1
Fig. 17, *Matonisporites* sp. Sample CC 34
Fig. 18, *Ornamentifera baculata,* Sample CC 46
Fig. 19, *Densoisporites velatus,* Sample CC 52
Fig. 20, *Retitriletes* sp. Sample CC 34
Fig. 21, *Podocarpidites* sp. Sample CC78
Fig. 22, *Alisporites* sp. Sample CC 62
Fig. 23, *Classopollis* sp. in Sample CC 76
Fig. 24, *Sestrosporites pseudoalveolatus,* Sample LM 1
Fig. 25, *Trilobosporites* cf. *apiverrucatus,* Sample CC 34
Fig. 26, *Concavissimisporites minimus,* Sample CC127
Fig. 27, *Trisaccites* sp. Sample CC127
Fig. 28, Gymnosperm woody matrix, Sample CC 62
Fig. 29, *Vitreisporites pallidus,* Sample CC 12
Fig. 30, *Neoraistrickia* sp. Sample, CC 12
Fig. 31, Gymnosperm woody matrix, Sample CC127
Fig. 32, Wood matrix, Sample CC127
Fig. 33, Leaf epidermal tissue, Sample CC127

Note: Scale bar represent 31µm for all figures

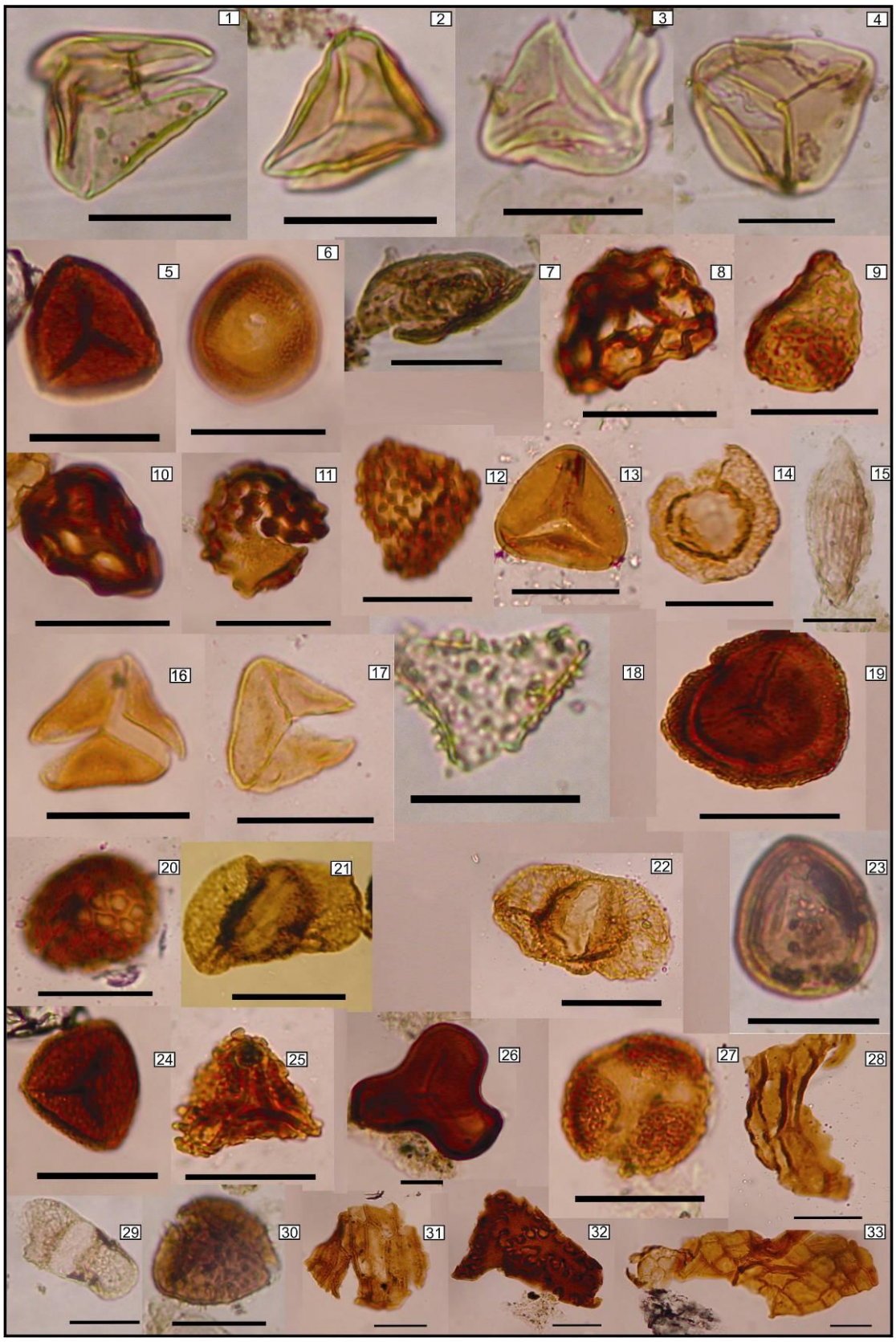
1
2
3
4
5
6
7
8
9
10
11
12
13
14
15
16
17
18
19
20
21
22
23
24
25
26
27
28
29
30
31
32
33

Plate 4

Plate 5

Fig. 1, *Cicatricosisporites* sp. Sample CC 52
Fig. 2, *Araucariacites australis,* Sample CC 46
Fig. 3, *Chromotriletes* cf. *minor*, Sample CC 102
Fig. 4, *Concavisporites* sp. Sample CC 76
Fig. 5, *Matonisporites* sp. Sample CC127
Fig. 6, *Callialasporites microvelatus,* Sample CC127
Fig. 7, *Converrucosisporites* sp. Sample CC 46
Fig. 8, *Pilosisporites* sp. Sample CC 94
Figs. 9-10, *Aequitriradites* sp. Sample CC127
Fig. 11, *Trilobosporites* sp. Sample CC 34
Fig. 12, *Impardecispora* sp. Sample CC 46
Fig. 13, *Kleithriasphaeridium* cf. eoinodes, Sample CC 94
Fig. 14, *Oligosphaeridium* sp. Sample CC 102
Fig. 15, *Surculosphaeridium* sp. Sample CC 94
Fig. 16, *Egmontodinium torynum,* Sample CC 102
Fig. 17, *Oligosphaeridium* cf. *complex*, Sample CC 102
Fig. 18, *Oligosphaeridium asterigerum,* Sample CC 102
Fig. 19, *Systematophora areolata,* Sample CC 102
Fig. 20, *Ctenidodinium* sp. Sample CC127
Fig. 21, *Sentusidinium pelionense,* Sample CC 34
Fig. 22, *Perisseiasphaeridium pannosum,* Sample CC 102
Fig. 23. *Systematophora* sp. Sample CC127

Note: Scale bar represent 31µm for all figures

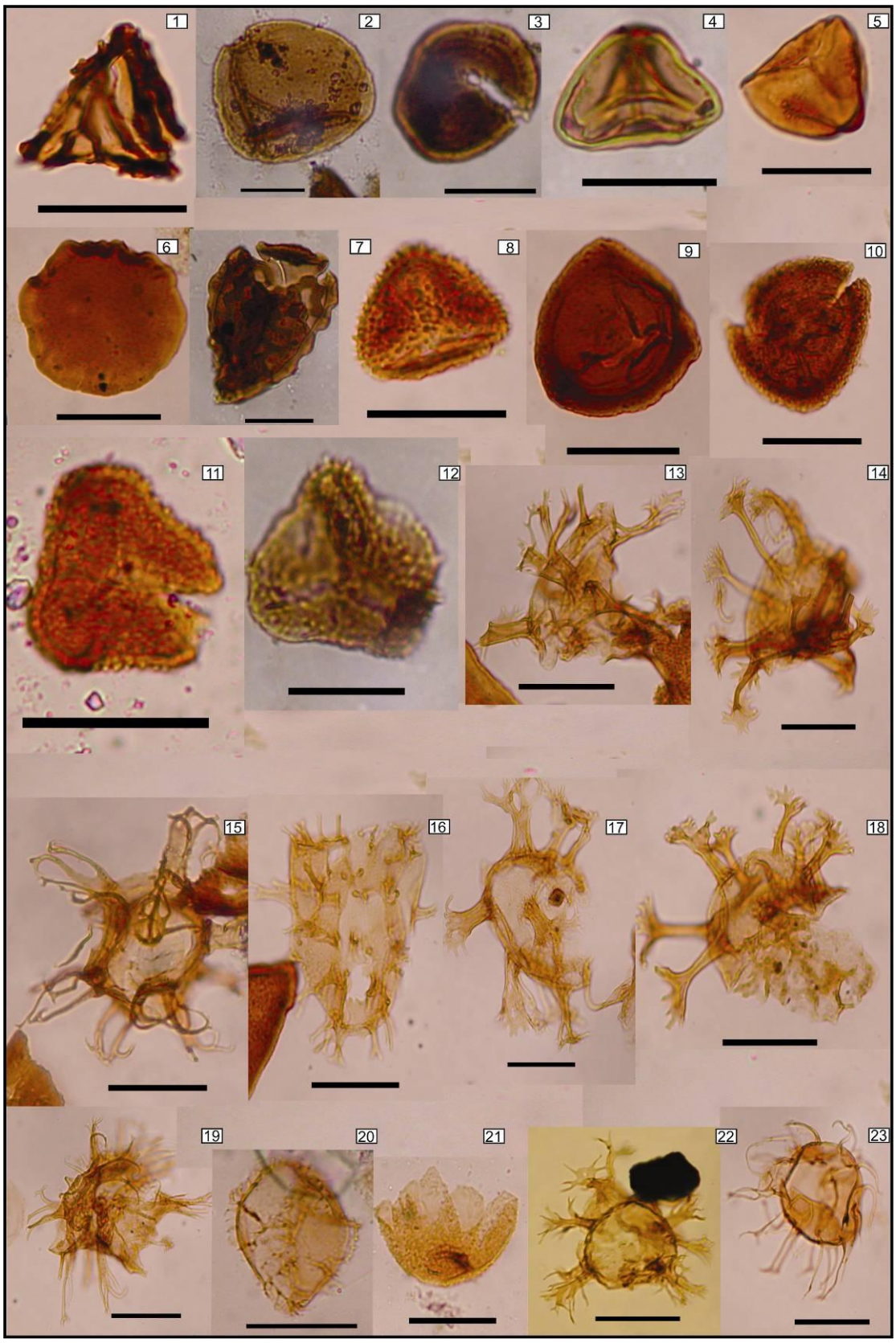

Plate 5

Plate 6

Figs. 1, 4, 5, *Oligosphaeridium complex,* Sample CC 12
Figs. 2-3, *Oligosphaeridium* sp. Sample CC12
Fig. 6, *Oligosphaeridium complex*, Sample CC 102
Fig. 7, *Oligosphaeridium complex*, Sample CC 102
Fig. 8, *Oligosphaeridium complex*, Sample CC 34
Fig. 9, *Oligosphaeridium complex*, Sample CC 52
Fig. 10, *Rigaudella* cf. *aemula*, Sample CC 12
Fig. 11, *Rigaudella aemula*, Sample CC 52
Fig. 12, *Oligosphaeridium* cf. *pulcherrimum,* Sample CC 94
Fig. 13, *Hystrichosphaerina schindewolfii,* Sample CC 12
Fig. 14, *Sentusidinium* sp. Sample CC 94
Fig. 15, *Prolixosphaeridium* sp. Sample CC 94
Fig. 16, *Cyclonephelium* cf. *distinctum,* Sample CC 102
Fig. 17, *Cyclonephelium* sp. Sample CC 102
Fig. 18, *Cyclonephelium* sp. Sample CC 12
Fig. 19, *Systematophora*, in Sample CC 34
Fig. 20, *Cyclonephelium* sp. Sample CC 102
Fig. 21, *Cymososphaeridium* cf. *validum*, Sample CC 94
Fig. 22, *Achomosphaera neptuni,* Sample CC 62
Figs.23-24, *Systematophora* cf. *areolata,* Sample CC 102
Fig. 25, *Sirmiodinium* cf. *grossi*, Sample CC 116
Fig. 26, *Sentusidinium* sp. Sample CC 12

Note: Scale bar represent 31µm for all figures

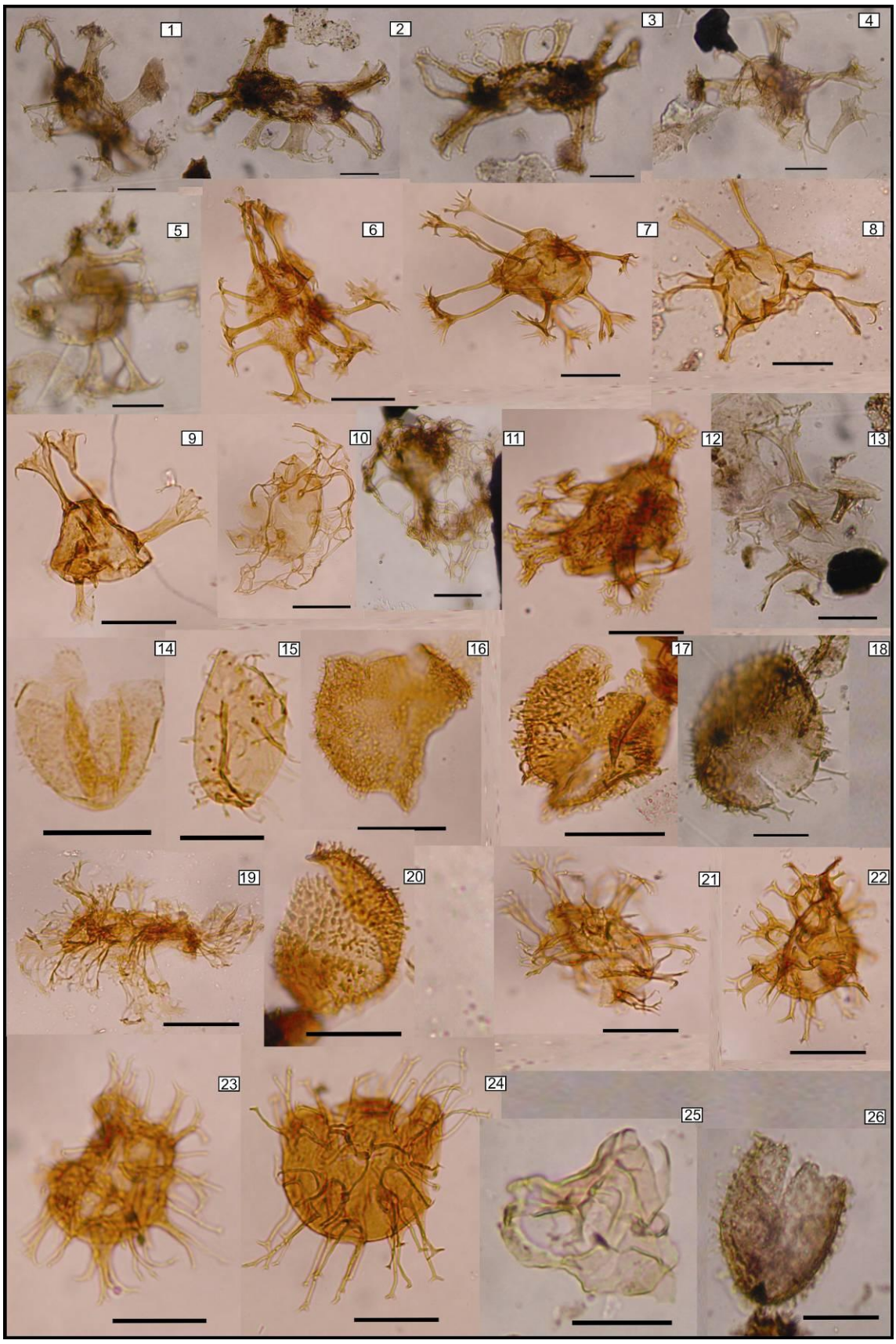

Plate 6

Plate 7

Figs. 1, 4, *Gonyaulacysta jurassica*, Sample CC 02
Figs. 2, 3, 5-10, *Cribroperidinium globatum*, Sample CC 02
Fig. 4, *Gonyaulacysta jurassica*, Sample CC 02
Fig. 11, *Scriniodinium* sp. Sample CC 105
Fig. 12, *Sirmiodinium* sp. Sample CC 116
Fig. 13, *Egmontodinium* cf. *expiratum*, Sample CC 12
Fig. 14, *Leptodinium subtile*, Sample CC 02
Fig. 15, *Ctenidodinium* sp. Sample CC 02
Fig. 16, *Ctenidodinium* sp. Sample CC 94
Fig. 17, *Systematophora* sp. Sample CC 102
Fig. 18, *Stiphrosphaeridium* sp. Sample CC 12
Fig. 19, *Pterospermella* sp. Sample CC 46
Fig. 20, *Pterospermella* sp. Sample CC 116
Fig. 21, *Oligosphaeridium complex*, Sample CC 116
Fig. 22, *Oligosphaeridium cf. complex* Sample CC12
Fig. 23, *Sentusidinium* sp. in Sample CC 12
Fig. 24, Acritarch

Note: Scale bar represent 31µm for all figures

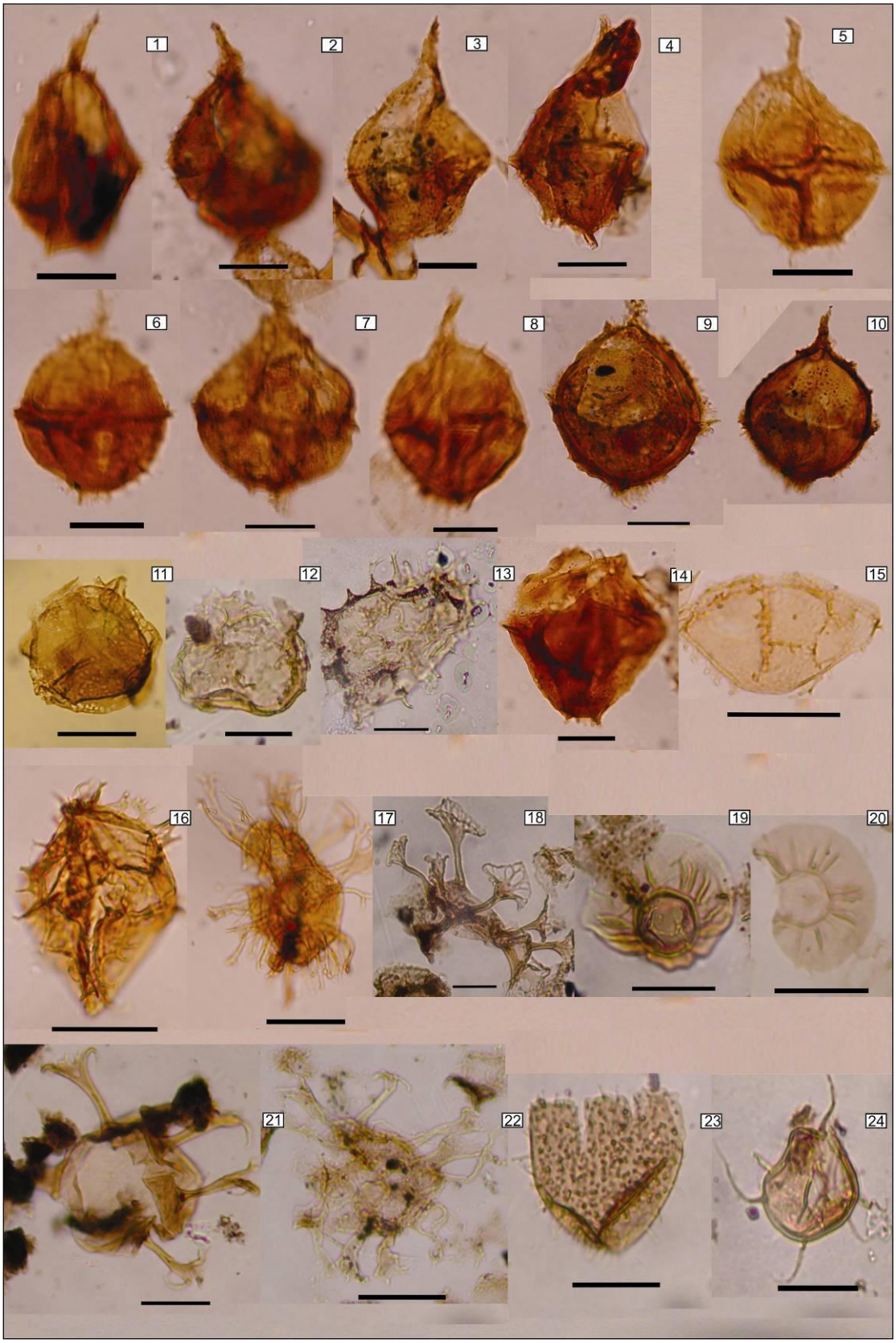

Plate 7

Plate 8

Fig. 1, *Prolixosphaeridium parvispinum*, Sample CC 102
Fig. 2, *Prolixosphaeridium parvispinum*, Sample C 52
Fig. 3, *Prolixosphaeridium parvispinum*, Sample CC 102
Fig. 4, *Prolixosphaeridium* sp. Sample CC 94
Fig. 5, *Cribroperidinium* sp. Sample CC 02
Fig. 6, *Batioladinium* sp. Sample CC 12
Fig. 7, *Wallodinium* sp. Sample CC 46
Fig. 8, *Sirmiodinium grossi*, Sample CC 12
Fig. 9, *Hystrichosphaerina schindewolfii*, Sample CC 12
Fig. 10, *Kleithriasphaeridium porospinosum*, Sample CC 02
Fig. 11, *Scriniodinium* sp. Sample CC 102
Fig. 12, *Pseudoceratium* sp. Sample CC 102
Figs. 13, 15, *Cyclonephelium distinctum*, Sample CC 91
Fig. 14, *Cyclonephelium distinctum*, Sample CC 78
Fig. 16, *Cyclonephelium* sp. Sample CC 91

Note: Scale bar represent 31µm for all figures

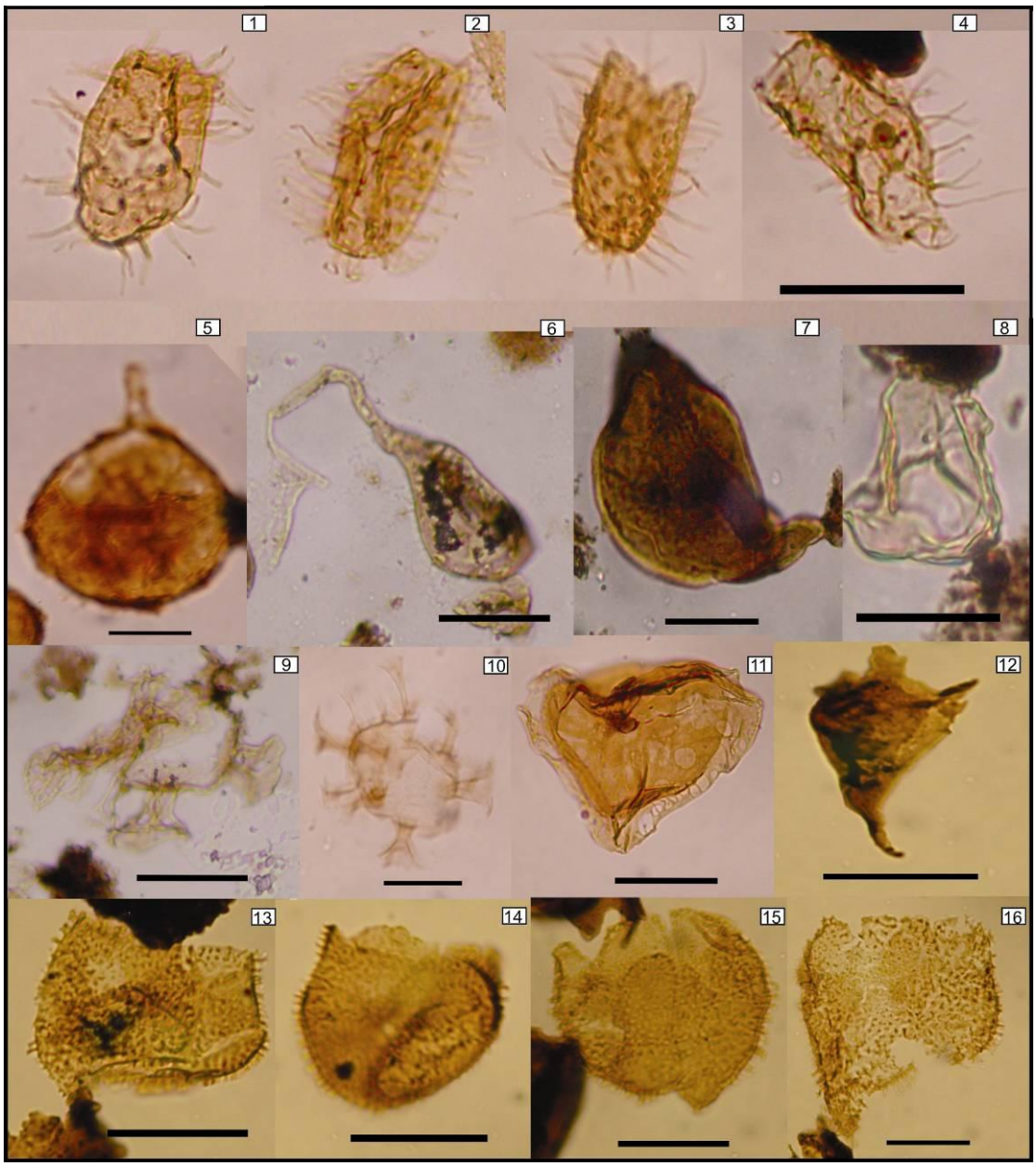

Plate 8

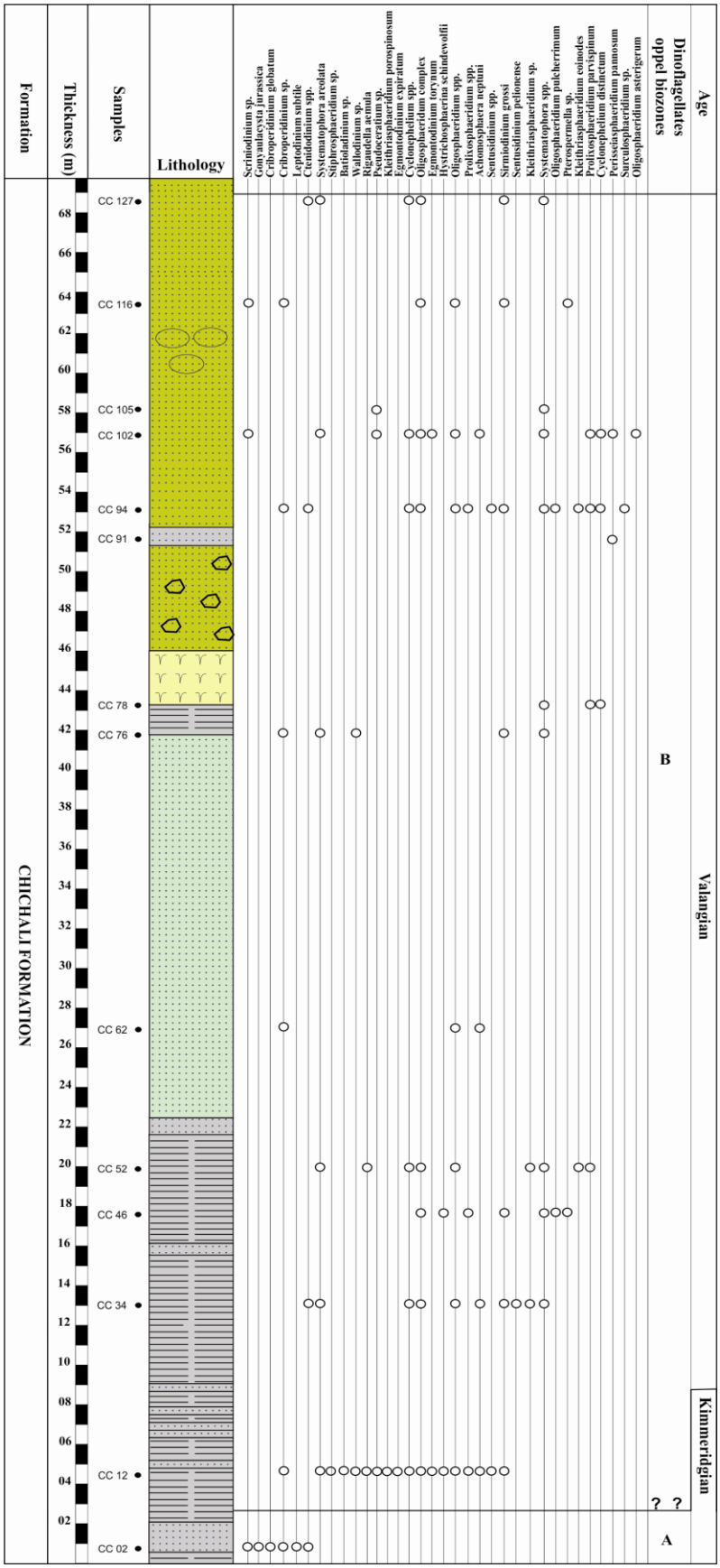

Figure 4.1: Dinoflagellates presence/absence and biozonation chart of the Chichali Formation, Chichali Nala Section.

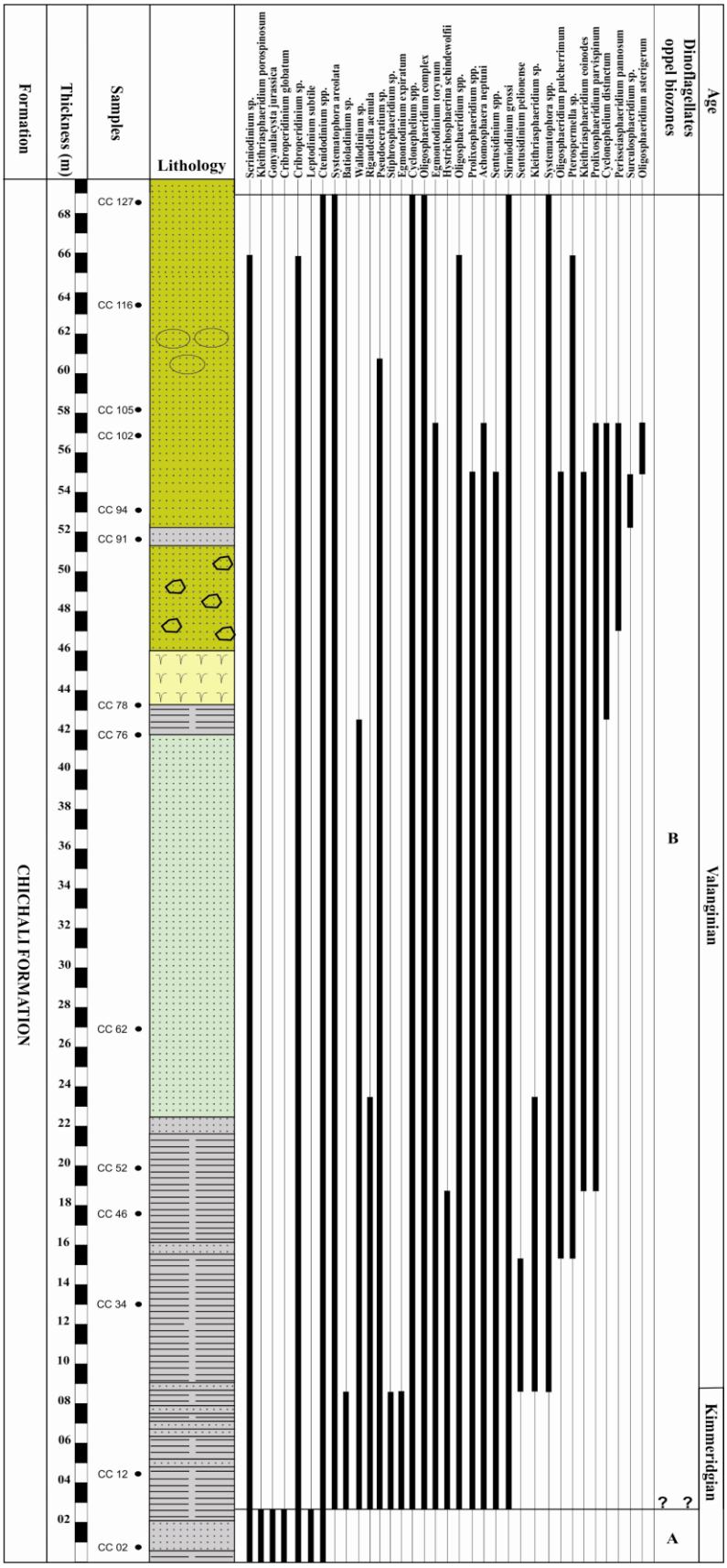

Figure 4.2: Dinoflagellates range and biozonation chart of the Chichali Formation, Chichali Nala Section.

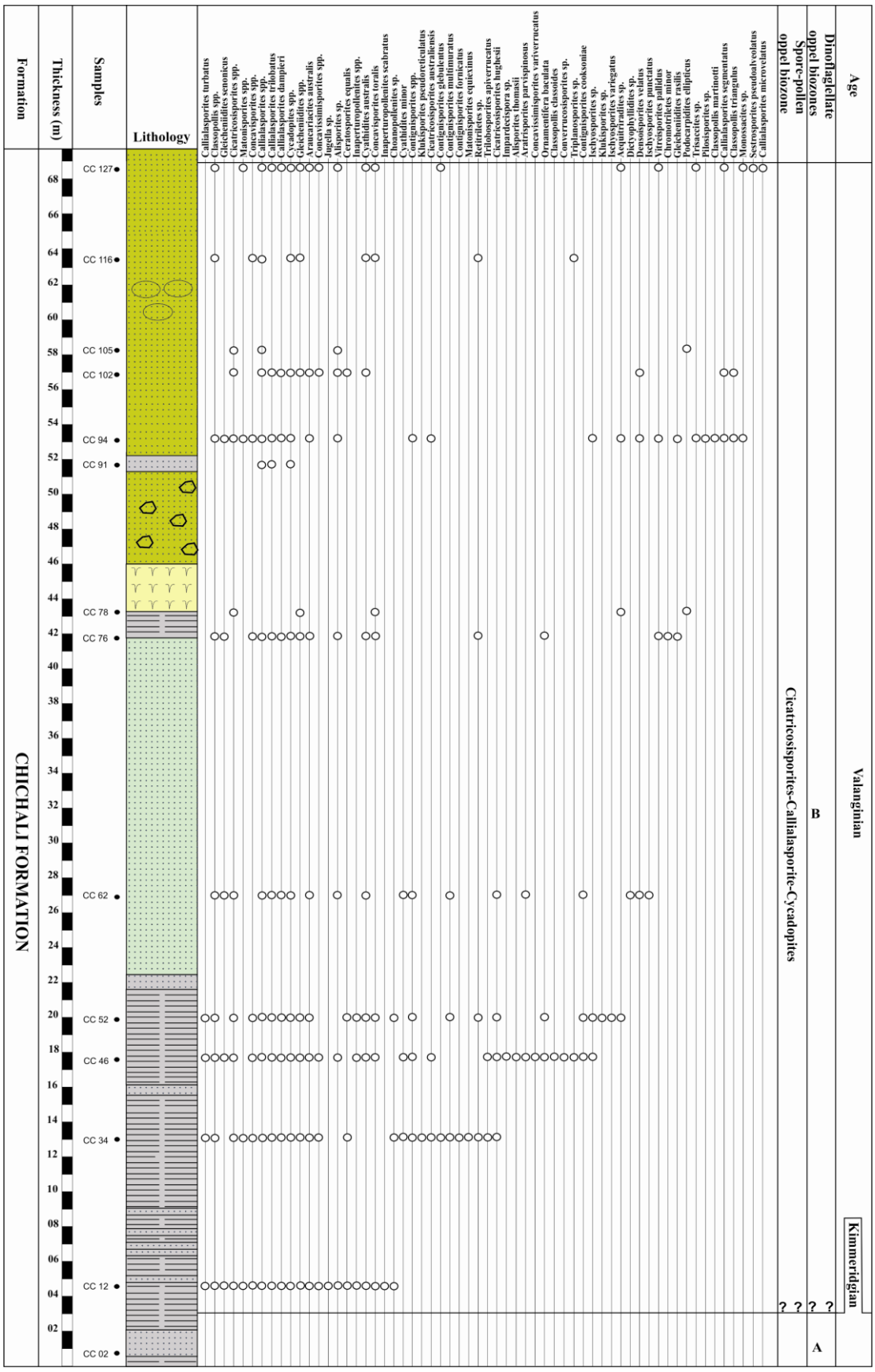

Figure 4.3: Spores-Pollens presence/absence and biozonation chart of the Chichali Formation, Chichali Nala Section.

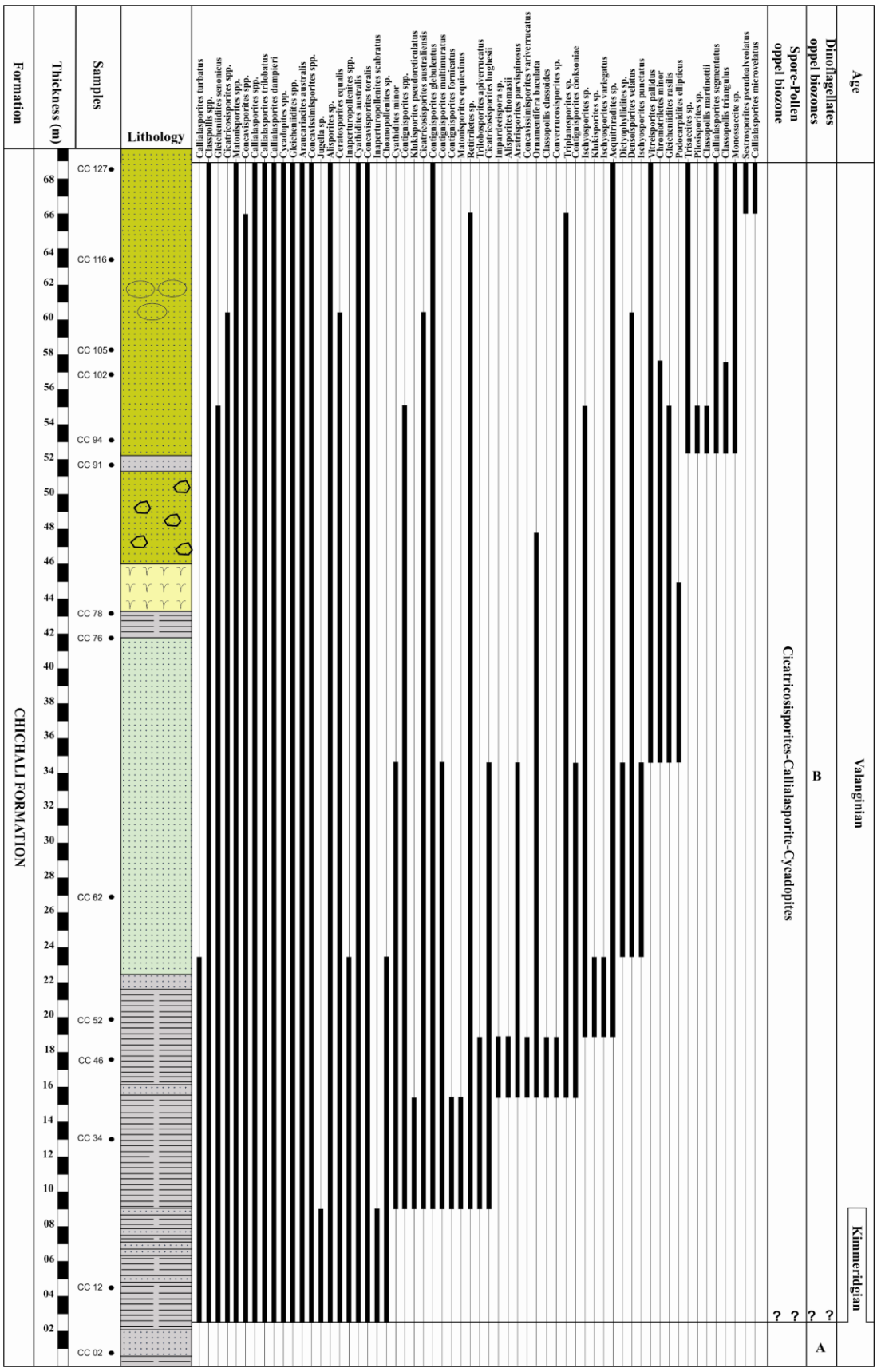

Figure 4.4: Spores-Pollens range and biozonation chart of the Chichali Formation, Chichali Nala Section

4.2.1 Palynomorphs Biozones

Biostratigraphers used different approaches to define dinoflagellate biozones in the Mesozoic. William (1977) described concurrent dinoflagellate range zones and subzones of global extent for the Cretaceous, while Helby (1987) defined Oppel, range, and interval zones for the Australian sections. Heilmann-Clausen (1987) plotted stratigraphic ranges of Early Cretaceous dinoflagellates against standard ammonite zones in a sedimentary sequence of the Danish Central Trough for correlation purposes.

The approach to build a dinofllagellate and spore-pollen biozonation in this study is slightly different from the aforementioned studies. An attempt is made to define Oppel biozones using a maximum number of age diagnostic species. This approach was taken because some of the key dinoflagellates, and spore-pollen species, used in these studies, are either missing due to rare occurrences or their poor preservation. The low sampling resolution may have further hampered the actual stratigraphic record of such species. The stratigraphic ranges of species used in defining these biozones are correlated with the stratigraphic ranges given in Williams & Bujak (1985), Helby et al., (1987), Riding & Thomas, (1992), and Costa & Davey (1992). Three Oppel biozones (two dinoflagellate biozones and one spore-pollen biozone) are defined based on important dinoflagellates and spore-pollens taxa (figs. 4.1-4.4). The details of these biozones are given as below.

4.2.1.1 Dinoflagellate Oppel Zone A

Age: Kimmeridgian

Author: Khan (this thesis)

Definition: The base of the zone is not exposed while the top of the biozone is defined by the last appearance levels of *Cribroperidinium globatum, Leptodinium subtile, Gonyaulacysta jurassica,* and other *Cribroperidinium* species.

Species assemblages: Cribroperidinium globatum, Leptodinium subtile, Gonyaulacysta jurassica, Kleithriasphaeridium porospinosum, Cribroperidinium sp., *Ctenidodinium spp.* and *Scriniodinium* sp.

Remarks: The *Cribroperidinium globatum, Leptodinium subtile,* and *Gonyaulacysta jurassica* occur in the Jurassic, more specifically their last occurrence are in the Kimmeridgian (Riding & Thomas, 1992; Riding et al. 1999 and Williams & Bujak; 1985). The first appearances of *Hystrichosphaerina schindewolfii* and *Oligosphaeridum complex* occur just 4m above the current zone. These species have their first occurrences in the Early Valanginian (Costa & Davey, 1992). Collectively, taking the stratigraphic information of all these species, it appears that the Tithonian stage of the Jurassic, and Berriasian stage of the Early Cretaceous are either condensed in just 4m of strata, or these two stages are truncated by an unconformity.

4.2.1.2 Dinoflagellate Oppel Zone B

Age: Valanginian

Author: Khan (this thesis)

Definition: The interval between the first appearances of the *Hystrichosphaerina schindewolfii, Oligosphaeridium complex, Egmontodinium torynum* and the end of the section.

Species assemblages: Hystrichosphaerina schindewolfii, Oligosphaeridium complex, Egmontodinium torynum, Egmontodinium cf. *expiratum, Rigaudella aemula, , Oligosphaeridum asterigerum, Oligosphaeridium* cf. *pulcherrimum, Oligosphaeridum* spp., *Kleithriasphaeridium* cf. eoinodes, *Achomosphaera neptuni, Perisseiasphaeridium pannosum, Cyclonephelium distinctum, Cyclonephelium* spp., *Prolixosphaeridium parvispinum, Prolixosphaeridium* spp., *Systematophora areolata, Systematophora* spp., *Sirmiodinium grossi, Pseudoceratium* sp., *Sentusidinium pelionense, Cymososphaeridium* cf. *validum, Stiphrosphaeridium* sp., S*urculosphaeridium* sp., *Batioladinium* sp., *Ctenidodinium* spp., *Pterospermella* sp., *Scriniodinium* sp., *Sentusidinium* spp., *Sirmiodinium* sp., *Wallodinium* sp. *Cribroperidinium* sp.

Remarks: The First Appearance Datums (FADs) of the *Hystrichosphaerina schindewolfii, Oligosphaeridum complex* represent Valanginian age (Harding et al. 2011, Schrank, 2005). More precisely the co-occurrences of *Hystrichosphaerina schindewolfii, Oligosphaeridum complex,* and *Egmontodinium torynum* in the basal most part of the zone indicate the Early Valanginian.

Notably, the last occurrences of *Hystrichosphaerina schindewolfii* (19m), *Rigaudella aemula* (~23m), and *Egmontodinium torynum* (57m) are within the Chichali Formation, which are know to disappear globally in the Early Valanginian (Helby et al., 1987; Costa & Davey, 1992). The top of the sequence is difficult to assign to either the Early Valanginian or Late Valanginian because the last occurrences of *Hystrichosphaerina schindewolfii, Rigaudella aemula,* and *Egmontodinium torynum* may be not their 'true' last occurrences as preservation and sampling resolution limit interpretation of the biostratigraphy. Therefore the Valanginian age is assigned to this whole biozone.

4.2.1.3 Cicatricosisporites-Callialasporites-Cycadophytes spore-pollen Oppel biozone

Author: Khan (this thesis)

Definition: The assemblage of spores and pollen comprising the species *Cicatricosisporites, Callialasporites,* and *Cycadophyte* spp.

Spores and pollens assemblages: Spores include, *Cicatricosisporites australiensis, Cicatricosisporites hughesii, Cicatricosisporites* spp., *Ischyosporites variegatus, Ischyosporites punctatus, Ischyosporites* sp., *Concavissimisporites minimus,* C*oncavissimisporites* sp., C*oncavissimisporites variverrucatus, Klukisporites* cf. *pseudoreticulatus, Klukisporites* sp., *Contignisporites cooksoniae, Contignisporites fornicatus, Contignisporites glebulentus, Contignisporites multimuratus, Contignisporites* spp., *Matonisporites equiexinus, Matonisporites* spp., *Concavisporites toralis, Concavisporites* spp., *Trilobosporites* cf. *apiverrucatus, Trilobosporites* sp., *Gleicheniidites rasilis, Gleicheniidites senonicus, Gleicheniidites* spp., *Ornamentifera baculata, Cyathidites australis, Cyathidites minor, Sestrosporites pseudoalveolatus, Aratrisporites parvispinosus, Densoisporites velatus, Ceratosporites equalis, Chomotriletes minor, Impardecispora* sp., *Triplanosporites* sp., *Pilosisporites* sp., *Dictyophyllidites* sp., *Deltoidospora* sp., *Converrucosisporites* sp., *Aequitriradites* sp., *Neoraistrickia* sp.

Pollens include, *Callialasporites microvelatus, Callialasporites segmentatus, Callialasporites dampieri, Callialasporites turbatus, Callialasporites dampieri-trilobatus, Callialasporites trilobatus, Callialasporites* spp., *Araucariacites*

australis, Classopollis martinottii, Classopollis triangulus, Classopollis classoides, Classopollis spp., *Alisporites grandis, Alisporites thomasii, Alisporites* sp., *Podocarpidites* cf. *ellipticus, Vitreisporites pallidus, Inaperturopollenites* spp., *Trisaccites* sp., *Cycadopites* spp., *Jugella* sp., *Choanopollenites* sp.

Remarks: The pollen and spores assemblage indicates an Early Cretaceous age. For instance, the base of the section contains the *Cicatricosisporites* spp. and the *Impardecispora* sp., indeed of Early Cretaceous age (Helby et al., 1987). These assemblages are accompanied by *Concavissimisporites*, *Pilosisporites* sp, and *Jugella* sp. suggesting further that the Chichali Formation was deposited during Early Cretaceous more specifically during the Valanginian to Barremian interval (Li & Batten, 2004). The *Monosaccites* sp., *Arcuatipollenites ovatus, Verticipollenites gibbosus* are reworked Permo-Triassic pollens assemblages, hence are not used for stratigraphy here.

4.2.2 Conclusions on the age of the section

The combined presence of species of dinoflagellates and spores and pollens indicate that the Chichali Formation is Kimmeridgian to Valanginian in age. However, there is potentially a hiatus or, condensed section, in the lowermost part of the section. The Tithonian and Berriasian are possibly missing.

4.3 Vegetation and paleoclimate

The plants are very sensitive to any change in climatic conditions therefore specific type of vegetation provides evidence for the prevailing climate during its growth (Traverse, 2007). For example the Mesozoic ferns of Cyatheaceae, Dicksoniaceae, and Schizaeaceae families are un-doubtfully agreed to represent warm humid climatic conditions (Van Konijnenburg-van Cittert, 2002). These ferns dwell in lowland marshes, along river banks or as understory in canopy forests. Also the plants of Selaginellaceae family thrived in shaded lowlands under warm humid conditions during Early Cretaceous (Prakash, 2008; Volkheimer et al., 2009). On the other hand the Jurassic and Early Cretaceous ferns of Matoniaceae and Gleicheniaceae families indicate warmer and drier conditions (Van Konijnenburg-Van Cittert, 2002).

The gymnosperms of Araucariaceae family such as *Callialasporites* spp. and *Araucariacites* spp. in the Early Cretaceous were common in lowland coastal areas (Volkheimer et al., 2009). The prominence of such species in the Early Cretaceous deposits of the Satpura Basin India indicates comparatively warm conditions (Prakash, 2008).

The dominant occurrence of other gymnosperms i.e. *Classopollis* spp. (Cheirolepidiaceae family) in Jurassic and Early Cretaceous can be explained by dry subtropical climate (Wang et al., 2005; Mendes et al., 2011). The *Classopollis* spp. were also restricted to low land coastal areas.

4.3.1 Spore-pollen assemblages of the Chichali Formation and Paleoclimate

It is important for the paleoclimate reconstruction to classify the spore and pollen assemblages according to their botanical affinities (e.g. families). The botanical affinities for each spore and pollen taxon of the Chichali Formation are derived from the published literature (Timmcke, 1981, Martin & McMinn, 1993, Wang et al., 2005, Barrón et al., 2006, Ziaja, 2006, Peyrot et al., 2007, Yang et al., 2007, Jiang et al., 2008, Prakash, 2008, Volkheimer et al., 2009). Consult figure 4.4 for the distribution of stratigraphic ranges of spores and pollens species. A list of these spores and pollens species with their botanical affinities is given in tables 4.1-4.2.

Based on the above literature pertaining to the Early Cretaceous climate based on vegetation of that time, it is evident from the spore and pollen assemblages of the Chichali Formation that warm humid to dry conditions prevailed during the Valanginian time on the Indian continent. The warm humid conditions are supported by the dominant occurrences of ferns (Cyatheaceae, Dicksoniaceae, and Schizaeaceae families), members of Selaginellaceae family, and gymnosperms i.e. *Callialasporites* spp. and *Araucariacites* sp. (Araucariaceae family). While the warm drier conditions are supported by the occurrences of specific ferns (i.e. members of Matoniaceae and Gleicheniaceae families) and gymnosperm i.e. *Classopollis* spp.

4.4 Discussion

It is very important to establish reliable ages for the Chichali Formation before any other paloenvironmental investigations are made. The established ages for the Chichali Formation vary from place to place in the Upper Indus Basin (Spath, 1930;

Fatmi, 1972; 1977; Badshah et al., 2000; Masood et al. 2008 see details in Chapter 2). The age for the lower and middle members of the Chichali Formation in the current Section is documented as Late Oxfordian to Neocomian (Spath, 1930; Fatmi, 1972; 1977) based on ammonites, however detailed biozonation is missing.

It was important to refine and confirm the age of the Chichali Formation using a different fossil group (i.e. palynomorphs), before any further paloenvironmental investigations are made. Based on the dinoflagellates and associated spores and pollen the basal part of the Chichali Formation is Kimmeridgian in age, while the rest of the Chichali Formation is Valanginian in age. The Valanginian strata overly the Kimmeridgian strata in the basal part of the Chichali Formation, hence it appears that the Tithonian stage of the Jurassic and the Berriasian stage of the Early Cretaceous are either condensed or truncated by an unconformity. The palynomorphs based biostratigraphy show that the bulk of the Chichali Formation is deposited in the Valanginian time (see figs 4.3-4.4), which makes this stratigraphic section very important for the paleoclimatic studies.

Apart from the stratigraphy, the purpose of this chapter is to document paleoclimatic data from the Indian Plate, based on the reconstruction of vegetation of the Valanginian time. This data will help in addressing the ongoing controversy regarding the paleoclimate of the Valanginian. Different data sets suggest global cooling during the Valanginian (Price & Nunn, 2010; Rogov & Zakharov, 2010; Alley & Frakes, 2003; (Dichfield, 1997; Price et al., 2000; Van de Schootbrugge et al., 2000; McArthur et al., 2007), however a consistently warm climate is suggested as an alternative possibility for this time period (Littler et al., 2011).

The Indus Basin was located at the ~-35^{o} during the Valanginian time (see figs 4.5) hence it was part of the sub-tropical climate belt. The vegetation reconstruction of the Indus Basin during the Valanginian time will tell us about the climate of that time because plants are very sensitive to any change in climatic conditions (Traverse, 2007).

Based on spore and pollen assemblages of the Chichali Formation it is evident that the warm humid to dry conditions prevailed during the Valanginian time on the Indian continent. Based on similar spores and pollen assemblages, warm to hot and dry climate, alternating with wet conditions have been suggested for the Early

Cretaceous time in China and India (Li & Batten, 2004; Prakash, 2008). Thus the current and the previous studies conclude that warm humid to dry climate was prevailing on the Indian and surrounding continents. Such kind of climatic conditions support the subtropical climate. The lack of temperate to polar vegetation in the subtropical climatic belt (the Indus Basin was located in the subtropical climatic belt i.e. ~-35^{o} during the Valanginian) supports strongly that global cooling didn't happen during the Valanginian time.

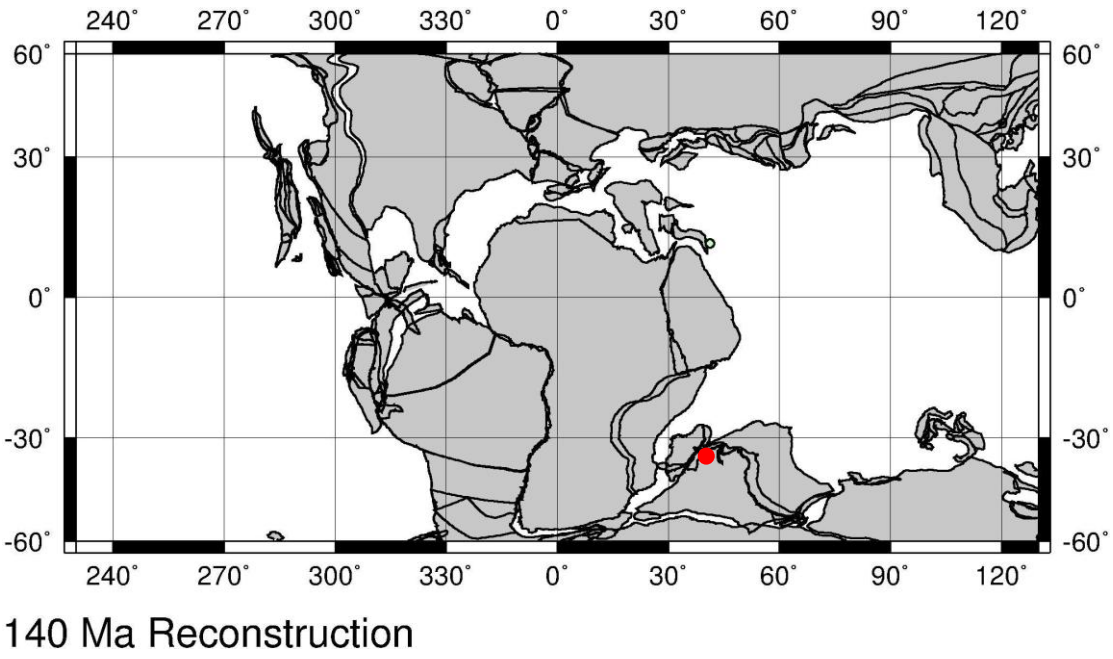

Figure 4.5: Shows the paleolatitude of the Chichali Nala Section during Valanginian time. Adapted from Ocean Drilling Stratigraphic Network (ODSN) Paleomap project (http://www.odsn.de/odsn/services/paleomap/paleomap.html).

4.5 Conclusions

- Two local dinoflagellates Oppel biozones are established in the Chichali Formation.
- One Oppel biozone is introduced in the Chichali Formation based on spore and pollen assemblages.
- Based on palynomorphs, Kimmeridgian to Valanginian age is assigned to the Chichali Formation.

- The Tithonian to Berriasian strata are either condensed in the 4m interval between the dinoflagellate Oppel Zones A and B, or are missing.

- Spore and pollen assemblages suggest that warm humid to dry climatic conditions prevailed on the Indian continent during the Valanginian time.

Spores		
Major division	**Botanical affinity**	**Genera/Species**
Pteridophyta	Schizaeaceae	*Cicatricosisporites australiensis*
	Schizaeaceae	*Cicatricosisporites hughesii*
	Schizaeaceae	*Cicatricosisporites* spp.
	Schizaeaceae	*Impardecispora* sp.
	Schizaeaceae	*Ischyosporites variegatus*
	Schizaeaceae	*Ischyosporites punctatus*
	Schizaeaceae	*Ischyosporites* sp.
	Schizaeaceae	*Concavissimisporites minimus*
	Schizaeaceae	C*oncavissimisporites* sp.
	Schizaeaceae	C*oncavissimisporites*
	Schizaeaceae	*Klukisporites* cf.
	Schizaeaceae	*Klukisporites* sp.
	Schizaeaceae	*Triplanosporites* sp.
	Schizaeaceae?	*Pilosisporites* sp.
	Pteridaceae/ Schizaeaceae	*Contignisporites cooksoniae*
	Pteridaceae/ Schizaeaceae	*Contignisporites fornicatus*
	Pteridaceae/ Schizaeaceae	*Contignisporites glebulentus*
	Pteridaceae/ Schizaeaceae	*Contignisporites multimuratus*
	Pteridaceae	*Contignisporites* spp.
	Matoniaceae	*Matonisporites equiexinus*
	Matoniaceae	*Matonisporites* spp.
	Matoniaceae	*Concavisporites* spp.
	Matoniaceae	*Concavisporites toralis*
	Matoniaceae	*Trilobosporites* sp.
	Matoniaceae	*Trilobosporites* cf. *apiverrucatus*
	Matoniaceae/Dicksoniaceae	*Dictyophyllidites* sp.
	Gleicheniaceae	*Gleicheniidites rasilis*
	Gleicheniaceae	*Gleicheniidites senonicus*
	Gleicheniaceae	*Gleicheniidites* spp.
	Gleicheniaceae	*Ornamentifera baculata*
	Cyatheaceae	*Cyathidites australis*
	Cyatheaceae	*Cyathidites minor*

Table 4.1: Showing the spore assemblages of the Chichali Formation along with their botanical affinities

	Cyatheaceae/Dicksoniaceae	*Deltoidospora* sp.
	Cyatheaceae/Dipteridaceae	*Converrucosisporites*
	Selaginellaceae	*Ceratosporites equalis*
	Selaginellaceae	*Aequitriradites* sp.
	Selaginellaceae	*Densoisporites velatus*
	Selaginellaceae	*Neoraistrickia* sp.
	Pleuromeiaceae	*Aratrisporites parvispinosus*
Bryophytes	Sphagnaceae	*Sestrosporites pseudoalveolatus*
Algae	Fresh water algae	*Chomotriletes minor*
Pollen		
Major division	**Botanical affinity**	**Genera/Species**
Gymnosperms	Araucariaceae	*Callialasporites microvelatus*
	Araucariaceae	*Callialasporites segmentatus*
	Araucariaceae	*Callialasporites turbatus*
	Araucariaceae	*Callialasporites trilobatus*
	Araucariaceae	*Callialasporites* spp.
	Araucariaceae	*Choanopollenites* sp.
	Araucariaceae	*Araucariacites australis*
	Araucariaceae	*Callialasporites dampieri-trilobatus*
	Cheirolepidiaceae	*Classopollis martinottii*
	Cheirolepidiaceae	*Classopollis triangulus*
	Cheirolepidiaceae	*Classopollis classoides*
	Cheirolepidiaceae	*Classopollis* spp.
	Pteridospermophyta	*Alisporites grandis*
	Pteridospermophyta	*Alisporites* sp.
	Pteridospermophyta	*Alisporites thomasii*
	Podocarpaceae	*Trisaccites* sp.
	Podocarpaceae	*Podocarpidites* cf. *ellipticus*
	Taxodiaceae–Cupressaceae	*Inaperturopollenites scabratus*
	Taxodiaceae–Cupressaceae	*Inaperturopollenites* sp.
	Cycadaceae	*Cycadopites* sp.
	Pteridospermophyta	*Vitreisporites pallidus*
Angiosperms	Araceae	*Jugella* sp.
Reworked pollens		
Monosaccites sp.		
Arcuatipollenites ovatus		
Verticipollenites gibbosus		

Table 4.2: Showing the spores and pollen assemblages of the Chichali Formation along with their botanical affinities

CHAPTER 5

5. Planktonic Foraminiferal Biostratigraphy of the Parh Formation

5.1 Introduction

The Parh Formation mainly comprises limestone and shales in all sections throughout the Lower Indus Basin of Pakistan, but the age range of the sections varies according to geographical location within the basin (see chapter 2 for details).

In the Moghal Kot Section an undisturbed stratigraphic record of the Parh Formation is exposed. The limestones and shales of this section span almost the entire Cretaceous. This section offers a unique opportunity to study the biostratigraphic succession of planktonic foraminifers in this part of the Tethys Ocean. In this chapter a new detailed planktonic foraminiferal biostratigraphy is presented. Most importantly, the distribution of organic rich horizons (black shales/limestones) can now be placed within this new detailed biostratigraphic framework. The planktonic biostratigraphic framework concerns the upper part of the Moghal Kot Section (Parh Formation), which comprises mainly limestones, having an age range of Early Aptian to Early Maastrichtian.

The planktonic foraminiferal biostratigraphy of the Moghal Kot Section is practically unknown because of its location. This section is located in the tribal belt of the Frontier Region of the district Dera Ismail Khan, implying serious safety concerns for entering the area, because there is no police for protection. However, I managed to enter the area and sample the section. As a resident of the tribal area, I had the full knowledge of the tribal affairs. I also had the opportunity of engaging students, who live in this area. These students helped me in hiring private security men on a daily wage basis. The Parh Formation was sampled in detail for the current study (see chapter 2 for details of the stratigraphic column of the section).

5.2 Biostratigraphy

5.2.1 Identification of planktonic foraminiferal species

Due to the nature of the sediments of the Parh Formation in Moghal Kot Section, that is mainly limestones and occasional shale horizons (see Chapter 2), ~95 % of the total foraminiferal specimens were mainly identified in thin section and as extracted specimens. Test size, growth-ratio patterns, chamber shape, and size of umbilicus, wall thickness, margin, profile shape and ornamentation were taken into account to identify species. However, in thin section it can be difficult to examine such parameters, because identification and quantification of such parameters can be hampered by non-favourable cuts through the specimens.

Most of the specimens in thin sections were studied by comparing the Moghal Kot Section specimens with those of species, in the standard published literature. I used a compilation of literature as reference for identification (see Appendix 2), particularly those studies in which various cuts through specimens are presented (e.g. Sliter, 1989; Pessagno, 1967; Premoli-Silva & Sliter, 1994; Robaszynski et al. 2010; Postuma 1971). A taxonomic list of species is included in this chapter, the type reference is mentioned, and occasionally a reference with details on the latest species name change. Photographs of specimens in the thin sections, showing various orientations, of each species are organised in Plates 1-23.

To enhance the accuracy of the biostratigraphy, planktonic foraminiferal shells were extracted from the limestone in certain intervals (for methods, see Chapter 1). The samples for extraction of the foraminifera were selected for confirmation of some of the species of *Hedbergella, Rotalipora, Whiteinella, Praeglobotruncana, Dicarinella, and Globotruncana* etc. particularly those species that occur in the Late Albian to Early Maastrichtian, because there is the possibility of missing rare specimens of certain foraminiferal species in thin section. These extracted specimens were extremely useful to further ascertain the presence and absence of species, because of their three-dimensional nature, and morphologies. Extracted specimens are presented to aid the reader for further definition of species names (see Plates 24-30).

5.2.2 Taxonomic Remarks of the Planktonic Foraminiferal species

In this section taxonomic remarks of species are given, including the type reference and in some cases, the most important synonym is given to highlight its latest name change.

Hedbergella delrioensis (Carsey), Plate 1, figs. 11-15; Plate 24, figs. 1-3

-Type reference: *Globigerina cretacea* d'Orbigny var. *delrioensis* Carsey, 1926, p. 43

-*Hedbergella delrioensis* Loeblich & Tappan, 1961, p. 275, pl. 2, figs. 11 (a)-13 (c)

Diagnosis: Test is arranged in a low trochospiral with five chambers in the last whorl. Chambers are inflated and increase in size as added. Sutures are straight to slightly curve and depressed. Wall is perforated, and without keels. The umbilicus is deep.

Hedbergella sigali Moullade, Plate, 1, fig. 1

-Type reference: *Hedbergella sigali* Moullade, 1966, p.87 pl. 7, figs. 24-25

Diagnosis: Small sized low trochospiral test, with tiny globular chambers. It can be differentiated from other *Hedbergella* species by its small size.

Hedbergella hispaniae Longoria, Plate 1, fig. 18

- Type reference: *Hedbergella hispaniae* Longoria, 1974, p.58 pl. 19, figs. 4-8, 19-20

Diagnosis: Trochospiral test, with spherical inflated chambers. Sutures look radial in thin section, and are depressed. The last chamber is titled towards the umbilicus.

Hedbergella trocoidea (Gandolfi), Plate 1, figs. 3-10

-Type reference: *Anomalina lorneiana* d'Orbigny var. *trocoidea* Gandolfi, 1942, p. 98, pl. 2, figs. la-c; pl. 4, figs. 2-3; pl. 13, figs. 2a, b, 5 (a, b)

-*Hedbergella trocoidea* Brönnimann & Brown, 1958, p. 16, fig. l (a-c)

Diagnosis: Test slightly elevated trochospiral with 7 to 8 chambers in the last whorl. The outline in some specimens is angular. The test wall is thick. This species is larger in size than other hedbergellids except *H. gorbachikae*.

Hedbergella gorbachikae Longoria, Plate 1, figs. 19-21

Type reference: *Hedbergella gorbachikae* Longoria, 1974, p. 58 pl. 15, figs. 11-13

Diagnosis: Trochospiral test with a thick wall. This species can be distinguished from *Hedbergella delrioensis* by its larger test size, and the nature of its last chamber. The last chamber of this species is less rounded in thin section and penetrates into the umbilical area.

Hedbergella rischi Moullade, Plate 4, figs. 17, 19-20

-Type reference: *Hedbergella rischi* Moullade, 1974, p. 1816

Diagnosis: It resembles *Hedbergella gorbachikae* but can be differentiated from it, by having larger test size.

Hedbergella planispira (Tappan), Plate 5, figs. 1-4; Plate 24, figs. 4-5

-Type reference: *Globigerina planispira* Tappan, 1940, p. 122, pl. 19, fig. 12

-*Hedbergella planispira* Loeblich & Tappan, 1961, p. 276, pl. 5, figs. 4-1l (c)

Diagnosis: Test is low trochospiral with six spherical inflated chambers in the last whorl. The chambers increase rapidly in size as added. Equatorial outline is more or less rounded. Wall is macroperforate. The sutures are straight and depressed on the umbilical side, while they are not very clear on the spiral side. The umbilicus is wide.

Globigerinelloides ferreolensis (Moullade), Plate 2, figs. 1-11

-Type reference: *Biticinella ferreolensis* Moullade, 1961, p. 214, pl. 1, figs. 1-5

-*Globigerinelloides ferreolensis* Moullade, 1966, p. 123, pl. 9, figs. 1-3

Diagnosis: Test is planispiral with elongated chambers. It can be differentiated from the stratigraphically younger planispiral *Globigerinelloides algerianus* by smaller numbers of chambers in its last whorl, its small size, and its uniform wall thickness of the test. The test wall shows dark and light bands in thin section.

Globigerinelloides algerianus (Cushman & Ten Dam), Plate 2, figs. 12-13; Plate 3, figs. 1-9; Plate 24, figs. 6-7

-Type reference: *Globigerinelloides algeriana* Cushman & Ten Dam, 1948, p. 43, pl. 8, figs. 4–6

-*Globigerinelloides algerianus* Moullade, 1966, p. 125, pl. 9, fig. 15

Diagnosis: Planispiral test with ten to twelve elongated chambers in the final whorl. The chambers can be better observed in thin section specimens, which increase in size as added. The thickness of the wall of the test varies. The test wall has dark and light bands in thin section.

Planomalina cheniourensis (Sigal), Plate 3, figs. 11-13

-Type reference: *Planulina cheniourensis* Sigal, 1952, p. 21, fig. 17

-*Planomalina cheniourensis* Moullade, 1966, p. 130-131, text fig. 3

Diagnosis: It has elongated and angular chambers, which gives the test an angular outline. It evolved from *Globigerinelloides algerianus* by developing a peripheral keel. In thin section, it differs from the *Planomalina buxtorfi* by having internal dark bands on the test wall.

Globigerinelloides barri (Bolli, Loeblich & Tappan), Plate 1, figs, 16-17

-Type reference: *Biglobigerinella barri* Bolli, Loeblich & Tappan, 1957, p. 25, pl. 1, figs. 13-18

-*Globigerinelloides barri* Longoria, 1974, p. 80-82, pl. 4, figs. 1-3, 8, 14; pl. 5, figs. 9-16; pl. 27, fig. 19

Diagnosis: Planispiral biumbilicate test, with spherical bulbous chambers. It can be differentiated from the *G. ferreolensis* and *G. algerianus* by its spherical chambers and a broad thicker test.

Ticinella primula Luterbacher, Plate 4, fig. 9; Plate 5, figs. 8-10

-Type reference: *Ticinella primula* Luterbacher in Renz et al. 1963, p.1085, fig. 4

Diagnosis: Test is arranged in a low trochospiral with six to seven chambers in the last whorl. The globular to subglobular chambers increase in size as added, while the final chamber is somewhat ovate. The sutures are curved on the spiral side and are radial and depressed on the umbilical side. Umbilicus is shallow and wide.

Ticinella roberti (Gandolfi), Plate 4, figs. 6-8; Plate 5, figs. 5-7; Plate 24, fig. 9

-Type reference: *Anomalina roberti* Gandolfi, 1942, p. 100-101, fig. 22, pl. 2, fig. 2; pl. 4, figs. 5–7; pl. 13, figs. 3, 6

-*Ticinella roberti* Moullade, 1966, p. 99-100, pl. 9, figs. 9–11

Diagnosis: Test low trochospiral, and is nearly circular in outline. Chambers are inflated and increase slowely in size as added. The test is pustulose. The sutures are depressed and are radial on the spiral side.

Ticinella raynaudi (Sigal), Plate 6, figs. 14-15; Plate 24, fig. 11

-Type reference: *Ticinella raynaudi* var. *raynaudi* Sigal, 1966, p. 201-202, pl. 5, fig. 10; pl. 6, figs. 1-5

Diagnosis: It has a similar test as *Ticinella primula,* however it has a slightly higher trochospire, and the periphery is more lobulate. The final chambers are seen elongated in thin section.

Ticinella madecassiana Sigal, Plate 6, fig. 12; Plate 7, figs. 3-4; Plate 24, fig. 12

-Type reference: *Ticinella madecassiana* Sigal, 1966, p.197, pl. 3, figs. 7 (a-b)

Diagnosis: Test trochospiral and umbilicate with 6 globular to ovate chambers. The equatorial view is circular. Wall is calcareous, and the surface is rugose. Sutures are radial and depressed on the umbilical side.

The wall is thick in thin section specimens. It is differentiated from other *Ticinella* members by having fewer chambers in the final whorl.

Ticinella bejaouaensis Sigal, Plate 4, figs. 1-4

Type reference: *Ticinella bejaouaensis* Sigal, 1966, p. 103, pl. 9, figs. 4-5

Diagnosis: Test is low trochospiral, with globular to ovate overlapping chambers in thin section. The peripheral outline is elongated and ovate. The wall is very thick and umbilicus is wide.

Biticinella breggiensis (Gandolfi), Plate 6, figs. 8-11

-Type reference: *Anomalina breggiensis* Gandolfi, 1942, p. 102-103, pl. 3, fig. 6, pl. 5, fig. 3; pl. 9, fig. 1,; pl. 13, figs. 7-8

-*Biticinella breggiensis* Sigal, 1956, p. 35

Diagnosis: The test is planispiral, biumbilicate. The peripheral outline is sub-circular and lobulate in transverse section. The final whorl has seven chambers which increase in size gradually as added. The test surface is hispid. The sutures are straight and radial on the spiral side.

Hedbergella simplex (Morrow), Plate 6, figs. 1-6; Plate 24, fig. 8

-Type reference*: Hastigerinella simplex* Morrow, 1934, p. 198, pl. 30, fig. 6

-*Hedbergella simplex* Robaszynski & Caron, 1979, p. 145, pl. 29, figs. 1- 3; pl.30, figs. 1-2

Diagnosis: Test trochospiral, five to six chambers in final whorl. The initial chambers are globular and the final chamber is more elongated and clavate. The sutures on the spiral side are radial and depressed. The outline in thin section specimen is ovate.

Globigerinellodies bentonensis (Morrow), Plate 4, fig. 16; Plate 5, figs. 12-15;

-Type reference: *Anomalina bentonensis* Morrow, 1934, p.201 pl. 30 figs. 4 (a-b)

-*Globigerinelloides bentonensis* Loeblich & Tappan, 1961, p.267, pl. 2, fig. 8-10

Diagnosis: Planispiral test, biumbilicate, and is elongated in thins section.

Ticinella praeticinensis Sigal, Plate 4, fig. 18

-Type reference: *Ticinella praeticinensis* Sigal, 1966, p. 195, pl. 2, figs. 3-8, pl. 3, figs. 1-6

Diagnosis: This species falls in between *Ticinella* and *Rotalipora* and the chambers are rounded to sub-rounded, which will eventually convert to the angular periphery of *Rotalipora*.

Rotalipora subticinensis (Gandolfi), Plate 6, fig.16

-Type reference: *Globotruncana (Thalmanninella) ticinensis subticinensis* Gandolfi, 1957, p.59 pl. 8 figs. 1 (a-c)

-*Rotalipora subticinensis* Caron, 1985, p.73, pl. 33, figs. 1-2

Diagnosis: Trochospiral test with angular to subangular chambers. Sutures are curved and thickened, while periphery is angular and keeled.

Rotalipora ticinensis (Gandolfi), Plate 6, fig. 17; Plate 7, figs. 1-2

-Type reference: *Globotruncana ticinensis* Gandolfi, 1942, p. 113, pl. 2, fig. 3 (a-c)

-*Rotalipora ticinensis* Caron & Luterbacher, 1969, p. 25, pl. 8, fig. 6 (a-c)

Diagnosis: Trochospiral test with angular chambers, which also give the test an angular outline. Angular periphery is keeled. Sutures are elevated and thick.

Planomalina buxtorfi (Gandolfi), Plate 7, figs. 7-13; Plate 24, fig. 13

-Type reference:*Planulina buxtorfi* Gandolfi, 1942, p. 103, pl. 3, fig. 7; pl. 5, figs. 3–6; pl. 6, figs. 1–3; pl. 8, fig. 8; pl. 9, fig. 2; pl. 12, fig. 2; pl. 13, figs. 13, 15; pl. 35, figs. 1–11

-*Planomalina buxtorfi* Loeblich & Tappan, 1961, p. 269, pl. 2, figs. 1-2

Diagnosis: Test is planispiral, which is partly evolute, having eight to ten chambers in the final whorl. Sutures are thick, elevated, and curved, giving ornamenation to the perforated calcareous wall. It has a well developed peripheral keel. The keeled and the biumbilicate nature can be observed in the thin section specimens.

Praeglobotruncana delrioensis (Plummer), Plate 7, figs. 14-15; Plate 24, fig. 14

-Type reference: *Globorotalia delrioensis* Plummer, 1931, p. 199-200, pl. 13, figs. 2a-c

-*Praeglobotruncana delrioensis* Bermudez, 1952, p.52 pl. 7; fig. 1

Diagnosis: Test is trochospiral with 5 chambers in the last whorl. The chambers look ovate in thin section with carina on the early chambers, which is less distinct in the final chambers. The sutures are straight, and radial in pattern on the spiral. Calcareous, perforated wall, with pustules on the surface. The early chambers are rugose with a keel.

Rotalipora appenninica (Renz), Plate 8, figs. 1-6; Plate 25, figs. 4-5

-Type reference: *Globotruncana appenninica* Renz, 1936, p. 20, pl. 6, figs. 1-11; pl. 7, fig. 1; pl. 8, fig. 4

-*Rotalipora appenninica* Caron & Luterbacher, 1969, p.26 pl. 8; fig. 8

Diagnosis: Test low trochospiral, six to nine chambers in last whorl. The initial chambers are not clearly visible. Chambers are broad, inflated, and are lunate in outline on the spiral side. Periphery is angular and keeled. Sutures are thick, raised, curved, and oblique on the spiral side. The final chamber is more elongated.

Hedbergella lybica Barr, Plate 25, figs. 1-3

-Type reference: *Hedbergella libyca* Barr, 1972, p. 14, pl. 10, figs. 5a-c

Diagnosis: Test is low to medium trochospiral, with an almost rounded periphery. The chambers are spherical. The surface is pustulose. These pustules fuse meridonally, which results in costellae. Sutures are radial and depressed on both sides.

Heterohelix moremani (Cushman), Plate 4, fig. 15; Plate 7, figs. 16-17

-Type reference: *Guembelina moremani* Cushman, 1938, p. 10, pl.2, figs. 1-3

-*Heterohelix moremani,* Pessagno, 1967, p. 260-261, pl. 48; figs. 10-11; pl.89, figs. 1-2

Diagnosis: Slender biserial test with six to nine chambers arranged biserially.The surface is smooth.

Globigerinelloides ultramicrus (Subbotina), Plate 4, figs. 12-14; Plate 7, fig. 18

-Type reference: *Globigerinella ultramicra* Subbotina, 1949, p.33, pl. 1; figs. 17-18

- *Globigerinelloides ultramicrus* Leckie, 1984, p. 614, pl. 11, figs. 10-11

Diagnosis: Test planispiral, biumbilicate, and elongated. It is laterally compressed with elongated chambers in thin section as compared to *G. bentonensis*.

Rotalipora balernaensis (Gandolfi), Plate 7, figs. 19-20

-Type reference: *Globotruncana appenninica balernaensis* Gandolfi 1957, p. 60, pl. 8, figs. 3 (a-c)

-*Rotalipora balernaensis* Sigal 1969, p. 635, pl. 2, figs. 2, 4, 5-8

Diagnosis: Test is trochospiral, with angular and keeled periphery. The chambers have slightly greater breadth than height, which gives a wedge shape to these chambers. The sutures are raised.

Praeglobotruncana stephani (Gandolfi), Plate 8, figs. 7-13; Plate 26, fig. 2

-Type reference: *Globotruncana stephani* Gandolfi, 1942, p.130, pl. 3, figs. 4 (a-c)

-*Praeglobotruncana stephani* Bolli et al. 1957, p. 39, pl. 9, fig. 2

Diagnosis: Trochospiral test, which is highly convex on the spiral side. The initial chambers are sub-rounded, while chambers become sub-angular in final stage. Sutures are thick, raised, and curved. The peripheral keel is prominent in early chambers and becomes less distinct in last chambers.

Globigerinelloides caseyi (Bolli, Loeblich, and Tappan), Plate 8, figs. 15-16

-Type reference: *Planomalina caseyi* Bolli et al. 1957, p.24, pl. 1, figs. 4-5

-*Globigerinelloides caseyi* Low, 1964, p.122-123

Diagnosis: Planispiral test, biumbilicate with spherical to sub-globular chambers.

Rotalipora gandolfi (Luterbacher & Premoli-Silva), Plate 9, figs. 1-3; Plate 25, fig. 8

-Type reference: *Rotalipora appenninica gandolfi* Luterbacher & Premoli-Silva, 1962, p.267

-*Rotalipora gandolfi* Caron & Luterbacher, 1969, p. 26-27, pl. 9, fig. 9

Diagnosis: Test is low trochospiral with 6 to 7 chambers in the last whorl. The periphery is angular and keeled. Chambers are inflated and are angular to ovate in outline on umbilical side. Sutures are radial and depressed on umbilical side. Umblicus shallow and wide.

Rotalipora brotzeni (Sigal), Plate 9, figs. 4-7, 16; Plate 25, figs. 6-7

-Type reference: *Thalmanninella brotzeni* Sigal, 1948, p.102, pl. 1, figs. 5(a-c)

-*Rotalipora brotzeni* Robaszynski & Caron, 1979, p. 65, pl. 6, figs. 1-2

Diagnosis: Test is low trochospiral, and is convex on umbilical side. Periphery is slightly lobulate and keeled. Five chambers occur in the last whorl, which are more or less triangular on umbilical side. Calcareous, faintly perforated. The umbilicus is moderately wide and deep**.**

Rotalipora montsalvensis (Mornod), Plate 9, figs. 8-10

-Type reference: *Globotruncana* (*Rotalipora*) *montsalvensis* Mornod, 1949, p. 584-5, fig. 4 (I a-c)

-*Rotalipora montsalvensis* Caron, 1976, p. 329-330, figs. 1 (a-c)

Diagnosis: Test is low trochospiral with inflated, elongated chamber. The sutures are straight to slightly curved and elevated.

Praeglobotruncana gibba (Klaus), Plate 9, figs. 11-14; Plate 26, fig. 3

-Type reference: *Praeglobotruncana stephani* var. *gibba* Klaus, 1960, p. 304

- *Praeglobotruncana gibba,* Caron, 1985, p. 68-69, figs. 30 (5-6)

Diagnosis: Test is slightly higher trochospiral, with angulae and keeled periphery. Spiral side is less convex than *Praeglobotruncan stephani*. The central area on the spiral side is raised. The sutures are thickened, curved and elevated.

Rotalipora reicheli Mornod, Plate 9, fig. 15

-Type reference: *Globotruncana* (*Rotalipora*) *reicheli* Mornod, 1949, p. 583-4, figs. 5 (IV a-c)

Diagnosis: Test is low trochospiral, which can be readily recognised by its distinct plano-convex test shape, which can be seen in thin section.

Rotalipora greenhornensis (Morrow), Plate 9, figs. 17-21; Plate 25, fig. 12; Plate 26, fig. 1

-Type reference: *Globorotalia greenhornensis* Morrow, 1934, p. 199-200, pl. 31, fig. 1

-*Rotalipora greenhornensis* Pessagno, 1967, p. 295-297, pl. 51, figs. 13-21

Diagnosis: Test is low trochospiral, having six crescent-shaped chambers in the last whorl. The spiral side is convex with strongly curved and raised sutures. Wall is calcareous, finely perforated.

Rotalipora cushmani (Morrow), Plate 10, figs. 1-17; Plate 25, figs. 9-11

-Type reference: *Globorotalia cushmani* Morrow, 1934, p.199, pl.31, figs. 2, 4

-*Rotalipora cushmani* Sigal, 1948, p. 96, pl. 1, fig. 2; pl.2, fig. 1

Diagnosis: Test low to medium trochospiral, having 4 to 6 inflated chambers in the last whorl. The periphery is strongly lobulate with a thick beaded protruding keel. The umbilicus is wide and deep.

Dicarinella algeriana (Caron), Plate 11, figs. 12-21

-Type reference: *Praeglobotruncana algeriana* Caron, 1966, p. 74-75, for figs. see

Reichel, 1950, pl. 16, fig. 8; pl. 17, fig. 8

-*Dicarinella algeriana* Robaszynski & Caron, 1979, p. 57, pl. 50, figs. 1-2

Diagnosis: This species is ancestral to the Genus *Dicarinella* and it is transitional from *Praeglobotruncana stephani* to *Dicarinella imbricata* and has therefore an in between morphology, however it lacks a true thick keel. This species has rectanglar peripheral margins in thin section.

Dicarinella imbricata (Mornod), Plate 12, figs. 1-2; Plate 26, figs. 4-5

-Type reference: *Globotruncana imbricata* Mornod, 1949, p. 581, fig. 5 (IIIa-d)

-*Dicarinella imbricata* Caron, 1976, p. 332-333, fig. 3

Diagnosis: Test is trochospiral with five chambers. A diverging beaded keel results in an imbricated pattern.

Rotalipora deekei (Franke) Plate 12, figs. 3-6

-Type reference: *Rotalia deeckei* Franke, 1925 p. 90, pl. 8, fig. 7 (a-c)

-Robaszynski & Caron, 1979, p. 75, pl. 9, figs. 1 (a-e), 2 (a-c); pl.10, figs.1 (a-e), 2 (a-c)

Diagnosis: Trochospiral test with angular to wedge shaped chambers. The periphery is angular with a thick keel. It closely resembles *R. greenhornensis* but it is smaller in size.

Rotalipora globotruncanoides Sigal, Plate 12, figs. 7-8

-Type reference: *Rotalipora globotruncanoides,* Sigal, 1948, p. 100, pl. 1, figs. 4 (a-c)

Diagnosis: Trochospiral test with trapezoidal to angular shaped chambers. The last chambers are more angular, and are petaloid in outline. The periphery is angular with a thick keel. It can be differentiated from the *Rotalipora greenhornensis* by its small and compressed test.

Whiteinella praehelvetica (Trujillo), Plate 11, figs. 4-6

-Type reference: *Rugoglobigerina praehelvetica* Trujillo, 1960, p.340, pl. 49, fig. 6.

-*Whiteinella praehelvetica* Peryt, 1983, p.477, pl. 31, fig. 2

Diagnosis: Test is low trochospiral, while the chambers are globular. Wall is thick and pustulose.

Whiteinella aumalensis (Sigal), Plate 11, figs. 1-3

-Type reference: *Globigerina aumalensis* Sigal, 1952, p. 28, fig. 29

-*Whiteinella aumalensis*: Premoli-Silva, 1994, p. 55, pl. 11, figs. 4-5

Diagnosis: Test is low trochospiral; chambers are angular and fork-like in thin section specimens. Wall is thick and pustulose. The sutures are elevated.

Whiteinella paradubia (Sigal), Plate 12, figs. 9-10

-Type reference: *Globigerina paradubia* Sigal, 1952, p.28. fig. 28

-*Whiteinella paradubia,* Robaszynski & Caron, 1979, p. 181-184, pl. 39, figs. 1a-2c

Diagnosis: Test is slightly higher trochospiral, with globular chambers. Wall is thick and pustulose. It is differentiated from other *Whiteinella* species by having a higher trochospire and large number of chambers.

Whiteinella archaeocretacea (Pessagno), Plate 12, figs. 11-13; Plate 26, figs. 8-9

-Type reference: *Whiteinella archaeocretacea* Pessagno, 1967, p. 298, pl. 54, figs. 22-24

Diagnosis: Test is low trochospiral with 5 to 6 chambers in the last whorl, which increase rapidly in size as added. The periphery is rounded. Chambers are separated by curved to straight depressed sutures. Surface of the test is coarsely rugose. Umbilicus is shallow and wide. The chambers look ovate in thin section.

Helvetoglobotruncana helvetica (Bolli). Plate 12, figs. 14-22; Plate 26, figs. 10-12

-Type reference: *Globotruncana helvetica* Bolli, 1945, p. 226, pl. 9, fig. 6

-*Helvetoglobotruncana helvetica* Caron, 1985, p. 68-69, figs. 30 (7-8)

Diagnosis: Test is arranged in a low trochospire. The spiral side is flat while the chamber on the umbilical side, inflated. The chambers on the spiral side have a hemispherical shape, which give rise to staircase-like imbricate pattern. The peripheral margin is marked by a single keel. The surface is rugose. The sutures are curved and elevated on the spiral side while radial and depressed on the umbilical side.

Whiteinella baltica Douglas & Rankin, Plate 11, figs. 8-11

-Type reference: *Whiteinella baltica* Douglas & Rankin, 1969, p.198, figs. 9a-c

Diagnosis: It can be distinguished from the *Whiteinella archaeocretacea* by the shape of its chambers which are more globular in *Whiteinella baltica* while ovate in *Whiteinella archaeocretacea* in thin section.

Whiteinella aprica (Loeblich & Tappan), Plate 13, figs. 1-2

-Type reference: *Ticinella aprica* Loeblich & Tappan, 1961, p. 292, pl. 4, figs. 14-16

-*Whiteinella aprica* Eicher & Worstell, 1970, p. 314, pl. 11, figs. 7(a-c); pl. 12, figs. 1-2

Diagnosis: Trochospiral test with globular chambers and thick pustulose wall. It resembles *Whiteinella brittonensis* in thin section. It can be distinguished from *Whiteinella brittonensis* by its low trochospire, while its larger size differentiates it form other members of this genus.

Whiteinella brittonensis (Loeblich & Tappan), Plate 13, figs. 3-4

-Type reference: *Hedbergella brittonensis* Loeblich & Tappan, 1961, p. 274-275, pl. 4, figs. 1-8

-*Whiteinella brittonensis* Robaszynski & Caron, 1979, p. 175, pl. 37, fig. 1; pl. 38, figs. 1, 2

Diagnosis: It can be distinguished from *Whiteinella aprica* by its high spiral chambers which are more globular, and by a thick rugose wall.

Whiteinella inornata (Bolli) Plate 13, figs. 12-13

-Type reference: *Globotruncana inornata* Bolli, 1957, p.57 pl. 13 figs. 5a-c

-*Whiteinella inornata* Caron, 1985, p.78 figs. 37 (6-7)

Diagnosis: It resembles morphology of *Whiteinella archaeocretacea* and can be differentiated from it by having a sharp angled periphery.

Dicarinella canaliculata (Reuss), Plate 13, figs. 5-7

-Type reference: *Rosalina canaliculata* Reuss, 1854, p.70, pl. 26 figs. 4 (a-b)

-*Dicarinella canaliculata* Caron, 1985, p.44 figs. 17 (5-6)

Diagnosis: The two parallel keels are visible as one thick keel in thin section. As both sides are flat, the peripheral outline is parallelogram shaped in thin section. The sutures on the spiral side are raised and can be observed in thin section.

Dicarinella hagni (Scheibnervoa), Plate 13, figs. 8-10

-Type reference: *Praeglobotruncana hagni* Scheibnerova, 1962, p.219, figs. 6(a-c)

-*Dicarinella hagni* Robaszynski & Caron, 1979, p. 79, pl. 56, figs.1-2; pl. 57, figs.1-2. pl. 57, figs.1-2

.*Diagnosis:* Trochospiral test with a thick peripheral keel. The chambers are angular with slightly curved elevated sutures. It can be distinguished from *Dicarinella algeriana* and *Dicarinella imbricata* by its large size.

Marginotruncana sigali (Reichel), Plate 14, figs. 1-4; Plate 27 fig. 3

-Type reference: *Globotruncana* (*Globotruncana*) *sigali* Reichel, 1950, p.610, figs. 5 (a-c)

-*Marginotruncana sigali* Caron, 1985, p. 63, 64 figs. 27 (7-8)

Diagnosis: Moderate trochospiral test with 4 to 5 elongated, lunate chambers. The periphery is angular in thin section specimen. Thick single peripheral keel is seen. Thick, raised, and beaded sutures give the chambers depressed appearance.

Marginotruncana pseudolinneiana (Pessagno), Plate 14, figs. 10-11; Plate 27, figs. 7-9

-Type reference: *Marginotruncana pseudolinneiana* Pessagno, 1967, p. 310, pl. 65, figs. 24-27

Diagnosis: Test is trochospiral and has close resemblance with *Globotruncana linneiana*. Test is plain on both sides. The chambers are 5 to 6 in number and are lunate on the spiral side and subrectangular shaped on umbilical side. These chambers increase in size gradually when added. The periphery has a double keel. The sutures are curved, beaded, and elevated on spiral side, and are straight on umbilical side. The wall is hyaline. The subrectangular shape of chambers can also be observed in thin section.

Marginotruncana sinuosa Porthault, Plate 15, fig. 3; Plate 27, figs. 4-5

-Type reference: *Marginotruncana sinuosa* Porthault, 1970, p. 81-82, pl. 11, figs.11-13

Diagnosis: Trochospiral test, with 6 to 7 lunate chambers in the last whorl. The spiral side is convex with a raised central part. The beaded carinae are distinct on the early chambers, which become less pronounced in the last chambers. Sutures curved, thick, beaded, and raised on the spiral side. This species is transitional to *Contusotruncana fornicata* but differs from it by having a lower trochospire and by lacking early globular chambers.

Marginotruncana renzi (Gandolfi), Plate 14, figs. 9,18; Plate 27, fig. 10

-Type reference: *Globotruncana renzi* Gandolfi, 1942, p.124-125 pl. 3 fig. 1; pl. 4 fig. 16

-*Marginotruncana renzi* Caron, 1985, p. 63-4, figs. 27.1-2

Diagnosis: Test is low trochospiral with lobulate periphery having 5 to 6 chambers in the final whorl. The chambers are elongate, and petaloid in shape on spiral side. Spiral side is planiform with curved, elevated, beaded sutures. Peripheral keel present on the spiral side.

Marginotruncana coronata (Bolli) Plate 14, figs. 13-17, 19-21

-Type reference: *Globotruncana lapparenti coronata* Bolli, 1945, p. 233, pl. 9, fig. 15

-*Marginotruncana coronata* Pessagno, 1967, p. 305-306, pl. 65 figs., 11-13, pl. 100 fig. 6

Diagnosis: Trochospiral test with angular to rhomboid chambers. The outline in thin section is more or less rectangular with a peripheral keel. It differs from *Marginotruncana pseudolinneiana* by its larger size and strongly compressed test profile.

Marginotruncana marianosi (Douglas), Plate 14, fig. 12

-Type reference: *Globotruncana marianosi* Douglas, 1969, p.183, figs. 5 (a-c)

-*Marginotruncana marianosi* Caron, 1985, p.62 figs. 26 (5-6)

Diagnosis: Trochospiral test with an angular, sharp, and keeled, periphery. The sutures are raised. In thin section it resembles *Rotalipora* in test outline.

Marginotruncana marginata (Reuss), Plate 14, fig. 22

-Type reference: *Rosalina marginata* Reuss, 1845, p. 36, pl. 8, figs.54 (a, b), 74 (a, b); pl, 13, figs. 68 (a-b)

-*Marginotruncana marginata* Pessagno, 1967, p. 307-310, pl. 54, figs. 7-12, 16-18; pl. 56, fig. 10; pl. 99, figs. 5-7

Diagnosis: Trochospiral test with keeled periphery and raised sutures. The last chambers are seen as polygonal in thin section.

Marginotruncana schneegansi (Sigal), Plate 14, figs. 5-8

-Type reference: *Globotruncana schneegansi* Sigal, 1952, p.33, fig. 34

-*Marginotruncana schneegansi* Caron, 1985, p. 63-64, figs. 27 (3-4)

Diagnosis: Trochospiral test with keeled periphery, and has petaloid-shaped chambers, which are seen as angular in thin section.

Hedbergella flandrini Porthault, Plate 14, figs. 23-25

-Type reference: *Hedbergella flandrini* Porthault, 1970, p.64, pl. 10, figs. 1-3

Diagnosis: Test low trochospiral with rapidly enlarging chambers as added. The initial chambers are globular and last chambers are ovate in outline in thin section and hence the overall outline also looks ovate.

Heterohelix reussi (Cushman), Plate 13, figs. 14-21; Plate 29, figs. 10-12

-Type reference: *Guembelina reussi* Cushman, 1938, p.11, pl. 2 figs. 6 (a-b)

-*Heterohelix reussi* Pessagno, 1967, p. 263, pl. 85, figs. 1-9; pl. 86, figs. 1-2

Diagnosis: Test biserial, tapering, with inflated to globular chambers. Chambers increase regularly as added. The aperture is located high as narrow arc at the base of

final chamber. The sutures are depressed. It can be differentiated from the *Heterohelix globulosa* by its slightly compressed chambers and from *H. striata* by its finer costae.

Archaeoglobigerina cretacea (D' Orbigny) Plate 15, figs. 8-9

-Type reference: *Globigerina cretacea* D' Orbigny, 1840, p.34 pl. 3 figs. 12-14

-*Archaeoglobigerina cretacea* Rodriguez, 1977, p. 72-77, pl. figs.1-2

Diagnosis: Test is trochospiral with globular chambers. The periphery is sub-rounded to rectangular with two faint keels which merge into one thick keel in thin section.

Dicarinella concavata (Brotzen) Plate 15, figs. 10-13

-Type reference: *Rotalia concavata* Brotzen, 1934, p. 66, pl. 3, fig. b

-*Dicarinella concavata* Caron, 1985, p. 45, figs. 17 (7–8)

Diagnosis: Test is trochospiral, peripheral outline lobulate with two closely spaced keels which merge into one thick keel in thin section. The chambers are hemispherical and look lunate in outline. The sutures are curved and raised.

Contusotruncana fornicata (Plummer), Plate 15, figs. 14, 17-18; Plate 21, figs. 1, 13; Plate 28, figs. 9-11; Plate 29, figs. 1-2

-Type reference: *Globotruncana fornicata* Plummer, 1931, p. 130, pl. 13, figs. 4 (a-c)

-*Contusotruncana fornicata*, Loeblich & Tappan, 1988, p. 468; pl. 503, figs. 4-7

Diagnosis: Test is moderately high trochospiral with 5 to 6 chambers in the final whorl. The chambers are elongated and subcrescentic on spiral side, while subrectangular on umbilical side. The sutures are thick, beaded, and raised on the spiral side and strongly depressed on the umbilical side. The subrectangular shape of the chambers, keel, and thick raised sutures can be observed in thin section. It is transitional from *Marginotruncana sinuosa* and can be differentiated from it, by its large chamber size and slightly higher trochospire.

Dicarinella primitiva (Dalbiez), Plate 15, figs. 4-7; Plate 27, fig. 2

-Type reference: *Globotruncana* (*Globotruncana*) *ventricosa primitiva* Dalbiez, 1955, p.171, fig. 6

-*Dicarinella primitiva* Robaszynski & Caron, 1979, p. 96, pl. 60, 47 figs. 1 (a-c)

Diagnosis: Trochospiral test with inflated chambers on umbilical side. It differs from *Dicarinella concavata* by having less inflated chambers on umbilical side and from *Marginotruncana schneegansi* by having two well developed keels which however look like one in thin section. The umbilicus is wide and shallow.

Pseudoguembelina costulata (Cushman) Plate 15, figs. 15-16; Plate 29, fig. 9

-Type reference: *Guembelina costulata* Cushman, 1938, p.16, pl. 3, figs. 7 (a-b)

-*Pseudoguembelina costulata*, Douglas, 1969, p.160, pl. 11, fig. 6

Diagnosis: Biserial test with subtriangular outline. Wall with irregular, raised, and imperforate costae. The intercostae areas are perforated.

Dicarinella asymetrica (Sigal), Plate 15, figs. 19-20; Plate 27, fig. 6

-Type reference *Globotruncana asymetrica* Sigal, 1952, p. 34–35, fig. 35

-*Dicarinella asymetrica* Caron, 1985, p. 43, figs. 17 (3–4)

Diagnosis: The test is low trochospiral and is flat with double keels which merge into one in thin section specimens. The early chambers are raised and globular and later chambers become petaloid in shape.

Globotruncana linneiana (D' Orbigny), Plate 16, figs. 1-3, 5-6; Plate 27, figs. 11-12

-Type reference: *Rosalina linneiana* D' Orbigny, 1839, p.101, pl.15, figs. 10-12

-*Globotruncana linneiana* Bronnimann & Brown, 1956, p.542 pl. 20 figs. 13-15

Diagnosis: Test is low trochospiral with near circular outline. The final whorl shows 6 chambers which increase gradually in size as added, overlapping one another, and

is lunate in spiral view. The wall is finely perforated. The spiral side is almost flat with lobulate periphery. Sutures are curved, elevated and thick on spiral side. It can be differentiated from *Globotruncana lapparenti* by its thick keel. The peripheral outline in thin section is subrectangular and so are the shapes of final chambers.

Globotruncanita elevata (Brotzen), Plate 16, figs. 7-12; Plate 22, fig. 12; Plate, 23, figs. 4-5

-Type reference: *Rotalia elevata* Brotzen, 1934, p. 66, pl. 3, fig. c

-*Globotruncanita elevata* Robaszynski et al. 1984, p. 228, 230, pl. 27, figs. 1–3; pl. 28, figs. 1–3

Diagnosis: Test is low trochospiral, chambers angular to subangular. The pointed periphery is keeled with elevated and thick sutures.

Globotruncana leupoldi Bolli, Plate, 21, fig. 4

Type reference: *Globotruncana leupoldi,* Bolli, 1945, p. 235

Diagnosis: Trochospiral test, with chamber showing rectangular outline in thin section. Strong thick keel peripheral is developed. The raised sutures give irregular outline to the periphery of the test in thin section. It can be differentiated from *Globotruncana arca* by having low trochospire.

Globotruncana orientalis El Naggar, Plate 22, fig. 2

Type reference: *Globotruncana orientalis, El Naggar,* 1966, p. 125, pl. 12, figs. 4 a-d

Diagnosis: Trochospiral test, with lobulate to irregular peripheral outline. Thick keel and raised sutures are present. It can be differenciated from *Globotruncana leupoldi* by its high trochospire.

Globotruncana dupeublei Caron et al. Plate, 22, fig. 3

-Type reference *Globotruncana dupeublei,* Caron in Robaszynski et al., 1984, p. 188, pl. 1, figs. 1,5; p. 190, pl. 7, figs. 1,2; pl. 8, figs. 1–3

Diagnosis: Moderate trochospiral, biconvex test. The umbilical side is more convex than the spiral side. Sutures are thick, curved, and raised. Chambers have rectangular to rounded outline in thin section. The unmbilicus is deep and wide.

Globotruncana lapparenti Brotzen Plate 16, figs. 13-14; Plate 21, fig. 3; Plate 28, fig. 8

-Type reference: *Globotruncana lapparenti* Brotzen, 1936, p.175-176, pl.5, fig. 2 (a, d, m, n)

Diagnosis: Test is very low trochospiral with flat to slightly convex spiral side. The spiral side carries 6 to 7 chambers, which are almost rectangular in thin section, giving rectangular periphery. The equatorial periphery is lobulate. Wall is all perforated, with raised, thick, and beaded sutures particularly in initial chambers. It is similar in appearance to *Globotruncana linneiana* and can be differentiated from it by having a slightly weaker keel.

Ventilabrella glabrata Cushman, Plate 18, fig. 3; Plate 23, fig. 15

-Type reference: *Ventilabrella eggeri* var. *glabrata* Cushman, 1938, p. 26, pl. 4, figs. 15-17

Diagnosis: Laterally compressed, tapering test. The side view is showing only uniserial arrangement of chambers. Wall is thick, while the sutures are straight and depressed.

Ventilabrella eggeri Cushman, Plate 22, fig. 7; Plate 29, fig. 8

-Type reference: *Ventilabrella eggeri*, Cushman, 1928, p. 2, pl. 1, figs. 10-12

Diagnosis: Test is biserial in early stages, while the globular chambers proliferate in late stage making fan shaped geometry. The sutures are depressed. The test is heavily costate. The costae are meridionally arranged. Aperture is present at the base of chambers in multiserial stage. It can be differentiated from the species of *Planoglobulina* by having appressed test in proliferation stage.

Ventilabrella multicamerata de Klasz, Plate 16, fig. 16

-Type reference: *Ventilabrella multicamerata* de Klasz, 1953, p. 230, pl. 5, figs. L (a-lb)

Diagnosis: Test is subtriangular to flabelliform or fan like, chambers pyriform or pear like, early stage chambers are arranged biserially while in late chambers there is rapid growth of chambers in the plane of biseriality. The sutures are distinct and depressed.

Globotruncana bulloides (Vogler), Plate 17, figs. 1-4; Plate 28, figs. 1-3

-Type reference: *Globotruncana linnei bulloides* Vogler, 1941, p.287 pl. 23 figs. 32-39

-*Globotruncana bulloides*, Pessagno, 1967, p.325, fig. 33

Diagnosis: The biconvex, low trochospiral, test carries five to six angular, inflated chambers in the last whorl, which increase in size as added. The chambers make an imbricated pattern on the spiral side. The central part of chambers is slightly rugose. The equatorial periphery is lobulate with two widely spaced beeded keels. Sutures on the spiral side are curved, raised and beaded.

Globotruncana arca (Cushman), Plate 17, figs. 5-10; Plate 29, figs. 3-6

-Type reference: *Pulvinulina arca* Cushman, 1926, p. 23, pl. 3, figs. 1 (a–c)

-*Globotruncana arca* Robaszynski et al., 1984, p. 182-84, pl. 1, figs. 2–3; pl. 4, figs. 1–3

Diagnosis: Test is low trochospiral with 6 angular chambers in last whorl, which are inflated on the spiral side. The chambers increase in size gradually as added. The spiral side is convex, while the equatorial periphery is lobulate. The beeded keels are present in the early chambers, and are not developed on the final chambers. The sutures are curved, strongly elevated, and beaded on spiral side. The wall is perforated with smooth surface. Thick keel, raised sutures, and angular chambers can also be well seen in the thin section.

Globotruncanita stuartiformis (Dalbiez), Plate 20, fig. 2; Plate 23, fig. 8; Plate 28, figs. 4-7

-Type reference: *Globotruncana elevata stuartiformis* Dalbiez, 1955, p.169, figs. 10 (a-c)

-*Globotruncanita stuartiformis* Caron, 1985, p. 55-56 figs. 23 (4-5)

Diagnosis: Test is very low trochospiral with 6 to 8 subangular chambers in the last whorl. The chambers increase in size as added and are slightly inflated, overlapping one another. The spiral side is slightly convex in its centre. The equatorial periphery is circular to slightly lobulate with one beaded keel. These beads are absent on the last chamber. The wall is perforate with smooth surface. The sutures are raised, beaded, curved becoming straight and tangential in the last whorl.

Heterohelix striata (Ehenberg), Plate 30, figs. 3-5

-Type reference: *Textularia striata* Ehenberg 1840, p.135, pl.4 figs. 1a, 2a, 3a

-*Heterohelix striata* Olvera, 1959, p. 71-72, pl.2, figs. 4, 8

Diagnosis: Biserially arranged globular chambers, flattened in the earlier part and later become spherical. The chambers increase in size as added. The periphery is lobulate. The wall is calcareous, perforated and costate. The sutures are distinct, straight, depressed. The primary aperture broad, low arc with a lip. It differs from *Heterohelix globulosa* in having fewer and strongly developed costae.

Heterohelix globulosa (Ehrenberg) Plate 17, figs. 11-17

-Type reference: *Textularia globulosa* Ehrenberg, 1840, p.135, pl. 4, figs. 2-8

-*Heterohelix globulosa* Montanaro Gallitelli, 1957, p. 137, pl. 31, figs. 12-15

Diagnosis: Biserial elongate test with globular chambers, which increase gradually in size as added. The final chambers increase very rapidly in size. The sutures are thick curved and depressed in thin section.

Heterohelix planata (Cushman), Plate 18, figs. 1-2

-Type reference: *Guembelina planata* Cushman, 1938, p. 2, pl. 2, figs. 13-14

-*Heterohelix planata* Huber, 1990, pl. 1, figs. 5-6

Diagnosis: Test biserial, elongated, with 6 to 7 globular chambers arranged in pairs. The sutures curved and depressed. Wall is thick. It can be differentiated from *H. globulosa* by its more compressed test.

Heterohelix carinata (Cushman), Plate 21, fig. 9

-Type reference: *Gümbelina carinata* Cushman, 1938, p. 18, pl. 3, fig. 10

- Premoli-Silva & Sliter, 1994, p. 81, pl. 24, figs. 13-14

Diagnosis: Test biserial having four to five chambers arranged in pairs but only one set of chambers is visible in thin sections. The periphery is elongated and carinate. The sutures are straight and depressed.

Laeviheterohelix glabrans (Cushman), Plate 16, fig. 15; Plate 20, fig. 17; Plate 21, figs. 8, 11

-Type reference: *Guembelina glabrans* Cushman, 1938, p. 15, pl. 3, figs. 1, 2

-*Laeviheterohelix glabrans* Nederbragt, 1991, p. 353, pl. 5, figs. 6 (a-b)

Diagnosis: Test is biserial with five to six chambers, but only one set of chambers is visible in thin section specimen. The periphery is slender. The chambers are reniform in thin section specimens.

Globotruncana hilli Pessagno Plate 18, figs. 4-7

-Type reference: *Globotruncana hilli* Pessagno, 1967, p. 343, pl. 64, figs. 9-14; p. 21-3, pl. 94, fig. 1

Diagnosis: Test is low trochospiral, chambers increasing rapidly in size. These chambers are globular initially, while it becomes subrectangular later. The sutures are raised to depressed. The peripheral outline is subrectangular with a thick keel.

Pseudotextularia elegans (Rzehak), Plate 20, figs. 4-6; Plate 30, fig. 7

-Type reference: *Cuneolina elegans* Rzehak, 1891, p.4

-*Pseudotextularia elegans* Caron, 1985, p. 55-56 fig. 24 (20-21)

Diagnosis: Slender elongated biserial test with lobulate periphery. The inflated chambers increase in size as added. Calcareous, finely perforated wall, while the sutures are depressed.

Rugoglobigerina rugosa (Plummer), Plate 18, fig. 8

-Type reference: *Globigerina rugosa* Plummer, 1926, p.38, pl.2, figs. 10 (a-d)

-*Rugoglobigerina rugosa*, Caron, 1985, p.74, figs 34.9-10

Diagnosis: The test has rounded periphery, with globular chambers. The surface is rugose. The sutures are curved and depressed.

***Rugoglobigerina milamensis* Smith & Pessagno, Plate, 23, fig. 10**

Type reference: *Rugoglobigerina milamensis* Smith & Pessagno, 1973, p. 56, pl. 24,

figs. 4-7

Diagnosis: Biconvex, trochospiral test with spherical to ovoidal chambers. Sutures are straight and depressed. Surface rugosities are not visible in thin section. Test with thick peripheral keel present. It has higher trochospire than the other members of the same genus.

Globotruncana ventricosa (White) Plate 19, figs. 1-9

-Type reference: *Globotruncana canaliculata* (Reuss) var. *ventricosa* White, 1928, p. 284, pl. 38, figs. 3 (a–c)

-*Globotruncana ventricosa* Robaszynski et al., 1984, p. 214-16, pl. 20, figs. 1–3; pl. 21, figs. 1–4

Diagnosis: Test is very low trochospiral with angular chambers. The sutures are thick, curved, raised. According to Robaszynski et al (1984) it evolved from *G. linneiana* and that is why it has slight resemblance with it in some thin section specimen.

Globotruncana carinata Dalbiez Plate 18, figs. 9-16

-Type reference: *Globotruncana* (*Globotruncana*) *ventricosa carinata* Dalbiez, 1955, p. 168, fig. 8

Diagnosis: Test is very low trochospiral with trapezoidal to subconical chmabers. Each chamber develops carina on top. The sutures are raised, straight to curve. The periphery has a thick keel. The straight sutures portioning the chambers are well seen in the thin section.

Globigerinelloides prairiehillensis Pessagno, Plate 19, figs. 11-15; Plate 29, fig. 7

-Type reference: *Globigerinelloides prairiehillensis* Pessagno, 1967, p. 267, pl. 83, fig. 1; pl. 90, figs. 1-2, 4; pl. 97, figs. 3-4

Diagnosis: Test is planispiral coiled, with lobulate periphery, and is umbilicate. The test has 7 chambers in the last whorl which are gradually increasing in size. The sutures are radial, straight to slightly curved, and depressed. Umbilicus is wide and shallow.

Contusotruncana plummerae Gandolfi Plate 19, fig. 16

-Type reference: *Globotruncana fornicata plummerae* Gandolfi, 1955, p. 42, pl. 2, figs. 3 (a-c)

-*Contusotruncana plummerae* Robaszynski et al., 2000, p. 481, p. 20, fig. 6

Diagnosis: Test is trochospiral with cylindrical to box shaped chambers. The sutures are thick, curved, and raised. The periphery is subrectangular and keeled.

Contusotruncana patelliformis Gandolfi, Plate 19, fig. 18; Plate, 21, fig. 2

Type reference: *Contusotruncana patelliformis*, Gandolfi, 1955, p. 54, pl. 4, figs. 2 (a-c)

Diagnosis: High trochospiral test with flat umbilical side. Initial chambers are spherical in outline while the last chambers are trapezoidal in shape. Thick peripheral keel is present. The sutures are curved and raised. This species can be differentiated from *Contusotruncana contusa* by having comparatively low

trochospiral and less convex test. It can be differentiated from *Contusotruncana fornicata* by having high trochospire.

Contusotruncana contusa Cushman, Plate 20, fig. 3; Plate 23, fig. 1

-Type reference: *Pulvinulina arca* Cushman var. *contusa* Cushman, 1926, p. 23

-*Contusotruncana contusa* Premoli-Silva & Sliter, 1994, pl. 17, fig. 6; pl. 23, fig. 8

Diagnosis: Test is high trochospiral, with strongly convex asymmetrical tilted spiral side. The umbilical side is concave. Sutures are thick and raised. It is differentiated form the *Contusotruncana patelliformis* by having more strongly convex spiral side and its large size.

Globigerinelloides volutus (White), Plate 21, fig. 6

-Type reference: *Globigerina voluta* White, 1928, p. 197-198, pl. 28, figs. 5 (a-b)

-*Globigerinelloides volutus* Pessagno, 1967, p. 403, pl. 62, figs. 9-11; pl. 100, fig. 9

Diagnosis: Planispiral compressed test, with inflated subspherical petaloid chambers.

Globotruncanita subspinosa (Pessagno), Plate 20 fig. 7

-Type reference: *Globotruncana* (*Globotruncana*) *subspinosa* Pessagno, 1960, p.101 pl.1, figs. 4-6

-*Globotruncanita subspinosa* Caron, 1985, p.55-56 figs. 22 (5-8)

Diagnosis: Test is trochospiral with lunate overlapping chambers which give irregular outline to the keel. The peripheral outline is saucer shaped in thin section.

Globotruncana rosetta (Carsey), Plate 20, fig. 8; Plate 21, fig. 12

-Type reference: *Globigerina rosetta* Carsey, 1926, p. 44, pl. 5, figs. 3 (a-c)

-*Globotruncana rosetta* Brönniman & Brown, 1956, p. 545, pl. 21, figs. 11-13

Diagnosis: Test is trochospiral with lunate chambers spirally, which look very angular in thin section. The sutures are raised. It can be differentiated from *Globotruncana ventricosa* by its sharper periphery, extremely narrow double keel,

and more important by lacking the *Globotruncana linneiana* shape in thin section. It can be differentiated from *Globotruncana elevata* by having a narrow keel and raised chamber at the one end.

Globotruncanita conica White, Plate 16, fig. 4; Plate 20, figs. 9-10; Plate, 23, figs. 2-3, 14

-Type reference: *Globotruncana conica* White, 1928, p. 280, pl. 38, figs. 7 (a-c)

Diagnosis: Test is trochospiral with angular, rhomboid chambers. The sutures are very thick, elevated, and curved. The periphery is lobulate and keeled.

Planoglobulina acervulinoides (Egger), Plate 20, figs. 12, 19; Plate 22, fig.10; Plate 30, fig. 6

-Type reference: *Guembelina acervulinoides* Egger, 1899, p.35 pl. 14, figs. 20-22

-*Planoglobulina acervulinoides* Cushman, 1946, p. 111, pl. 47: 12, 13

Diagnosis: Test is biserial in the early stages, becomes multiserial later, with subglobulor chambers. It is inflated in the biserial arrangement and becomes somewhat flattened in the end region. The sutures are distinct, and depressed. The longitudinal costae are more pronounced and continuous in early chambers, becoming faint and discontinous in later portion of the test. The apertures are highly arched openings.

Globotruncana stephensoni Pessagno, Plate 22, fig. 1

-Type reference: *Globotruncana stephensoni* Pessagno, 1967, p. 408, pl. 69, figs. 1-3, 7; p. 437, pl. 96, figs. 5-6

Diagnosis: Diagnosis: Trochospiral test with trapezoidal chambers, and having sharp angular periphery. Sutures are slightly curved, thick and raised. It looks like *Globotruncana arca* in thin section and can be differentiated from it by its trapezoidal chambers. Thick peripheral keel is present.

Globotruncanita calcarata (Cushman), Plate 20, figs. 13-14; Plate 23, figs. 11-13

-Type reference: *Globotruncana calcarata* Cushman, 1927, p. 115, pl. 23, figs. 10 (a-b)

-*Globotruncanita calcarata* Robaszynski et al., 1984, p. 224, pl. 22, fig. 4; pl. 25, figs. 1–3

Diagnosis: Test is low trochospiral with setellate (start-like) equatorial periphery is keeled and has spines. The chambers are angular. The sutures, curved to almost straight, and elevated.

Globotruncana aegyptiaca Nakkady, Plate 20, fig. 16

-Type reference: *Globotruncana aegyptiaca* Nakkady, 1950, p. 690, pl. 90, fig. 20

Diagnosis: Trochospiral, test with angular chambers. The sutures are curved and elevated. The half of the test surface is rugose or coarsely spinose. The periphery has a thick keel.

Globotruncanella havanensis (Voorwijk), Plate 22, fig. 5

-Type reference: *Globotruncana havanensis* Voorwijk, 1937, p.195 pl.1, figs. 25, 26, 29

-*Globotruncanella havanensis* Caron, 1985, p. 52, figs. 21 (3-4)

Diagnosis: Test is low trochospiral, compressed, having petaloid chambers. The sutures are depressed. The periphery is lobulate.

Globigerinelloides messinae (Brönnimann), Plate 20, fig. 20

-Type reference: *Globigerinella messinae*, Brönnimann, 1952, p. 42, pl. 1, figs. 6-7

-*Planomalina* (*Globigerinelloides*) *messinae* Berggren, 1962, p. 44, pl. 8, figs. 4-8

Diagnosis: Test is planispiral, biumbilicate with a lobulate peripheral outline. The chambers are ovate, and elongated. The sutures are depressed, straight to slightly

curved. The wall is calcareous and thick in early chambers and become finer in final chambers. Tets is laterally borader as compared to other *Globigerinelloides*.

Globigerinelloides bollii Pessagno Plate 15, figs. 1-2; Plate, 21 fig. 7

-Type reference: *Globigerinelloides bollii* Pessagno, 1967, p. 403, pl. 62, fig.5; p. 420, pl. 81, figs. 7-8; p. 436, pl. 97, figs. 1-2; p. 441, pl. 100, fig. 3

Diagnosis: Test is planispiral, biumbilicate, earlier chambers spherical, and later become ovoid, and tilted. The test surface smooth, it can be differentiated from *G. prairiehillensis* by more compressed test, shallow umbilicus, and by being smaller in size.

Sigalia carpathica Salaj and Samuel, Plate 30, figs. 1-2

-Type reference: *Sigalia carpatica* Salaj and Samuel, 1966, pl. 37, fig. 2

Diagnosis: Biserial flat test, compressed with a serrated periphery. The peripheral outline is conical to subrectangular. Biserially arranged chambers to the top, while in the later stage the rounded chamber proliferate enormously.The sutures are beaded and granular. The test surface is heavily ornamented, and shows low discontinous ribs.

Globotruncanita stuarti (De Lapparent), Plate, 23, figs.6-7

-Type reference: *Rosalina stuarti* De Lapparent 1918, p. 11-13, pl. 1, figs. 5, 6, 7

-*Globotruncanita stuarti* Caron, 1985, p. 54, figs. 23 (1-3)

Diagnosis: The rhomboid chambers look angular in thin section, and give a pointed periphery on both edges of the test on all its corners. The peripheral outline is polygonal and is keeled. The sutures on the spiral sides are elevated and curved.

Planoglobulina carseyae (Plummer), Plate 22, fig. 9

-Type reference: *Ventilabrella carseyae* Plummer, 1931, p. 178-179, pl. 9, figs. 7-10

-*Planoglobulina carseyae* Keller, 1988, p. 250, pl.1, fig. 16

Diagnosis: Test is flabelliform, early chambers are biserially arranged which proliferate drastically in the final stage. Chambers are inflated, subglobular. The sutures are are depressed and distinct.

Plate 1

Fig. 1, *Hedbergella sigali* (Moullade), Sample MP-10

Fig. 2, *Hedbergella praetrocoidea* (Kretchmar & Gorbachik), Sample MP-9

Fig. 3, *Hedbergella trocoidea* (Gandolfi), Sample MP-3

Fig. 4, *Hedbergella trocoidea* (Gandolfi), Sample MP 30

Fig. 5, *Hedbergella trocoidea* (Gandolfi), Sample MP 40

Fig. 6 *Hedbergella trocoidea* (Gandolfi), Sample MP 42

Fig. 7, *Hedbergella trocoidea* (Gandolfi), Sample MP-44

Fig. 8, *Hedbergella trocoidea* (Gandolfi), Sample MP-44

Fig. 9, *Hedbergella trocoidea* (Gandolfi), Sample MP-31

Fig. 10, *Hedbergella trocoidea* (Gandolfi), Sample MP-3

Fig. 11, *Hedbergella delrioensis* (Carsey), Sample MP-9

Fig. 12 *Hedbergella delrioensis* (Carsey), Sample MP-127

Fig. 13, *Hedbergella delrioensis* (Carsey), Sample MP-9

Fig. 14, *Hedbergella delrioensis* (Carsey), Sample MP-123

Fig. 15, *Hedbergella delrioensis* (Carsey), Sample MP-118

Fig. 16, *Globigerinelloides barri* (Bolli, Loeblich and Tappan), Sample MP-72

Fig. 17, *Globigerinelloides barri* (Bolli, Loeblich and Tappan), Sample MP-72

Fig. 18, *Hedbergella hispaniae*, (Longoria), Sample MP-9

Fig. 19, *Hedbergella gorbachikae* (Longoria), Sample MP-133

Fig. 20, *Hedbergella Gorbachikae* (Longoria), Sample MP-32

Fig. 21, *Hedbergella* Gorbachikae (Longoria), Sample MP-114

Note: Scale for all figs. =125 micrometer. Figs. 2, 4, 5-6, 14-15, transverse sections; all other figs. are axial to subaxial sections. All samples are from the Moghal Kot Section.

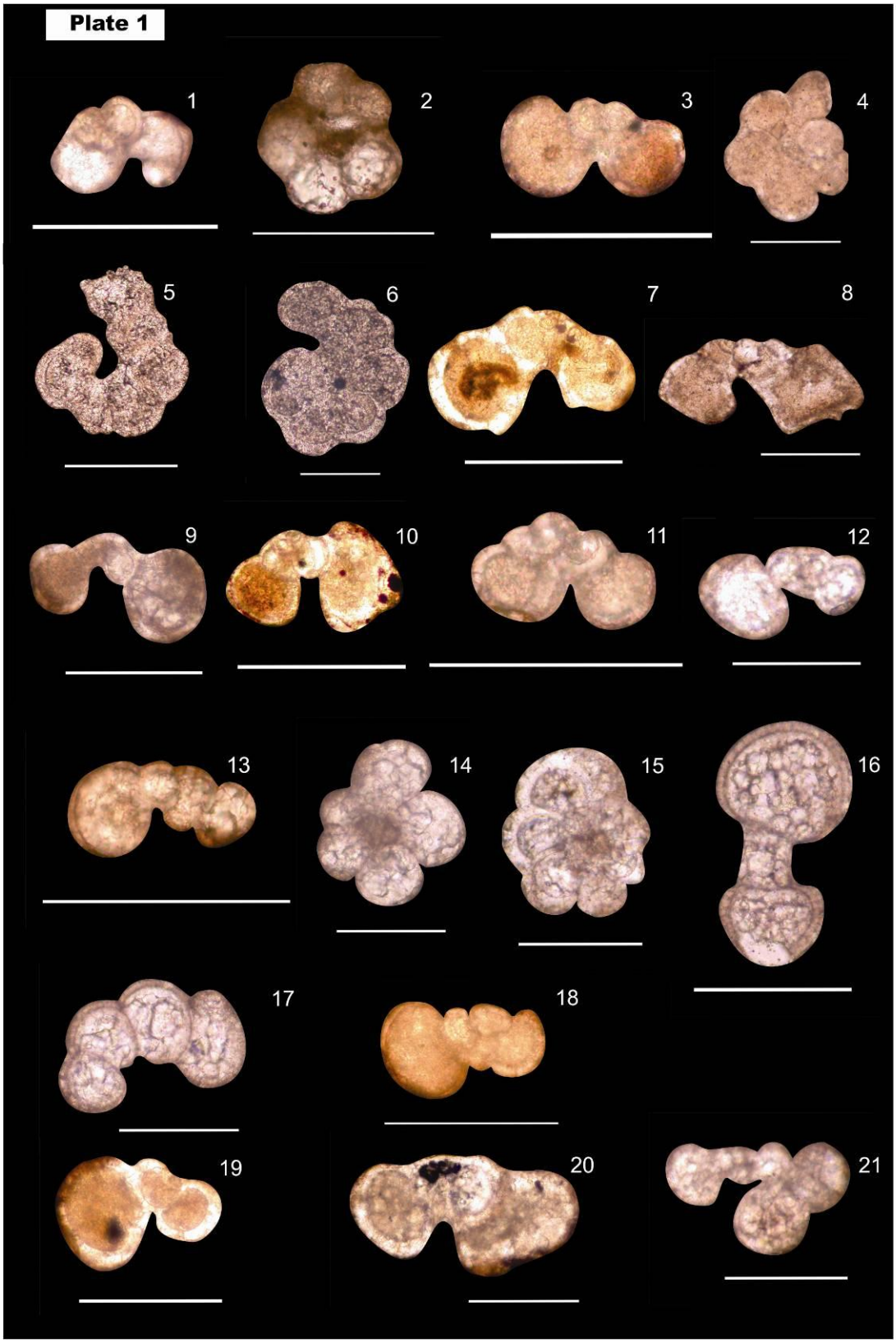
Plate 1
1
2
3
4
5
6
7
8
9
10
11
12
13
14
15
16
17
18
19
20
21

Plate 2

Figs. 1, *Globigerinelloides ferreolensis* (Moullade), Sample MP 26

Figs. 2, *Globigerinelloides ferreolensis* (Moullade), Sample MP 28

Fig. 3, *Globigerinelloides ferreolensis* (Moullade), Sample MP 28

Fig. 4, *Globigerinelloides* cf. *ferreolensis* (Moullade), Sample MP 28

Fig. 5, *Globigerinelloides ferreolensis* (Moullade), Sample MP 24

Fig. 6, *Globigerinelloides ferreolensis* (Moullade), Sample MP 24

Fig. 7, *Globigerinelloides ferreolensis* (Moullade), Sample MP 31

Fig. 8, *Globigerinelloides ferreolensis* (Moullade), Sample MP 30

Fig. 9, *Globigerinelloides ferreolensis* (Moullade), Sample MP 33

Fig. 10, *Globigerinelloides ferreolensis* (Moullade), Sample MP 23

Fig. 11, *Globigerinelloides* cf. *ferreolensis* (Moullade), Sample MP 26

Fig. 12, *Globigerinelloides algerianus* (Cushman & Ten Dam), Sample MP 30

Fig. 13, *Globigerinelloides algerianus* (Cushman & Ten Dam), Sample MP 30

Note: Scale for all figs. =125 micrometer. Fig. 8, transverse section; all other figs. are axial to subaxial sections. All samples are from the Moghal Kot Section.

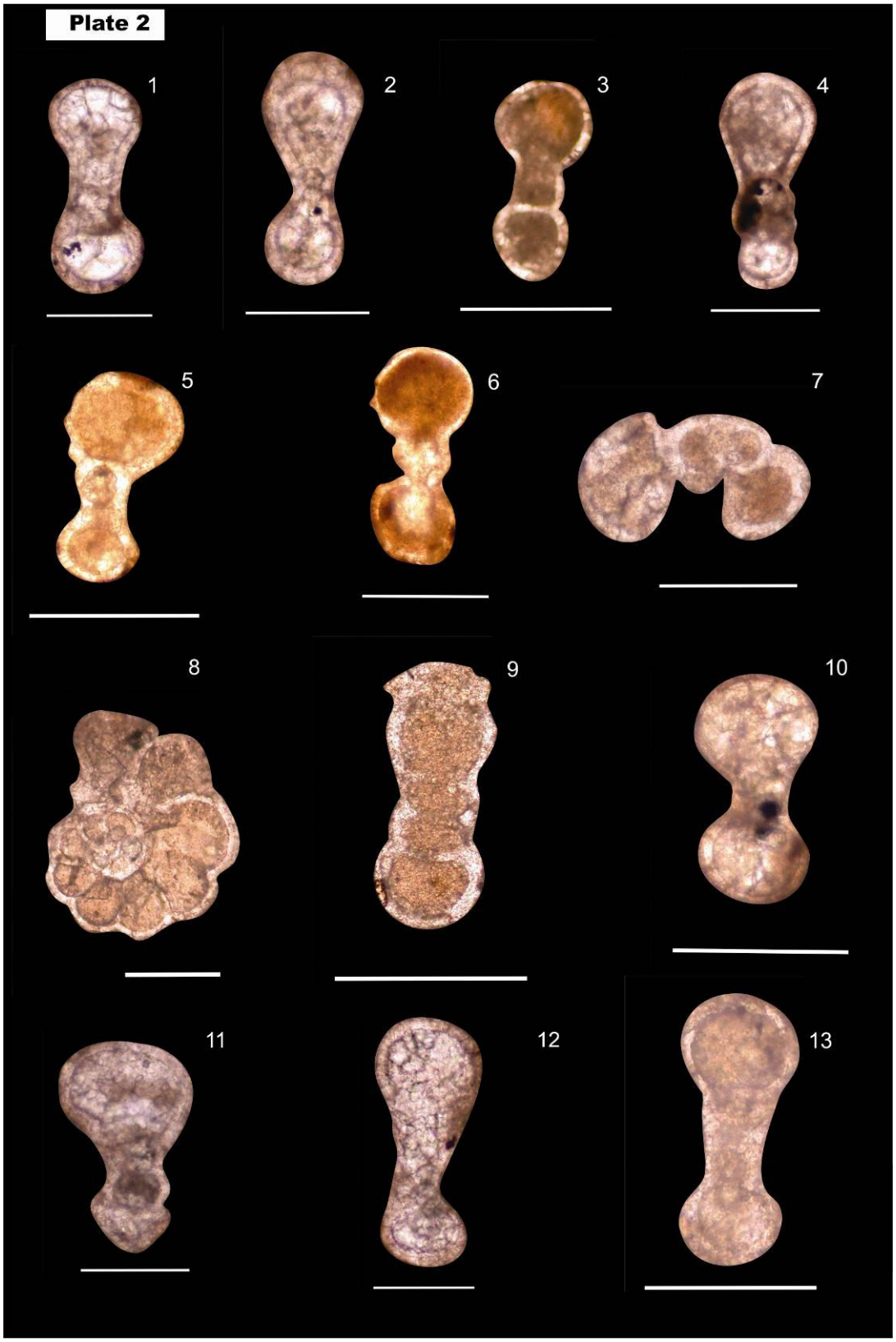
Plate 2
1
2
3
4
5
6
7
8
9
10
11
12
13

Plate 3

Fig. 1, *Globigerinelloides algerianus* (Cushman & Ten Dam), Sample MP 30

Fig. 2, *Globigerinelloides algerianus* (Cushman & Ten Dam), Sample MP 30

Fig. 3, *Globigerinelloides algerianus* (Cushman & Ten Dam), Sample MP 28

Fig. 4, *Globigerinelloides algerianus* (Cushman & Ten Dam), Sample MP 26

Fig. 5, *Globigerinelloides algerianus* (Cushman & Ten Dam), Sample MP 30

Fig. 6, *Globigerinelloides algerianus* (Cushman & Ten Dam), Sample MP 28

Fig. 7, *Globigerinelloides algerianus* (Cushman & Ten Dam), Sample MP 24

Fig. 8, *Globigerinelloides algerianus* (Cushman & Ten Dam), Sample MP 28

Fig. 9, *Globigerinelloides algerianus* (Cushman & Ten Dam), Sample MP 29

Fig.10, Transitional between *Globigerinelloides algerianus* and *Planomalina cheniourensis* , Sample MP 32

Fig. 11, *Planomalina cheniourensis* (Sigal), Sample MP 37

Fig. 12, *Planomalina cheniourensis* (Sigal), Sample MP 37

Fig. 13, *Planomalina cheniourensis* (Sigal), Sample MP 37

Note: Scale for all figs. =125 micrometer. Fig. 1, transverse section; all other figs. are axial to subaxial sections. All samples are from the Moghal Kot Section.

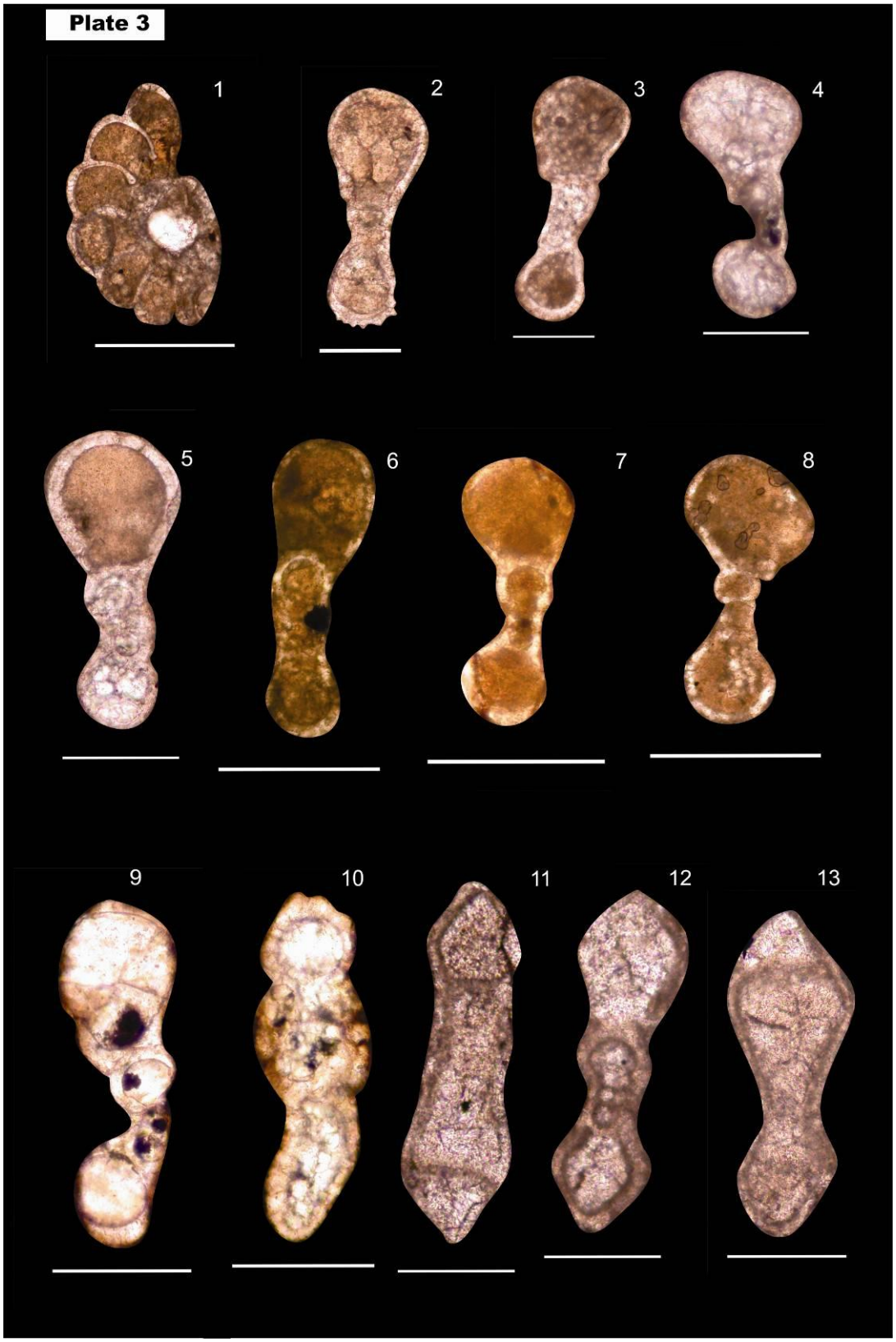
Plate 3
1
2
3
4
5
6
7
8
9
10
11
12
13

Plate 4

Fig. 1, *Ticinella bejaouaensis*, (Sigal), Sample MP 42

Fig. 2, *Ticinella bejaouaensis* (Sigal), Sample MP 42

Fig. 3, *Ticinella bejaouaensis* (Sigal), Sample MP 89

Fig. 4, *Ticinella bejaouaensis* (Sigal), Sample MP 89

Fig. 5 *Ticinella* sp. in Sample MP 96

Fig. 6, *Ticinella roberti* (Gandolfi), Sample MP 127

Fig. 7, *Ticinella roberti* (Gandolfi), Sample MP 125

Fig. 8, *Ticinella roberti* (Gandolfi), Sample MP 102

Fig. 9, *Ticinella primula* (Luterbacher), Sample MP122

Fig. 10, *Hedbergella rhinoceros* (Coccinoni & Cocon), Sample MP 77

Fig. 11, *Planomalina praebuxtorfi* (Wonders), Sample MP 127

Fig. 12, *Globigerinelloides ultramicrus* (Subbotina), Sample MP 120

Fig. 13, *Globigerinelloides ultramicrus* (Subbotina), Sample MP 119

Fig. 14, *Globigerinelloides ultramicrus* (Subbotina), Sample MP 121

Fig. 15, *Heterohelix moremani* (Cushman), Sample MP 127

Fig. 16, *Globigerinelloides bentonensis* (Morrow), Sample MP 118

Fig. 17, *Hedbergella rischi* (Moullade), Sample MP 73

Fig. 18, *Ticinella praeticinensis* (Sigal), Sample MP 118

Fig. 19, *Hedbergella rischi* (Moullade), iSample MP 110

Fig. 20, *Hedbergella rischi* (Moullade), Sample MP 89

Note: Scale for all figs. =125 micrometer. Fig. 10, transverse section; fig. 15, edge section; all other figs. are axial to subaxial sections. All samples are from the Moghal Kot Section.

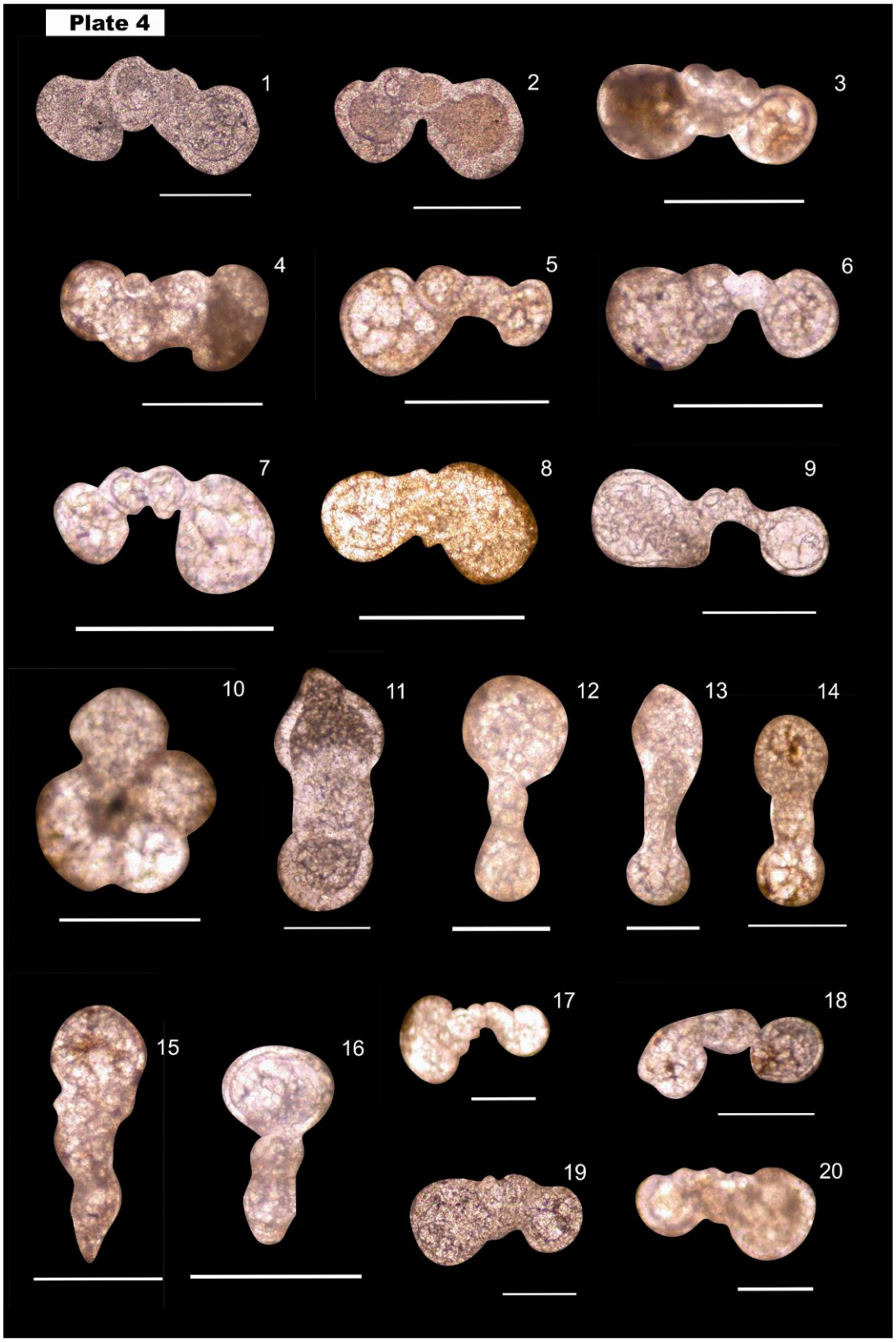
Plate 4
1
2
3
4
5
6
7
8
9
10
11
12
13
14
15
16
17
18
19
20

Plate 5

Fig. 1, *Hedbergella planispira* (Tappan), Sample MP 109

Fig. 2, *Hedbergella planispira* (Tappan), Sample MP 121

Fig. 3, *Hedbergella planispira* (Tappan), Sample MP 109

Fig. 4, *Hedbergella planispira* (Tappan), Sample MP 107

Fig. 5, *Ticinella roberti* (Gandolfi), Sample MP 101

Fig. 6, *Ticinella roberti* (Gandolfi), Sample MP 111

Fig. 7, *Ticinella roberti* (Gandolfi), Sample MP 109

Fig. 8, *Ticinella primula* (Luterbacher), Sample MP 125

Fig. 9, *Ticinella primula* (Luterbacher), Sample MP 123

Fig. 10, *Ticinella primula* (Luterbacher), Sample MP 120

Fig. 11, *Ticinella* cf. *roberti*, Sample MP 119

Fig. 12, *Globigerinelloides bentonensis*, Sample MP 139

Fig. 13, *Globigerinelloides bentonensis*, Sample MP 140

Fig. 14, *Macroglobigerinelloides bentonensis*, Sample MP 120

Fig. 15, *Globigerinelloides bentonensis* (Morrow), Sample MP 137

Fig. 16, *Macroglobigerinelloides bentonensis* (Morrow), Sample MP 119

Note: Scale for all figs. =125 micrometer. Figs. 8-9, transverse sections; all other figs. are axial to subaxial sections. All samples are from Moghal Kot Section.


Plate 5
1
2
3
4
5
6
7
8
9
10
11
12
13
14
15
16

Plate 6

Fig. 1, *Hedbergella simplex* (Morrow), Sample MP 122

Fig. 2, *Hedbergella simplex* (Morrow), Sample MP 196

Fig. 3, *Hedbergella simplex* (Morrow), Sample MM 23

Fig. 4, *Hedbergella* cf. *simplex* (Morrow), Sample MM 25

Fig. 5, *Hedbergella simplex* (Morrow), Sample MP 113

Fig. 6, *Hedbergella simplex* (Morrow), Sample MP 124

Fig. 7, *Ticinella* sp. Sample MP 113

Fig. 8, *Biticinella breggiensis* (Gandolfi), Sample MP 111

Fig. 9, *Biticinella breggiensis* (Gandolfi), Sample MP 113

Fig.10, *Biticinella breggiensis* (Gandolfi), Sample MP 125

Fig.11, *Biticinella breggiensis* (Gandolfi), Sample MP 126

Fig.12, *Ticinella madecassiana* (Sigal), Sample MP 123

Fig.13, *Biticinella subbreggiensis* (Sigal), Sample MP 125

Fig.14, *Ticinella raynaudi* (Sigal), Sample MP 121

Fig.15, *Ticinella raynaudi* (Sigal), Sample MP 121

Fig.16, *Rotalipora* cf. *subticinensis* (Gandolfi), Sample MP 127

Fig.17, *Rotalipora ticinensis* (Gandolfi), Sample MP 122

Note: Scale for all figs. =125 micrometer. Fig. 9, transverse section; all other figs. are axial to subaxial sections. All samples are from the Moghal Kot Section.

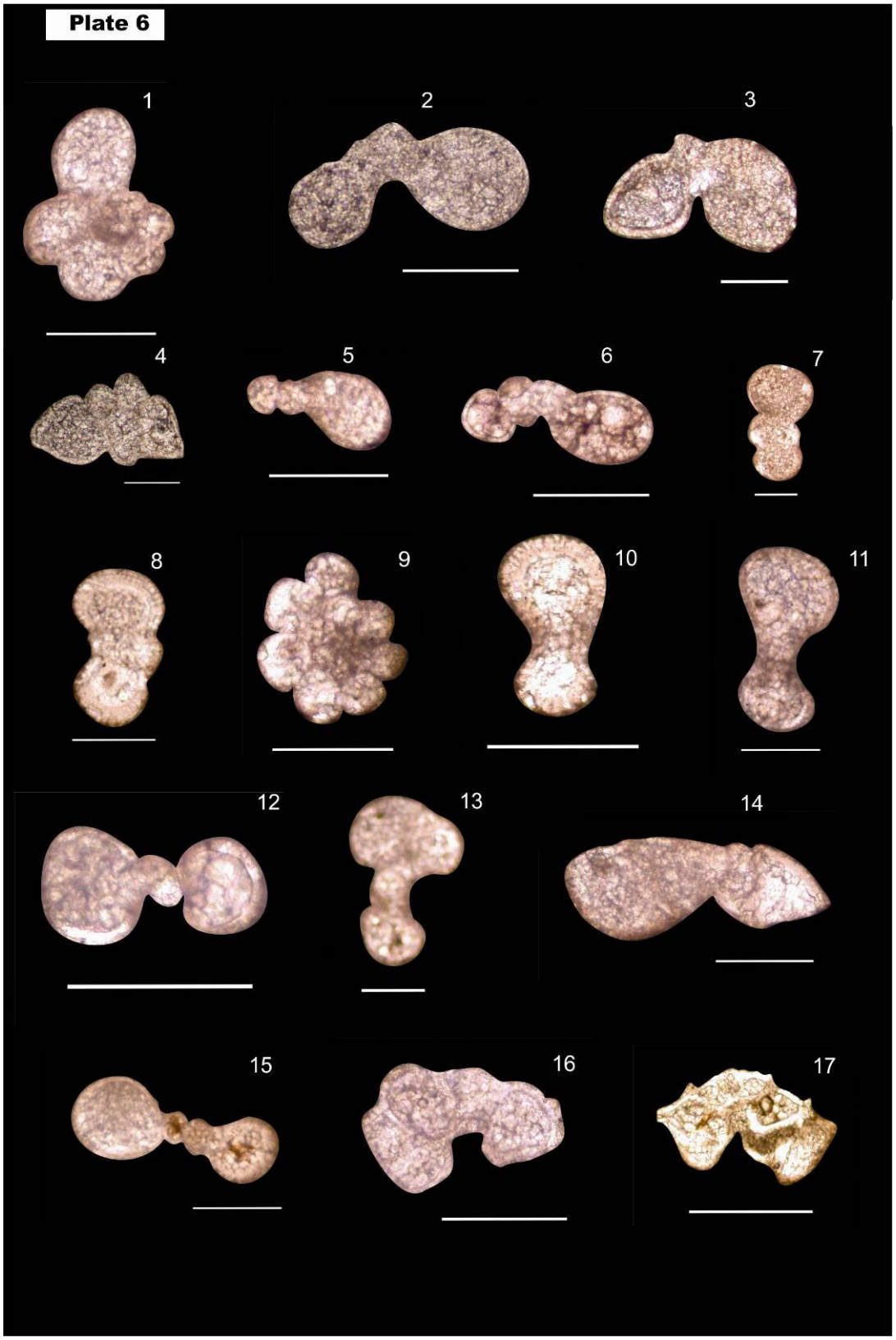
Plate 6
1
2
3
4
5
6
7
8
9
10
11
12
13
14
15
16
17

Plate 7

Fig. 1, *Rotalipora ticinensis* (Gandolfi), Sample MM 23

Fig. 2, *Rotalipora ticinensis* (Gandolfi), Sample MP 124

Fig. 3, *Ticinella madecassiana* (Sigal), Sample MP 119

Fig. 4, *Ticinella madecassiana* (Sigal), Sample MP 117

Fig. 5, *Rotalipora praeappenninica* (Sigal), Sample MM 24

Fig. 6, *Rotalipora praeappenninica*? (Sigal), Sample MP 127

Fig. 7, *Planomalina buxtorfi* (Gandolfi), Sample MP 129

Fig. 8, *Planomalina buxtorfi* (Gandolfi), Sample MM 23

Fig. 9, *Planomalina buxtorfi* (Gandolfi), Sample MP 130

Fig. 10, *Planomalina buxtorfi* (Gandolfi), Sample MM 23

Fig. 11, *Planomalina buxtorfi* (Gandolfi), Sample MP 128

Fig. 12, *Planomalina buxtorfi* (Gandolfi), Sample MP 128

Fig. 13, *Planomalina buxtorfi* (Gandolfi), Sample MP 129

Fig. 14, *Praeglobotruncana delrioensis* (Plummer), Sample MM 25

Fig. 15, *Praeglobotruncana delrioensis* (Plummer), Sample MM 23

Fig. 16, *Heterohelix moremani* (Cushman), Sample MP-203

Fig. 17, *Heterohelix moremani* (Cushman), Sample MP 127

Fig. 18, *Globigerinelloides ultramicrus* (Subbotina), Sample MP 120

Fig. 19, *Rotalipora balernaensis* (Gandolfi), Sample MP 132

Fig. 20, *Rotalipora balernaensis* (Gandolfi), Sample MM 24

Note: Scale for all figs. =125 micrometer. Figs. 7, 12, transverse sections; fig. 16, lateral section; fig. 17, edge section; all other figs.are axial to subaxial sections. All samples are from Moghal Kot Section

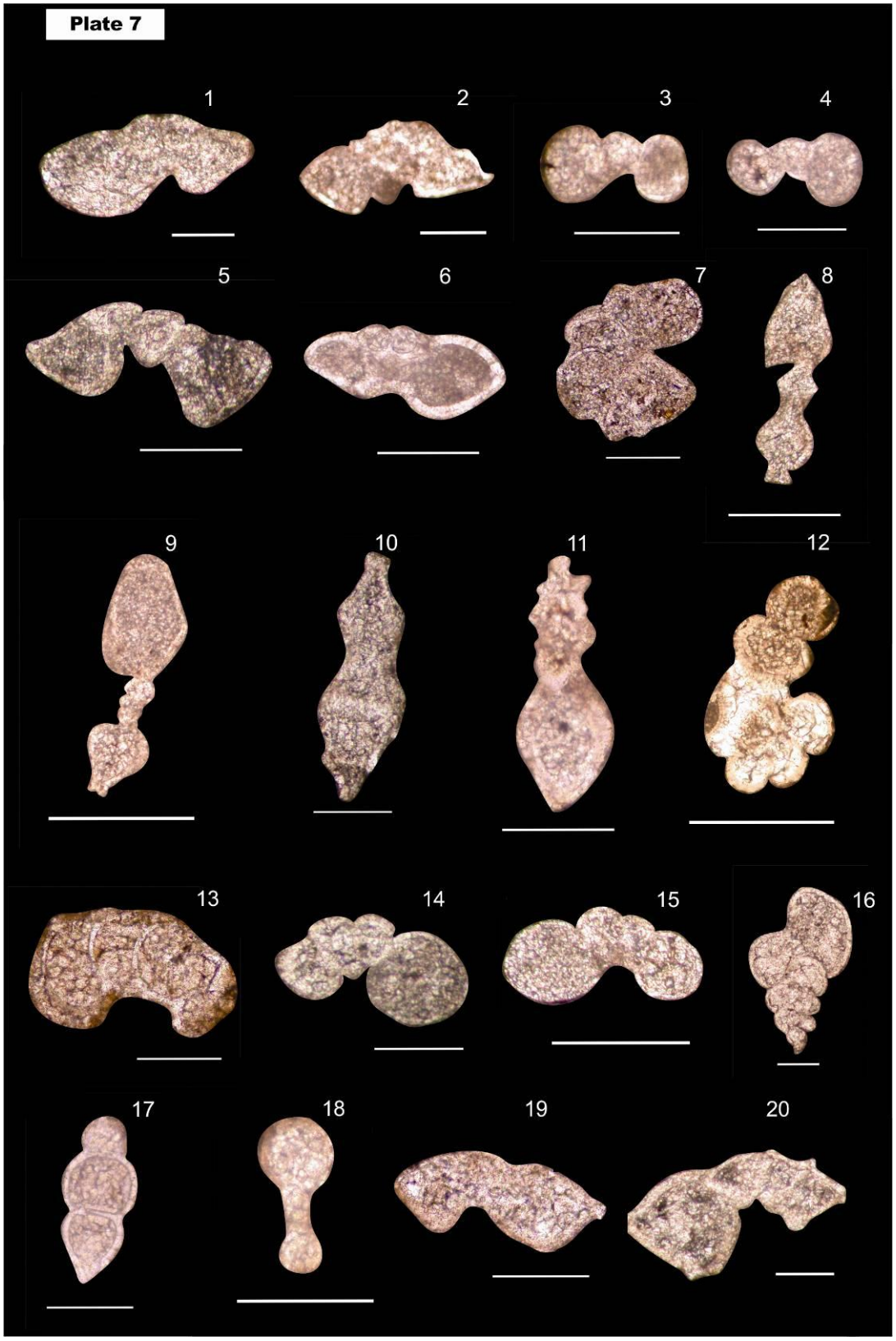
Plate 7
1
2
3
4
5
6
7
8
9
10
11
12
13
14
15
16
17
18
19
20

Plate 8

Fig. 1, *Rotalipora appenninica* (Renz), Sample MP 129

Fig. 2, *Rotalipora appenninica* (Renz), Sample MP 140

Fig. 3, *Rotalipora appenninica* (Renz), Sample MP 137

Fig. 4, *Rotalipora appenninica* (Renz), Sample MP 137

Fig. 5, *Rotalipora appenninica* (Renz), Sample MP 127

Fig. 6, *Rotalipora appenninica* (Renz), Sample MP 129

Fig. 7, *Praeglobotruncana stephani* (Gandolfi), Sample MP 137

Fig. 8, *Praeglobotruncana stephani* (Gandolfi), Sample MP 140

Fig. 9, *Praeglobotruncana stephani* (Gandolfi), Sample MM 23

Fig.10, *Praeglobotruncana stephani* (Gandolfi), Sample MP 138

Fig.11, *Praeglobotruncana stephani* (Gandolfi), Sample MP 139

Fig.12, *Praeglobotruncana stephani* (Gandolfi), Sample MM 25

Fig.13, *Praeglobotruncana stephani* (Gandolfi), Sample MP 191

Fig.14, *Globigerinelloides ultramicrus* (Subbotina), Sample MP 126

Fig.15. *Globigerinelloides caseyi* (Bolli, Loeblich and Tappan), Sample MP 124

Fig.16. *Globigerinelloides caseyi* ((Bolli, Loeblich and Tappan), Sample MP 126

Note: Scale for all figs. =125 micrometer. All figs. are axial to subaxial sections. All samples are from Moghal Kot Section

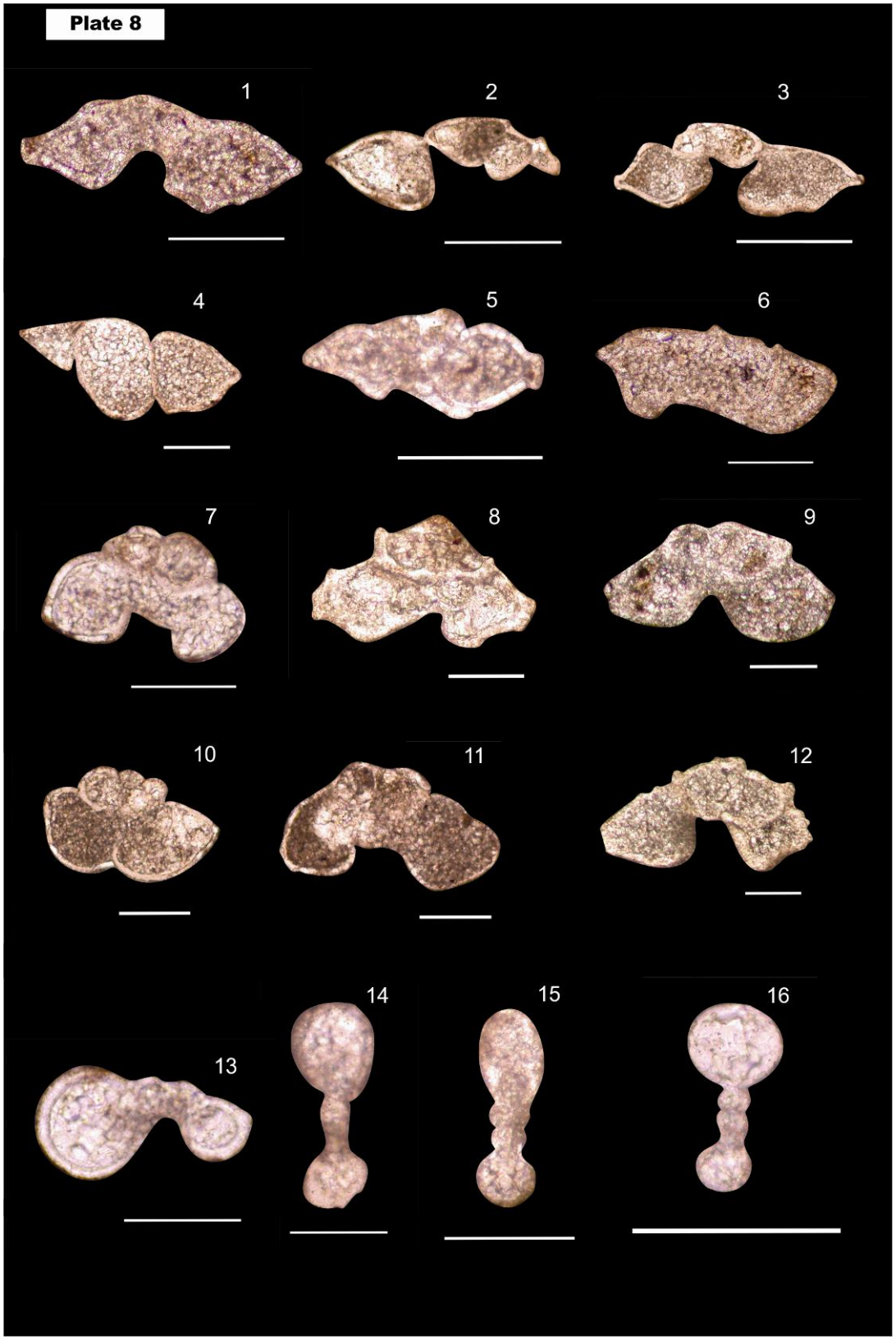
Plate 8
1
2
3
4
5
6
7
8
9
10
11
12
13
14
15
16

Plate 9

Fig. 1, *Rotalipora gandolfi* (Luterbacher & Premoli-Silva), Sample MP 129

Fig. 2, *Rotalipora gandolfi* (Luterbacher & Premoli-Silva), Sample MP 137

Fig. 3, *Rotalipora gandolfi* (Luterbacher & Premoli-Silva), Sample MP 132

Fig. 4, *Rotalipora brotzeni* (Sigal), Sample MP 139

Fig. 5, *Rotalipora brotzeni* (Sigal), Sample MP 138

Fig. 6, *Rotalipora brotzeni* (Sigal), Sample MP 137

Fig. 7, *Rotalipora brotzeni* (Sigal), Sample MP 137

Fig. 8, *Rotalipora montsalvensis* (Mornod), Sample MP 130

Fig. 9, *Rotalipora montsalvensis* (Mornod), Sample MM 23

Fig. 10, *Rotalipora montsalvensis* (Mornod), Sample MM 25

Fig. 11, *Praeglobotruncana gibba* (Klaus), Sample MP 182

Fig. 12, *Praeglobotruncana gibba* (Klaus), Sample MP 182

Fig. 13, *Praeglobotruncana gibba* (Klaus), Sample MP 193

Fig. 14, *Praeglobotruncana gibba* (Klaus), Sample MP 183

Fig. 15, *Rotalipora reicheli* (Mornod), Sample MP 132

Fig. 16, *Rotalipora brotzeni* (Sigal), Sample MP 137

Fig. 17, *Rotalipora greenhornensis* (Morrow), Sample MP 137

Fig. 18, *Rotalipora greenhornensis* (Morrow), Sample MP 137

Fig. 19, *Rotalipora greenhornensis* (Morrow), Sample MM 23

Fig. 20, *Rotalipora greenhornensis* (Morrow), Sample MP 137

Fig. 21, *Rotalipora greenhornensis* (Morrow), Sample MM24

Note: Scale for all fig. =125 micrometer. Fig. 10, transverse section, all other fig. are axial to subaxial sections. All samples are from Moghal Kot Section

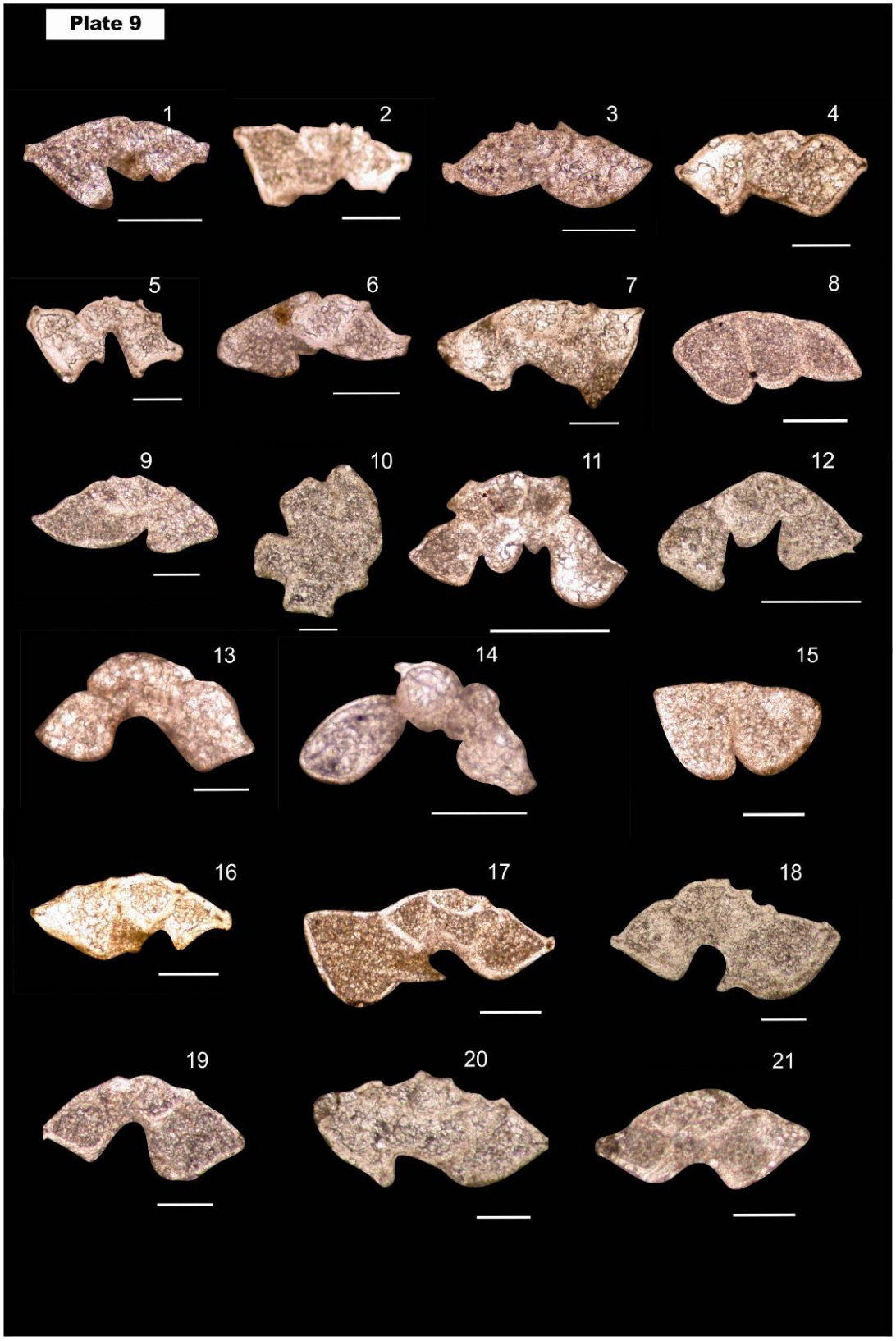
Plate 9
1
2
3
4
5
6
7
8
9
10
11
12
13
14
15
16
17
18
19
20
21

Plate 10

Fig. 1, *Rotalipora cushmani* (Morrow), Sample MM25

Fig. 2, *Rotalipora cushmani* (Morrow), Sample MM 25

Fig. 3 *Rotalipora cushmani* (Morrow), Sample MP 139

Fig. 4, *Rotalipora cushmani* (Morrow), Sample MP 139

Fig. 5, *Rotalipora cushmani* (Morrow), Sample MM 25

Fig. 6, *Rotalipora cushmani* (Morrow), Sample MM 25

Fig. 7, *Rotalipora cushmani* (Morrow), Sample MP 140

Fig. 8, *Rotalipora cushmani* (Morrow), Sample MP 138

Fig. 9, *Rotalipora cushmani* (Morrow), Sample MP 139

Fig. 10, *Rotalipora cushmani* (Morrow), Sample MM 25

Fig. 11, *Rotalipora cushmani* (Morrow), Sample MP138

Fig. 12, *Rotalipora cushmani* (Morrow), Sample MP138

Fig. 13, *Rotalipora cushmani* (Morrow), Sample MP138

Fig. 14, *Rotalipora cushmani* (Morrow), Sample MP138

Fig. 15, *Rotalipora cushmani* (Morrow), Sample MP138

Fig. 16, *Rotalipora cushmani* (Morrow), Sample MM 25

Fig. 17, *Rotalipora cushmani* (Morrow), Sample MP139

Note: Scale for all figs. =125 micrometer. All figs. are axial to subaxial sections. All samples are from Moghal Kot Section

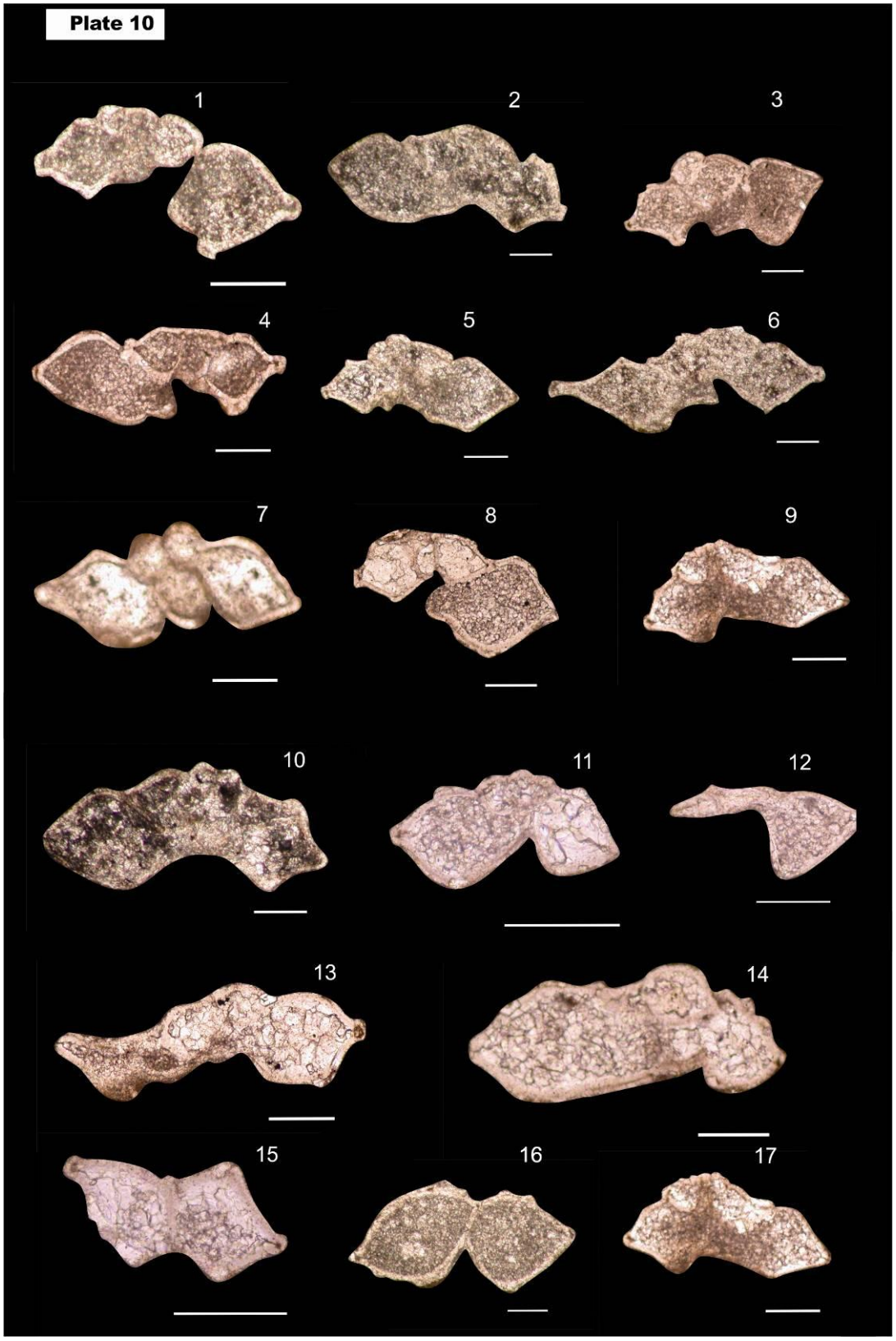
Plate 10
1
2
3
4
5
6
7
8
9
10
11
12
13
14
15
16
17

Plate 11

Fig.1, *Whiteinella aumalensis* (Sigal), Sample MP 181

Fig.2, *Whiteinella aumalensis* (Sigal), Sample MP 179

Fig.3, *Whiteinella aumalensis* (Sigal), Sample MP 189

Fig.4, *Whiteinella praehelvetica* (Trujillo), Sample MP 195

Fig.5, *Whiteinella praehelvetica* (Trujillo), Sample MP 138

Fig.6, *Whiteinella praehelvetica* (Trujillo), Sample MP 181

Fig.7, Transitional form between *Whiteinella baltica* and *Whiteinella praehelvetica*, Sample MP 191

Fig.8, *Whiteinella baltica* (Douglas & Rankin), Sample MP 137

Fig.9, *Whiteinella baltica* (Douglas & Rankin), Sample MP 181

Fig.10, *Whiteinella baltica* (Douglas & Rankin), Sample MP 180

Fig.11, *Whiteinella baltica* (Douglas & Rankin), Sample MP 194

Fig.12, *Dicarinella algeriana* (Caron), Sample MP 137

Fig.13, *Dicarinella algeriana* (Caron), Sample MP 181

Fig.14, *Dicarinella algeriana* (Caron), Sample MP 193

Fig.15, *Dicarinella algeriana* (Caron), Sample MP 138

Fig.16, *Dicarinella algeriana* (Caron), Sample MP 194

Fig.17, *Dicarinella algeriana* (Caron), Sample MM 25

Fig.18, *Dicarinella algeriana* (Caron), Sample MP 137

Fig.19, *Dicarinella algeriana* (Caron), Sample MP 179

Fig. 20, *Dicarinella algeriana* (Caron), Sample MP 191

Fig. 21, *Dicarinella algeriana* (Caron), Sample MP 138

Note: Scale for all figs. =125 micrometer. All figs.are axial to subaxial sections. All samples are from Moghal Kot Section

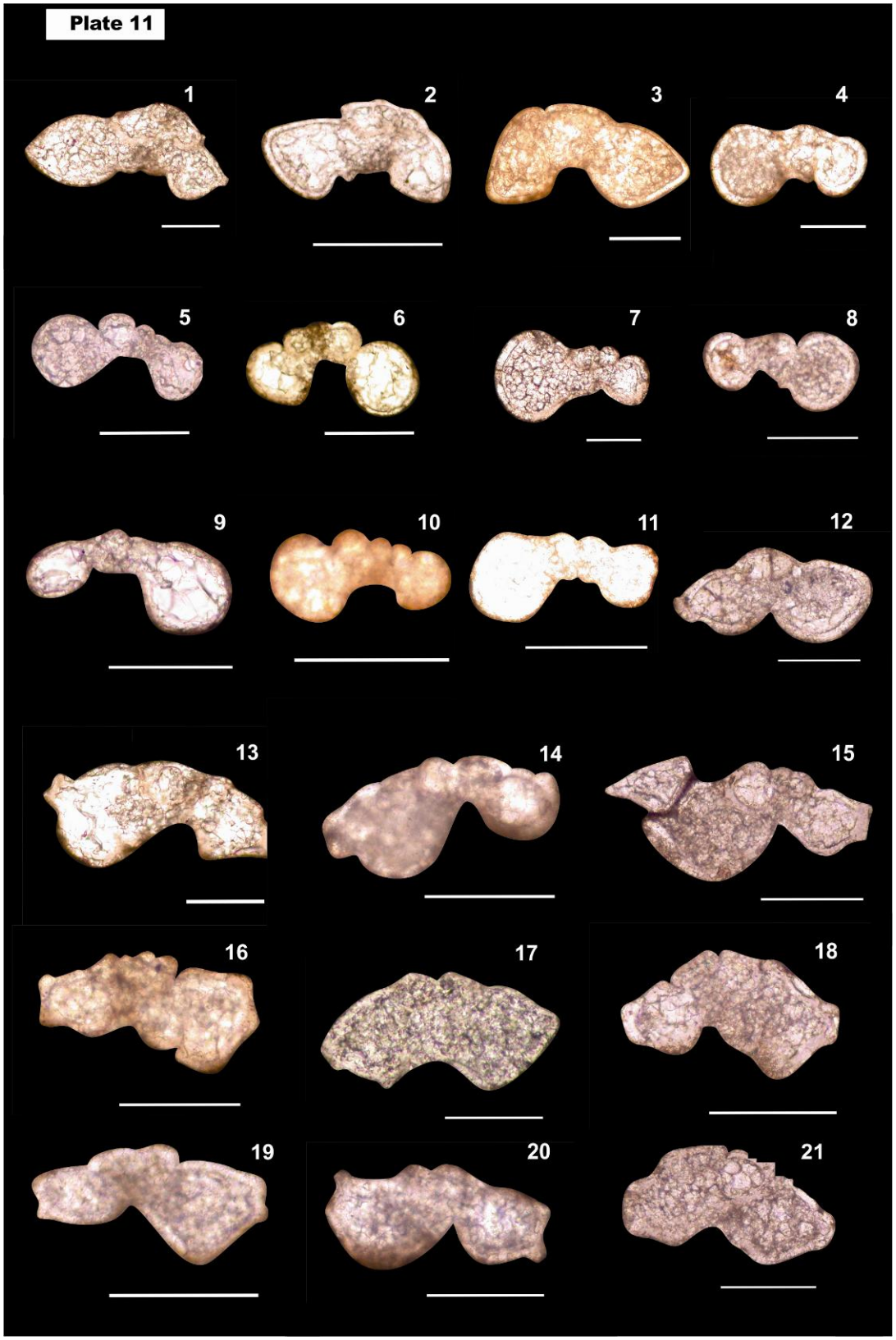
Plate 11
1
2
3
4
5
6
7
8
9
10
11
12
13
14
15
16
17
18
19
20
21

Plate 12

Fig. 1, *Dicarinella imbricata* (Mornod), Sample MP 140

Fig. 2, *Dicarinella imbricata* (Mornod), Sample MP 182

Fig. 3, *Rotalipora deekei* (Franke), Sample MP 138

Fig. 4, *Rotalipora deekei* (Franke), Sample MP 137

Fig. 5, *Rotalipora deekei* (Franke), Sample MM 25

Fig. 6, *Rotalipora deekei* (Franke), Sample MP 140

Fig. 7, *Rotalipora globotruncanoides* (Sigal), Sample MP 140

Fig. 8, *Rotalipora globotruncanoides* (Sigal), Sample MP 140

Fig. 9, *Whiteinella paradubia* (Sigal), Sample MP 179

Fig.10, *Whiteinella paradubia* (Sigal), Sample MP 189

Fig.11, *Whiteinella archaeocretacea* (Pessagno), Sample MP 182

Fig.12, *Whiteinella archaeocretacea* (Pessagno), Sample MP 182

Fig.13, *Whiteinella archaeocretacea* (Pessagno), Sample MP 191

Fig.14, *Helvetoglobotruncana helvetica* (Bolli), Sample MP 181

Fig.15, *Helvetoglobotruncana helvetica* (Bolli), Sample MP 197

Fig.16, *Helvetoglobotruncana helvetica* (Bolli), Sample MP 196

Fig.17, *Helvetoglobotruncana helvetica* (Bolli), Sample MP 179

Fig. 18, *Helvetoglobotruncana helvetica (*Bolli), Sample MP 196

Fig. 19, *Helvetoglobotruncana helvetica* (Bolli), Sample MP 187

Fig. 20, *Helvetoglobotruncana helvetica* (Bolli), Sample MP 182

Fig. 21, *Helvetoglobotruncana helvetica* (Bolli), Sample MP 182

Fig. 22, *Helvetoglobotruncana helvetica* (Bolli), Sample MP 195

Note: Scale for all figs. =125 micrometer. All figs. are axial to subaxial sections. All samples are from Moghal Kot Section

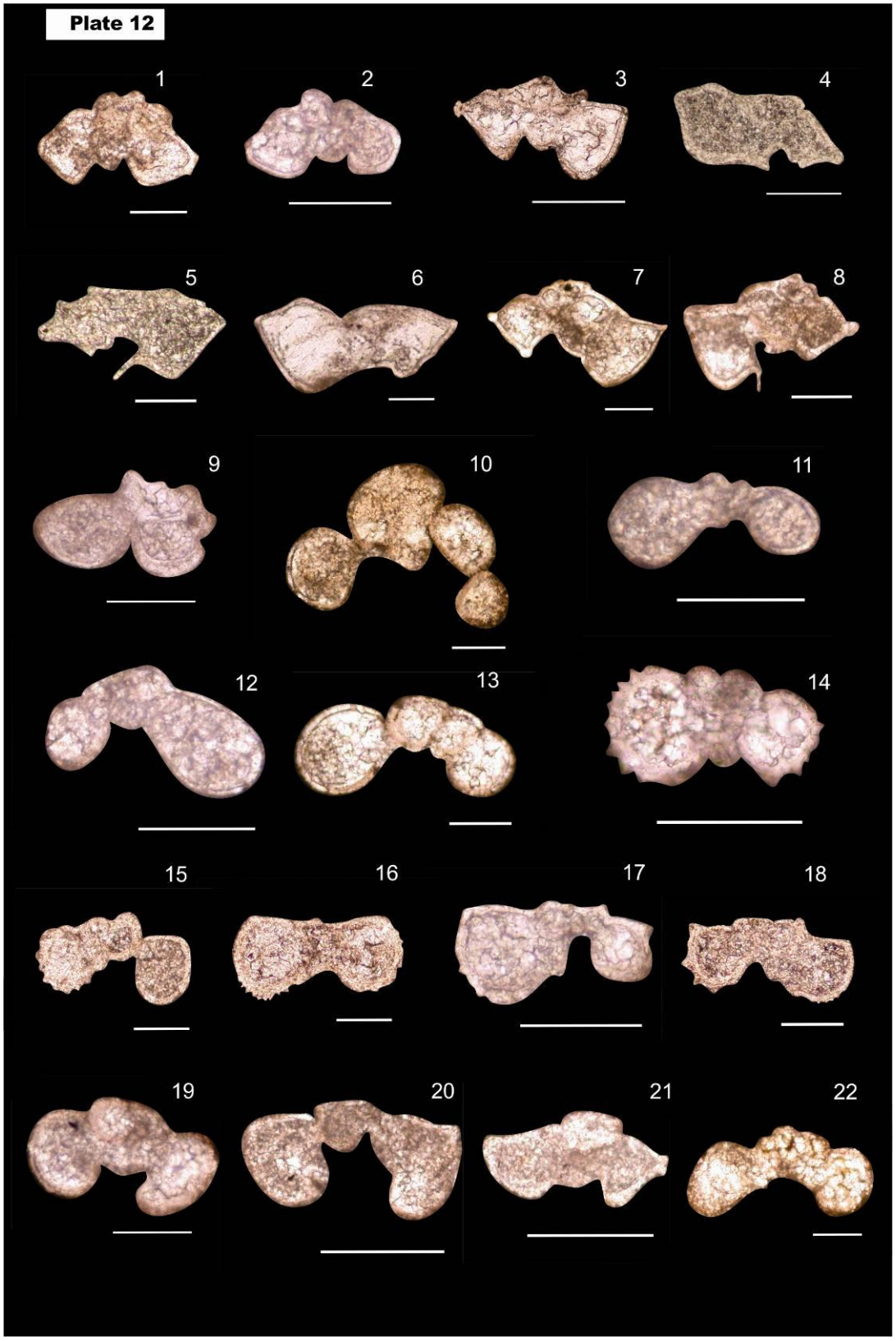
Plate 12
1
2
3
4
5
6
7
8
9
10
11
12
13
14
15
16
17
18
19
20
21
22

Plate 13

Fig. 1, *Whiteinella aprica* (Loeblich & Tappan), Sample MP 188

Fig. 2, *Whiteinella aprica* (Loeblich & Tappan), Sample MP 185

Fig. 3, *Whiteinella brittonensis* (Loeblich & Tappan), Sample MP 185

Fig. 4, *Whiteinella brittonensis* (Loeblich & Tappan), Sample MP 132

Fig. 5, *Dicarinella canaliculata* (Reuss), Sample MP 196

Fig. 6, *Dicarinella canaliculata* (Reuss), Sample MP 185

Fig. 7, *Dicarinella canaliculata* (Reuss), Sample MP 137

Fig. 8, *Dicarinella hagni* (Scheibnerova), Sample MP 194

Fig. 9, *Dicarinella hagni* (Scheibnervoa), Sample MP 182

Fig. 10, *Dicarinella hagni* (Scheibnervoa), Sample MP 195

Fig. 11, *Dicarinella hagni/imbricata*, Sample MP 181

Fig. 12, *Whiteinella (?) inornata* (Bolli), Sample MP 193

Fig. 13, *Whiteinella (?) inornata* (Bolli) Sample MP 181

Fig. 14, *Heterohelix reussi* (Cushman), Sample MP 201

Fig. 15, *Heterohelix reussi* (Cushman), Sample MP 193

Fig. 16, *Heterohelix reussi* (Cushman), Sample MP 203

Fig. 17, *Heterohelix reussi* (Cushman), Sample MP 205

Fig. 18, *Heterohelix reussi* (Cushman), Sample MP 206

Fig. 19, *Heterohelix reussi* (Cushman), Sample MP 203

Fig. 20, *Heterohelix reussi* (Cushman), Sample MP 203

Fig. 21, *Heterohelix reussi* (Cushman), Sample MP 207

Note: Scale for all figs. =125 micrometer. Figs. 14-18, 20-21, edge sections; fig. 19, lateral section; all other figs. are axial to subaxial sections. All samples are from Moghal Kot Section

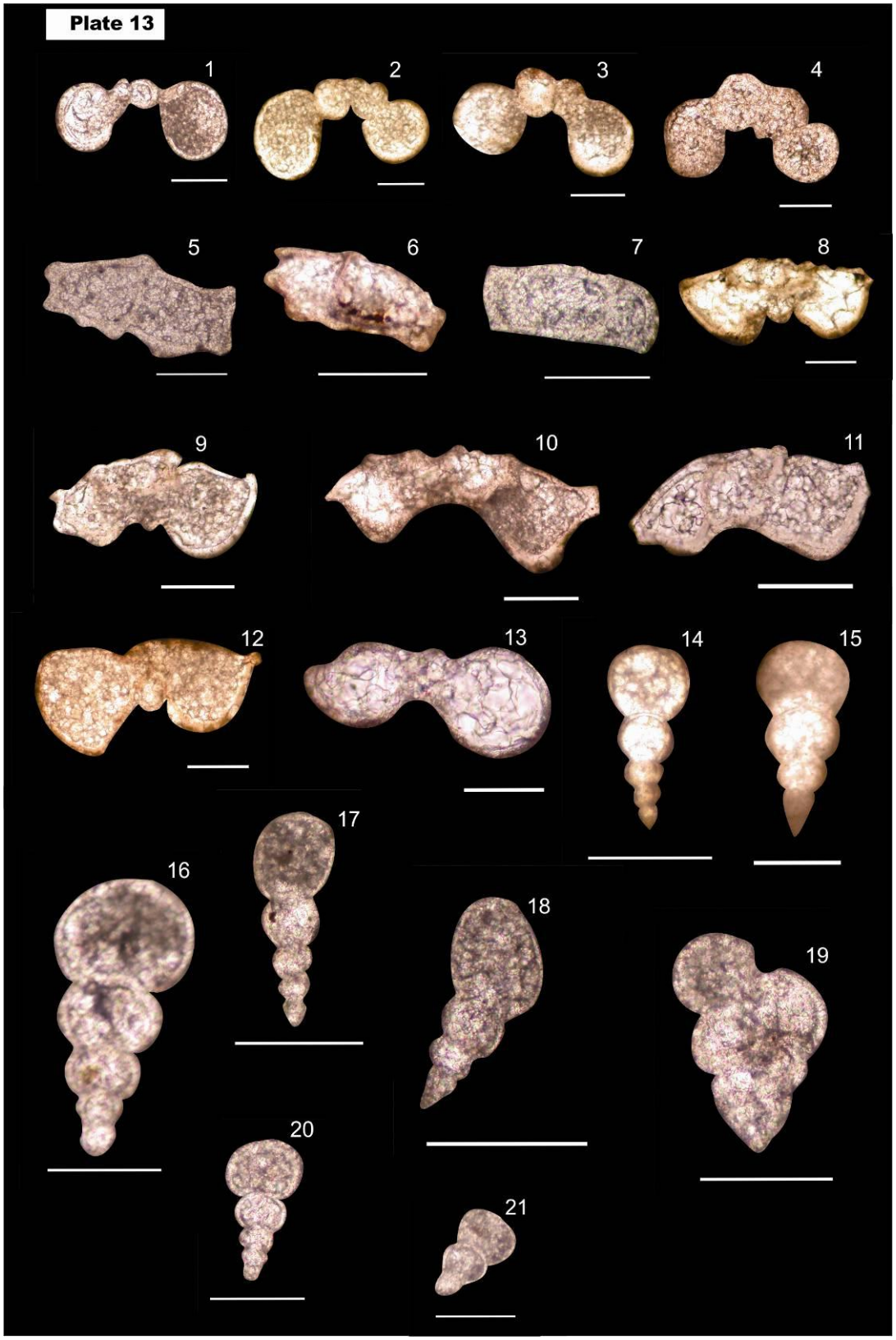
Plate 13
1
2
3
4
5
6
7
8
9
10
11
12
13
14
15
16
17
18
19
20
21

Plate 14

Fig. 1, *Marginotruncana sigali* (Reichel), Sample MP 195

Fig. 2, *Marginotruncana sigali* (Reichel), Sample MP 194

Fig. 3, *Marginotruncana sigali* (Reichel), Sample MP 187

Fig. 4, *Marginotruncana sigali* (Reichel), Sample MP 194

Fig. 5, *Marginotruncana schneegansi* (Sigali), Sample MP 187

Fig. 6, *Marginotruncana schneegansi* (Sigali), Sample MP 196

Fig. 7, *Marginotruncana schneegansi* (Sigali), Sample MP 186

Fig. 8, *Marginotruncana schneegansi* (Sigali), Sample MP 180

Fig. 9, *Marginotruncana renzi* (Gandolfi), Sample MP 185

Fig. 10, *Marginotruncana pseudolinneiana* (Pessagno), Sample MP 196

Fig. 11, *Marginotruncana pseudolinneiana* (Pessagno), Sample MP 198

Fig. 12, *Marginotruncana marianosi* (Douglas), Sample MP 191

Fig. 13, *Marginotruncana coronata* (Bolli), Sample MP 204

Fig. 14, *Marginotruncana coronata* (Bolli), Sample MP 205

Fig. 15, *Marginotruncana coronata* (Bolli), Sample MP 181

Fig. 16, *Marginotruncana coronata* (Bolli), Sample MP 181

Fig. 17, *Marginotruncana coronata* (Bolli), Sample MP 196

Fig. 18, *Marginotruncana renzi* (Bolli), in Sample MP 202

Fig. 19, *Marginotruncana coronata* (Bolli), Sample MP 196

Fig. 20, *Marginotruncana coronata* (Bolli), Sample MP 209

Fig. 21, *Marginotruncana coronata* (Bolli), Sample MP 204

Fig. 22, *Marginotruncana marginata* (Reuss) Sample MP 191

Fig. 23, *Hedbergella flandrini* (Porthault), Sample MP 192

Fig. 24, *Hedbergella flandrini* (Porthault), Sample MP 195

Fig. 25, *Hedbergella flandrini* (Porthault), Sample MP 198

Note: Scale for all figs. =125 micrometer. All figs. are axial to subaxial sections. All samples are from the Moghal Kot Section

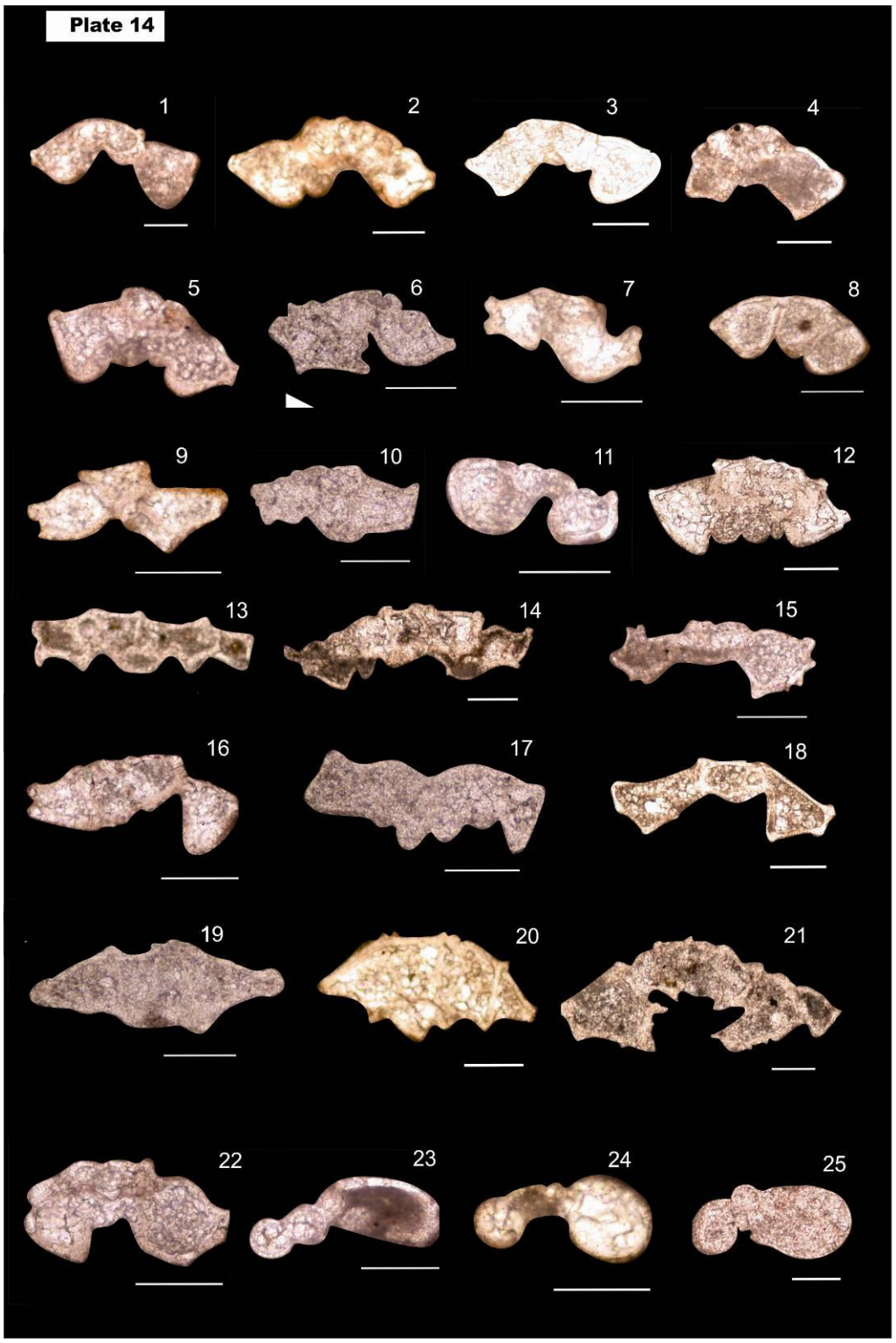
Plate 14
1
2
3
4
5
6
7
8
9
10
11
12
13
14
15
16
17
18
19
20
21
22
23
24
25

Plate 15

Fig. 1, *Globigerinelloides bollii* (Pessagno) Sample MP 195

Fig. 2, *Globigerinelloides bollii* (Pessagno), Sample MP 194

Fig. 3, *Marginotruncana sinousa* (Porthault), Sample MP 185

Fig. 4, *Dicarinella primitiva* (Dalbiez), Sample MP 195

Fig. 5, *Dicarinella primitiva* (Dalbiez), Sample MP 197

Fig. 6, *Dicarinella primitiva* (Dalbiez), Sample MP 196

Fig. 7, *Dicarinella primitiva* (Dalbiez), Sample MP 196

Fig. 8, *Archaeoglobigerina cretacea* (D' Orbigny), Sample MP 196

Fig. 9, *Archaeoglobigerina cretacea* (D' Orbigny), Sample MP 196

Fig. 10, *Dicarinella concavata* (Brotzen), Sample MP 196

Fig. 11, *Dicarinella concavata* (Brotzen), Sample MP 193

Fig. 12, *Dicarinella concavata* (Brotzen), Sample MP 191

Fig. 13, *Dicarinella concavata* (Brotzen), Sample MP 194

Fig. 14, *Contusotruncana fornicata* (Plummer), Sample MP 193

Fig. 15, *Pseudoguembelina costulata* (Cushman), Sample MP 203

Fig. 16, *Pseudoguembelina costulata* (Cushman), Sample MP 203

Fig. 17, *Contusotruncana fornicata* (Plummer), Sample MP 200

Fig. 18, *Contusotruncana fornicata* (Plummer), Sample MP 204

Fig. 19, *Dicarinella* cf. *asymetrica* (Sigal), Sample MP 195

Fig. 20, *Dicarinella asymetrica* (Sigal), Sample MP 195

Note: Scale for all figs. =125 micrometer. All figs.are axial to subaxial sections. All samples are from the Moghal Kot Section

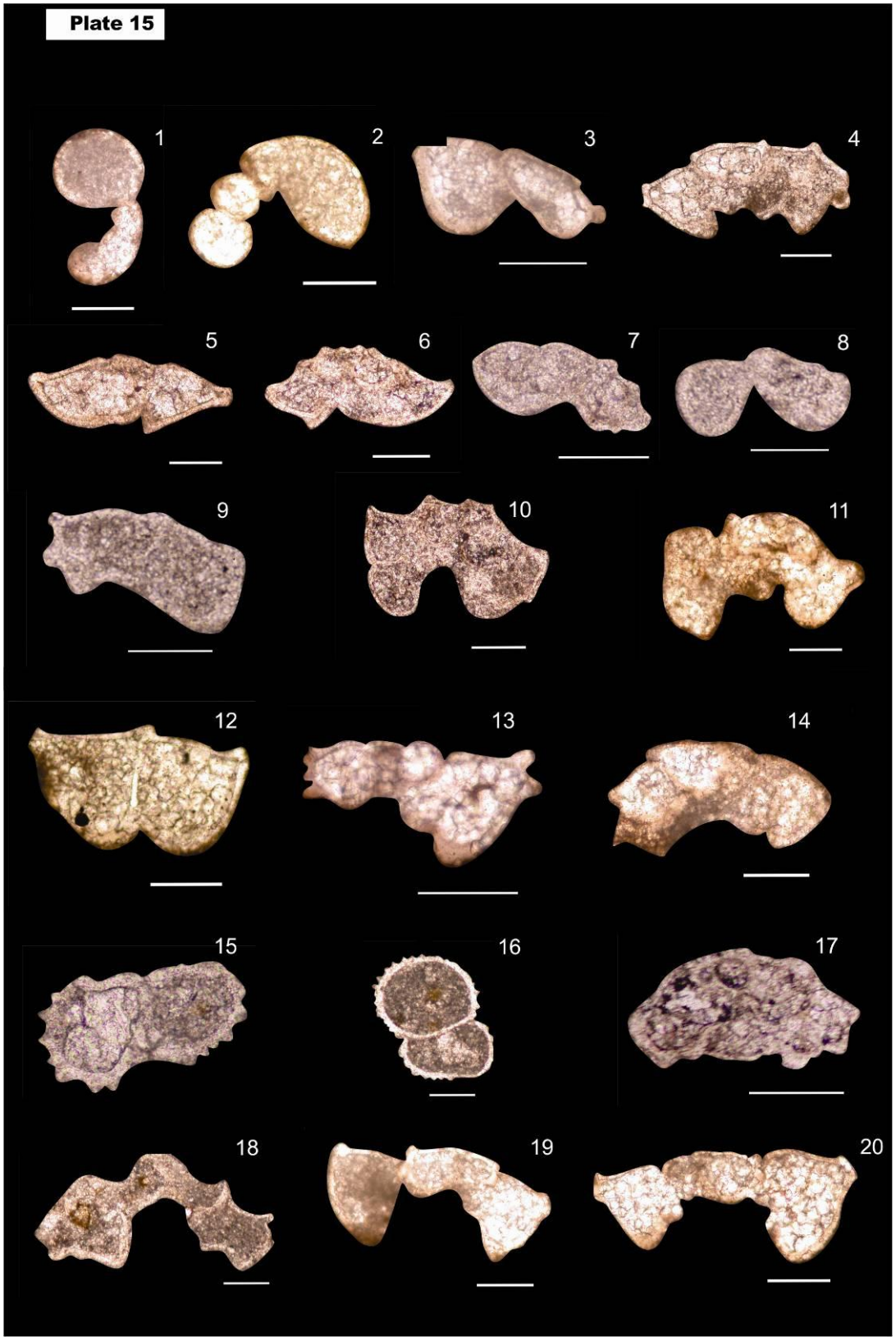
Plate 15
1
2
3
4
5
6
7
8
9
10
11
12
13
14
15
16
17
18
19
20

Plate 16

Fig.1, *Globotruncana linneiana* (D' Orbigny), Sample MP 209
Fig.2, *Globotruncana linneiana* (D' Orbigny), Sample MP 202
Fig.3, *Globotruncana linneiana* (D' Orbigny), Sample MP 200
Fig.4, *Globotruncanita conica* (White), Sample MP 204
Fig.5, *Globotruncana linneiana* (D' Orbigny), Sample MP 209
Fig.6, *Globotruncana linneiana* (D' Orbigny), Sample MP 209
Fig.7, *Globotruncanita elevata* (Brotzen), Sample MP 207
Fig. 8, *Globotruncanita elevata* (Brotzen), Sample MP 200
Fig. 9, *Globotruncanita elevata* (Brotzen), Sample MP 200
Fig. 10, *Globotruncanita elevata* (Brotzen), Sample MP 204
Fig. 11, *Globotruncanita elevata* (Brotzen), Sample MP 207
Fig. 12, *Globotruncanita elevata* (Brotzen), Sample MP 201
Fig. 13, *Globotruncana lapparenti* (Brotzen), Sample MP 201
Fig. 14, *Globotruncana lapparenti* (Brotzen), Sample MP 204
Fig. 15, *Laeviheterohelix glabrans* (Cushman), Sample MP 206
Fig. 16, *Ventilabrella multicamerata* (Klasz), Sample MP 204

Note: Scale for all figs. =125 micrometer. Fig. 15, edge section, fig. 16, lateral section; all others figs. are axial to subaxial sections. All samples are from the Moghal Kot Section

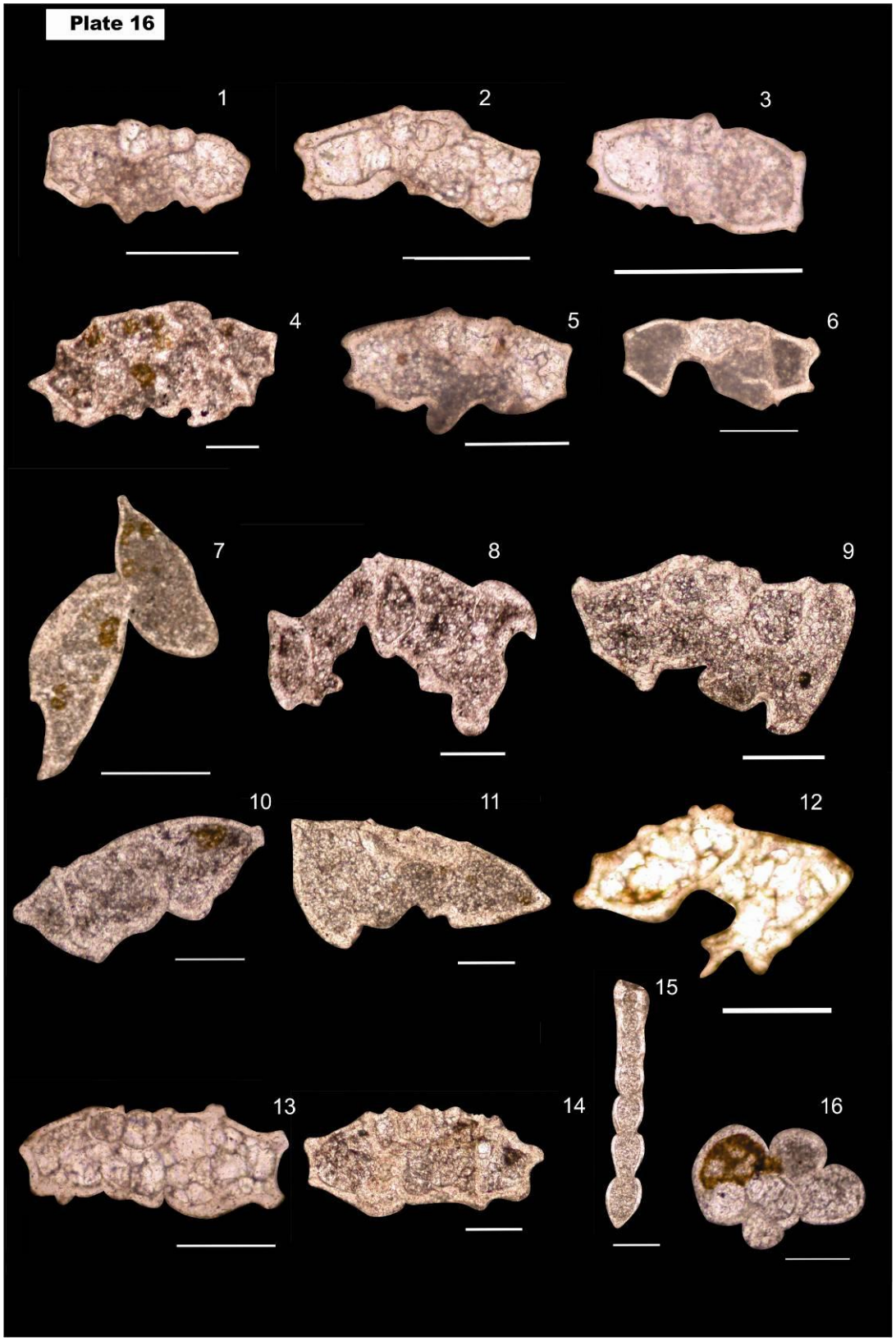
Plate 16
1
2
3
4
5
6
7
8
9
10
11
12
13
14
15
16

Plate 17

Fig. 1, *Globotruncana bulloides* (Vogler), Sample MP 204
Fig. 2, *Globotruncana bulloides* (Vogler), Sample MP 207
Fig. 3, *Globotruncana bulloides* (Vogler), Sample MP 206
Fig. 4, *Globotruncana bulloides* (Vogler), Sample MP 207
Fig. 5, *Globotruncana arca* (Cushman), Sample MP 203
Fig. 6, *Globotruncana arca* (Cushman), Sample MP 203
Fig. 7, *Globotruncana arca* (Cushman), Sample MP 206
Fig. 8, *Globotruncana arca* (Cushman), Sample MP 206
Fig. 9, *Globotruncana arca* (Cushman), Sample MP 204
Fig.10, *Globotruncana arca* (Cushman), Sample MP 203
Fig.11, *Heterohelix globulosa* (Ehrenberg), Sample MP 207
Fig.12, *Heterohelix globulosa* (Ehrenberg), Sample MP 206
Fig.13, *Heterohelix globulosa* (Ehrenberg), Sample MP 203
Fig.14, *Heterohelix globulosa* (Ehrenberg), Sample MP 203
Fig.15, *Heterohelix globulosa* (Ehrenberg), Sample MP 204
Fig.16, *Heterohelix globulosa* (Ehrenberg), Sample MP 207
Fig.17, *Heterohelix globulosa* (Ehrenberg), Sample MP 203

Note: Scale for all figs. =125 micrometer. Figs. 11-17, lateral sections; all others figs. are axial to subaxial sections. All samples are from the Moghal Kot Section

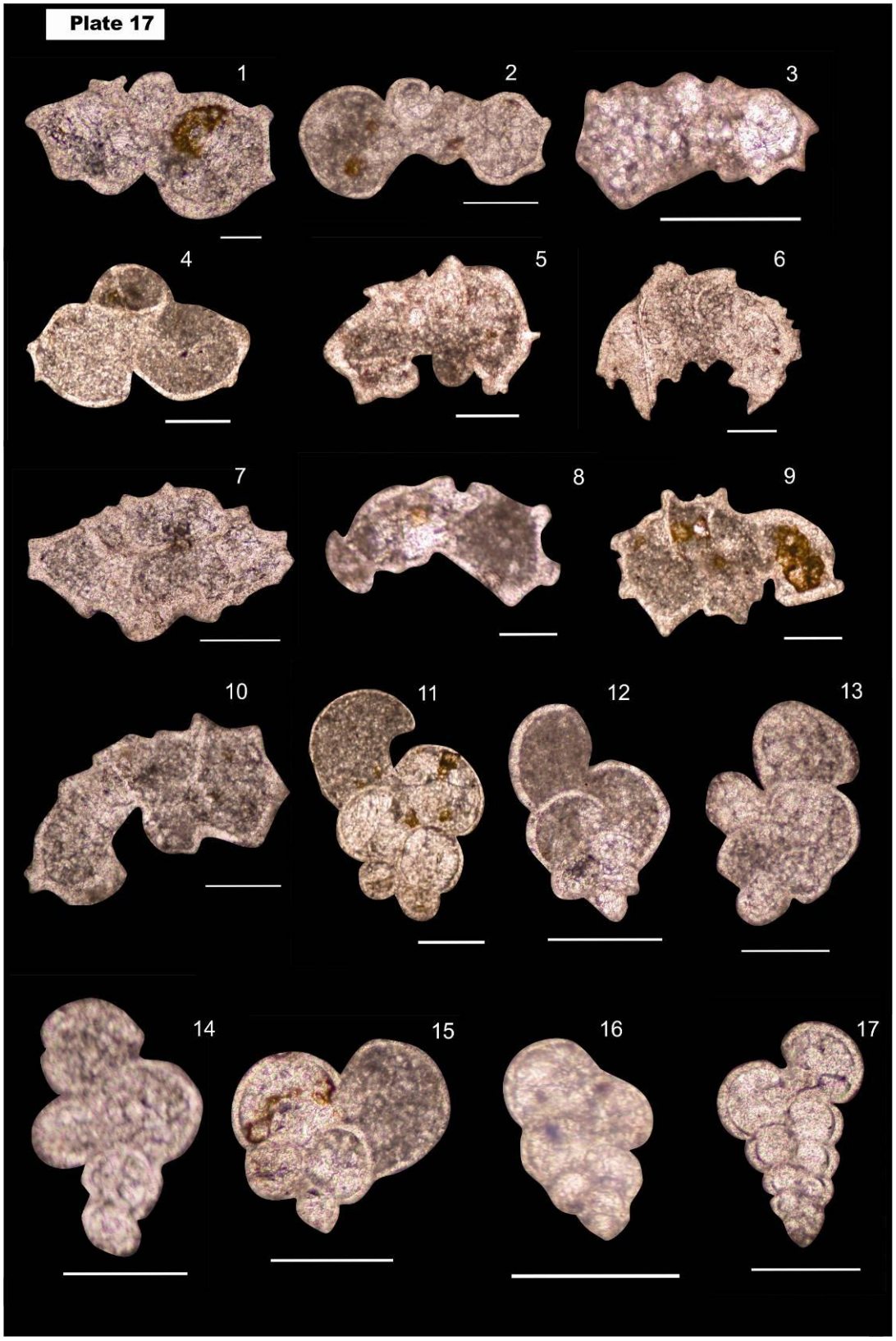
Plate 17
1
2
3
4
5
6
7
8
9
10
11
12
13
14
15
16
17

Plate 18

Fig. 1, *Heterohelix planata* (Cushman), Sample MP 202

Fig. 2, *Heterohelix planata* (Cushman), Sample MP 203

Fig. 3, *Ventilabrella glabrata* (Cushman), Sample MP 204

Fig. 4 *Globotruncana hilli* (Pessagno), Sample MP 200

Fig. 5, *Globotruncana hilli* (Pessagno), Sample MP 200

Fig. 6, *Globotruncana hilli* (Pessagno), Sample MP 200

Fig. 7, *Globotruncana hilli* (Pessagno), Sample MP 206

Fig. 8, *Rugoglobigerina rugosa* (Plummer), Sample MP 207

Fig. 9, *Globotruncana carinata* (Dalbiez), Sample MP 204

Fig.10, *Globotruncana carinata* (Dalbiez), Sample MP 201

Fig.11, *Globotruncana carinata* (Dalbiez), Sample MP 200

Fig.12, *Globotruncana carinata* (Dalbiez), Sample MP 204

Fig.13, *Globotruncana carinata* (Dalbiez), Sample MP 204

Fig.14 *Globotruncana carinata* (Dalbiez), Sample MP 204

Fig.15 *Globotruncana carinata* (Dalbiez), Sample MP 204

Fig.16 *Globotruncana carinata* (Dalbiez), Sample MP 204

Note: Scale for all figs. =125 micrometer. Figs. 1-2 lateral sections; fig. 3, edge section; all others figs. are axial to subaxial sections. All samples are from the Moghal Kot Section


Plate 18
1
2
3
4
5
6
7
8
9
10
11
12
13
14
15
16

Plate 19

Fig. 1, *Globotruncana ventricosa* (White), Sample MP 202

Fig. 2, *Globotruncana ventricosa* (White), Sample MP 206

Fig. 3, *Globotruncana ventricosa* (White), Sample MP 200

Fig. 4, *Globotruncana ventricosa* (White), Sample MP 203

Fig. 5, *Globotruncana ventricosa* (White), Sample MP 207

Fig. 6, *Globotruncana ventricosa* (White), Sample MP 203

Fig. 7, *Globotruncana ventricosa* (White), Sample MP 204

Fig. 8, *Globotruncana ventricosa* (White), Sample MP 207

Fig. 9, *Globotruncana ventricosa* (White), Sample MP 204

Fig. 10, *Globotruncana* sp. Sample MP 204

Fig. 11, *Globigerinelloides prairiehillensis* (Pessagno), Sample MP 206

Fig. 12, *Globigerinelloides prairiehillensis* (Pessagno), Sample MP 205

Fig. 13, *Globigerinelloides prairiehillensis* (Pessagno), Sample MP 205

Fig. 14, *Globigerinelloides prairiehillensis* (Pessagno), Sample MP 198

Fig. 15, *Globigerinelloides prairiehillensis* (Pessagno), Sample MP 202

Fig. 16, *Contusotruncana plummerae* (Gandolfi), Sample MP 200

Fig.17. Transitional between *Contusotruncana patelliformis* and *Contusotruncana contusa,* Sample MP 200

Fig. 18 *Contusotruncana patelliformis* (Gandolfi), Sample MP 199

Note: Scale for all figs. =125 micrometer. Figs. 14-15, transverse sections; all other figs. are axial to subaxial sections. All samples are from the Moghal Kot Section

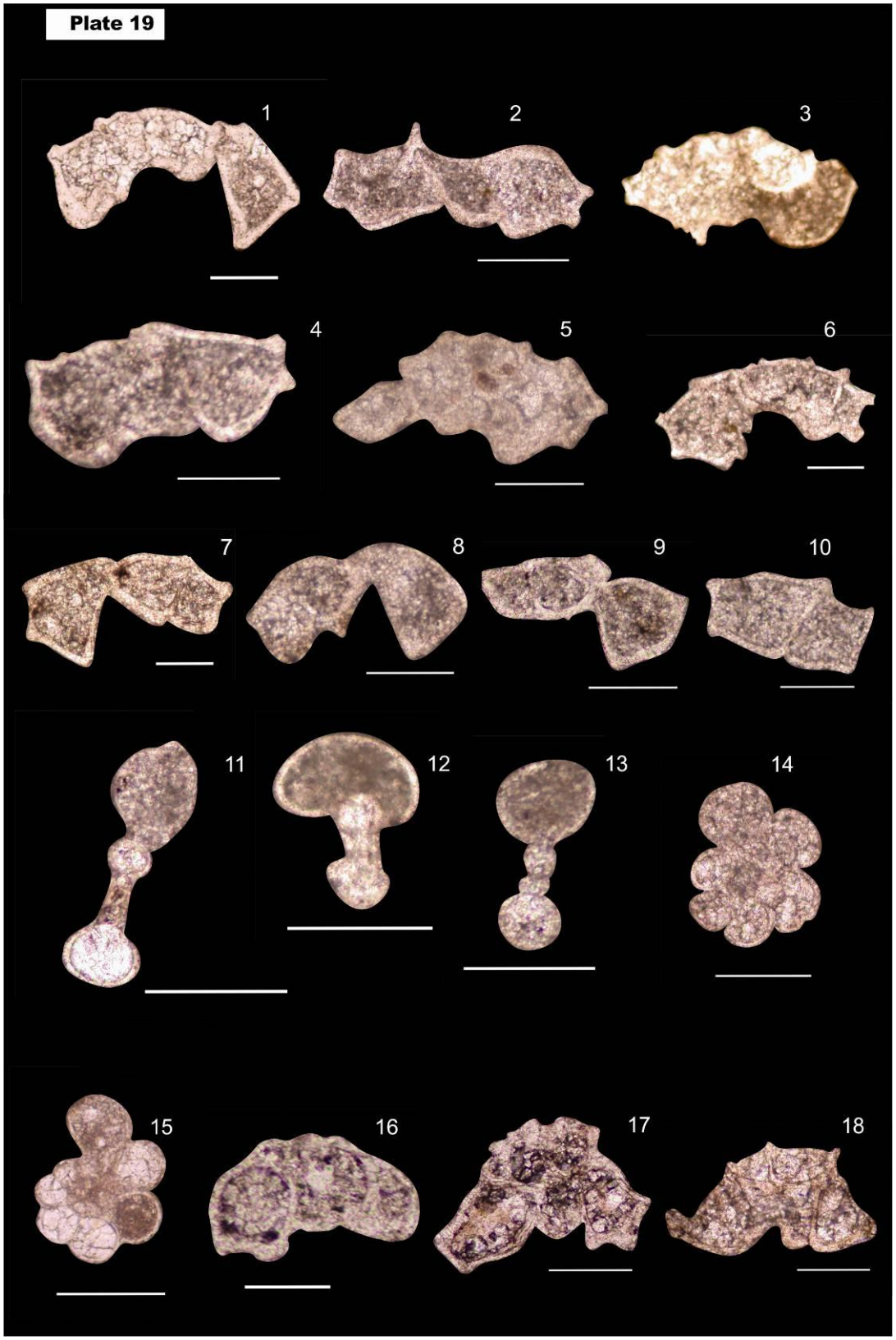
Plate 19
1
2
3
4
5
6
7
8
9
10
11
12
13
14
15
16
17
18

Plate 20

Fig. 1 *Globotruncanita stuarti* (de Lapparent), Sample MP 207

Fig. 2, *Globotruncanita stuartiformis* (Dalbiez), Sample MP 209

Fig. 3, *Contusotruncana contusa* (Cushman), Sample MP 207

Fig. 4, *Pseudotextularia elegans* (Rezehak), Sample MP 204

Fig. 5, *Pseudotextularia elegans* (Rezehak), Sample MP 206

Fig. 6, *Pseudotextularia elegans* (Rezehak), Sample MP 202

Fig. 7, *Globotruncanita subspinosa* (Pessagno), Sample MP 208

Fig. 8, *Globotruncana rosetta* (Carsey), Sample MP 200

Fig. 9, *Globotruncanita conica* (White), Sample MP 204

Fig. 10, *Globotruncanita conica* (White), Sample MP 204

Fig. 11, *Planoglobulina* sp. Sample MP 208

Fig. 12, *Planoglobulina acervulinoides* (Egger), Sample MP 209

Fig. 13, *Globotruncanita calcarata* (Cushman), Sample MP 204

Fig. 14, *Globotruncanita calcarata* (Cushman), Sample MP 204

Fig. 15, *Globotruncana arca* (Cushman), Sample MP 207

Fig. 16, *Globotruncana* cf. *aegyptiaca* (Nakkady), Sample MP 209

Fig. 17, *Laeviheterohelix glabrans* (Cushman), Sample MP 205

Fig. 18, *Gublerina* cf. *robusta* (de Clasz), Sample MP 204

Fig. 19, *Planoglobulina acervulinoides* (Egger), Sample MP 204

Fig. 20, *Globigerinelloides messinae* (Bronnimann), Sample MP 205

Note: Scale for all figs. =125 micrometer. Figs., 4-6, 17-19, edge sections; all other figs. are axial to subaxial section. All samples are from the Moghal Kot Section

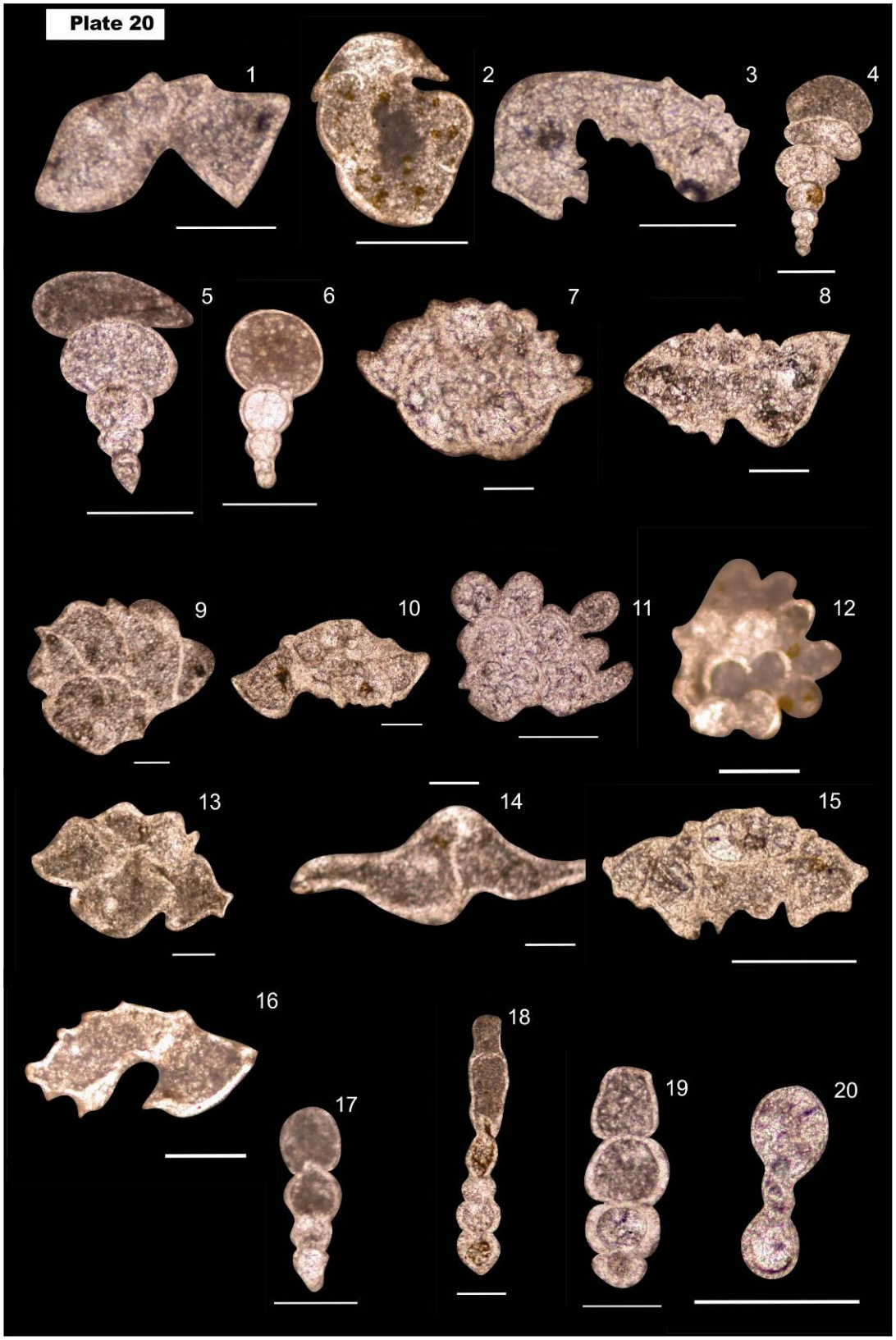
Plate 20
1
2
3
4
5
6
7
8
9
10
11
12
13
14
15
16
17
18
19
20

Plate 21

Fig. 1, *Contusotruncana fornicata* (Plummer), Sample MP 203

Fig. 2, *Contusotruncana patelliformis* (Gandolfi), Sample MP 200

Fig. 3, *Globotruncana lapparenti* (Brotzen), Sample MP 206

Fig. 4, *Globotruncana leupoldi* (Bolli), Sample MP 208

Fig. 5, *Globotruncanella* sp., Sample MP 200

Fig. 6, *Globigerinelloides volutus* (White), Sample MP 203

Fig. 7, *Globigerinelloides bollii* (Pessagno), Sample MP 201

Fig. 8, *Laeviheterohelix glabrans,* Sample MP 204

Fig. 9, *Heterohelix carinata,* Sample MP 200

Fig. 10, *Gublerina* cf. robusta, Sample MP 204

Fig.11, *Laeviheterohelix glabrans* (Cushman), Sample MP 208

Fig. 12, *Globotruncana rosetta* (Carsey), Sample MP 208

Fig. 13, *Contusotruncana fornicata* (Plummer), Sample MP 200

Note: Scale for all figs. =125 micrometer. Figs., 8, 11, lateral sections; figs., 9-10, edge sections; all other figs. are axial to subaxial sections. All samples are from the Moghal Kot Section

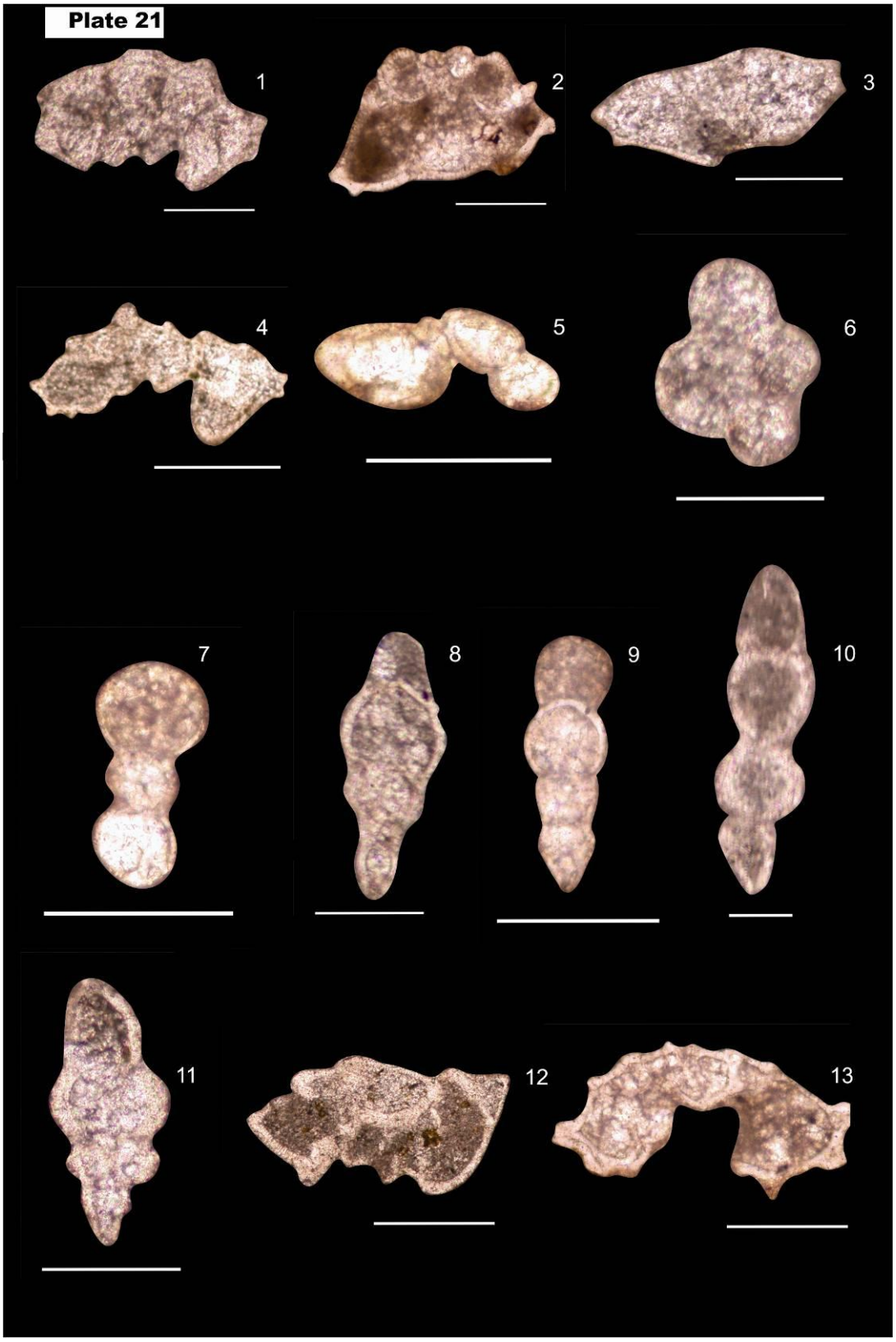
Plate 21
1
2
3
4
5
6
7
8
9
10
11
12
13

Plate 22

Fig. 1, *Globotruncana stephensoni* (Pessagno), Sample MP 207

Fig. 2, *Globotruncana orientalis* (El Naggar), Sample MP 202

Fig. 3, *Globotruncana dupeublei* (Caron), Sample MP 209

Fig. 4, *Contusotruncana* sp. Sample MP 204

Fig. 5, *Globotruncanella havanensis* (Voorwijk), Sample MP 206

Fig. 6, *Sigalia* sp. Sample MP 208

Fig. 7, *Ventilabrella eggeri* (Cushman), Sample MP 208

Fig. 8, *Heterohelix* sp. in Sample MP 202

Fig. 9, *Planoglobulina carsey* (Plummer), Sample MP 208

Fig. 10, *Planoglobulina acervulinoides* (Egger), Sample MP 209

Fig. 11, *Aragonia* sp. in Sample MP 208

12, *Globotruncanita elevata* (Brotzen), Sample MP 207

Note: Scale for all figs. =125 micrometer. Figs., 6-7, 10, edge sections; figs. 8-9, 11, lateral sections; all other figs. are axial to subaxial sections. All samples are from the Moghal Kot Section

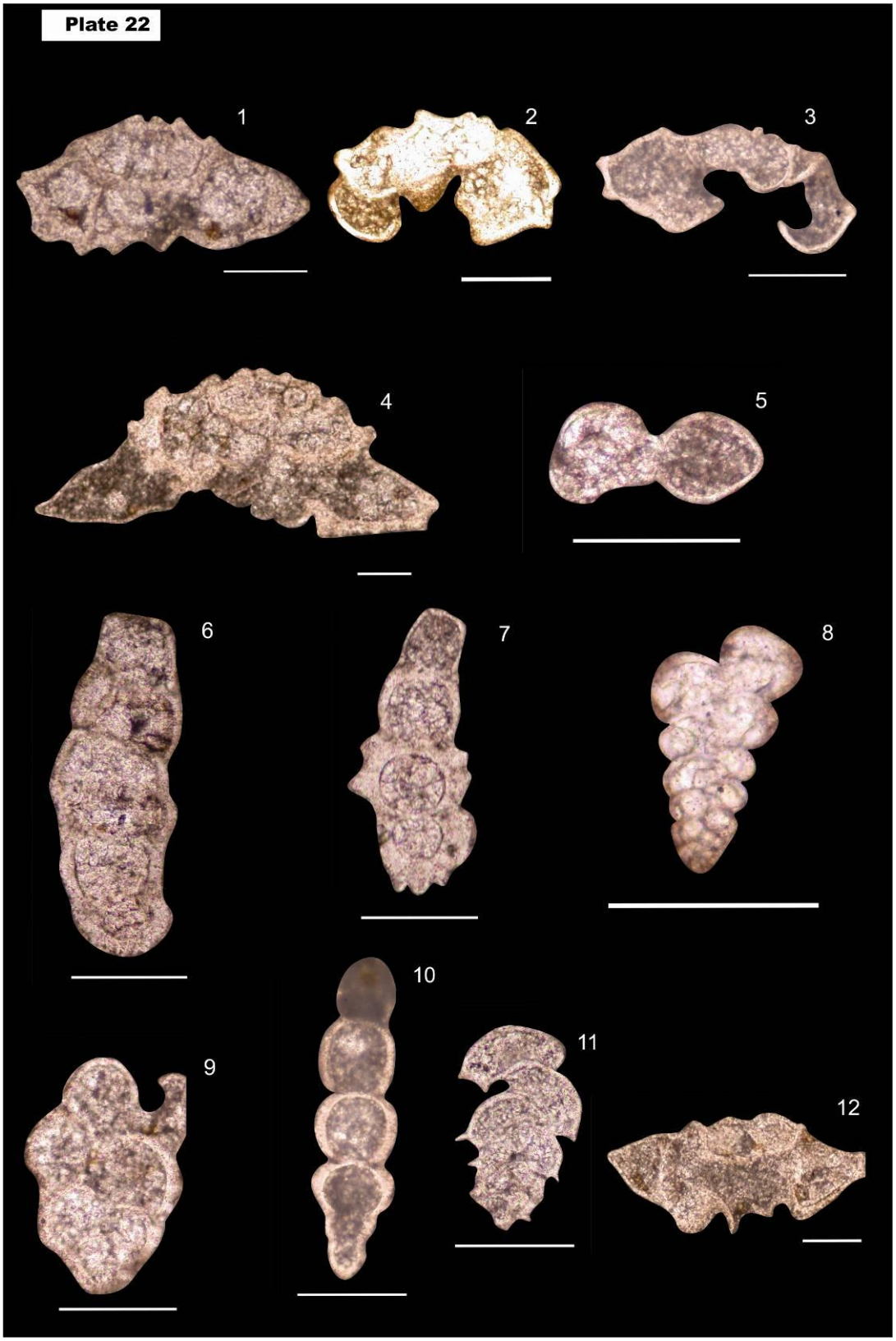
Plate 22
1
2
3
4
5
6
7
8
9
10
11
12

Plate 23

Fig. 1, *Contusotruncana contusa* (Cushman), Sample, MP-207

Fig. 2, 3, *Globotruncanita conica* (White), Sample, MP-210

Fig. 4, *Globotruncanita elevata* (Brotzen), Sample, 210

Fig. 5, *Globotruncanita elevata* (Brotzen), Sample, 208

Fig. 6, *Globotruncanita stuarti* (de Lapparent), Sample, 208

Fig. 7, *Globotruncanita stuarti* (de Lapparent), Sample, 208

Fig. 8, *Globotruncanita stuartiformis* (Dalbiez) , Sample 208

Fig.9,Transitional form between *Globotruncanita subspinosa* and *Globotruncanita calcarata,* Sample MP-208

Fig. 10, *Rugoglobigerina milamensis* (Smith & Pessagno), Sample, 208

Fig. 11, *Globotruncanita calcarata*, (Cushman), Sample MP-209

Fig. 12, *Globotruncanita calcarata*, (Cushman), Sample MP-209

Fig. 13, *Globotruncanita calcarata* (Cushman), Sample 208

Fig. 14, *Globotruncanita conica,* (White), Sample MP-210

Fig. 15, *Ventilabrella glabrata* (Cushman), Sample MP-209

Note: Scale for all figs. =125 micrometer. Fig., 15, lateral sections; all other figs. are axial to subaxial sections. All samples are from the Moghal Kot Section

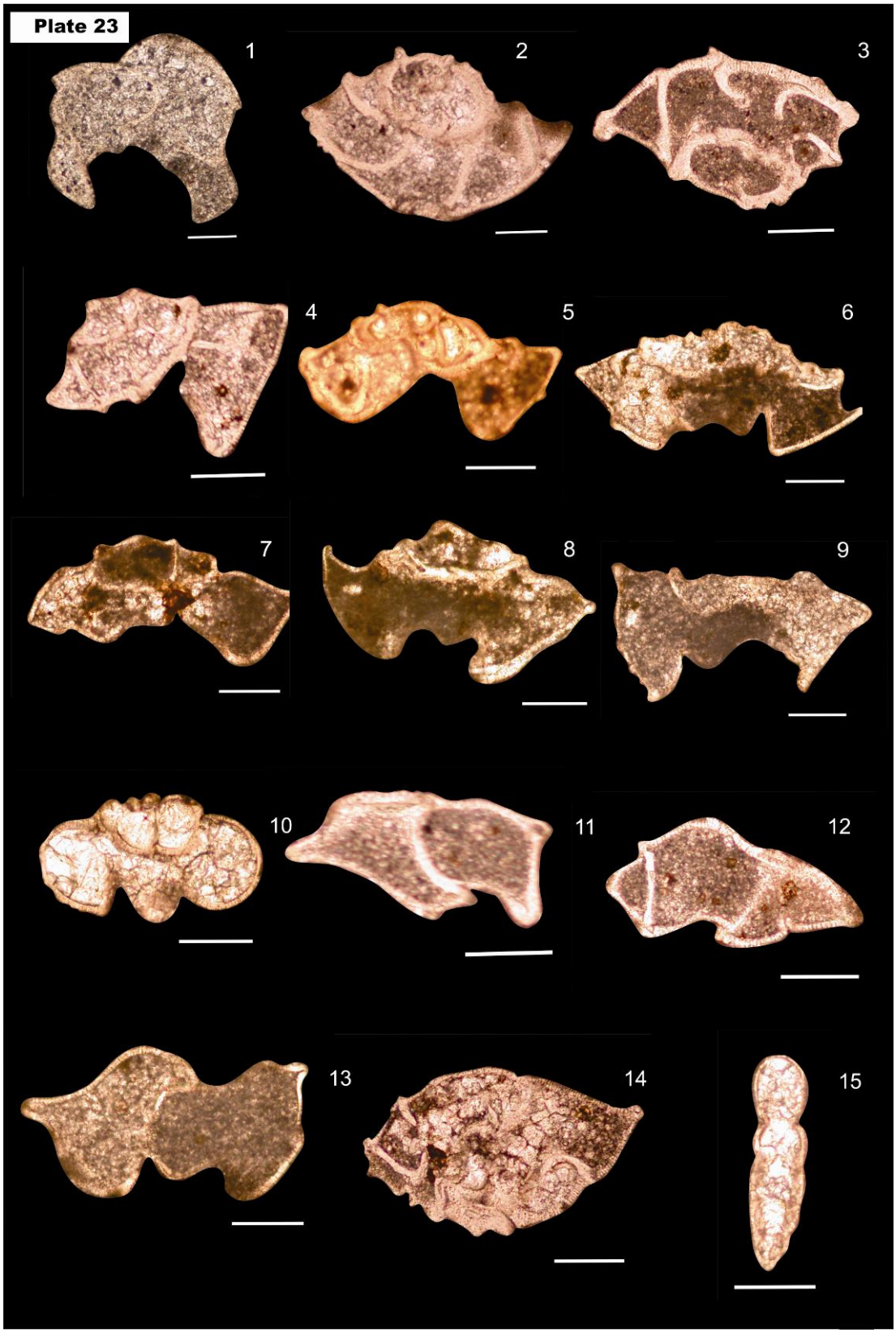
Plate 23
1
2
3
4
5
6
7
8
9
10
11
12
13
14
15

Plate 24

Fig. 1, *Hedbergella delrioensis* (Carsey), Spiral view, Sample MP 9

Fig. 2, *Hedbergella delrioensis* (Carsey), Umbilical view, Sample MP 9

Fig. 3, *Hedbergella delrioensis* (Carsey), Umbilical view, Sample MP 95

Fig. 4, *Hedbergella planispira* (Tappan), Umbilical view, Sample MP 66

Fig. 5, *Hedbergella planispira* (Tappan), Spiral view, Sample MP 66

Fig. 6, *Globigerinelloides algerianus* (Cushman & Ten Dam), Umbilical view, Sample MP 28

Fig. 7, *Globigerinelloides algerianus* (Cushman & Ten Dam), Spiral view, Sample MP 28

Fig. 8, *Hedbergella simplex* (Morrow), Spiral view, Sample MM 23

Fig. 9, *Ticinella roberti*, (Gandolfi), Spiral view, Sample MM 23

Fig.10, *Praeglobotruncana gibba*, (Claus), Umbilical view, Sample 23

Fig.11, *Ticinella raynaudi*, (Sigal), Spiral view, Sample MM23

Fig.12, *Ticinella madecassiana*, (Sigal), Umbilical view, Sample MM 23

Fig.13, *Planomalina buxtorfi*, (Gandolfi), Spiral view, Sample MM 23

Fig.14, *Praeglobotruncana delrioensis*, (Plummer), Spiral View, Sample MM 23

Note: All samples are from the Moghal Kot Section

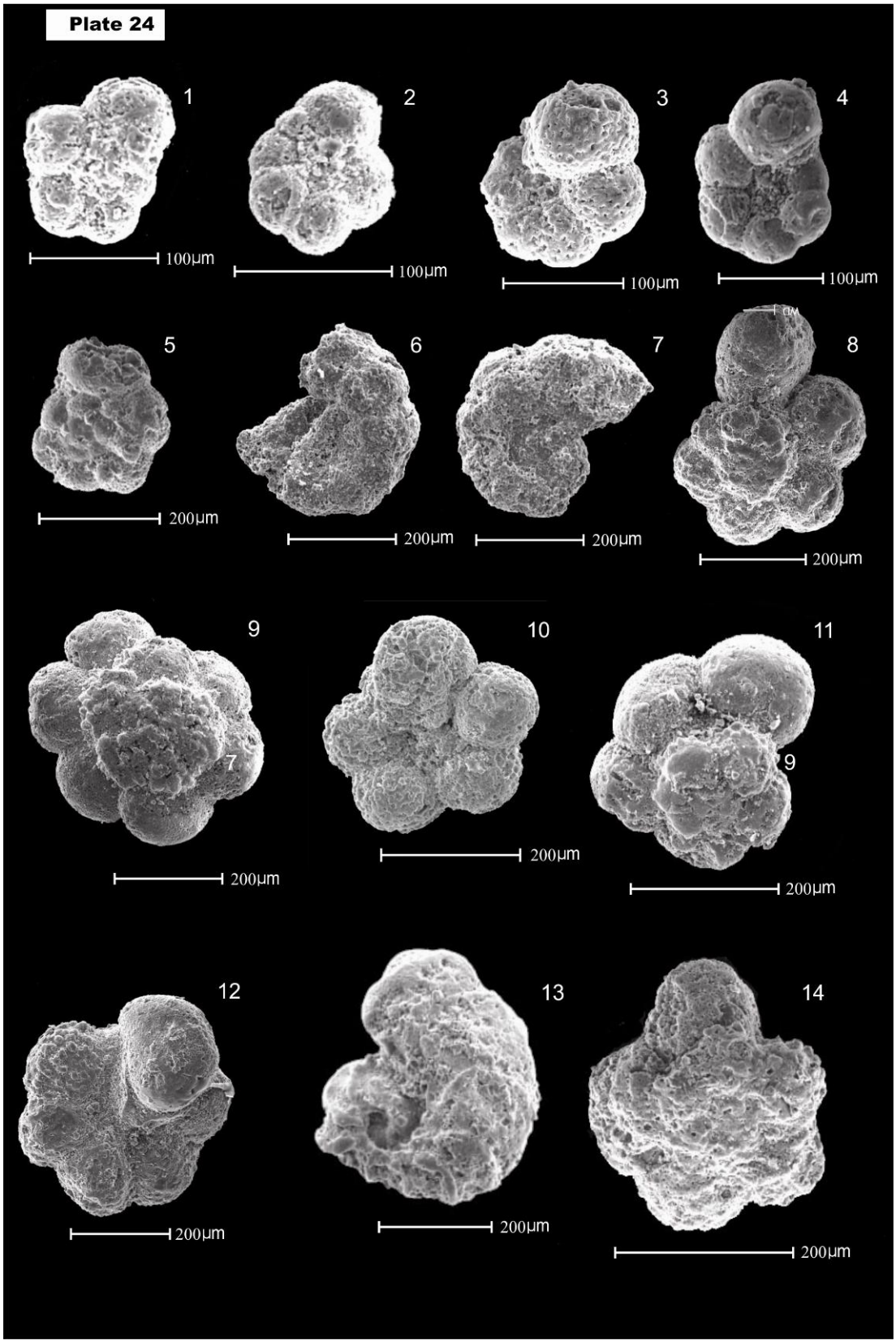
Plate 24
1
100µm
2
100µm
3
100µm
4
100µm
5
200µm
6
200µm
7
200µm
8
200µm
9
200µm
10
200µm
11
200µm
12
200µm
13
200µm
14
200µm

Plate 25

Fig. 1, *Hedbergella libyca* (Barr), Spiral view, Sample MM 23

Fig. 2, *Hedbergella libyca*, (Barr), Umbilical view, Sample MM 23

Fig. 3, *Hedbergella libyca*, (Barr), Top view, Sample MM 23

Fig. 4, *Rotalipora appenninica*, (Renz), Spiral view, Sample MM 23

Fig. 5, *Rotalipora appenninca*, (Renz), Umbilical view, Sample MM 23

Fig. 6, *Rotalipora brotzeni*, (Sigal), Umbilical view, Sample MM 23

Fig. 7, *Rotalipora brotzeni*, (Sigal), Umbilical view, Sample MM 23

Fig. 8, *Rotalipora gandolfi*, (Luterbacher & Premoli-Silva), Umbilical view, Sample MM23

Fig. 9, *Rotalipora cushmani*, (Morrow), Spiral View, Sample MM 25

Fig.10, *Rotalipora cushmani*, (Morrow), Spiral view, Sample MM 25

Fig.11, *Rotalipora cushmani*, (Morrow), Umbilical view, Sample MP 139

Fig.12, *Rotalipora greenhornensis*, (Morrow), Spiral view, Sample MP 139

Note: All samples are from the Moghal Kot Section

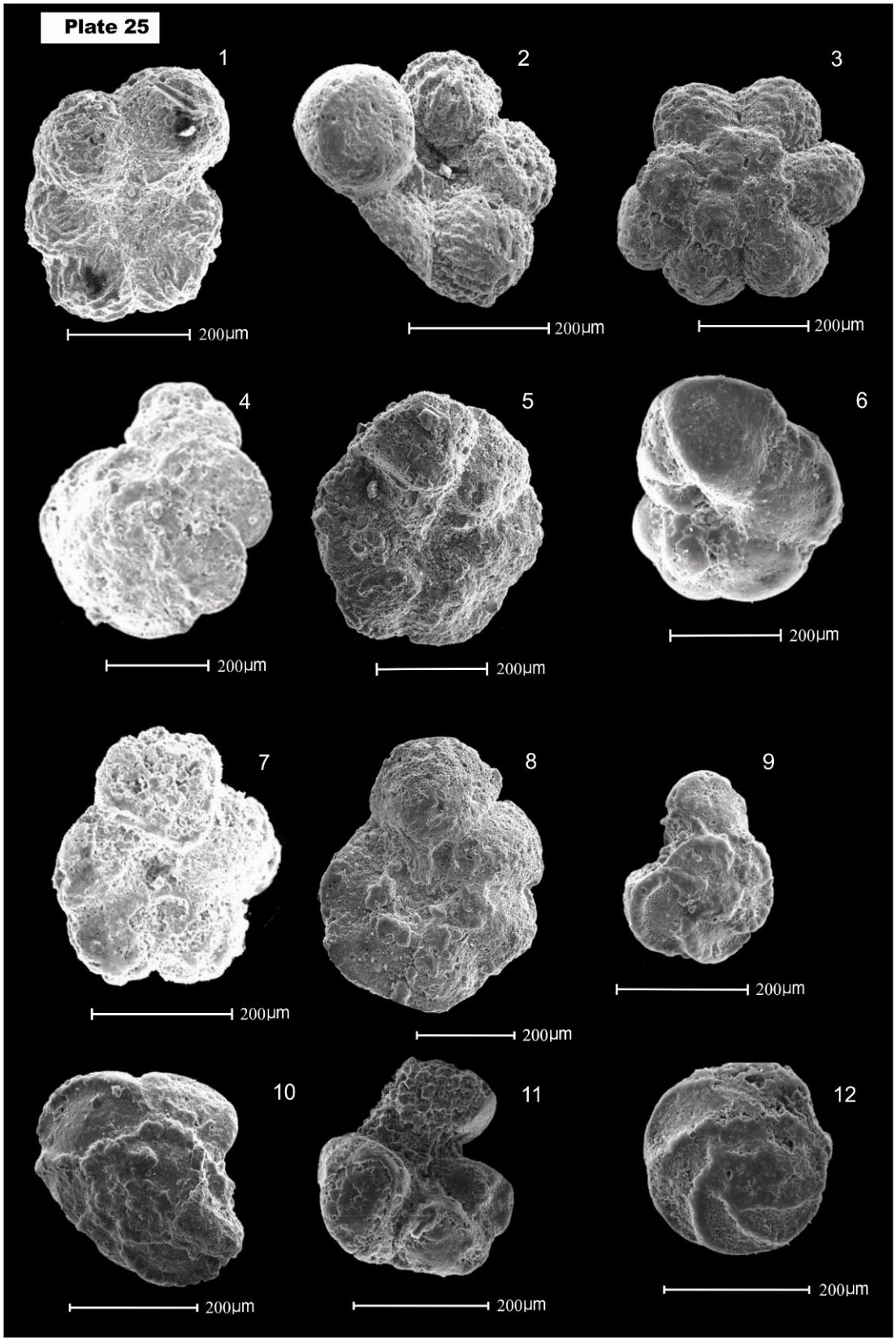
Plate 25
1
200µm
2
200µm
3
200µm
4
200µm
5
200µm
6
200µm
7
200µm
8
200µm
9
200µm
10
200µm
11
200µm
12
200µm

Plate 26

Fig. 1, *Rotalipora greenhornensis* (Morrow), Spiral view, Sample MP 139

Fig. 2, *Praeglobotruncana stephani* (Gandolfi), Spiral view, Sample MP 139

Fig. 3, *Praeglobotruncana gibba* (Klaus) Spiral view, Sample MP 139

Fig. 4, *Dicarinella imbricata* (Mornod), Spiral view, Sample MM 25

Fig. 5, *Dicarinella imbricata* (Mornod), Spiral view, Sample MM 25

Fig. 6, *Marginotruncana* sp., Spiral view, Sample MP 200

Fig. 7 *Praeglobotruncana* sp., Umbilical view, Sample MM 23

Fig. 8, *Whiteinella archaeocretacea* (Pessagno), Umbilical view, Sample MP 196

Fig. 9, *Whiteinella archaeocretacea* (Pessagno), Umbilical view, Sample MP 188

Fig.10, *Helvetoglobotruncana helvetica* (Bolli), Spiral view, Sample MP 188

Fig.11, *Helvetoglobotruncana helvetica* (Bolli), Spiral view, Sample MP 196

Fig.12, *Helvetoglobotruncana helvetica* (Bolli), Umbilical view, in Sample MP 191

Note: All samples are from the Moghal Kot Section

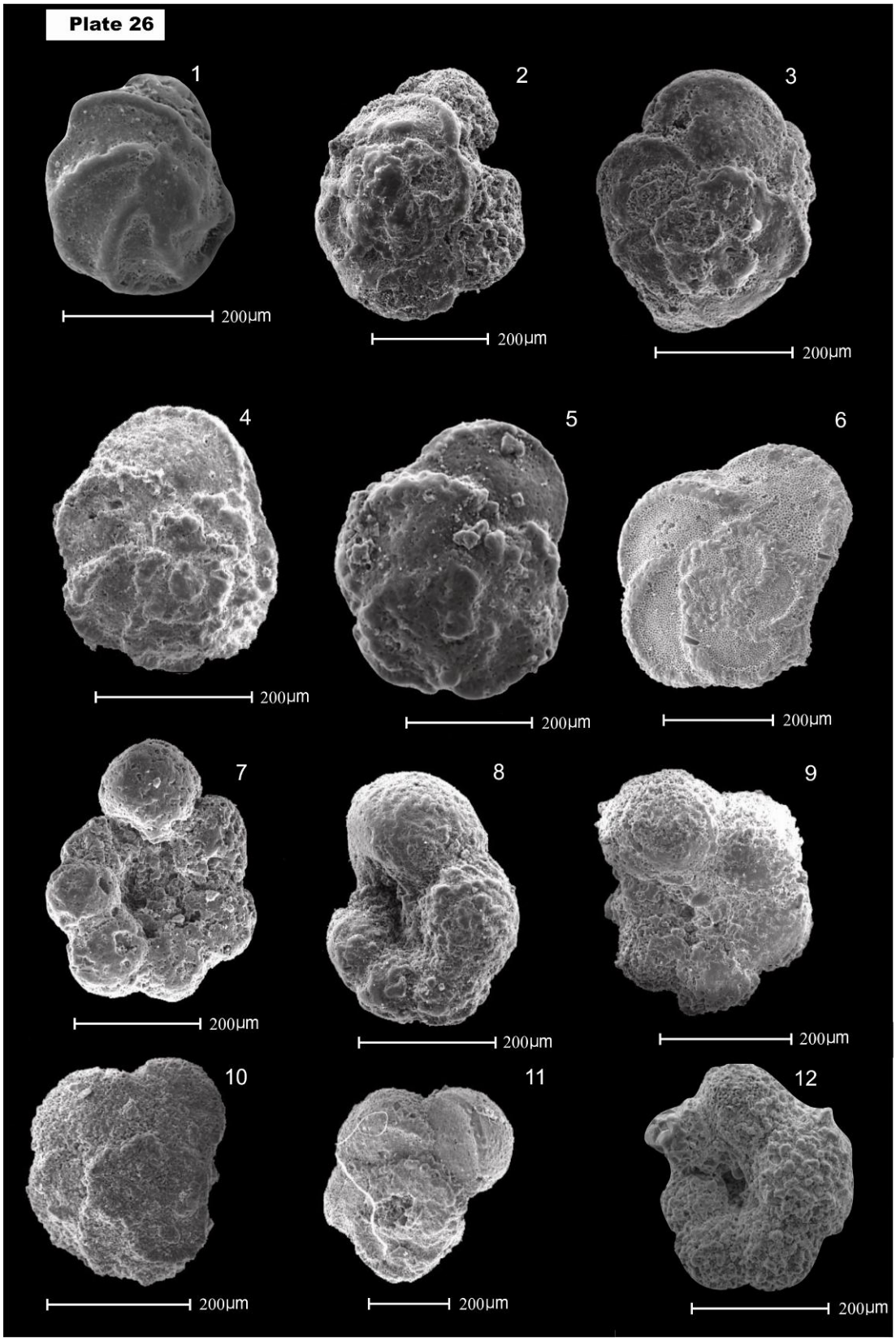
Plate 26
1
200µm
2
200µm
3
200µm
4
200µm
5
200µm
6
200µm
7
200µm
8
200µm
9
200µm
10
200µm
11
200µm
12
200µm

Plate 27

Fig. 1, *Praeglobotruncana difformis*, Spiral view, Sample MP 196

Fig. 2, *Dicarinella primitiva* (Dalbiez), Umbilical view, Sample MP 196

Fig. 3, *Marginotruncana sigali* (Reichel), Spiral view, Sample MP 196

Fig. 4, *Margintruncana sinousa* (Porthault), Spiral view, Sample MP 188

Fig. 5, *Marginotruncana sinousa* (Porthault), Spiral view, Sample MP 196

Fig. 6, *Dicarinella* cf. *asymetrica* (Sigal), Spiral view, Sample MP 200

Fig. 7, *Marginotruncana pseudolinneiana* (Pessagno), Spiral view, Sample MP 205

Fig. 8, *Marginotruncana pseudolinneiana* (Pessagno), Spiral view, Sample MP 200

Fig. 9, *Marginotruncana pseudolinneiana* (Pessagno), Umbilical, Sample MP 200

Fig.10, *Marginotruncana renzi* (Bolli), Spiral, Sample MP 200

Fig.11, *Globotruncana linneiana* (D' Orbigny), Spiral view, Sample MP 205

Fig.12, *Globotruncana linneiana* (D' Orbigny), Spiral view, Sample MP 200

Note: All samples are from the Moghal Kot Section

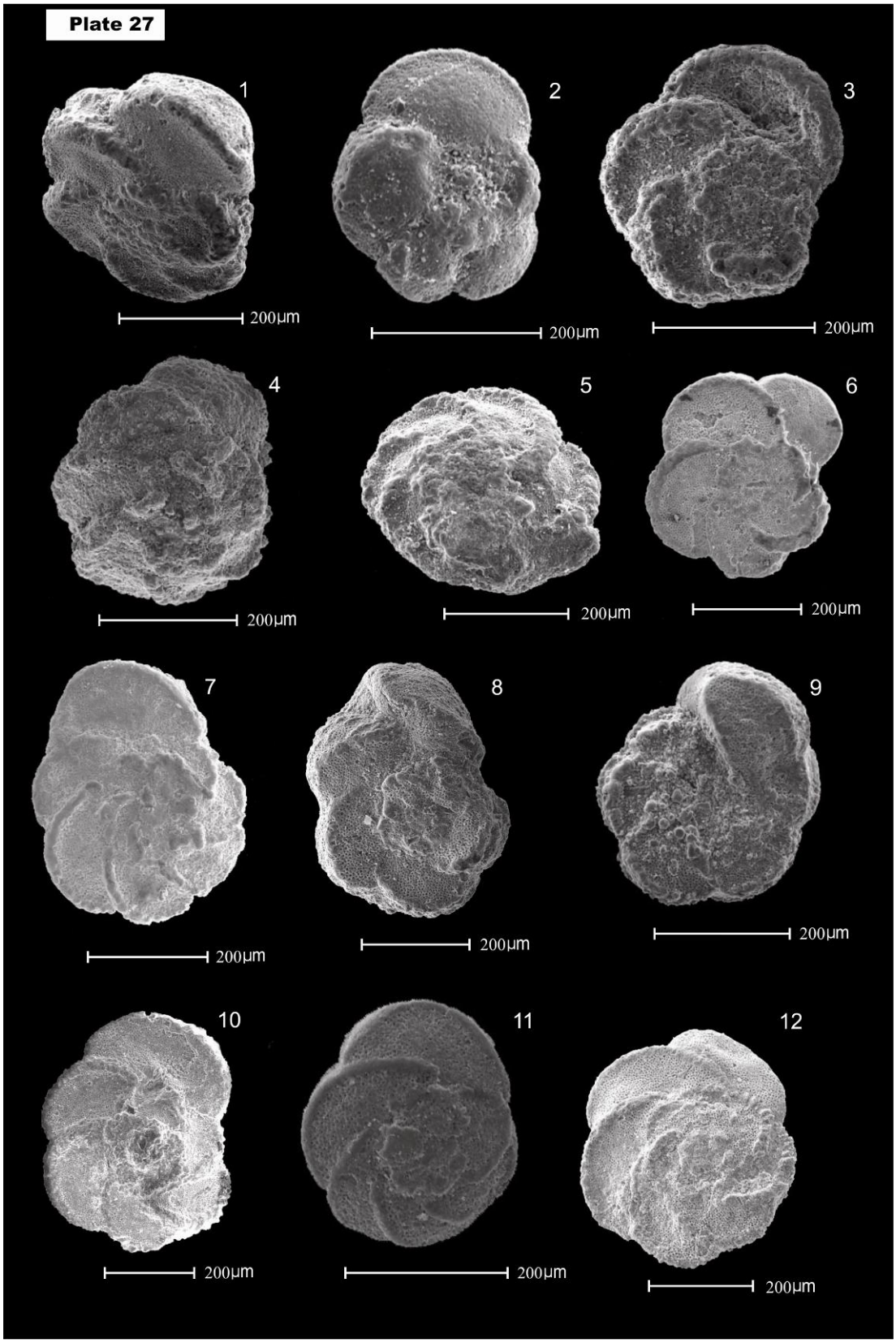
Plate 27
1
200µm
2
200µm
3
200µm
4
200µm
5
200µm
6
200µm
7
200µm
8
200µm
9
200µm
10
200µm
11
200µm
12
200µm

Plate 28

Fig. 1, *Globotruncana bulloides* (Vogler), Spiral view, Sample MP 205

Fig. 2, *Globotruncana bulloides* (Vogler), Spiral view, Sample MP 205

Fig. 3, *Globotruncana bulloides* (Vogler), Umbilicla view, Sample MP 205

Fig. 4, *Globotruncanita stuartiformis* (Dalbiez), Spiral view, Sample MP 205

Fig. 5, *Globotruncanita stuartiformis* (Dalbiez),, Spiral view, Sample MP 205

Fig. 6, *Globotruncanita stuartiformis* (Dalbiez), Spiral view, Sample MP 205

Fig. 7, *Globotruncanita stuartiformis* (Dalbiez), Spiral view, Sample MP 205

Fig. 8, *Globotruncana lapparenti* (Brotzen), Spiral view, Sample MP 205

Fig. 9, *Contusotruncana fornicata* (Plummer), Spiral view, Sample MP 207

Fig.10, *Contusotruncana fornicata* (Plummer), Spiral view, Sample MP 200

Fig.11, *Contusotruncana fornicata* (Plummer), Spiral view, Sample MP 200

Fig. 12, *Rugoglobigerina* sp. Spiral view, Sample MP 200

Note: All samples are from the Moghal Kot Section

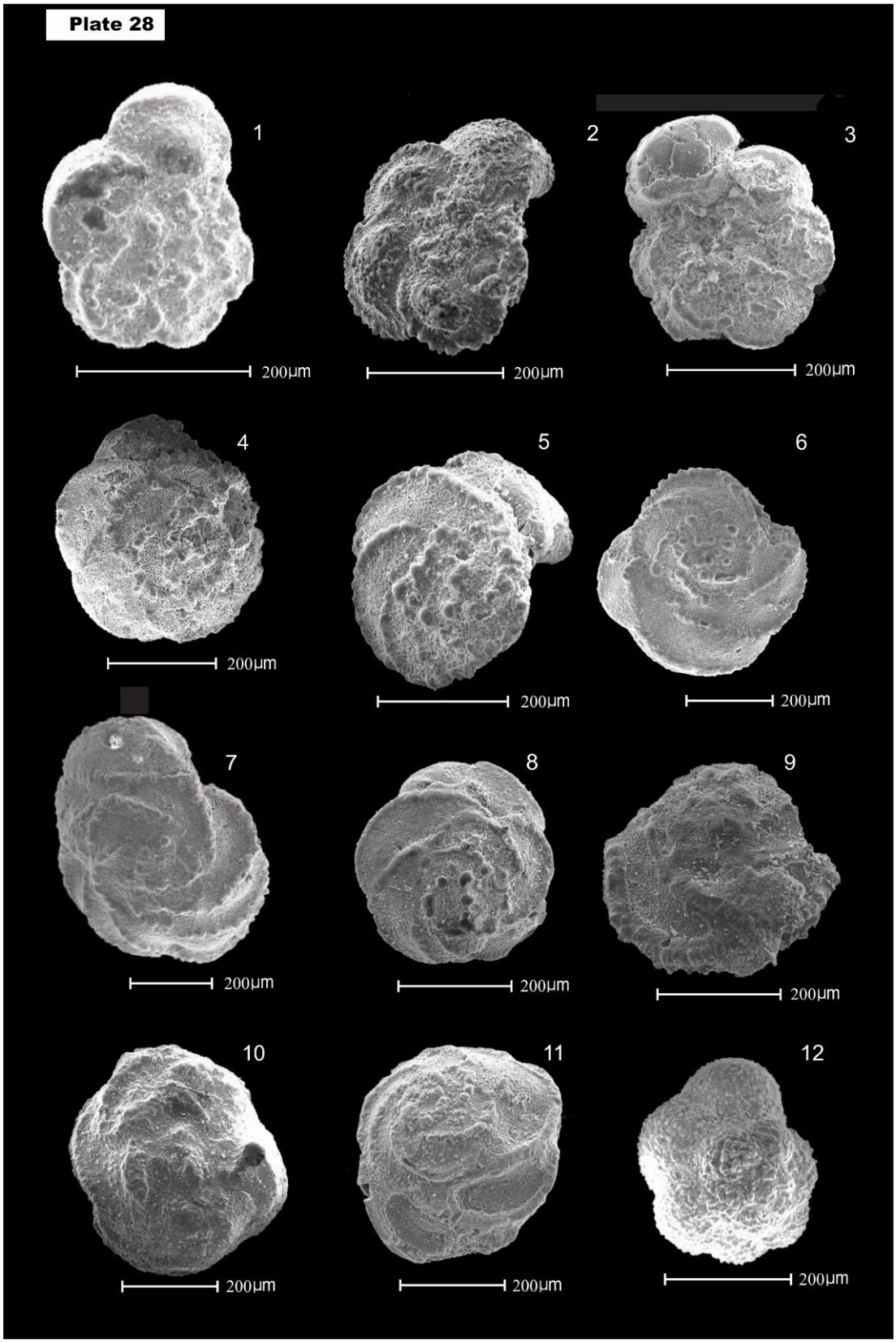
Plate 28
1
200µm
2
200µm
3
200µm
4
200µm
5
200µm
6
200µm
7
200µm
8
200µm
9
200µm
10
200µm
11
200µm
12
200µm

Plate 29

Fig. 1, *Contusotruncana fornicata* (Plummer), Spiral side, Sample MP 205

Fig. 2, *Contusotruncana fornicata*, (Plummer) Spiral side, Sample MP 200

Fig. 3, *Globotruncana arca* (Cushman), Spiral side, Sample MP 200

Fig. 4, *Globotruncana arca* (Cushman), Spiral side, Sample MP 205

Fig. 5, *Globotruncana arca* (Cushman), Spiral side, Sample MP 200

Fig. 6, *Globotruncana arca* (Cushman), Spiral side, Sample MP 200

Fig. 7, *Globigerinelloides prairiehillensis* (Pessagno), Spiral side, MP 200

Fig. 8, *Ventilabrella eggeri* (Cushman), Side view, Sample MP 206

Fig. 9, *Pseudoguembelina costulata* (Cushman), Side view, Sample MP 207

Fig.10, *Heterohelix reussi* (Cushman), Side view, Sample MP 200

Fig.11, *Heterohelix reussi* (Cushman), Side view, Sample MP 200

Fig.12, *Heterohelix reussi* (Cushman), Side view, Sample MP 200

Note: All samples are from the Moghal Kot Section

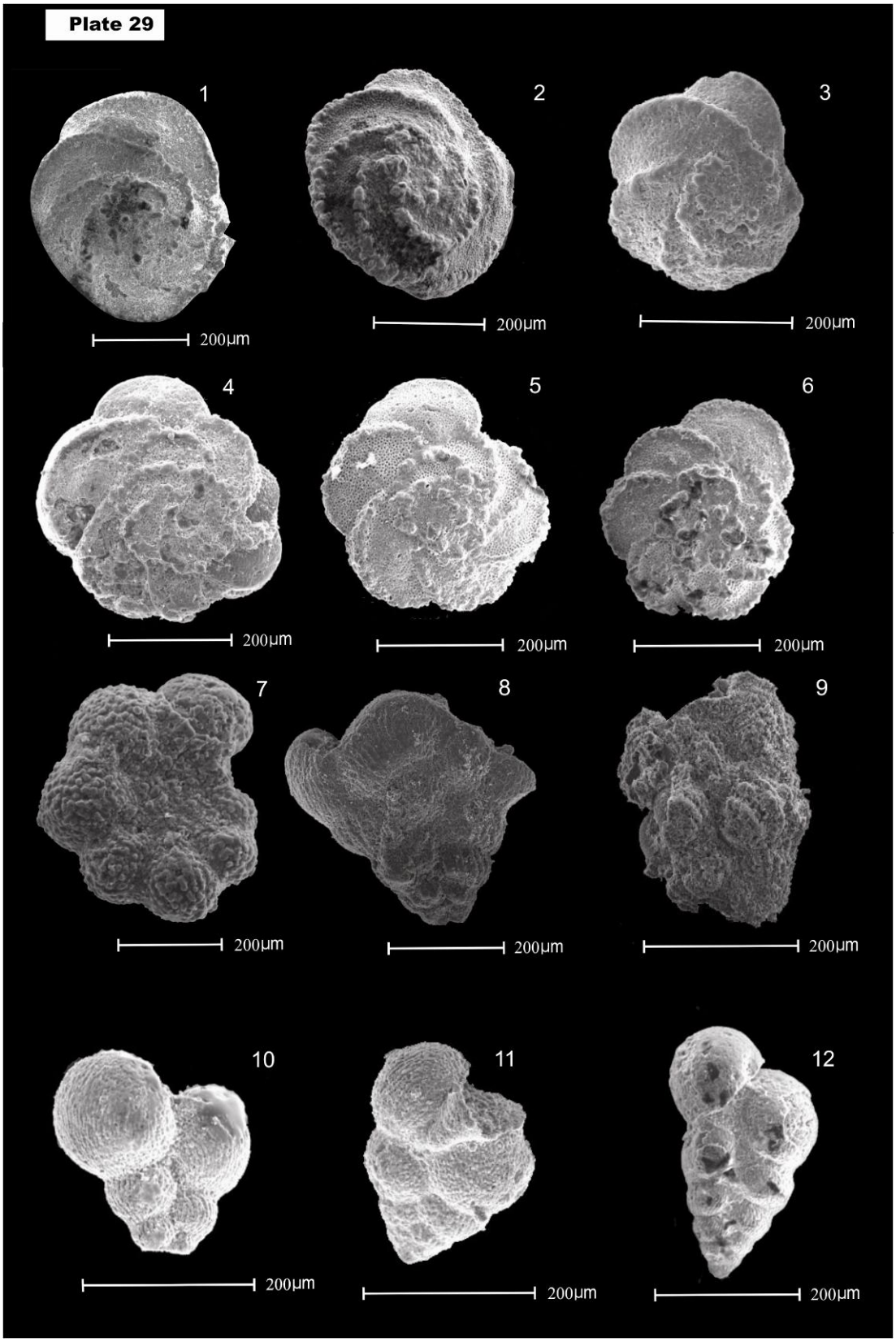
Plate 29
1
200µm
2
200µm
3
200µm
4
200µm
5
200µm
6
200µm
7
200µm
8
200µm
9
200µm
10
200µm
11
200µm
12
200µm

Plate 30

Fig. 1, *Sigalia carpathica* (Salaj & Samuel) Side view, Sample MP 200

Fig. 2, *Sigalia cf. carpathica* (Salaj & Samuel), Side view, Sample MP 200

Fig. 3, *Heterohelix striata* (Ehrenberg), Side view, Sample MP 205

Fig. 4, *Heterohelix striata* (Ehrenberg), Side view, Sample MP 203

Fig. 5, *Heterohelix striata* (Ehrenberg), Side view, Sample MP 200

Fig. 6, *Planoglobulina acervulinoides* (Egger), Side View, Sample MP 205

Fig. 7, *Pseudotextularia elegans* (Rezehak), Side view, Sample MP 205

Fig. 8, *Ammobaculites wenonahae*, Side view, Sample MP 72

Fig. 9, *Ammobaculites cf. reophacoides*, Side view, Sample MP 101

Fig. 10, *Marginopsis curuisepta*, Side view, Sample MP 205

Fig.11, *Frondicularia jarvesi*, Side view, Sample MP 208

Fig. 12, *Pyramidulina obscura*, Side view, Sample MP 196

Fig. 13, *Ammobaculites* sp., Side view, Sample MP 101

Fig.14, *Dentalina frontierensis*, Side view, Sample MP 196

Note: All samples are from the Moghal Kot Section. Figs. 8-12 are benthic foraminiferal taxa.

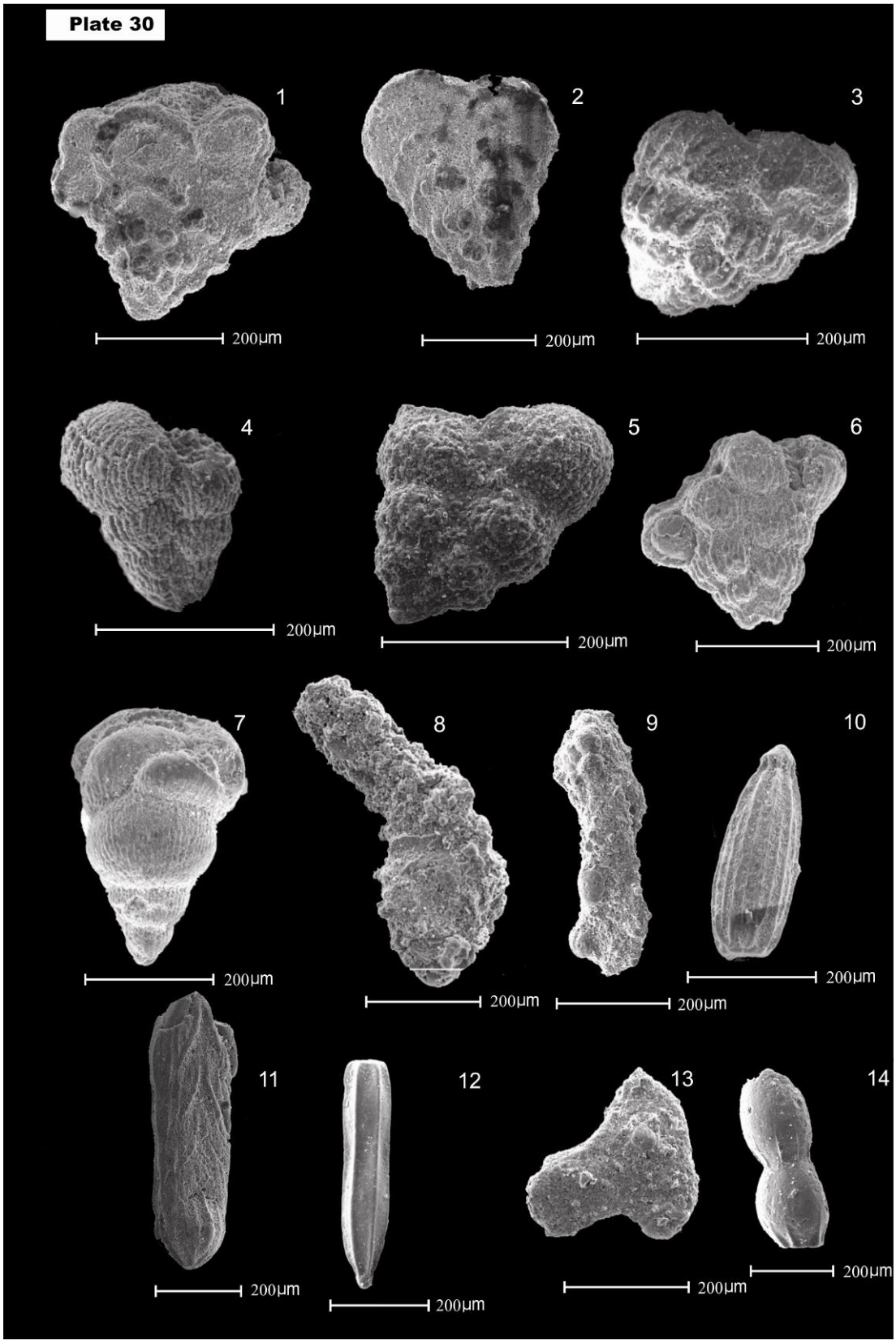
Plate 30
1
200µm
2
200µm
3
200µm
4
200µm
5
200µm
6
200µm
7
200µm
8
200µm
9
200µm
10
200µm
11
200µm
12
200µm
13
200µm
14
200µm

5.2.3 Biozones (fig. 5.1)

Biostratigraphy is the study of fossil contents of the layered sedimentary rocks. A stratigraphic interval defined by its fossil content, along with the evironmental factors are often taken into account in marking and interpreting the biozones (Nichols, 2009). Contrary to the formation, a biozone varies greatly in its thickness and geographical extent. The zonal categories designated in this work are as follows:

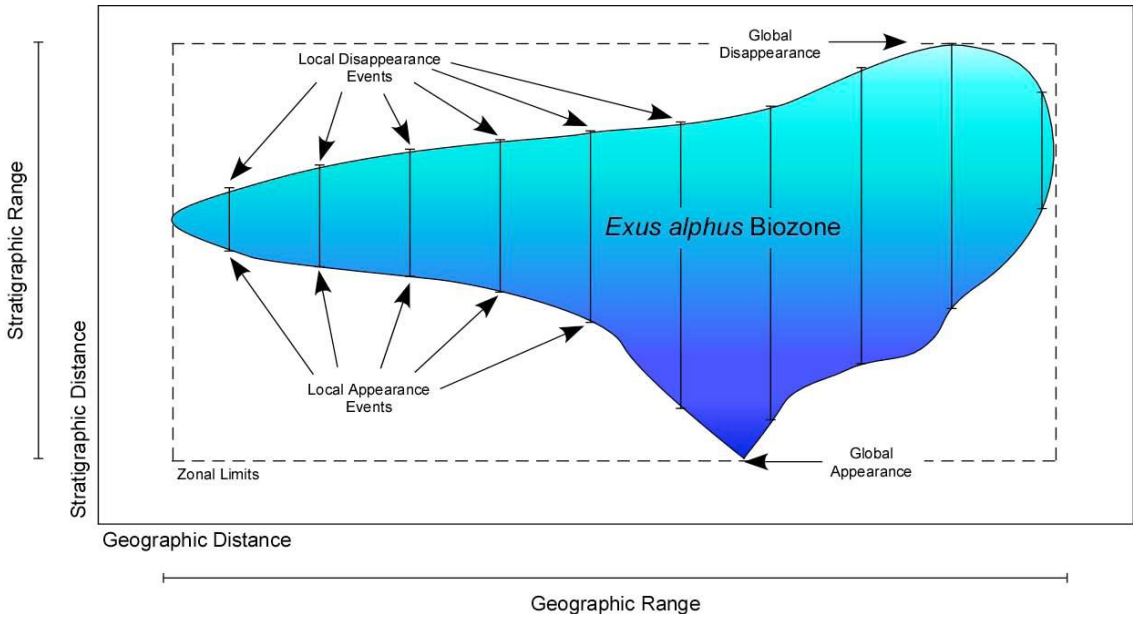

Figure 5.1: Relation between the spatio-temporal concept of a biozone and various local and global appearance and disappearance events, (MacLeod, 2005).

5.2.3.1 Taxon Range Zone (fig.5.2)

The Taxon Range Zone is the stratigraphic interval marked by the total stratigraphic range of a particular taxon. The biozone may have essentially diachronous boundaries as the speciation and extinction of a defining taxon vary geographically (MacLeod, 2005). The sampling size and frequency at both the upper and lower boundaries may affect the appearance and disappearance of a taxon (MacLeod, 2005). The higher sampling frequency and larger size of the samples at both ends will better encompass the taxon range zone. The local bondaries of taxon range zone are often correlated across the sedimentary successions in order to better constrain the boundaries of taxon range zone. The defining taxon gives its name to the taxon range zone.

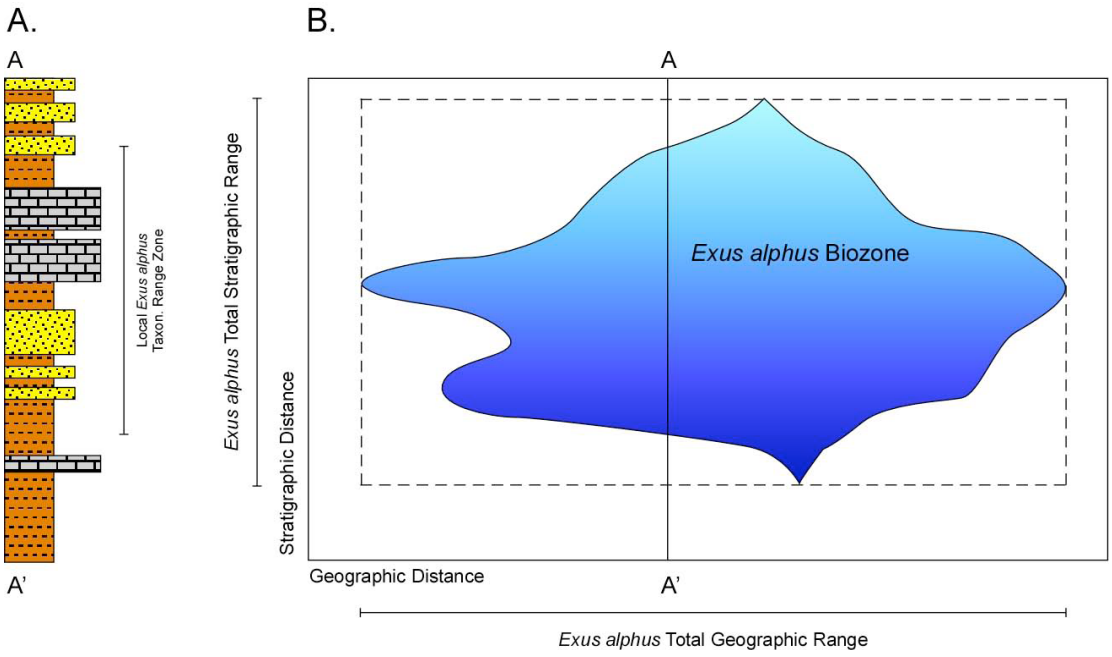

Figure 5.2: One-dimensional (A) and two-dimensional (B) representations of a taxon range biozone (MacLeod, 2005).

5.2.3.2 Interval Zone or Partial Range Zone (fig.5.3)

An interval zone or partial range zone is an undefined zone between other biozones and its boundaries are marked by a wide range of criteria (MacLeod, 2005). It includes two extinction events, two origination events, or one origination event and one extinction event etc. The biozone is also named after the taxon which occurs in the interval.

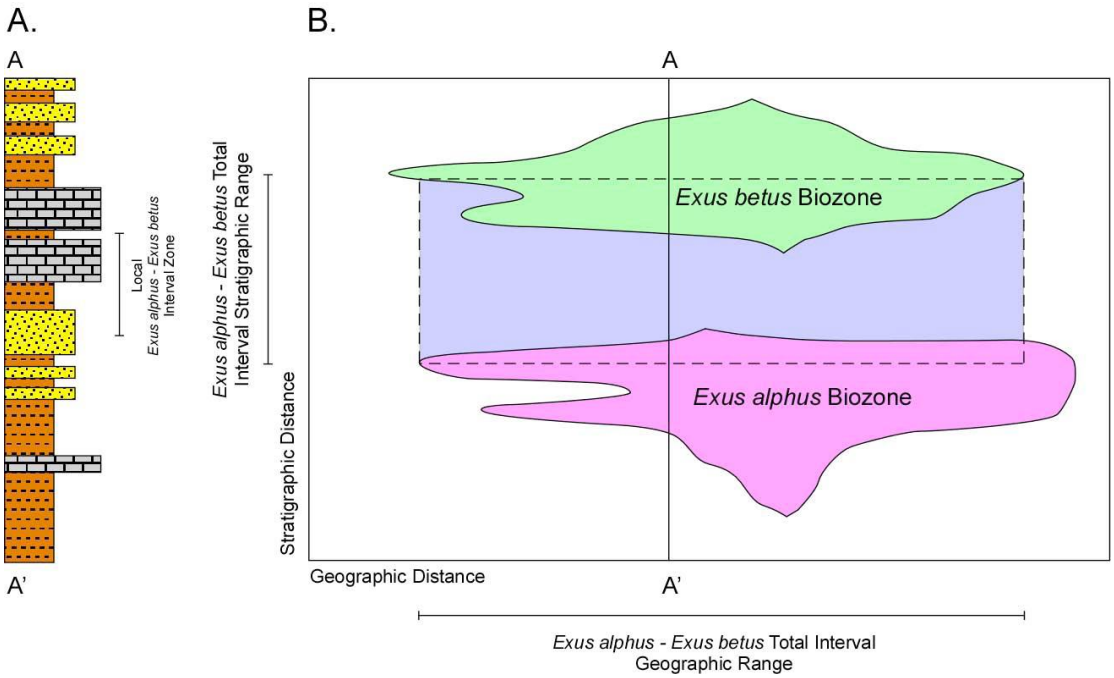

Figure 5.3: One-dimensional (A) and two-dimensional (B) representations of an interval biozone (MacLeod, 2005).

5.2.4 Principal sections through the planktonic foraminiferal test

The type of section through the specimens is important for the recognition of the species. Various sections are defined as follows (fig.5.4)

Axial section: A section passing through the axis of coiling.

Subaxial section: A section passing parallel to the axis of coiling but not passing through the proloculus.

Transverse section: A section passing perpendicular to the axis of coiling.

Oblique section: A section passing neither parallel nor perpendicular to the axis of coiling.

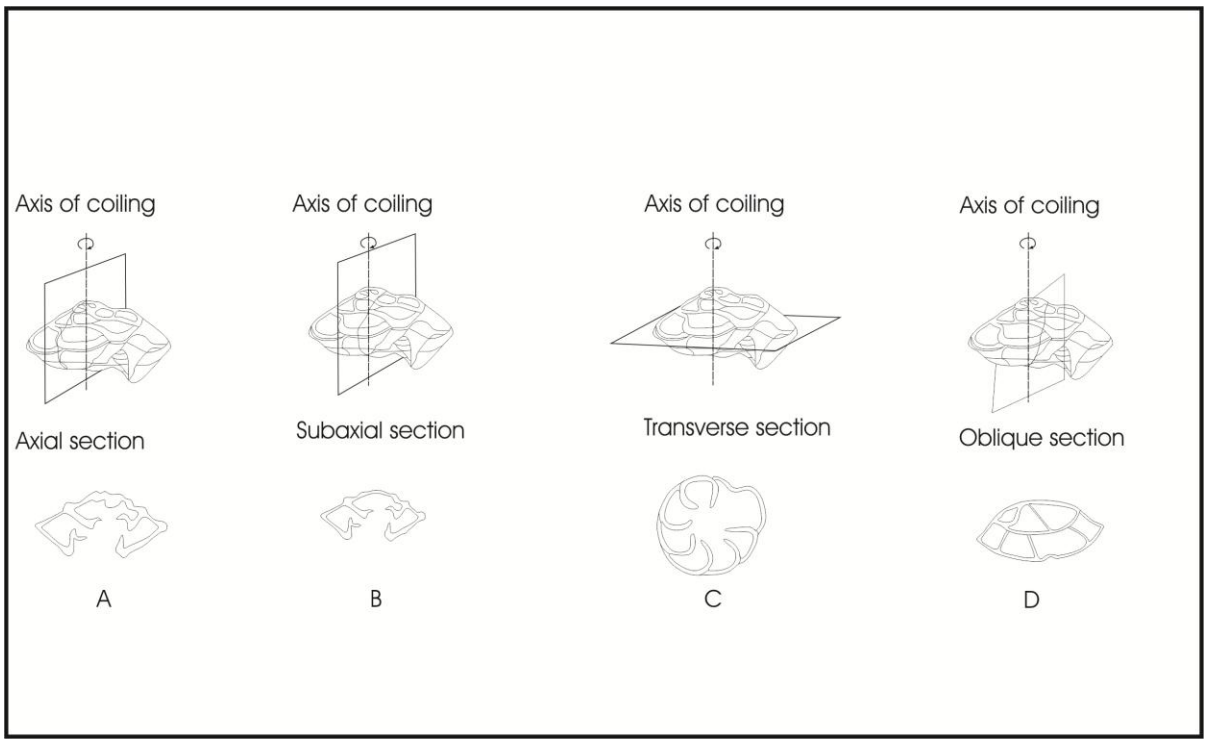

Figure 5.4: Principal sections through a planktonic foraminiferal test modified after Sari (2006).

5.2.5 Planktonic foraminiferal biozones in the Moghal Kot section

The upper part of the Moghal Kot Section (i.e. Parh Formation) is investigated for the planktonic foraminiferal content using 217 samples. Most of the samples have the MP code (M stands for Moghal Kot and P stands for Parh). Some of the samples have a different code, i.e MM 23, MM 24, MM 25, and MM 26, because these samples were collected at a different time, where the MM code stands for Moghal Kot Mela (Mela in the local language means village). Presence and absence of species are recorded in each sample, and species distribution charts are reconstructed (figs. 5.5, 5.6, 5.7 & 5.8, arrows within these charts indicate the First Appeance Datums (FADs) and Last Appeance Datums (LADs). At the same time, these charts provide a framework for the planktonic foraminiferal range charts based on the FADs and LADs (figs.5.9, 5.10, 5.11 & 5.12). The correlation of the planktonic foraminiferal biozones of the Parh Formation with the various global biozonation schemes is made (see fig. 5.13). The formainfera taxa which have small stratigraphic ranges and/are have lesser stratigraphic importance are not shown in the presense/absence and range charts i.e. *Hedbergella rhinoceros, Hedbergella hispaniae, Hedbergella libyca, Praeglobotruncana difformis, Sigalia carpathica, Aragonia* sp., *Biticinella*

subbreggiensis, Globigerinelloides messinae, Globigerinelloides volutus, Macroglobigerinelloides bentonensis, Contusotruncana contusa, Globotruncana dupeublei, Globotruncana stephensoni, Gublerina cf. *robusta.*

The criteerion for defining the biozone is based on the FAD and LAD of index species. The FAD and LAD of an index species represents a specific geological time at which the species appeared globally. Although sometime there is a mismatch in the FAD or LAD of a particular species in different parts of the globe. In order to precisely define the biozonal boundaries, the FADs and LADs of index species are used in combination with FADs and LADs of associated species assemablges. These locally erected biozones including the species assemblages of biozones are compared with the standard literature of Sliter (1989) and Caron (1985). The detailed biozonal criterion is further discussed in the remarks section of a biozone. A total of 15 biozones were identified, of which 5 are local biozones and 10 are global biozones. The previously recognised global *Rotalipora reicheli*, *Whiteinella archaeocretacea*, *Marginotruncana sigali*, and *Globotruncanita elevata* Biozones were not found. The subzones of Sliter (1989), i.e. the *Ticinella praeticinensis*, *Rotalipora subticinensis*, *Rotalipora greenhornensis*, and *Dicarinella algeriana* Subzones were not identified, because of the rarity of the key species despite many samples in these intervals. Based on this study the following biozones were found.

5.2.5.1 Local Hedbergella delrioensis Partial Range Zone

Age: Early to Late Aptian

Author: Khan (this thesis)

Definition: It is the interval described by presence of *Hedbergella delrioensis* and absence of *Globigerinelloides algerianus*. This is a partial range zone of *Hedbergella delrioensis.* The first presence of *Hedbergella delrioensis* occurs at the bottom of the limestone section, and thus its 'true' first occurrence may be older.

Species assemblage of the zone: *Hedbergella delrioensis, Hedbergella sigali, Hedbergella trocoidea, Hedbergella praetrocoidea, Hedbergella planispira*.

Remarks: The *Hedbergella delrioensis* Zone is most likely equivalent to the globally recognised *Leupoldina cabri* and *Globigerinelloides ferreolensis* Zones of Sliter (1989). The species *Leupoldina cabri* is not present in the Moghal Kot Section, probably its absence can be explained by the delicate nature of its test, and thus specimens of this species are not preserved here. The occurrence of *Globigerinelloides algerianus* above the *Hedbergella delrioensis* Zone confirms that the age of this local zone is equivalent to that of the combined age of the *Leupoldina cabri* and *Globigerinelloides ferreolensis* Biozones (Sliter, 1989), implying Early to Late Aptian.

The presence of *Hedbergella trocoidea* in the *Hedbergella delrioensis* Zone is anomalously early compared to its distribution in other sections, where mostly it appears in the younger *Globigerinelloides algerianus* Zone (Caron, 1985; Sliter, 1989; Sliter, 1999). Hence, this species shows an early appearance in this part of the Tethys Ocean.

5.2.5.2 Globigerinelloides algerianus Total Range Zone

Age: Late Aptian

Author: Moullade (1966)

Definition: This zone is based on the entire stratigraphic range of *Globigerinelloides algerianus*.

Species assemblages of the zone: Globigerinelloides algerianus, Globigerinelloides ferreolensis, Hedbergella trocoidea, Hedbergella planispira, Hedbergella delrioensis, Hedbergella gorbachikae.

Remark: The FAD of *Hedbergella gorbachikae* is documented here in this biozone. The FAD occurs also in this biozone elsewhere (Sliter, 1989; 1999; Caron, 1985).

5.2.5.3 Hedbergella Gorbachikae Partial Range Zone

Age: Late Aptian

Author: Longoria (1974)

Definition: This interval spans from the LAD of *Globigerinelloides algerianus* to the FAD of *Ticinella bejaouaensis*.

Species assemblages of the zone: Hedbergella planispira, Hedbergella gorbachikae, Hedbergella delrioensis, Globigerinelloides ferreolensis, Planomalina cheniourensis, and Hedbergella trocoidea.

Remark: The species *Planomalina cheniourensis* appears in this zone in the Moghal Kot Section.

5.2.5.4 Ticinella bejaouaensis Partial Range Zone

Age: Late Aptian to Early Albian

Author: Moullade (1966)

Definition: The interval ranges from the FAD of *Ticinella bejaouaensis* to the FAD of *Ticinella primula*.

Species assemblage of the zone: Ticinella bejaouaensis, Hedbergella trocoidea, Hedbergella planispira, Hedbergella delrioensis, Hedbergella gorbachikae, Hedbergella rischi, Planomalina cheniourensis, Globigerinelloides barri, Globigerinelloides ferreolensis.

Remarks: The rocks covering this zone generally contain low abundances of planktonic foraminifera. The planktonic foraminiferal fauna also shows a low diversity. The *Globigerinelloides ferreolensis* and *Planomalina cheniourensis* have their Last Appearance Datum levels (LAD) in this zone, while *Globigerinelloides bentonensis* and *Hedbergella rischi*, and *Globigerinelloides barri* have their FADs in the current zone. The timing of the FAD of *Hedbergella rischi* in the section is different from that in other areas, where it occurs later in the *Ticinella primula* Zone. (Sliter, 1989; 1999).

5.2.5.5 Ticinella primula Partial Range Zone

Age: Middle Albian

Author: Moullade (1966)

Definition: This interval ranges from the FAD of *Ticinella primula* to the FAD of *Biticinella breggiensis*.

Species assemblages of the zone: Ticinella primula, Ticinella roberti, Ticinella bejaouaensis, Hedbergella planispira, Hedbergella gorbachikae, Hedbergella trocoidea, Hedbergella rischi, Hedbergella delrioensis, Hedbergella simplex, Globigerinelloides bentonensis.

Remarks: The rocks show increased abundances of planktonic foraminifera in this zone. *Hedbergella simplex* and *Ticinella roberti* have their FADs in this zone. Elsewhere, Sliter (1989) and Caron (1985) documented an earlier appearance of *Ticinella roberti*, more specifically in the *Ticinella bejaouaensis* Zone.

5.2.5.6 Local Biticinella breggiensis Partial Range Zone

Age: Middle Albian

Author: Khan (this thesis)

Definition: This interval ranges from the FAD of *Biticinella breggiensis* to the FAD of *Planomalina buxtorfi*.

Species assemblage of the zone: Biticinella breggiensis, Ticinella raynaudi, Ticinella roberti, Ticinella primula, Ticinella praeticinensis, Ticinella bejaouaensis, Ticinella madecassiana, Hedbergella planispira, Hedbergella rischi, Hedbergella simplex, Hedbergella trocoidea, Hedbergella gorbachikae, Hedbergella delrioensis, Globigerinelloides bentonensis.

Remarks: The rocks show a dramatic increase in abundance and diversity of planktonic foraminiferal species in this zone. *Ticinella madecassiana, Ticinella praeticinensis,* and *Ticinella raynaudi* appear in this zone. The upper boundary of this zone is defined here by the FAD of the *Planomalina buxtorfi* instead of the FAD of *Rotalipora ticinensis*, which has been used to define the boundary elsewhere (Moullade, 1966; Caron, 1985; Sliter, 1989). In this section, the FAD of *Rotalipora ticinensis* is thought to be less reliable because of its irregular appearance in the early part of its range.

5.2.5.7 Local Planomalina buxtorfi Partial Range Zone

Age: Late Albian

Author: Khan (this thesis)

Definition: This interval ranges from the FAD of *Planomalina buxtorfi* to the FAD of *Rotalipora appenninica*.

Species assemblage of the zone: Rotalipora ticinensis, Biticinella breggiensis, Ticinella raynaudi, Ticinella praeticinensis, Ticinella madecassiana, Ticinella roberti, Ticinella primula, Hedbergella planispira, Hedbergella gorbachikae, Hedbergella delrioensis, Hedbergella trocoidea, Hedbergella simplex, Hedbergella rischi, Praeglobotruncana delrioensis, Planomalina buxtorfi, Globigerinelloides bentonensis, Globigerinelloides ultramicrus, Globigerinelloides caseyi.

Remarks: Increased diversification occurs in the early part of the zone. In contrast, diversification in this zone started in the upper half elsewhere (Sliter, 1989). The FADs of *Globigerinelloides ultramicrus* and *Praeglobotruncana delrioensis* occur in this zone. This local biozone correlates with the *Rotalipora ticinensis* Zone of Dalbiez (1955).

5.2.5.8 Rotalipora appenninica Partial Range Zone

Age: Late Albian

Author: Brönnimann (1952)

Definition: This interval zone spans from the FAD of *Rotalipora appenninica* to the FAD of *Rotalipora brotzeni*.

Species assemblage of the Zone: Rotalipora appenninica, Rotalipora praeappenninica, Rotalipora gandolfi, Rotalipora ticinensis, Rotalipora subticinensis, Ticinella raynaudi, Ticinella primula, Ticinella robertii, Ticinella madecassiana, Ticinella praeticinensis, Planomalina buxtorfi, Praeglobotruncana delrioensis, Planomalina praebuxtorfi, Hedbergella simplex, Hedbergella trocoidea, Hedbergella delrioensis, Hedbergella planispira, Heterohelix moremani,

Globigerinelloides bentonensis, Globigerinelloides ultramicrus, Globigerinelloides caseyi.

Remarks: In this biozone the planktonic foraminiferal abundance and diversity increase further. For instance, *Rotalipora praeappenninica, Ticinella praeticinensis, and Globigerinelloides caseyi* are present in this zone, and the FADs of *Rotalipora gandolfi and Heterohelix moremani* occur. Noteworthy is that the FAD of *Rotalipora praeappenninica* occurs also in this zone, synchronously with the FAD of *Rotalipora appenninica*. Possibly specimens of *R. praeappenninica* are rare in the early part of its range. Specimens of *Planomalina buxtorfi* are abundant in this zone, which dominates the planktonic foraminiferal assemblage. *Rotalipora ticinensis, Rotalipora subticinensis, Ticinella raynaudi, Ticinella praeticinensis, and Ticinella primula* have their LADs in this biozone. Elsewhere, the *Rotalipora subticinensis, Ticinella praeticinensis,* and *Ticinella primula* disappear earlier, more specifically in the *Rotalipora ticinensis* Zone (e.g. Caron, 1985; Sliter 1989). Conversely, the *Rotalipora ticinensis* has its LAD later, more specifically in the *Rotalipora brotzeni* Zone (Sliter, 1989).

5.2.5.9 Rotalipora brotzeni Partial Range Zone

Age: Early Cenomanian

Author: Khan (this thesis)

Definition: The interval ranges from the FAD of *Rotalipora brotzeni* to the FAD of *Rotalipora cushmani*.

Species assemblage of the zone: Rotalipora brotzeni, Hedbergella delrioensis, Hedbergella planispira, Hedbergella simplex, Ticinella roberti, Ticinella medecassiana, Planomalina buxtorfi, Rotalipora balernaensis, Rotalipora gandolfi, Rotalipora appenninica, Rotalipora ticinensis, Rotalipora montsalvensis, Globigerinelloides bentonensis, Globigerinelloides ultramicrus, Globigerinelloides caseyi, Heterohelix moremani, Praeglobotruncana delrioensis, and Praeglobotruncana stephani.

Remarks: This zone is defined by the FAD of the zonal marker. Noteworthy is that the FAD of *Rotalipora montsalvensis* occurs at the same time. The FAD of *Rotalipora balernaensis* and *Praeglobotruncana stephani* occur in this zone. In other areas, the latter species occurred earlier in the *Rotalipora appenninica* Zone Caron (1985). *Heterohelix* is absent from the rocks in this interval, indicating low abundance of *Heterohelix in* the ocean at this time.

Rotalipora reicheli is an important species in most global zonation schemes, but here, it occurs just once, in Sample MP 132, synchronously with the FAD of *Rotalipora cushmani*. Because of its rarity, the global *Rotalipora reicheli* Zone was not identified here (Caron, 1985; Sliter, 1989), and consequently the *Rotalipora reicheli* Zone is included in the *Rotalipora cushmani* Zone.

5.2.5.10 Rotalipora cushmani Total Range Zone

Age: Middle to late Cenomanian

Author: Borsetti (1962)

Definition: The zone covers the entire range of *Rotalipora cushmani*.

Species assemblage of the biozone: Rotalipora cushmani, Rotalipora greenhornensis, Rotalipora brotzeni, Rotalipora deekei, Rotalipora appenninica, Rotalipora gandolfi, Rotalipora montsalvensis, Rotalipora brotzeni, Rotalipora balernaensis, Rotalipora reicheli, Dicarinella algeriana, Dicarinella imbricata, Dicarinella canaliculata, Whiteinella aprica, Whiteinella brittonensis, Whiteinella praehelvetica, Praeglobotruncana delrioensis, Praeglobotruncana stephani, Globigerinelloides bentonensis, Globigerinelloides ultramicrus, Hedbergella delrioensis, Hedbergella planispira, Hedbergella simplex, Heterohelix reussi, Rotalipora globotruncanoides, Heterohelix moremani, Praeglobotruncana gibba.

Remarks: The *Dicarinella algeriana* and whiteinellids show their FADs in the lower most part of the zone. The *Dicarinella imbricata*, *Dicarinella canaliculata*, *Rotalipora deekei*, *Praeglobotruncana gibba*, and *Heterohelix reussi* have their FADs in the upper part of the zone. *Rotalipora globotruncanoides* has rare occurrences in the upper part of the zone. The rotaliporids are dominant in this zone, which has been seen also elsewhere (Premoli-Silva & Sliter, 1994). The abundance

of the *Rotalipora cushmani* decreases towards the top of this zone. Rotaliporids disappear at the onset of black shale formation in the Early Turonian. This black shale unit obviously correlates with the global Bonarelli Event (OAE 2), taking the current planktonic foraminiferal stratigraphy into account. Noteworthy is that all the planktonic foraminifera disappeared at the onset of the black shale unit including *Whiteinella archaeocretacea,* therefore the global zone based on the partial range of of the *Whiteinella archaeocretacea* is defined arbitararliy between the *Rotalipora cushmani* and *Helvetolobotrucnana helvetica* Biozones (according to Sliter, 1989; Caron, 1985; and Premoli-Silva, 1994). This arbitaray zone is barren of planktonic foaminifera, therefore it is not described in detail. The late appearance of the *Whiteinella archaeocretacea* is most likely influenced by adverse environmental conditions in this part of the ocean.

5.2.5.11 Local Helvetoglobotruncana helvetica Partial Range Zone

Age: Early to middle Turonian

Author: Khan (this thesis)

Definition: The interval ranges from the FAD of *Helvetoglobotruncana helvetica* to the FAD of the *Dicarinella concavata*.

Species assemblage in this zone: Helvetoglobotruncana helvetica, Dicarinella algeriana, Dicarinella canaliculata, Dicarinella imbricata, Dicarinella hagni, Marginotruncana renzi, Marginotruncana schneegansi, Marginotruncana marianosi, Marginotruncana coronata, Marginotruncana marginata, Marginotruncana sigali, Marginotruncana sinousa, Whiteinella baltica, Whiteinella inornata, Whiteinella paradubia, Whiteinella aprica, Whiteinella brittonensis, Whiteinella praehelvetica, Whiteinella archaeocretacea, Whiteinella aumalensis, Whiteinella baltica, Hedbergella simplex, Praeglobotruncana stephani, Praeglobotruncana gibba, Heterohelix moremani, Heterohelix reussi.

Remarks: The *Helvetoglobotruncana helvetica* Zone is usually defined as a total range zone (Dalbiez, 1955). However, the zonal marker extends upwards into the *Dicarinella asymetrica* Zone in this part of the Tethys Ocean. Therefore the upper boundary is redefined in this study. The FAD of the zonal marker occurs above the interval where several species, e.g. rotaliporids, became extinct in the early Turonian.

The *Globigerinelloides bentonensis*, whiteinellids and dicarinellids have survived this extinction. The marginotruncanids appeared for the first time in this zone and diversified rapidly. Small sized planktonic foraminifera include *Heterohelix reussi* while large size foraminifera include praeglobotruncanids, marginotruncanids, and whiteinellids.

5.2.5.12 Local Dicarinella concavata Partial Range Zone

Age: Middle Turonian to Early Santonian

Author: Khan (this thesis)

Definition: This interval spans from the FAD of *Dicarinella concavata* to the FAD of *Dicarinella asymetrica*.

Species assemblage of the zone: Dicarinella concavata, Dicarinella paraconcavata, Dicarinella imbricata, Dicarinella primitiva, Hedbergella flandrini, Helvetoglobotruncana helvetica, Dicarinella algeriana, Dicarinella canaliculata, Dicarinella hagni, Marginotruncana renzi, Marginotruncana schneegansi, Marginotruncana marianosi, Marginotruncana pseudolinneiana, Marginotruncana coronata, Marginotruncana marginata, Marginotruncana sigali, Marginotruncana sinousa, Whiteinella baltica, Whiteinella inornata, Whiteinella paradubia, Whiteinella aprica, Whiteinella brittonensis, Whiteinella archaeocretacea, Whiteinella aumalensis, Whiteinella baltica, Hedbergella simplex, Contusotruncana fornicata, Globigerinelloides bollii, Praeglobotruncana stephani, Praeglobotruncana gibba, Heterohelix moremani and Heterohelix reussi.

Remarks: The planktonic foraminiferal diversity and abundances are high, e.g. whiteinellids, marginotruncanids, hedbergellids are common. *Hedbergella flandrini* shows its FAD in the upper lower part of the biozone, followed by the synchronous FADs of *Contusotruncana fornicata*, *Marginotruncana pseudolinneiana*, *Dicarinella primitiva*, and *Contusotruncana fornicata*. Upwards, the FAD of *Globigerinelloides bollii* occurs. The age of the lower boundary of the biozone is in the Late Coniacian according to Caron (1985) and Sliter (1989). However, according to Sarri (2006) the lower limit of this biozone corresponds to the Turonian/Coniacian boundary. In this study, the associated assemblages, e.g. *Praeglobotruncana stephani*, *Whiteinella*

praehelvetica, *Helvetoglobotruncana helvetica*, and *Whiteinella aumalensis*, suggest that this biozone extends further downwards, most probably into the Mid Turonian.

5.2.5.13 Dicarinella asymetrica Total Range Zone

Age: Late Santonian

Author: (Postuma, 1971, = *Globotruncana concavata carinata* Zone)

Definition: This zone spans the entire range of *Dicarinella asymetrica*

Species assemblage of the zone: *Dicarinella asymetrica, Dicarinella primitiva, Dicarinella concavata, Dicarinella imbricata, Dicarinella hagni, Dicarinella primitiva, Contusotruncana fornicata, Globotruncana bulloides, Archaeoglobigerina cretacea, Globotruncana linneiana, Globotruncanita stuartiformis, Hedbergella flandrini, Globigerinelloides bolli, Marginotruncana schneegansi, Marginotruncana marginata, Marginotruncana sinuosa, Marginotruncana sigali, Marginotruncana pseudolinneiana, Marginotruncana coronata, Whiteinella aprica, Whiteinella paradubia, Marginotruncana renzi, Whiteinella baltica, Helvetoglobotruncana helvetica, Globigerinelloides prairiehillensis, Heterohelix globulosa, Heterohelix reussi, Heterohelix moremani, Hedbergella simplex.*

Remarks: The FAD of the zonal marker is almost synchronous with the FADs of *Globotruncana bulloides*, *Archaeoglobigerina cretacea*, *Globotruncanita stuartiformis*, *Heterohelix globulosa*, *Globigerinelloides prairiehillensis*, and *Globotruncana linneiana*. The whiteinellids, dicarinellids, and most of the marginotruncanids became extinct in this zone.

The upper part of this zone has been probably truncated, because the globally recognized *Globotruncanita elevata* Partial Range Zone is missing, or is highly condensed. This hiatus, or condensed interval, is indicated by the almost co-occurrences of the LAD of *Dicarinella asymetrica* and FADs of *Globotruncanita elevata* and *Globotruncana ventricosa*. Such hiatus also exists in the western Taurides, Turkey, where both the *Globotruncana elevata* and *Globotruncana ventricosa* Zones were truncated (Sarri, 2006).

5.2.5.14 Globotruncana ventricosa Partial Range Zone

Age: Middle to Late Campanian

Author: Dalbiez (1955)

Definition: This interval spans from the FAD of *Globotruncana ventricosa* to the FAD of *Globotruncanita calcarata*.

Species assemblage of the zone: Globotruncana ventricosa, Globotruncana hilli, Globotruncana linneiana, Globotruncanita elevata, Globotruncana carinata, Marginotruncana coronata, Marginotruncana renzi, Marginotruncana sigali, Marginotruncana pseudolinneiana, Contusotruncana fornicata, Globigerinelloides bollii, Archaeoglobigerina cretacea, Globotruncana stuartiformis, Heterohelix reussi, Heterohelix globulosa, Globotruncana bulloides, Globotruncana lapparenti, Globotruncana arca, Pseudotextularia elegans, Contusotruncana plummerae, Archaeoglobigerina blowi, Pseudoguembelina costulata, Globigerinelloides prairiehillensis, Ventilabrella glabrata, Heterohelix carinata, Heterohelix striata, Globotruncana rosetta, Globotruncana orientalis, Contusotruncana patelliformis, Heterohelix planata, Ventilabrella multicamerata.

Remarks: The lower boundary of the biozone is marked by the FADs of the zonal marker, *Globotruncana carinata* and *Globotruncana hilli*. The planktonic foraminiferal fauna diversified rapidly in this zone. The absence of the globally underlying *Globotruncanita elevata* zone indicates that the lower boundary of the current biozone has been truncated.

5.2.5.15 Globotruncanita calcarata Total Range Zone

Age: Late Campanian

Author: Herm (1962)

Definition: This biozone spans the entire range of *Globotruncanita calcarata*.

Species assemblage of the zone: Globotruncanita calcarata, Globotruncana ventricosa, Globotruncana arca, Globotruncana bulloides, Globotruncana carinata, Globotruncanita conica, Globotruncana orientalis, Globotruncana lapparenti, Globotruncana rosetta, Globotruncana coronata, Globotruncana linneiana, Globotruncana hilli, Laeviheterohelix glabrans, Ventilabrella glabrata, Ventilabrella eggeri, Heterohelix carinata, Planoglobulina acervulinoides, Marginotruncana pseudolinneiana, Marginotruncana coronata, Heterohelix globulosa, Ventilabrella multicamerata, Heterohelix reussi, Heterohelix striata, Heterohelix planata, Gublerina sp.*, Pseudoguembelina costulata, Globigerinelloides prairiehillensis, Globotruncanella havanensis, Globotruncanita stuartiformis, Globotruncanita elevata, Globotruncana aegyptiaca, Globotruncanita subspinosa, Globotruncanita stuarti, Rugoglobigerina rugosa, Rugoglobigerina milamensis, Archaeoglobigerina blowi, Planoglobulina acervulinoides, Planoglobulina carseyae, Pseudotextularia elegans, Contusotruncana fornicata, Contusotruncana patelliformis.*

Remarks: The FAD of the zonal marker co-occurs with the FADs of *Globotruncanita conica, Globotruncanella havanensis, Ventilabrella eggeri, Globotruncanita subspinosa*. The *Globotruncana aegyptiaca, Rugoglobigerina milamensis Planoglobulina acervulinoides*, and *Planoglobulina carseyae* occur at different levels in this zone. In other areas, the FADs of *Globotruncanita conica, Planoglobulina acervulinoides*, and *Planoglobulina carseyae* occur later in the *Gansserina gansseri* Zone (Caron, 1985; and Premoli-Silva & Sliter, 1994). Similarly, the *Globotruncana aegyptiaca* and *Rugoglobigerina milamensis* have their FADs later in the *Globotruncana aegyptiaca* Zone elsewhere (Caron, 1985; and Premoli-Silva & Sliter, 1994). Based on these associated younger foraminiferal assemblages the upper boundary of this biozone may extend into the Early Maastrichtian. The foraminiferal abundance and diversity are very high in this zone. Unfortunately the zonal marker is very rare in the samples, and thus the precise location of the lower boundary of this biozone is difficult to determine (see also Premoli-Silva & Sliter, 1994).

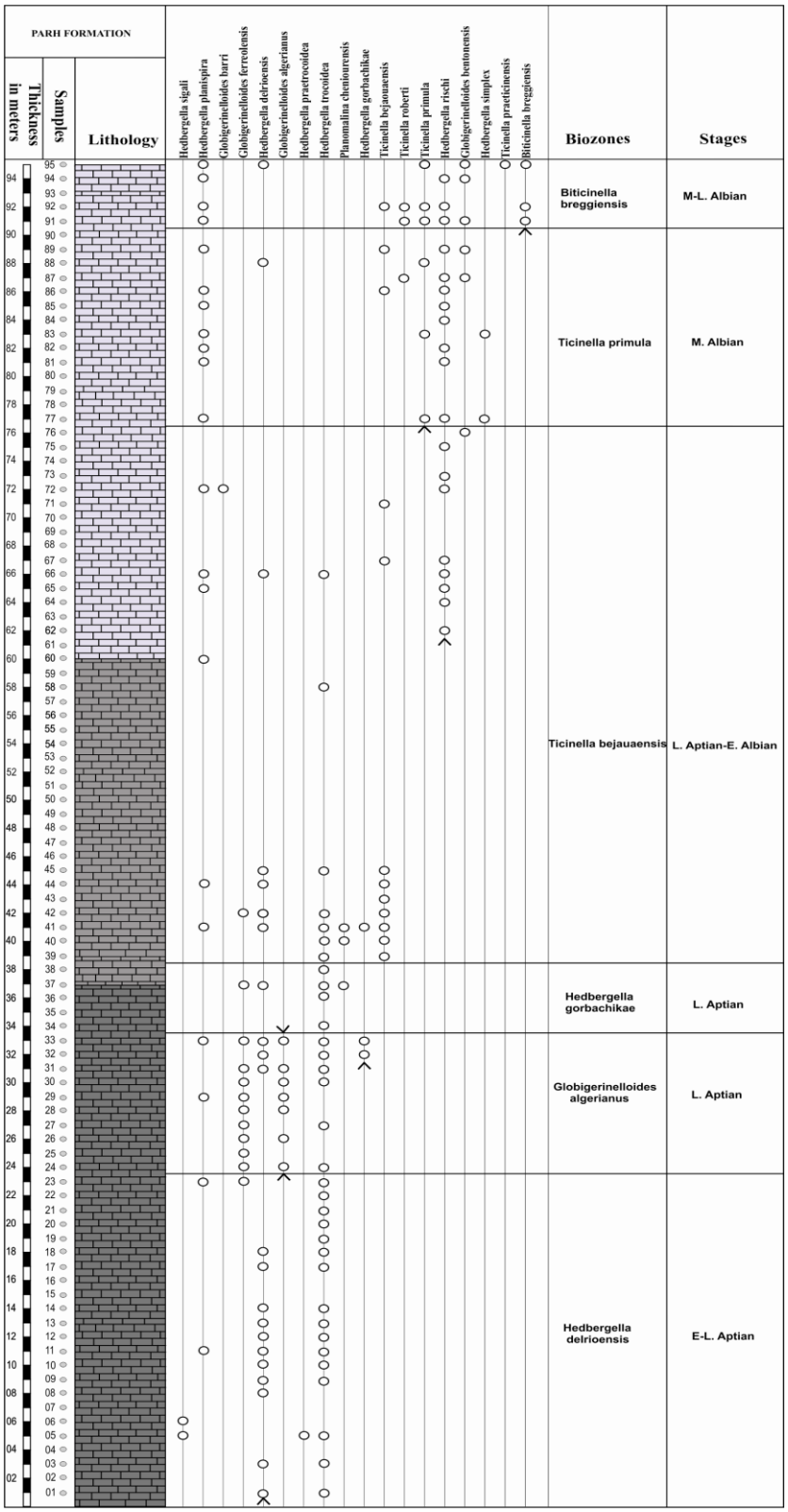

Figure 5.5: Planktonic foraminifera presence/absence chart of the Parh Formation, Moghal Kot Section. Species are arranged according to Sliter, 1989; Caron, 1985

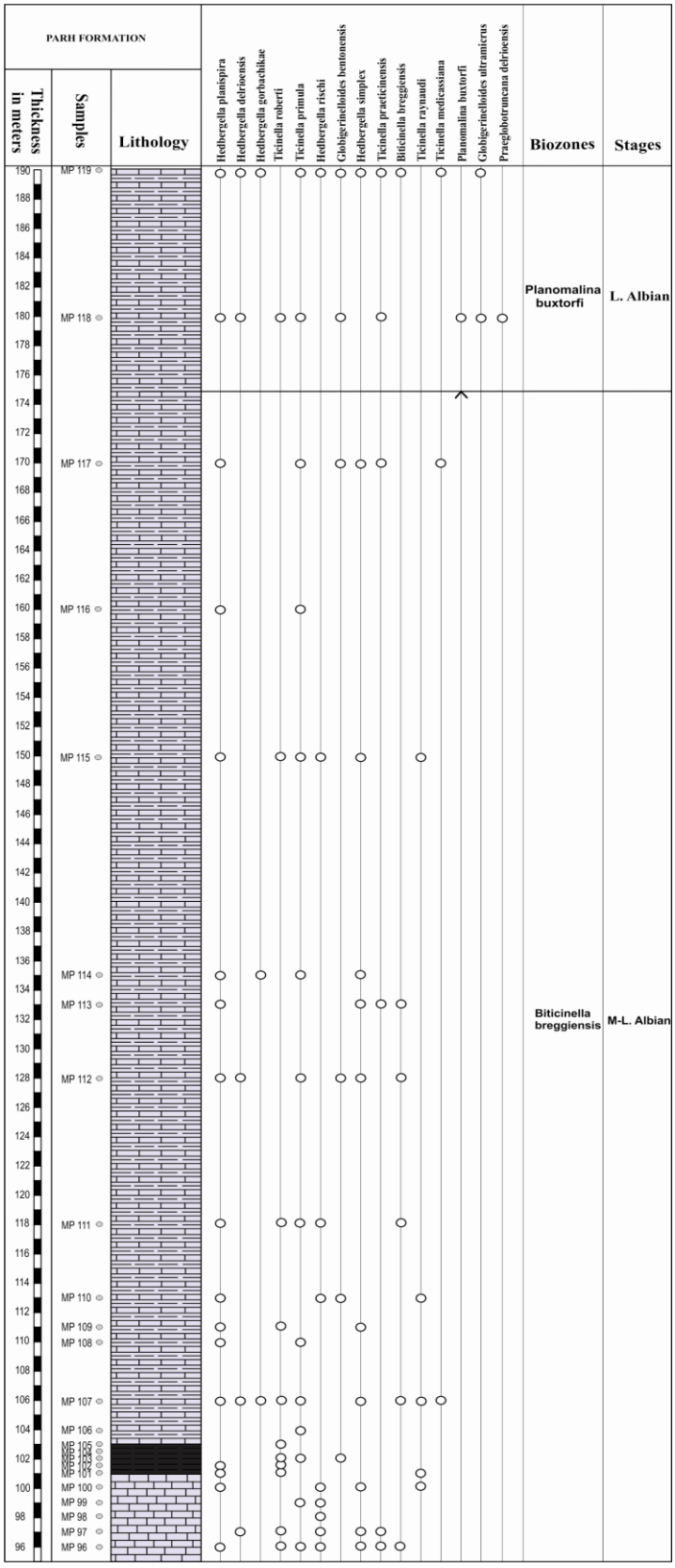

Figure 5.6: Planktonic foraminifera presence/absence chart of the Parh Formation, Moghal Kot Section. Species are arranged according to Sliter, 1989; Caron, 1985

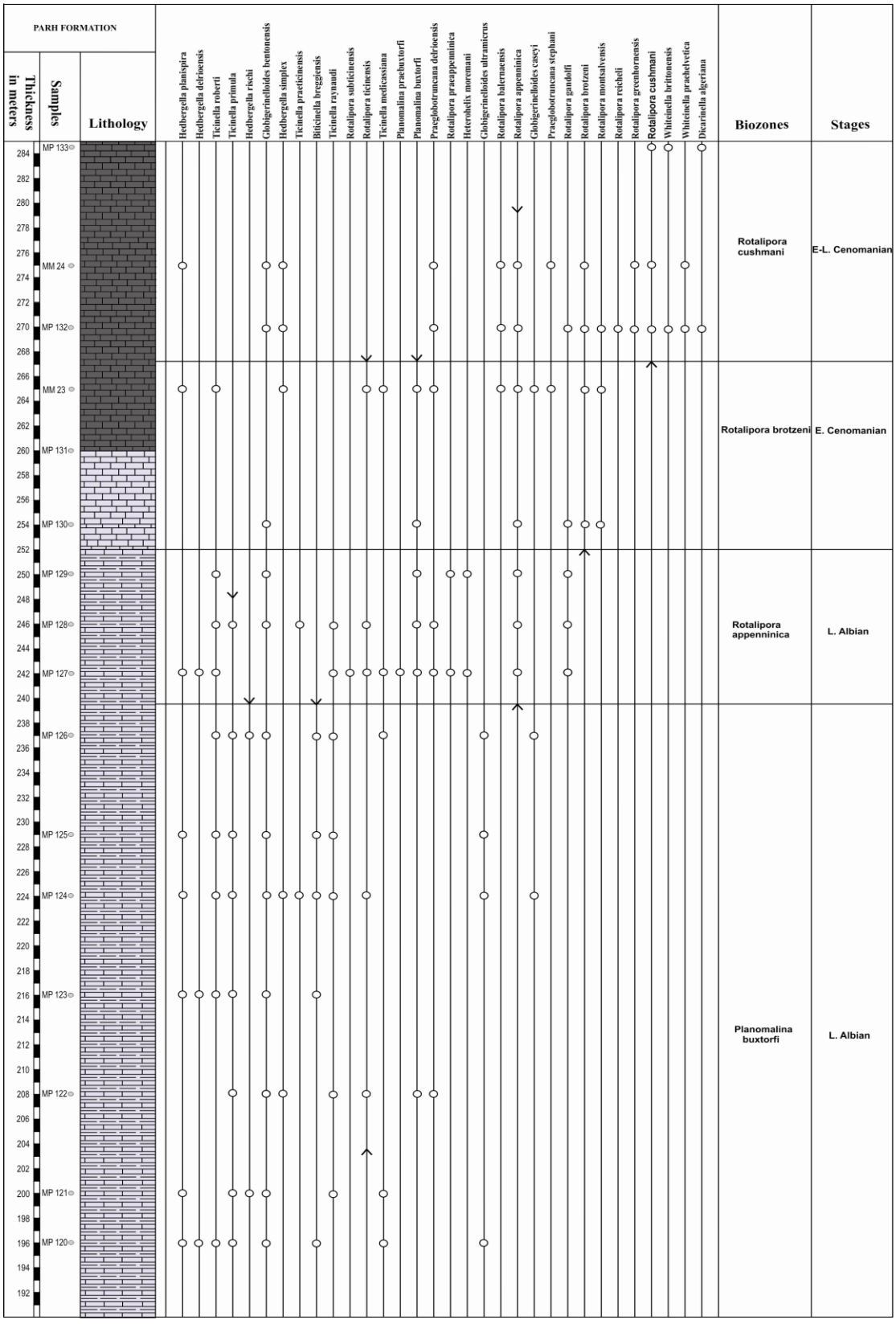

Figure 5.7: Planktonic foraminifera presence/absence chart of the Parh Formation, Moghal Kot Section. Species are arranged according to Sliter, 1989; Caron, 1985

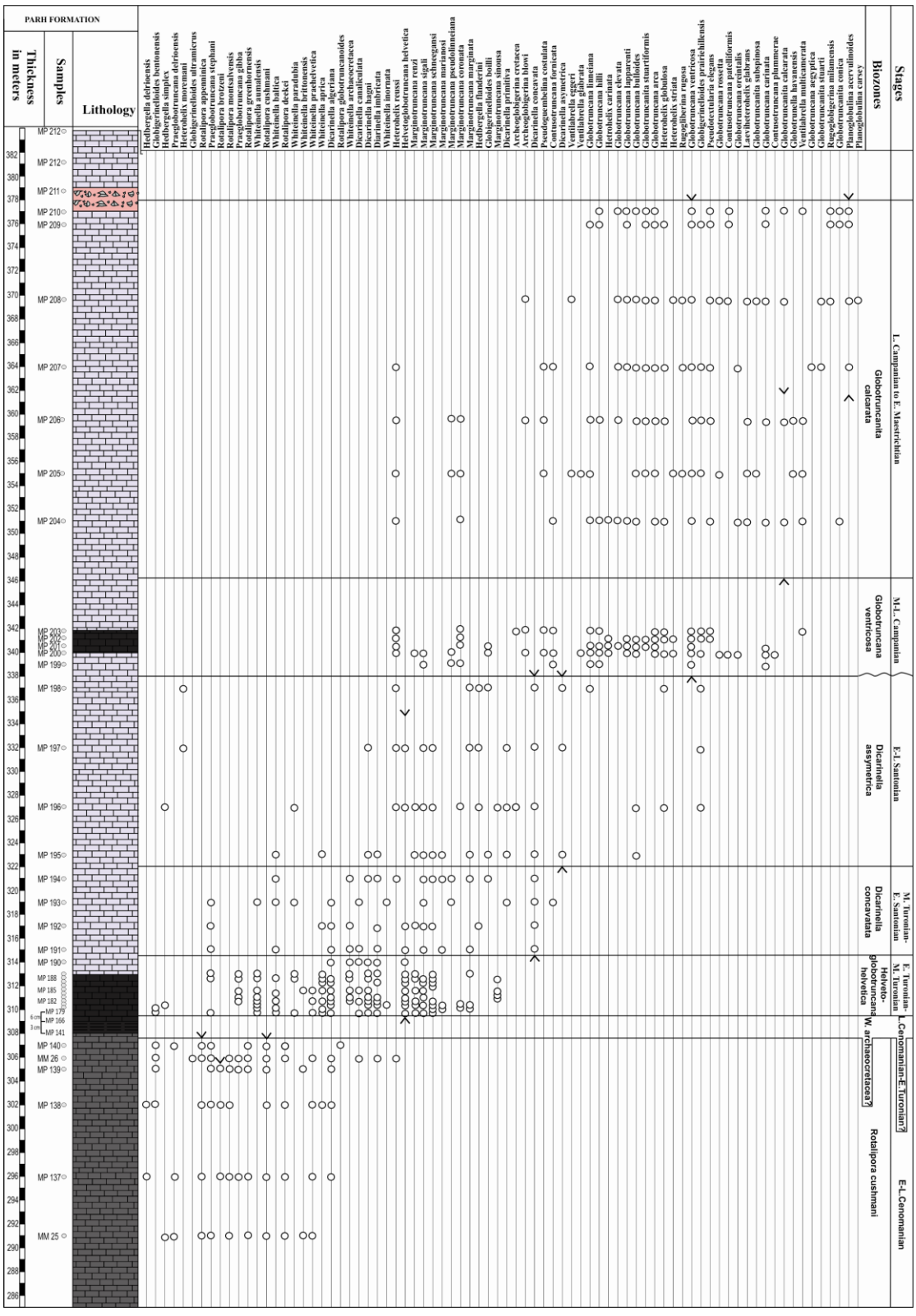

Figure 5.8 Planktonic foraminifera presence/absence chart of the Parh Formation, Moghal Kot Section. Species are arranged according to Sliter, 1989; Caron, 1985

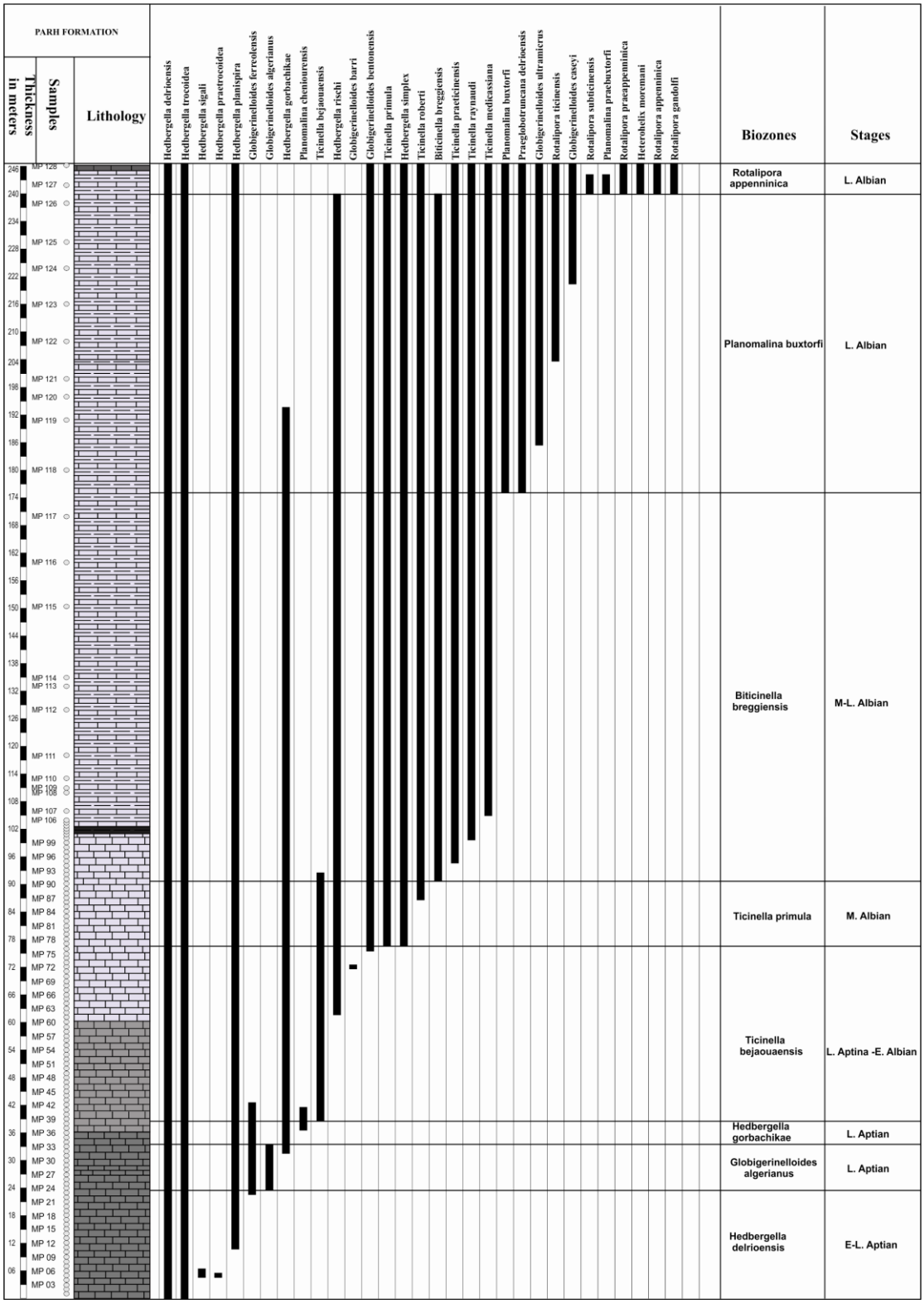

Figure 5.9: Planktonic foraminifera range chart base on the First Appearance Datum (FADs) of the Parh Formation, Moghal Kot Section.

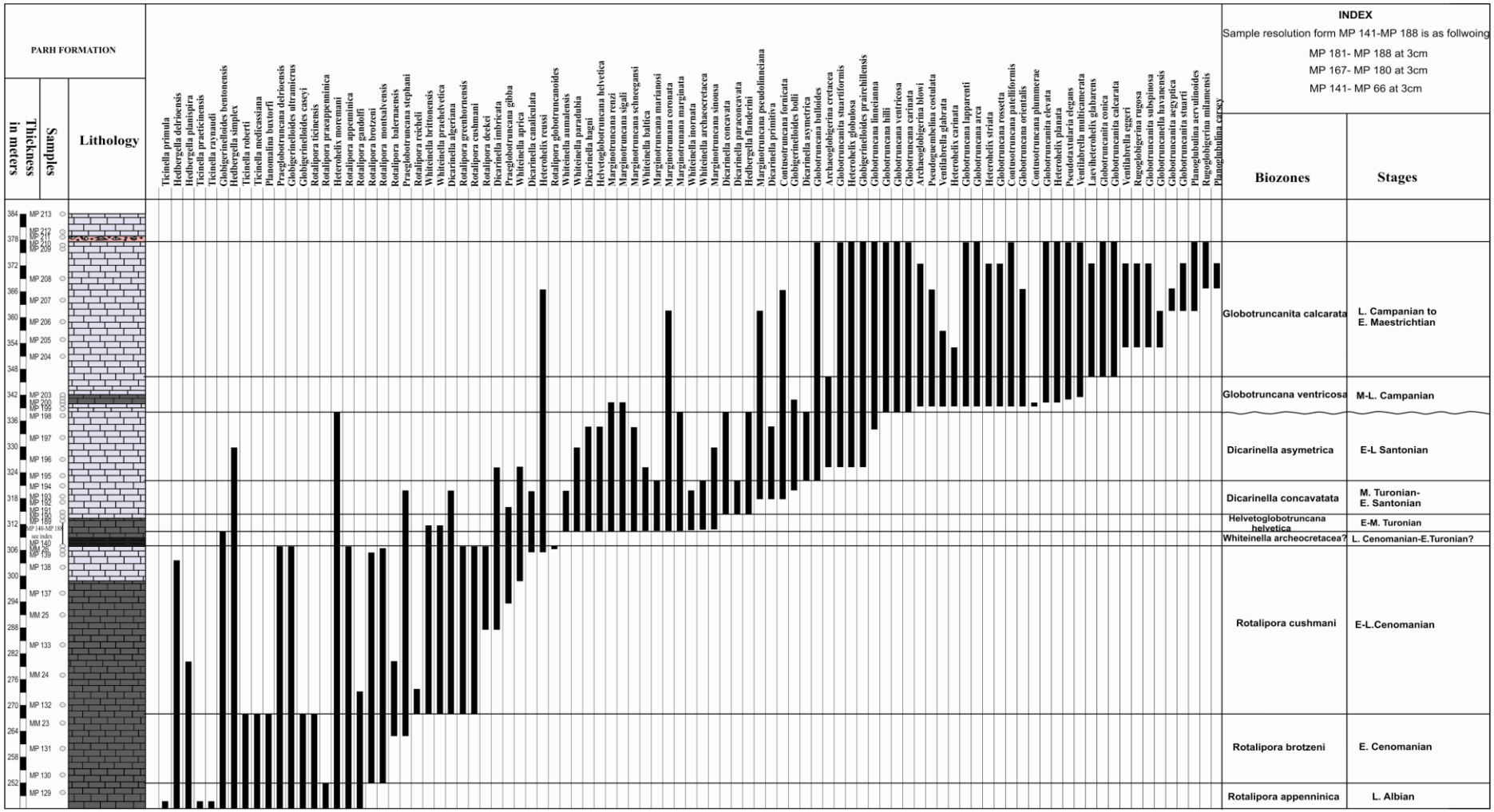

Figure 5.10: Planktonic foraminifera range chart base on the First Appearance Datum (FADs) of the Parh Formation, Moghal Kot Section.

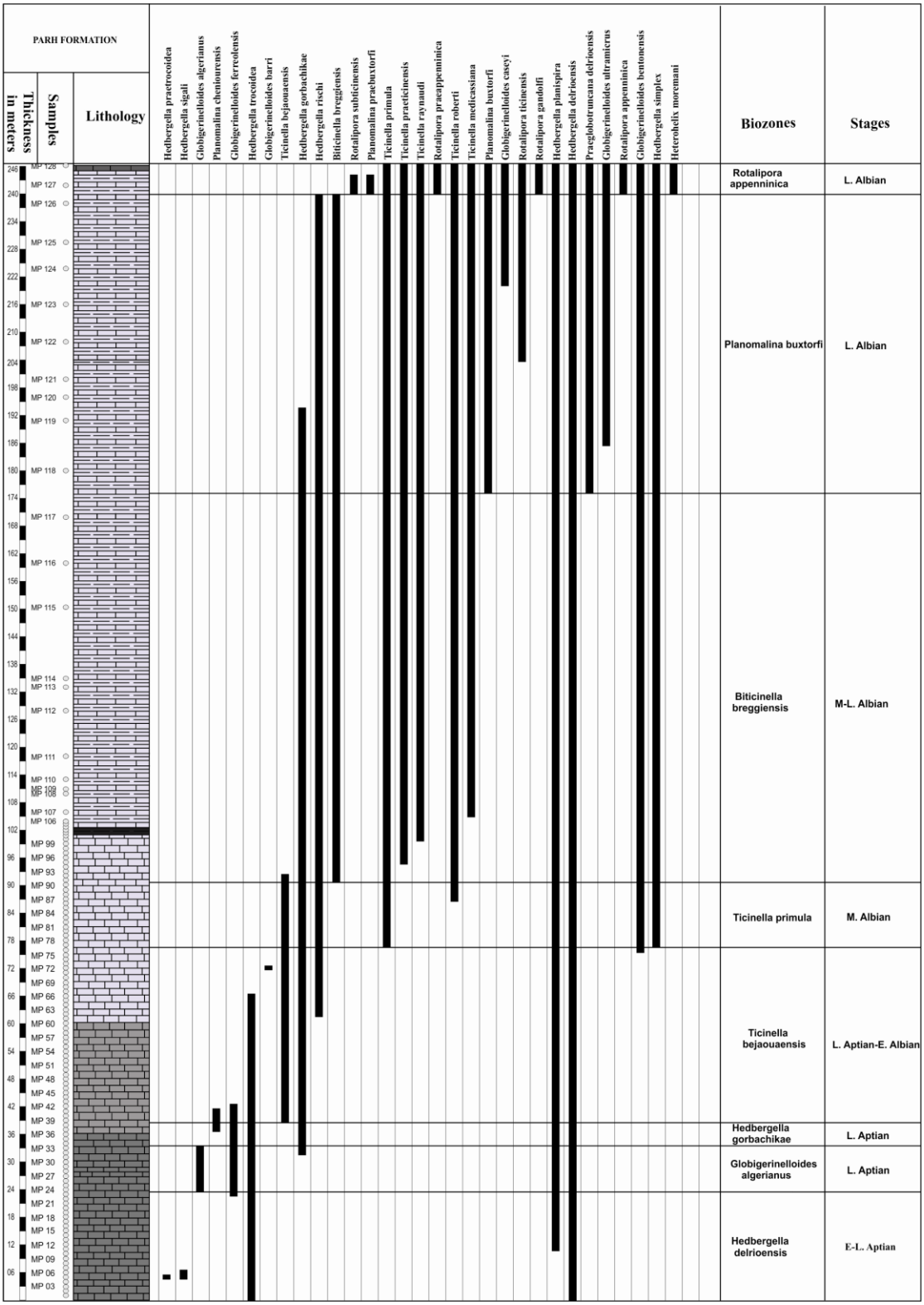

Figure 5.11: Planktonic foraminifera range chart base on the Last Appearance Datum (LADs) of the Parh Formation, Moghal Kot Section.

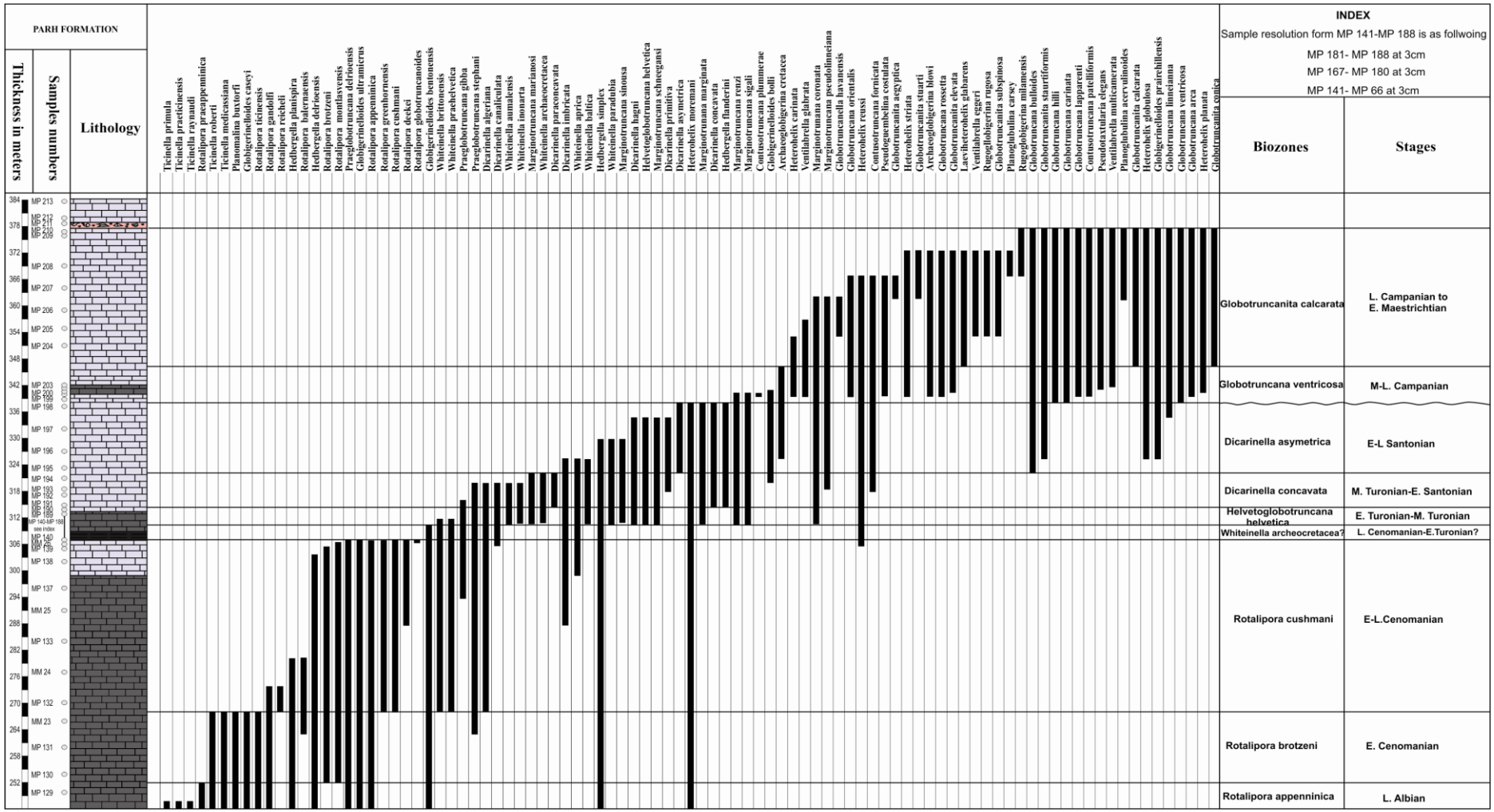

Figure 5.12: Planktonic foraminifera range chart base on the Last Appearance Datum (LADs) of the Parh Formation, Moghal Kot Section.

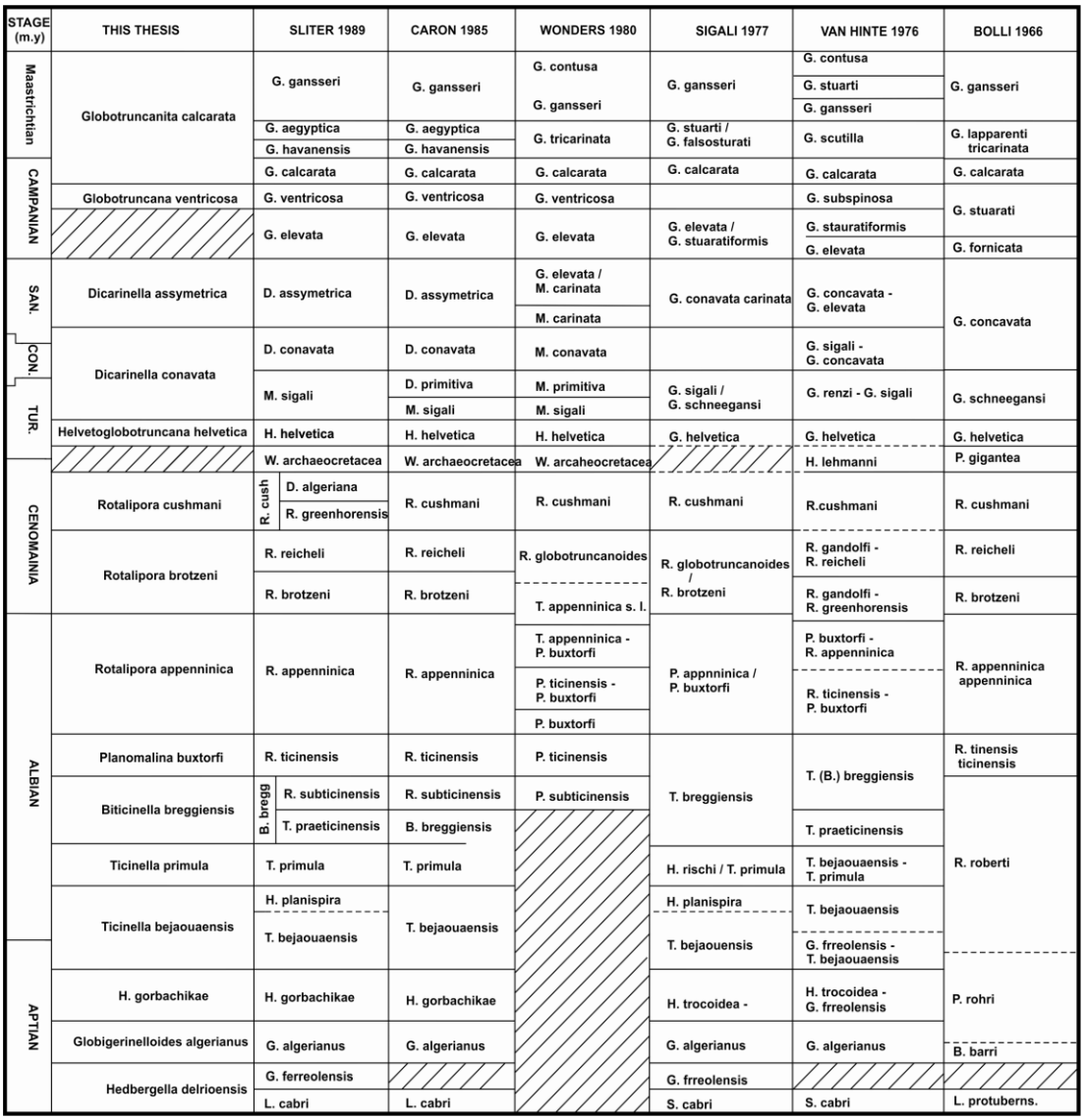

Figure 5.13: Comparison of Cretaceous planktonic foraminiferal biozonation of the Parh Formation, Mohal Kot Section with the global biozonation schemes. The global biozonation schem is modified after Sliter (1989)

5.3 Discussion

Previous studies on the biostratigraphy of the Parh Formation are not complete; hence the main aim of the study is to put the pelagic sediments of the Parh Formation into reliable time frame. More importantly the organic rich horizons within the Parh Formation need to be properly dated as these horizons may represent the Oceanic Anoxic Events (OAEs). The subdivision of the Parh Formation into high resolution biostratigraphic time intervals will help to constrain the stratigraphic position of (OAEs), as recorded in the Parh Formation. For this purpose planktonic foraminifera were studied both in thin sections and as extracted specimens in order to establish Planktonic foraminiferal biozones of global significance.

The detailed planktonic foraminiferal biostratigraphy suggest an Early Aptian to Early Maastrichtian age for the Parh Formation. Most of the biozones of the Parh Formation are global in nature, i.e. the *Globigerinelloides algerianus, Hedbergella gorbachikae, Ticinella bejaouaensis, Ticinella primula, Biticinella breggiensis, Rotalipora appenninica, Rotalipora brotzeni, Rotalipora cushmani, Dicarinella asymetrica, Globotruncana ventricosa* Biozones, while 5 local biozones are described such as the *Hedbergella delrioensis, Planomalina buxtorfi, Helvetoglobotruncana helvetica, Dicarinella concavata, Globotruncanita calcarata* Biozones (see Caron, 1985 and Sliter 1989 for confirmation). These 5 local biozones correlate well with the global biozones of the Sliter (1989) and Caron (1985), see the remarks of these biozones for details. The biostratigraphy of the Parh Formation suggests further that the sedimentation in the Eastern Tethys was almost continuous throughout most of the Cretaceous.

The organic rich horizons which are observed both on the outcrop and microfacies level can now be placed into a reliable time frame. The lowermost organic-rich (abundant) interval (base of the section up to 32m) occurs in the *Hedbergella delrioensis* and *Globigerinelloides algerianus* Zones of Early to Late Aptian which corresponds to the Selli Event (OAE 1a) and Fallot Event (see Microfacies MP1-MP8 in Chapter 3). The Selli Event (OEA1) is recorded elsewhere in the Early Aptian (Weissert et al., 1998; Erbacher et al., 1996; Menegatti et al., 1998; Erba, 1994) while the Fallot Event is recorded in the Late Aptian (Friedrich et al. 2003 and Takashima et al. 2006). The precise demarcation of the stratigraphic positions of

these OAEs will be documented in Chapter-6. The next interval with abundant presence of organic matter along with minor occurrence of pyrite occurs at 44-45m in the *Ticinella bejaouaensis* Zone (latest Aptian), which correlates with OAE1b (see Microfacies, MP4, Chapter 3). This event is reported elsewhere in the *Ticinella bejaouaensis* to *Hedbergella planispira* Biozones, of Latest Aptian to Early Albian age (Erbacher et al., 2001 and Kuypers et al., 2002). Another interval with abundant organic matter along with minor to moderate presence of pyrite occurs at 101-103m in the *Biticinella breggiensis* Zone of the middle to late Albian (see Microfacies MP6 & MP11, Chapter 3). This interval correlates with the OAE1c because in the type locality (Central Italy) of the current OAE, it is recorded in the *Ticinella praeticinensis* Biozone (which is a subzone of *Biticinella breggiensis*) of the Middle Albian. The precise stratigraphic position of the OAE1c is outlined in Chapter 6. Moderate amounts of organic matter and pyrite are present within the latest Albian-Cenomanian, in the interval 244-274m along with the moderate presence of the pyrite (see Microfacies MP13 & MP14, Chapter 3). Upwards, black shales/limestone in the interval 308-309m occurs with high abundance of organic matter and pyrite (see Microfacies MP17-MP20, Chapter 3). This interval straddles the Cenomanian-Turonian boundary and corresponds to OAE2. This event is documented in Cenomanian-Turonian sections elsewhere (Schlanger and Jenkyns 1976; Scholle and Arthur; 1980; Tsikos et al., 2004; Paul et al, 1999). Within the Middle to Late Campanian, the interval from 340-342m in the *Globotruncana ventricosa* Zone contains abundant organic matter and moderate to abundant amounts of pyrite (see Microfacies, MP22, Chapter 3). This interval may correlate with one of the Campanian isotopic events, which have been reported in the literature (Jarvis, 2002; Thibault et al. 2012) but currently the biostratigraphy is not precisely enough to decide on detailed correlation to one of the two Campanian OAE events. Perhaps the integrated stratigraphy in Chapter-6 may be useful in this respect.

The evolution of the Cretaceous planktonic foraminifera is forced by the short time paleoceanographic changes brought about by the OAEs (Leckie et al, 2002) because the highest rates of speciation and extinction are associated with such such OAEs. The complete record of the planktonic foraminifera in the Parh Formation provides strong basis for understanding the planktonic foraminiferal evolution under the influence of such paleoceanographic changes. The evolution of planktonic foraminifera will be discussed in Chapter-8.

5.4 Conclusions

The planktonic foraminiferal biostratigraphic study of the Parh Formation reveals the following conclusions:

- The presence of well preserved planktonic foraminifera provides the possibility to build a reliable, detailed biostratigraphy of the Parh Formation.

- The biostratigraphic results based on global correlation of most of the the planktonic foraminiferal biozones, suggest that the Parh Formation ranges in age from Early Aptian to Early Maastrichtian.

- 10 global Cretaceous planktonic foraminiferal biozones, while 5 local biozones are reprted from the Parh Formation.

- The absence of the *Globotruncanita elevata* Zone indicates a hiatus in this part of the section. Also, the lower part of the *Globotruncana ventricosa* Zone may be missing due to this hiatus.

- The stratigraphic positions of the Cretaceous OAEs i.e OAE1, OAE2, and one of the Campanian Events, are tenatitively defined; however the precise positions of these OAEs will be clear after the integrated stratigraphy in Chapter-6.

- The Parh Formation records almost the entire history of the Cretaceous sedimentation in the area, including the evolution of the planktonic foraminifera, and synchronous paleoceanographic changes.

CHAPTER 6

Integrated Stratigraphy of the Parh Formation

6.1 Aims of this chapter

The aim of this chapter is to define the accurate stratigraphic positions of the Oceanic Anoxic Events (OAEs), preserved in the Parh Formation. For this purpose, microfacies and biostratigraphic details are combined with the $\delta^{13}C$ record of bulk pelagic carbonates (see tables. 6.1 & 6.2) spanning from Early Aptian to Early Maastrichtian, resulting in an integrated stratigraphy, highlighting the ages of the OAEs. The microfacies data are used here to demarcate the organic rich horizons which reflect the OAE intervals. The biostratigraphic data demarcate the ages of the OAEs, while the $\delta^{13}C$ variability records carbon perturbations which are also useful in defining the accurate stratigraphic positions of the OAEs in the Parh Formation.

6.2 Stratigraphy of the OAEs

Both the high abundances of organic matter and pyrite represent periods during which ocean waters were anoxic, i.e. these intervals represent the OAEs. The OAEs are also marked by the high clastic influx to the basin due to enhanced weathering of the continents. Based on the integrated stratigraphic approach the following observations are made about the stratigraphic positions of the OAEs.

The lowermost organic-rich (abundant) interval (base of the section up to 32m) occurs in the *H. delrioensis* and *Globigerinelloides algerianus* Zones in the Aptian and stratigraphically corresponds to the Selli Event (OAE 1a) and Fallot Event (see fig. 6.1 and Microfacies MP1-MP8, Chapter 3). This interval is also marked by moderate to abundant detrital quartz input (see Microfacies MP2 & MP 5, Chapter 3). The $\delta^{13}C$ record, corresponding to this interval, indicates positive (C1 to C3) and subsequent negative (C4) excursions (fig. 6.1). The positive excursion (C1 to C3) is recorded in the lower *Hedbergella delrioensis* Zone of Early Aptian age (for age see Chapter 5) and corresponds to the Selli Event (OAE 1a). The Selli Event (OAE 1a) is also recorded as organic-rich horizon marked by a positive $\delta^{13}C$ excursion

elsewhere

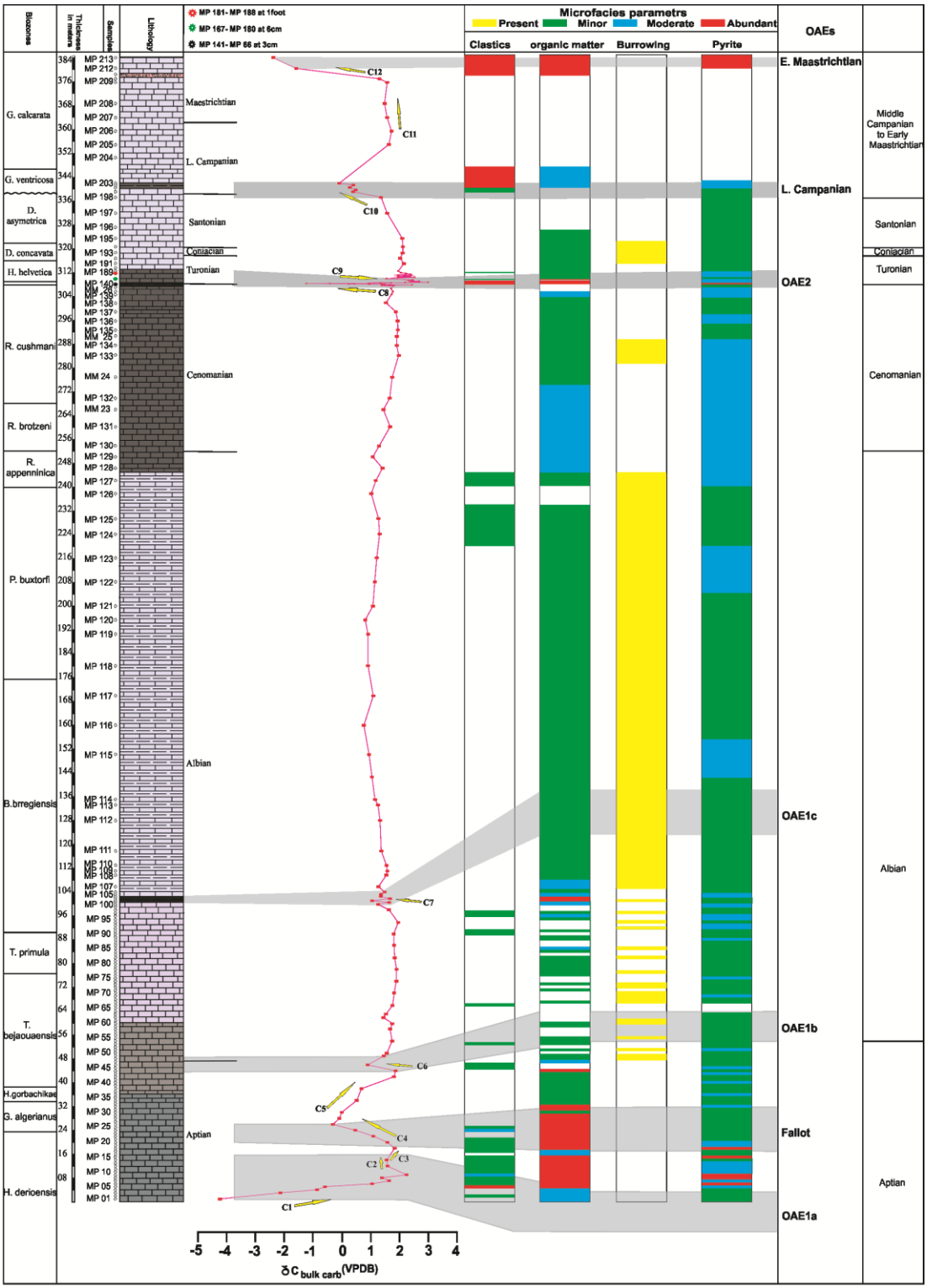

Figure 6.1: The integrated stratigraphic chart showing biozones, biostratigraphic ages, $\delta^{13}C$ isotope curve, and microfacies parameters of the Parh Formation.

in the Early Aptian (Menegatti et al., 1998; Erba et al., 1999). The negative $\delta^{13}C$ excursions (C4) in the Parh Formation straddle the boundary between the upper

Hedbergella delrioensis to lower *Globigerinelloides algerianus* Zones of Late Aptian (fig. 6.1) and correspond to the Fallot Event. The Fallot Event is also marked by a negative $\delta^{13}C$ excursion elsewhere in the Late Aptian (Friedrich et al. 2003).

The next interval with abundant presence of organic matter along with minor occurrence of pyrite occurs at 44-45m in the *Ticinella bejaouaensis* Zone of latest Aptian, which correlates with the OAE1b (see Microfacies MP4, Chapter 3). The OAE1b is marked by a small negative $\delta^{13}C$ excursion (C6) in the Parh Formation. A similar small negative $\delta^{13}C$ excursion is reported elsewhere in the *Ticinella bejaouaensis* to *Hedbergella planispira* Zones interval (Karakitsios et al. 2004; Erbacher et al., 2001; Kuypers et al., 2002).

Another interval with abundant organic matter along with minor to moderate presence of pyrite occurs at 101-103m in the *Biticinella breggiensis* Zone of the Middle to Late Albian (see Microfacies MP11, Chapter 3). This interval correlates with the OAE1c. The $\delta^{13}C$-record corresponding to this event in the Parh Formation shows small cyclic negative and positive excursions (C7) see figure 6.1. In its type locality, i.e. Amadeus Segment (Central Italy), the $\delta^{13}C$ profile shows a similar cyclic record in the *Biticinella breggiensis* Zone (Galeotti et al., 2003).

Samples	$\delta^{13}C$	$\delta^{18}O$	Samples	$\delta^{13}C$	$\delta^{18}O$
MP 1	-4.212	-6.042	MP 100	1.293	-5.862
MP 2	-7.907	-8.118	MP 101	1.631	-5.620
MP 3	-2.144	-6.360	MP 102	1.040	-5.751
MP 4	-0.822	-6.131	MP 103	1.671	-5.140
MP 5	-0.594	-5.550	MP 104	1.377	-5.559
MP 6	1.040	-6.051	MP 105	1.377	-5.439
MP 7	1.685	-5.812	MP 106	1.495	-5.150
MP 8	1.398	-7.195	MP 107	1.274	-6.247
MP 9	2.279	-5.760	MP 108	1.555	-5.428
MP 10	1.069	-5.947	MP 109	1.587	-6.167
MP 12	1.598	-5.606	MP 110	1.566	-6.176
MP 14	1.556	-5.986	MP 111	1.370	-6.207
MP 16	-0.448	-5.956	MP 112	1.340	-5.671
MP 18	1.831	-5.900	MP 113	1.241	-6.000
MP 20	1.598	-5.884	MP 114	1.163	-5.606
MP 22	1.111	-6.545	MP 115	0.944	-6.177
MP 24	0.480	-5.920	MP 116	0.758	-5.822
MP 26	-0.301	-5.713	MP 117	1.110	-5.322
MP 28	-0.082	-5.304	MP 118	0.918	-5.361
MP 30	0.014	-4.582	MP 119	0.925	-5.648
MP 34	0.530	-3.980	MP 120	0.832	-6.087
MP 38	0.677	-6.199	MP 121	1.113	-5.824
MP 42	1.801	-6.338	MP 122	1.174	-5.886
MP 44	1.981	-6.042	MP 123	1.233	-5.915
MP 46	0.932	-6.415	MP 124	1.321	-5.599
MP 49	1.415	-5.962	MP 125	1.272	-5.566
MP 50	1.547	-6.272	MP 126	1.044	-6.038
MP 54	1.722	-6.293	MP 127	1.184	-5.782
MP 58	1.689	-6.255	MP 128	1.434	-6.117
MP 60	1.864	-5.946	MP 129	1.111	-6.097
MP 62	1.462	-6.177	MP 130	1.304	-6.112
MP 63	1.542	-5.902	MP 131	1.688	-6.050
MP 66	1.771	-6.256	MP 132	1.687	-5.819
MP 70	1.836	-5.832	MP 133	1.962	-5.443
MP 74	1.890	-6.219	MP 134	1.911	-6.072
MP 78	1.899	-6.142	MP 135	1.955	-5.348
MP 82	1.832	-6.226	MP 136	1.951	-5.714
MP 86	1.822	-5.861	MP 137	1.900	-5.888
MP 90	1.787	-6.199	MP 138	1.557	-5.885
MP 94	1.951	-5.967	MP 139	1.732	-5.507
MP 98	1.654	-6.105	MP 140	1.710	-5.899

Table 6.1: Showing $\delta^{13}C$ and $\delta^{18}O$-values (VPDB) of bulk carbonates of the Parh Formation, Moghal Kot Section.

Samples	$\delta^{13}C$	$\delta^{18}O$	Samples	$\delta^{13}C$	$\delta^{18}O$
MP 141	0.662	-5.022	MP 177	2.486	-6.446
MP 142	1.782	-5.835	MP 178	2.487	-5.240
MP 143	1.637	-5.288	MP 180	1.585	-4.754
MP 144	1.415	-4.116	MP 181	1.977	-3.430
MP 145	1.487	-4.442	MP 182	2.558	-5.848
MP 146	1.769	-4.878	MP 183	2.001	-5.843
MP 147	1.721	-4.916	MP 184	2.412	-5.838
MP 148	1.537	-4.313	MP 185	2.017	-5.918
MP 149	2.452	-4.989	MP 186	2.385	-5.839
MP 150	1.687	-4.365	MP 187	2.250	-5.672
MP 151	1.465	-4.125	MP 188	2.102	-5.823
MP 152	1.431	-4.116	MP 189	2.011	-5.348
MP 153	1.496	-4.836	MP 191	2.191	-5.218
MP 154	1.388	-4.173	MP 192	2.069	-5.676
MP 155	0.986	-5.978	MP 193	2.170	-5.553
MP 156	0.262	-5.253	MP 194	2.165	-5.327
MP 157	0.428	-5.644	MP 195	2.116	-5.416
MP 158	-0.401	-5.859	MP 197	1.624	-5.552
MP 159	-1.218	-6.926	MP 198	1.389	-5.684
MP 160	0.911	-5.886	MP 199	0.425	-5.594
MP 162	1.339	-4.077	MP 200	0.528	-5.801
MP 163	1.344	-4.038	MP 201	0.314	-6.125
MP 164	1.697	-5.400	MP 202	0.439	-5.903
MP 165	0.962	-6.305	MP 203	1.938	-5.363
MP 166	2.232	-4.917	MP 304	-0.055	-5.657
MP 167	3.000	-5.931	MP 305	1.685	-5.072
MP 168	2.679	-5.708	MP 306	1.755	-4.677
MP 169	2.396	-5.747	MP 307	1.614	-4.623
MP 171	2.698	-5.130	MP 308	1.530	-4.164
MP 172	2.686	-5.708	MP 309	1.619	-5.484
MP 173	2.473	-5.094	MP 310	1.353	-4.922
MP 174	2.487	-5.378	MP 311	-1.804	-4.931
MP 175	2.493	-4.602	MP 312	-1.560	-5.029
MP 176	2.338	-5.278	MP 313	-2.329	-4.619

Table 6.2: Showing $\delta^{13}C$ and $\delta^{18}O$-values (VPDB) of bulk carbonates of the Parh Formation, Moghal Kot Section.

Upwards, high abundance of organic matter and pyrite occurs in the black shales/limestone interval 308-309m (see Microfacies MP17-MP20, Chapter 3). This interval straddles the Cenomanian-Turonian boundary and corresponds to the OAE2. This interval is also marked by abundant detrital angular quartz, which indicates enhanced clastic influx to the basin (Microfacies MP19, Chapter 3). The $\delta^{13}C$ record of the Parh Formation shows alternating negative (C8) and positive (C9) excursions across the Cenomanian-Turonian boundary (fig. 6.1). The OAE2 is recorded as a positive $\delta^{13}C$ excursion elsewhere in the Late Cenomanian to Early Turonian (Parente et al., 2007; Takashima et al, 2009). Here, a unique negative $\delta^{13}C$ excursion resides in the middle of the event, which has not been recorded elsewhere. Notably, a prominent positive $\delta^{13}C$, which is recorded usually elsewhere, is not present in the Parh Formation. The unique negative $\delta^{13}C$ excursion coupled with the lack of a prominent positive $\delta^{13}C$ excursion in the Parh Formation, are difficult to reconcile with global $\delta^{13}C$ records around this time. Other factors may have come into play in shaping the local $\delta^{13}C$ profile around the OAE2 interval in the Parh Formation. One such factor may be diagenesis; another may be the presence of a considerable hiatus explaining the absence of the prominent OAE2 positive excursion.

Within the Middle to Late Campanian, the interval from 340-342m in the *Globotruncana ventricosa* Zone contains abundant organic matter and moderate to abundant amounts of pyrite (see Microfacies MP22, Chapter 3). This interval has also recorded high clastic influx to the basin (see Microfacies MP22, Chapter 3). There is a conspicuous negative $\delta^{13}C$ excursion (C10) in this interval. The negative $\delta^{13}C$ event correlates with the Late Campanian Isotopic Event, which has also been reported in the literature (Jarvis, 2002; Thibault et al. 2012). Notably, there is no positive $\delta^{13}C$ excursion of middle Campanian, recorded in the $\delta^{13}C$ of the Parh Formation. Keeping the middle to late Campanian age of the *Globotruncana ventricosa* in mind, and the absence of the middle Campanian $\delta^{13}C$ positive event, it is concluded that the middle Campanian part of the current biozone is missing. In other words, the $\delta^{13}C$ record suggests that the lower part of the *Globotruncana ventricosa* Zone is Late Campanian in age, while the middle Campanian is missing, probably due to hiatus (see *Globotruncana ventricosa* biozone in Chapter 5 for detail). The uppermost interval, 379-384m, with abundant organic matter and pyrite is recorded in the Early Maastrichtian (see Microfacies MP19, Chapter 3). This interval is also marked by high clastic influx to the basin (see fig. 6.1 and

Microfacies MP19, Chapter 3). The $\delta^{13}C$ curve associated with the Early Maastrichtian shows a negative $\delta^{13}C$ excursion. Such a negative $\delta^{13}C$ excursion is common in records in other parts of the world in the Early Maastrichtian (e.g. Jarvis et al., 2002; Thibault et al. 2012).

6.2 Conclusions

- Based on the microfacies, biostratigraphy, and $\delta^{13}C$ the stratigraphic positions of the Cretaceous OAEs within the Parh Formations i.e. Selli Event (OAE1a), Paquier Event (OAE1b), OAE1c, Bonarelli Event (OAE 2), Late Campanian, and Early Maastrichtian are defined.
- The pronounced negative $\delta^{13}C$ excursion corresponding to the Bonarelli Event (OAE2) is reported for the first time from the Cenomanian-Turonian interval in the Parh Formation. Such a negative $\delta^{13}C$ is lacking elsewhere. However a pronounced positive $\delta^{13}C$ excursion recorded elsewhere is missing in the Parh Formation. The pronounced negative $\delta^{13}C$ and lack of prominent positive $\delta^{13}C$ excursion in the Parh Formation could be explained by diagenetic overprints on the $\delta^{13}C$ record or a possible hiatus, which might have eroded the characteristic positive $\delta^{13}C$ excursion in current stratigraphic section.
- The Late Campanian Isotopic Event recorded at the base of the *Globotruncana ventricosa* (Middle to Late Campanian) Zone of the Parh Formation suggests a Late Campanian age. The Middle Campanian part of this Zone has been eroded, resulting in a hiatus. The absence of *Globotruncanita elevata* of early Campanian is thought to be truncated by the same hiatus (see *Globotruncana ventricosa* biozone in Chapter 5 for detail).

CHAPTER 7

7. Palaeoenvironmental Analysis the Cretaceous Strata of the Indus Basin

7.1 Aim of this Chapter

The aim of this chapter is to carry out palaeoenvironmental analysis of the Cretaceous strata of the Indus Basin i.e. the Chichali and Parh Formations. It was extremely important to establish reliable ages for the Chichali and Parh Formations in order to put these formations in reliable time frame before any further investigations are made. Hence based on palynomorphs and planktonic foraminifera, the ages for the Chichali and Parh Formations were established respectively (see Chapters 4 & 5). The palynomorphs based biostratigraphy (see Chapter 4) suggest Kimmeridgian to Valanginian age for the Chichali Formation, while the planktonic foraminiferal biostratigraphy suggest Aptian to Early Maastrichtian age for the Parh Formation (see Chapter 5). Furthermore the integrated study based on the combination of microfacies, planktonic foraminifera and carbon isotope curve of the Parh Formation was helpful to define the stratigraphic positions of the OAEs (see Chapter 6). In this chapter, the presence of marine organic matter and belemnites in the Chichali Formation will be used for reconstructing the Sea Surface Temperature (SST) of the Valanginian time. Also the OAEs will be discussed in details. The palaeoenvironmental analysis of the Chichali and Parh Formations are given as below.

7.2 TEX_{86} and $\delta^{18}O$ Based Sea Surface Temperatures in the Kimmeridgian to Valanginian

7.2.1 Background to the study

The aim of this chapter is to reconstruct Sea Surface Temperatures (SSTs) for the Kimmeridgian to Valanginian sediments of the Chichali Formation using TEX_{86} and $\delta^{18}O$ paleothermometries (i.e. Schouten et al., 2002 and Epstein et al., 1953). Why is this important? Currently, there is much debate about the climate development, based on various proxy data, in the Valanginian period (Föllmi, 2012). The recently developed biomarker based proxy, $TEX_{86,}$ has proved its potential as proxy for

paleotemperature reconstructions in the Cretaceous (e.g. Schouten et al., 2003, Forster et al., 2007, and Littler et al., 2011). The $\delta^{18}O$ based paleothermometry is extensively used for the reconstruction of paleotemperature of the oceans, particularly during the Early Cretaceous (Van de Schootbrugge et al., 2000; Price et al. 2000; McArthur et al., 2007). However the combined use of TEX_{86} and $\delta^{18}O$ paleothermometries for the Early Cretaceous sections is still missing. The use of both these proxies in current study may help in resolving the long standing controversies of the Early Cretaceous climate.

Within the Early Valanginian, the occurrence of polar ice is suggested by the presence of ikaite (hydrated carbonate which form below 7 ^{o}C) in sediments of Svalbard and Russia (Price & Nunn, 2010; Rogov & Zakharov, 2010). The direct evidence in the form of glacial diamictite has been documented in the Eromanga Basin, southern Australia, during the Berriasian to Valanginian interval (Alley & Frakes, 2003). The $\delta^{18}O$-based paleotemperatures from belemnites suggest cool temperatures during the Lower Valanginian period in Svalbard, Russia (Dichfield, (1997). Conversely, Littler et al. (2011) recorded very high SSTs based on TEX_{86} paleothermometry in the low and high latitudes during the Early Valanginian.

Within the Middle-Late Valanginian time period, the SST development surrounding the Valanginian Oceanic Anoxic Event has been of particular interest. This event is marked by a $\delta^{13}C$ excursion of 1.5-2‰ in various basins across the globe (Föllmi, 2012). The Valanginian event is marked by sea level rise and subsequent drowning of the carbonate platforms (Föllmi et al., 1994). Conversely, McArthur et al. (2007) are of the view that sea level fell due to polar ice formation during this time. Such cooling in the Middle Valanginian to Early Hauterivian is supported by $\delta^{18}O$-based paleotemperatures in various localities of the world (Dichfield, 1997; Van de Schootbrugge et al., 2000; Price et al. 2000; McArthur et al., 2007). Also, the presence of the boreal nannofossil species *Kokia borealis* during the positive $\delta^{13}C$ excursion in ODP Hole 1149B (Pacific) suggests low latitude surface water cooling during the Valanginian Event (Erba et al., 2004). But again, in contrast, Littler et al. (2011) recorded very high SSTs based on TEX_{86} paleothermometry in low and high latitudes in the Middle-Late Valanginian period.

The Valanginian sediments in the Upper Indus Basin of Pakistan are recorded in the Chichali Formation which range in age from the Kimmeridgian to Valanginian. In

this study, paleotemperatures are reconstructed based on the $\delta^{18}O$ of belemnites and TEX_{86} in the Kimmeridgian to Valanginian interval. This new data add to the discussion whether cooling or warming occurred during the Valanginian period.

7.2.2 δ 18O Proxy

7.2.2.1 Introduction

The $\delta^{18}O$ is an important paleotemperature proxy used for reconstructing past ocean temperatures. This proxy was introduced by Urey (1947), and was later on used by many other scientists (e.g. Epstein et al. 1953; Dichfield, 1997; Price et al., 2000; Van de Shootbrugge et al., 2000; McArthur et al., 2007). In this study, the paleotemperatures from the oxygen isotope data of belemnite calcite were calculated by using the equation of Epstein et al. (1953) and Craig (1965), modified by Anderson & McArthur (1983) (see table. 7.1). The equation is given below.

$$T\ (^{o}C) = 16.0 - 4.14\ (\delta c - \delta w) + 0.13\ (\delta c - \delta w)^{2}$$

The δc is the oxygen isotopic composition of belemnite calcite with respect to VPDB, while the δw is the oxygen isotopic composition of water from which the belemnite precipitated their shells. In order to calculate paleotemperatures for the Early Cretaceous the value of δw is needed, which is thought to be -1 ‰ (Shackleton & Kennett 1975) for ice free world.

7.2.3 The TEX86 proxy

7.2.3.1 Introduction

The recently introduced Sea Surface Temperature (SST) proxy TEX_{86}, based on marine organic matter depends on the relative distribution of glycerol dibiphytanyl glycerol tetraethers (GDGTs), which can be measured by high-performance liquid chromatography/atmospheric pressure chemical ionization mass spectrometry (HPLC/APCI-MS) (Schouten et al., 2002; Schouten et al., 2007). These lipids are produced by a Crenarchaeota, which are widely present in the marine realm (Karner, et al., 2001).

The GDGTs 0-3 are biosynthesised by marine Crenarchaeota; contain 0-3 cyclopentane moieties (fig.7.1), while crenarchaeol carries a cyclohexane ring in addition to the 4 cyclopentane moieties (Schouten et al., 2000; Schouten et al., 2007). The Crenarchaeota also synthesise a small amount of regio-isomer of crenarchaeol (Schouten et al., 2007).

The cultural experiments on the membrane composition of the Crenarchaeota showed that the increase in temperature causes an increase in the relative number of cyclopentane moieties (Uda et al., 2001, Schouten et al., 2007). This temperature dependency is also proved from the marine Crenarchaeota analysis of the Holocene core top sediments (Schouten et al., 2002; Schouten et al., 2007). Other mesocosm (experiments in which environmental parameters are controlled) by Wuchter et al., 2004) also confirmed that the increase in temperature causes change in the membrane composition of Crenarchaeota. Salinity, nutrients, and redox conditions of the water don't significantly affect the membrane composition of the Crenarchaeota (Schouten et al., 2007; Kim et al., 2008). It is therefore that measuring the relative amounts of GDGTs in marine sediments can be successfully used for SSTs reconstructions. This proxy is more reliable for reconstructing the past SSTs from relatively immature organic matter (Schouten et al., 2004), as highly mature organic matter cause bias in SSTs or it completely destroy the GDGTs. This new paleotemperature proxy is used to efficiently reconstruct the sea surface temperature as old as old as 160 My (Jenkyns et al., 2012).

7.2.3.2 Branched Isoprenoid Tetraether (BIT)

There are two groups of structurally similar GDGTs i.e. branched GDGTs and isoprenoid GDGTs. The branched GDGTs are present in the membranes lipids of soil bacteria, while the isoprenoid GDGTs are mainly derived from the marine Crenarchaeota (for the structures of both GDGTs see fig. 7.1). The relative amounts of these two types of GDGTs can be used to track the source of the organic matter. Branched and Isoprenoid Tetraether (BIT) index is a measure for the relative fluvial input of soil organic matter in marine sediments, based on the amount of branched GDGTs in marine sediments relative to the isoprenoid GDGT crenarchaeol (Hopmans et al., 2004; Weijers et al., 2006b).

BIT= [I+II+III] / [I+II+III] + [IV]

which can also be written as

BIT = ([1022]+[1036]+[1050]) / ([1022]+[1036]+[1050]+[Cren])

The BIT–index ranges from 0 (no branched GDGT content, or pure marine organic matter) to 1 (no crenarchaeol, pure soil/peat bog organic matter) (Hopmans et al., 2004).

7.2.3.3 TEX_{86} and Sea surface Temperature (SST) calculations

Ten samples from the Chichali Formation were selected for the TEX_{86} analysis. Samples were prepared in the Organic Geochemistry Laboratory of the Department of Earth Sciences, Utrecht University, after which the GDGTs were analysed on the HPLC-MS, stationed at the Department of Marine Organic Biogeochemistry, NIOZ Royal Netherlands, Institute for Sea Research-Texel (see Chapter 1 for the detailed methodology). The data for the TEX_{86} calculation are given in tables 7.2 and 7.3. The TEX_{86} can be calculated by the following equation introduced by Schouten et al. (2002).

TEX_{86}= [GDGT 2] + [GDGT 3] + [GDGT 4]/ [GDGT 1] + [GDGT 2] + [GDGT 3] + [GDGT 4]

which could also be rewritten as follows:

TEX_{86} = ([1298]+[1296]+[1292']) / (([1300]+[1298]+[1296]+[1292'])

The obtained TEX_{86}-value could subsequently be translated into a SST estimate using the following calibration formula provided by Kim et al., (2008):

T= (TEX_{86}-0.28)/0.015 (r^2=0.92, n=44).

For samples from the greenhouse world, Kim et al., (2010) introduced a new calibration, known as TEX_{86}^{H}, which can be used to calculate GDGT index-2 by the following equation:

GDGT index-2 = LOG (TEX_{86})

This calibration can also be used to calculate Paleo-SSTs as follows:

Paleo-SST = 68.4 x GDGT index-2 + 38.6 (r^2 = 0.87, n = 255, p < 0.0001)

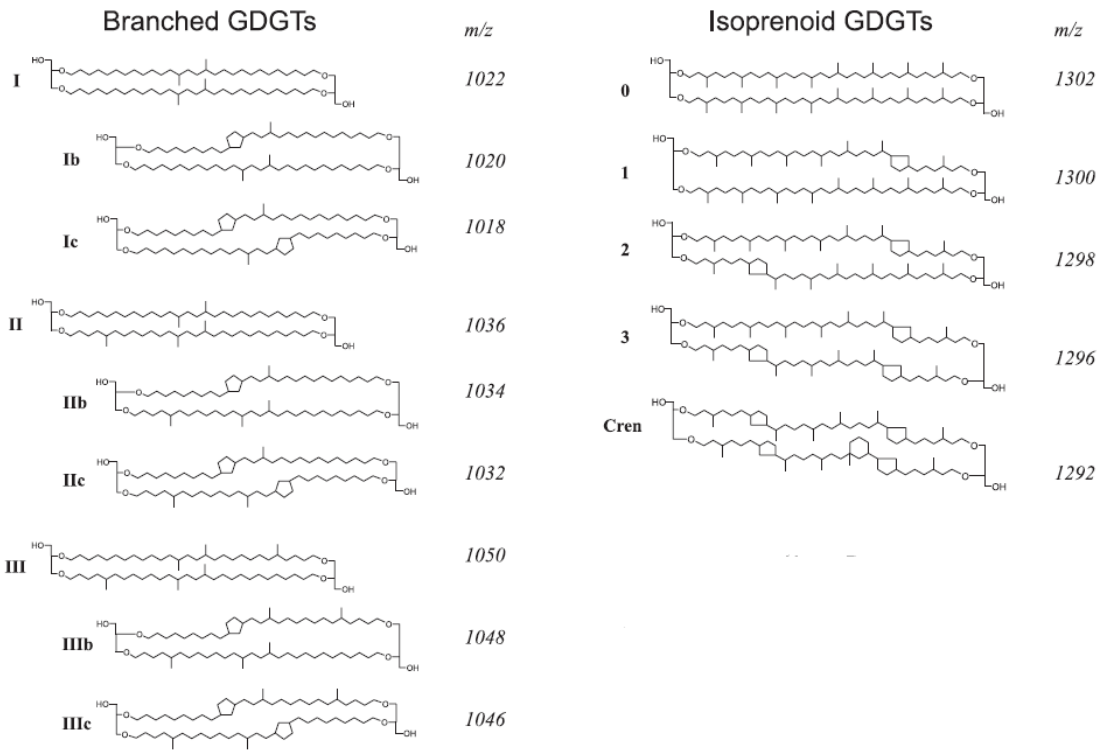

Figure 7.1: Structures of Branched and Isoprenoid GDGTs produced by soil bacteria and marine Crenarchaeota respectively. (Structure of branched GDGT is taken from Weijers, et al., 2007, while structure of Isoprenoid GDGT is taken from Schouten et al., 2007).

7.2.4 Results

7.2.4.1 $\delta^{18}O$ belemnite paleotemperatures

The $\delta^{18}O$ record, which is based on thirty belemnites throughout the section, in the Chichali Formation fluctuates between 0.83 to -2.49 ‰ (excluding the three samples with very light $\delta^{13}C/\delta^{18}O$ see table 7.1). The average $\delta^{18}O$ value of the Chichali Formation is -0.5 ‰. The paleotemperatures constructed from the $\delta^{18}O$ fluctuate between 8.7°C to 22.4 °C with an average of ~14.1 °C.

7.2.4.2 Belemnite Diagenesis

Diagenesis may have altered the primary carbon isotope values, or even more so oxygen isotope values. It is well known that stable isotopes in carbonates

(belemnites) change their values according to diagenetic processes (e.g. Hudson, 1977). To test whether significant diagensis has affected the primary isotopic signals, cross-plots of $\delta^{13}C$ and $\delta^{18}O$ can be a very useful tool. Importantly, a significant positive covariant trend between the $\delta^{13}C$ and $\delta^{18}O$ values implies that the carbonates have been substantially diagenetically altered (Lohmann, 1988; Marshall, 1992).

The cross plot, using all $\delta^{13}C$ and $\delta^{18}O$ values from all samples, shows a strong positive covariance, indicating that there has been a meteoric diagenetic overprint of the carbonate that constitutes the shells of these belemnites (r^2=0.45 see fig. 7.2A). Excluding, three belemnite samples (CC-69, CC-104, and CC-109) with very light $\delta^{13}C/\delta^{18}O$ values doesn't change this interpretation, because the scatter plot still shows a strong positive covariance (r^2=0.26 see fig. 7.2B).

Two visually well preserved belemnites (carrying light $\delta^{18}O$-values) were selected for Cathodoluminescence (CL) microscopy to screen further for diagenesis (figs. 7.3 & 7.4). The CL microscopy of these two samples (CC20 & CC50) shows diagenetic alteration along and across the growth bands. Diagensis can be seen as dark (pyrite-rich) and bright (Mn-rich) luminescence. The diagenetic alteration is common along the linear and wavy micro-cracks. The sediment infillings in the apical region may also affect the original isotopic signals of the rostrum (7.4B-C). However, the apical region was avoided during drilling of the rostrum for stable isotope analysis.

Collectively, the strong positive covariance of the $\delta^{13}C$ and $\delta^{18}O$ values and the CL images show that strong diagenetic overprinting has severely biased the primary isotopic signals of the belemnite calcite; hence these isotopic values are excluded from the paleotemperatures calculations, and are not taken into consideration into the discussion.

Samples	$\delta^{13}C$	$\delta^{18}O$	T(^{o}C)
CC 1	-0.07	0.16	11.36
CC 4	-0.73	0.60	9.71
CC 7	-1.23	-0.11	12.41
CC 11	-0.93	-0.09	12.34
CC 14	-0.91	-0.72	14.86
CC 17	-1.49	0.83	8.87
CC 20	-2.95	-2.49	22.47
CC 23	-1.33	0.75	9.15
CC 26	-2.29	-0.47	13.84
CC 29	-2.59	-1.33	17.37
CC 31	-1.59	-0.33	13.29
CC 36	-0.99	0.49	10.14
CC 38	-2.24	-0.12	12.46
CC 41	-2.85	-1.02	16.07
CC 44	-3.11	-0.85	15.38
CC 47	-2.47	0.01	11.94
CC 50	-2.59	-1.78	19.30
CC 53	-2.42	-0.66	14.60
CC 56	-1.94	-0.58	14.29
CC 59	-3.93	-1.47	17.98
CC 63	-3.08	-0.52	14.05
CC 65	-2.82	-0.70	14.75
CC 69	-3.28	-6.71	--------
CC 71	-3.42	-1.62	18.61
CC 73	-2.13	-0.43	13.68
CC 98	0.03	-1.13	16.53
CC 104	-14.03	-5.08	--------
CC 109	-11.68	-3.81	--------
CC 112	-0.59	-0.98	15.90
CC 119	-2.14	0.17	11.35

Table7.1: Showing $\delta^{13}C$ and $\delta^{18}O$-values of belemnites, and $\delta^{18}O$ based paleotemperature values for the Chichali Formation, in Chichali Nala Section

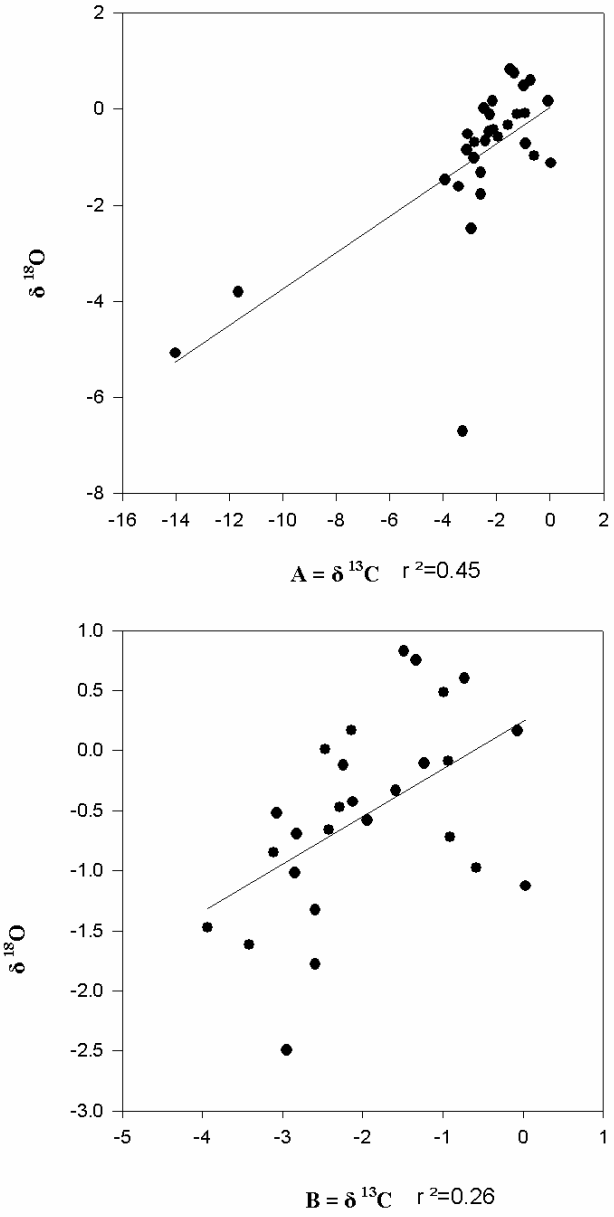

Figure 7.2: A = Kimmeridgian to Valanginian δ ^{13}C and δ ^{18}O scatter plot for all belemnite samples, showing strong covariance; B = Kimmeridgian to Valanginian ^{13}C and δ ^{18}O scatter plot showing strong covariance even after excluding the apparently diagenetically altered samples i.e. CC-69, CC-104, and CC-109.

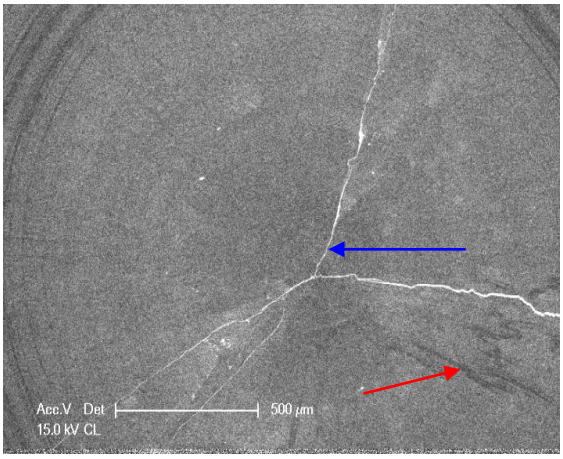

A

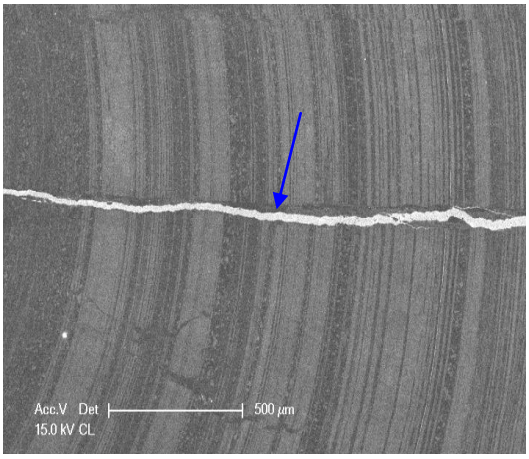

B

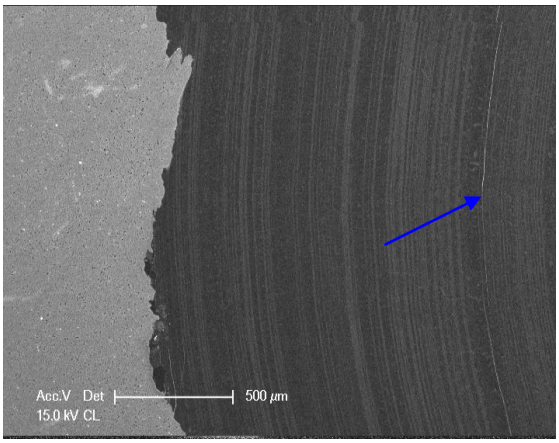

C

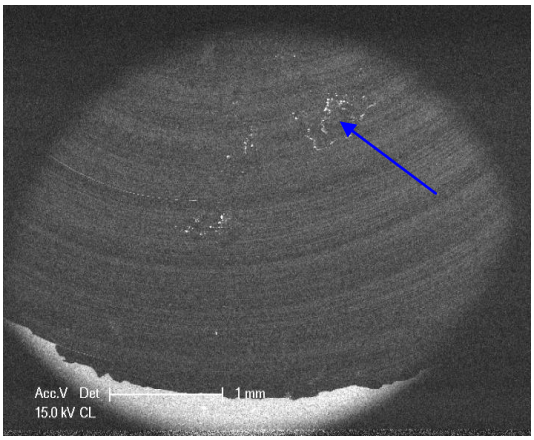

D

Figure 7.3: Cathodoluminescence images of sample CC50. A. Bright white luminescence developed along triple junction of crakcs representing digenetic Mn development, B. Diagenetically altered cracks showing bright luminescence (Mn rich) in a well preserved growth bands of belemnite rostrum, C. well preserved concentric bands in the outer periphery of rostrum with minor bright luminescence (blue arrow) developed along growth bands due to diagenetic Mn enrichment, D. Small patches of bright luminescence (blue arrow) represent digenetic addition of Mn to the rostrum.

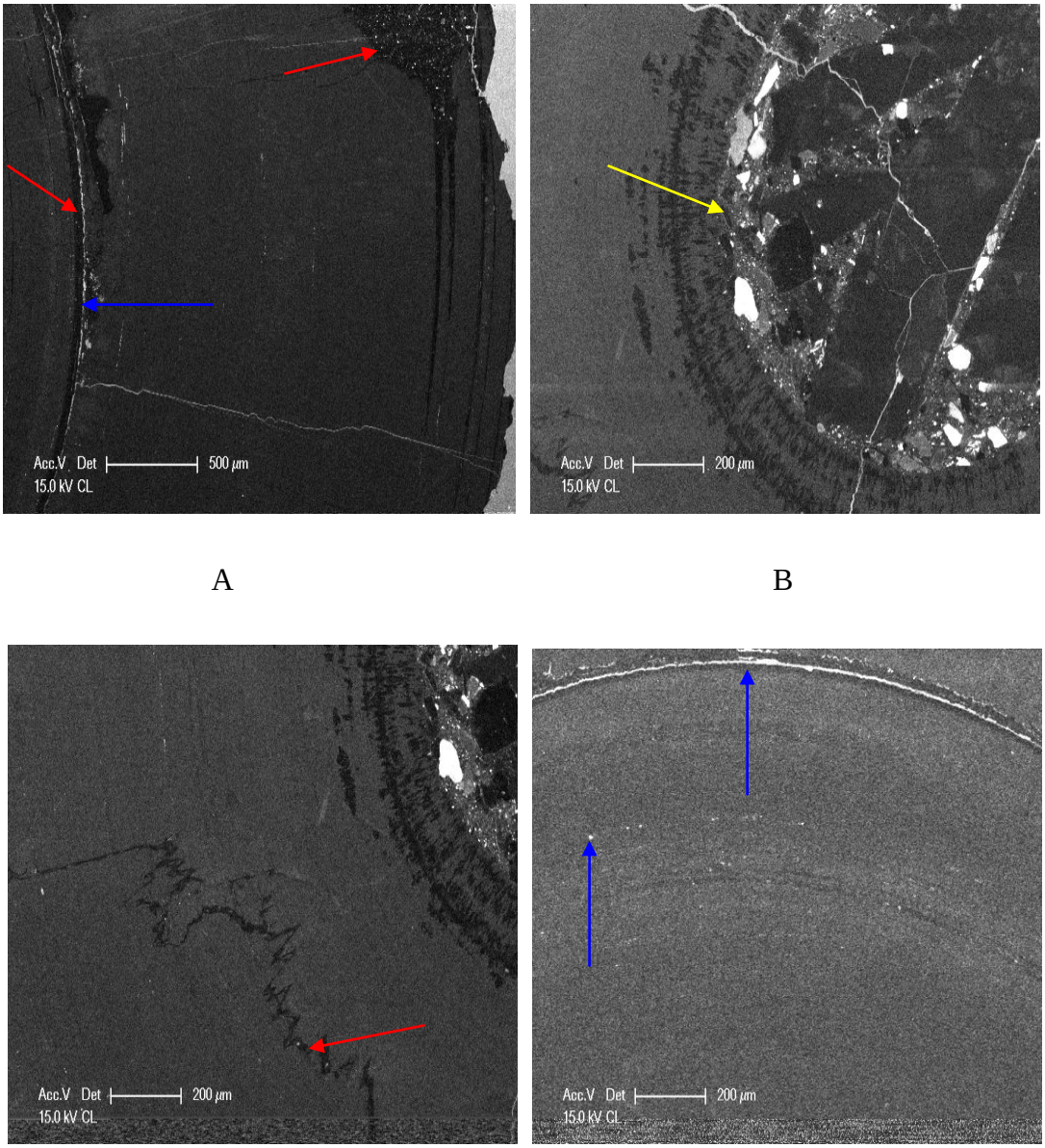

Figure 7.4: Cathodoluminescence images of belemnite rostrum from sample CC20. A. Development of dark black colour caused by digenetic pyrite development along the periphery and along growth bands in the centre (red arrows); bright luminescence show the diagenetic Mn addition to the belemnite rostrum (blue arrow) B. Sediment filled apical region, which show bright white, and black luminescence (yellow arrow) C. Pyritisation in the middle of rostrum along a wavy stylolitic crack (red arrow), D. Bright white luminescence due to Mn development along growth bands and small patches throughout the rostrum (blue arrow).

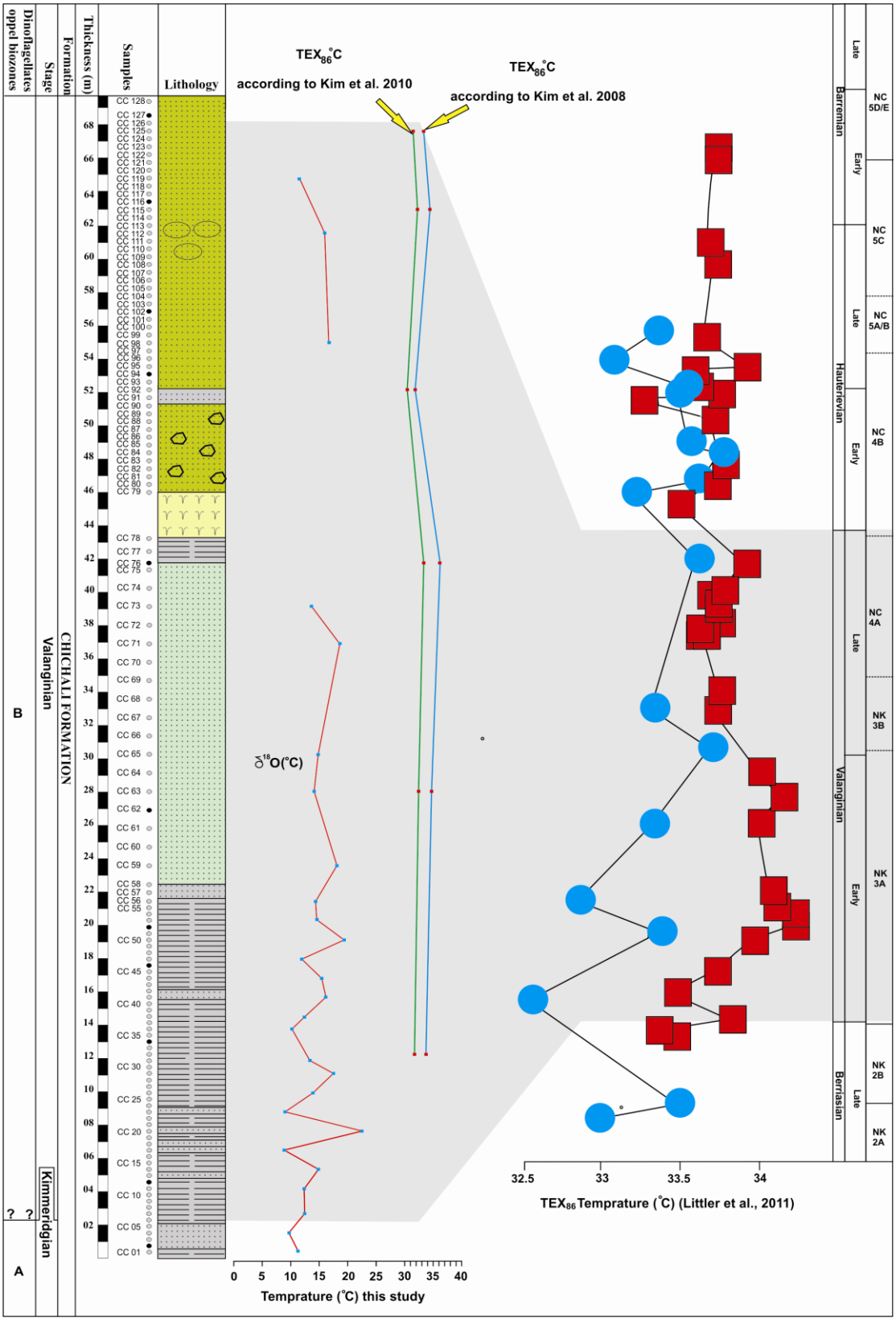

Figure 7.5: The Kimmeridgian to Valanginian δ ^{18}O (belemnites) paleotemperatures, and TEX_{86} derived SSTs (Valanginian only) of the Chichali Formation correlated with the Valanginian TEX_{86} SSTs of the Littler et al., (2011).

7.2.4.3 TEX86 SSTs

Ten samples were processed for the TEX_{86} paleothermometry. The GDGTs concentrations for four of the samples (CC3, CC44, CC52, & CC104) were too low for reliable SST reconstructions (tables 7.2-7.3). The exclusion of these samples was further supported by the high BIT-index values (0.52, 0.64, 0.76, 0.91 respectively), which indicates that these four samples contain too much terrestrial organic matter (Hopmans et al., 2004), indeed rendering them useless for the SST reconstruction. These four samples are therefore excluded from the SST discussions. The six remaining samples are distributed throughout the entire Valanginian of the Chichali Formation (fig. 7.5).

SSTs calculated according to the Kim et al., (2008) TEX_{86} calibration, range from 31.9^{o}C to 36.1^{o}C with an average of 34^{o}C for the Valanginian sediments of the Chichali Formation while SSTs calculated according to Kim et al. (2010) TEX_{86}^{H} calibration, range from 30.4 to 33.2^{o}C with an average of 31.8^{o}C (fig.7.5).

7.2.5 Discussion

The objective of this study is to add new SST data to the discussion of climate development during the Valanginian. The new data can only be meaningful if the Indus Basin is relocated to its position much further south than today in the Valanginian. The Indus Basin was located at the paleolatitude of ~-35^{o} (fig.7.6) during the Valanginian. Today, SSTs at this latitude are ~22 ^{o}C (Littler et al., 2011). Thus, the question arises whether the SSTs were higher or lower than today at this latitude during the Valanginian.

Were temperatures possibly higher than today's temperatures in the Valanginian? First of all greenhouse gases content of the atmosphere was much higher generally in the Cretaceous than today (Menegatti et al., 1998; Leckie, 2002, Takashima et al., 2006.), which would have led to warmer temperatures of the ocean, and in particular to a less steep temperature gradient from low to high latitudes (Leckie, 2002).

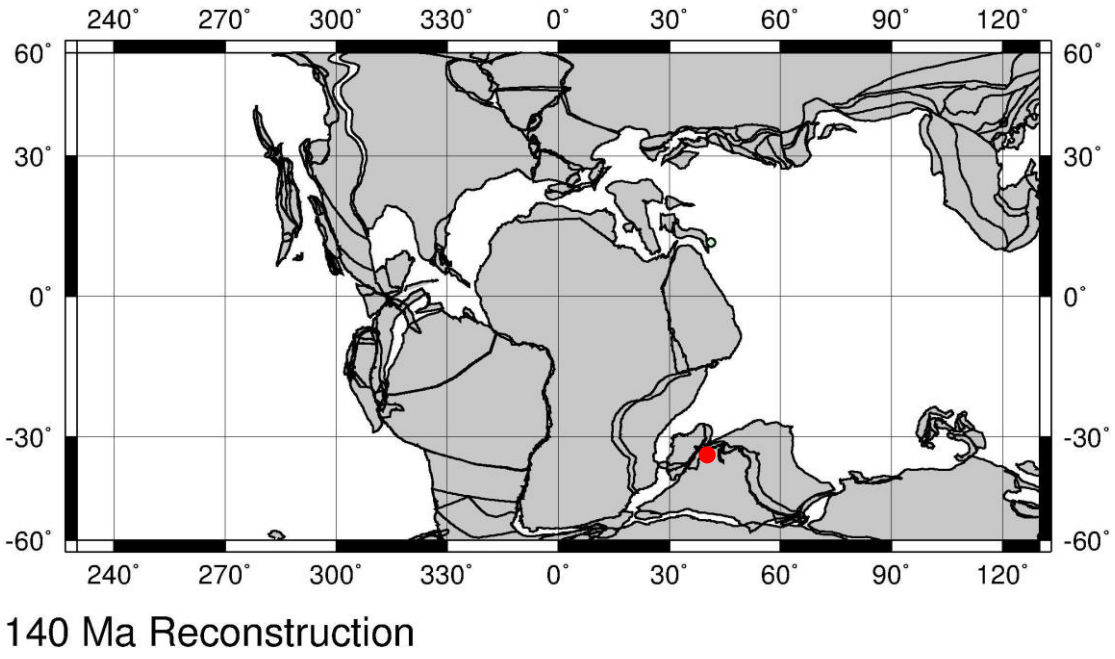

Figure 7.6: Shows the paleolatitude of the Chichali Nala Section during Valanginian time. Adapted from Ocean Drilling Stratigraphic Network (ODSN) Paleomap project (http://www.odsn.de/odsn/services/paleomap/paleomap.html).

Thus, the Indus Basin reconstructed SSTs, are ideally placed to test the hypothesis that there was a reduced SST gradient as a result from the high greenhouse content in the atmosphere in the Valanginian. Were temperatures possibly lower than today's in the Valanginian? The presence of ikaite and glacial diamictite during the Valanginian suggest that cooling occurred (Price & Nunn, 2010; Rogov & Zakharov, 2010; Alley & Frakes, 2003) in the Valanginian. Paleotemperatures based on $\delta^{18}O$ also suggest cooling during the Valanginian, particularly during the positive $\delta^{13}C$ excursion of the Valanginian Event (Dichfield, 1997; Price et al., 2000; Van de Schootbrugge et al., 2000; McArthur et al., 2007). The cooling during the Late Valanginian is also supported by the distribution of the boreal nannofossil during the peak of the $\delta^{13}C$ excursion (Erba et al., 2004). Thus, the Indus Basin reconstructed SSTs, are ideally placed to test the hypothesis that cooling occurred in the Valanginian.

The SST results based on the TEX_{86} analysis show that the surface ocean was consistently much warmer than today at the paleolatitude of ~-35^{o}. The current SSTs are about 22^{o}C at the latitude of about 35^{o} South (Littler et al., 2011). Thus, the Valanginian SSTs based on TEX_{86} were about 10-12 ^{o}C higher than today. Littler et al. (2011), using various sites distributed over the globe, reconstructed similar (high) temperatures based on the same proxy occurred. Here, the new data fit perfectly

within the data set produced by Littler et al. (2011) (fig. 7.5). Notably, the SSTs at the paleolatitude of about 35^{o} South were equally warm as those in the low latitudes of 15-20^{o} North, implying that surface ocean waters were exceedingly hot from low to middle latitudes. Therefore, our new data set confirms that higher SSTs prevailed at low to middle paleolatitude than today during the Early Cretaceous as was already concluded by Littler et al. (2011).

The reconstruction of the meridional SSTs gradient is very important for understanding the past climate (Leckie et al. 2202). The new data provide a significant insight into such meridional reconstruction, and it provides the opportunity to compare the Valanginian SST gradient from mid to high latitudes with similar gradients during the warm Late Cretaceous and early Cenozoic periods (See figure 7.7). Such comparison suggests that the SST gradient during the Valanginian was basically similar to the gradients in the, Late Cretaceous and early Cenozoic. This suggests that extreme warmth occurred during the Valanginian.

The spore-pollen record of the Chichali Formation also indicates warm, humid to dry conditions at the 35^{o} South paleolatitude during Valanginian (see Chapter 4 for details).

Collectively, all these datasets indicate strongly that the Valanginian world was overall very warm and the first hypothesis as mentioned above seems correct. But how can we reconcile the notion of a super warm world with suggestions that cooling occurred in the Valanginian? Perhaps the $\delta^{18}O$ paleotemperatures based on carbonate from the belemnite rostrum is biased because of the uncertainties regarding the life

habitat of belemnites. It is still uncertain whether they have lived in the

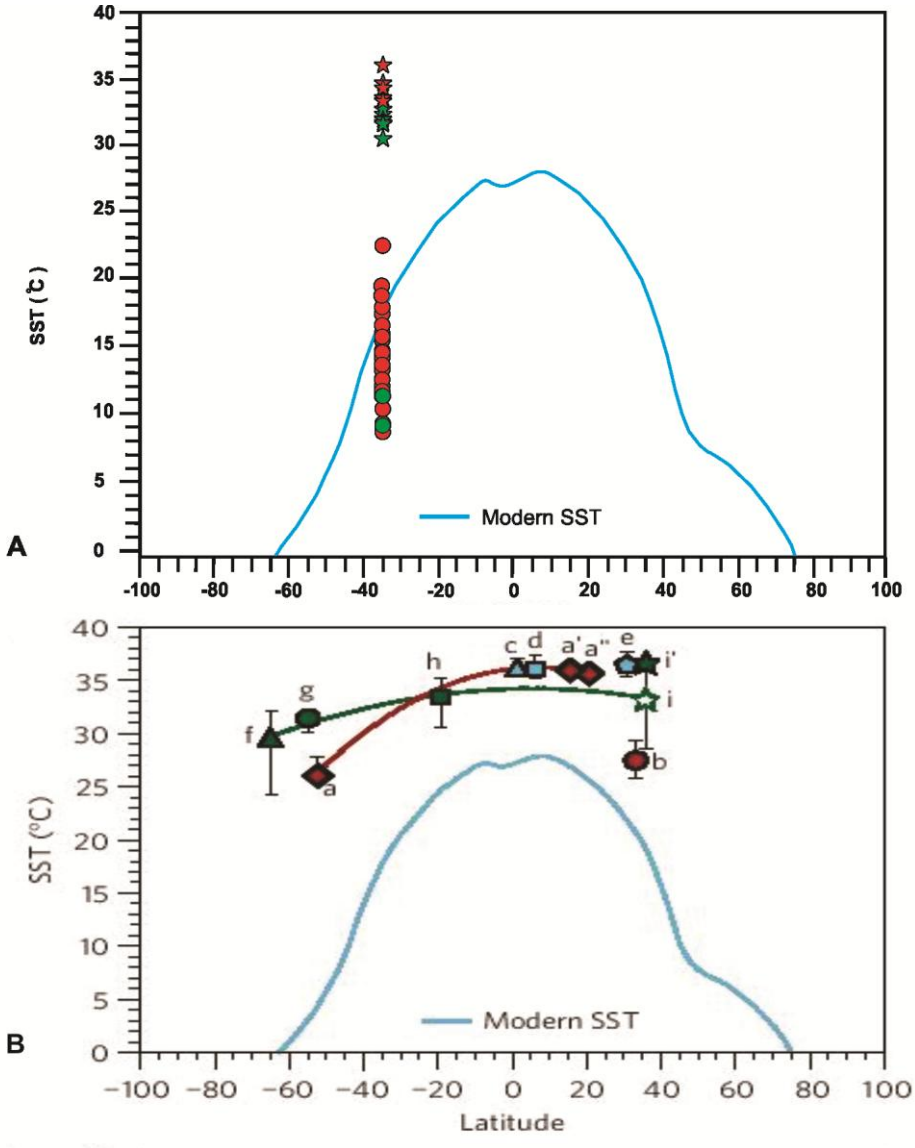

Figure 7.7: Showing the Meridional temperature gradients. A, The TEX_{86} based Valanginian SSTs of the Chichali Formation (green stars represent calculation of SSTs according to Kim et al. 2010 while red stars represent calculation of SSTs according to Kim et al. 2008); belemnites based Kimmeridgian to Valanginian SSTs of the Chichali Formation (green circles represent the Kimmeridgian SSTs while red circle represent the Valanginian SSTs). B, Hauterivian TEX_{86} based SSTs (a, a' and a") Early Eocene SSTs (green symbols), Late Cretaceous SSTs (blue symbols) and Early Barremian SSTs (red circle). These SSTs are from different parts of the globe (see Littler et al. 2011 for details). In these SSTs (d) represents Cenomanian-Turonian, while the peak SST of Palaeocene-Eocene Thermal Maximum is shown as (i').

nektonic or benthic environments, but if so, their carbonate would have recorded colder temperatures (McArthur et al., 2007; Mutterlose et al., 2010). The calculated temperatures from the oxygen isotope results suggest they may have lived in deep environments. Another reason for the cold temperatures may relate to diagenesis affecting the primary isotope signals. The cross plots of $\delta\ ^{13}C$ and $\delta\ ^{18}O$ values show a positive correlation suggesting that diagenesis occurred (fig. 7.2). Diagenesis of the carbonates results into cold temperatures if the shells are recrystallized on the sea floor in the deep ocean. It is therefore, perhaps not surprising that the $\delta^{18}O$ paleotemperatures based on carbonate from the belemnite rostrum are very different from the reconstructed SSTs based on the TEX_{86}.

Perhaps, the contrast between warm SSTs based on TEX_{86} and other data which support cooling during the Valanginian can be further explained in terms of the regional difference in climate sensitivity, especially at high latitudes as discussed by Littler et al. (2011).

Samples	Weight (g)	M/Z Areas										BIT	TEX86	GDGT index-2	SST1 °C	SST2 °C
		744 (y) C46 GDGT	1302 or GDGT 0	1300 or GDGT 1	1298 or GDGT 2	1296 or GDGT 3	1292 (x) or GDGT 4	1292' or GDGT	1050 or GDGT	1036 or GDGT	1022 or GDGT I					
CC3	12.3	1.36E+07	7.45E+04	2.42E+04	3.39E+04	2.23E+04	1.16E+05	1.98E+04	4.53E+03	5.88E+04	6.27E+04	0.52	0.76	-0.12	------	------
CC32	14.6	1.61E+07	3.88E+05	1.49E+05	1.53E+05	1.01E+05	1.41E+06	3.21E+05	2.19E+04	1.89E+05	2.89E+05	0.26	0.79	-0.10	31.76	33.85
CC44	13.3	1.50E+07	1.36E+04	4.56E+03	3.37E+03	3.45E+03	6.07E+04	1.18E+04	7.49E+04	1.42E+04	1.67E+04	0.64	0.80	-0.10	-----	------
CC52	12.4	1.42E+07	2.27E+04	4.74E+03	3.09E+03	1.10E+03	2.87E+04	1.24E+03	1.00E+04	3.57E+04	4.56E+04	0.76	0.53	-0.27	------	------
CC63	16	1.53E+07	4.54E+04	2.99E+04	2.32E+04	3.31E+04	8.55E+05	7.21E+04	5.22E+03	3.51E+04	5.11E+04	0.10	0.81	-0.09	32.38	34.80
CC76	15.1	1.61E+07	9.01E+04	5.09E+04	5.89E+04	5.69E+04	1.18E+06	1.42E+05	3.81E+04	2.35E+05	1.66E+05	0.27	0.84	-0.08	33.25	36.15
CC92	13.4	1.61E+07	4.41E+05	6.10E+04	3.20E+04	3.17E+04	6.42E+05	1.29E+05	1.27E+04	1.06E+05	2.19E+05	0.34	0.76	-0.12	30.43	31.91
CC104	15.1	1.47E+07	1.63E+04	4.03E+03	4.31E+03	4.41E+03	8.60E+03	1.00E+03	6.70E+03	3.92E+04	3.84E+04	0.91	0.71	-0.15	------	------
CC115	15.7	1.41E+07	5.38E+04	2.70E+04	1.84E+04	2.15E+04	6.25E+05	7.04E+04	2.33E+03	1.25E+04	7.63E+03	0.03	0.80	-0.10	32.10	34.37
CC125	16.3	1.30E+07	1.12E+05	3.24E+04	1.99E+04	2.26E+04	5.34E+05	7.56E+04	3.53E+04	1.08E+05	6.23E+04	0.28	0.78	-0.11	31.40	33.32

Table 7.2: Shows all the parameters used for the TEX_{86} SSTs calculations for the Chichali Formation: C46 GDGT is internal standard i.e. Crenoarcheol/C46 and is equal to 0.974382; SST1 calculated according to Kim et al., (2010), SST2 calculated according to Kim et al., (2008). GDGT index-2 is calculated according to Kim et al. (2010).

Depth	Concentration ng/g sediments								
	1302 or GDGT 0	**1300 or GDGT 1**	**1298 or GDGT 2**	**1296 or DGT 3**	**1292 or GDGT 4**	**1292' or GDGT 4'**	**1050 or GDGT III**	**1036 or GDGT II**	**1022 or GDGT I**
CC3	0.114268	0.037118	0.051996	0.034204	0.17792	0.030369	0.006945	0.090187	0.096169
CC32	0.42351	0.162637	0.167003	0.110244	1.539044	0.350378	0.023904	0.206297	0.31545
CC44	0.017491	0.005863	0.004338	0.004441	0.078065	0.015176	0.096327	0.018262	0.021478
CC52	0.033077	0.006913	0.004498	0.001598	0.04182	0.0018	0.014571	0.05202	0.066445
CC63	0.047583	0.031338	0.024316	0.034692	0.896119	0.075567	0.005468	0.036788	0.053557
CC76	0.09509	0.053719	0.062162	0.060051	1.245346	0.149864	0.04021	0.248014	0.175193
CC92	0.524468	0.072545	0.038057	0.0377	0.763511	0.153416	0.015104	0.126063	0.26045
CC104	0.018841	0.004658	0.004985	0.005096	0.009942	0.001156	0.007739	0.045311	0.044386
CC115	0.062355	0.031294	0.021326	0.024919	0.724389	0.081595	0.002698	0.014488	0.008838
CC125	0.135249	0.039231	0.024095	0.027365	0.646578	0.091538	0.042742	0.130769	0.075434

Table 7.3: Show the concentrations of Isoprenoid and branched GDGTs.

7.3 Palaeoenvironmental Analysis of the Parh Formation

7.3.1 General Introduction

The Oceanic Anoxic Events (OAEs) were most likely caused by perturbations of the carbon cycle, e.g. by volcanic CO_2 out-gassing or methane release from the continental margin sediments (Menegatti et al., 1998; Dickens et al. 1995; Hesselbo et al., 2000). Such perturbations in the carbon cycle can be recorded in the $\delta^{13}C$ of the marine carbonate and organic matter (Scholle & Arthur, 1980; Gröcke et al., 2005; Menegatti et al., 1998; Hesselbo, et al., 2000). The aim of this Chapter 7 is to present the $\delta^{13}C$ record of bulk pelagic carbonates of the Parh Formation which spans from Early Aptian to Early Maastrichtian (see tables. 7.4 & 7.5). The $\delta^{13}C$ record would be useful to shed light on processes surrounding carbon perturbations and to assign the precise stratigraphic positions of the OAEs in the Parh Formation.

7.3.2 Carbon cycle and carbon isotope excursions

The carbon isotopes get fractionated when carbon moves from one reservoir to another, see figure 7.8. These reservoirs contain carbon species each with its own isotopic value. For instance, marine organic carbon has a $\delta\ ^{13}C$-value of -22‰, while marine inorganic carbon $\delta\ ^{13}C$-values range from 1‰ in the surface ocean to 0‰ in the deep ocean. Carbons in volcanic gases and icy methane hydrates (not shown on the fig. 7.8) have $\delta^{13}C$ values of -5‰ and -60‰ (Scholle & Arthur, 1980; Dickens et al.1995), respectively.

The marine inorganic carbon $\delta^{13}C$ records usually show positive excursions across OAEs, i.e. the OAE2 Bonarelli Event (see Chapter-1, figure 1.1) shows a pronounced positive excursion that has been globally recorded in the major oceans. This is explained by massive burial of organic matter enriched in ^{12}C (e.g. Scholle & Arthur, 1980). However, negative excursions occasionally occurred across OAEs, when high amounts of carbon driven by massive degassing from hydrates were added to the ocean. There is no such OAE example as yet from the Cretaceous, but massive degassing from hydrates might have occurred at the base of the important OAE in the Toarcian (e.g. Hesselbo, 2000). However, unlike the Paleocene-Eocene Thermal Maximum (PETM), the methane outburst feedback mechanism for the OAEs is still debatable, e.g. Schootbrugge et al. (2005) believe that the large $\delta^{13}C$ excursion along

the Toarcian Anoxic Event can also be explained by the recycling of the dissolved inorganic carbon from the deeper stratified water masses.

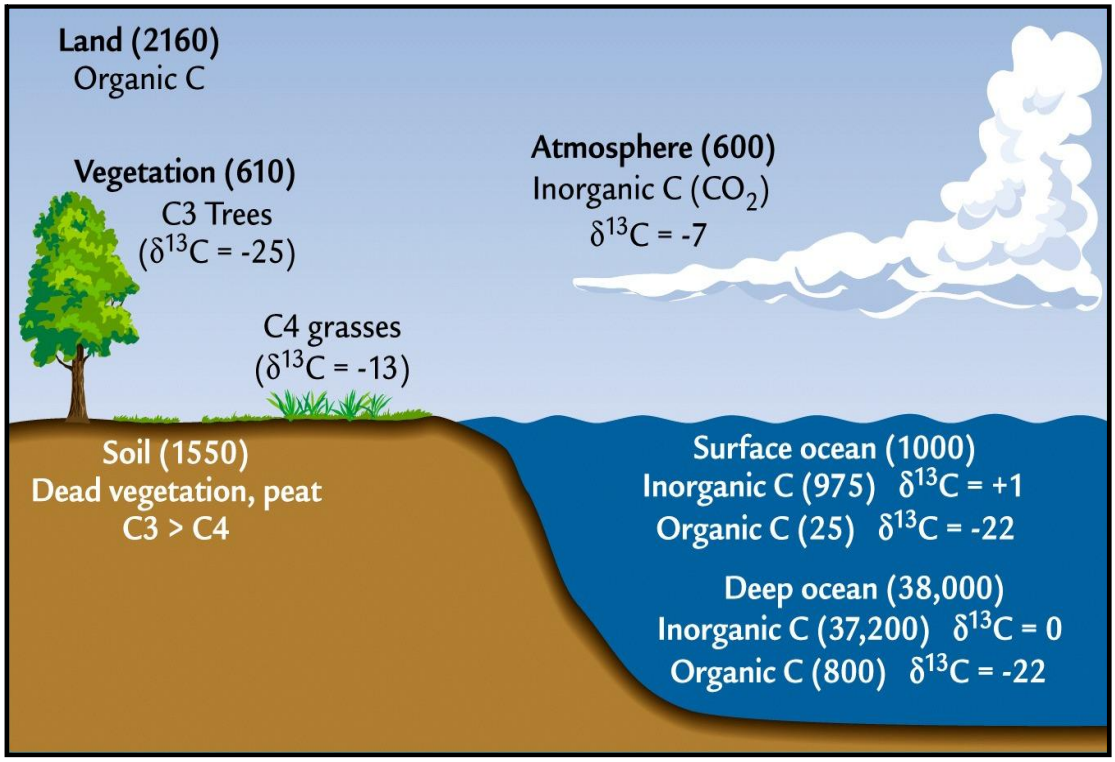

Figure 7.8: Showing major carbon reservoirs, along with $\delta^{13}C$ values. The amounts of carbon in these reservoirs are in gigatons. (Modified after Ruddiman, 2007).

7.3.3 Diagenesis

Diagenesis may have altered the primary carbon isotope values, or even more so oxygen isotope values. It is well known that stable isotopes in limestones change their values according to diagenetic processes (e.g. Hudson, 1977). To test whether significant diagensis has affected the primary isotopic signals, cross-plots of $\delta^{13}C$ and $\delta^{18}O$ can be a very useful tool. Importantly, a significant positive covariant trend between the $\delta^{13}C$ and $\delta^{18}O$ values implies that the carbonates have been substantially diagenetically altered (Lohmann, 1988; Marshall, 1992; Heydari et al., 2001).

Samples	$\delta^{13}C$	$\delta^{18}O$	Samples	$\delta^{13}C$	$\delta^{18}O$
MP 1	-4.212	-6.042	MP 100	1.293	-5.862
MP 2	-7.907	-8.118	MP 101	1.631	-5.620
MP 3	-2.144	-6.360	MP 102	1.040	-5.751
MP 4	-0.822	-6.131	MP 103	1.671	-5.140
MP 5	-0.594	-5.550	MP 104	1.377	-5.559
MP 6	1.040	-6.051	MP 105	1.377	-5.439
MP 7	1.685	-5.812	MP 106	1.495	-5.150
MP 8	1.398	-7.195	MP 107	1.274	-6.247
MP 9	2.279	-5.760	MP 108	1.555	-5.428
MP 10	1.069	-5.947	MP 109	1.587	-6.167
MP 12	1.598	-5.606	MP 110	1.566	-6.176
MP 14	1.556	-5.986	MP 111	1.370	-6.207
MP 16	-0.448	-5.956	MP 112	1.340	-5.671
MP 18	1.831	-5.900	MP 113	1.241	-6.000
MP 20	1.598	-5.884	MP 114	1.163	-5.606
MP 22	1.111	-6.545	MP 115	0.944	-6.177
MP 24	0.480	-5.920	MP 116	0.758	-5.822
MP 26	-0.301	-5.713	MP 117	1.110	-5.322
MP 28	-0.082	-5.304	MP 118	0.918	-5.361
MP 30	0.014	-4.582	MP 119	0.925	-5.648
MP 34	0.530	-3.980	MP 120	0.832	-6.087
MP 38	0.677	-6.199	MP 121	1.113	-5.824
MP 42	1.801	-6.338	MP 122	1.174	-5.886
MP 44	1.981	-6.042	MP 123	1.233	-5.915
MP 46	0.932	-6.415	MP 124	1.321	-5.599
MP 49	1.415	-5.962	MP 125	1.272	-5.566
MP 50	1.547	-6.272	MP 126	1.044	-6.038
MP 54	1.722	-6.293	MP 127	1.184	-5.782
MP 58	1.689	-6.255	MP 128	1.434	-6.117
MP 60	1.864	-5.946	MP 129	1.111	-6.097
MP 62	1.462	-6.177	MP 130	1.304	-6.112
MP 63	1.542	-5.902	MP 131	1.688	-6.050
MP 66	1.771	-6.256	MP 132	1.687	-5.819
MP 70	1.836	-5.832	MP 133	1.962	-5.443
MP 74	1.890	-6.219	MP 134	1.911	-6.072
MP 78	1.899	-6.142	MP 135	1.955	-5.348
MP 82	1.832	-6.226	MP 136	1.951	-5.714
MP 86	1.822	-5.861	MP 137	1.900	-5.888
MP 90	1.787	-6.199	MP 138	1.557	-5.885
MP 94	1.951	-5.967	MP 139	1.732	-5.507
MP 98	1.654	-6.105	MP 140	1.710	-5.899

Table 7.4: Showing $\delta^{13}C$ and $\delta^{18}O$-values (VPDB) of bulk carbonates of the Parh Formation, Moghal Kot Section.

Samples	$\delta^{13}C$	$\delta^{18}O$	Samples	$\delta^{13}C$	$\delta^{18}O$
MP 141	0.662	-5.022	MP 177	2.486	-6.446
MP 142	1.782	-5.835	MP 178	2.487	-5.240
MP 143	1.637	-5.288	MP 180	1.585	-4.754
MP 144	1.415	-4.116	MP 181	1.977	-3.430
MP 145	1.487	-4.442	MP 182	2.558	-5.848
MP 146	1.769	-4.878	MP 183	2.001	-5.843
MP 147	1.721	-4.916	MP 184	2.412	-5.838
MP 148	1.537	-4.313	MP 185	2.017	-5.918
MP 149	2.452	-4.989	MP 186	2.385	-5.839
MP 150	1.687	-4.365	MP 187	2.250	-5.672
MP 151	1.465	-4.125	MP 188	2.102	-5.823
MP 152	1.431	-4.116	MP 189	2.011	-5.348
MP 153	1.496	-4.836	MP 191	2.191	-5.218
MP 154	1.388	-4.173	MP 192	2.069	-5.676
MP 155	0.986	-5.978	MP 193	2.170	-5.553
MP 156	0.262	-5.253	MP 194	2.165	-5.327
MP 157	0.428	-5.644	MP 195	2.116	-5.416
MP 158	-0.401	-5.859	MP 197	1.624	-5.552
MP 159	-1.218	-6.926	MP 198	1.389	-5.684
MP 160	0.911	-5.886	MP 199	0.425	-5.594
MP 162	1.339	-4.077	MP 200	0.528	-5.801
MP 163	1.344	-4.038	MP 201	0.314	-6.125
MP 164	1.697	-5.400	MP 202	0.439	-5.903
MP 165	0.962	-6.305	MP 203	1.938	-5.363
MP 166	2.232	-4.917	MP 304	-0.055	-5.657
MP 167	3.000	-5.931	MP 305	1.685	-5.072
MP 168	2.679	-5.708	MP 306	1.755	-4.677
MP 169	2.396	-5.747	MP 307	1.614	-4.623
MP 171	2.698	-5.130	MP 308	1.530	-4.164
MP 172	2.686	-5.708	MP 309	1.619	-5.484
MP 173	2.473	-5.094	MP 310	1.353	-4.922
MP 174	2.487	-5.378	MP 311	-1.804	-4.931
MP 175	2.493	-4.602	MP 312	-1.560	-5.029
MP 176	2.338	-5.278	MP 313	-2.329	-4.619

Table 7.5: Showing $\delta^{13}C$ and $\delta^{18}O$-values (VPDB) of bulk carbonates of the Parh Formation, Moghal Kot Section.

7.3.3.1 Scatter plot based on the entire sequence of the Parh Formation

The scatter plot, using all measured samples throughout the Parh Formation (Aptian-Maastrichtian), shows a very weak positive covariance ($r^{2=}$0.053 see fig. 7.9A). This weak positive covariance, however, is a result of one outlier (Sample MP-2), which shows very low values for both $\delta^{13}C$ (-7.9 ‰) and $\delta^{18}O$ (-8 ‰). The scatter plot without the sample MP-2 (fig. 7.9B) shows insignificant covariance ($r^{2=}$0.003). Therefore, the insignificant covariance, between the $\delta^{13}C$ and $\delta^{18}O$ values for the whole section suggests that diagenesis has not affected the primary signals except for Sample MP-2 that has been significantly affected by diagenesis.

7.3.3.2 Scatter plots based on samples from individual subsections of the Parh Formation

The $\delta^{13}C$ and $\delta^{18}O$ scatter plot for the Aptian sequence shows moderate covariance ($r^{2=}$0.171) (fig. 7.10A). But again, there is no significant covariance ($r^{2=}$0.004) if sample MP-2 is excluded from the cross plot (fig. 7.10B). The cross plots of the Albian (r^2=0.07 see fig. 7.11A), Turonian (r^2=0.003 see fig. 7.12A), and Coniacian-Maastrichtian (r^2=0.011 see fig. 7.12B) intervals show no significant covariance, reassuringly suggesting that no significant diagenetic overprints affected the isotopic signals. The $\delta^{13}C$ and $\delta^{18}O$ scatter plot of the Cenomanian carbonates shows strong covariance (r^2=0.311, see fig. 7.11B), suggesting that diagenetic overprints may have affected the isotope signals. Such covariant trends can also be caused by the kinetic fractionation during the biological calcification (Mconnaughey, 1988). In such fractionation the organisms discriminate against heavy isotopes of carbon and oxygen during the hydration and hydroxylation of C02 (Mconnaughey, 1988). However the bulk carbonates of the Parh Formation during the Cenomanian are not entirely biogenic (see Chapter 3 for details), i.e. the microfacies show that the planktonic foraminifera are incorporated in the micrite, while micrite can also be formed by chemical precipitation (Flügel, 2004). Also the planktonic foraminifera evolved to dwell in different depth habitats during the Cenomanian (Premoli-Silva & Sliter, 1999). Therefore different species will have recorded different isotopic signals depending upon their depth habitats. Based on the above factors the covariant trend of $\delta^{13}C$ and $\delta^{18}O$ scatter plots of bulk carbonates can't be explained by the kinetic fractionation.

In conclusion, although some diagenetic overprinting cannot be ruled for the sediments of the Parh Formation, the cross plots of the $\delta^{13}C$ and $\delta^{18}O$ values suggest that the carbon isotopic values retained their primary signals. As mentioned earlier, the $\delta^{18}O$ signature is very prone to diagenetic overprints; hence $\delta^{18}O$ signals are not used for the paleoenvironmental interpretation in this study.

7.3.4 The bulk stable carbon isotope record of the Parh Formation

The bulk stable carbon isotope record of the Parh Formation, Moghal Kot Section of Pakistan is presented together with the global composite carbon isotope curve (fig. 7.13). Here, the global composite curve comprises carbon isotope records from several stratigraphic sections around the world, summarizing data from several authors (Erbacher et al., 1996, fig. 2; Weissert et al., 1998, fig. 2; Jenkyns & Wilson, 1999, fig. 6; Jarvis et al, 2006, fig. 15; Jarvis et al., 2002, fig. 2, and Thibault et al. 2012, fig. 4). This comparison was thought to be useful because the bulk stable carbon isotope records are global in nature. Any large reservoir shift of carbon associated with a large shift in carbon isotope values of bulk carbonates should be present in both curves.

7.3.4.1 OAE1a or Selli Event

The name of the Selli Event is derived from the organic-rich horizon called Livello Selli, in Umbria-Marche, Central Italy (Coccioni et al., 1987). The complete $\delta^{13}C$ record of the Selli Event is documented globally in the combined *Globigerinelloides blowi*/*Leupoldina cabri* Biozones in the Early Aptian (e.g. Weissert et al., 1998; Erbacher et al., 1996; Menegatti et al., 1998; Erba, 1994). Importantly, the base of the Selli Event (OAE1a) is marked by a large negative $\delta^{13}C$ excursion while the end of the Selli Event is characterized by a $\delta^{13}C$ positive excursion (Menegatti et al., 1998; Erba et al., 1999). The basal negative $\delta^{13}C$-excursion of the Selli Event is mainly considered to be the result of the volcanic outgassing of CO_2 from the Ontong-Java and Manihiki plateaus (Weissert et al., 1998; Larson & Erba, 1999), whilst Jahren et al. (2005) suggested methane hydrate melting as a possible cause for this negative $\delta^{13}C$ excursion.

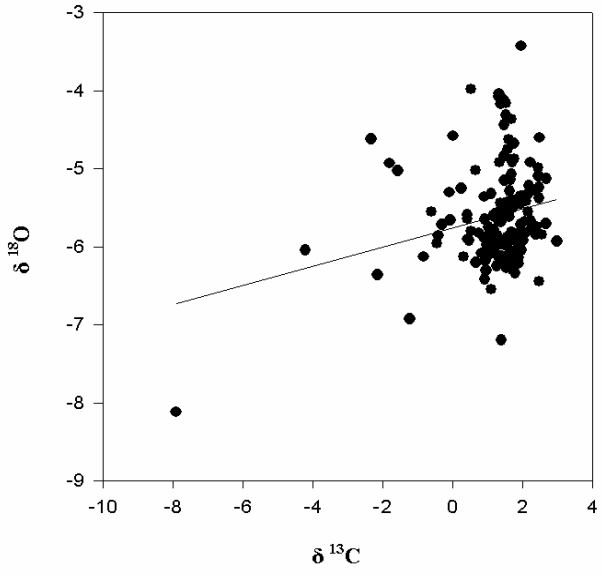

A = Aptian to Maastrichtian, r ^{2}=0.053

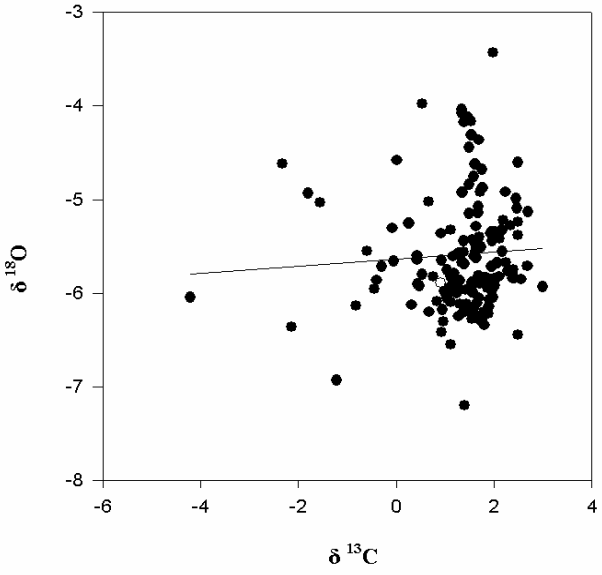

B = Aptian to Maastrichtian, r ^{2}=0.003

Figure 7.9: A = Weak covariant scatter for δ^{13}Cand δ^{18}O, B = insignificant covariant scatter for δ^{13}C carbon and δ^{18}O after removing sample MP-2 with very lighter δ^{18}O-value.

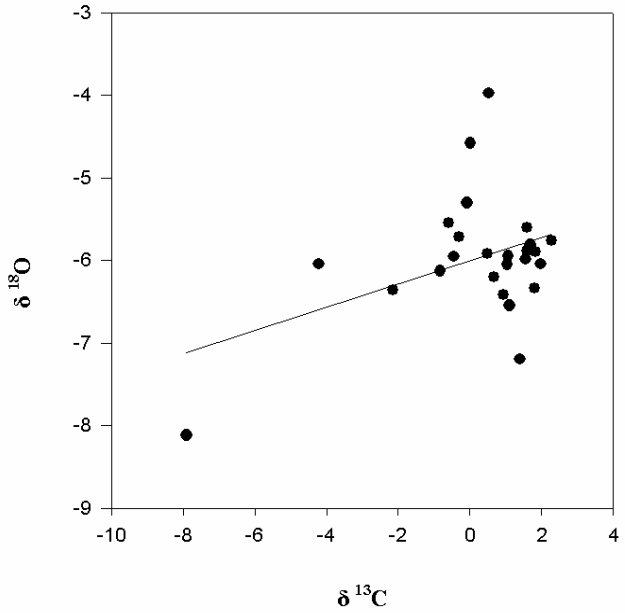

A = Aptian, r ^{2}=0.171

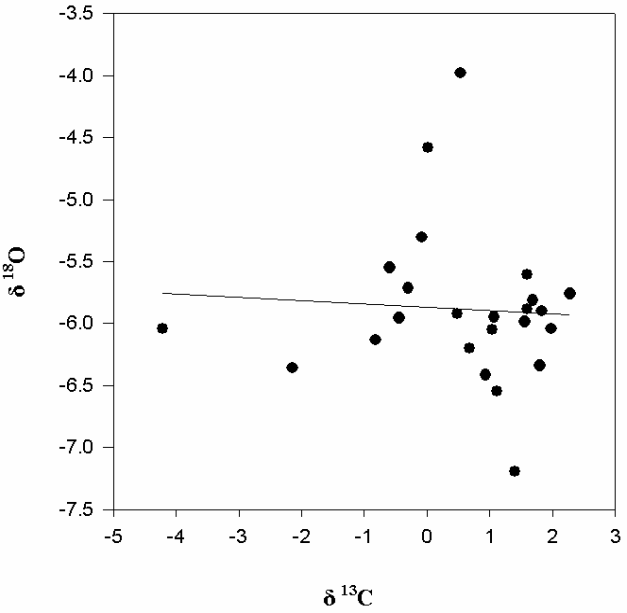

B= Aptian, r ^{2}=0.004

Figure 7.10: A = Aptian moderately covariant scatter for $\delta^{13}C$ and $\delta^{18}O$, B = Aptian insignificant covariant scatter for $\delta^{13}C$ and $\delta^{18}O$ excluding MP-2 with very lighter $\delta^{18}O$-value

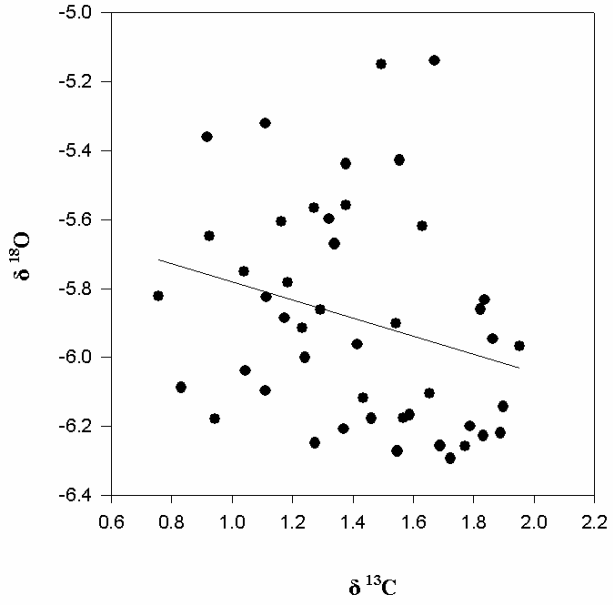

A = Albian, r ^{2}=0.07

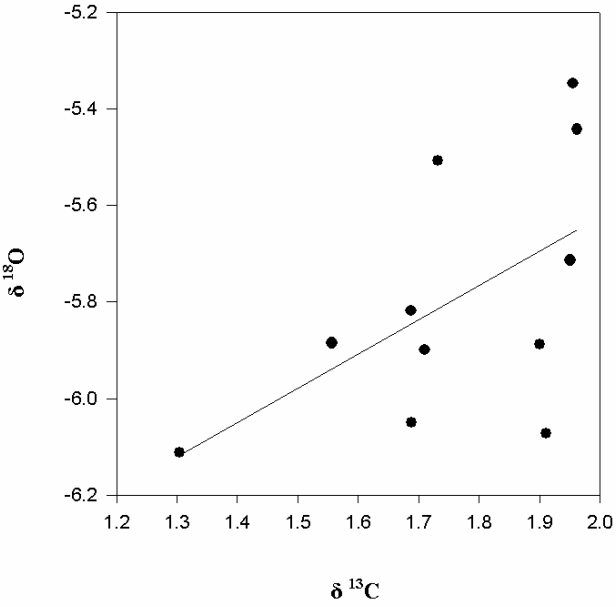

B = Cenomanian, r ^{2}= 0.311

Figure 7.11: A = Albian very weak covariant scatter for δ ^{13}C and δ ^{18}O, B = Cenomanian strong covariant scatter for δ ^{13}C and δ ^{18}O

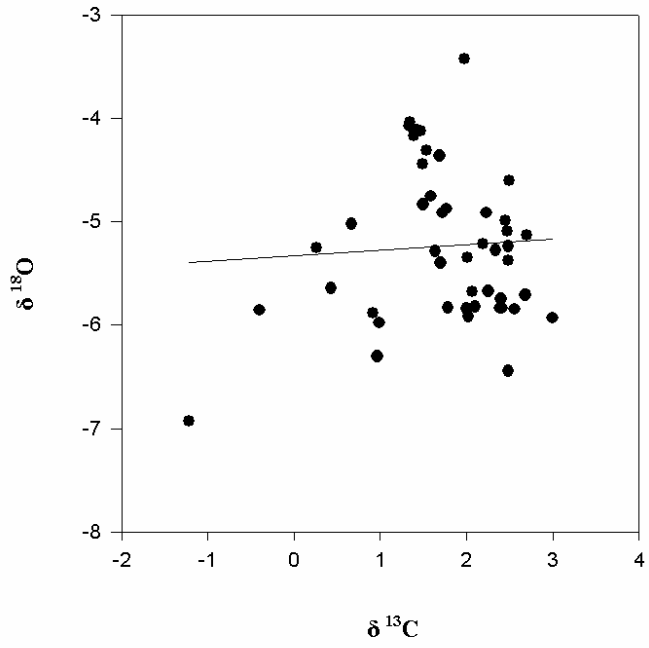

A = Turonian, r ²=003

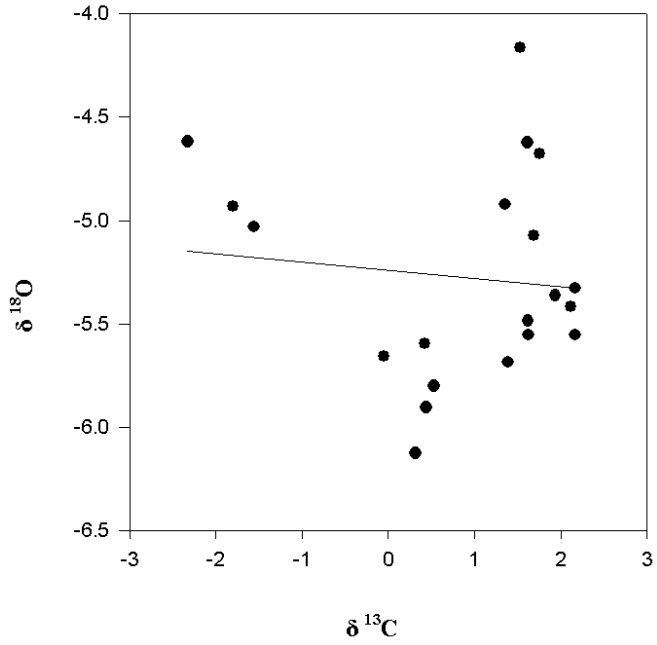

B = Coniacian to Maastrichtian, r ²=0.011

Figure 7.12: A = Turonian insignificant covariant scatter for δ^{13}Ccarb and δ^{18}O, B = Coniacian to Maastrichtian insignificant covariant scatter for δ^{13}C and δ^{18}O

Carbon isotope results:

In the current study the Selli Event (OAE1a) in the Parh Formation is recorded in the *Hedbergella delrioensis* (equivalent to the *Leupoldina cabri* and *Globigerinelloides ferreolensis* biozones of Sliter, 1989, see Chapter 6 for details) Biozone. Here, the Selli Event shows a high amplitude positive $\delta^{13}C$ excursion (C1) of 6.6‰ in the basal part of the Parh Formation (fig. 7.13). The lowermost part of the excursion is not exposed here, because the contact between the Sembar Formation and the Parh Formation is alluvium covered. Hence, it is unclear whether a negative $\delta^{13}C$ excursion precedes the positive $\delta^{13}C$ excursion in the Parh Formation.

After this positive excursion (C1) the $\delta^{13}C$ record displays a short negative $\delta^{13}C$ excursion of 0.6‰ (2.2‰ to 1.6‰). Above this short-lived negative excursion, the $\delta^{13}C$ profile shows a plateau (C2) with average $\delta^{13}C$ values of 1.6‰. This plateau ends with a subsequent 0.2‰ positive excursion (C3), which is stratigraphically coinciding with the end of the organic-rich interval of the OAE1a, in the Parh Formation.

In summary, the $\delta^{13}C$ record from the Parh Formation shows similar $\delta^{13}C$-excursions as in the composite $\delta^{13}C$ curve along the Selli Event (OAE1a) (fig.7.13). The Selli Event has biostratigraphically the same age in the Parh Formation as elsewhere, namely Early Aptian.

7.3.4.2 Fallot Oceanic Anoxic Event

The Fallot black shales occurs in Late Aptian between the *Globigerinelloides ferreolensis* and *Globigerinelloides algerianus* Biozones in the Vocontian Basin, SE France (Friedrich et al. 2003), which is marked by negative $\delta^{13}C$ excursion. Takashima (2006) called this negative excursion, as Fallot Event (Chapter 1, fig. 1.1). An organic rich horizon which is marked by negative $\delta^{13}C$ excursion occurs in the upper part of *Hedbergella delrioensis*, and *Globigerinelloides algerianus* biozones of the Parh Formation; hence it corresponds to the Fallot Event.

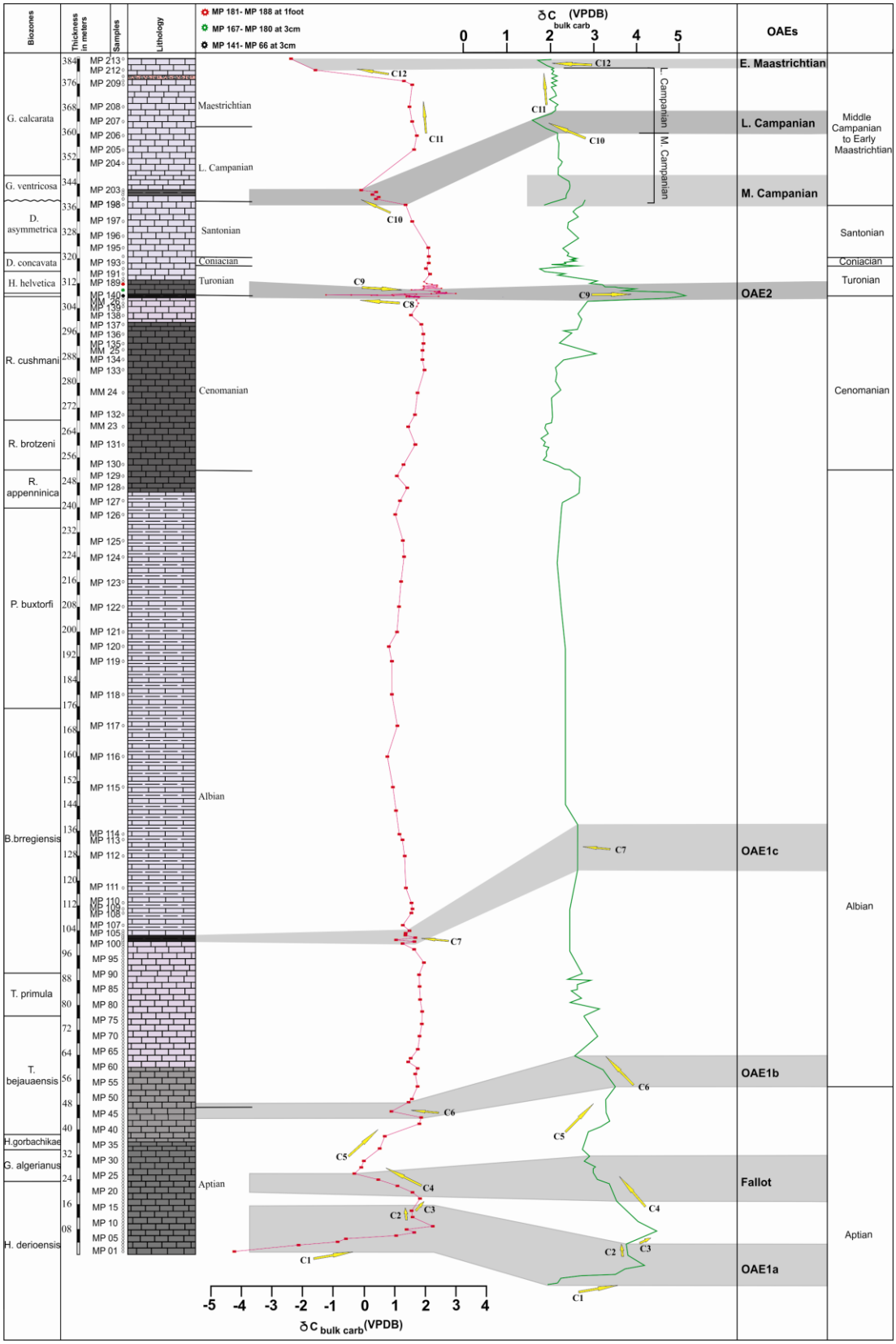

Figure 7.13: The $\delta^{13}C$ isotope curve (red colour on the left side) of the Moghal Kot Section correlated with the global composite curve (green on the right side).

Carbon isotope results:

The $\delta^{13}C$ record in this part of the Parh Formation is marked by a negative 2‰ (1.8 to -0.2‰) $\delta^{13}C$-excursion (C4), which straddles the boundary between the upper *Hedbergella delrioensis* to lower *Globigerinelloides algerianus* Biozones of Late Aptian (fig. 7.13).

In summary, the negative $\delta^{13}C$ excursion (C4) of the Parh Formation correlates with a similar negative excursion in the composite $\delta^{13}C$ curve, suggesting that the organic-rich horizon in the Parh Formation is synchronous with the Fallot Event as defined by Takashima (2006).

7.3.4.3 OAE1b or Paquier Event

The Early Albian anoxic shales found in the Vocontian Trough, SE France, Germany, and Austria represents the so-called Paquier Event (Bréhéret, 1985). This event occurs in the *Ticinella bejaouaensis* to *Hedbergella planispira* Biozones, which ranges in age from Late Aptian to Early Albian (Erbacher et al., 2001; Kuypers et al., 2002). This event has also been documented in various localities in the Tethyan and the Atlantic Oceans (Karakitsios et al. 2004, and references therein). The OAE1b is marked by a small negative $\delta^{13}C$ excursion in various places (fig. 7.14).

Carbon isotope Results:

After the Fallot Event, the $\delta^{13}C$ record recovered from the negative excursion to a new peak value of 1.8‰ (C5, fig. 7.13). The onset of the OAE1b in the Parh Formation is recorded in the *Ticinella bejaouaensis* Biozone based on the integrated stratigraphy (see Chapter 6). This event is marked by a small negative $\delta^{13}C$ excursion of 0.9‰ from 1.8‰ to 0.9‰ in the Parh Formation. This excursion occurs in between the two organic rich horizons i.e. organic rich horizons which correspond to OAE1b (see Chapter 6, fig. 6.1).

In summary**,** a small negative $\delta^{13}C$ excursion (C6) of the Parh Formation correlates with a similar negative excursion in the composite $\delta^{13}C$ curve, and other Atlantic Sections (see fig. 7.14) suggesting that the organic-rich horizon in the Parh Formation is synchronous with the OAE1b Event.

7.3.4.4 OAE1c

The OAE1c is recorded in the *Ticinella praeticinensis* Biozone (which is a subzone of *Biticinella breggiensis*) of the Middle Albian in central Italy. The Amadeus segment in the Umbria-Marche Basin (Coccioni & Galeotti (1993) is considered as the type locality of OAE1c. In the type locality the OAE1c is recorded as rhythmic black shales, calcareous marl, and radiolarian-rich layers (Erbacher et al., 1996; Galeotti et al. 2003).

Carbon Isotope Results:

The $\delta^{13}C$-record corresponding to this event in the Parh Formation shows small cyclic negative and positive excursions (C7) see figures 7.13 & 7.15. These excursions are fluctuating between $\delta^{13}C$ values of 1 to 1.6‰.

In summary, there is no prominent $\delta^{13}C$ excursion associated with the organic-rich horizon in the Parh Formation. The lack of a prominent $\delta^{13}C$ excursion is not surprising because there is none elsewhere either.

7.3.4.5 OAE2 or Bonareli Event

The OAE2 (Bonarelli Event) is marked by enhanced organic carbon burial world wide, causing positive $\delta^{13}C$ excursions in both carbonates and organic matter (Schlanger and Jenkyns 1976; Scholle and Arthur; 1980; Tsikos et al., 2004; Paul et al, 1999). In the Livello Bonarelli Section of the Marche-Umbria Basin, the 1 meter thick organic-rich interval is considered the type locality of the OAE2 (Tsikos et al., 2004).

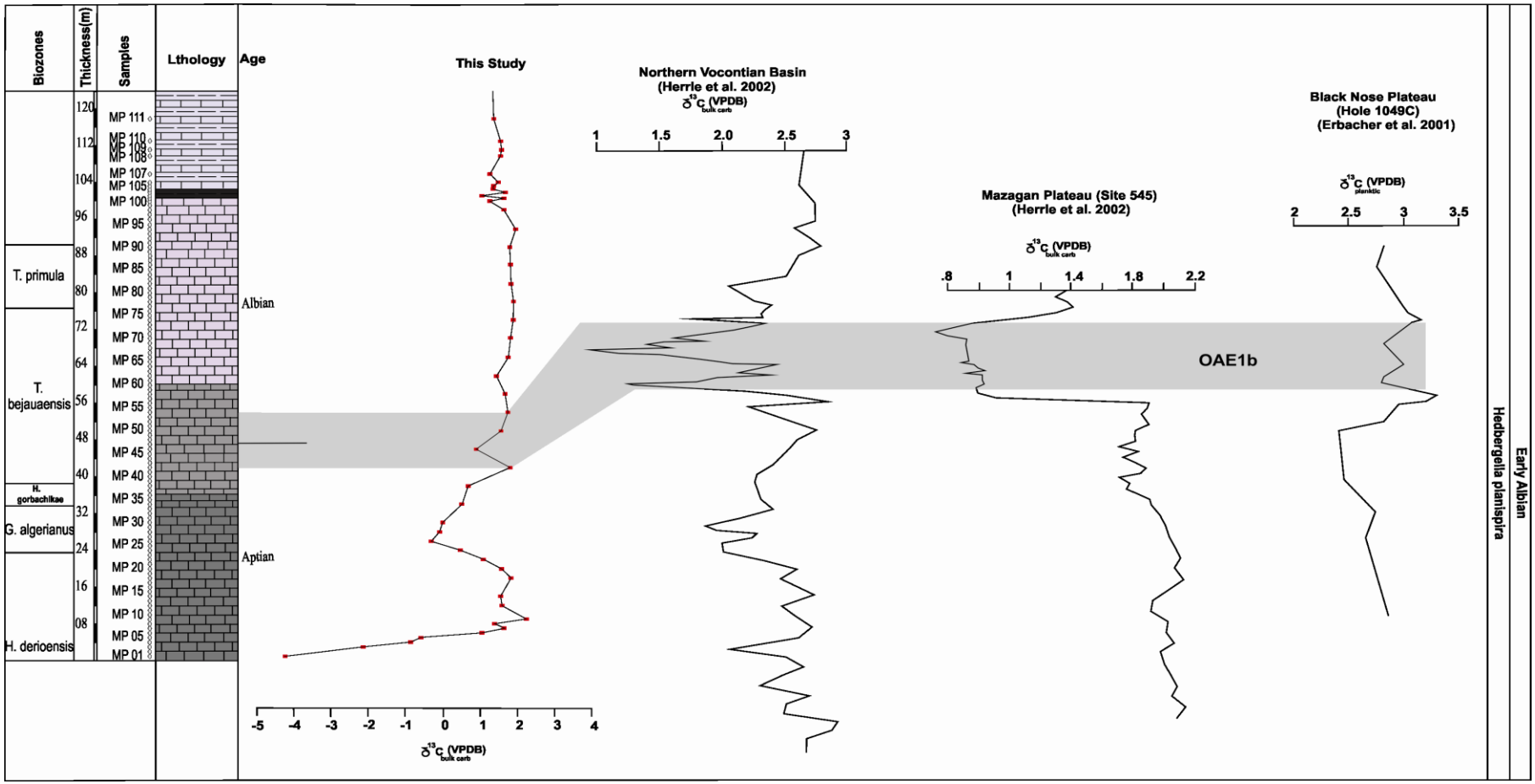

Figure 7.14: Correlation of the OAE1b in Pakistan with Atlantic (Mazagan Plateau, and Blake Nose) and Northern Vocontian Basin. The correlation chart of Atlantic and Northern Vocontian is modified after Friedrich et al. (2005). The three curves (from Atlantic and Vocontian) are plotted according to the age model of Friedrich et al. (2005), while the Moghal Kot Section is plotted according to the age model of current study. Due to difference in biozonation schemes.

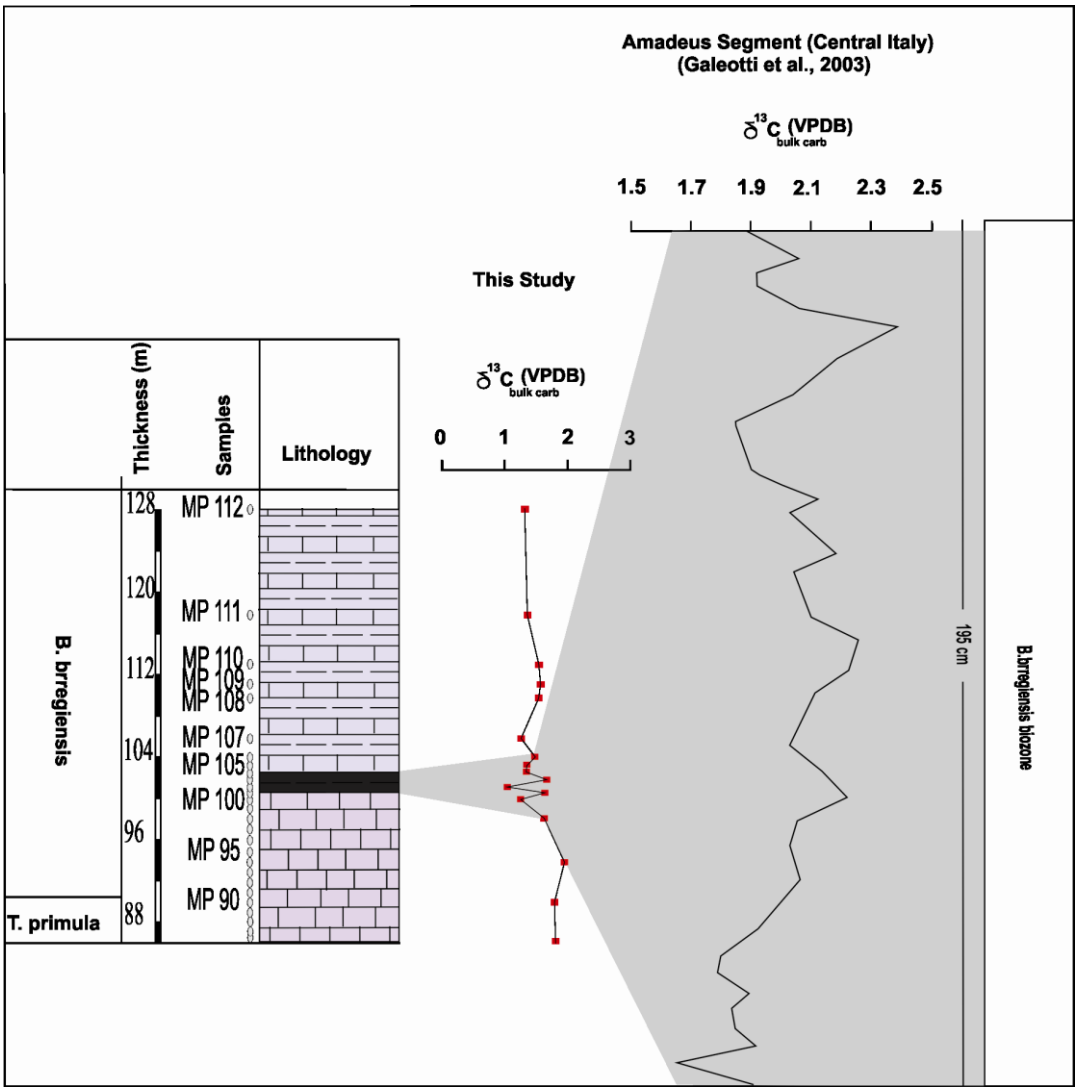

Figure 7.15: Correlation of the OAE1c in Moghal Kot Section with Amadeus Segment (Central Italy (Galeotti et al., 2003). The δ ^{13}C of the Moghal Section and Amadeus Segment are plotted according to the current, and Galeotti et al., (2003) age model. Both fall in the same biozone.

Carbon isotope results:

The $\delta^{13}C$ record of the Parh Formation shows alternating negative (C8) and positive (C9) excursions across the Cenomanian-Turonian boundary, which coincides with the OAE2 (fig. 7.13). In the composite curve, only the positive $\delta^{13}C$ excursion (C9)

is recorded (fig. 7.13), but this positive excursion is not as pronounced as recorded elsewhere (Scholle and Arthur; 1980; Tsikos et al., 2004; Paul et al, 1999). Locally a more complex $\delta^{13}C$ curve occurs, e.g. the Eastbourne section in the United Kingdom. A tentative correlation scheme can be designed between the two sections. In detail, the high resolution $\delta^{13}C$ record in the Parh Formation shows 5 major excursions, which are comparable to events, for instance, as recorded in the Eastbourne section (fig. 7.16). Thus, a simple visual correlation between the two sections appears possible (fig. 7.16), however the characteristic positive $\delta^{13}C$ excursion is missing in the Parh Formation. Also the independent evidence from planktonic foraminiferal biostratigraphy for this correlation is difficult, because the *Whiteinella archaeocretacea* biozone is not defined in this study due to the complete absence of the planktonic foraminifera at the onset of OAE2, elsewhere it is present.

In summary, prominent $\delta^{13}C$ excursions corresponding to the OAE2 (Bonarelli Event) are missing in the Parh Formation. This could be caused by diagenetic overprinting of the isotopic signals or there is a possible hiatus which might have truncated the characteristic positive excursion of OAE2. Both of these possibilities are usually associated with sea level fall. It is interesting to note that a drastic sea level fall is recorded the OAE 2 interval (see figs. 3.32-3.33, Chapter 3). A pronounced negative $\delta^{13}C$ excursion corresponding to OAE2 can also be diagenetic in nature.

7.3.4.6 Campanian and Maastrichtian Events

In the Campanian-Maastrichtian interval, three carbon isotopic events are recorded, i.e. the Middle Campanian, the Late Campanian, and the Early Maastrichtian Events. All of these events are thought to be associated with sea level fluctuations (Jarvis et al., 2002; Thibault et al. 2012). The lack of common planktonic foraminiferal biozonation across the globe in the Campanian makes the $\delta^{13}C$ events very useful for global stratigraphic correlation (Jarvis et al., 2002).

Carbon isotope results:

An organic-rich laminated limestone occurs in the *Globotruncana ventricosa* Zone (Middle to Late Campanian, lower part of the zone has been truncated by a hiatus) of

the Parh Formation**.** Here a negative $\delta^{13}C$ excursion occurs (C10 see fig. 7.13). Upwards, the $\delta^{13}C$-values for the remainder of the Campanian form a broad plateau (C11), followed again by another negative carbon isotope excursion during the Early Maastrichtian (C12). The two negative $\delta^{13}C$ excursions coincide with organic-rich intervals, suggesting the presence of two OAEs.

In the composite curve (fig. 7.13), the Middle Campanian Event shows a 0.5‰ positive $\delta^{13}C$ excursion, while the Late Campanian Event is marked by a 0.5‰ negative excursion. Using simple visual correlation, the negative $\delta^{13}C$ excursion in the Parh Formation would correspond to the negative $\delta^{13}C$ excursion of the Late Campanian Event in the composite curve. Such a pronounced negative $\delta^{13}C$ excursion is also recorded in the *Globotruncana ventricosa* Zone of Tibet (Li et al., 2006). Thus, with regards to timing of this event, based on comparison of the $\delta^{13}C$ records the middle Campanian is missing in the Parh Formation. In the Parh Formation, the $\delta^{13}C$ curve associated with the Early Maastrichtian correlates with the $\delta^{13}C$ excursion in the composite curve.

In summary, the $\delta^{13}C$ negative excursions of the Late Campanian and Early Maastrichtian in the Parh Formation correlate with their equivalent excursions in the composite curve. Therefore, these isotopic events have similar ages, i.e. Late Campanian and Early Maastrichtian, respectively. Although the cause of these isotopic events is assigned to the sea level fluctuations (Jarvis et al., 2002; Thibault et al. 2012), however the organic enrichment along these isotopic events in the Parh Formation suggest strongly that Oceanic Anoxic Conditions prevailed during these events. The widespread record of these carbon isotope events and the higher amplitudes of $\delta^{13}C$ excursions in the Parh Formation (corresponding to these events) suggest global perturbations of the carbon cycle in Late Campanian and Early Maastrichtian.

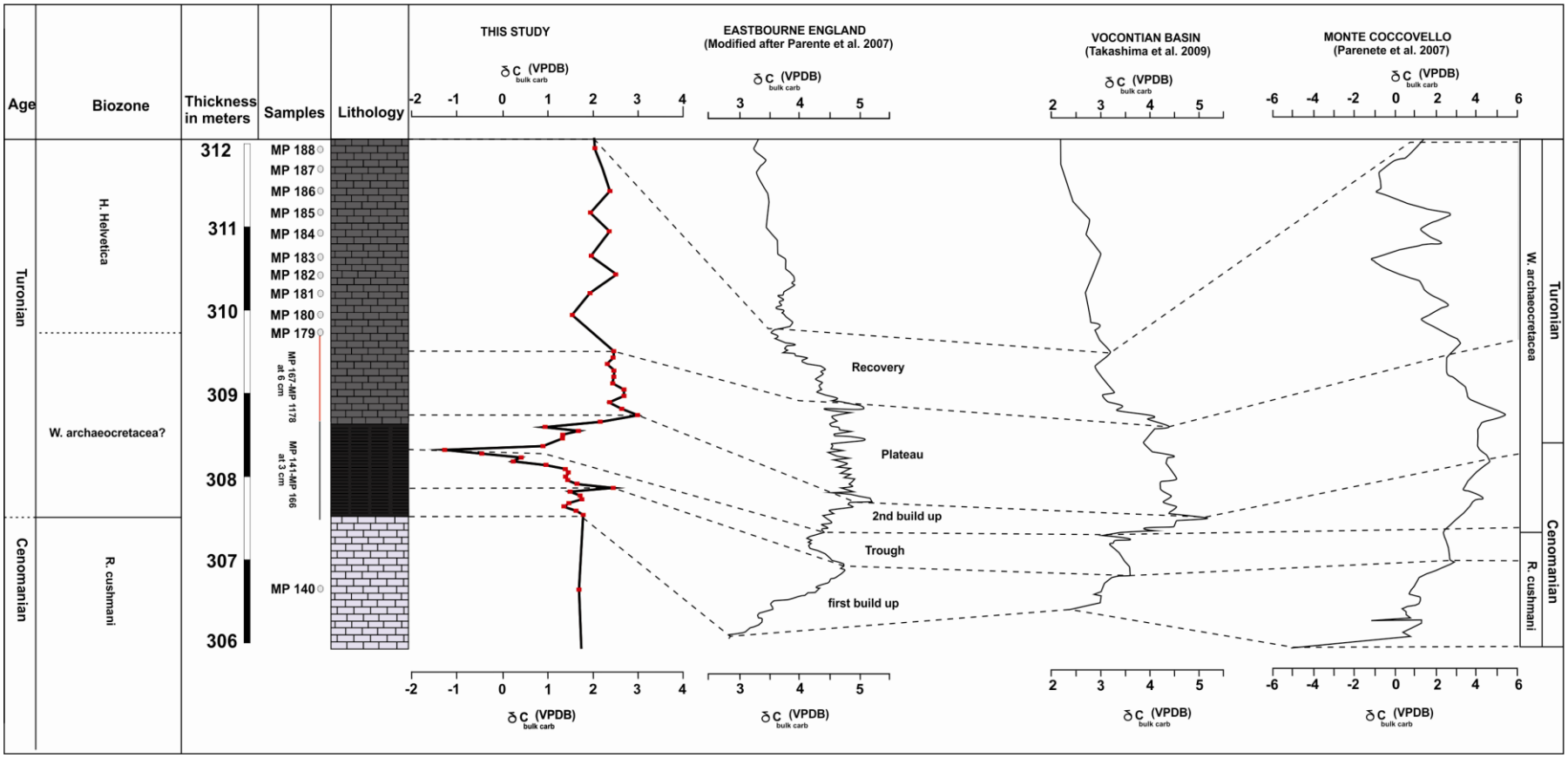

Figure 7.16: Correlation of the OAE2 in Moghal Kot Section with Monte Coccovello, southern Apennines, Italy (Parente et al., 2007), Eastbourne Chalk (modified, after Parente et al., 2007), and Vocontian Basin (Takashima et al, 2009).

7.4 Conclusions

- SST reconstruction results based on recently developed TEX_{86} paleo-SST proxy show that the surface ocean was consistently much warmer (10-12 ^{o}C) than today at the paleolatitude of ~-35^{o}. Similar SSTs were documented by Littler et al. (2011), using the same proxy for low to high latitudes. Therefore, our new data set confirms that higher SSTs prevailed at low to middle paleolatitude than today during the Early Cretaceous.

- The cooler $\delta^{18}O$ paleotemperatures based on carbonate from the belemnite rostrum for the same time period, can be explained by the uncertainty related to the life habitat, species specific vital affect, and digenetic alteration of belemnites. Such cooling can also can be further explained in terms of the regional difference in climate sensitivity, especially at high latitudes as discussed by Littler et al. (2011).

- The distinction between the Selli Event (OAE1a) and Fallot Event is clear based on the $\delta^{13}C$ record.

- A pronounced negative $\delta^{13}C$ of 3.6‰ corresponding to the OAE2 is recorded in the section However, a positive $\delta^{13}C$ excursion is often associated with OAE2 elsewhere, which is absent in the Parh Formation. The absence of such positive $\delta^{13}C$ and the presence of pronounced negative $\delta^{13}C$ excursion can be explained by the diagenetic overprinting. On the other hand, the absence of a positive $\delta^{13}C$ can also be explained by a possible hiatus within the OAE2 interval. Both the diagenetic overprinting and/or a hiatus may have been caused by the sea level fall during OAE2.

- Based on the $\delta^{13}C$ record, a Late Campanian age is assigned to the OAE in this interval, and this implies that the *Globotruncana ventricosa* Zone of the Parh Formation has been truncated at its lower boundary.

- Almost all OAEs present in the Parh Formation correlate with OAEs as observed elsewhere. The new record of the OAEs in the Parh Formation confirms the widespread occurrence of these events, possibly all global in nature.

CHAPTER 8

6. A quantitative review of the Planktonic Foraminiferal Evolution

8.1 Introduction

The planktonic foraminiferal evolution in the Cretaceous is marked by alternating periods of diversification and stasis, interrupted by extinctions and turnovers (Leckie, 1989, Leckie et al., 2002; Premoli-Silva & Sliter, 1999; Premoli-Silva et al., 1999). This planktonic foraminiferal evolution may have been controlled by periods of significant paleoceanographic changes, specifically those which occurred during the Oceanic Anoxic Events (e.g. Premoli-Silva & Sliter, 1999; Leckie, et al., 2002). Here in this chapter, the link between planktonic foraminiferal evolution and OAEs is explored further in the Parh Formation using a quantitative approach.

The biostratigraphy using the planktonic foraminifera (see Chapter 5) shows that the pelagic sedimentary sequence of the Parh Formation comprises almost the entire Cretaceous succession. The microfacies (see Chapter 3) and the stable carbon isotope stratigraphies (see Chapter 6) revealed the presence of the OAEs in the same sequence. Therefore, all these observations collectively allow the link between planktonic foraminiferal evolution and changing conditions during OAEs to be explored.

8.2 Methodology

The range charts of planktonic foraminiferal species are used to calculate the specific evolutionary parameters as defined below. The age model of Sliter (1989) is used for assigning absolute ages to the planktonic foraminiferal biozone boundaries (figs. 8.1 & 8.2). In order to arrive at a continuous age model, age estimates are based on linear interpolation between age control points.

The evolutionary parameters of the planktonic foraminifera include species richness, rate of speciation, rate of extinction, rate of diversity, and rate of turnover. These are calculated according to the equations used by Leckie et al. (2002) as follows:

Rate of speciation (rs): rs=((1/S) FO),

Rate of extinction (re): re=((1/(S) LO),

Rate of diversification (rd): rd=rs–re,

Rate of turnover (rt): rt=rs+re.

In these equations S is species richness (number of species), FO is number of First Occurrence Events, and LO is number of Last Occurrence Events.

These quantitative parameters of evolution are assessed in between successive samples, and results are presented in tables 8.1-8.4, and are plotted in figures, 8.3 and 8.4. In order to improve the robustness of the results a time-controlled moving average 200ka filter was applied. The filter acts by moving a specific time window across the sample set (FO/LO), each time assigning the mean value of all data points within the time window to the sample (FO/LO) currently being processed. The advantage of this method is that the peaks and troughs of the rates of extinction, speciation, turnover and diversification are well pronounced.

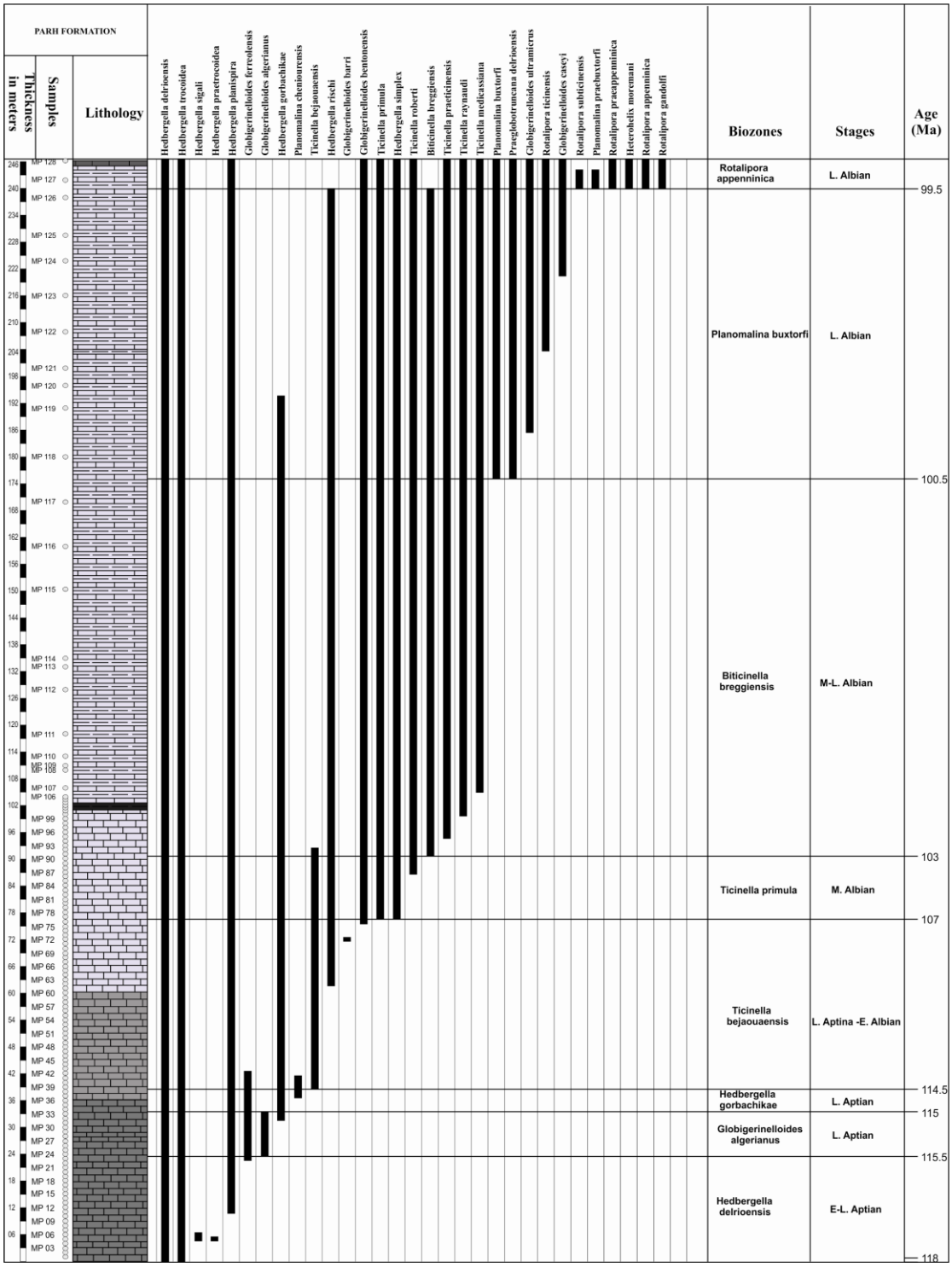

Figure 8.1: Showing stratigraphic range/biozonation chart of the Parh Formation, Moghal Kot Section. Ages are assigned to the biozonal boundaries according to Sliter (1989).

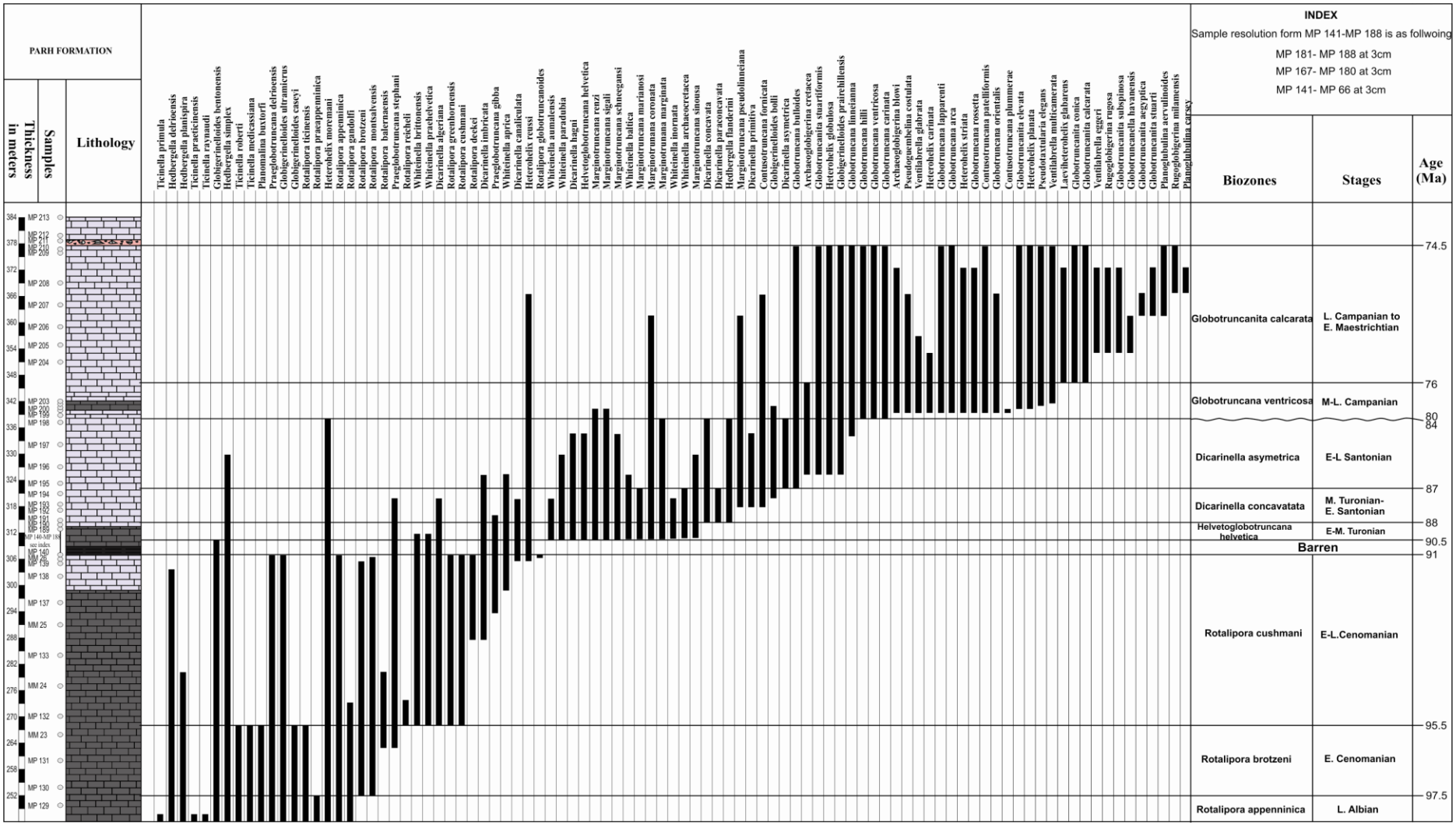

Figure 8.2: Showing stratigraphic range/biozonation chart of the Parh Formation, Moghal Kot Section. Ages are assigned to the biozonal boundaries according to Sliter (1989).

Age(Ma)	Height (m)	S	FADs	LADs	rs	re	rd	rt
74.30	379.5	8	0	0	0.00	0.00	0.00	0.00
74.50	376.5	19	0	0	0.00	0.00	0.00	0.00
74.70	372.5	27	0	8	0.00	0.30	-0.30	0.30
75.00	366.5	32	2	5	0.06	0.16	-0.09	0.22
75.23	362	33	3	3	0.09	0.09	0.00	0.18
75.48	357	32	0	2	0.00	0.06	-0.06	0.06
75.68	353	33	4	1	0.12	0.03	0.09	0.15
76.00	346.5	30	3	1	0.10	0.03	0.07	0.13
78.35	341.5	27	1	0	0.04	0.00	0.04	0.04
78.59	341	27	1	1	0.04	0.04	0.00	0.07
78.82	340.5	29	2	3	0.07	0.10	-0.03	0.17
80.00	338	27	11	0	0.41	0.00	0.41	0.41
84.00	337.5	21	3	5	0.14	0.24	-0.10	0.38
84.40	335.5	22	1	4	0.05	0.18	-0.14	0.23
85.50	330	24	0	3	0.00	0.13	-0.13	0.13
86.40	325.5	27	4	3	0.15	0.11	0.04	0.26
87.00	322.5	26	2	3	0.08	0.12	-0.04	0.19
87.31	320	29	1	5	0.03	0.17	-0.14	0.21
87.58	317.9	28	3	0	0.11	0.00	0.11	0.11
87.81	316	26	0	1	0.00	0.04	-0.04	0.04
88.00	314.5	26	3	0	0.12	0.00	0.12	0.12
88.66	313.5	23	0	0	0.00	0.00	0.00	0.00
89.78	311.8	25	0	2	0.00	0.08	-0.08	0.08
90.37	310.9	25	3	0	0.12	0.00	0.12	0.12
90.50	310.7	22	4	0	0.18	0.00	0.18	0.18
90.56	310.5	19	7	1	0.37	0.05	0.32	0.42
91.03	309	12	0	0	0.00	0.00	0.00	0.00
91.50	307.5	19	0	7	0.00	0.37	-0.37	0.37
91.60	306.5	20	1	1	0.05	0.05	0.00	0.10
91.70	305.5	20	2	1	0.10	0.05	0.05	0.15
91.85	304	19	0	1	0.00	0.05	-0.05	0.05
92.36	299	19	1	0	0.05	0.00	0.05	0.05
92.87	294	18	1	0	0.06	0.00	0.06	0.06
93.49	287.8	17	2	0	0.12	0.00	0.12	0.12
94.23	280.5	17	0	2	0.00	0.12	-0.12	0.12
94.89	274	19	0	2	0.00	0.11	-0.11	0.11
95.50	268	24	6	5	0.25	0.21	0.04	0.46
96.13	263	18	2	0	0.11	0.00	0.11	0.11
96.88	257	16	0	0	0.00	0.00	0.00	0.00
97.50	252	17	2	1	0.12	0.06	0.06	0.18
98.33	247	18	0	3	0.00	0.17	-0.17	0.17
98.83	244	21	0	2	0.00	0.10	-0.10	0.10
99.50	240	23	6	2	0.26	0.09	0.17	0.35
99.59	234	17	0	0	0.00	0.00	0.00	0.00
99.70	227	17	0	0	0.00	0.00	0.00	0.00

Table 8.1: Showing the ages of the FADs/LADs in million years, while stratigraphic heights are meters. Species richness (S), rates of speciation (rs), extinction (re), diversification (rd), and turn over (rt) are also shown.

Age(Ma)	Height (m)	S	FADs	LADs	rs	re	rd	rt
99.79	221	17	1	0	0.06	0.00	0.06	0.06
99.93	212	16	0	0	0.00	0.00	0.00	0.00
100.05	204	16	1	0	0.06	0.00	0.06	0.06
100.15	198	15	0	0	0.00	0.00	0.00	0.00
100.22	193.5	16	0	1	0.00	0.06	-0.06	0.06
100.33	186	16	1	0	0.06	0.00	0.06	0.06
100.50	175	15	2	0	0.13	0.00	0.13	0.13
100.80	165	13	0	0	0.00	0.00	0.00	0.00
101.08	155.5	13	0	0	0.00	0.00	0.00	0.00
101.48	142	13	0	0	0.00	0.00	0.00	0.00
101.70	134.5	13	0	0	0.00	0.00	0.00	0.00
101.80	131	13	0	0	0.00	0.00	0.00	0.00
102.04	123	13	0	0	0.00	0.00	0.00	0.00
102.26	115.5	13	0	0	0.00	0.00	0.00	0.00
102.36	112	13	0	0	0.00	0.00	0.00	0.00
102.41	110.5	13	0	0	0.00	0.00	0.00	0.00
102.48	108	13	0	0	0.00	0.00	0.00	0.00
102.57	105	13	1	0	0.08	0.00	0.08	0.08
102.63	103	12	0	0	0.00	0.00	0.00	0.00
102.66	102	12	0	0	0.00	0.00	0.00	0.00
102.67	101.5	12	0	0	0.00	0.00	0.00	0.00
102.69	101	12	0	0	0.00	0.00	0.00	0.00
102.70	100.5	12	0	0	0.00	0.00	0.00	0.00
102.72	100	12	0	0	0.00	0.00	0.00	0.00
102.73	99.5	12	1	0	0.08	0.00	0.08	0.08
102.76	98.5	11	0	0	0.00	0.00	0.00	0.00
102.79	97.5	11	0	0	0.00	0.00	0.00	0.00
102.82	96.5	11	0	0	0.00	0.00	0.00	0.00
102.85	95.5	11	0	0	0.00	0.00	0.00	0.00
102.88	94.5	11	1	0	0.09	0.00	0.09	0.09
102.91	93.5	10	0	0	0.00	0.00	0.00	0.00
102.94	92.5	11	0	1	0.00	0.09	-0.09	0.09
102.97	91.5	11	0	0	0.00	0.00	0.00	0.00
103.00	90.5	11	1	0	0.09	0.00	0.09	0.09
103.29	89.5	10	0	0	0.00	0.00	0.00	0.00
103.57	88.5	10	0	0	0.00	0.00	0.00	0.00
103.86	87.5	10	0	0	0.00	0.00	0.00	0.00
104.14	86.5	10	1	0	0.10	0.00	0.10	0.10
104.43	85.5	9	0	0	0.00	0.00	0.00	0.00
104.71	84.5	9	0	0	0.00	0.00	0.00	0.00
105.00	83.5	9	0	0	0.00	0.00	0.00	0.00
105.29	82.5	9	0	0	0.00	0.00	0.00	0.00
105.57	81.5	9	0	0	0.00	0.00	0.00	0.00

Table 8.2: Showing the ages of the FADs/LADs in million years, while stratigraphic heights are meters. Species richness (S), rates of speciation (rs), extinction (re), diversification (rd), and turn over (rt) are also shown.

Age(Ma)	Height (m)	S	FADs	LADs	rs	re	rd	rt
105.86	80.5	9	0	0	0.00	0.00	0.00	0.00
106.14	79.5	9	0	0	0.00	0.00	0.00	0.00
106.43	78.5	9	0	0	0.00	0.00	0.00	0.00
106.71	77.5	9	0	0	0.00	0.00	0.00	0.00
107.00	76.5	9	2	0	0.22	0.00	0.22	0.22
107.20	75.5	7	1	0	0.14	0.00	0.14	0.14
107.39	74.5	6	0	0	0.00	0.00	0.00	0.00
107.59	73.5	6	0	0	0.00	0.00	0.00	0.00
107.79	72.5	7	0	1	0.00	0.14	-0.14	0.14
107.99	71.5	7	1	0	0.14	0.00	0.14	0.14
108.18	70.5	6	0	0	0.00	0.00	0.00	0.00
108.38	69.5	6	0	0	0.00	0.00	0.00	0.00
108.58	68.5	6	0	0	0.00	0.00	0.00	0.00
108.78	67.5	6	0	0	0.00	0.00	0.00	0.00
108.97	66.5	6	0	0	0.00	0.00	0.00	0.00
109.17	65.5	6	0	0	0.00	0.00	0.00	0.00
109.37	64.5	6	0	0	0.00	0.00	0.00	0.00
109.57	63.5	6	0	0	0.00	0.00	0.00	0.00
109.76	62.5	6	0	0	0.00	0.00	0.00	0.00
109.96	61.5	6	1	0	0.17	0.00	0.17	0.17
110.16	60.5	5	0	0	0.00	0.00	0.00	0.00
110.36	59.5	5	0	0	0.00	0.00	0.00	0.00
110.55	58.5	5	0	0	0.00	0.00	0.00	0.00
110.75	57.5	5	0	0	0.00	0.00	0.00	0.00
110.95	56.5	5	0	0	0.00	0.00	0.00	0.00
111.14	55.5	5	0	0	0.00	0.00	0.00	0.00
111.34	54.5	5	0	0	0.00	0.00	0.00	0.00
111.54	53.5	5	0	0	0.00	0.00	0.00	0.00
111.74	52.5	5	0	0	0.00	0.00	0.00	0.00
111.93	51.5	5	0	0	0.00	0.00	0.00	0.00
112.13	50.5	5	0	0	0.00	0.00	0.00	0.00
112.33	49.5	5	0	0	0.00	0.00	0.00	0.00
112.53	48.5	5	0	0	0.00	0.00	0.00	0.00
112.72	47.5	5	0	0	0.00	0.00	0.00	0.00
112.92	46.5	5	0	0	0.00	0.00	0.00	0.00
113.12	45.5	5	0	0	0.00	0.00	0.00	0.00
113.32	44.5	5	0	0	0.00	0.00	0.00	0.00
113.51	43.5	5	0	0	0.00	0.00	0.00	0.00
113.71	42.5	6	0	1	0.00	0.17	-0.17	0.17
113.91	41.5	7	0	1	0.00	0.14	-0.14	0.14
114.11	40.5	7	0	0	0.00	0.00	0.00	0.00
114.30	39.5	7	0	0	0.00	0.00	0.00	0.00

Table 8.3: Showing the ages of the FADs/LADs in million years, while stratigraphic heights are meters. Species richness (S), rates of speciation (rs), extinction (re), diversification (rd), and turn over (rt) are also shown.

Age(Ma)	Height (m)	S	FADs	LADs	rs	re	rd	
114.50	38.5	7	1	0	0.14	0.00	0.14	0.14
114.60	37.5	6	0	0	0.00	0.00	0.00	0.00
114.70	36.5	6	1	0	0.17	0.00	0.17	0.17
114.80	35.5	5	0	0	0.00	0.00	0.00	0.00
114.90	34.5	5	0	0	0.00	0.00	0.00	0.00
115.00	33.5	6	0	1	0.00	0.17	-0.17	0.17
115.05	32.5	6	0	0	0.00	0.00	0.00	0.00
115.10	31.5	6	1	0	0.17	0.00	0.17	0.17
115.15	30.5	5	0	0	0.00	0.00	0.00	0.00
115.20	29.5	5	0	0	0.00	0.00	0.00	0.00
115.25	28.5	5	0	0	0.00	0.00	0.00	0.00
115.30	27.5	5	0	0	0.00	0.00	0.00	0.00
115.35	26.5	5	0	0	0.00	0.00	0.00	0.00
115.40	25.5	5	0	0	0.00	0.00	0.00	0.00
115.45	24.5	5	0	0	0.00	0.00	0.00	0.00
115.50	23.5	5	1	0	0.20	0.00	0.20	0.20
115.61	22.5	4	1	0	0.25	0.00	0.25	0.25
115.73	21.5	3	0	0	0.00	0.00	0.00	0.00
115.84	20.5	3	0	0	0.00	0.00	0.00	0.00
115.95	19.5	3	0	0	0.00	0.00	0.00	0.00
116.07	18.5	3	0	0	0.00	0.00	0.00	0.00
116.18	17.5	3	0	0	0.00	0.00	0.00	0.00
116.30	16.5	3	0	0	0.00	0.00	0.00	0.00
116.41	15.5	3	0	0	0.00	0.00	0.00	0.00
116.52	14.5	3	0	0	0.00	0.00	0.00	0.00
116.64	13.5	3	0	0	0.00	0.00	0.00	0.00
116.75	12.5	3	0	0	0.00	0.00	0.00	0.00
116.86	11.5	3	0	0	0.00	0.00	0.00	0.00
116.98	10.5	3	1	0	0.33	0.00	0.33	0.33
117.09	9.5	2	0	0	0.00	0.00	0.00	0.00
117.20	8.5	2	0	0	0.00	0.00	0.00	0.00
117.32	7.5	2	0	0	0.00	0.00	0.00	0.00
117.43	6.5	3	0	1	0.00	0.33	-0.33	0.33
117.55	5.5	4	0	1	0.00	0.25	-0.25	0.25
117.66	4.5	4	2	0	0.50	0.00	0.50	0.50
117.77	3.5	2	0	0	0.00	0.00	0.00	0.00
117.89	2.5	2	0	0	0.00	0.00	0.00	0.00
118.00	1.5	2	0	0	0.00	0.00	0.00	0.00

Table 8.4: Showing the ages of the FADs/LADs in million years, while stratigraphic heights are meters. Species richness (S), rates of speciation (rs), extinction (re), diversification (rd), and turn over (rt) are also shown.

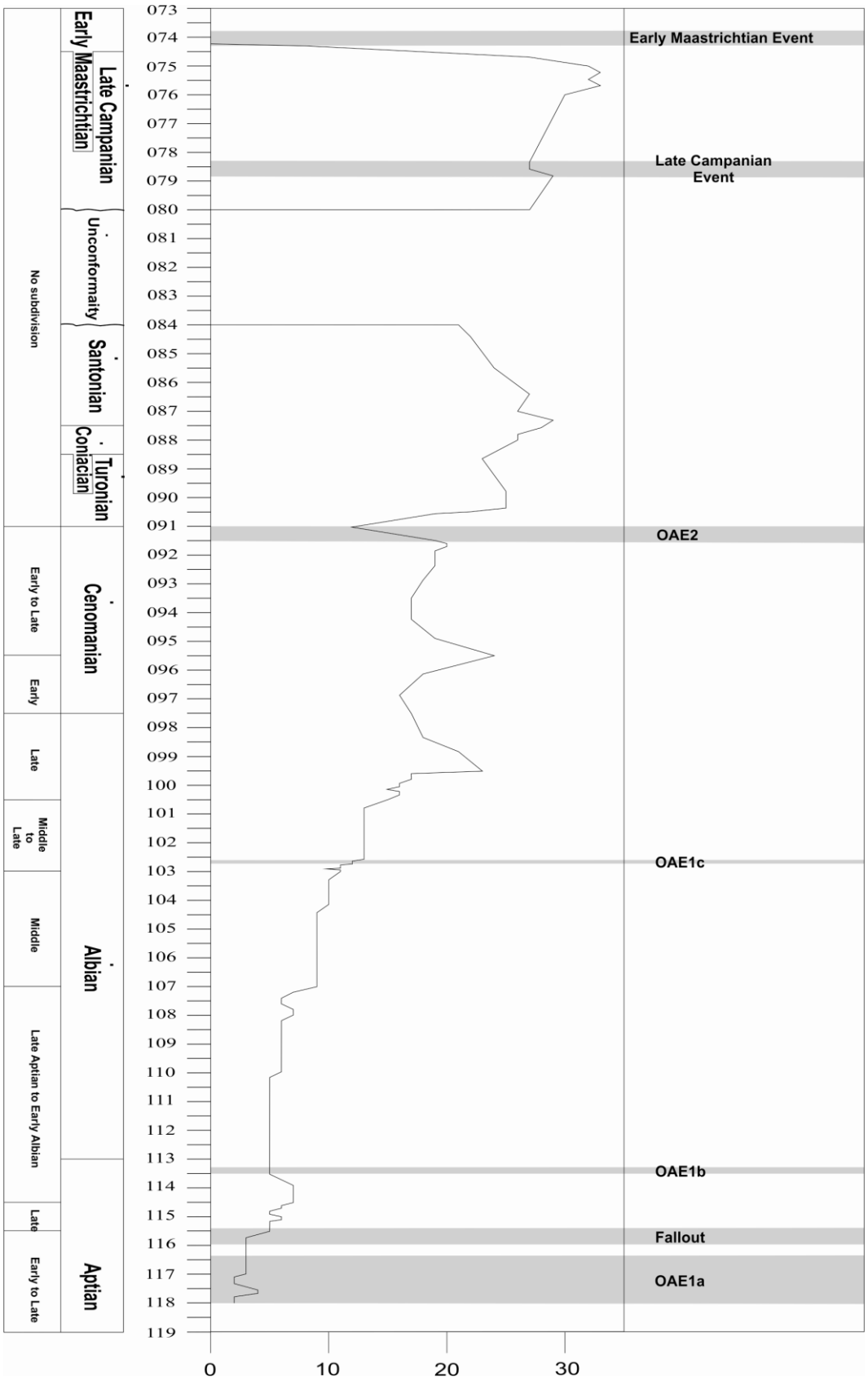

Figure 8.3: Cretaceous planktonic foraminiferal species richness record of the Parh Formation, Moghal Kot Section.

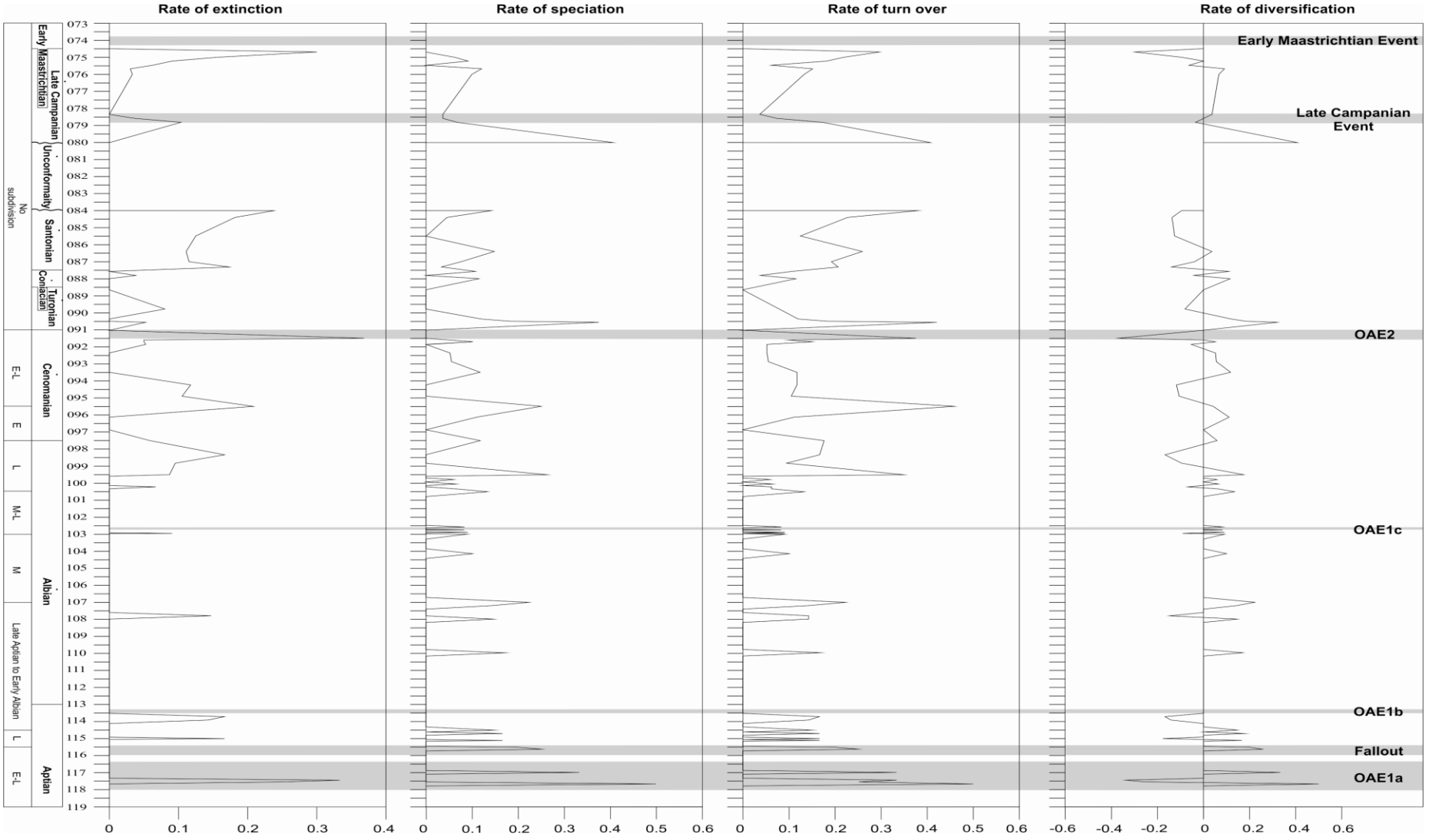

Figure 8.4: Showing the rates of speciation, extinction, diversity, and turn over of the Cretaceous planktonic foraminifera in Parh Formation, Moghal Kot Section.

8.3 Results

8.3.1 Species Richness (fig. 8.3)

The species richness (number of species) increased throughout the Cretaceous. In more detail, the species richness was lowest in the Early to Late Aptian (fig. 8.3). The species richness rose in the Late Aptian, specifically during the Fallot Event, and rose further until it dropped before the OAE1b. It remained unchanged in the Early Albian, but it rose again in the Middle Albian, and then reached its peak in the Late Albian at about 99.5 Ma. This is followed by a major fall in species richness in the Early Cenomanian, but reached another peak within the Early Cenomanian at about 95.5 Ma. The most conspicuous reduction in Species richness occurred at the base of the Bonarelli Event (OAE2). This drop was followed by a rise within the Turonian, culminating in another peak in the Santonian at about 87.5 Ma. There is a hiatus of ~4 million years between the Santonian and Late Campanian, and thus species richness is not recorded for this interval. The species richness kept rising in the Campanian until it reached its maximum peak in the Late Campanian at about 75.5 Ma. The overlain sandstone/conglomerate deposition caused an artificial drop in species richness in the Early Maastrichtian. The maximum peaks in species richness are obviously driven by a high rate of speciation and reduced rate of background extinction. The contribution from distinct planktonic foraminiferal genera to these peaks, either speciation or extinction, is mentioned in Rates of Speciation, Extinction, Turnover and Diversity see below.

8.3.2 Rates of Speciation, Extinction, Turnover and Diversification (fig. 8. 4)

In the Aptian, a double peak in speciation rates occurs at about 117.6 Ma and 117 Ma) with in between a high rate of extinction (~117.5 Ma). These high rates of speciation and extinction are an artefact of the fact that the first occurrences of the planktonic foraminifera in the lowermost part of the studied section are not their true FADs. Another reason for these high rates of speciation is the low number of species at this time, which exaggerates the relative importance of the FADs and LADs in the equations of the parameters. Notably, this part of the section in the Early Aptian is the time when OAE1a occurred. The rates of evolution in all parameters seem fast, but as mentioned above, these are artificial, and basically very modest rates of extinction and speciation occurred. Thus, the environmental conditions of OAE1a

did not adversely affect planktonic foraminiferal evolution. The robust *Globigerinelloides ferreolensis*, *Globigerinelloides algerianus*, and *Hedbergella gorbachikae* have their FADs but rapidly disappeared later in the Aptian. The FADs of these species are linked with the Fallot Event. There is a rate of extinction peak prior to the OAE1b Event. It is not clear whether this peak event is really prior to the OAE1b, because the sampling resolution is low in this part of the section. As mentioned above the number of species is low in the Aptian part of the section, which results in exaggerated rates of extinction and speciation. Nevertheless, this pattern of speciation and extinction is also recorded elsewhere (Premoli-Silva & Sliter, 1999; Leckie et al., 2002), and thus the Aptian evolutionary rates of change in the planktonic foraminifera occurred globally.

In the Late Aptian to Early Albian (113.5-108 Ma), the hedbergellids dominated the planktonic foraminiferal fauna, but evolutionary rates remained subdued. This long period of stasis was followed by high rates of speciation and turnover, leading to increased diversity in the Early to Late Albian (108-103 Ma). In this period, new morphotypes appeared, i.e. *Ticinella*, and new *Globigerinelloides* sp., in a stepwise pattern (see figs. 8.1).

In the Late Albian to Late Cenomanian (100.5-91 Ma), high rates of extinction and speciation occurred. The *Ticinella* spp. have their last appearances in this period, resulting in two extinction peaks (see figs. 8.1 & 8.2). The *Rotalipora* spp. developed in the same period, resulting in a series of peaks in rates of speciation. The *Rotalipora* became the most dominant taxa in the Cenomanian. The parallel development of extinction and speciation of taxa led to two distinct peaks of species richness in the Late Albian to Late Cenomanian as mentioned above (fig. 8.3). *Ticinella* developed predominantly in the lower Albian peak, whilst *Rotalipora* was important in the higher Cenomanian peak (figs. 8.1 & 8.2).

At the base of OAE2 the highest rate of extinction occurred, resulting in a mass extinction of foraminiferal species, mainly species of the *Rotalipora*. Notably, this extinction is exactly synchronous with the onset of OAE2 conditions.

In the Turonian, after the presence of the OAE2, the fastest rate in speciation took place, characterized by simultaneous appearance of the whiteinellids,

marginotruncanids, and dicarinellids along with the *Helvetoglobotruncana* sp. (see fig. 8.2) Thus, a high rate of extinction at the onset of OAE2 was followed by a high rate of speciation after the OAE2 in the Turonian.

The Campanian Eastern Tethys Ocean is dominated by the *Globotruncana* and *Heterohelix* as recorded in the Parh Formation (see fig. 8.2). The high rates of speciation and extinction in the Santonian and Late Campanian, just below and above the hiatus, are not real because they are an artefact of the hiatus.

8.4 Discussion

The objective of this chapter is to identify relationships between planktonic foraminiferal evolution and the OAEs. I aim to answer the question whether maximum or minimum rates of change in the planktonic foraminiferal evolutionary parameters, i.e. extinction and speciation, and in turn turnover and diversification are synchronous with OAEs. This question is important, because such synchroneity would verify the link between evolution of planktonic foraminifera and changing ocean conditions at the onset and/or during the OAE development irrespective of the cause of the OAE. Leckie et al. (2002) made earlier such an attempt of linking planktonic foraminiferal evolution with OAE history in the Middle Cretaceous by using planktonic foraminiferal data from various sections around the world. They subdivided the planktonic foraminiferal range charts in 1-million years increments to obtain the rates of evolutionary parameters. However, such a large time window isn't appropriate for establishing the link between planktonic foraminiferal evolution and the occurrences of OAEs. The time used in calculations of above parameters in this study, is the exact age of each FADs and LADs, which make it more appropriate for such exercise. Also, the planktonic foraminiferal record of the Parh Formation gives unique information from the Eastern Tethys Ocean.

8.4.1 Aptian and Albian OAEs

To discuss a potential link between planktonic foraminiferal evolution and OAEs in the Aptian and Albian is very difficult, because the low number of species exaggerates the rates of extinction and speciation. However, the very low species richness in the entire Aptian and Lower Albian record may be enhanced by the small size of the tests which makes recognition in thin sections exceedingly difficult. Moreover, poor preservation may be another reason for not detecting all species. It is

important to note that species richness was increasing throughout this interval, but even more so in the Late Albian when the *Ticinella* thrived, culminating in the distinct species richness peak at 99.5 Ma. This was followed later by another species richness peak in the Cenomanian when the *Rotalipora* became dominant in the planktonic foraminiferal record (figs. 8.2 & 8.3). Perhaps the evolution from hedbergellids to ticinellids and rotaliporids has been driven by long term changes in nutrient content of the ocean waters (e.g. Premoli-Silva & Sliter, 1999).

8.4.2 OAE2

The highest rate of extinction, resulting in the lowest rate of diversification, occurred exactly at the onset of the OAE2 (91 Ma). All the rotaliporids became extinct along this event. This extinction of the rotaliporids has been observed elsewhere (Premoli-Silva & Sliter, 1999; Leckie, et al., 2002). Remarkably, all other planktonic foraminiferal species disappear at the base of OAE2 and remained absent during the OAE2 in the Parh Formation. After the OAE2, they appeared again. This is different from observations in other sections around the world where some species continued during the adverse conditions of OAE2. At this stage, I can only speculate on the cause of the disappearance of all planktonic foraminiferal species, but perhaps a sea level fall played a role here, and the ocean became too shallow at this site for the planktonic foraminifera (see paleoenvironments of Microfacies MP17-20, Chapter 4), but such a sea level fall may have been accompanied by other environmental changes as described in the literature. For instance, the cause of extinction of the rotaliporids is generally attributed to the eutrophication of the ocean (Premoli-Silva & Sliter, 1999; Leckie, et al., 2002), and thus eutrophication may have played a role in the Eastern Tethys as well in addition to the sea level fall. The suggestion of eutrophication of the oceans stems from the idea that the OAE at the Cenomanian/Turonian boundary (91 Ma) was related to submarine volcanism, including the formation of the Caribbean Plateau [Leckie, et al., 2002 and references therein). The release of greenhouse gases would have enhanced the hydrological cycle with increased nutrient run-off. Such surface water eutrophication can also be caused by enhanced upwelling, associated with the loss of density structure of oceans, hence pumping up of the nutrient to the surface water from the deeper eutrophic parts of the ocean (e. Premoli-Silva & Sliter, 199). Others mention the possibility that acidification of the ocean as a result of the enhance concentrations of

green house gases may have also influenced the extinction of the rotaliporids. However, there is no evidence for this as yet.

8.5 Conclusion

In summary, the synchroneity of the extinction of the planktonic foraminifera with the adverse conditions of the OAE2 is clearly recorded in the Parh Formation. This is the only evolutionary event of the planktonic foraminifera that is strongly related to climate change. This event is clearly global in nature which suggests that environmental changes along the OAE2 have strongly forced the evolution of the planktonic foraminifera across the world, although it is not clear as yet what the exact nature is of those environmental changes.

References

Ahamd et al. 1999: Structural geometry of the Himalayan Frontal Thrust Zone: Surghar Range, Pakistan.

Alley, N.F., Frakes, L.A., 2003: First known Cretaceous glaciation. Livingston Tillite Member of the Cadne-owie Formation, South Australia. *Australian Journal of Earth Sciences,* v. 50, pp.139-144.

Amorosi, A., 1995: Glauony and sequence stratigraphy. Conceptual framework of distribution in siliciclastic sequences. *Journal of Sedimentary Research*, v. 65, pp. 419-425.

Anderson, T.F., Arthur, M.A., 1983. Stable isotopes of oxygen and carbon and their application to sedimentological and environmental problems. In: Arthur, M.A., Anderson, T.F., Kaplan, I.R., Veizer, J., Land, L.S., (Eds.), *Stable Isotopes in Sedimentary Geology, Society of Economic Paleontologists and Short Course*, v. 10, pp. 1-151.

Baccelle, L., Bosellini. A., 1965: Diagrammi per la stima visiva della composizione percentuale nelle rocce sedimentarie. *Annali della Università di Ferrara, Sezione IX, Science Geologiche e Paleontologiche*, v. 1, pp. 59-62.

Badshah, M.S., Gnos, E., Jan, M.Q., Afridi, M.I. 2000: Stratigraphic and tectonic evolution of the northwestern Indian plate and Kabul Block. In: Khan, M.A., Treloar, P.J., Searle, M.P., Jan, M.Q. (Eds.), Tectonics of the Nanga Parbat Syntaxis and the Western Himalaya. *Geological Society London, Special Publication,* v. 170, pp. 467-475.

Banks, C.J., Warburton. J., 1986: Passive roof duplex geometry in the frontal structures of the Kirthar and Sulaiman Mountain belts: Pakistan. *Journal of Structural Geology*, v. 8, pp. 229-237.

Bannert, D., Raza, H.A., 1992: The segmentation of the Indo-Pakistan Plate. *Pakistan Journal of Hydrocarbon Research*, v. 4, no.2, pp. 5-18.

Barr, F.T., 1972: Cretaceous biostratigraphy and planktonic foraminifera of Libya. *Micropaleontology,* v. 18, no.1, pp. 1-46.

Barrón, E., Gómez, J.J., Goy, A., Pieren, A.P., 2006: The Triassic-Jurassic boundary in Asturias (northern Spain): palynological characterisation and facies. *Review of Palaeobotany and Palynology*, v.138, pp. 187-208.

Berggren, W.A., 1 962: Some planktonic foraminifera from the Maestrichtian and type Danian Stages of southern Scandinavia. *Acta University Stockholm, Stockholm Contributions in Geology*, v. 9, no. 1, pp. 1-106.

Bermudez, P.J., 1952: Estudio sistematico de los foraminiferos rotaliformes. *Boletin de Geologia, Venezuela* v. no. 4, pp.1-230.

Besse, J., Courtillot V., 1988: Paleogeographic maps of the Indian Ocean bordering continents since the Upper Jurassic. *Jornal of Geophysical Research,* v. 93, pp. 11791- 11808.

Blanford, W.T., 1876: On the Geology of Sindh. *India Geological Survey, Records*, v. 9, pp. 8-22.

Bodin S., Godet A., Follmi K.B., Vermeulen J., Arnaud H., Strasser A., 2006: The late Hauterivian Faraoni oceanic event in the western Tethys: evidence from phosphorus burial rates. *Palaeogeography Palaeoclimatology Palaeoecology*, v. 235, pp. 238-257.

Bolli, H. M., 1945: Zur Stratigraphie der Oberen Kreide in den höheren helvetischen Decken. *Ecoglae geologicae Helvetiae,* v. 37, pp. 217-328.

Bolli, H.M., 1957: The genera *Praeglobotruncana*, *Rotalipora*, *Globotruncana*, and *Abathomphalus* in the Upper Cretaceous of Trinidad. *U.S. National Museum Bulletin*, v. 215, pp. 51-60.

Bolli, H.M., Loeblich, A.R., Tappan, H., 1957: Planktonic foraminiferal families Hantkeninidae, Orbulinidae, Globorotaliidae and Globotruncanidae. *U.S. National Museum Bulletin*, v. 215, pp. 3-50.

Borsetti, A.M., 1962: Foraminiferi planctonici di una serie cretacea dei Dintorni di Piobbico (Prov. di Pesaro). *Giornale di Geology Series 2*, v. 29, pp. 19-75.

Bouilhol, P., Jagoutz, O., M. Hanchar, M. J., Dudas, O. F., 2013: A refined scenario of the India-Eurasia collision derived from the magmatic evolution of NW Himalaya. *Geophysical Research Abstracts,* v. 15.

Bralower, T.J., Thierstein, H.R., 1984: Low productivity and slow deep-water circulation in mid-Cretaceous oceans. *Geology*, v. 12, pp. 614-618.

Bréhéret, J.G., 1985: Indices d'un evenement anoxique etendu a la Tethys alpine, a l' Albien inferieur (evement Paquier). *Comptes Rendus De L Academie Des Sciences Paris Serie II*, v. 300, pp. 355-358.

Brönnimann, P., 1952: Globigerinidae from the Upper Cretaceous (Cenomanian-Maestrichtian) of Trinidad. B.W.I. *Bulletins of American Palaeontology*, v. 34, no. 140, pp. 1-70.

Brönnimann, P., Brown, N.K., 1956: Taxonomy of the Globotruncanidae. *Ecoglae geologicae Helvetiae*, v. 48, pp. 503-561.

Brönnimann, P., Brown, N.K., 1958: *Hedbergella*, a new name for a Cretaceous planktonic foraminiferal genus. *Journal of the Washington Academy of Sciences*, v. 48, pp.15-17.

Brotzen, F., 1934: Foraminiferen aus dem Senon Palastinas. *Zeitschrift des Deutschen Palastina-Vereins*, v. 57, pp. 28-72.

Brotzen, F., 1936: Foraminiferen aus dem schwedischen untersten Senon von Eriksdal in Schonen. *Sveriges geologiska undersökning*, v.30, pp. 1-206.

Butler, R.W.H., Coward, M.P., Harwoodm, G.M., Knipe, R.J., 1987: Salt control on the thrust geometry, structural style and gravitational collapse along the Himalayan mountain front in the salt range of northern Pakistan. In: Lerche, I., O'Brien, J.J. (Eds.), Dynamical Geology of Salt and Related Structures. *Academic Press*, Inc, pp. 339-418

Caron, M., 1966: Globotruncanidae du Crétacé supérieur du synclinal de la Gruyère (Préalpes Médianes, Suisse). *Revue de Micropaléontologie*, v. 9, pp. 68-93.

Caron, M., 1985: Cretaceous planktic foraminifera. In: Bolli, H.M., Saunders, J.B., Perch-Nielsen, K. (Eds.). *Plankton Stratigraphy: Cambridge University Press, Cambridge*, pp. 17-86.

Caron, M., Luterbacher, H., 1969: On some type specimens of Cretaceous planktonic foraminifera Cretaceous planktonic foraminifera, *Cushman Foundation for Foraminiferal Research*, v. 20, pp. 23-29.

Caron, M., 1976: Révision des types de Foraminiféres planctoniques décrits dans la région du Montsalvens (Préalpes fribourgeoises): *Eclogae Geologicae Helvetiae*, v. 69, no. 2, p. 327-333.

Carsey, D. O., 1926: Foraminifera of the Cretaceous of Central Texas. *University of Texas Bulletin*, v. 2612, pp. 1-56.

Cassaigneau, C., 1979: Contribution a l'Etude des Suture Inde-Eurasie: La Zone de Suture de Khost dans le Sud-Est de l'Afghanistan, l'Obduction Paleocene et la Tectonique Teriare. *Ph.D. dissertation, University of Sciences and Techniques of Languedoc*, pp. 1-145.

Coccioni, R., Nesci, O., Tramontana, C.F., Wezel, C.F., Moretti, E., 1987: Descrizione di un Livello guida 'Radiolaritico-Bituminoso-Ittiolitico' alla base delle Marne a Fucoidi nell'Appennino Umbro-Marchigiano. *Bollettino Societa Geologica Italiana*, v. 106, pp. 183-192.

Coccioni, R., Galeotti, S., 1993: Orbitally induced cycles in benthonic foraminiferal morphogroups and trophic structures distribution patterns from the Late Albian 'Amadeus Segment' (Central Italy). *Journal of Micropaleontology*, v. 12, pp. 227-239.

Costa, L.I., Davey, R.J., 1992: Dinoflagellate cysts of the Cretaceous System. In: Powell, A.J. (ed.): A stratigraphic index of dinoflagellate cysts. *British Micropalaeontological Society London*. pp. 99-131.

Coward, M.P., Windley, B.F., Broughton, R.D., Luff, I. W., Petterson, M.G., Pudsey, C.J., Rex, D.C., Asif Khan, M., 1986: Collision tectonics in the NW Himalayas. In: Collision Tectonics (M.P. Coward and A.C. Ries, eds). *Geological Society London, Special Publication*, v. 19, pp. 203-219.

Craig, H., 1965: Measurement of oxygen isotope paleotemperatures. In: Stable Isotopes in Oceanographic Studies and Paleotemperatures. *Consiglio Nazionale delle Ricerche,* pp. 161-182.

Cushman, J.A., 1926: Some Foraminifera from the Mendez Shale of eastern Mexico. *Cushman Foundation for Foraminiferal Research,* v. 2, no. 1, pp. 16-26.

Cushman, J.A.**,** 1927: New and interesting foraminifera from Mexico and Texas**.** *Cushman Foundation for Foraminiferal Research***,** v. 3, no. 2, pp. 111-119.

Cushman, J.A., 1928: Additional genera of the Foraminifera. *Contributions from the Cushman Laboratory for Foraminiferal Research,* v. 4, no. 1, pp. 1-8.

Cushman, J.A., 1938: Cretaceous species of *Guembelina* and related genera. *Cushman Laboratory for Foraminiferal Research,* v. 14, pp. 2-27.

Cushman, J.A., 1946: Upper Cretaceous foraminifera of the Gulf Coastal region of the United States and adjacent Areas. *U.S. Geological Survey Professional Paper,* v. 206, pp. 1-241.

Cushman, J.A., Ten, Dam, A., 1948: Globigerinelloides, a new genus of the Globigerinidae. *Cushman Foundation for Foraminiferal Research***,** v. 24, pp. 42-44.

Dalbiez, F., 1955: The genus *Globotruncana* in Tunisia. *Micropaleontology,* v. 1, pp. 161-171.

Danilchik, W., 1961: The Iron formation of the Surghar and western Slat Range, Mianwali District, West Pakistan. *U.S. Geological Survey, Professional. Paper,* v. 424-D, pp. 228-231.

de Klasz, I., 1953: Einige neue oder wenig bekannte Foraminiferen aus der helvetischen Oberkreide der bayerischen Alpen südlich Traunstein (Oberbayern). *Geologica Bavarica,* v. 17, pp. 233-244.

De Lapparent, J., 1918: Étude lithologique des terrains crétacés de la région d'Hendaye. *Mémoires pour servir à l'explication de la carte géologique détaillée de la France*. pp. 1-155.

Dickens, G.R., O'Neil, J.R., Rea, D.K., Owen, R.M., 1995: Dissociation of oceanic methane hydrate as a cause of the carbon isotope excursion at the end of the Palaeocene. *Paleoceanography,* v. 10, pp. 965-971.

Ditchfield, P.W., 1997: High northern paleolatitude Jurassic-Cretaceous paleotemperature variation, new data from Kong Karls Land, Svalbard. *Palaeogeography, Palaeoclimatology, Paleoecology,* v. 130, pp. 163-175.

d'Orbigny, A., 1839: Foraminifères. In: Histoire Physique, Politique et Naturelle de l'ile de Cuba. *Atlas, de la Sagra,* v. pp. 1-224.

d'Orbigny, A., 1840: Mémoires sur les foraminifères de la craie blanche du bassin de Paris. *Mémoires de la Société Géologique de France*, v. pp. 1-51.

Douglas, R.G., 1969: Upper Cretaceous planktonic foraminifera in northern California. Part 1-Systematic. *Micropaleontology*, v. 15, pp. 151-209.

Douglas, R.G., Rankin, C., 1969: Cretaceous planktonic foraminifera from Bornholm and their zoogeographic significance. *Lethaia*, v. 2, pp. 185-217.

Egger, J.G., 1899: Foraminiferen und Ostracoden aus den Kreidemergeln der oberbayerischen Alpen. *Abhandlungen der Bayerische Akademie der Wissenschaften, Mathematisch-naturwissenschaftliche Klasse*, v. 21, pp. 1-230.

Ehrenberg, G.C., 1840: Über die Bildung der Kreidefelsen und des Kreidemergels durch unsichtbare Organismen. *Abhandlungen der Königliche Akademie der Wissenschaften zu Berlin*, v. 1838, pp. 59-147.

Eicher, D.L., Worstell. P., 1970: Cenomanian & Turonian, foraminifera from the Great Plains, United States. *Micropaleontology*, v. 16, pp. 296-324.

El Naggar, Z. R.M., 1966: Stratigraphy and planktonic foraminifera in the Upper Cretaceous-Lower Tertiary succession in the Esna-Idfu region, Nile Valley, Egypt. *Bulletin of the British Museum (Natural History), Geology Supplement*, v. 2, pp. 1-279.

Epstein, S., Buchsbaum, R., Lowenstam, H.A., Urey, H.C., 1953: Revised carbonate-water isotopic temperature scale. *Geological Society of America Bulletin*, v. 64, pp. 1315-1325.

Erba, E., 1994: Nannofossils and superplumes: the early Aptian ‘‘nannoconid’’ crisis. *Paleoceanography*, v. 9, pp. 483-501.

Erba, E., 2004: Calcareous nannofossils and Mesozoic oceanic anoxic events. *Marine Micropaleontology*, v. 52, p. 85-106.

Erba, E., Bartolini, A., Larson Roger, L., 2004: Valanginian Weissert oceanic anoxic event. *Geological Society of America*, v. 32, no. 2, pp. 149-152.

Erba, E., Channell, J. E. T., Claps, M., Jones, C., Larson, R., Opdyke, B., Premoli-Silva, I., Riva, A., Salvini, G., Torricelli, S., 1999: Integrated stratigraphy of the Cismon Apticore (southern Alps, Italy): a “reference section” for the Barremian-Aptian interval at low latitudes, *Journal of Foraminiferal Research*, v. 29, pp. 371-391.

Erbacher, J., Huber, B.T., Norris, R.D., Markey, M., 2001: Increased thermohaline stratification as a possible cause for an ocean anoxic event in the Cretaceous period. *Nature*, v. 409, pp. 325-327.

Erbacher, J., Thurow, J., 1997: Influence of oceanic anoxic events on the evolution of mid-Cretaceous radiolaria in the North Atlantic and western Tethys. *Marine Micropaleontology*, v. 30, pp. 139-158.

Erbacher, J., Thurow, J., Littke, R., 1996: Evolution patterns of radiolaria and organic matter variations: a new approach to identify sea level changes in mid-Cretaceous pelagic environments. *Geology*, v. 24, pp. 499-502.

Fatmi, A.N., 1972: Stratigraphy of the Jurassic and Lower Cretaceous rocks and Jurassic ammonites from northern areas of West Pakistan. *Bulletin of the British Museum (Natural History) Geology*, v. 20, no. 7, pp. 297-380.

Fatmi, A.N., 1977: Mesozoic. In: Shah, S.M.I., (Ed.), Stratigraphy of Pakistan. *Geological Survey, Pakistan, Memoirs*, v. 12, pp. 1-138.

Fensome, R.A., Gocht, H., Stover, L.E., Williams, G.L., 1991: The Eisenack Catalog of Fossil Dinoflagellates. New Series. *Schweizerbart'sche Verlagsbuchhandlung, Stuttgart, Germany*. v. 1. pp. 1-829.

Fensome, R.A., Gocht, H., Stover, L.E. Williams, G.L., 1993: The Eisenack Catalog of Fossil Dinoflagellates. New Series. *Schweizerbart'sche Verlagsbuchhandlung, Stuttgart, Germany*. v. 2. pp. 829-1461.

Flügel, E., 2004: Microfacies of Carbonate Rocks-Analysis, interpretation and application. *Springer-Verlag Berlin Heidelberg*, pp. 1-976.

Föllmi, K.B., 2012: Early Cretaceous life, climate and anoxia. *Cretaceous Research*, v. 35, pp. 230-257.

Föllmi, K.B., Weissert, H., Bisping, M., Funk, H., 1994: Phosphogenesis, carbon-isotope stratigraphy, and carbonate-platform evolution along the Lower Cretaceous northern Tethyan margin. *Geological Society of America, Bulletin*, v. 106, pp. 729-746.

Forster, A., Schouten, S., Baas, M., Sinninghe Damsté, J.S., 2007: Mid-Cretaceous (Albian-Santonian) sea surface temperature record of the tropical Atlantic Ocean. *Geology*, v. 35, pp. 919-922.

Franke, A., 1925: Die Foraminiferen der pommerschen Kreide. *Abhandlungen aus dem Geologisch-Palaeontologischen Institut der Universitat Greifswald*, v. 6, pp. 1-96.

Friedrich, O., Reichelt, K., Herrle, J.O., Lehmann, J., Pross, J., Hemleben, C., 2003: Formation of the Late Aptian Niveau Fallot black shales in the Vocontian Basin (SE France): Evidence from planktic and benthic foraminifera and stable isotopes. *Marine Micropaleontology*, v. 49, pp. 65-85.

Friedrich, O., Nishi, H., Pross, J.O., Schmiedl, G., Hemleben, C., 2005: Centennial-scale interruptions of the Oceanic Anoxic Event lb (Early Albian, mid-Cretaceous) inferred from benthic foraminiferal repopulation events. *Palaios*, v. 20, pp. 64-77.

Fürsich, F. T., Pandey, D. K., 2003: Sequence stratigraphic significance of sedimentary cycles and shell concentrations in the Upper Jurassic-Lower Cretaceous of Kachchh, western India. *Palaeogeography, Palaeoclimatology, Palaeoecology*, v. 193, pp. 285-309.

Galeotti, S., Sprovieri, M., Coccioni, R., Bellanca, A., Neri, R., 2003: Orbitally modulated black shale deposition in the upper Albian Amadeus Segment (central Italy): a multi-proxy reconstruction. *Palaeogeography, Palaeoclimatology, Palaeoecology*, v. 190, pp. 441-458.

Gallitelli, E.M., 1957: A revision of the Family Heterohelicidae. *Bulletin-United States National Museum*, v. 215, pp. 133-154.

Gandolfi, R., 1942: Ricerche micropaleontologiche e stratigrafiche sulla scaglia e sul flysch Cretacici dei Dintorni di Balerna (Canton Ticino). *Rivista Italiana di Paleontologia Memoria,* v. 4, pp. 1-160.

Gandolfi, R., 1955: The genus *Globotruncana* in Northeastern Colombia. *Bulletins of American Paleontology,* v. 36, pp. 7-118.

Gandolfi, R., 1957: Notes on some species of Globotruncana. *Contributions from the Cushman Foundation for Foraminiferal Research*, v. 8, no. 2, pp. 59-65.

Gansser, A., 1981: The geodynamic history of the Himalaya. In: Gupta, H.K., Delany, F.M., (Eds.), Zagros, Hindu Kush, Himalaya, Geodynamic Evolution. *American Geophysical Union Geodynamic Series,* v. 3, pp. 111-121.

Gansser, O., 1970: Zur Geologie von Südost–Afghanistan; 1. Geologie des Gebietes von Ghazni-Gardez-Urgun; 2. Geologie des Gebietes um Mukur und Ob-i-Istada Bh. Translated Title: Geology of southeastern Afghanistan; 1, Geology of the Ghazni-Gardez-Urgun area; 2, Geology of the Mukur and Ob-i-Istada area. *Geologisches Jahrbuch, Beihefte*, v. 84, pp. 1-203.

Gröcke, D.R., Price, G.D., Robinson, S.A., Baraboshkin, E.Y., Mutterlose, J., Ruffel, A.H., 2005: The Upper Valanginian (Early Cretaceous) positive carbon-isotope event recorded in terrestrial plants. *Earth and Planetary Science Letters*, v. 240, pp. 495-509.

Haq, S.S.B., Davis, D.M., 1997: Oblique convergence and the lobate mountain belts of western Pakistan. *Geology*, v. 25, pp. 23-26.

Harding, I.C., Smith G.A., Riding J.B., Wimbledon W.A.P., 2011: Inter-regional correlation of Jurassic/Cretaceous boundary strata based on the Tithonian-Valanginian dinoflagellate cyst biostratigraphy of the Volga Basin, western Russia. *Review of Palaeobotany and Palynology*, v. 167, pp. 82-116.

Heilmann-Clausen, C., 1987: Lower Cretaceous dinoflagellate biostratigraphy in the Danish Central Trough. *Danmarks Geologiske Undersøgelse Serie*, v. 17, pp. 1-89.

Helby, R., McMinn, A., 1992: A preliminary report of Early Cretaceous dinocyst floras from Site 765, Argo Abyssal Plain, Northwest Australia. In Gradstein, F.M., Ludden, J.N., et al. (Eds.), *Proceedings of the ODP Scientific Results*, v. 123, pp. 407-420.

Helby, R., Morgan, R., Partridge, A.D., 1987: A palynological zonation of the Australian Mesozoic. *Memoir of the Association of Australasian Paleontologists*, v. 4, pp. 1-94.

Heldt, M., Bachmann, M., Lehmann, J., 2008: Microfacies, biostratigraphy, and geochemistry of the hemipelagic Barremian–Aptian: influence of the OAE 1a on the southern Tethys margin. *Palaeogeography, Palaeoclimatology, Paleoecology*, v. 261, pp. 246-260.

Herm, D., 1962: Stratigraphische und miktopala¨ontologische Untersuchungen der Oberkreide im Lattengebirge und im Nierental. *Abhandlungen der Bayerischen Akademie der Wissenschaften zu München New Series*, v. 104, pp. 1-119.

Hesselbo, S.P., Gröcke, D.R., Jenkyns, H.C., Bjerrum, C.J., Farriomond, P., Morgans Bell, H.S., Green, O. R., 2000: Massive dissociation of gas hydrate during a Jurassic oceanic anoxic event. *Nature*, v. 406, pp. 392-395.

Heydari, E., Wade, W.J., Hassanzadeh, J., 2001: Diagenetic origin of carbon and oxygen isotope compositions of Permian-Triassic boundary strata. *Sedimentary Geology*, v. 143, pp. 191-197.

Hönisch, B., Ridgwell, A., Schmidt, D. N., Thomas, E., Gibbs, S. J., Sluijs, A., Zeebe, R., Kump, L., Martindale, R. C., Greene, S. E., Kiessling, W., Ries, J., Zachos, J. C., Royer, D. L., Barker, S., Marchitto Jr., T. M., Moyer, R., Pelejero, C., Ziveri, P., Foster, G. L., and Williams, B., 2012: The Geological Record of Ocean Acidification, *Science*, v. 335, pp. 1058-1063.

Hopmans, E.C., Schouten, S., Pancost, R.D., Van Der Meer, M.J.T., Sinninghe Damste´, J.S., 2000: Analysis of intact tetraether lipids in archaeal cell material and sediments using high performance liquid chromatography/atmospheric pressure ionization mass spectrometry. *Rapid Communications in Mass Spectrometry*, v. 14, pp. 585-589.

Hopmans E.C., Weijers J.W.H., Schefuß E., Herfort L., Sinninghe Damste´ J.S., Schouten S., 2004: A novel proxy for terrestrial organic matter in sediments based on branched and isoprenoid tetraether lipids. *Earth Planetary Science. Letters*, v. 224, pp. 107-116.

Huber, B.T., 1990: Maestrichtian planktonic foraminifer biostratigraphy of the Maud Rise (Weddell Sea, Antarctica): ODP Leg 113 Holes 689B and 690C. In Barker, P. F., Kennett, J. P., et al., *Proceedings of the ODP Scientific Results*, v. 113, pp. 489-513.

Hudson, J. D., 1977: Stable isotopes and limestone lithification. *Journal of the Geological Society of London*, v. 133, pp. 637-660.

Hughes, A.D., Whitehead, D., 1987: Glauconitization of detrital silica substrates in the Bantom Formation (Upper Eocene) of the Hampshire Basin, southern England. *Sedimentlogy*, v. 34, pp. 825-835.

Jahren, A.H., Conrad, C.P., Arens, N.C., Mora, G., Lithgow-Bertelloni, C., 2005: A plate tectonic mechanism for methane hydrates release along subduction zones. *Earth and Planetary Science Letters*, v. 236, pp. 691-704.

Jarvis, I., Mabrouk, A., Moody, R.T.J., de Cabrera, S.C., 2002: Late Cretaceous (Campanian) carbon isotope events, sea-level change and correlation of the Tethyan and Boreal realms. *Palaeogeography, Palaeoclimatology, Paleoecology*, v. 168, pp. 311-336.

Jarvis, I., Gale, A.S., Jenkyns, H.C., Pearce, M.A., 2006: Secular variation in Late Cretaceous carbon isotopes: a new $\delta^{13}C$ carbonate reference curve for the Cenomanian-Campanian (99.6-70.6 Ma). *Geological Magazine*, v.143, pp. 561-608.

Jenkyns H.C., Wilson, P.A., 1999: Stratigraphy, paleoceanography and evolution of Cretaceous Pacific guyots: relics from a greenhouse earth. *American Journal of Science*, v. 299, pp. 341-392.

Jenkyns, H.C., 2003: Evidence for rapid climate change in the Mesozoic-Paleogene greenhouse world. *Philosophical Transactions of the Royal Society*, v. 361, pp. 1885-1916.

Jenkyns, H.C., 2010: Geochemistry of Oceanic Anoxic Events. *Geochemistry, Geophysics, Geosystems*, v. 11, no. 3, pp. 1-30.

Jenkyns, H.C., Gale, A.S., Corfield, R.M., 1994: Carbon-and oxygen-isotope stratigraphy of the English Chalk and Italian Scaglia and its palaeoclimatic significance. *Geological Magazine*, v. 131, pp. 1-34.

Jenkyns, H., Schouten-Huibers, L., Schouten, S., Sinninghe Damsté, J.S., 2012: Warm Middle Jurassic-Early Cretaceous high-latitude sea-surface temperatures from the Southern Ocean. *Climate of the Past*, v. 8, pp. 215-226.

Jiang, D.X., Wang, Y, D., Robbins, E.I., Wei, J., Tian, N., 2008: Mesozoic non-marine petroleum source rocks determined by palynomorphs in the Tarim Basin, Xinjiang, northwestern China. *Geological Magazine*, v. 145, pp. 868-885.

Johnson, G.D., Powell C.M.A., Veevers J.J., 1976: Spreading history of the eastern Indian Ocean and Greater India's northward flight from Antarctica and Australia. *Geological Society of America Bulletin*, v. 87, pp. 1560-1566.

Jones, A.G., 1960: Reconnaissance geology of part of West Pakistan. A Colombo Plan cooperative project conducted and compiled by the *Hunting Survey Corporation, Limited, Toronto, Canada*, pp. 1-550.

Kadri, I.B., 1995: Petroleum Geology of Pakistan. *Pakistan Petroleum Limited, Karachi, Pakistan*, pp. 1-275.

Kaever, M., 1967: Untersuchungen zur Schichtfolge im Gebiet Quasim-Khel-Ali-Khel, E-Afghanistan. *Neues Jahrbuch Geologische und Paldiontologische Monatshefte*, v. 5, pp. 284-304.

Karakitsios, K., Kafousia, N., Tsikos, H., 2004: A Review of Oceanic Anoxic Events as recorded in the Mesozoic sedimentary record of mainland Greece. *Hellenic Journal of Geosciences,* v. 45, pp. 123-132.

Karner M., DeLong E. F., Karl D.M., 2001: Archaeal dominance in the mesopelagic zone of the Pacific Ocean. *Nature*, v. 409, pp. 507-510.

Kazmi, A.H., 1955: Geology of Ziarat-Kach-Zardalu area of Balochistan. *D.I.C. thesis, Imperial College London*, pp. 1-157.

Kazmi, A.H., 1988: Stratigraphy of the Dungan Group in Kach-Ziaratt area northeastern Baluchistan. *Geological Bulletin University of Peshawar*, v. 21, pp. 117-130.

Kazmi, A.H., Rana, R.A., 1982: Tectonic map of Pakistan at a scale of 1:2,000,000. *Geological Survey of Pakistan,* 1 sheet.

Kazmi, A.H., Jan, M.Q., 1997: Geology and Tectonics of Pakistan. *Graphic Publishers, Karachi, Pakistan*. pp. 1-545.

Keller, G., 1988: Extinction, survivorship and evolution of planktic foraminifera across the Cretaceous/Tertiary boundary at El Kef Tunisia. *Marine Micropaleontology*, v. 13, pp. 239-263.

Khan, U.S., 2010: Climate Classification of Pakistan. *Balwois-Ohrid, Republic of Macedonia*, v. 25.

Kim, J.H., Schouten, S., Hopmans, E.C., Donner, B., Sinninghe Damste, J.S., 2008: Global sediment core-top calibration of the TEX_{86} palaeothermometer in the ocean. *Geochimica et Cosmochimica Acta*, v. 72, pp. 1154-1173.

Kim, J.H., Van der Meer, J., Schouten, S., Helmke, P., Willmott, V., Sangiorgi, F., Koç, N., Hopmans, E.C., Sinninghe Damsté, J.S., 2010: New indices and calibrations derived from the distribution of crenarchaeal isoprenoid tetraether lipids: implications for past sea surface temperature reconstructions. *Geochimica et Cosmochimica Acta*, v. 74, pp. 4639-4654.

Klaus, J., 1960: Etude biometrique et statistique de quelques espèces de Globotruncanidés. 1. Les espéces du genre Praeglobotruncana dans le Cenomanien de la Breggia . *Ecoglae geologicae Helvetiae*, v. 53, pp. 285-308.

Kotova, I.Z., 1983: Palynological study of Upper Jurassic and Lower Cretaceous sediments, Site 511, Deep Sea Drilling Project Leg 71 (Falkland Plateau). In Ludwig, W. J., Krasheninnikov, V. A., et al. *Initial Report of the DSDP*, v. 71, pp. 879-906.

Kuypers, M.M.M., Blokker, P., Hopmans, E.C., Kinkel, H., Pancost, R.D., Schouten, S., Sinninghe Damsté, J.S., 2002: Archaeal remains dominate marine organic matter from the early Albian oceanic anoxic event 1b. *Palaeogeography, Palaeoclimatology, Palaeoecology*, v.185, pp. 211-234.

Larson, R.L., 1991: Latest pulse of Earth: evidence for a mid-Cretaceous superplume. *Geology* v.19, pp. 547-550.

Larson, R.L., Erba, E., 1999, Onset of the mid-Cretaceous greenhouse in the Barremian-Aptian: Igneous events and the biological, sedimentary, and geochemical responses: *Paleoceanography*, v. 14, pp. 663-678.

Leckie, M.R., 1984: Mid-Cretaceous planktonic foraminiferal biostratigraphy off Central Morocco, Deep Sea Drilling Project Leg 79, Sites 545 and 547.- *Initial Reports of the DSDP*, v. 79, pp. 579-620.

Leckie, R. M., 1989: An oceanographic model for the early evolutionary history of planktonic foraminifera, *Palaeogeography, Palaeoclimatology, Palaeoecology*, v. 73, pp. 107-138.

Leckie, R.M., Bralower, T.J., Cashman, R., 2002: Oceanic anoxic events and plankton evolution: Biotic response to tectonic forcing during the mid-Cretaceous. *Paleoceanography*, v. 17, no. 3, pp. 1-29.

Lehmann, C., Osleger, D.A., Montañez, I.P., 1998: Controls on cyclostratigraphy of Lower Cretaceous carbonates and evaporites, Cupido and Coahuila platforms, northeastern Mexico. *Journal of Sedimentary Research*. v. 68, pp. 1109-1130.

Lézin, C., Andreu, B., Ettachfini, El M., Wallez, M. J., Lebedel, V., Ch. Meister, Ch., 2012: The Upper Cenomanian-Lower Turonian of the Preafrican Trough, Morocco. *Sedimentary Geology*, v. 245-246, pp. 1-16.

Li, J., Batten, D.J., 2004: Early Cretaceous palynofloras from the Tanggula Mountains of the northern Qinghai–Xizang (Tibet) Plateau, China. *Cretaceous Research*, v. 25, pp. 531-542.

Li, X., Jenkyns, H.C., Wang, C., Hu, X., Chen, X., Wei, Y., Huang, Y., Cui, J., 2006: Upper Cretaceous carbon- and oxygen-isotope stratigraphy of hemipelagic carbonate facies from southern Tibet, China. *Journal of the Geological Society, London*, v. 163, pp. 375-382.

Lim, D.I., Park, Y.A., Choi, J.Y., Cho, J.W., Khim, B.K., 2000: Glauconite grains in continental shelf sediments around the Korean Peninsula and their depositional implications, *Geo-Marine Letters*, v. 20, no. 2, pp. 80-86.

Lindström, S., Erlström, M., 2011: The Jurassic-Cretaceous transition of the Fårarp-1 core, southern Sweden: sedimentological and phytological indications of climate change. *Palaeogeography, Palaeoclimatology, Palaeoecology*, v. 308, pp. 445-475.

Lirer, F., 2000: A new technique for retrieving calcareous microfossils from lithified lime deposits. *Micropaleontology*, v. 46, pp. 365-369.

Littler, K., Robinson, S.A., Bown, P. R., Nederbragt, A.J., Pancost, R.D., 2011: High sea-surface temperatures during the Early Cretaceous Epoch, *Nature Geoscience*, v. 4, pp. 169-172.

Loeblich, A.R., Tappan, H., 1961: Cretaceous planktonic foraminifera. Part. 1. Cenomanian. *Micropaleontology* v. 7, pp. 257-304.

Loeblich, A. Tappan, H., 1988: Foraminiferal Genera and Their Classification: *Van Nostrand Reinhold Company, New York*, pp. 1-970.

Lohmann, K.C., 1988, Geochemical patterns of meteoric diagenetic systems and their application to studies of paleokarst. In: Choquette, P.W., and James, N.P., eds., *Paleokarst: New York, Springer-Verlag*, pp. 58–80.

Longoria, J.F., 1974: Stratigraphic, morphologic and taxonomic studies of Aptian planktonic foraminifera. *Revista Espanola de Micropaleontología Num*. extraord, pp. 1-107.

Low, D., 1964: Redescription of Anomalina eaglefordensis Moreman. *Contributions from the Cushman Foundation for Foraminiferal Research,* v. 15, pp. 122, 123.

Luterbacher, H.P., Premoli-Silva, I., 1962: Note preliminaire sur une revision du profil de Gubbio. *Rivista Italiana di Paleontologia*, v. 68, pp. 1-253.

McCann, T., Saintot, A., 2003: Tracing tectonic deformation using the sedimentary record. *Geological Society London Special Publication*, v. 208, p. 1-28.

McDougal, J. W. and S. H. Khan, 1990, Strike slip faulting in a Foreland Fold-Thrust Belt: the Kalabagh Fault and western Salt Range, Pakistan. *Tectonics*, v. 9, no. 5, pp.1061-1075.

MacLeod, N., 2005: Biozones, in Selley, R.C., Cocks, L.R.M., Plimer, I.R., (eds.), Encyclopaedia of geology: *London, Academic Press*, pp. 294-306.

Marshall, J.D., 1992: Climatic and oceanographic isotopic signals from carbonate rock record and their preservation. *Geological Magazine*, v.129, pp. 143-160.

Martin, H.A., McMinn, A., 1993: Palynology of Sites 815 and 823: the Neogene vegetation history of coastal northeastern Australia. In: McKenzie, J.A., Davies, P.J., Palmer-Julson, A., et al., *Proceedings of the ODP Scientific Results*, v. 133, pp. 115-125.

Masood, K.R., Qureshi, K.A., Hussain, Z. Butt A.A., Ghazi, S., 2008: Palyonology of the Mesozoic succession of the Kala Chitta Range Pakistan. *Geological Bulletin of the Punjab University*, v. 43, pp. 83-99.

McArthur, J.M., Janssen, N.M.M., Reboulet, S., Leng, M.J., Thirlwall, M.F., Van de Schootbrugge, B., 2007: Early Cretaceous ice-cap volume, palaeo-temperatures (Mg, $\delta^{18}O$), and isotope stratigraphy ($\delta^{13}C$, $^{87}Sr/^{86}Sr$) from Tethyan belemnites. *Palaeogeography, Palaeoclimatology, Paleoecology*, v. 248, pp. 391-430.

Mendes, M.M., Dinis, J., Pais, J., Friis, E.M., 2011: Early Cretaceous flora from Vale Painho (Lusitanian basin, western Portugal): An integrated palynological and mesofossil study. *Review of Palaeobotany and Palynology*, v. 166, pp. 152-162.

Menegatti, A.P., Weissert, H., Brown, R. S., Tyson, R.V., Farrimond, P., 1998: High-resolution $\delta^{13}C$ stratigraphy through the early Aptian "Livello Selli" of the Alpine Tethys. *Paleoceanography*, v. 13, pp. 530-545.

Mohseni, H., Al-Aasm, I.S., 2004: Tempestite deposits on a storm-influenced carbonate ramp: An example from the Pabdeh formation (Paleogene), Zagros Basin, SW. *Journal of Petroleum Geology*, v. 27, no. 2, pp. 163-178.

Montanaro-Gallitelli, E., 1957: A revision of the foraminiferal Family Heterohelicidae. *Bulletin of the United States National Museum*, v. 215, pp. 133-154.

Mornod, L., 1949: Les Globorotalides du Cretace superieur du Montsalvens (Prealpes fribourgeoises). *Ecoglae geologicae Helvetiae*, v. no. 2, pp. 573-596.

Morrow, A.L., 1934. Foraminifera and Ostracoda from the Upper Cretaceous of Kansas. *Journal of Paleontology*, v. 8, no. 2, pp. 186-205.

Moullade, M., 1961: Quelques Foraminifères et Ostracodes nouveaux du Crétacé inférieur des Baronnies (Drome). *Revue de Micropaleontología,* v.3, pp. 213-216.

Moullade, M., 1966: Etude stratigraphique et micropaléontologique du Crétacé inférieur de la "fosse vocontienne". *Documents des Laboratoires de Géologie de la Faculté des Sciences de Lyon,* v. 15, pp. 1-369.

Moullade, M., 1974: Zones de Foraminifères du Crétacé inférieur mésogéen. Comptes Rendus de l'Académie des Sciences, Paris (Série D), v. 278, pp. 1813-1816.

Mutterlose, J., Malkoc, M., Schouten, S., Sinninghe Damsté, J.S., Foster, A., 2010: TEX_{86} and stable δ18O paleothermometry of Early Cretaceous sediments: implications for belemnite ecology and paleotemperature proxy application. *Earth and Planetary Science Letters* v. 298, pp. 286-298.

Nakkady, S.E., 1950: A new foraminiferal fauna from the Esna shales and Upper Cretaceous chalk of Egypt. *Journal of Paleontology*, v. 24, pp. 675-692.

Nederbragt, A.J., 1991: Late Cretaceous biostratigraphy and development of Heterohelicidae (planktic foraminifera). *Micropaleontology*, v. 37, pp. 329-372.

Nichols, G., 2009: Sedimentology and stratigraphy, 2nd ed., *Wiley- Blackwell Publishing Company, UK*, pp. 1-419.

Odin, G.S., Matter, A., 1981: De glauconiarum origine. *Sedimentology,* v. 28, pp. 611-641.

Olvera, Y.E., 1959: Foraminiferos del Cretacico superior Tampico Tuxpan. *Bulletin of Mexican Association of Petroleum Geologists***,** v**.** 11, nos. 3, 4, pp. 63-134.

Parente, M., Frijia, G., Di Lucia, M., 2007: Carbon-isotope stratigraphy of Cenomanian–Turonian platform carbonates from the Southern Apennines (Italy): a chemostratigraphic approach to the problem of correlation between shallow water and deep-water successions. *Journal of the Geological Society, London*, v. 164, pp. 609-620.

Paul, C.R.C., Lamolda, M.A., Mitchell, S.F., Vaziri, M.R., Gorostidi, A., Marshall, J.D., 1999: The Cenomanian-Turonian boundary at Eastbourne (Sussex, UK): a proposed European reference section. *Palaeogeography, Palaeoclimatology, Palaeoecology*, v.150, pp. 83-121.

Pederson, T.F., Calvert. S.E., 1990: Anoxia vs. productivity: what controls the formation of organic-carbon rich sediments and sedimentary rocks? *American Association of Petroleum Geoscientists* v. 74, pp. 454-466.

Peryt, D., 1983: Mid-Cretaceous microbiostratigraphy and foraminifers of the NE margins of the Swietokrzyskie Holy Cross Mts, Poland. *Palaeontologica*, v. 28, pp. 417-466.

Pessagno, E.A. Jr., 1960: Stratigraphy and micropalaeontology of the Cretaceous and lower Tertiary of Puerto Rico. *Micropaleontology,* v. 6, pp. 87-110.

Pessagno, E.A., Jr., 1967: Upper Cretaceous planktonic foraminifera from the Western Gulf Coastal Plain. *Paleontographica Americana*, v. 5, pp. 245-445.

Peyrot, D., Rodríguez-López, J.P., Barrón, E., Meléndez, N., 2007: Palynology and biostratigraphy of the Escucha Formation in the early Cretaceous Oliete Sub-basin, Teruel, Spain. *Revista Española de Micropaleontología*, v. 39, no. 1-2, pp. 135-154.

Peyrot, D., Rodríguez-López, J.P., Lassaletta, L., Meléndez, N., Barrón, E., 2007: Contributions to the palaeoenvironmental knowledge of the Escucha Formation in the Lower Cretaceous Oliete Sub-basin, Teruel, Spain. *C. R. Palevol,* v. 6, pp. 469-481.

Plummer, H.J. 1926: Foraminifera of the Midway Formation in Texas. *University of Texas Bulletin*, v. 2644, no. 1, pp.1-206.

Plummer, H.J., 1931: Some Cretaceous foraminifera in Texas. *University of Texas Bulletin*, v. 3101, pp.109-203.

Porthault, B., 1970: Foraminifér*s*. In: P. Donze, B., Porthault, G., Thomel, O. de Villout reys, Le Sénonien inférieur de Puget Théniers (Alpes Maritimes) et sa microfaune. *Geobios,* v. 3, pp. 41-106.

Postuma, J., 1971: Manual of Planktonic Foraminifera. *Elsevier Publishing Co., Amsterdam*, pp. 1-420

Powell, C. McA., 1979: A speculative tectonic history of Pakistan and surroundings: Some constraints from the Indian Ocean. In: Farah, A. & DeJong, K.A., eds. Geodynamics of Pakistan. *Geological Survey of Pakistan, Quetta*, pp. 5-24.

Prakash, N., 2008: Biodiversity and palaeoclimatic interpretation of Early Cretaceous flora of Jabalpur Formation, Satpura Basin, India. *Palaeoworld,* v. 17, pp. 253-263.

Premoli Silva, I., Sliter, W.V., 1994: Cretaceous planktonic foraminiferal biostratigraphy and evolutionary trends from the Bottaccione section, Gubbio, Italy. *Palaeontographica Italica*, v. 82, pp. 1-89.

Premoli Silva, I., Sliter W.V., 1999: Cretaceous paleoceanography: evidence from planktonic foraminiferal evolution. In: Barrera E., Johnson C.C., (eds), Evolution of the Cretaceous ocean-climate system. *Geological Society of America Special Paper*, v. 332, pp. 301-328.

Premoli Silva, I., Erba, E., Salvini, G., Locatelli, C., Verga, D., 1999: Biotic changes in Cretaceous oceanic anoxic events of the Tethys, *Journal of Foraminiferal Research*, v. 29, pp. 352-370.

Price, G.D., Ruffell, A.H., Jones, C.E., Kalin, R.M., Mutterlose, J., 2000: Isotopic evidence for temperature variation during the early Cretaceous (late Ryazanian-mid-Hauterivian). *Journal of the Geological Society*, v. 157, pp. 335-343.

Price, G.D., Nunn, E.V., 2010: Valanginian isotope variation in glendonites and belemnites from Arctic Svalbard: Transient glacial temperatures during the Cretaceous greenhouse, *Geology*, v. 38, pp. 251-254.

Reichel, M. 1950: Observations sur les Globotruncana du grisement de la Breggia (Tessin). *Ecoglae geologicae Helvetiae*, v. 42, pp. 596-617.

Renz, O., 1936: Stratigraphie und mikropaläontologische Untersuchung der Scaglia (Obere Kreide-Tertiär) im zentralen Apennin. *Ecoglae geologicae Helvetiae*, v. 29, pp. 1-149.

Renz, O., Luterbacher, H., Schneider, A., 1963: Stratigraphisch-paläontologische Untersuchungen im Albien un Cenomanien der Neuenburger Jura. *Ecoglae geologicae Helvetiae*, v. 56, pp. 1073-1116.

Reuss, A.E., 1845: Die Versteinerungen der Böhmischen Kreideformation. *E. Schweizerbart, Stuttgart, Abtheilung*, v. 1, pp. 1-58.

Reuss, A.E., 1854: Beiträge zur Charakteristik der Kreide-Schichten in den Ostalpen, besonders im Gosauthale und dem Wolfgangsee. Sitzaber. Kon. *Akad. Wissensch. Wien, Math- Naturw. Kl. Denkschrift*, v. 7, pp. 1-156.

Riding, J.B., Thomas, J.E., 1988: Dinoflagellate cyst stratigraphy of the Kimmeridgian Clay (Upper Jurassic) from the Dorset coast, southern England. *Palynology*, v. 12, pp. 65-88.

Riding, J.B., Thomas, J.E., 1992: Dinoflagellate cysts of the Jurassic System. In: Powell, A.J. (ed.): A stratigraphic index of dinoflagellate cysts. *London: British Micropalaeontological Society London*. pp. 7-97.

Riding, J.B., Fedorova, V.A., Ilyina, V.I., 1999: Jurassic and lowermost Cretaceous dinoflagellate cyst biostratigraphy of the Russian Platform and northern Siberia, Russia. *American Association of Stratigraphic Palynologists Contributions Series*, v. 36, pp. 1-183.

Riley, L.A., Fenton, J.P.G., 1984: Palynostratigraphy of the Berriasian to Cenomanian sequence at Deep Sea Drilling Project, Site 535, LEG 77, south eastern Gulf of Mexico: *Initial Reports of DSDP*, v. 77, pp. 675-690.

Robaszynski, F., Caron, M., (coordinators), 1979: Atlas des foraminiferes planctoniques du cretace moyen (mer boreale et Tethys). *Cahiers de Micropaleontologie*, v. 1, pp. 1-185.

Robaszynski, F., Caron, M., Gonzalez Donoso, J.M., Wonders, A.A.H., 1984: Atlas of Late Cretaceous Globotruncanids. *Revue de Micropaléontologie*, v. 26, pp. 145-305.

Robaszynski, F., Gonzáles Donoso, J.M., Linares, D., Amédro, F., Caron, M., Dupuis, C. V., Dhondt, A. Gartner, S., 2000: Le Crétacé supérieur de la région de Kalaat Senan, Tunesie centrale. Lithobiostratigraphie intégrée: zones d'ammonites, de foraminiféres planctoniques et de nannofossils du Turonien supérieur au Maastrichtien. *Bulletin du Centre de Recherches Elf Exploration-Production*, v. 22, pp. 359-490.

Robaszynski, F., Zagrani, M.F., Caron, M., Amédro, F., 2010: The global bio-events at the Cenomanian-Turonian transition in the reduced Bahloul Formation of Bou Ghanem (central Tunisia). *Cretaceous Research*, v. 31, no. 1, pp. 1-15.

Rodriguez, D.L., 1977: Foraminíferos planctónicos del cretácico superior de las Cordilleras Béticas (sector central). *Ph.D. thesis*, pp. 1-410.

Rogov, M.A., Zakharov, V.A., 2010: Jurassic and Lower Cretaceous glendonite occurrences and their implication for Arctic paleoclimate reconstructions and stratigraphy. *Earth Science Frontiers, Special Issue*, v.17, pp. 345-347.

Ruddiman, W.F., 2007: Earth's Climate: Past and Future: *New York, W.H. Freeman & Company*, pp. 1-465.

Rzehak, A., 1891: Die Foraminiferenfauna der altertiären Ablagerungen von Bruderndorf in Niederösterreich, mit Berücksichtigung des angleblichen Kreidevorkommens von Leitzersdorf. *Annalen des K.K. naturhistorischen Hofmuseums*, v. 6, pp. 1-12.

Salaj, J., Samuel, O., 1966: Foraminifera der Westkarpaten Kreide (Slowakai). *Geologicky Ustav Dionyza Stura in Bratislava*, pp. 1-292.

Sari, B., 2006: Upper Cretaceous planktonic foraminiferal biostratigraphy of the Bey Dağları autochthon in the Korkuteli Area, Western Taurides, Turkey. *Journal of Foraminiferal Research*, v. 36, pp. 241-261.

Scheibnerova, V., 1962: Stratigraphy of the Middle and Upper Cretaceous of the Mediterranean province on the basis of the Globotruncanoids. *Geologicky Sbornik, Bratislava*, v.13, pp. 197-226.

Schlanger, S.O., Jenkyns, H.C., 1976: Cretaceous oceanic anoxic events: Causes and consequences: *Geologie en Mijnbouw*, v. 55, pp. 179-184.

Scholle, P.A., Arthur, M. A., 1980: Carbon isotope fluctuations in Cretaceous pelagic limestones: Potential stratigraphic and petroleum exploration tool: *American Association of Petroleum Geologists Bulletin*, v. 64, pp. 67-87.

Schouten, S., Hopmans E.C., Pancost, R.D., Sinninghe Damste´ J.S., 2000: Widespread occurrence of structurally diverse tetraether membrane lipids: evidence for the ubiquitous presence of low-temperature relatives of hyperthermophiles. *Proceedings of the National Academy of Science of the USA*, v. 97, pp. 14421-14426.

Schouten, S., Hopmans, E.C., Schefuß, E., Sinninghe Damste´ J.S., 2002: Distributional variations in marine crenarchaeotal membrane lipids: a new organic proxy for reconstructing ancient sea water temperatures? *Earth and Planetary Science Letters*, v. 204, pp. 265-274.

Schouten, S., Hopmans, E.C., Forster, A., van Breugel, Y., Kuypers, M.M.M., Sinninghe Damsté, J.S., 2003: Extremely high sea-surface temperatures at low latitudes during the middle 30 Cretaceous as revealed by archaeal membrane lipids, *Geology*, v. 31, pp. 1069–1072.

Schouten, S., Hopmans E.C., Sinninghe Damste´ J.S., 2004: The effect of maturity and depositional redox conditions on archaeal tetraether lipid paleothermometry. *Organic Geochemistry*, v. 35, pp. 567-571.

Schouten, S., Forster A., Panato E., Sinninghe Damste´ J.S., 2007: Towards the calibration of the TEX_{86} paleothermometer in ancient green house worlds. *Organic Geochemistry*, v. 38, pp. 1537-1546.

Schouten, S., Huguet C., Hopmans E.C., Kienhuis M., Sinninghe Damste´ J.S., 2007: Analytical Methodology for TEX_{86} paleothermometry by high-performance liquid chromatography/atmospheric pressure chemical ionization-mass spectrometry. *Analytical Chemistry*, v. 79, pp. 2940-2944.

Schrank, E., 2005: Dinoflagellate cysts and associated aquatic palynomorphs from the Tendaguru Beds (Upper Jurassic-Lower Cretaceous) of southeast Tanzania. *Palynology*, v. 29, pp. 49-85.

Schrank, E., 2010: Pollen and Spores from the Tendaguru Beds, Upper Jurassic and Lower Cretaceous of Southeast Tanzania: Palynostratigraphical and Paleoecological Implications, *Palynology*, v. 34, no. 1, pp. 3-42.

Searle, M.P., 1991: Geology and Tectonics of the Karakoram Mountains, *John Wiley & Sons*, pp. 1-358.

Shackleton, N.J., Kennett, J.P., 1975: Paleotemperature history of the Cenozoic and the initiation of Antarctic glaciation: Oxygen and carbon isotopic analyses in DSDP Sites 277, 279, and 281, *Initial Report of the DSDP*, v. 29, 743-756.

Shafique, N.A., 2001: Spatial Biostratigraphy of NW Pakistan. *PhD thesis, Miami University*, pp. 1-137.

Shah, S.M.I., 1977: Stratigraphy of Pakistan. *Geological Survey of Pakistan, Memoirs, Quetta*, v. 12, pp. 1-138.

Shah, S.M.I., 2009: Stratigraphy of Pakistan, *Memoir of the Geological Survey of Pakistan*, v. 22, pp. 1-381.

Sigal, J., 1948: Notes sur les genres de foraminifères *Rotalipora* Brotzen, 1942 et *Thalmanninella*, famille des Globorotaliidae. *Révue de l' Institut français du Pétrole*, v. 3, pp. 95-103.

Sigal, J., 1952: Aperçu stratigraphique sur la micropaléontologie du Crétace´: 19th Congrés Géologique International, *Monographies régionales, series. 1, Algérie*, no. 26, pp. 1-47.

Sigal, J., 1956: Notes micropaléontologiques nord-africaines. 4. Biticinella breggiensis (Gandolfi), nouveau morphogenre. *Comptes Rendu Sommaire des Séances de la Société Géologique de France*, v. 3, pp. 35-36.

Sigal, J., 1966: Contribution à une monographie des Rosalines 1.Le genre Ticinella Reichel, souche des Rotalipores. *Ecoglae geologicae Helvetiae,* v. 59, pp. 185-217.

Sigal, J., 1969: Contribution a une nonographie des Rosalines: 2. L'espece Rotalipora appenninica (O.Renz) 1936 origine phyletique et taxinomique. Proceedings of the First International Conference on Planktonic Microfossils. *Geneve* 1967, pp. 622-639.

Sliter, W.V., 1989: Biostratigraphic zonation for Cretaceous planktonic foraminifers examined in thin section. *Journal of Foraminiferal Research,* v. 19, 1-19.

Sliter, W.V., 1999: Cretaceous planktic foraminiferal biostratigraphy of the Calera Limestone, northern California, USA. *Journal of Foraminiferal Research*, v. 29, pp. 318-339.

Smewing, J.D., Warburton, T., Daley, T., Copestake, P., Ul Haq, N., 2002: Sequence stratigraphy of the southern Kirthar Fold Belt and middle Indus basin, Pakistan. In: Clift, P.D., Kroon, D., Gaedicke, C., Craig, J., (Eds.), The tectonic and climatic evolution of the Arabian Sea region. *Geological Society London Special Publication*. v. 195, pp. 273-299.

Smith, C.C., Pessagno, E.A., 1973: Planktonic foraminifera and stratigraphy of the Corsicana Formation (Maastrichtian), north-central Texas. In: *Cushman Foundation for Foraminiferal Research, Special Publication*, v. 112, pp. 1-68.

Spath L.F., 1930: The fossil fauna of the Samana Range and some neighbouring areas. The Lower Cretaceous Ammonoidea, with notes on Albian Cephalopoda from Hazara. *Geological Survey of India, Palaeontologica Indica Memoirs (New Series),* v. 15, pp. 50-66.

Subbotina, N, N., 1949: Microfauna of the Cretaceous deposits of the southern slope of the Caucasus. Microfauna of the oil fields of the USSR. Trudy Vsesoyuznogo Neftyanogo Nauchno-Isledovatelskogo Geologo-Razvedochnogo Instituta (VNIGRI), *Novaya Seriya*, v. 34, pp. 5-36.

Tahirkheli, R.A.K., 1982: Geology of the Himalaya, Karakoram and Hindukush in Pakistan. *Geological Bulletin, University of Peshawar* v. 15, pp. 1-51.

Takashima R., Nishi, H., Huber, B. T., Leckie, R.M., 2006: Greenhouse world and the Mesozoic ocean. *Oceanography*, v. 19, pp. 64-74.

Takashima, R., Nishi, R., Hayashi, K., Okada, H., Kawahata, H., Yamanaka, T., Fernando, A.G., Mampuku, M., 2009: Litho-, bio- and Chemostratigraphy across the Cenomanian/Turonian boundary (OAE 2) in the Vocontian Basin of southeastern France. *Palaeogeography Palaeoclimatology Palaeoecology*, v. 273, 61-74.

Tappan, H., 1940: Foraminifera from the Grayson Formation of northern Texas. *Journal of Paleontology*, v. 14, pp. 93-126.

Thibault, N.R., Harlou, R., Schovsbo, N., Schiøler, P., Minoletti, F., Galbrun, B., Lauridsen, B.W., Sheldon, E., Stemmerik, L., Surlyk, F., 2012: Upper Campanian-Maastrichtian nannofossil biostratigraphy and high-resolution carbon-isotope stratigraphy of the Danish Basin: towards a standard $\delta^{13}C$ curve for the Boreal Realm, *Cretaceous Research*, v. 33, pp. 72-90.

Thierstein, H.R., 1979: Paleoceanographic implications of organic carbon and carbonate distribution in Mesozoic deep sea sediments. In: M. Talwani, W. Hay and W.B.F. Ryan (Editors), Deep Drilling Results in the Atlantic Ocean: Continental Margins and Paleo- environment. *American Geophysical Union, Washington, D.C*, pp.249-274.

Timmcke, T., 1981: Palynology of the Lower Cretaceous Pebble Shale Unit, Point Barrow, Alaska, *M. S. thesis, Arizona State University*, pp. 1-115.

Traverse, A., 2007, Paleopalynology (2d edition), *Springer, Dordrecht, The Netherlands*, pp. 1-813.

Treloar, P.J., Coward, M.P., Chambers, A.F., Izatt, C.N., Jackson, K.C., 1992: Thrust geometries, interferences and rotations in the northwest Himalaya. In: McClay, K.R. (Ed.), *Thrust Tectonics. Chapman and Hall, London*, pp. 325-342

Trujillo, E.F., 1960: Upper Cretaceous foraminifera from near Redding, California. *Journal of Paleontology*, v. 34, pp. 290-346.

Tsandev,I.,Slomp, C.P., 2009. Modeling phosphorus cycling and carbon burial during Cretaceous Oceanic Anoxic Events. *Earth Planetary Science Letters*, v. 286, pp. 71-79.

Tsikos, H., Jenkyns, H.C., Walsworth-Bell, B., Petrizzo, M.R., Forster, A., Kolonic, S., Erba, E., Premoli-Silva, I., Baas, M., Wagner, T., and Sinninghe Damst´e, J.S., 2004: Carbon-isotope stratigraphy recorded by the Cenomanian-Turonian oceanic anoxic event: Correlation and implications based on three key localities, *Journal of the Geological Society of London*, v. 161, pp. 711-719.

Uda, A., Sugai, Y.H., Itoh, T., 2001: Variation on molecular species of polar lipids from Thermoplasma acidophilum depends on growth temperature. *Lipids*, v. 36, pp. 103-105.

Urey, H. C., 1947: The thermodynamic properties of isotopic substances. *Journal of Chemical Society London*, pp. 562-581.

Van de Schootbrugge, B., Föllmi, K.B., Bulot, L.G., Burns, S.J., 2000: Paleoceanographic changes during the Early Cretaceous (Valanginian-Hauterivian): evidence from oxygen and carbon stable isotopes. *Earth and Planetary Science Letters*, v. 181, pp. 15-31.

Van Konijnenburg Van Cittert, J.H.A., 2002: Ecology of some Late Triassic to Early Cretaceous ferns in Eurasia. *Review of Palaeobotany and Palynology*, v. 119, pp. 113-124.

Vijaya, 1997: Palynoflora from subsurface Lower Cretaceous Intertrappean beds in Domra Sub-basin of the Raniganj Gondwana Basin, West Bengal, India. *Cretaceous Research*, v. 18, pp. 37-50.

Vijaya, 2009: Palynofloral changes in the Upper Paleozoic and Mesozoic of the Deocha-Pachami area, Birbhum Coalfield, West Bengal, India. Science in China Series D: *Earth Sciences*, v. 52, no. 12, pp. 1932-1952.

Vogler, J., 1941: Ober-Jura und Kreide von Misol (Niederländisch-Ostindien). *Palaeontographica*, v. 4, pp. 243-293.

Volkheimer, W., Gallego, O.F., Cabaleri, N.G., Armella, C., Narvaez, P.L., Silva Nieto, D.G., Paez, M.A., 2009: Stratigraphy, palynology, and conchostracans of a Lower Cretaceous sequence at the Canadon Calcareo locality, Extra-Andean central Patagonia: age and palaeoenvironmental significance. *Cretaceous Research*, v.30, pp. 270-282.

Voorwijk, G.H., 1937: Foraminifera from the Upper Cretaceous of Havana, Cuba. *Koninklijke Nederlandse Akademie van Wetenschappen, Proceedings*, v. 40, pp. 190-198

Wang, Y, Mosbrugger, V., Zhang H., 2005: Early to Middle Jurassic vegetation and climatic events in the Qaidam Basin, Northwest China. *Palaeogeography, Palaeoclimatology, Palaeoecology*, v. 224, pp. 200-216.

Weissert, H., Lini, A., Föllmi, K.B., Kuhn, O., 1998: Correlation of Early Cretaceous carbon isotope stratigraphy and platform drowning events: a possible link? *Palaeogeography, Palaeoclimatology, Palaeoecology*, v. 137, pp. 189-203.

Weijers, J.W.H., Schouten, S., Spaargaren, O.C., Sinninghe Damsté, J.S., 2006b: Occurrence and distribution of tetraether membrane lipids in soils: implications for the use of the TEX_{86} proxy and the BIT index. *Organic Geochemistry*, v. 37, pp. 1680-1693.

Weijers, J.W.H., Schouten, S., Van den Donker, J.C., Hopmans, E.C., Sinninghe Damste, J.S., 2007: Environmental controls on bacterial tetraether membrane lipid distribution in soils, *Geochimica et Cosmochimica Acta*, 71: 703-713.

White, M.P., 1928: Some index foraminifera of the Tampico embayment of Mexico, Parts 1-2. *Journal of Paleontology*, v. 2, no.4, pp. 177-215, 280-313.

William, M., Dean, 1959: Stratigraphy of the Lower Indus Basin, West Pakistan. *World Petroleum Congress, 5th, New York, Proceedings, Section I, paper*, v. 19, pp. 377-390.

Williams, G.L., 1977: Dinocysts: their paleontology, biostratigraphy and paleoecology. In: A.T.S. Ramsay (ed.), *Oceanic Micropalaeontology, Academic Press, New York*, v. 2, pp. 1231-1325.

Williams, G.L., Bujak, J. P., 1985: Mesozoic and Cenozoic dinoflagellates. In: H.M Bolli, J.B. Saunders, and K. Perch-Nielsen (eds.), *Plankton Stratigraphy, Cambridge University Press*, pp. 847-964.

Wilson, J.L., 1975: Carbonate Facies in Geologic History. *New York, springerverlag*, pp. 1-472.

Wuchter C., Schouten S., Coolen M.J.L., Sinninghe Damste´ J.S., 2004: Temperature-dependent variation in the distribution of tetraether membrane lipids of marine Crenarchaeota: implications for TEX86 paleothermometry. *Paleoceanography*, v. 19, pp. 1-10.

Yang, X., Li, W., Batten, D.J., 2007: Biostratigraphic and palaeoenvironmental implications of an Early Cretaceous miospore assemblage from the Muling Formation. *Cretaceous Research*, v. 28, no. 2, pp. 339-347.

Zachos, J.C., Röhl, U., Schellenberg, S.A., Sluijs, A., Hodell, D.A., Kelly, D.C., Thomas, E., Nicolo, M., Raffi, I., Lourens, L.J., McCarren, H. & Kroon, D. , 2005: Rapid Acidification of the Ocean during the Paleocene-Eocene Thermal Maximum, *Science*, v. 308, no. 5728, pp. 1611-1615.

Ziaja, J., 2006: Lower Jurassic spores and pollen grains from Odrowąż, Mesozoic margin of the Holy cross Mountains, Poland. *Acta Palaeobotanica*, v. 46, no. 1, pp. 3-83.

Appendix 1

Dinoflagellates

Achomosphaera neptuni (Eisenack, 1958a) Davey and Williams, 1966

***Batioladinium* sp.**

Cribroperidinium globatum (Gitmez & Sarjeant, 1972) Helenes 1984

***Cribroperidinium* sp.**

***Ctenidodinium* spp.**

Cyclonephelium distinctum Deflandre and Cookson, 1955

***Cyclonephelium* spp.**

Cymososphaeridium* cf. *validum Davey, 1982

Egmontodinium* cf. *expiratum Davey, 1982

Egmontodinium torynum (Cookson & Eisenack, 1960) Davey, 1979

Gonyaulacysta jurassica (Deflandre 1938) Norris & Sarjeant 1965

Hystrichosphaerina schindewolfii Alberti 1961

***Kleithriasphaeridium* cf. eoinodes** (Eisenack 1958) Davey 1974

Kleithriasphaeridium porospinosum Davey 1982

Leptodinium subtile Klement 1960

Oligosphaeridium asterigerum (Gocht, 1959) Davey & Williams, 1969b

Oligosphaeridium* cf. *pulcherrimum (Deflandre and Cookson, 1955) Davey & Williams, 1966

Oligosphaeridium complex (White, 1842) Davey & Williams, 1966b

***Oligosphaeridium* spp.**

Perisseiasphaeridium pannosum Davey & Williams 1966

Prolixosphaeridium parvispinum (Deflandre, 1937) Davey *et al.*, 1969

Prolixosphaeridium **spp.**

Pseudoceratium **sp.**

Pterospermella **sp.**

Rigaudella aemula (Deflandre 1939) Below 1982

Scriniodinium **sp.**

Sentusidinium pelionense Fensome 1979

Sentusidinium **spp.**

Sirmiodinium grossi Alberti 1961

Sirmiodinium **sp.**

Stiphrosphaeridium **sp.**

Surculosphaeridium **sp.**

Systematophora areolata Klement 1960

Systematophora **spp.**

Wallodinium **sp.**

Spores

Aequitriradites **sp.**

Aratrisporites parvispinosus Leschik, 1955

Ceratosporites equalis Cookson & Dettmann, 1958

Chomotriletes minor (Kedves, 1961) Pocock, 1970

Cicatricosisporites australiensis (Cookson 1953) Potonié, 1956

Cicatricosisporites hughesii Dettmann, 1963

Cicatricosisporites **spp.**

Concavisporites **spp.**

Concavisporites toralis (Leschik 1955) Nilsson 1958

Concavissimisporites minimus Herngreen, 1970

C*oncavissimisporites* sp.

C*oncavissimisporites variverrucatus* (Couper, 1958) Brenner 1963

Contignisporites cooksoniae (Balme, 1957) Dettmann, 1963

Contignisporites fornicatus Dettmann 1963

Contignisporites glebulentus Dettmann, 1963

Contignisporites multimuratus Dettmann, 1963

***Contignisporites* spp.**

***Converrucosisporites* sp.**

Cyathidites australis Couper, 1953

Cyathidites minor Couper, 1953

***Deltoidospora* sp.**

Densoisporites velatus Weyland & Krieger, 1953

***Dictyophyllidites* sp.**

Gleicheniidites rasilis Bolkhovitina, 1968

Gleicheniidites senonicus Ross, 1949

***Gleicheniidites* spp.**

***Impardecispora* sp.**

Ischyosporites punctatus Cookson and Dettmann, 1958

***Ischyosporites* sp.**

Ischyosporites variegatus (Couper, 1958) Schulz 1967

Klukisporites* cf. *pseudoreticulatus Couper, 1958

***Klukisporites* sp.**

Matonisporites equiexinus Couper, 1958

***Matonisporites* spp.**

***Neoraistrickia* sp.**

Ornamentifera baculata Singh 1971

***Pilosisporites* sp.**

***Retitriletes* sp.**

Sestrosporites pseudoalveolatus (Couper, 1958) Dettmann, 1963

Trilobosporites* cf. *apiverrucatus Couper, 1958

***Trilobosporites* sp.**

***Triplanosporites* sp.**

Pollen

Alisporites grandis (Cookson, 1953) Dettmann, 1963

***Alisporites* sp.**

Alisporites thomasii (Couper 1958) Nilsson 1958

Araucariacites australis Cookson, 1947

Callialasporites dampieri-trilobatus

Callialasporites dampieri (Balme 1957), Dev, 1961

Callialasporites microvelatus Schulz, 1966

Callialasporites segmentatus (Balme, 1957) Srivastava, 1963

***Callialasporites* spp.**

Callialasporites trilobatus (Balme 1957), Dev, 1961

Callialasporites turbatus (Balme, 1957) Schulz, 1967

***Choanopollenites* sp.**

Classopollis classoides (Pflug, 1953) Pocock & Jansonius, 1961

Classopollis martinottii Reyre, 1970

***Classopollis* spp.**

Classopollis triangulus (Zhang 1978) Lei 1981

***Cycadopites* spp.**

Inaperturopollenites scabratus Muller, 1968

***Inaperturopollenites* sp.**

Inaperturopollenites laevigatus Takahashi, 1957

***Jugella* sp.**

Podocarpidites* cf. *ellipticus Cookson**,** 1947

***Trisaccites* sp.**

Vitreisporites pallidus (Reissinger, 1958) Nilsson, 1958

Reworked Permo-Triassic older pollens

***Monosaccites* sp.**

Arcuatipollenites ovatus (Goubin) Twari & Vijaya 1995

Verticipollenites gibbosus Bharadwaj 1962

Appendix-2

Species details in this thesis				Identification references
Plate	Figures	Species	Samples	
1	1	*Hedbergella sigali*	MP-10	Sliter, 1989, p. 12, pl. 1, fig. 4.
	2	*Hedbergella praetrocoidea*	MP-9	Sliter, 1999, p. 333, pl. 1, fig. 5.
	3	*Hedbergella trocoidea*	MP-3	Sliter, 1999, p. 333, pl. 1, fig. 14.
	4,5,6, 8, 10 with minor differences	*Hedbergella trocoidea*	MP-30, MP-40, MP-42, MP-44, MP-3	Mandic & Lukeneder, 2008, p. 906, figs 7 (2-3).
	7	*Hedbergella trocoidea*	MP-44	Sliter, 1992, p. 290, fig. 7 (3)
	9	*Hedbergella trocoidea*	MP-31	Sliter, 1992, p. 290, fig. 7(5)
	11	*Hedbergella delrioensis*	MP-9	Sliter & Leckie, 1993, p. 81, pl. 2, fig. 14.
	12,13 with minor differences	*Hedbergella delrioensis*	MP-127, MP-9	Rojay & Altiner, 1998, p. 175, pl. 1, fig. 21.
	14	*Hedbergella delrioensis*	MP-123	Pessagno, 1967, p. 389, pl. 48, fig. 3
	15	*Hedbergella delrioensis*	MP-118	----------
	16	*Globigerinelloides barri*	MP-72	Sliter, 1999, p. 334, pl. 2, fig. 20
	17	*Globigerinelloides barri*	MP-72	----------
	18	*Hedbergella hispaniae*	MP-9	Sliter, 1992, p. 288, fig. 6(15)
	19	*Hedbergella gorbachikae*	MP-133	Sliter, 1999, p. 333, pl. 1, fig. 25
	20,21 with minor Differences	*Hedbergella gorbachikae*	MP-32, MP-114	Sliter, 1999, p. 333, pl. 1, fig. 22
2	1, 3, 6, 9, 10 with minor differences	*Globigerinelloides ferreolensis*	MP-26, P-28, MP-24,MP-33, MP-23	Sliter, 1992, p. 288, fig. 6 (6)
	4	*Globigerinelloides* cf. *ferreolensis*	MP 28	----------
	2, 5	*Globigerinelloides ferreolensis*	MP 28, MP 24	Sliter, 1989, p. 12, pl. 1, fig. 11-12
	7	*Globigerinelloides ferreolensis*	MP 31	Rojay & Altiner, 1998, p. 175, pl. 1, fig. 29
	8	*Globigerinelloides ferreolensis*	MP 30	Mandic & Lukeneder, 2008, p. 906. fig. 7 (7)

2	12	*Globigerinelloides algerianus*	MP 30	Sliter, 1999, p. 334, pl. 2, fig. 23
	13	*Globigerinelloides algerianus*	MP 30	Sliter, 1999, p. 334, pl. 2, fig. 24
3	1	*Globigerinelloides algerianus*	MP-30	Mandic & Lukeneder, 2008, p. 906, fig. 7 (9)
	2	*Globigerinelloides algerianus*	MP-30	Sliter, 1999, p. 334, pl. 2, fig. 17
	3,6 with minor differences	*Globigerinelloides algerianus*	MP-28	Mandic & Lukeneder, 2008, p. 906, fig. 7 (9)
	4,5 with minor differences	*Globigerinelloides algerianus*	MP-26, MP-30	Sliter, 1999, p. 334, pl. 2, fig. 23
	7,8 with minor differences	*Globigerinelloides algerianus*	MP-24, MP-28	Sliter, 1999, p. 334, pl. 2, figs. 17, 26
	9	*Globigerinelloides algerianus*	MP-29	Sliter, 1999, p. 334, pl. 2, fig. 17, 26
	10	Transitional between *Globigerinelloides algerianus* and *Planomalina cheniourensis*	MP-32	----------
	11,13 with minor differences	*Planomalina cheniourensis*	MP-37	Sliter, 1992, p. 288, fig 6 (11)
	12	*Planomalina cheniourensis*	MP-37	Sliter, 1999, p. 334, pl. 2, figs. 17, 27; Wonders, 1980, p. 155, pl. 9, fig. 6.
4	1,3 with minor differences	*Ticinella bejaouaensis*	MP-42, MP-89	Sliter, 1992, p. 290, fig. 7 (8)
	2	*Ticinella bejaouaensis*	MP-42	Sliter, 1992, p. 290, fig. 7 (9)
	4	*Ticinella bejaouaensis*	MP-89	Sliter, 1992, p. 290, fig. 7 (14)
	5	*Ticinella* sp.	MP-96	Okay & Altiner, 2007, p. 273, pl. 3, fig. 32
	6	*Ticinella roberti*	MP-127	Premoli-Silva & Sliter, 1994, pl. 4, fig. 2
	7	*Ticinella roberti*	MP-125	Okay & Altiner, 2007, p. 273, pl. 3, fig. 36
	8	*Ticinella roberti*	MP-102	Sliter, 1999, p. 336. pl. 4, fig. 4.
	9	*Ticinella primula*	MP-122	Sliter, 1999, p. 335, pl. 3, fig. 11
	10	*Hedbergella rhinoceros*	MP-77	Sliter, 1999, p. 333, pl. 1, fig. 23

4	11	*Planomalina praebuxtorfi*	MP-127	Sliter & Premoli, 1990, p. 652, fig. 12 (12)
	14	*Globigerinelloides ultramicrus*	MP-121	Premoli-Silva & Sliter, 1994, p. 39, pl. 3, fig. 3
	15	*Heterohelix moremani*	MP-127	----------
	16	*Globigerinelloides bentonensis*	MP-118	Premoli-Silva & Sliter, 1994, p. 39, pl. 3, fig. 15
	17	*Hedbergella rischi*	MP-73	Premoli-Silva & Sliter,1994, p. 35, pl. 1, fig. 12
	18	*Ticinella praeticinensis*	MP-118	Okay & Altiner, 2007, p. 278, pl. 3, fig. 22
	19	*Hedbergella rischi*	MP-110	----------
	20	*Hedbergella rischi*	MP 89	Sliter, 1999, p. 333, pl. 1, figs. 16, 21
5	1	*Hedbergella planispira*	MP-109	Premoli-Silva & Sliter, 1994, p. 34, pl. 1, fig. 1.
	2	*Hedbergella planispira*	MP-121	Premoli-Silva & Sliter, 1994, p. 34, pl. 1, fig. 10
	3	*Hedbergella planispira*	MP-109	Sliter, 199, p. 333, pl. 1, fig. 13
	4	*Hedbergella planispira*	MP-107	Sliter, 1992, p. 288, fig. 6 (19)
	5	*Ticinella roberti*	MP-101	Premoli-Silva & Sliter, 1994, p. 41, pl. 4, fig. 2
	6	*Ticinella roberti*	MP-111	Sliter, 1999, p. 336, pl. 4, fig. 1
	7	*Ticinella roberti*	MP-109	Sliter, 1999, p. 336, pl. 4, fig. 4.
	8	*Ticinella primula*	MP-125	Premoli-Silva & Sliter, 1994, p. 41, pl. 4, fig. 11
	9	*Ticinella primula*	MP-123	Premoli-Silva & Sliter, 1994, p. 41, pl. 4, fig. 6
	10	*Ticinella primula*	MP-120	Sliter, 1999, p. 335, pl. 3, fig. 11
	11	*Ticinella* cf. *roberti*	MP-119	----------
	12, 13 with minor differences	*Globigerinelloides bentonensis*	MP-139, MP-140	Sliter & Premoli-Silva 1990, p. 652, fig. 12 (6).
	14	*Macroglobigerinello-ides bentonensis*	MP-120	Okay & Altiner, 2007, p. 272, pl. 3, fig. 47.
	15	*Globigerinelloides bentonensis*	MP-137	Premoli-Silva & Sliter, 1994, p. 37, pl. 2, fig. 7
	16	*Macroglobigerinelloi des bentonensis*	MP-119	Okay & Altiner, 2007, p. 272, pl. 3, figs. 45, 47.
6	1	*Hedbergella simplex*	MP-122	Sliter, & Premoli, 1990, p. 652, fig. 12 (9)
	2	*Hedbergella simplex*	MP-196	Sliter, 1999, p. 335, pl. 3, fig. 14
	3	*Hedbergella simplex*	MM-23	Li et al. 2009, p. 1010, fig. 4 (6).
	4	*Hedbergella* cf. *simplex*	MM-25	----------
	5	*Hedbergella simplex*	MP-113	Sliter, 1999, p. 335, pl. 3, fig. 14
	6	*Hedbergella simplex*	MP-124	Premoli-Silva & Sliter, 1994, p. 35, pl. 1, fig. 9
	7	*Ticinella* sp.	MP-113	----------
	8	*Biticinella breggiensis*	MP-111	Premoli-Silva & Sliter, 1994, p. 43, pl. 5, figs. 9-10

6	9	*Biticinella breggiensis*	MP-113	Premoli-Silva & Sliter, 1994, p. 43, pl. 5, figs. 1, 3
	10	*Biticinella breggiensis*	MP-125	----------
	11	*Biticinella breggiensis*	MP-126	Sliter, 1999, p. 336, pl. 4, figs. 8, 13
	12	*Ticinella madecassiana*	MP-123	Premoli-Silva & Sliter, 1994, p. 41, pl. 4, fig. 5
	13	*Biticinella subbreggiensis*	MP-125	Sliter, 1999, p. 336, pl. 4, fig. 9
	14	*Ticinella raynaudi*	MP-121	Premoli-Silva & Sliter, 1994, p. 41, pl. 4, fig. 8
	15	*Ticinella raynaudi*	MP-121	Sliter, 1999, p. 335, pl. 3, fig. 17
	16	*Rotalipora* cf. *subticinensis*	MP-127	Premoli-Silva & Sliter, 1994, p. 47, pl. 7, fig. 3
	17	*Rotalipora ticinensis*	MP-122	Premoli-Silva & Sliter, 1994, p. 49, pl. 8, fig. 9
7	1	*Rotalipora ticinensis*	MM-23	Li et al. 2009, p. 1008, fig. 3 (3).
	2	*Rotalipora ticinensis*	MP-124	Bertle & Suttner, 2005, p. 886, fig. 3 (F, G)
	3,4 with minor differences	*Ticinella madecassiana*	MP-119, MP-117	Premoli-Silva & Sliter, 1994, p. 41, pl. 4, figs. 4-5
	5	*Rotalipora praeappenninica*	MM-24	Premoli-Silva & Sliter, 1994, p. 47, pl. 7, fig. 1
	6	*Rotalipora praeappenninica?*	MP-127	Sliter 1999, p. 336, pl. 4, fig. 5
	7	*Planomalina buxtorfi*	MP-129	Carron, 1985, p. 66, fig. 29 (2b)
	8-11with minor differences	*Planomalina buxtorfi*	MM-23 MP-130 MM-23 MP-128	Premoli-Silva & Sliter, 1994, p. 43, pl. 5, figs, 6,7; Sliter, 1992, p. 288, fig. 6 (8)
	12	*Planomalina buxtorfi*	MP-128	----------
	13	*Planomalina buxtorfi*	MP-129	----------
	14,15 with minor differences	*Praeglobotruncana delrioensis*	MM-25, MM-23	Premoli-Silva & Sliter, 1994, p. 45, pl. 6. fig.11; Okay & Altiner, 2007, p. 275, pl. 4, fig. 16
	16	*Heterohelix moremani*	MP-203	Premoli-Silva & Sliter, 1994, p. 81, pl. 24, fig. 12
	17	*Heterohelix moremani*	MP-127	----------
	18	*Globigerinelloides ultramicrus*	MP-120	Sliter & Premoli, p. 652, fig. 12 (7)
	19	*Rotalipora balernaensis*	MP-132	Sliter & Premoli, p. 654, fig. 13 (3)
	20	*Rotalipora balernaensis*	MM-24	Premoli-Silva & Sliter, 1994, p. 47, pl. 7, fig. 2

8	1	*Rotalipora appenninica*	MP-129	Sliter 1999, p. 336, pl. 4, fig. 12
	2	*Rotalipora appenninica*	MP-140	Li et al. 2009, p. 1008, fig. 3 (9)
	3	*Rotalipora appenninica*	MP-137	----------
	4	*Rotalipora appenninica*	MP-137	Li et al. 2009, p. 1008, fig. 3 (8).
	5	*Rotalipora appenninica*	MP-127	----------
	6	*Rotalipora appenninica*	MP-129	Li et al. 2009, p. 1008, fig. 3 (12).
	7	*Praeglobotruncana stephani*	MP-137	Premoli-Silva & Sliter, 1994, p. 51, pl. 9, fig. 1
	8,9,12 with minor differences	*Praeglobotruncana stephani*	MP-140, MM-23, MM-25	Premoli-Silva & Sliter, 1994, p. 51, pl. 9, fig. 3
	10	*Praeglobotruncana stephani*	MP-138	Premoli-Silva & Sliter, 1994, p. 51, pl. 9, fig. 8
	11	*Praeglobotruncana stephani*	MP-139	Premoli-Silva & Sliter, 1994, p. 51, pl. 9, fig. 2
	13	*Praeglobotruncana stephani*	MP-191	Premoli-Silva & Sliter, 1994, p. 51, pl. 9, fig. 2
	14	*Globigerinelloides ultramicrus*	MP-126	Sliter & Premoli, p. 652, fig. 12 (7)
	15	*Globigerinelloides caseyi*	MP-124	Premoli-Silva & Sliter, 1994, p. 37, pl. 2, fig. 11
	16	*Globigerinelloides caseyi*	MP-126	Premoli-Silva & Sliter, 1994, p. 37, pl. 2, fig. 5
9	1	*Rotalipora gandolfi*	MP-129	Premoli-Silva & Sliter, 1994, p. 49, pl. 8, fig. 1
	2	*Rotalipora gandolfi*	MP-137	Li et al. 2009, p. 1008, fig. 3 (25)
	3	*Rotalipora gandolfi*	MP-132	Sliter & Premoli, 1990, p. 654, fig. 13 (6)
	4	*Rotalipora brotzeni*	MP-139	Li et al. 2009, p. 1008, fig. 3 (17)
	5	*Rotalipora brotzeni*	MP-138	----------
	6	*Rotalipora brotzeni*	MP-137	Sliter, 1999, p. 336, pl. 4, fig. 6
	7	*Rotalipora brotzeni*	MP-137	Li et al. 2009, p. 1008, fig. 3 (23)
	8	*Rotalipora montsalvensis*	MP-130	Premoli-Silva & Sliter, 1994, p. 45, pl. 6, fig. 8
	9	*Rotalipora montsalvensis*	MM-23	Bertle & Suttner, 2005, p. 886, fig. 3 (L)
	10	*Rotalipora montsalvensis*	MM-25	Li et al. 2009, p. 1008, fig. 3 (29)
	11,13,14 with minor difference	*Praeglobotruncana gibba*	MP-182, MP-193, MP-183	Premoli-Silva & Sliter, 1994, p. 51, pl. 9, fig. 6.
	12	*Praeglobotruncana gibba*	MP-182	Sliter & Premoli, 1990, p. 652, fig. 12 (18)

9	15	*Rotalipora reicheli*	MP-132	Premoli-Silva & Sliter, 1994, p. 48, pl. 8, fig. 6
	16	*Rotalipora brotzeni*	MP-137	Premoli-Silva & Sliter, 1994, p. 48, pl. 6, fig. 9; Li et al. 2009, p. 1008, fig. 3 (19).
	17	*Rotalipora greenhornensis*	MP-137	Li et al. 2009, p. 1008, fig. 3 (35)
	18	*Rotalipora greenhornensis*	MP-137	Okay & Altiner, p. 275, pl. 4, fig. 14
	19	*Rotalipora greenhornensis*	MM-23	Premoli-Silva & Sliter, 1994, p. 47, pl. 7, fig. 9.
	20	*Rotalipora greenhornensis*	MP-137	Li et al. 2009, p. 1008, fig. 3 (40)
	21	*Rotalipora greenhornensis*	MM-24	Li et al. 2009, p. 1008, fig. 3 (41)
10	1,3	*Rotalipora cushmani*	MM-25, MP-139	Okay & Altiner, 2007, p. 275, pl. 4, fig. 3
	2	*Rotalipora cushmani*	MM-25	Okay & Altiner, 2007, p. 275, pl. 4, fig. 2
	4	*Rotalipora cushmani*	MP-139	Premoli-Silva & Sliter, 1994, p. 47, pl. 7, fig. 6
	5	*Rotalipora cushmani*	MM-25	Premoli-Silva & Sliter, 1994, p. 47, pl. 7, fig. 5
	6	*Rotalipora cushmani*	MM-25	Sliter 1989, p. 14, pl. 2, fig. 6
	7,8,9,17 with minor difference	*Rotalipora cushmani*	MP-140,MP-138, MP-139 MP-139	Li et al. 2009, p. 1010, fig. 4 (3).
	10	*Rotalipora cushmani*	MM-25	Premoli-Silva & Sliter, 1994, p. 47, pl. 7, fig. 6
	11	*Rotalipora cushmani*	MP-138	Premoli-Silva & Sliter, 1994, p. 47, pl. 7, fig. 5
	12	*Rotalipora cushmani*	MP-138	Li et al. 2009, p. 1010, fig. 4 (4)
	13	*Rotalipora cushmani*	MP-138	Premoli-Silva & Sliter, 1994, p. 49, pl. 8, fig. 10
	14	*Rotalipora cushmani*	MP-138	----------
	15	*Rotalipora cushmani*	MP-138	Li et al. 2009, p. 1010, fig. 4 (1)
	16	*Rotalipora cushmani*	MM-25	Okay & Altiner, 2007, p. 275, pl. 4, fig. 1
11	1-3 with minor differences	*Whiteinella aumalensis*	MP-181,MP-179,MP-189	Premoli-Silva & Sliter, 1994, p. 55, pl. 11, fig. 4
	4	*Whiteinella praehelvetica*	MP-195	Premoli-Silva & Sliter, 1994, p. 55, pl. 11, fig. 1
	5	*Whiteinella praehelvetica*	MP-138	Robaszynski et al. 2010, p. 11, fig. 13 (P)
	6	*Whiteinella praehelvetica*	MP-181	Aguilera, 2003, p. 208, pl. 1, fig. 16
	7	Transitional form between *Whiteinella baltica* and *Whiteinella praehelvetica*	MP-191	Premoli-Silva & Sliter, 1994, p. 53, pl. 10, fig. 10.

11	8, with different orientation	*Whiteinella baltica*	MP-137	Premoli-Silva & Sliter, 1994, p. 55, pl. 11, fig. 11
	9	*Whiteinella baltica*	MP-181	Ifrim & Stinnesbeck, 2008, p. 954, fig. 12 (h)
	10,11 with different orientation	*Whiteinella baltica*	MP-180, MP-194	Premoli-Silva & Sliter, 1994, p. 55, pl. 11, fig. 11; Sliter & Premoli-Silva, 1990, p. 656, fig. 14 (5)
	12	*Dicarinella algeriana*	MP-137	Okay & Altiner, 2007, p. 275, pl. 4, fig. 25
	13, 14, 15, with minor differences	*Dicarinella algeriana*	MP 181. MP 193, MP 138	Premoli-Silva & Sliter, 1994, p. 57, pl. 12, fig. 4
	16, 18, 19, 20, with minor differences	*Dicarinella algeriana*	MP-194, MP-137, MP179, MP-191	Premoli-Silva & Sliter, 1994, p. 57, pl. 12, fig. 9
	17	*Dicarinella algeriana*	MM-25	Premoli-Silva & Sliter, 1994, p. 57, pl. 12, fig. 7
	21	*Dicarinella algeriana*	MP -138	Premoli-Silva & Sliter, 1994, p. 57, pl. 12, fig. 10
12	1,2	*Dicarinella imbricata*	MP-140, MP-182	Sliter & Premoli-Silva, 1990, p. 653, fig 12 (3)
	3	*Rotalipora deekei*	MP-138	Premoli-Silva & Sliter, 1994, p. 49, pl. 8, fig. 7
	4,5	*Rotalipora deekei*	MP-137, MM-25	Sliter & Premoli, 1990, fig. 13 (9); Okay & Altiner, 2007, p. 275, pl. 4, fig. 8
	6	*Rotalipora deekei*	MP -140	----------
	7,8 with minor differences	*Rotalipora globotruncanoides*	MP-140	Bertle & Suttner, 2005, p. 886, figs. 3 (M, N)
	9	*Whiteinella paradubia*	MP-179	Premoli-Silva & Sliter, 1994, p. 53, pl. 10, figs. 5, 7
	10	*Whiteinella paradubia*	MP-189	Premoli-Silva & Sliter, 1994, p. 53, pl. 10, fig. 1
	11,13, with minor differences	*Whiteinella archaeocretacea*	MP-182, MP-191	Premoli-Silva & Sliter, 1994, p. 55, pl. 11, fig. 6.
	12	*Whiteinella archaeocretacea*	MP-182	Sliter & Premoli-Silva, 1990 p. 656, fig. 14 (3)
	14	*Helvetoglobotruncana helvetica*	MP-181	Okay & Altiner, 2007, p. 277, pl. 5, fig. 2
	15	*Helvetoglobotruncana helvetica*	MP-197	Okay & Altiner, 2007, p. 277, pl. 5, fig. 1; Premoli-Silva & Sliter 1995, p. 55, pl. 11, fig. 9
	16,19,20,22 with minor differences	*Helvetoglobotruncana helvetica*	MP-196,MP-187,MP-182,MP-195	Premoli-Silva & Sliter, 1994, p. 55, pl. 11, fig. 3
	17	*Helvetoglobotruncana helvetica*	MP-179	Premoli-Silva & Sliter, 1994, p. 55, pl. 11, fig. 9
	18	*Helvetoglobotruncana helvetica*	MP-196	Premoli-Silva & Sliter, 1994, p. 55, pl. 11, fig. 10
	21	*Helvetoglobotruncana helvetica*	MP-182	Okay et al. 2010, p. 1262, fig. 12 (E).

13	1,2	*Whiteinella aprica*	MP-188, MP-185	Premoli-Silva & Sliter, 1994, p. 53, pl. 10, fig. 8
	3,4 with minor differences	*Whiteinella brittonensis*	MP-185, MP-132	Premoli-Silva & Sliter, 1995, p. 53, pl. 10, fig. 2
	5,6 with minor differences	*Dicarinella canaliculata*	MP-196, MP-185	Premoli-Silva & Sliter, 1994, p. 57, pl. 12, fig. 14
	7	*Dicarinella canaliculata*	MP-137	Sliter & Premoli, 1990, p. 652, fig. 12 (8)
	8	*Dicarinella hagni*	MP-194	Caron et al. 2006, p.16, fig. 8 (9)
	9	*Dicarinella hagni*	MP-182	Premoli-Silva & Sliter, 1994, p. 57, pl. 12, fig. 3
	10	*Dicarinella hagni*	MP-195	Robaszynski et al. 2010, p. 11, fig. 13 (N)
	11	*Dicarinella hagni/imbricata*	MP-181	Robaszynski et al. 2010, p. 11, fig. 13 (M)
	12,13 with minor differences	*Whiteinella* (?) *inornata*	MP-193, MP-181	Bellier, 1998, p. 345, pl. 5, fig. 4
	14, 15, 16, 17, 18, 19, 20, with minor differences	*Heterohelix reussi*	MP-201, MP-193, MP-203, MP-205, MP-206, MP-203, MP-203	Premoli-Silva & Sliter, 1994, p. 81, pl. 24, figs. 7-9
	21	*Heterohelix reussi*	MP-207	Li et al. 2009, p. 1012, fig. 5 (36)
14	1	*Marginotruncana sigali*	MP-195	----------
	2,3	*Marginotruncana sigali*	MP-194, MP-187	Radoičić & Buser, 2004, p. 161, pl. 2, fig. 1; Bandini et al. 2007, pl. 3, fig. 5
	4	*Marginotruncana sigali*	MP-194	Okay et al. 2010, p. 1262, fig. 12 (J).
	5	*Marginotruncana schneegansi*	MP-187	Okay & Altiner, 2007, p. 277, pl. 5, fig. 21; Radoicic & Buser, 2004, pl. 1, fig. 12
	6	*Marginotruncana schneegansi*	MP-196	Radoičić & Buser, 2004, p. 161, pl. 2, fig. 10
	7	*Marginotruncana schneegansi*	MP-186	Premoli-Silva & Sliter, 1994, p. 60, pl. 14, fig. 8
	8	*Marginotruncana schneegansi*	MP-180	Premoli-Silva & Sliter, 1994, p. 61, pl. 14, fig. 3
	9	*Marginotruncana renzi*	MP-185	Premoli-Silva & Sliter, 1994, p. 61, pl. 14, fig. 1
	10	*Marginotruncana pseudolinneiana*	MP-196	Okay et al. 2010, p. 1262, fig. 12 (M)
	11	*Marginotruncana pseudolinneiana*	MP-198	----------
	12	*Marginotruncana marianosi*	MP-191	Premoli-Silva & Sliter, 1994, p. 49, pl. 8, fig. 8.
	13	*Marginotruncana coronata*	MP-204	Altiner & özcan, 1999, p. 292, fig. 4 (2)
	14	*Marginotruncana coronata*	MP-205	Farinacci & Yeniay, 1986, p. 271, pl. 4, fig. 3

14	15	*Marginotruncana coronata*	MP-181	Okay & Altiner, 2007, p. 277, pl. 5, fig. 16
	16	*Marginotruncana coronata*	MP-181	Radoičić & Buser, 2004, p. 171, pl. 7, fig. 8
	17	*Marginotruncana coronata*	MP-196	----------
	18	*Marginotruncana renzi*	MP-202	Okay et al. 2010, p. 1262, fig. 12 (G)
	19	*Marginotruncana coronata*	MP-196	Radoičić & Buser, 2004, p. 161, pl. 2, fig. 5
	20	*Marginotruncana coronata*	MP-209	Willems et al. 1996, p. 742, fig. 17 (f)
	21	*Marginotruncana coronata*	MP-204	Postuma 1971, p. 33
	22	*Marginotruncana marginata*	MP-191	Premoli-Silva & Sliter, 1994, p. 59, pl. fig. 6
	23, 24, 25 with minor differences	*Hedbergella flandrini*	MP-192, MP-195, MP-198	Okay et al. 2010, p. 1262, fig. 12 (I); Li et al. 2010, p. 6, figs. 5 (1-3)
15	1,2 with minor differences	*Globigerinelloides bollii*	MP-195, MP-194	Premoli-Silva & Sliter, 1994, p. 39, pl. 3, fig. 13.
	3	*Marginotruncana sinousa*	MP-185	Li et al. 2009, p. 1010, fig. 4 (13).
	4	*Dicarinella primitiva*	MP-195	Willems et al. 1996, p. 742, fig. 17 (g).
	5,6	*Dicarinella primitiva*	MP-197, MP-196	Bertle & Suttner, 2005, p 887, fig. 4 (M).
	7	*Dicarinella primitiva*	MP 196	----------
	8	*Archaeoglobigerina cretacea*	MP-196	Premoli-Silva & Sliter, 1994, p. 75, pl. 21, fig. 2
	9	*Archaeoglobigerina cretacea*	MP-196	Premoli-Silva & Sliter 1995, p. 75, pl. 21, fig. 5
	10,11	*Dicarinella concavata*	MP-196, MP-193	Sliter, 1989, p. 14, pl. 2, fig. 11; Premoli-Silva & Sliter 1995, p. 57, pl. 12, fig. 1
	12	*Dicarinella concavata*	MP-191	Sari & özer, 2002, p. 57, pl. 1, fig. 3
	13	*Dicarinella concavata*	MP-194	Willems et al. 1996, p. 742, fig. 17 (h)
	14	*Contusotruncana fornicata*	MP-193	Li et al. 2009, p. 1010, fig. 4(42)
	15	*Pseudoguembelina costulata*	MP-203	Premoli-Silva & Sliter, 1994, p. 82, pl. 25, fig. 9
	16	*Pseudoguembelina costulata*	MP-203	Premoli-Silva & Sliter, 1994, p. 82, pl. 25, fig. 10
	17	*Contusotruncana fornicata*	MP-200	Farinacci & Yeniay, 1986, pl. 5, fig. 2
	18	*Contusotruncana fornicata*	MP-204	Farinacci & Yeniay, 1986, pl. 5, fig. 1
	19	*Dicarinella* cf. *asymetrica*	MP-195	Radoičić & Buser, 2004, p. 177, pl. 10, fig. 7
	20	*Dicarinella asymetrica*	MP-195	Altiner & özcan, 1999, p. 292, fig. 4 (1); Sliter 1989, p. 16, pl. 3, fig. 1

16	1,2,3,5,6 with minor differences	*Globotruncana linneiana*	MP-209,MP-202,MP-200,MP-209,MP-209	Sari & özer, 2002, p. 57, pl. 1, fig. 7; Sari, 2006, p. 252, pl. I, fig, 1; Premoli-Silva & Sliter 1994, p. 65, pl. 16, fig. 6
	4	*Globotruncanita conica*	MP-204	Vaziri, 2002, p. 351, pl. 6, fig, 7
	7	*Globotruncanita elevata*	MP-207	Radoičić & Buser, 2004, p. 177, pl. 10, fig, 1
	8	*Globotruncanita elevata*	MP-200	Radoičić & Buser, 2004, p. 177, pl. 10, fig, 3
	9	*Globotruncanita elevata*	MP-200	Postuma 1971, p. 35; Radoičić & Buser, 2004, p. 177, pl. 10, fig, 6
	10	*Globotruncanita elevata*	MP-204	Pessagno, 1967, p. 432, pl. 93, fig. 8
	11	*Globotruncanita elevata*	MP-207	Premoli-Silva & Sliter, 1994, p. 69, pl. 18. fig. 5
	12	*Globotruncanita elevata*	MP-201	Sari, 2006, p. 254, pl. II, fig. 14; Sari & özer, 2002, p. 57, pl. 1, fig. 4
	13	*Globotruncana lapparenti*	MP-201	Postuma, 1971, p. 49
	14	*Globotruncana lapparenti*	MP-204	Li et al. 2009, p. 1010, 4(28)
	15	*Laeviheterohelix glabrans*	MP-206	Premoli-Silva & Sliter, 1994, p. 81, pl. 24, fig. 16
	16	*Ventilabrella multicamerata*	MP-204	Premoli-Silva & Sliter, 1994, p. 85, pl. 26, fig. 9
17	1,3 with minor differences	*Globotruncana bulloides*	MP-204,MP-206	Premoli-Silva & Sliter, 1994, p. 63, pl. 15, fig. 8
	2	*Globotruncana bulloides*	MP-207	Li et al. 2010, p. 5, figs. 4 (15-16); Sari, 2006, p. 254, pl. II, fig. 1
	4	*Globotruncana bulloides*	MP-207	Li et al. 2009, p. 1010, fig. 4 (23)
	5	*Globotruncana arca*	MP-203	Li et al. 2009, p. 1010, fig. 4 (31)
	6	*Globotruncana arca*	MP-203	Vaziri, 2002, p. 352, pl. 7, fig. 7
	7	*Globotruncana arca*	MP-206	Sari, 2009, p. 1112, fig. 8 (40).
	8,9,10 with minor differences	*Globotruncana arca*	MP-206,MP-204,MP-203	Premoli-Silva & Sliter, 1994, p. 65, pl. 16, fig. 7; Li et al. 2009, p. 1010, fig. 4 (30)
	11,12,14,16 with minor difference	*Heterohelix globulosa*	MP-207,MP-206, MP-203,MP-207	Li et al. 2009, p. 1012, fig. 5 (32)
	13,15 with minor differences	*Heterohelix globulosa*	MP-203,MP-204	Li et al. 2009, p. 1012, figs. 5 (30-31)
	17	*Heterohelix globulosa*	MP-203	Premoli-Silva & Sliter, 1994, p. 81, pl. 24, fig. 3

18	1	*Heterohelix planata*	MP-202	Li et al. 2009, p. 1012, fig. 5 (33)
	2	*Heterohelix planata*	MP-203	Li et al. 2009, p. 1012, fig. 5 (34)
	3	*Ventilabrella glabrata*	MP-204	Premoli-Silva & Sliter, 1994, p. 82, pl. 25, fig. 4
	4	*Globotruncana hilli*	MP-200	Sliter & Leckie, 1993, p. 82, pl. 3, fig. 7; Premoli-Silva & Sliter, 1994, p. 65, pl. 16, fig. 3
	5,6 with minor differences	*Globotruncana hilli*	MP-200	Premoli-Silva & Sliter, 1994, p. 65, pl. 16, fig. 4
	7	*Globotruncana hilli*	MP-206	Premoli-Silva & Sliter, 1994, p. 65, pl.16, fig. 3
	8	*Rugoglobigerina rugosa*	MP-207	Sari, 2006, p. 256, pl. III, fig. 12
	9,10,14,15,16 with minor differences	*Globotruncana carinata*	MP-204, MP-201, MP-204, MP-204, MP-204	Li et al. 2009, p. 1010, figs. 4 (38-39)
	11	*Globotruncana carinata*	MP-200	Li et al. 2007, p. 924, pl.1, fig. 14
	12,13 with minor differences	*Globotruncana carinata*	MP-204, MP-204	Li et al. 2007, p. 924, pl.1, fig. 13
19	1	*Globotruncana ventricosa*	MP-202	Premoli-Silva & Sliter, 1994, p. 63, pl. 15, fig. 4
	2	*Globotruncana ventricosa*	MP-206	Li et al. 2010, p. 4, fig. 3 (5)
	3	*Globotruncana ventricosa*	MP-200	Willems et al. 1996, p. 742, fig. 17 (m)
	4	*Globotruncana ventricosa*	MP-203	Vaziri, 2002, p. 352, pl. 7, fig. 2
	5	*Globotruncana ventricosa*	MP-207	Li et al. 2010, p. 4, fig. 3 (4)
	6	*Globotruncana ventricosa*	MP-203	Li et al. 2009, p. 1012, fig. 5 (3).
	7	*Globotruncana ventricosa*	MP-204	Li et al. 2009, p. 1012, fig. 5 (2)
	8	*Globotruncana ventricosa*	MP-207	Li et al. 2010, p. 4, fig. 3 (2); Li et al. 2009, p. 1012, fig. 5 (7)
	9	*Globotruncana ventricosa*	MP-204	Li et al. 2009, p. 1012, fig. 5 (7)
	10	*Globotruncana* sp.	MP-204	Li et al. 2010, p. 4, fig. 3 (1)
	11	*Globigerinelloides prairiehillensis*	MP-206	Li et al. 2010, p. 6, fig. 5 (8).
	12	*Globigerinelloides prairiehillensis*	MP-205	Li et al. 2010, p. 6, fig. 5 (9); Premoli-Silva & Sliter, 1994, p. 39, pl. 3, fig. 8

19	13	*Globigerinelloides prairiehillensis*	MP-205	Li et al. 2010, p. 6, fig. 5 (7)
	14,15 with minor differences	*Globigerinelloides prairiehillensis*	MP-198, MP-202	Li et al. 2009, p. 1012, fig. 5 (51)
	16	*Contusotruncana plummerae*	MP-200	Premoli-Silva & Sliter, 1994, p. 67, pl. 17, fig. 5
	17	Transitional between *Contusotruncana patelliformis* and *Contusotruncana contusa*	MP-200	Premoli-Silva & Sliter, 1994, p. 67, pl. 17, fig. 3
	18	*Contusotruncana patelliformis*	MP-199	Premoli-Silva & Sliter, 1994, p. 67, pl. 17, fig. 4
20	1	*Globotruncanita stuarti*	MP-207	Li et al. 2009, p. 1012, fig. 5 (21)
	2	*Globotruncanita stuartiformis*	MP-209	Premoli-Silva & Sliter, 1994, pl. 18, fig. 6
	3	*Contusotruncana contusa*	MP-207	Premoli-Silva & Sliter, 1994, p. 67, pl. 17, fig. 6
	4,6 with minor differences	*Pseudotextularia elegans*	MP-204,MP-202	Li et al. 2009, p. 1012, fig. 5 (42)
	5	*Pseudotextularia elegans*	MP-206	Li et al. 2009, p. 1012, fig. 5 (41); Pessagno, 1967, p. 436, pl.97, fig. 18.
	7	*Globotruncanita subspinosa*	MP-208	Sari, 2009, p. 1114, fig. 9 (28)
	8	*Globotruncana rosetta*	MP-200	Sari, 2009, p. 1112, fig. 8 (52)
	9	*Globotruncanita conica*	MP-204	Premoli-Silva & Sliter, 1994, p. 69, pl. 18, fig. 3
	10	*Globotruncanita conica*	MP-204	Pessagno 1967, p. 432, pl.93, fig. 13; Postuma, 1971, p. 29
	11	*Planoglobulina* sp.	MP-208	Sari, 2009, p. 1114, fig. 9 (47)
	12	*Planoglobulina acervulinoides*	MP-209	Altiner & özcan, 1999, p. 292, fig. 4 (9)
	13	*Globotruncanita calcarata*	MP-204	Altiner & özcan, 1999, p. 292, fig. 4 (3)
	14	*Globotruncanita calcarata*	MP-204	Sari, 2009, p. 1114, fig. 9 (24)
	15	*Globotruncana arca*	MP-207	Tertis et al. 2002, p.82, pl. III, fig. 12
	16	*Globotruncana* cf. *aegyptiaca.*	MP-209	----------
	17	*Laeviheterohelix glabrans*	MP-205	Premoli-Silva & Sliter, 1994, pl. 24, fig. 16

20	18	*Gublerina* cf. *robusta*	MP-204	Premoli-Silva & Sliter, 1994, p. 85, pl. 26, fig. 13
	19	*Planoglobulina acervulinoides*	MP-204	Premoli-Silva & Sliter, 1994, p. 85, pl. 26, fig. 10
	20	*Globigerinelloides messinae*	MP-205	Premoli-Silva & Sliter, 1994, p. 73, pl. 20, fig. 3
21	1	*Contusotruncana fornicata*	MP-203	Postuma, 1971, p. 39
	2	*Contusotruncana patelliformis*	MP-200	Premoli-Silva & Sliter, 1994, p. 67, pl. 17, fig. 4
	3	*Globotruncana lapparenti*	MP-206	Li et al. 2009, p. 1010, fig. 4 (29)
	4	*Globotruncana leupoldi*	MP-208	Radoičić & Buser, 2004, p. 173, pl. 8, fig. 10
	5	*Globotruncanella* sp.	MP-200	----------
	6	*Globigerinelloides volutus*	MP-203	Pessagno, 1967, p. 441, pl. 100, fig. 9
	7	*Globigerinelloides bollii*	MP-201	Premoli-Silva & Sliter, 1994, p. 39, pl. 3, fig. 7
	8	*Laeviheterohelix glabrans*	MP-204	Premoli-Silva & Sliter, 1994, p. 81, pl. 24, fig. 16
	9	*Heterohelix carinata*	MP-200	Premoli-Silva & Sliter, 1994, p. 81, pl. 24, fig. 14
	10	*Gublerina* cf. *robusta*	MP-204	Premoli-Silva & Sliter, 1994, p. 85, pl. 26, fig. 13
	11	*Laeviheterohelix glabrans*	MP-208	----------
	12	*Globotruncana rosetta*	MP-208	Sari, 2009, p. 112, fig. 8 (52)
	13	*Contusotruncana fornicata*	MP-200	Postuma, 1971, p. 39
22	1	*Globotruncana stephensoni*	MP-207	Pessagno, 1967, p. 437, pl. 96, fig. 5.
	2	*Globotruncana orientalis*	MP-202	Premoli-Silva & Sliter, 1994, p. 63, pl. 15, fig. 3
	3	*Globotruncana dupeublei*	MP-209	Altiner & özcan, 1999, p. 292, fig. 4 (7)
	4	*Contusotruncana* sp.	MP-204	----------
	5	*Globotruncanella havanensis*	MP-206	Premoli-Silva & Sliter, 1994, p. 71, pl. 19, fig. 12
	6	*Sigalia* sp.	MP-208	Premoli-Silva & Sliter, 1994, p. 83, pl. 25, fig. 2
	7	*Ventilabrella eggeri*	MP-208	Premoli-Silva & Sliter, 1994, p. 83, pl. 25, fig. 5
	8	*Heterohelix* sp.	MP-202	----------
	9	*Planoglobulina carseyae*	MP-208	Premoli-Silva & Sliter, 1994, p. 85, pl. 26, fig. 1
	10	*Planoglobulina acervulinoides*	MP-209	Premoli-Silva & Sliter, 1994, p. 85, pl. 26, fig. 11.
	11	*Aragonia sp.*	MP-208	Sliter & Leckie, 1993, p. 82, pl. 4, fig. 6
	12	*Globotruncanita elevata*	MP-207	Pessagno, 1967, p. 432, pl. 93, fig. 4

23	1	*Contusotruncana contusa*	MP-207	Pessagno, 1967, p. 437, pl. 96, fig. 15
	2,3	*Globotruncanita conica*	MP-210	Premoli-Silva & Sliter, 1994, p.69, pl. 18, fig. 3
	4,5	*Globotruncanita elevata*	MP-210, MP-208	Premoli-Silva & Sliter, 1994, p. 69, pl. 18, figs, 5, 7.
	6	*Globotruncanita stuarti*	MP-208	Sari, 2009, p. 1114, fig. 9(16).
	7	*Globotruncanita stuarti*	MP-208	Premoli-Silva & Sliter, 1994, p. 69, pl. 18, fig. 2.
	8	*Globotruncanita stuartifromis*	MP-208	Premoli-Silva & Sliter, 1994, p. 69, fig. 4.
	9	Transitional form between *Globotruncanita subspinosa* and *Globotruncanita calcarata*	MP-208	Premoli-Silva & Sliter, 1994, p. 69, pl. 18, fig. 1.
	10	*Rugoglobigerina milamensis*	MP-208	Premoli-Silva & Sliter, 1994, p. 79, pl, 23, fig. 2
	11, 12	*Globotruncanita calcarata*	MP-209	Chen et al., 2011, p. 104, fig. 3(21).
	13	*Globotruncanita calcarata*	MP-208	Pessagno, 1967, p. 432, pl. 93, fig. 14
	14	*Globotruncanita conica*	MP-210	Pessagno, 1967, p. 432, pl. 93, fig. 13
	15	*Ventilabrella glabrata*	MP-209	Premoli-Silva & Sliter, 1994, p. 83, pl. 25, fig. 4